

TECHNIQUES AND INSTRUMENTATION IN ANALYTICAL CHEMISTRY—VOLUME 8

NUCLEAR ANALYTICAL TECHNIQUES IN MEDICINE

Edited by

Roberto Cesareo

*Università degli Studi di Roma "La Sapienza", Centro per l'Ingegneria Biomedica, 00186
Rome, Italy*



ELSEVIER

Amsterdam – Oxford – New York – Tokyo 1988

ELSEVIER SCIENCE PUBLISHERS B.V.
Sara Burgerhartstraat 25
P.O. Box 211, 1000 AE Amsterdam, The Netherlands

Distributors for the United States and Canada:

ELSEVIER SCIENCE PUBLISHING COMPANY INC.
52, Vanderbilt Avenue
New York, NY 10017, U.S.A.

ISBN 0-444-42911-5 (Vol. 8)
ISBN 0-444-41744-3 (Series)

© Elsevier Science Publishers B.V., 1988

All rights reserved. No part of this publication may be reproduced, stored in a retrieval system or transmitted in any form or by any means, electronic, mechanical, photocopying, recording or otherwise, without the prior written permission of the publisher, Elsevier Science Publishers B.V./ Science & Technology Division, P.O. Box 330, 1000 AH Amsterdam, The Netherlands.

Special regulations for readers in the USA – This publication has been registered with the Copyright Clearance Center Inc. (CCC), Salem, Massachusetts. Information can be obtained from the CCC about conditions under which photocopies of parts of this publication may be made in the USA. All other copyright questions, including photocopying outside of the USA, should be referred to the publisher.

No responsibility is assumed by the Publisher for any injury and/or damage to persons or property as a matter of products liability, negligence or otherwise, or from any use or operation of any methods, products, instructions or ideas contained in the material herein. Because of rapid advances in the medical sciences, the Publisher recommends that independent verification of diagnoses and drug dosages should be made.

Printed in The Netherlands

CONTRIBUTORS

H.J.M. BOWEN, Department of Chemistry, University of Reading, P.O. Box 224,
Reading RG6 2AD, U.K.

R. CESAREO, Centro per l'Ingegneria Biomedica e Cattedra di Fisica, Facoltà di
Farmacia, Università di Roma "La Sapienza", Corso Vittorio Emanuele
II, 244, 00186 Rome, Italy

K.V. ETTINGER, Department of Internal Medicine, University of Rome "Tor Vergata",
Via O. Raimondo, 00173 Rome, Italy

G.E. GIGANTE, Centro per l'Ingegneria Biomedica, Università di Roma "La
Sapienza" e Dipartimento di Scienze Biomediche, Facoltà di Medicina e
Chirurgia, 67100 L'Aquila, Italy

B. GONSIOR, Ruhr Universität Bochum, Institut für Experimentalphysik III,
Postfach 102148, D-4630 Bochum, F.R.G.

N. MOLHO, Dipartimento di Fisica, Sezione di Fisica Medica, Università di
Milano, Via Celoria 16, 20122 Milan, Italy

Chapter 1

TRACE ELEMENTS IN BIOLOGICAL SAMPLES

H.J.M. BOWEN

Dept. of Chemistry

University of Reading

PO BOX 224, Reading RG6 2AD (England)

1.1 INTRODUCTION

A trace element is taken to mean an element which constitutes less than one per cent of the wet weight of biological material. Carbon, hydrogen, oxygen, nitrogen, phosphorus and sulphur are major elements of vital importance in biology but will not be considered in this chapter. Calcium is a major element in tissues such as bone and tooth, but a minor element in soft tissues and blood. Sodium, potassium and chlorine constitute more than one per cent of a few tissues, but are treated as trace elements here.

Trace elements are classified as inessential or essential according to whether an organism can grow and complete its life cycle in their absence (ref. 1). However it is technically impossible to remove every atom of a particular element from the diet and environment of an organism, and extremely difficult to produce deficiency symptoms in humans or even small mammals in most cases. Even for essential elements there is always an optimum range of concentration in the diet, below which deficiency symptoms such as stunting of growth occur, and above which symptoms of toxicity begin. Our current knowledge of elements essential to mammals is imperfect and somewhat controversial, as shown by the following groups (refs. 1,2).

Essential: Ca, Cl, Co, Cu, Fe, I, K, Mg, Mn, Mo, Na, Ni, Se, Zn

Probably essential: As, Cr, F, Si, Sn, V

Evidence for essentiality lacking: B, Ba, Br, Cd, Li, Rb, Sr

Inessential: All other elements?

Researchers in medicine have mostly concentrated on essential trace elements, especially Cu, Se and Zn in recent years. There has also been much interest in those inessential elements which have been increasing in the environment as a result of man's activities. The fashionable elements to study have been Cd, Hg and Pb, but Ag, As, Cr, Mn, Sb, Sn and V also fall in this

category. In very few cases do we know the functions of essential trace elements, or the manner in which toxic elements cause dysfunction.

1.2 FUNCTIONS OF TRACE ELEMENTS

These functions can be classified as inorganic/structural, electrochemical, catalytic and miscellaneous or unknown. Examples of inorganic/structural functions include apatite, or calcium phosphate, in vertebrate bone and tooth; the barium sulphate crystals which may act as gravity sensors in *Loxodid* cells (ref. 3); magnetite (triferric tetroxide) crystals which act as magnetic field sensors in bacteria and bees (refs. 4, 5); and silica or unknown derivatives which may help to stiffen collagen (ref. 6).

Electrochemical functions are associated with the metal cations Ca^{++} , K^+ , Mg^{++} , Na^+ and the Cl^- anion. All living cells maintain high concentrations of K^+ and Mg^{++} inside their cytoplasm, while excluding Ca^{++} and Na^+ in the extracellular fluid. In this way they can keep a supply of potential energy on tap. Most of the calcium and magnesium inside cells appears to be bound rather than as free ions. The free calcium ion has many important messenger functions within and between cells (ref. 7).

The essential trace elements Ca, Cl, Co, Cu, Fe, Mg, Mn, Mo, Ni, Se and Zn form compounds with proteins which have a wide range of catalytic functions. Cu, Fe, Mn and Mo catalyse many redox reactions in vitro, but do so far more specifically and efficiently when the metal occupies a specific site in an enzyme molecule.

Miscellaneous functions include the production of toxic molecules containing halogen or fluorine atoms by sponges, algae, fungi, lichens and a few higher plants (refs. 1, 8). These are believed to discourage predators. Arsenobetaine from marine animals, boromycin from *Streptomyces*, selenomethionine and homologues from higher plants and fungi, and amavanadine from the fungus *Amanita muscaria* may have similar functions (ref. 1).

In many animals excessive or toxic amounts of certain metals may be shunted into very large proteins, such as iron in ferritin, or into granular bodies in the cytoplasm, possibly as a mechanism of excretion. Examples are the calcium carbonate or calcium phosphate granules in many tissues, sulphide-rich granules which may contain Bi, Cd, Cu, Hg, Pb or Zn found in the kidney, and mercury-selenium granules found in the livers of whales (refs. 9, 10). Such granules represent a form of internal contamination, and make the interpretation of analyses of whole organs such as kidneys more difficult.

1.3 CONTAMINATION AND LOSS BEFORE ANALYSIS

So far no mention has been made of the technical difficulties of analysing biological material in general and human tissues in particular. Most human tissues are taken from victims of accidents as soon as possible after death, to avoid the inevitable post-mortem changes. A major problem is the universal presence of trace elements in environmental dust, sampling tools and containers which frequently contaminate samples. Where the element sought is present in concentrations of 1 - 10 ppm or more, reasonably clean handling before analysis is adequate. However many soft tissues have been handled or cut with stainless steel instruments, which can cause gross contamination with Co, Cr, Fe, Mn, Mo, W and other elements whose true concentration may be extremely low. Contamination can be reduced by using instruments made of titanium or silica, and by working in a clean-room with a supply of filtered air. Samples of skin and lung will have been exposed to the environment for some time, however carefully they are collected. Bone and tooth samples are difficult to cut, and may have been contaminated by chronic exposure to metal implants, tooth fillings or false teeth. Hair and nail are likely to be contaminated with environmental dust, sweat, and materials derived from ornaments and washing treatments. How they should be cleaned before analysis is a matter of controversy. Perhaps the most difficult samples to collect without contamination are blood, serum, plasma and erythrocytes. Versieck (ref. 12) has shown that ordinary hypodermic needles are quite unsuitable for collecting blood samples in which Co, Cr, Mn or Mo are to be determined. If they are used, the values obtained are a measure of the solubility of hypodermic needles in blood. Any sort of anticoagulant, notably heparin, is a likely contaminant and should be avoided. The centrifugal separation of erythrocytes from plasma needs care as the cells easily break up, as they do on exposure to pure water. The iron content of the plasma is a useful guide to the efficiency of removing red cells without rupturing them. The collection of human milk and urine also have their problems, such as bacterial attack or precipitation on storage. Any sort of preservative is a source of contamination.

Losses of elements before analysis can also occur. If samples are dried in freeze-driers or ovens, volatile derivatives of non-metallic elements may be lost. Such losses are even more likely if samples are ashed at about 500 °C to reduce their volume. Testing losses by spiking with radionuclides is not satisfactory when, as is usually the case, the chemical form of the natural element is unknown. Many noble metals and metalloids such as As, Hg, Pb, Sb, Se, Sn and Te may occur naturally as methyl derivatives whose volatility is uncertain (ref. 13).

1.4 METHODS OF ANALYSIS AND THEIR RELIABILITY

Tremendous improvements in analytical sensitivity have occurred in the last thirty years, so that it is now possible to determine most elements in ng if not pg amounts. Practising analysts need to emphasize the following limitations of their skills when talking to their biological and medical colleagues:

- a. Improvements in sensitivity mean that previously unrecognised sources of contamination become significant or even dominant.
- b. No single method of determination can be used for all the elements, and all methods have wide variations in sensitivity between different elements.
- c. Extremely sensitive determinations require a large capital investment in equipment.

Nuclear methods of analysis form the subject matter of subsequent chapters. Their disadvantages include slowness, inadequate sensitivity for some elements and a number of potential errors. Slow methods are not used in routine clinical work. Inadequate sensitivity is shown by the limited number of reliable determinations in the literature for the following elements, as amplified in Tables 1.2 - 1.4 below. For essential elements, good data is scarce for Si, Sn and V. Among the inessential elements, there appear to be no data for Ir, Os, Re, Rh, Ru and Ta in human tissues, and reliable data for the following is sparse: B, Be, Bi, Ga, Ge, Hf, In, La - Lu, Li, Nb, Pd, Pt, Te, Th, Ti, Tl, U, W, Y and Zr.

All methods of analysis can have systematic errors, which appear to increase in frequency when the analyte occurs at concentrations below 1 ppm. The best method of discovering and then avoiding systematic errors is the regular use of certified reference materials (CRM) to check that ones own results agree with those of others (ref. 14). I have circulated one such CRM, Kale, and the accuracy of over a thousand determinations on this material can be summarised by saying that over 40% differ from the best mean by more than 10% (ref. 15). Other reviewers have found equally unsatisfactory agreement between different analysts. Reported concentrations of chromium in SRM Bovine Liver from the U.S. National Bureau of Standards range from less than 5 to 3500 ng g⁻¹, although the certified value is 88 ± 12 ng g⁻¹ (ref. 12). Similar disagreements are unfortunately common. According to Parr (ref. 16), a reasonable number of biological CRMs with certified values of the following elements are available for testing accuracy: As, Ca, Cd, Cl, Cr, Cu, Fe, Hg, K, Mg, Mn, Mo, Na, Ni, Pb, Se and Zn. The situation is far less satisfactory for all the other elements, which makes it hard to assess the accuracy of published work. The absence or paucity of CRMs for elements thought to be essential, such as Co, F, I, Si, Sn and V, represents a real obstacle to progress in our knowledge of their abundance in human tissues.

Striking improvements in the reliability of determinations of cadmium have been achieved by circulating CRMs and then feeding outlier results back to the analysts concerned for re-appraisal (ref. 17). Some sort of quality control in analytical work should be mandatory.

1.5 COMPOSITION OF SELECTED TISSUES

The literature on the elemental composition of tissues from healthy, adult humans is vast. Iyengar et al. (ref. 18) listed 1026 references giving data in a compilation published in 1978, and at least as many papers on the topic have appeared in the succeeding eight years. These have not been fed into the data bank of an accessible computer, and selection of reliable data is both arduous and subjective. Versieck has made a good attempt at objectivity by rejecting data for which there is no means of assessing accuracy (ref. 12), while Iyengar has assembled a mass of new data from many different countries (ref. 19).

A useful concept, Reference Man, has been introduced by Snyder (ref. 20), who gives average data for fresh weights, dry weights and ash weights of most tissues. These data are invaluable for recalculating figures from the literature, which are given in a great variety of units. Some values for Reference Man are given in Table 1.1.

TABLE 1.1

Fresh weights, dry weights and ash weights of some tissues in Reference Man (ref. 20).

Tissue	FM/kg	DM/kg	Ash/g
Whole Man	70	28	3700
Muscle	28	6	340
Liver	1.8	0.5	23
Lung	1	0.22	11
Kidney	0.31	0.07	3.4
Blood	5.5	0.825	55
Hair	0.02	0.018	0.1
Nail	0.003	0.003	0.016
Bone (+ marrow)	10	7	2800
Tooth	0.046	0.042	34

In the succeeding Tables 1.2 - 1.4, I have attempted to summarise current knowledge of the elemental composition of the tissues listed in Table 1.1, together with serum (or plasma), erythrocytes and milk. In a short chapter of this kind it would be impractical to list all the references on which this

highly subjective summary is based, beyond saying that Chemical Abstracts has been scanned up to the end of Vol. 99. Since disagreements are numerous in the literature, values are given as ranges with outliers omitted. Whether these can be termed 'normal ranges' requires some discussion. For several essential elements such as Ca, Cu, Fe, K, Na, Se and Zn, and perhaps for all the essential group, the ranges of composition are well-established, rather narrow and more or less known to be controlled by homeostatic mechanisms in healthy people. These are certainly normal ranges. For inessential elements such as Ag, Al, Br, Cd, Hg, Pb, Sb, Ti etc there is no need to postulate a 'normal' lower limit of concentration, though the upper limit may be constrained by toxic symptoms or by some method of detoxification involving either kidney or liver or both.

1.5.1 Comments on the data for soft tissues in Table 1.2

All soft tissues have rather closely similar elemental compositions, with a few notable exceptions. Muscle is rich in Cs, K and Mg and relatively poor in most other elements, which correlates well with the concept of K and Mg as sources of free energy in cells. Liver is enriched in Cu, Fe, Mn and Mo, all of which are important in the catalytic oxidation of soluble foods which is a major function of the organ. Kidney is notably enriched in Cd and Hg, and possibly also in Ag, Bi, Br, Mn, Pb, Sb, Se, Sn, Te, Tl, U and V. We know that kidney filters many elements from the bloodstream, and that it manufactures sulphur-rich proteins called metallothioneins which are powerful ligands for heavy metals such as Ag, Cd, Hg, Sn and Zn (ref. 21). Dysfunction of tubules in the kidney has been associated with increased intakes of Bi, Cd, Hg and Pb, while somewhat different kidney damage is caused by excessive Au and U (ref. 22).

The elements enriched in lung are mostly more or less inessential elements which are common in atmospheric dust and soil such as Al, Fe, Sc, Si, Ti and Zr, as well as elements which are characteristic of polluted aerosols such as As, Br, Sb and V (ref. 23). The limited data suggest that Be, Cr, In, La, Lu, Pt metals and Th may also be enriched in mature lung.

1.5.2 Comments on the data for blood components in Table 1.3

Data for whole blood and serum greatly outnumber those for plasma and erythrocytes. The differences in elemental content for serum and plasma seem to be small and are neglected here. The data show that erythrocytes have a higher concentration of As, Cd, Cr, Cs, F, Fe, K, Mg, Mn, Pb, Rb and Zn than does serum. The same is probably true for Hg, Mo, Ni, Sb and V but better data are needed for the content of these elements, and also Al, B, I and Si in

TABLE 1.2

Selected data for elements in human muscle, liver, kidney and lung: figures are concentrations in ppm dry matter.

Element	Muscle	Liver	Kidney	Lung
Ag	0.009-0.02	0.005-0.25	0.005-0.26	0.009-0.03
Al	0.7-28	3-300	1.5-27	80-230
As	0.009-0.23	0.018-0.039	0.007-0.03	0.034-0.5
Au		0.00006-0.003	0.0009-0.0017	0.0003-0.0073
B	0.33-1	0.4-2.5	0.9-2.6	2.7-36
Ba	0.09?	0.04-1.2	0.04-1	0.14-1.6
Be	0.00075	0.0016?	0.0002?	0.05-0.15
Bi	0.032?	0.015-0.1	0.17?	0.05?
Br	8	1-7	16-49	15-46
Ca	140-700	180-610	360-1500	770-1300
Cd	0.14-1.2	1.1-12	12-110	0.09-6.2
Ce		0.29?	0.013	0.1-0.4
Cl	2000-5000	900-9300	1000-12000	1700-11000
Co	0.005-0.028	0.021-0.081	0.018-0.068	0.009-0.073
Cr	0.002-0.37	0.02-0.53	0.04-0.45	0.15-1.4
Cs	0.07-1.6	0.036-0.065	0.028-0.057	0.021-0.08
Cu	3-4	19-28	9-14	5-13
F	0.05	0.2-7	0.04-10	0.8-16
Fe	180	170-1100	23-710	290-4000
Ga	0.0014	0.0025	0.004	0.02-0.23
Ge	0.14?	0.15?		0.18-0.4
Hg	0.02-0.18	0.04-1.7	0.14-12	0.03-2.4
I	0.05-0.5	0.7	0.15	0.3
K	16000	5000-12000	7000-8000	7000-11000
La	0.0004	0.014-0.072	0.00045-0.013	0.025-0.14
Li	0.023	0.025	0.016-0.044	0.14-0.27
Mg	900	390-750	510-670	450-820
Mn	0.23-0.48	1.8-8.1	1.5-5	0.2-5
Mo	0.018	1.3-2.9	0.5-3.1	0.1-1.2
Na	2600-7800	1000-10000	1000-10000	2200-11000
Nb	0.14?	0.15?	0.04-0.07	0.9?
Ni	0.37	0.03-0.39	0.43-0.68	0.3-1.2
Pb	0.23-0.95	0.34-8.3	1.2-6.8	0.06-5.5
Rb	12-18	14-33	14-35	8-19
Sb	0.0003-0.19	0.011-0.083	0.026-0.22	0.032-0.81
Sc	0.0002?	0.0004-0.0014	0.0007-0.0065	0.0023
Se	0.28-0.65	0.69-2	1.4-5.2	0.43-1.1
Si	100-200	24-110	14-200	260-930
Sn	0.23-2.4	0.23-3.8	0.7-8.6	0.77-8
Sr	0.12-0.35	0.08-0.36	0.15-1.5	0.5-0.9
Te	0.017?	0.014?	0.07?	0.1?
Ti	0.9-2.2	0.37-4.7	0.27-1	2.3-38
Tl	0.07	0.004-0.033	0.013	0.006
U	0.0009	0.003	0.009-0.024	
V	0.02	0.006-0.025	0.03-0.67	0.032-0.64
Zn	180-220	180-250	180-320	40-77
Zr	0.08?	0.11?	0.066-0.09	0.23-2.3

Values for other elements: Muscle; Y 0.02. Liver; Pt 0.00013-0.00086. Lung; Dy 0.009, Er 0.009, Eu 0.001-0.004, Gd 0.09, Ho 0.004, In 2.8?, Nd 0.028, Pd 0.22?, Rh 0.36?, Sm 0.005-0.014, Th 0.045

erythrocytes. Serum carries most of the Ba, Br, Ca, Cl, Na and Sr in blood. The high value for K and Mg, together with Cs and Rb, is typical for cells, as is the exclusion of Ca, Cl and Na in the extracellular plasma. Iron is high in cells because of its association with haemoglobin, but the reasons for the enrichment of other elements in cells are obscure. It is possible that toxic element such as Cd, Hg and Pb become incorporated in the mitochondria of cells, where they block sites normally occupied by essential metals such as Cu and Zn (ref. 24).

The amounts of Al, As, Cd, Pb, Sb and Se in whole blood seem to be more variable than other elements. Earlier data indicating high variability for Co, Cr, Mn, Mo, Ni and V are rejected here as they were probably due to sample contamination or other analytical errors (ref. 12). Apart from Se, where low values are only found in abnormal, selenium-deficient populations, the variable elements are inessential and so the wide range of concentrations found may be genuine.

There does not seem to be any reason other than tradition why whole blood is nearly always chosen for the determination of Cd, Hg and Pb, while serum is used for most other elements such as Al, Br, Co, F, I and V.

1.5.3 Comments on the data for hair and nail in Table 1.4

These tissues are quite unlike other soft tissues or bone in elemental content, but are not very different from one another; their main bulk is made of insoluble, sulphur-rich protein. They are depleted in K and Mg, but enriched in some noble metals such as Au, Cu and Pb and in the group of volatile elements which are markedly enriched in aerosols, such as As, Hg, I and Sb (ref. 23). The natural range of composition of hair and nail appears to be much wider than those of soft tissues, for example for As, Cd, Cr, Cu, Fe, Hg, Mn, Pb, Sb, Se and Sn, as well as for Cl and Na, whose content depends critically on the method used to wash the tissue before analysis (ref. 25). Some suggestions have been made that the body uses hair as a mode of excreting thiophilic elements such as As, Hg, Pb, Sb, Se and Te. While hair composition broadly reflects dietary habits and/or exposure to polluted atmospheres, it cannot be used as a fingerprint to identify individuals, as was once hoped by forensic scientists.

1.5.4 Comments on the data for bone and tooth in Table 1.4

Compared with soft tissues, bone is strongly enriched in Ba, Ca, F, Pb, Sc, Sr and probably also the rare earth elements and thorium, though data for the latter are scarce. All these bone-seeking elements form insoluble phosphates or fit readily into the crystal structure of apatite, which constitutes

TABLE 1.3

Selected data for elements in human blood, serum or plasma, erythrocytes and milk: figures are concentrations in ng ml⁻¹ fresh material

Element	Blood	Serum	Erythrocytes	Milk
Ag	0.3?	0.1?	10?	
Al	170-420	2-250	64?	250-2400
As	2-23	0.2-15	2.7	0.02-170
Au	0.01-0.25	0.04-0.32	0.63	
B	130-1300	120-490		240
Ba	1-250	50-600	7	6-42
Be	< 0.01	< 0.7		
Bi	0.002-0.011	< 0.6		
Br	1100-4700	2100-7500	1500	1500
Ca	40k-72k	88k-110k	600-3200	150k-480k
Cd	0.3-1.5	1.9-4	4.2	0.7-4.6
Cl	2900k	3800k	2000k	360k-1100k
Co	0.2-2.6	0.1-0.5	0.2-0.6	0.2-3
Cr	3-40	0.07-0.24	37	0.4-5
Cs	3	0.74-2.1	4.5-13	2-32
Cu	900-1200	800-1600	580-810	200-670
F	500?	12-62	450?	4-110?
Fe	430k-510k	760-1500	700k-1100k	200-1800
Ga	< 80	0.07-0.21		
Ge	400?	< 30	650?	
Hg	0.4-20	1.3-12	2.5-33	0.2-13
I	50	32-89		20-660
K	1500k	130k-200k	3500k	330k-740k
La	17?	1		
Li	4	7-30	7-28	3-100
Mg	33k-43k	18k-25k	57k	23k-48k
Mn	4-30	0.54-1	14-38	3-42
Mo	0.8-5	0.55-2.4	17?	1-20
Na	2000k	3100k-3400k	280k	120k-630k
Ni	4-10	0.4-3.6	83?	1.5-39
Pb	8-270	0.02-15	92-460	3.6-30
Pt	0.5	< 0.5		
Rb	2100-4200	84-290	3500-4700	420-1100
Sb	0.5-6	0.1-7.2	4.6	0.08-5
Sc	0.6-9	< 0.009-0.17		0.004-0.2
Se	30-300	66-140	68-220	10-62
Si	4000?	400-1400	4100?	280-650
Sm	8	3		
Sn	2-80	34-100	380?	0.2-0.5
Sr	35	35	7.2	20-290
Th	0.2-2		0.16	
Ti	30-50	10-110	110	20-910
Tl	0.45	< 2.5		
U	0.5-2	< 0.1	0.24	
V	< 0.1	0.017-0.047	5.6?	0.08-0.8
W	1	0.4		
Zn	3800-8800	610-1500	9200-16000	750-7100
Zr	11	1.7	12?	

Additional values: Blood; Hf 24, Nb 5?, Pd < 0.1, Ta 70?, Te 0.2, Y 4.7.
Milk; Eu 0.008-0.04.

TABLE 1.4

Selected data for elements in human hair, nail, bone and tooth enamel: figures are concentrations in ppm dry matter.

Element	Hair	Nail	Bone	Tooth enamel
Ag	0.05-0.8	0.003-0.5	0.01-0.4	0.005-0.6
Al	8-20	130-930	0.6-190	12-3000
As	0.04-0.85	0.2-3	0.005-1.6	0.02-0.07
Au	0.002-0.17	0.03-1.5	0.02-0.06	0.0001-0.1
B	1.6-5	33?	1-8	5
Ba	1-8	7.5	3-70	4-120
Be	0.006-0.02	< 0.01	0.003	< 0.01
Bi	2?	1.3?	< 0.2	0.006
Br	2-16	9	5-12	1-34
Ca	370-1800	370-3400	170k	370k
Cd	0.1-2	0.08-3.4	0.2	0.0001-0.5
Ce	0.25-0.57	0.6		0.07
Cl	210-4800	1000-3600	900	2200-6500
Co	0.04-0.5	0.055	0.01-0.4	0.004-0.13
Cr	0.06-4	5.5?	0.1	0.005-3.2
Cs	0.02-0.2		0.013-0.052	0.04
Cu	7-29	18	1-5	0.2-20
F	< 5-40		640-12k	290-2600
Fe	4-900	27-350	3-480	4-340
Ga	0.07			< 0.02
Ge	2.3?	1.2?		< 0.02
Hg	0.2-8.6	0.07-1.1	0.01-0.1	< 0.1-3
I	0.27-1.4			0.036
K	17-140	360-2800	500-2000	270-400
La	0.014-0.054	0.3?	0.021	< 0.02
Li	0.05-0.3		0.2	1.1?
Mg	30-350	16-120	1900-3100	1100-3100
Mn	0.3-17	0.04-2.1	0.13-1.6	0.03-1.1
Mo	0.05-0.4	< 0.15-16	< 0.02	0.05-7
Na	13-3000	330-3000	6k-11k	2k-12k
Nb	2?		< 0.07?	0.28
Ni	0.02-2.7	0.03-12	0.5-2	10?
Pb	2.3-56	14-170	0.7-25	0.16-36
Rb	0.2-1.7	3	0.1-5	0.4-7
Sb	0.013-0.26	< 0.03-0.75	0.007-0.1	0.08-0.96
Sc	0.002-0.007		0.001-6	
Se	0.2-6	0.75-8	< 0.06-0.34	0.27-0.87
Si	7-170	300-3500	17?	60?
Sn	0.4-0.7	12?	0.08-1.4	0.2
Sr	0.05-4.5	0.02-0.65	40-150	80-120
Th	0.08		0.002-0.01	
Ti	1-12	0.28	0.5	0.19
Tl	0.016	0.0022	0.002	< 0.04
U	0.0001-0.22		0.0002-0.07	
V	0.005-0.18		0.0035	0.0037-0.017
W	0.016		0.0025	0.24?
Zn	140-250	70-300	90-140	100-370
Zr	0.05-0.3	1.4?	< 0.1	< 0.1

Additional data: Hair; Hf 0.011, Eu 0.0035, In 0.001-0.005, Pd < 0.2, Pt < 0.05, Sm 0.002-0.006, Te 0.95.

Bone; Y 0.07.

Tooth enamel; Nd 0.045, Pr 0.027.

the mineral part of bone. Bone is depleted in Cl, K, Rb and Se compared to soft tissues. Tooth differs from bone in its lower content of proteinaceous, marrow-like material, so that it is even more depleted in K. The data here suggest that tooth is slightly enriched in Al, Hg, Mo and Sb with respect to bone, but this may represent contamination from artificial fillings or dentures. Data for Cd, I and Sn in both tissues are extremely scanty, while data for As, Cr, F, Fe, Mn and Pb show considerable variation, some of which may be caused by analytical errors.

1.5.5 Comments on the data for milk in Table 1.3

Data for many rare and inessential elements are missing for milk. Its elemental composition does not differ greatly from that of whole blood, though it is enriched in calcium and much depleted in iron. It is also depleted in Cl, Cu, K, Na, Pb, Rb and Se compared to whole blood. The composition of milk, though buffered metabolically, must reflect the diet taken by the mother. This may account for the considerable variation in concentration in As, Cd, F, Fe, I, Mn, Mo, Se and Zn found in different countries (refs. 19, 26). Another source of variability is the time elapsed since birth (ref. 26).

1.6 ABNORMAL CONCENTRATIONS OF ELEMENTS IN HUMAN TISSUES

This is such an enormous topic that only a brief overview can be attempted here. Abnormalities can be categorised under the presumed causative agent, which may be dietary (and hence often geographical), industrial, age-related or pathological. Some abnormalities in hair composition have no obvious cause (ref. 19).

1.6.1 Abnormalities due to diet

Following a review of the elemental composition of human diets, it was concluded that deficient and toxic diets are rare and local in the world, apart from deficiencies in iodine and iron (ref. 27). Symptoms of deficiency or toxicity are more often found in domestic animals, which have a diet restricted to locally-grown plants (ref. 28). Arsenic is very low, perhaps even deficient, in refined diets of rich countries, where it is mainly supplied by sea-foods. On the other hand arsenic is high in soil and waters in parts of Alaska, Chile, New Zealand and Taiwan, and this is reflected in the high concentrations of arsenic in the blood plasma and liver of local populations (ref. 19). There have been suggestions, but little hard evidence, that chromium may be deficient in the diets of richer countries (ref. 29). Deficiencies of copper, manganese and molybdenum in humans are extremely rare, but

have been found in a very few children on diets which are nutritionally inadequate (ref. 30). Fluorine deficiency is implicated in the increased incidence of tooth decay in children, and is sometimes added to drinking water, though not without local protests (ref. 31). Fluorine toxicity is associated with high concentrations of fluoride in waters of dry regions in parts of Madras in India, Kazakhstan and China (refs. 32, 33, 34). The toxic effects are associated with very high concentrations of fluorine in bones and teeth. Iron deficiency is rather common in the world to-day (ref. 35), and is indicated by the low iron concentrations in blood in some regions (ref. 19). Iron toxicity is a much rarer condition found in some African groups (refs. 35, 36), and may be correlatable with high iron in hair (ref. 19). High mercury concentrations in hair have often been associated with a high dietary intake of fish (refs. 37, 38), and are found in Japan where much fish is eaten (ref. 19), but an alternative explanation could be that mercury is elevated in the atmosphere of volcanic regions such as Japan. Iodine deficiency is a widespread condition in the internal parts of continents, whose diagnosis can be confirmed by measuring either free iodide or protein-bound iodine in plasma (ref. 35). One area of Japan has endemic goitre due to excessive amounts of iodine in the diet (ref. 39). The high level of molybdenum in human milk from India and the Philippines (ref. 19) may be caused by the high dietary intake of legumes, which are rich in molybdenum. Indeed it has been suggested that the small stature of tropical Asian populations compared to Europeans may be a consequence of the different Cu/Mo ratios in their diets (ref. 40). Selenium deficiency is a big problem in the Keshan region of China, where it is often fatal, and the local population have low concentrations of Se in blood, serum, hair, liver and milk: cardiomyopathy is likely to occur when selenium concentrations in an individuals blood fall below 26 ng ml^{-1} (ref. 41). Less severe selenium deficiency may be present in Egypt, Finland, New Zealand and elsewhere (refs. 19, 41). Selenium toxicity has long been known in animals living on the 'badlands' of central U.S.A. (ref. 42), but is much rarer in humans, though reported from parts of Columbia (ref. 43), Venezuela (ref. 44) and the Enshi region of China (refs. 45, 46). According to Clayton (ref. 30), zinc deficiency may be widespread in the world. It has caused problems in backward parts of Egypt and Iraq, where it seems to be the result of poor absorption rather than low intake of the metal (ref. 47). It gives rise to low zinc concentrations in plasma and hair, but cannot unequivocally be diagnosed by analysis of these tissues. Table 1.5 gives quantitative data to support some of these observations.

TABLE 1.5

Examples of unusual concentrations of elements in human tissues, probably related to diet or location. Figures in ppm fresh weight.

Element	Tissue	Location of population	Normal	Abnormal	Ref
As	Plasma	Taiwan, As-rich area	0.0024	0.015	(19)
As	Liver	New Zealand, As-rich area	0.005-0.016	0.042-0.062	(19)
Fe	Blood	Bangladesh	491 \pm 24	280-410	(19)
Fe	Hair	Male Botswana Bushmen	4-300	224-2370	(19)
Hg	Hair	Livorno, Italy: fish-eaters	0.3-4	17.5	(38)
Mo	Milk	Urban Philippines	1.7-3.8	10-30	(19)
Se	Blood	Keshan, China, Se-poor area	0.03-0.3	0.008-0.026	(41)
Se	Blood	Venezuela, Se-rich area	0.03-0.3	0.7-1.5	(44)
Se	Hair	Keshan, China, Se-poor area	0.11-0.52	< 0.11	(46)
Se	Hair	China, Se-rich area	0.11-0.52	> 0.52	(46)
Zn	Hair	Egypt; dwarves	140-250	30-75	(25)

1.6.2 Abnormalities due to industrial environments and pollution

Most heavy metals have been implicated in isolated cases of toxicity from time to time. Individuals are occasionally poisoned from absorption of As, Hg or Tl used as biocides, while As, Co, Cr, Cu, Hg, Mn, Ni, Pb and V can contaminate workers who are chronically exposed to them in specific industries (ref. 48). Concentrations of arsenic in excess of 2 ppm in hair indicate acute poisoning (ref. 25), but As and also Cr, Hg, Pb and Zn are usually elevated in the hair of city dwellers (refs. 19, 49). Cadmium is significantly higher in the blood of heavy smokers than in non-smokers (ref. 17), and industrial pollution of an estuary has caused toxicity problems, Itai Itai disease and fatalities in Japan (ref. 50). Cadmium toxicity is associated with concentrations of more than 900 ppm Cd in dry kidney tissue (ref. 51). Chromium was elevated to 1400 ppm in the dry lungs of one worker in the chromium industry (ref. 52). Both fluorine and manganese are elevated in the hair of workers exposed to these elements in their workplace (ref. 53). Lead poisoning as an industrial disease is now a declining problem through legislation; it can be diagnosed from increases in the lead content of blood, hair, soft tissues or bone (refs. 25, 48). The insidious effects of chronic low doses of lead from pollution of air, soil and crops are still a point of contention, but there is no doubt about the elevated concentrations of lead found in the blood of city-dwellers (ref. 19). Mercury concentrations in all tissues, especially the kidney, are raised by exposure to mercury salts or vapours of the metal (ref. 48), and have been used to diagnose the cause of accidental poisoning and Minamata disease in Japan (ref. 54). Chicago police firing-range instructors

have markedly elevated antimony in their blood (ref. 48): see Table 1.6.

TABLE 1.6

Examples of unusual concentrations of elements in human tissues, probably related to pollution in cities or factories. Figures in ppm fresh weight.

Element	Tissue	Location of population	Normal	Abnormal	Ref
Cd	Blood	Brussels: heavy smokers	1.1 ± 0.5	2.5 ± 1.7	(19)
Cr	Lung	Japan: Cr industry workers	0.3	48-310	(52)
F	Hair	Germany: F industry workers	44	440	(53)
Hg	Liver	Glasgow city dwellers	0.03-0.16	0.43	(19)
Mn	Hair	Germany: welders	0.4-4	0.7-39	(53)
Pb	Blood	Mexico city males	0.008-0.2	0.27 ± 0.08	(19)
Sb	Blood	Chicago gunnery instructors	0.0005-0.006	0.01-0.13	(48)
Zn	Hair	Warsaw city dwellers	140-250	71-622	(19)

1.6.3 Age-related abnormalities

A number of studies have involved analysing tissues of neonates or stillbirths, and the general conclusion is that concentrations of inessential heavy metals such as Cd, Hg and Pb are lower than those in adult organs. Newborns have high copper concentrations in their livers and low serum copper, both tissues becoming 'normal' after a few months (ref. 55). The increase in tissue cadmium with age was first discovered by Tipton et al. (ref. 56), and is a real phenomenon caused by the long residence time of this metal in the body, especially in the kidney. On the other hand chromium concentrations in most tissues are said to decline with age (ref. 57). In old age, the condition of osteoporosis involves losses of calcium from bone which can be clearly shown and diagnosed by regular in vivo analysis (ref. 58).

1.6.4 Pathological abnormalities

One symptom of the disease cystic fibrosis is the high concentration of Cl, K and Na in hair, nail and sweat from affected persons (ref. 59). Determination of these elements for diagnostic purposes has been superseded by other biochemical tests. Metabolic disorders due to deficiency or malabsorption of copper have been reviewed by Evans (ref. 60). In Wilson's disease copper is enriched in the liver but depleted in serum, while in Menke's syndrome the metal is depleted in liver, kidney, brain and especially serum. The common condition of anaemia caused by deficiency of iron can be diagnosed from concentrations of iron in plasma or serum down to about 25% of the normal value (ref. 61). Serum molybdenum is hard to determine, but appears to be

elevated in cirrhosis and viral hepatitis (ref. 62).

Although many workers have tried to find some distinction between normal cancerous tissues from their elemental composition, nothing of diagnostic value has resulted. The carcinogenic nature of several elements, especially arsenic, is controversial, but Be, Cd, Cr and Ni are believed to have caused cancers in man (ref. 63).

Drugs used to cure or alleviate disease sometimes contain rare elements and can have marked effects on the elemental content of tissues. Bismuth compounds, whose use in medicine is now obsolete, can elevate bismuth in blood to 5 ppm or more (ref. 64). Bromides used as soporifics elevate bromine in blood, serum and hair for some time. Compounds of gold used in rheumatic therapy can elevate gold in kidney and other soft tissues for a year or more after treatment (refs. 53, 65, 66). Lithium chloride is used to treat mental patients, but requires careful monitoring of concentrations in blood or plasma to avoid toxic effects (ref. 67). Anti-tumour drugs containing platinum, or rarely rhodium, increase tissue concentrations, especially in the kidney (ref. 68). Selenium sulphide is a component of some hair shampoos which can give rise to extraordinary concentrations of Se in hair (ref. 69).

High concentrations of aluminium in brain have been associated with Alzheimers disease (ref. 70) and with encephalopathy which develops in some patients treated by dialysis for chronic kidney failure (ref. 71), but both findings have been disputed (refs. 72, 73).

REFERENCES

- 1 H.J.M. Bowen, *Environmental Chemistry of the Elements*, Academic Press, London, 1979, p. 129.
- 2 M. Anke, B. Grappel and H. Kronemann, in P. Brätter and P. Schramel (Eds.), *Trace Element Analytical Chemistry in Medicine and Biology*, W. de Gruyter, Berlin, 3 (1984) 421-464.
- 3 G. Hubert, N. Rieder, G. Schmitt and W. Send, *Z. Naturforsch.* 30C (1975) 422.
- 4 R.B. Frankel, R.P. Blakemore and R.S. Wolfe, *Science*, 203 (1979) 1355-1356.
- 5 J.L. Gould, J.L. Kirschvink and K.S. Deffeyes, *Science*, 201 (1978) 1026-1028.
- 6 J.D. Birchall, in R.J.P. Williams and J.R.R.F. Da Silva (Eds.), *New Trends in Bio-inorganic Chemistry*, Academic Press, London, 1978, Chap. 7, 227-231 pp.
- 7 W.Y. Cheung (Ed.), *Calcium and cell function*, 2 vols, Academic Press, London, 1980-1982.
- 8 R.H. Thomson, *J. Indian Chem. Soc.*, 55 (1978) 1209-1220.
- 9 M.G. Taylor and K. Simkiss, *Environ. Chem.*, 3 (1984) 102-138.
- 10 R. Martoja and D. Viale, *C.R. Seanc. Acad. Sci. Paris*, D 285 (1977) 109-112.

- 11 B. Sansoni and G.V. Iyengar, in *Elemental Analysis in Biological Materials*, IAEA Techn. Rept. 197, IAEA, Vienna, 1980, Ch. 5, pp. 57-71.
- 12 J. Versieck, *CRC Crit.Rev.Clin.Lab.Sci.*, 22 (1985) 97-184.
- 13 H. Woggon and S. Klein, *Nahrung*, 27 (1983) 21-29.
- 14 W.R. Wolf (Ed.), *Biological Reference Materials*, J.Wiley, New York, 1985.
- 15 H.J.M. Bowen, *At.Energy Rev.*, 13 (1975) 451-477.
- 16 R.M. Parr, Rept IAEA/RL/103, IAEA, Vienna, 1983.
- 17 L. Friberg, C.G. Elinder, T. Kjellstrom and G.F. Nordberg, *Cadmium and Health*, 2 vols, Chemical Rubber Co, Palm Beach, Florida, 1985-1986.
- 18 G.V. Iyengar, W.E. Kollmer and H.J.M. Bowen, *The elemental composition of human tissues and body fluids*, Verlag Chemie, Weinheim and New York, 1978.
- 19 G.V. Iyengar, *Concentrations of 15 trace elements in some selected adult human tissues and body fluids*, Kernforschungsanlage Julich GmbH, Germany, 1985.
- 20 W.S. Snyder (Ed.), *Report of Task Group on Reference Man*, Pergamon Press, Oxford, 1975.
- 21 J.H.R. Kagi and M. Nordberg (Eds.), *Metallothionein*, Birkhauser Verlag, Basle, Switzerland, 1979.
- 22 G. Kazantzis, *Eur.J.Clin.Invest.*, 9 (1979) 3-4.
- 23 H.J.M. Bowen, *Environmental Chemistry of the Elements*, Academic Press, London, 1979, pp. 8-12.
- 24 M. Webb, *Dev. Toxicol. Environ. Sci.*, 1 (1977) 51-64.
- 25 V. Valkovic, *Trace Elements in Human Hair*, Garland STPM Press, New York, 1977.
- 26 G.V. Iyengar, *Elemental Composition of Human and Animal Milk*, IAEA - Tecdoc-269, IAEA, Vienna, 1982.
- 27 H.J.M. Bowen, *Environ.Chem.*, 2 (1982) 70-93.
- 28 E.J. Underwood, *Trace Elements in Human and Animal Nutrition*, Academic Press, London, 1977.
- 29 C.E. Casey and K.M. Hambidge, *Adv.Nutr.Res.*, 3 (1980) 23-63.
- 30 B.E. Clayton, *Adv.Clin.Chem.*, 21 (1980) 147-176.
- 31 World Health Organisation Monograph 59, *Fluorides and Human Health*, WHO, Rome, 1970.
- 32 K.V. Paliwal, *Proc.Indian Natl.Sci.Acad.*, A40 (1974) 331-341.
- 33 A.A. Zavoronkov and L.S. Strochkova, *Fluoride*, 14 (1981) 182-183.
- 34 D.S. Ling, Q.M. Chen and Z.C. Yu, *Ti Chua Hua Hsueh*, 1 (1980) 13-15.
- 35 D.J. Horvath, in P.M. Newberne (Ed.), *Trace Substances and Health*, M. Dekker, New York, 1976, p. 319.
- 36 C.I. Waslien, in A.S. Prasad and D. Oberleas (Eds.), *Trace Elements in Human Health and Disease*, vols 2, Academic Press, London, 1976, p. 347.
- 37 G. Birke, A.G. Johnels, L.O. Plantin, B. Sjostrand, S. Skerfving and T. Westermark, *Arch.Environ.Health*, 25 (1972) 77-91.
- 38 A. Buzzo, R. Biffoli, F. Chiti and B. Pisani, *Boll.Chim.Unione Ital.Lab. Prov., Parte Sci.*, 32 (1981) 167-184.
- 39 H. Suzuki, T.Higuchi, K.Sawa, S.Ohtaki and Y.Horiuchi, *Japan.Acta Endocrinol.*, 50 (1965) 161-170.
- 40 C.C. Pfeiffer, E.Siegert and A.H. Sohler, *Trace Elem.Med.*, 2 (1985) 33-36.
- 41 C.S. Li and M.L. Jackson, *Trace Subst.Environ.Health*, 19 (1985) 264-276.
- 42 I. Rosenfeld and O.A. Beath, *Selenium*, Academic Press, New York, 1964, 286 pp.
- 43 J. Ancizar-Sordo, *Soil Sci.*, 63 (1947) 437-438.
- 44 W.G. Jaffe, D. Raphael, M.C. Mondragon and M.A. Cuevas, *Arch.Latinamer. Nutr.*, 22 (1972) 595-599.
- 45 G. Yang, R. Zhou, S. Sun., S. Wang and S. Li, *Yingyang Xuebao*, 4 (1982) 81-89.
- 46 M. Wang, *Yingyang Xuebao*, 4 (1982) 201-207.
- 47 A.S. Prasad, *Trace elements and iron in human metabolism*, J. Wiley, New York, 1978.

- 48 E. Berman, Toxic metals and their analysis, Heyden, Philadelphia, 1980.
- 49 S.A. Katz, Amer.Lab. (Fairfield, Conn.), 11 (1979) 44-52.
- 50 J. Kobayashi, in F.W. Oehme (Ed.), Toxicity of Heavy Metals in Environment, Part 1, M. Dekker, New York, 1978, pp. 199-260.
- 51 E.C. Foulkes, Trace Subst. Environ. Health, 19 (1985) 129-133.
- 52 H. Teraoka, Arch. Environ. Health, 36 (1980) 155-165.
- 53 W. Wiesener, W. Geerner and S. Niese, Nuclear Activation in the Life Sciences 1978, IAEA, Vienna, 1979, pp. 307-320.
- 54 T. Tsubaki and K. Irukayama (Eds.), Minamata Disease, Elsevier, Amsterdam, 1977.
- 55 H Rupp and U. Weser, Biochem.Biophys.Res.Comm., 72 (1976) 223-229.
- 56 I.H. Tipton, J.C. Johns and M. Boyd, Proc. 1st Int.Congr.Radiation Protection, Pergamon Press, New York, 1968.
- 57 O.A. Levander, J.Amer.Diet.Assoc., 66 (1975) 338-344.
- 58 K.J. Ellis and S.H. Cohn, in J.R. Vogt (Ed.), Trans. 5th Int.Conf.Nucl. Meth.Environ.Energy Res., 1984, 191 pp.
- 59 L. Kopito, A. Mahmoodian, R.R.W. Townley, K.T. Khaw and H. Schwachman, New Engl. J.Med., 272 (1965) 504-511.
- 60 G.W. Evans, Adv.Nutr.Res., 1 (1977) 167-187.
- 61 M.M. Wintrobe, G.E. Cartwright and C.J. Gubler, J.Nutr., 50 (1953) 395-419.
- 62 J. Versieck, L. Vanballenberghe, G. Lerney, F. Barbier, R. Cornelis and J. De Rudder, in P. Brätter and P. Schramel (Eds.), Trace Element Analytical Chemistry in Medicine and Biology, W. de Gruyter, Berlin, vol. 1, 1980, pp. 273-282.
- 63 G. Pershagen, M. Kuschner, M. Piscator, T. Norseth, F.W. Sunderman and G. Kazantzis, Environ.Health Perspect., 40 (1981) 93-161.
- 64 G. Monseu, M. Struelens and M. Roland, Acta Neurol.Belg., 76 (1976) 301-306.
- 65 N.L. Gottlieb, P.M. Smith and E.M. Smith, Arth.Rheum., 15 (1972) 16-21.
- 66 B. Vernon-Roberts, J. Rheumatol., Suppl. 5 (1979) 120-129.
- 67 M. Peet, in F.N. Johnson (Ed.), Lithium Research and Therapy, Academic Press, London, 1975.
- 68 M.J. Cleare and P.C. Hydes, in H.Sigel (Ed.), Metal Ions in Biologic Systems, vol. 11, M. Dekker, New York, 1980, pp. 1-62.
- 69 T.S. Davies, Lancet, no. 2 (1982) 935.
- 70 D.R. Crapper, S.S. Krishnan and A.J. Dalton, Science, 180 (1973) 511-513.
- 71 A.C. Alfrey, A. Hegg and P. Craswell, Am.J.Clin.Nutr., 33 (1980) 1509-1516.
- 72 G. Dunea, S.D. Mahurkar, B. Mamdani and E.C. Smith, Ann.Int.Med., 88 (1978) 502-507.
- 73 S.G. Epstein, Trace Subst.Environ.Health, 18 (1984) 139-148.

Chapter 2

PHOTON INDUCED X-RAY EMISSION

ROBERTO CESAREO

Centro per l'Ingegneria Biomedica e
Cattedra di Fisica, Facoltà di Farmacia
Università di Roma "La Sapienza"
Corso Vittorio Emanuele II, 244, 00186 Roma (Italy)

2.1 INTRODUCTION

In recent years X-ray fluorescence induced by photons has emerged as a very powerful technique for the elemental analysis of biomedical and environmental samples.

X-ray fluorescence (XRF) analysis induced by photons consists of the excitation of a sample with radiation of adequate energy and intensity and the measurement of the characteristic X-rays emitted by the excited sample (see Fig. 2.1).

Traditionally, X-ray tubes have been used to excite the fluorescence, and crystal spectrometers were employed to analyze the characteristic X-rays according to their wavelength (wavelength dispersive X-ray Spectrometry). The apparatus is expensive, and limited to research where very high resolution is required.

The development of X-ray semiconductor detectors has made interesting the use of energy-dispersive spectrometry, which was previously restricted to investigation of a few elements at the time, with the use of gas proportional detectors or scintillation detectors.

In this Chapter, we shall describe energy dispersive X-ray fluorescence systems using photon excitation, which have been designed for analysis of thin biomedical and environmental samples.

In order to understand how the excitation process occurs and how atoms de-excite, and in order to better understand the spectral distribution of the emitted X-rays, it is necessary to gain some understanding of atomic structure (Section 2.2) and of the interaction of incident and emitted radiation with matter: absorption, attenuation and scattering of X-rays (Section 2.3).

In Section 2.4 the theoretical background for X-ray analysis will be given, as well as the theoretical detection limits, for both thick and thin samples.

The experimental methods will be described in Section 2.6. X-ray sources, detectors, electronic chains for amplifying the pulses and multi-channel

analyzers will be discussed in detail in this Section.

Then the most important biomedical and environmental applications will be discussed in Section 2.7; they include analysis of trace elements in water samples (Section 2.7.1) and in air particulate matter (Section 2.7.2), analysis of trace elements in blood (Section 2.7.3), analysis of forensic samples (Section 2.7.4) and analysis of urinary calculi (Section 2.7.5).

Finally, "in vivo" applications of XRF-analysis will be described (Section 2.7.6). The study of lead and strontium in bone, cadmium and mercury in kidney, iodine in the thyroid and lead in teeth will be discussed.

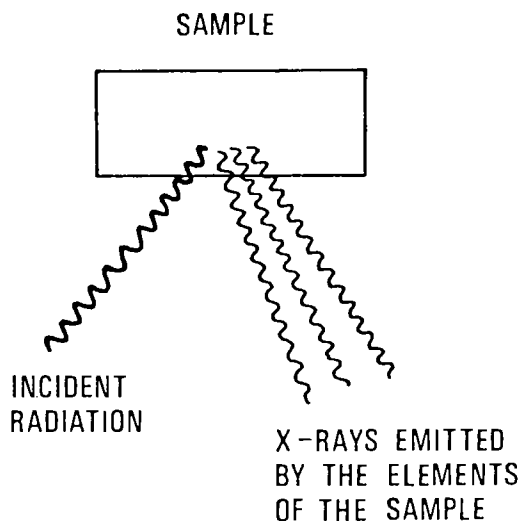


Fig. 2.1. Schematic diagram of the energy-dispersive X-ray fluorescence. Incident radiation (monoenergetic X-rays, bremsstrahlung or low-energy γ -rays) excites atoms of the sample which deexcite with the emission of X-rays, the energies of which are characteristic of the excited elements.

2.2 ATOMIC STRUCTURE

2.2.1 The atom

The spectroscopic properties of the elements are determined by the atomic number Z , which gives the total number of protons within the nucleus or the total number of electrons around the nucleus. The atomic model proposed by N. Bohr results in the distribution of electrons around the nucleus being confined to specific quantized shells. The quantum number $n=1$ is assigned to the most tightly bound shell and in X-ray terminology is referred to as K-shell. The next shells are $n=2$ or L shells, $n=3$ or M shells, $n=4$ or N shells and so on.

In Figure 2.2 the atomic level scheme is shown, which represents the electronic shells and the main X-ray transitions.

2.2.2 X-rays (energies and intensities)

All K-series X-rays correspond to the filling of a vacancy in the K-shell, all L-series to the filling of a vacancy in the L-shells and so on. In general, each X-ray is followed by a Greek letter, indicating both the shell from which the transition starts and the relative intensities (K_α is stronger than K_β).

For example, K_α -X rays correspond to a transition from the L-shells to the K-shell, and K_β to a transition from the M shells to the K-shell.

L_α -X-rays correspond to the filling of vacancies in the L subshell by electrons from M subshells, L_β to the filling of vacancies in the L subshells by electrons from M and N subshells, and L_γ to the filling of vacancies in the L subshells by electrons from N and O subshells (see Fig. 2.2).

There is a fine structure in the energy values of the X-rays; for example electron transitions from the L_{III} and L_{II} subshells to the K-shell correspond to two X-lines (K_1 and K_2 -X rays) and the same occurs for K_β , L_α , L_β , L_γ -X rays. Therefore, for practical purposes, the energy separation between, for example, $K_{\alpha 1}$ and $K_{\alpha 2}$ is, in general, not great enough to be resolved with detectors employed in X-ray analysis.

X-ray energy values of practical utility for X-ray analysis are shown in Table 2.1.

The energy of the X-rays is the most important parameter for the identification of an element in a given sample. For quantitative determination, the net peak intensity of the observed X-rays has to be measured. Thus, in some cases, a detailed knowledge of the K_α/K_β ratio or L_α/L_β ratio is required, which is reported in Table 2.2.

The intensity of any given X-ray line or component is governed by two fundamental atomic parameters, namely:

- the electronic population of higher lying levels, which may fill a lower lying vacancy;
- the mode of deexcitation or readjustment taken assumed by the atom.

The second parameter governing X-ray intensity is how the atom deexcites. Once a vacancy is formed, it is not always followed by the emission of an X-ray. The yield of X-rays emitted is known as the fluorescence yield and is denoted by ω .

2.2.3 Fluorescence yields

The fluorescence yield of an atomic shell or subshell is defined as the probability that a vacancy in that shell or subshell is filled through X-rays. Thus, the fluorescence yield of a shell corresponds to the number of photons emitted when vacancies in the shell are filled, divided by the number of primary vacancies in the shell. Emission of X-rays is in competition with emission of

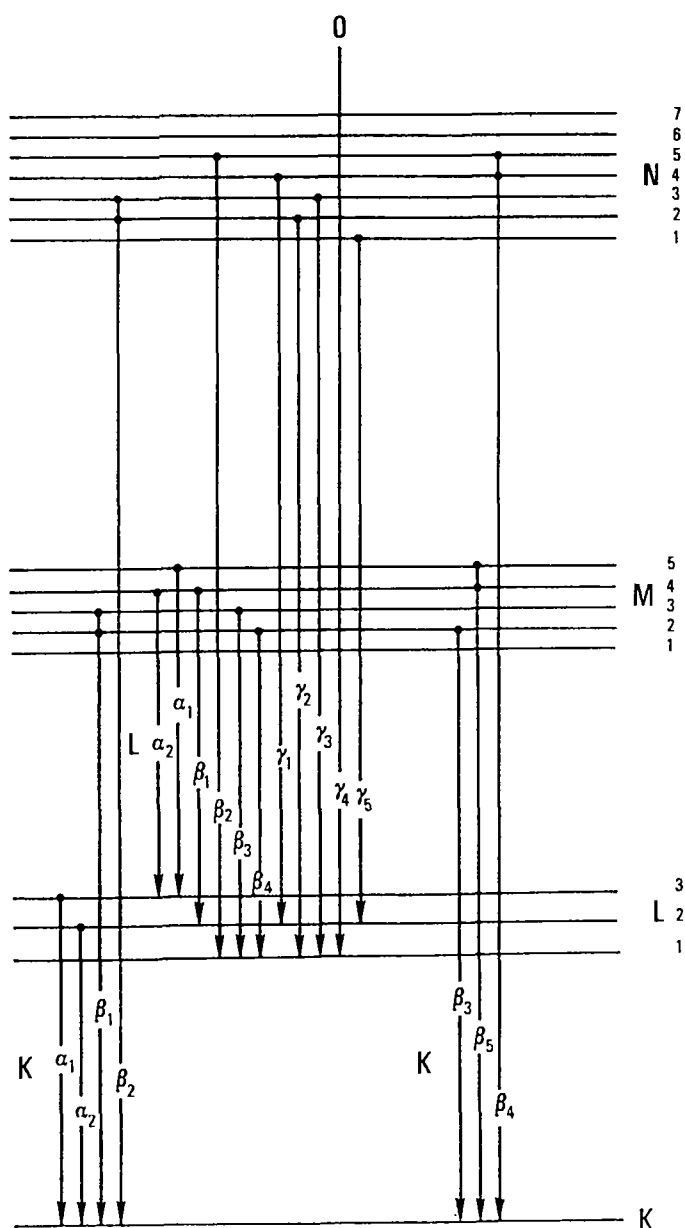


Fig. 2.2. Part of the energy-level diagram and most important possible X-ray transitions.

TABLE 2.1.

X-ray energy values (in keV) and absorption edge energy values (in keV) of selected elements for XRF-analysis

Atomic no. and element	K _α	K _β	K _{ab}	L _α	L _β	L _γ
15 P	2.015	2.136	2.142			
16 S	2.307	2.464	2.470			
17 Cl	2.622	2.815	2.819			
18 A	2.956	3.192	3.203			
19 K	3.312	3.589	3.607			
20 Ca	3.690	4.012	4.038			
22 Ti	4.507	4.931	4.964			
23 V	4.948	5.427	5.463			
24 Cr	5.410	5.946	5.988			
25 Mn	5.893	6.490	6.537			
26 Fe	6.398	7.057	7.111			
27 Co	6.922	7.649	7.709			
28 Ni	7.468	8.296	8.331			
29 Cu	8.037	8.940	8.980			
30 Zn	8.626	9.614	9.660			
31 Ga	9.242	10.314	10.368			
32 Ge	9.869	11.040	11.103			
33 As	10.525	11.794	11.863			
34 Se	11.201	12.573	12.652			
35 Br	11.900	13.377	13.475			
36 Kr	12.622	14.212	14.323			
37 Rb	13.364	15.072	15.201			
38 Sr	14.130	15.958	16.106			
39 Y	14.919	16.873	17.037			
40 Zr	15.732	17.817	17.998	2.04	2.18	2.30
41 Nb	16.567	18.786	18.987	2.16	2.31	2.46
42 Mo	17.425	19.785	20.002	2.29	2.46	2.62
44 Ru	19.211	21.86	22.19	2.56	2.72	2.96
45 Rh	20.141	22.95	23.22	2.69	2.86	3.14
46 Pd	21.196	24.06	24.35	2.84	3.02	3.33
47 Ag	22.073	25.19	25.51	2.98	3.20	3.60
48 Cd	23.075	26.36	26.71	3.13	3.35	3.73
49 In	24.102	27.56	27.94	3.28	3.52	4.0
50 Sn	25.153	28.79	29.20	3.44	3.71	4.20
51 Sb	26.233	30.05	30.49	3.60	3.89	4.45
52 Te	27.336	31.34	31.81	3.77	4.07	4.65
53 I	28.462	32.66	33.16	3.94	4.26	4.90
54 Xe	29.644	34.02	34.58	4.11	4.48	5.15
55 Cs	30.796	35.40	35.96	4.28	4.68	5.40
56 Ba	32.000	36.81	37.41	4.46	4.87	5.65
57 La	33.236	38.26	38.93	4.65	5.10	5.90
60 Nd	37.102	42.80	43.57	5.23	5.77	6.70
65 Tb	44.103	51.04	52.0	6.27	7.04	8.25
70 Yb	51.85	60.16	61.30	7.41	8.48	9.90
74 W	58.65	68.16	69.51	8.39	9.75	11.45
77 Ir	64.09	74.58	76.10	9.17	10.80	12.70
78 Pt	65.98	76.80	78.38	9.44	11.15	13.10
79 Au	67.90	79.07	80.71	9.71	11.53	13.55
80 Hg	69.86	80.24	82.53	9.98	11.90	14.0
82 Pb	73.89	84.92	87.34	10.55	12.70	14.90
83 Bi	75.96	87.33	89.83	10.84	13.10	15.40
92 U	98.44	94.66	115.59	13.61	17.35	20.35
		119.29	114.55			

TABLE 2.2.

Predicted K and L-X ray intensities for selected elements

Atomic no. and element	K_{α}	K_{β}	K_{α}/K_{β}	L_{α}	L_{β}	L_{γ}	L_{α}/L_{β}	L_{α}/L_{γ}
16 S	95.5	4.5	21					
18 A	92.5	7.5	12					
20 Ca	90.4	9.6	9.4					
22 Ti	89.8	10.2	8.8					
24 Cr	89.8	10.2	8.8					
25 Mn	89.6	10.4	8.5					
26 Fe	89.3	10.7	8.3					
27 Co	89.2	10.8	8.2					
28 Ni	89.2	10.8	8.2					
30 Zn	88.9	11.1	8.0					
32 Ge	88.3	11.7	7.6					
34 Se	87.5	12.5	7.0					
36 Kr	86.6	13.4	6.5					
38 Sr	85.9	14.1	6.1					
40 Zr	85.2	14.8	5.8					
42 Mo	84.7	15.3	5.5	54.9	42.1	2.9	1.3	18.9
44 Ru	84.2	15.8	5.5	53.7	42.6	3.7	1.26	14.5
46 Pd	83.8	16.2	5.2	52.7	43.0	4.3	1.22	12.2
48 Cd	83.3	16.7	5.0	51.8	43.4	4.8	1.19	10.8
50 Sn	83.0	17.0	4.9	50.9	43.6	5.5	1.17	9.3
52 Te	82.4	17.6	4.7	50.0	43.9	6.1	1.14	8.2
54 Xe	81.9	18.1	4.6	49.2	44.2	6.8	1.11	7.2
56 Ba	81.5	18.5	4.5	48.7	44.3	7.0	1.10	7.0
58 Ce	81.2	18.8	4.4	48.5	44.4	7.1	1.09	6.8
60 Nd	81.0	19.0	4.36	48.4	44.2	7.2	1.09	6.7
65 Tb	80.8	19.2	4.21	47.9	44.7	7.4	1.07	6.5
70 Y	80.3	19.7	4.08	47.5	44.9	7.6	1.06	6.2
74 W	80.0	20.0	4.0	46.6	45.3	8.1	1.03	5.7
75 Re	79.9	20.1	3.97	46.4	45.4	8.2	1.02	5.7
78 Pt	79.6	20.4	3.90	45.8	45.5	8.7	1.01	5.3
80 Hg	79.5	20.5	3.88	45.4	45.8	8.8	0.99	5.2
82 Pb	79.3	20.7	3.83	44.9	45.9	9.2	0.98	4.9
92 U	78.7	21.3	3.69	42.8	46.7	10.5	0.92	4.7

"Auger electrons".

Values of the ω_K and ω_L yields are reported in Table 2.3, as the most recent mixture of experimental, theoretical and fitted values (ref.1,2).

2.3 PHYSICAL PRINCIPLES OF X-RAY FLUORESCENCE

Radiation may interact with matter in various ways. The most important, in the energy range of interest for XRF-analysis, namely 10-150 keV, is the photo-electric effect, which gives rise to the emission of fluorescent X-rays, and elastic and inelastic scattering, which mainly contribute to the background.

In particular, when monoenergetic X-or gamma rays of energy between a few keV and about 150 keV interact with matter, these effects contribute to the absorption, attenuation or scattering of the radiation by the sample (see Fig. 2.3).

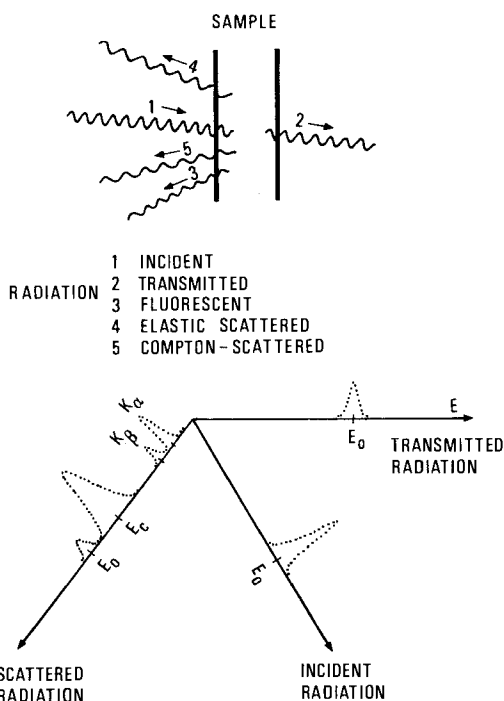


Fig. 2.3. Interaction of monoenergetic radiation with matter and resulting X-ray spectrum collected with a semiconductor detector.

1. incident radiation
2. transmitted radiation
3. fluorescent radiation
4. elastic scattered radiation
5. Compton scattered radiation.

TABLE 2.3.
K-shell (ω_K) and L-shell (ω_L) fluorescence yields

Atomic no. and element	ω_K	ω_L
15 P	0.060 \pm 0.01	
16 S	0.080 \pm 0.01	
17 Cl	0.096 \pm 0.005	
18 Ar	0.119 \pm 0.006	
19 K	0.138 \pm 0.013	
20 Ca	0.163 \pm 0.016	
22 Ti	0.22 \pm 0.02	
23 V	0.25 \pm 0.01	0.0023 \pm 0.00002
24 Cr	0.28 \pm 0.01	
25 Mn	0.31 \pm 0.02	0.003 \pm 0.0004
26 Fe	0.35 \pm 0.01	
27 Co	0.375 \pm 0.03	
28 Ni	0.43 \pm 0.03	
29 Cu	0.44 \pm 0.01	0.0056
30 Zn	0.48 \pm 0.03	
31 Ga	0.52 \pm 0.01	0.0064 \pm 0.0004
32 Ge	0.55 \pm 0.03	
33 As	0.58 \pm 0.03	
34 Se	0.60 \pm 0.03	
35 Br	0.62 \pm 0.03	
36 Kr	0.65 \pm 0.03	
37 Rb	0.67 \pm 0.01	0.01 \pm 0.002
38 Sr	0.69 \pm 0.02	
39 Y	0.71 \pm 0.03	0.03 \pm 0.003
40 Zr	0.73 \pm 0.03	
41 Nb	0.75 \pm 0.03	
42 Mo	0.76 \pm 0.03	
43 Tc	0.78 \pm 0.03	
44 Ru	0.79 \pm 0.03	
45 Rh	0.81 \pm 0.03	
46 Pd	0.82 \pm 0.03	
47 Ag	0.833 \pm 0.03	0.052 \pm 0.006
48 Cd	0.84 \pm 0.03	
49 In	0.85 \pm 0.03	
50 Sn	0.858 \pm 0.03	
51 Sb	0.869 \pm 0.03	
52 Te	0.875 \pm 0.03	
53 I	0.88 \pm 0.03	
54 Xe	0.887 \pm 0.02	0.107 \pm 0.010
55 Cs	0.892 \pm 0.015	0.089 \pm 0.013
56 Ba	0.90 \pm 0.03	0.093 \pm 0.012
57 La	0.906 \pm 0.03	0.101 \pm 0.015
60 Nd	0.92 \pm 0.03	0.131 \pm 0.017
65 Tb	0.94 \pm 0.025	0.194 \pm 0.027
70 Yb	0.95 \pm 0.02	
74 W	0.957 \pm 0.02	
77 Ir	0.962 \pm 0.02	0.30 \pm 0.04
78 Pt	0.965 \pm 0.015	0.32 \pm 0.02
79 Au	0.96 \pm 0.02	0.40 \pm 0.02
80 Hg	0.962 \pm 0.02	0.38 \pm 0.04
81 Tl	0.967 \pm 0.02	0.43 \pm 0.07
82 Pb	0.97 \pm 0.015	0.36 \pm 0.04
83 Bi	0.97 \pm 0.02	0.40 \pm 0.08
92 U	0.973 \pm 0.015	0.51 \pm 0.04

2.3.1 Attenuation of monoenergetic radiation in matter

When a narrow beam of monoenergetic photons of energy E_0 and intensity N_0 crosses a homogeneous absorber of thickness x (in cm.) and density δ (in g/cm^3), part of the beam may be completely absorbed by the sample (mainly through the photoelectric effect), part may not interact with the sample at all and part may be scattered either with or without some energy loss.

The emergent beam intensity N is given by:

$$N = N_0 \exp\{-\mu(\delta, E, Z)x\} \quad (1)$$

where μ is the linear attenuation coefficient (in cm^{-1}) for material of atomic number Z .

It is often more convenient to define the mass attenuation coefficient μ/δ (in cm^2/g) which is independent from the density of the material. The mass attenuation coefficient is related to the probability that radiation will interact with matter. This probability, or cross section σ , represents a measure of the atomic area involved in the interaction. The fundamental unit of atomic cross-section is the barn, which is 10^{-24} cm^2 . Mass absorption coefficients are often given in terms of barns/atom, that is:

$$\mu/\delta (\text{cm}^2/\text{g}) = \sigma (\text{barns/atom}) (N/A)$$

where N is Avogadro's number (6.03×10^{23} atoms/mol) and A is the atomic weight (g/mol).

The total mass attenuation coefficient is the sum of the attenuation coefficients from each mode of photon interaction, i.e. photoelectric effect, Compton scattering and Rayleigh scattering (ref. 3):

$$\mu_t/\delta = \mu_{\text{ph}}/\delta + \mu_{\text{C}}/\delta + \mu_{\text{R}}/\delta \quad (2)$$

Figure 2.4 shows the relative percentage of the three photon interactions versus energy E_0 , for water. It can be observed that the photoelectric effect is prevalent below about 25 keV. Between 5 and 25 keV may also be considered the ideal region for XRF-analysis of biological samples. Above 70 keV, the Compton effect contributes to more than 90% of the total attenuation coefficient. The elastic scattering does not, in general, play an important quantitative role, because its contribution never exceeds 10% in materials of biological interest.

In the following Sections, the modes of interaction of radiation with matter will be discussed in detail, since they are essential for the understanding of the XRF process.

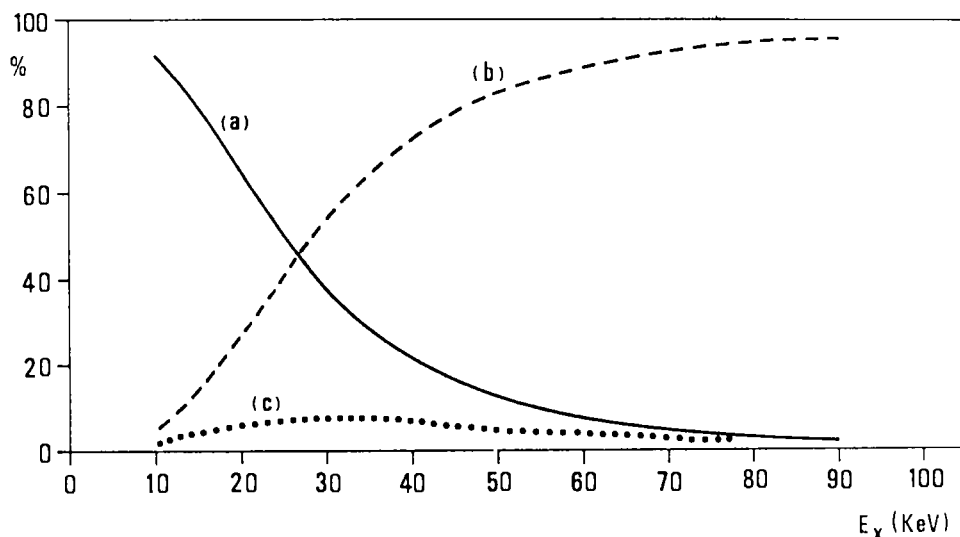


Fig. 2.4. Relative percentage of photoelectric effect (a), Compton scattering (b), and Rayleigh scattering (c) of water versus energy.

2.3.2 Photoelectric effect

As far as concerns the photoelectric effect, it gives rise to the absorption of an incident photon, the ejection of a bound electron from an inner shell of the atom and the simultaneous emission of an X-ray or of an Auger electron (depending on the fluorescence yield); the probability for electron vacancy production is greatest for photon energies immediately above the threshold for the ejection of the bound electron. The probability then decreases approximately as E_0^{-3} as the energy of the incident photon is increased above this threshold. This energy dependence has important consequences when one wishes to analyze a wide range of elements using a single energy photon source.

Due to the photoelectric effect, the atoms of the irradiated sample will, therefore, emit characteristic X-rays, the energy of which allows the identification of the constituent elements. A sample containing several elements will emit as many X-rays of different energy as there are elements, and the intensity of these X-rays is approximately proportional to the elemental composition of the sample itself.

Each element deexcites by emitting more than one typical X-ray. When an electron of the K-shell is excited, the atom deexcites by emitting, as observed in par. 2.2.2, K_α and K_β X-rays in a fixed intensity ratio (see Table 2.2).

When an electron of the L-shell is excited, the atom deexcites by emitting L_{α} , L_{β} , and L_{γ} -X rays, also in a fixed intensity ratio (see Table 2.2). Only in very special applications will M-X-rays be of interest for XRF analysis.

Some examples of X-rays emitted by pure elements and collected with a semiconductor detector are shown in Figure 2.5.

2.3.3 Compton scattering

In this process, the incident photon, of energy E_0 , interacts with a single loosely bound atomic electron. Part of the photon energy is transferred to the electron, and the incident photon will be, consequently, reduced in energy and scattered with respect to the initial direction.

The following relationship can be deduced between the incident photon energy E_0 and the scattered photon energy E_C :

$$E_C = E_0 \left\{ \frac{1}{1 + E_0/511(1 - \cos\theta)} \right\} \quad (3)$$

in which E_0 and E_C are expressed in keV, 511 (in keV) is the rest mass of the electron and θ the scattering angle. The energy shift (in keV) of Compton scattered photons versus scattering angle θ , at various photon energies, is shown in Figure 2.6.

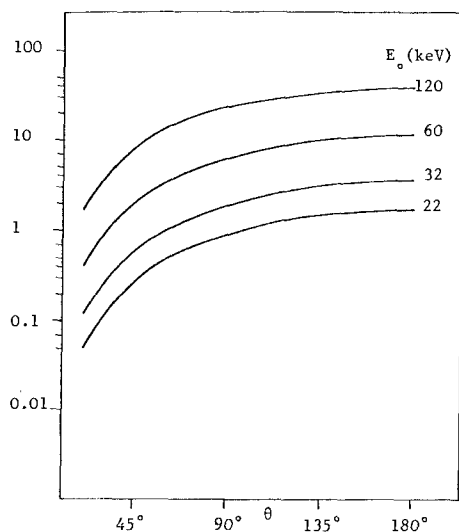


Fig. 2.6 Energy shift of Compton scattered photons versus scattering angle θ for incident energy of 22, 32, 60 and 122 keV.

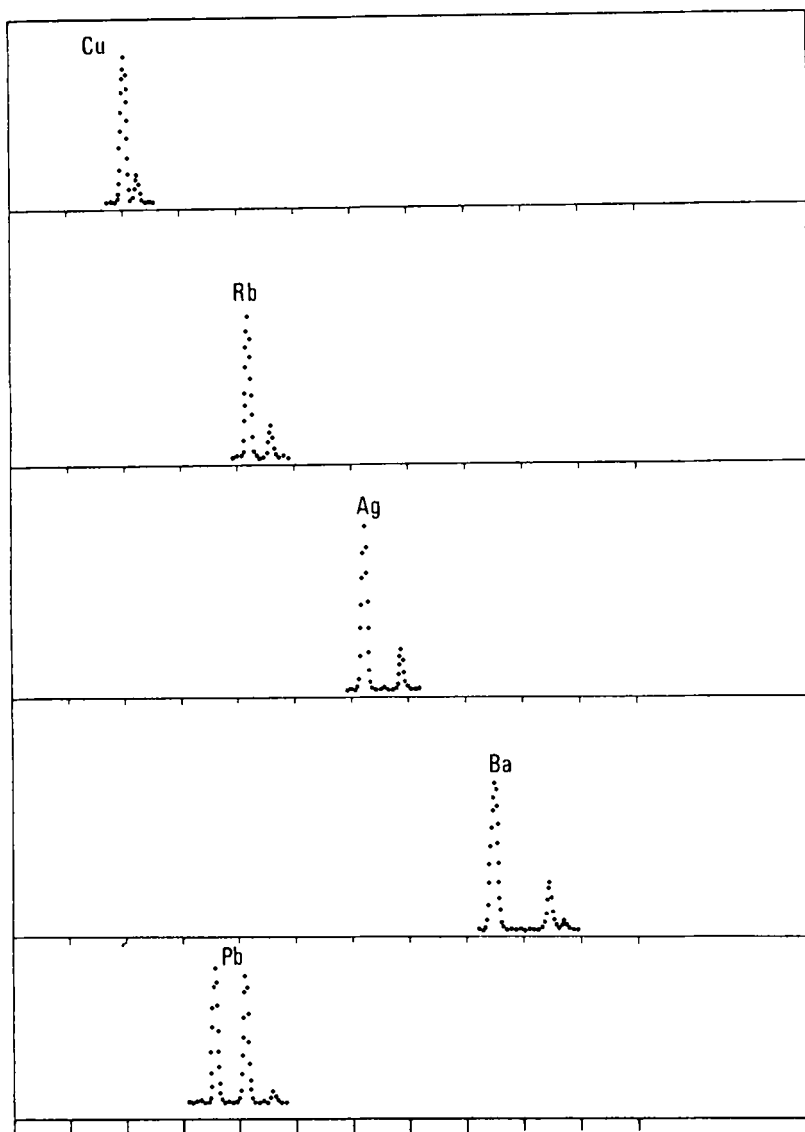


Fig. 2.5. X-Ray Fluorescence spectra of some typical pure elements collected with a HPGe semiconductor detector. From the top X_K -rays of Cu (8.04 and 8.94 keV), Rb (13.36 and 15.1 keV), Ag (22.1 and 25.2 keV) and Ba (32.0 and 36.8 keV), and X_L -rays of Pb (10.5 and 12.615 keV).

The differential cross section of Compton scattering is given by:

$$\frac{d\sigma_C}{d\Omega} = \frac{r_o^2}{2} S(y,Z) \left(\frac{1}{\{1 + \alpha(1 - \cos\theta)\}^2} \{1 + \cos^2\theta + \frac{\alpha^2(1 - \cos\theta)^2}{1 + \alpha(1 - \cos\theta)}\} \right) \quad (4)$$

where $d\Omega$ is the differential solid angle, $r_o = 2.8 \times 10^{-13}$ cm is the classical electron radius and $S(y,Z)$ represents the incoherent scattering function (ref.4) in which $y = (\sin\theta/2)/\lambda$ where λ is the photon wavelength in Ångströms = $12398/E(\text{eV})$. In the energy range of photons of interest for XRF-analysis, electron binding significantly alters the incoherent scattering cross-section, which can be expressed as:

$$\frac{d\sigma}{d\Omega} = \frac{d\sigma_C}{d\Omega} S(y,Z) \quad (5)$$

where $d\sigma_C/d\Omega$ is the Klein-Nishina cross section for a single free electron, as given by Eq. (4). Binding effects are important for energies less than 100 keV. For example, Figure 2.7 illustrates the deviation of $d\sigma'_C/d\Omega$ from $d\sigma_C/d\Omega$ as a function of photon energy for several elements.

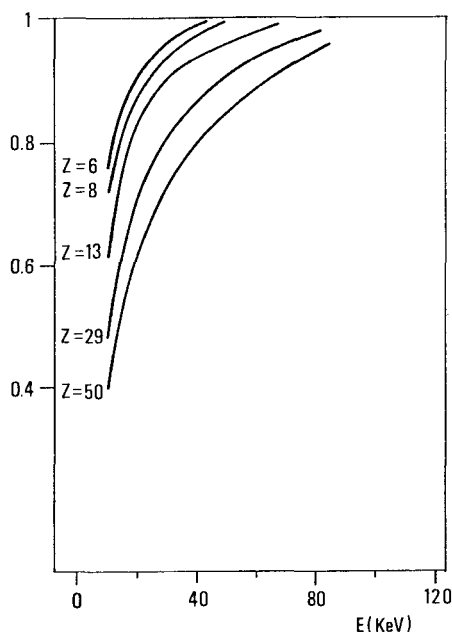


Fig. 2.7. Difference between incoherent scattering cross section $d\sigma'_C/d\Omega$ and Klein-Nishina cross section $d\sigma_C/d\Omega = 1$ for targets of different atomic number Z , at scattering angle $\theta = 90^\circ$.

In the approximation of radiation scattered at 90° and at 180° (usual geometrical disposition for XRF-analysis) Eqs. (3) and (4) can be written in the following form:

$$\frac{d\sigma_C}{d\Omega} = \frac{r_o^2}{2} S(y, Z) \frac{1+\alpha+\alpha^2}{(1+\alpha)^3} \quad (6)$$

and

$$\frac{d\sigma_C}{d\Omega} = r_o^2 S(y, Z) \left\{ \frac{1+2\alpha+2\alpha^2}{(1+2\alpha)^3} \right\} \quad (7)$$

respectively.

In the approximation $\alpha \approx 0$ (i.e. $E_o \ll 511$ keV):

$$\left(\frac{d\sigma_C}{d\Omega} \right)_{180} = 2 \left(\frac{d\sigma_C}{d\Omega} \right)_{90}$$

Angular distribution of Compton scattered X and gamma rays versus energy is shown in Figure 2.8.

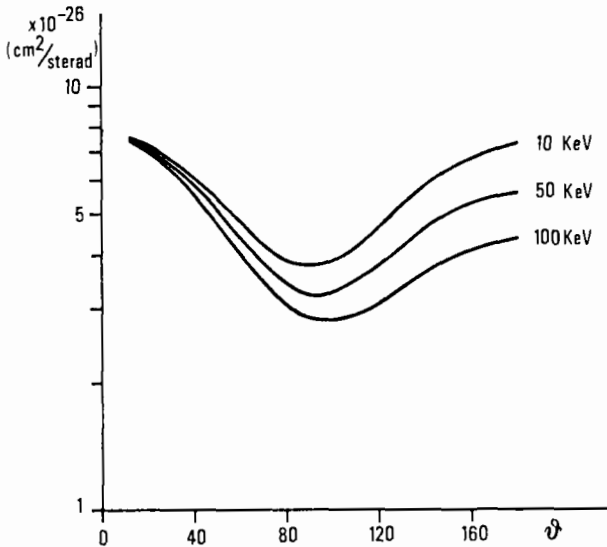


Fig. 2.8. Relative probability of Compton scattering differential cross section per electron versus scattering angle θ .

2.3.4 Rayleigh scattering

Rayleigh scattering, also called elastic or coherent scattering, takes place if the electron returns to its original state after the interaction. In this case, the atom as a whole absorbs the momentum change and the scattered photon has the same energy as the incident. Detailed Rayleigh scattering calculations have been made by several authors. In practice, it is necessary to consider the charge distribution of all Z electrons. This can be done approximately through use of an "atomic form factor" $F(y, Z)$. The square of this factor is the probability that the Z electrons of an atom take up a recoil momentum without absorbing any energy. The above probability is combined with the low-energy form of the Klein-Nishina formula to give the differential Rayleigh cross section:

$$\frac{d\sigma_R}{d\Omega} = \frac{r_0^2}{2} (1 + \cos^2 \theta) \{F(y, Z)\}^2 \quad (8)$$

The atomic form factor is tabulated in Ref. 4.

Angular dependence of Rayleigh and Compton attenuation coefficients at 30, 60, 120 and 200 keV is shown in Figure 2.9.

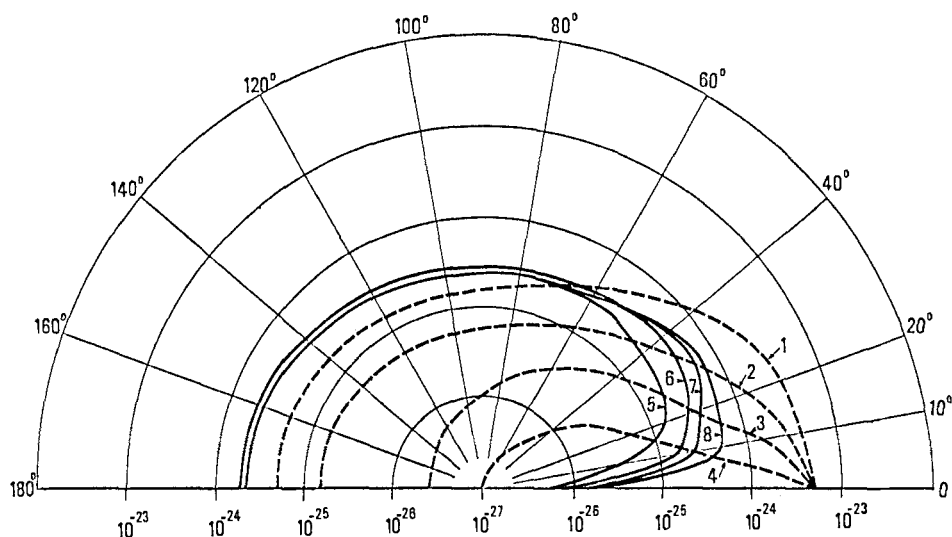


Fig. 2.9. Angular distribution of Rayleigh scattering differential cross section of water at 10 keV (1), 20 keV (2), 40 keV (3), and 100 keV (4) and of Compton scattering differential cross section of water at 10 keV (5), 20 keV (6), 40 keV (7) and 100 keV (8).

2.4 THEORETICAL BACKGROUND FOR XRF-ANALYSIS

By irradiating a sample containing an element a having concentration c_a with monoenergetic radiation of energy E_o and photon flux density (intensity) N_o , (see Fig. 2.10), the fluorescent intensity N_a of X-rays of element a emitted from the sample is given by:

$$N_a = \frac{N_o k \omega_a \mu_{ph,a} (1-1/J_a) c_a}{\{\mu_t(E_o) \text{cosec}\phi_o + \mu_t(E_a) \text{cosec}\phi_1\}} (1 - \exp\{-\mu_t(E_o) \text{cosec}\phi_o + \mu_t(E_a) \text{cosec}\phi_1\} m) \quad (9)$$

where the parameters of the above Equation have the significance and the dimensions listed in Table 2.4. For a sample irradiated and emitting normally with respect to the sample surface (backscattering geometry), $\text{cosec}\phi_o = \text{cosec}\phi_1 = 1$, and Eq. (9) could be written:

$$N_a = \frac{N_o k \omega_a \mu_{ph,a} (1-1/J_a) c_a}{\{\mu_t(E_o) + \mu_t(E_a)\}} (1 - \exp\{-\mu_t(E_o) + \mu_t(E_a)\} m) \quad (9')$$

For a 90° geometry ($\phi_o = \phi_1 = 45^\circ$):

$$N_a = \frac{N_o k \omega_a \mu_{ph,a} (1-1/J_a) 0.71 c_a}{\{\mu_t(E_o) + \mu_t(E_a)\}} (1 - \exp\{-\mu_t(E_o) + \mu_t(E_a)\} 1.41 m) \quad (9'')$$

By indicating in Eq. (9) the matrix term as (ref.5):

$$C = \frac{1 - \exp\{-\mu_t(E_o) \text{cosec}\phi_o + \mu_t(E_a) \text{cosec}\phi_1\} m}{\{\mu_t(E_o) \text{cosec}\phi_o + \mu_t(E_a) \text{cosec}\phi_1\} m} \quad (10)$$

Eq. (9) can be written as:

$$N_a = N_o k \omega_a \mu_{ph,a} (1-1/J_a) C m c_a$$

The matrix term C , for $\phi_o = 180^\circ, \phi_1 = 180^\circ$ is shown in Figure 2.11, versus sample thickness.

It is very useful to consider two extreme cases for the sample thickness, in the hypothesis of backscattering geometry (see Eq. 9').

2.4.1 Infinitely thick samples

This is the case with liquids, alloys, minerals and so on, when the thickness of the sample is more than a few tenths of a mm.

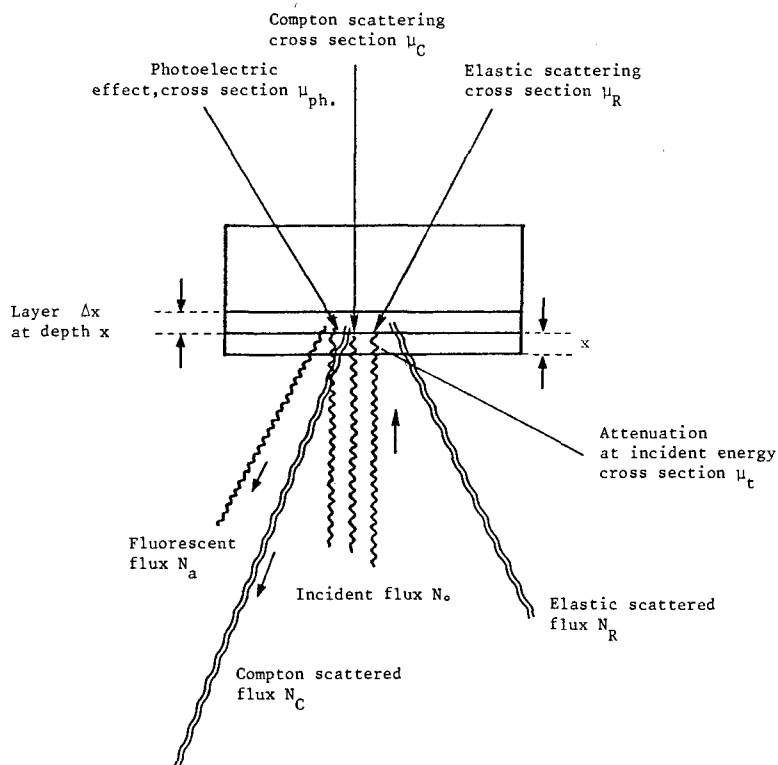


Fig. 2.10. Physical model of basic Equation for XRF-analysis

TABLE 2.4

List of parameters employed in Par.2.4

N_a (ph./cm ² s)	Fluorescent photon flux density (number of photons per unit area and time) of X-rays of element <u>a</u> ;
N_0 (ph./cm ² s)	Incident photon flux density;
k	Geometrical factor;
ω_a	Fluorescent yield of element <u>a</u> in the shell of interest (see Table 2.3);
$\mu_{ph.a}(E_0)$ (cm ² /g)	Photoelectric absorption coefficient of element <u>a</u> at incident energy E_0 ;
$(1-1/J_a)$	Branching factor which corresponds to the intensity of X-rays in the line of interest over the total X-ray intensity;
c_a (%)	Concentration (%) by weight) of element <u>a</u> ;
m_a (g/cm ²)	Mass per unit area of the sample;
$\mu_t(E_0)$ (cm ² /g)	Total mass absorption coefficient of the matrix at energy E_0 ;
$\mu_t(E_a)$ (cm ² /g)	Total mass absorption coefficient of the matrix at energy E_a ;
ϕ_0 (degrees)	Incident angle with respect to the sample surface;
ϕ_1 (degrees)	Outgoing angle with respect to the sample surface.

. In the following this factor will be approximated to 1.

For infinitely thick samples, no radiation crosses the sample, and, therefore, from Eq. (9') it is necessary to satisfy the condition:

$$m\{\mu_t(E_o) + \mu_t(E_a)\} \gg 1 \quad (11)$$

In this hypothesis Eq. (9') can be written in the form:

$$N_a = \frac{N_o k \omega_a \mu_{ph.a} c_a}{\mu_t(E_o) + \mu_t(E_a)} \quad (12)$$

showing a non linear dependence of the fluorescent counts N_a versus the elemental concentration c_a .

Incident radiation is also scattered by the sample. The flux of radiation scattered at 180° through the Compton effect and Rayleigh scattering is given, respectively, by:

$$N_C = \frac{N_o k \mu_C}{\{\mu_t(E_o) + \mu_t(E_2)\}} (1 - \exp\{-\{\mu_t(E_o) + \mu_t(E_2)\} m\}) \quad (13)$$

and

$$N_R = \frac{N_o k \mu_R}{2\mu_t(E_o)} (1 - \exp\{-2\mu_t(E_o)m\}) \quad (14)$$

where:

E_2 is the energy of Compton scattered radiation at 180° ;

μ_C is the attenuation coefficient of the sample for Compton effect;

μ_R is the attenuation coefficient of the sample for elastic scattering.

For infinitely thick samples, Eqs. (13) and (14) can be written as:

$$N_C = \frac{N_o k \mu_C}{\mu_t(E_o) + \mu_t(E_2)} \quad (15)$$

and

$$N_R = \frac{N_o k \mu_R}{2 \mu_t(E_o)} \quad (16)$$

The total flux of scattered radiation at 180° is, therefore, given by:

$$N_{sc} = \frac{N_o k \mu_{sc}}{2 \mu_t(E_o)} \quad (17)$$

where $\mu_{sc} = \mu_C + \mu_R$. Eq. (17) is valid in the approximation $E_2 \approx E_o$.

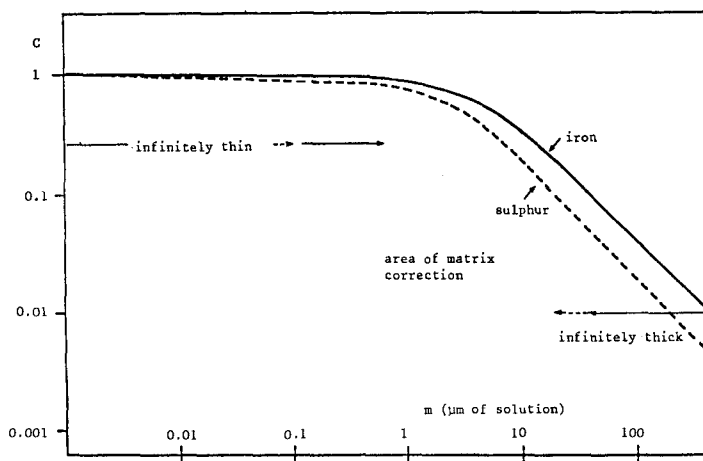


Fig. 2.11. Matrix correction term C (see Eq.(10)) of sulphur and iron in solution versus sample thickness

The effect of scattered counts on the XRF spectrum is shown in Figure 2.12 A, which refers to 0.1% copper in solution excited by 12 keV Br-X-rays. In the Figure 2.12 B is shown the XRF-spectrum of 50 μ l of the same solution deposited on a thin filter disk and dried. There is an evident great advantage when thin samples are analyzed (see Section 2.4.2).

2.4.2 Infinitely thin samples

A thin sample is obtained, for example, by depositing and drying liquids on thin filters, by vacuum deposition, by applying paints and so on.

For "infinitely thin" samples, the attenuation of incident and output radiation should be negligible. Therefore, the following condition should be satisfied (ref. 6):

$$m\{\mu_t(E_o) + \mu_t(E_a)\} \ll 1 \quad (18)$$

In this hypothesis $C=1$ and Eq. (9') can be written as:

$$N_a = N_o k \omega_a \mu_{ph,a} m c_a = N_o k \omega_a \mu_{ph,a} m_a \quad (19)$$

showing a linear relationship between fluorescent flux N_a and concentration c_a of element a . No matrix effects or interelement effects occur.

Following Eq. (19), the unknown content of element a can be determined if the geometrical coefficient k and the physical parameters ω_a and $\mu_{ph,a}$ are

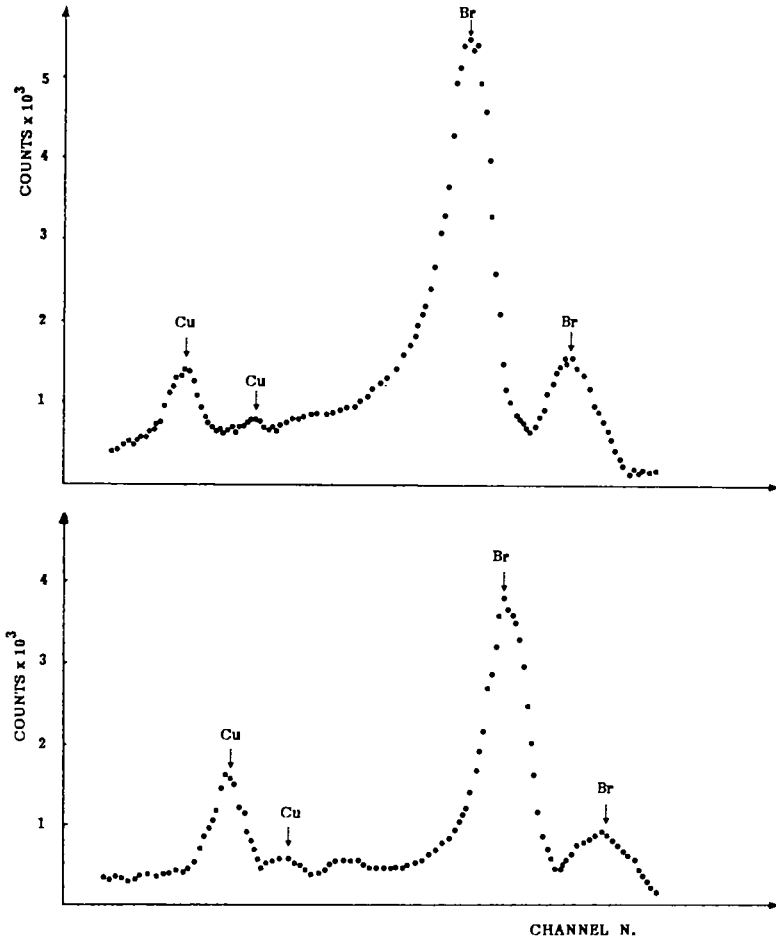


Fig. 2.12. XRF-spectrum of a 0.1% copper solution excited by 12 keV photons and directly analyzed (thick sample:A) and XRF-spectrum of 50 μ l of the same solution deposited on a filter paper disk and dried (thin sample:B).

known, in addition to the incident flux N_0 . In practice, it is easier to deduce the product of all these factors by analyzing in the same geometrical arrangement as the unknown sample, a standard sample having a morphology and composition similar to the unknown sample.

In the thin sample hypothesis, Eqs. (13) and (14) can be written as:

$$N_C = N_0 \cdot k \cdot \mu_C \cdot m \quad (20)$$

and

$$N_R = N_0 \cdot k \cdot \mu_R \cdot m \quad (21)$$

The total flux of scattered radiation at 180° , for thin samples, is, therefore, given by:

$$N_{sc} = N_0 k \mu_{sc} m \quad (21')$$

where $N_{sc} = N_C + N_R$ and $\mu_{sc} = \mu_C + \mu_R$

The optimization of the XRF-analysis for thin samples requires that fluorescent counts are increased as much as possible and scattered counts are lowered.

To increase photoelectric counts, the photoelectric attenuation coefficient $\mu_{ph.a}$ has to be increased. This can be done by selecting an optimal value of incident energy, close to the photoelectric edge of the element to be excited and analyzed (see Fig. 2.13). Numerical values of Fe-cross-section versus energy are shown in Table 5.(ref. 7).

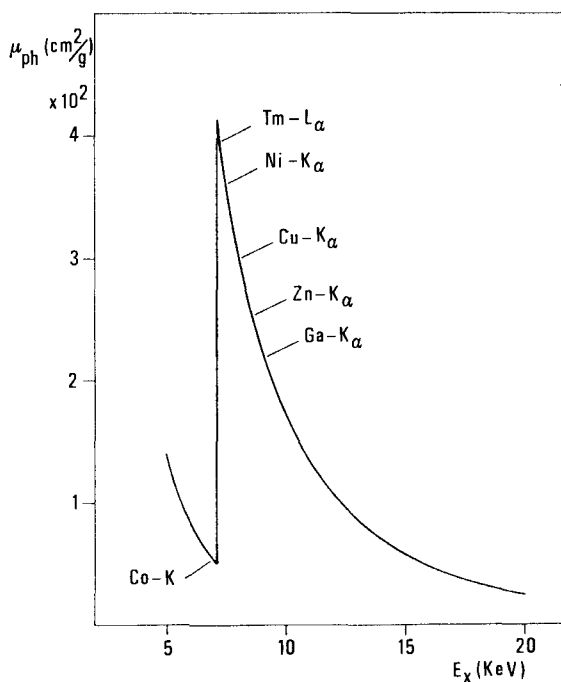


Fig. 2.13. Attenuation cross section of iron (cm^2/g) versus energy, near the photoelectric discontinuity $E(K_{ab})$ of iron. Energy values of K_α -X-rays of some secondary targets are shown (see also Table 2.5).

TABLE 2.5

Cross-section for Fe versus energy (keV) and corresponding secondary target when an X-ray tube is employed

Secondary target	E_0 (keV)	Fe-cross section (cm^2/g)
Co(K α)	6.93	56
Tm(L α)	7.15	400
Ni(K α)	7.47	360
Cu(K α)	8.05	300
Zn(K α)	8.64	252
Ga(K α)	9.25	210
Sr(K α)	14.1	66
Mo(K α)	17.5	37
Ag(K α)	22.0	23
Ba(K α)	32.0	7

Scattered counts can be reduced by lowering the term $m\mu_{\text{sc}}$, i.e. the mass per unit area of the sample and/or of the support; very thin substrates should be employed. Reduction of μ_{sc} requires the lowering of the mean atomic number of the sample and of the substrate, as can be deduced from the observation of the scattering attenuation coefficient of the matter versus mean atomic number Z (see Fig. 2.14).

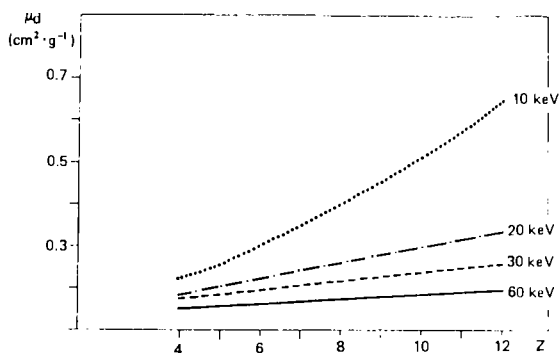


Fig. 2.14. Scattering cross-section of matter of mean atomic number Z at incident energies of 10, 20, 30 and 60 keV.

2.5 THEORETICAL MINIMUM DETECTION LIMITS FOR XRF-ANALYSIS

Following the derivations of Currie (ref. 8) based on Poisson counting statistics, a definition for the minimum detectable limit (MDL) with 95% confidence, is:

$$\text{MDL} = (3.29/S) \sqrt{(N_b/t)} \quad (22)$$

where S represents the sensitivity of the equipment expressed in counts/s per

$\mu\text{g}/\text{cm}^2$ of the element to be analyzed, R_b is the number of counts in the background and t is the measuring time.

If we now consider Eqs. (19) and (21') and the ratio between fluorescent counts (which are connected to the term S of Eq.(22)), and scattered counts (which are connected to the background term N_b), then:

$$\frac{N_a}{N_{sc}} = \frac{\omega_a \mu_{ph.a} m_a}{\mu_{sc} m} \quad (23)$$

To obtain the best MDL value, the number of fluorescent counts N_a should be as large as possible, and the number of scattered counts N_{sc} should be as low as possible.

To this end, we have deduced in Par. 2.4.2 that the energy of the incident radiation should be selected near the photoelectric edge of the element or elements to be analyzed, and that the mass of the sample and of the substrate should be as thin as possible. Substrates with a mass per unit area of $1 \text{ mg}/\text{cm}^2$ and less are obtainable.

Assuming that the background under the photoelectric peak is mainly due to the scattered radiation, and keeping in mind the definition of MDL, the following Equation can be deduced for thin samples, from Eqs. (19) and (21'):

$$(\text{MDL})_a = 3.29 \sqrt{\frac{\mu_{sc} m}{\alpha N_o k \omega_a^2 \mu_{ph.a}^2}} \quad (24)$$

where α is the fraction of scattered radiation under the photoelectric peak of element a , which is due primarily to incomplete collection of energy in the detector, and is proportional to the scattered radiation (ref. 9). Assuming, for example, to excite iron with an X-ray tube with a Zn-secondary target ($K_\alpha = 8.6 \text{ keV}$) and assuming: $N_{sc} = 10^4 \text{ ph./s}$ (see Par. 2.6.2c), $\mu_{sc} = 0.35 \text{ cm}^2/\text{g}$, and $m = 1 \text{ mg}/\text{cm}^2$, one obtains:

$$(\text{MDL})_a = 3.29 \times 10^{-2} \frac{\mu_{sc} m}{\omega_a \mu_{ph.a} \sqrt{\alpha}} \text{ g/s} \quad (24')$$

The value of α can be determined experimentally by irradiating the support only. If, for example, $\alpha = 100$, one obtains: $(\text{MDL})_{Fe} = 13 \text{ ng/s}$.

Therefore, a MDL of 0.4 ng could be obtained, theoretically, in a measuring time of 10^3 s . Values in the same range are obtained for elements with atomic number ranging from about 25 to about 40 (see Table 2.6). Experimental values of MDL are not unlike the calculated values.

TABLE 2.6

Calculated MDL values for some selected elements in thin samples.

Element	secondary target and exciting energy (keV)		coefficient α	MDL (ng/s)
Ti	Zn	8.6	50	34
Fe	Zn	8.6	100	13
Br	Mo	17.5	40	26
Ru	Sn	25.0	30	28
I	Ce	35.0	30	44

For thick samples, and considering Eqs. (12) and (17), the following Equation can be written for the minimum detectable limit, taking into account the hypothesis $N_{sc} = 10^4$ ph/s

$$(MDL)_a = 1.64 \times 10^{-2} \frac{\mu_{sc}}{\omega_a \mu_{ph.a} \sqrt{\alpha}} \times \left\{ \frac{\mu_t(E_o) + \mu_t(E_a)}{\mu_t(E_o)} \right\} \quad (25)$$

The MDL obtained in 10^3 s measuring time, when elements Fe, Ti, Br, Ru and I are considered, in the same conditions as those given for thin samples, are reported in Table 2.7.

TABLE 2.7

Calculated MDL values for some selected elements in solution

Element <u>a</u>	Secondary target and relative energy (keV)		$\mu_{ph.a}$	ω_a	MDL $\times \sqrt{\alpha}$ (ppm)
Ti	Zn	8.6	200	0.22	4.5
Fe	Zn	8.6	250	0.35	2.2
Br	Mo	17.5	75	0.62	3.0
Ru	Sn	25.0	50	0.78	3.0
I	Ce	35.0	30	0.88	4.3

2.6 EXPERIMENTAL ARRANGEMENT

2.6.1 Apparatus for XRF-analysis

A typical X-ray fluorescence analyzer consists of the following basic components: an excitation source (radioisotope or X-ray tube); a detector which selects the energies of the characteristic X-rays excited and measures their intensities; an electronic amplification chain and a readout system, the output of which can be correlated with the elements present in the specimen and their concentrations.

Figure 2.15 shows typical schema of two extreme versions of XRF-analyzers; the upper part (see Fig. 2.15a) refers to a very simple, portable, single-element analyzer, characterized by a sealed-off radioactive source, a gas-proportional detector or a NaI(Tl) scintillation detector, an amplifier and a single channel-analyzer with timer-scaler. The lower part (see Fig. 15b) shows a sophisticated multielement XRF-analyzer, characterized by an X-ray tube with various secondary targets, a semiconductor detector, a pre-amplifier, an amplifier, a multi-channel-analyzer coupled to a personal computer for automatic analysis of the spectra.

A practical source-detector arrangement for radioisotope X-ray excitation and spectrometry should have the following requisites:

- maximum geometrical efficiency;
- negligible background due to direct transmission of radiation from source to detector;
- minimum background due to scatter or fluorescence from the instrument structure;
- adequate shielding to reduce the radiation dose rate at accessible points outside the measuring head.

The "central source geometry" with the source placed over the centre of the detector window is the most suitable, reaching ten percent efficiency, and has been widely used with scintillation and gas proportional counters which have large windows. "Side source" geometry is a useful alternative, if the source and detector window diameters are comparable (ref. 10).

"Annular source" arrangements are desirable for small Si(Li) and Ge(Li) or HPGe detectors (ref. 10).

When the excitation source is an X-ray tube with secondary targets, the requisites for maximum geometrical efficiency are not so critical, because the X-ray emission from the tube is much more intense. Other above mentioned requisites are valid also for X-ray tubes, particularly the latter concerning the radiation dose.

In this paragraph, the single components of standard X-ray equipment will be discussed in detail.

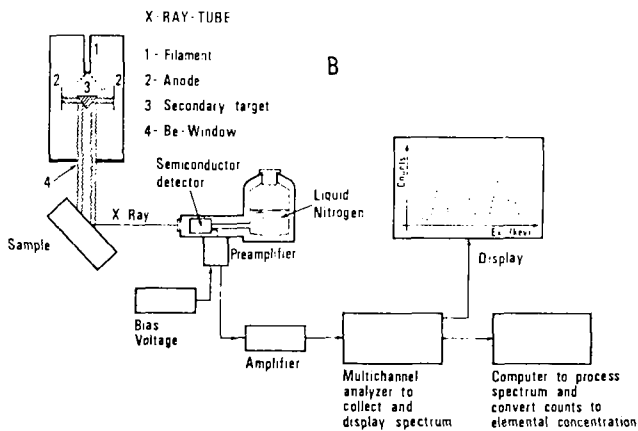
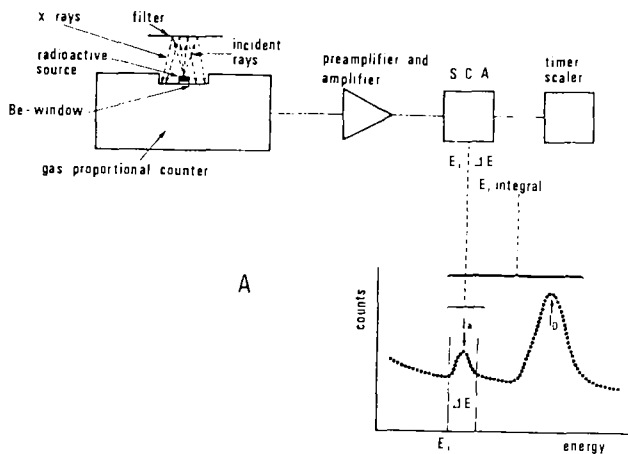


Fig. 2.15. Schema of two versions of XRF-analyzers. A: "single element" X-ray fluorescence system. A typical spectrum, collected with a multi-channel analyzer is shown. The X-rays of element *a* and the elastically scattered source peak (D) are shown. With the single-element XRF system, a single-channel analyzer is employed, instead of the multi-channel analyzer. The window (ΔE) of the single-channel analyzer (S.C.A.) is centered on the peak of interest; B: "multi-element" X-ray fluorescence system characterized by an X-ray tube with secondary targets, a semiconductor detector and a multi-channel-analyzer coupled to a computer.

2.6.2 Excitation sources

X- or gamma-ray sources from a few keV to about 150 keV can be usefully employed for X-ray excitation. As a general rule, the best excitation energy for a prefixed element is just above the photoelectric edge of the element, where the photoelectric coefficient for the excited shell is maximum (see Fig. 2.13). The energy of excitation should, however, be selected with reference to the detector resolution (it is essential to avoid partial superimposition of X-rays of elements to be excited, with the scattered radiation), and to whether one or more elements are to be analyzed.

(a) Radioactive sources

A radioactive source emitting radiation in the 5-150 keV range can be usefully employed for X-ray excitation when:

- it emits few X- or gamma-lines (quasi monoenergetic source) below about 150 keV without emitting high-energy beta or gamma radiation;
- it can be produced with a specific activity high enough to yield a source emission of almost $10^7 - 10^8$ photons;
- it has a half life of at least one year.

A very wide range of such sources are now available in the desired energy range, specific activities, half-lives and encapsulation.

Table 2.8 shows a list of suitable radioactive sources and the associated emission energy and typical intensity (ref. 11).

TABLE 2.8
Radioactive photon sources for fluorescent excitation.

Isotope	Half-life $T_{1/2}$	Principal photon emission (energy in keV)	Typical acti- vity (Bq) $\times 10^8$	Photon out- put* (ph/s.sr)
Fe-55	2.7 y	Mn-K-X-rays 5.9	3.7	$7 \cdot 10^6$
Cd-109	453 d	Ag-K-Xrays 22, 25	1.1	$7.5 \cdot 10^6$
Pu-238	80 y	U-L-X-rays 13.5, 16.8	7.4	$2.5 \cdot 10^6$
I-125	60 d	Te-K-X-rays 27.4, 31.3	18.5	$2 \cdot 10^8$
Am-241	433 y	59.6	37	$6 \cdot 10^7$
Co-57	270 d	122, 133	1.1	$3.5 \cdot 10^6$
Gd-153	241 d	97, 103	111	$4.2 \cdot 10^8$

* photon outputs are the values measured at the peak of the spatial distribution in photons per second per sterad. These represent the output which would be recorded in narrow beam geometry (ref. 11).

Elements which can be usefully excited by the above-mentioned sources are shown in Figure 2.16, together with the range of Compton scattered radiation, at which the source is of no use.

Sometimes, secondary sources can be employed, for fluorescent excitation, consisting of beta-emitters in which "bremsstrahlung" radiation is

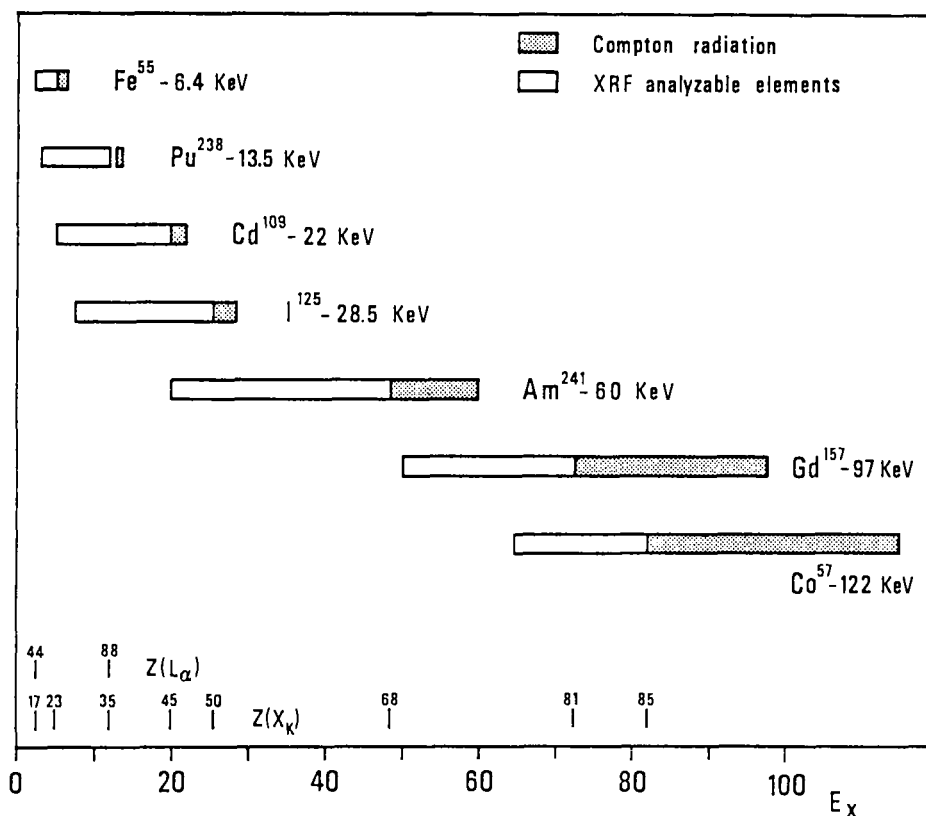


Fig. 2.16. Range of elements which can be analyzed employing radioactive sources (after Cesareo, ref. 45).

produced by scattering of beta-particles within the constituent material of the sources. The spectrum produced is continuous up to the maximum beta particle energy. Suitable bremsstrahlung sources (BS) are listed in Table 2.9 (ref. 11).

(b) X-ray tubes with secondary targets

The most common and intense photon sources are X-ray tubes. For a 1 mA

electron source, approximately $5 \cdot 10^{10}$ photons/s are generated, distributed between the characteristic X-rays of the anode material and the continuous bremsstrahlung radiation. A summary of X-ray tubes for XRF Spectrometry can be found in ref. 12, and the development of a portable one-piece generator and tube system, the kevox PXS, capable of producing 50 kV and 1 mA is described in ref. 13.

Direct X-ray excitation with bremsstrahlung radiation is not very useful when very high sensitivities are required. Monoenergetic radiation is preferable for this purpose. This can be obtained by employing secondary targets of

TABLE 2.9.
Useful bremsstrahlung sources for X-ray excitation

Isotope	Half-life $T_{1/2}$	Principal photon energies (keV)	Emission (%)	Typical Photon output (ph/s.sr)
Pm-147 + Zr target	2.6 y	Zr-X-rays + BS up to 225 keV	0.4%	$3 \cdot 10^5$
H-3 + Ti	12.35y	Ti-K-X-rays + BS up to 18.6 keV	0.01	"
H-3 + Zr	"	Zr-K-X-rays + BS up to 18.6 keV	0.01	"

pure elements at the output of the tube. The experimental arrangement for "converting" bremsstrahlung radiation in "quasi monoenergetic" radiation (i.e. X-rays of the target element) is shown in Figure 2.17. The primary bremsstrahlung radiation is guided to the target through a cylindrical collimator lined with a foil of the same target material. The primary radiation is converted into X-rays of the element of the target through a photoelectric effect. Since the target represents an "infinitely thick" sample, the conversion factor is given by:

$$\frac{\omega_t \mu_{ph.t}(E_o)}{\mu_{tt}(E_o) + \mu_{tt}(E_t)} \quad (26)$$

in which:

μ_t is the fluorescent yield of the target element;

$\mu_{ph.t}$ represents the attenuation coefficient of the target material at incident energy E_o ;

$\mu_{tt}(E_o)$ represents the total attenuation coefficient of the target material at incident energy E_o ;

$\mu_{tt}(E_t)$ represents the total attenuation coefficient of the target material at fluorescent energy of the target E_t .

Typical values of the "conversion factor" are 30-50%; a large part of the incident bremsstrahlung radiation is then "converted" into secondary, quasi monoenergetic radiation providing the high voltage value of the X-ray tube anode is well selected. Only a very small part of the incident radiation

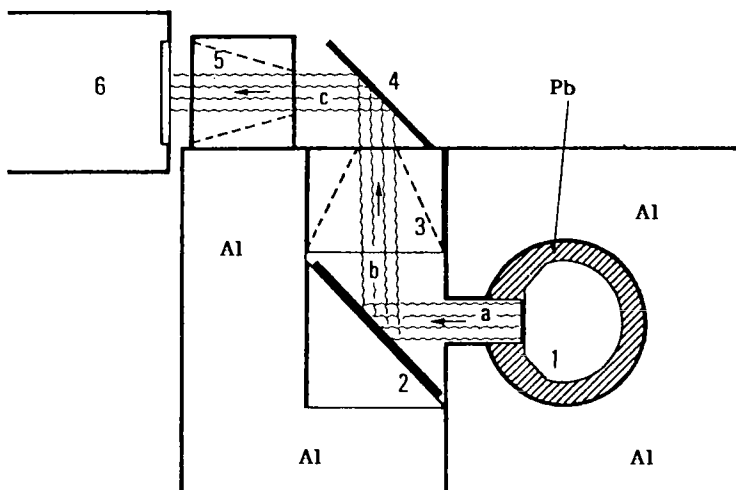


Fig. 2.17. Schematic set-up of the apparatus employed for generating monoenergetic X-rays for XRF-analysis.

1. X-ray tube;
2. secondary target of element t ;
3. conic collimator internally covered with a foil of element t ;
4. sample;
5. conic collimator internally covered with a foil of element t ;
6. detector;
- a. primary bremsstrahlung radiation;
- b. secondary radiation;
- c. X-rays emitted by the sample.

(after Cesareo and Viezzoli, ref. 14).

scattered by the secondary target. The major loss of radiation is, therefore, given by geometrical factor k . For example, if a Zn-target is employed, and the mean energy value of bremsstrahlung radiation is 15 keV, then:

$$N_{\text{Zn}}/kN_o = 0.3$$

$$N_{\text{sc.}}/kN_o = 6 \cdot 10^{-3}$$

The intensity of secondary Zn-X-rays is about 50 times higher than the elastic and inelastic scattered bremsstrahlung radiation, which is further

spread over a large energy interval.

The secondary radiation leaving the target is then collimated through a cylindrical or conic collimator lined with a foil of the same target material, in order to avoid undesired radiation produced by photoelectric effect of secondary radiation in the collimator.

The sample is, therefore, irradiated by a strong, collimated monoenergetic radiation, the energy of which can be varied by varying the secondary target, and the intensity of which can be varied by more or less collimation. When a great deal of collimation is employed both at the output of the X-ray tube, and at the output of the target, the intensity is reduced by about three-four orders of magnitude; the intensity of the secondary radiation then ranges between $10^8 - 10^9$ photons/s, depending also on the tube electron current.

Secondary radiation leaving the target is constituted essentially of K_α and K_β radiation emitted by the target element, superimposed on the background radiation due to elastic and inelastic scattering of primary and secondary radiation by the collimators and by the secondary target (ref. 9). Other peaks should be avoided, and for this reason all collimators are lined with a foil of target material, which should be extremely pure, in order to avoid any photoelectric effect due to "trace elements" present in the target material. The presence of the photoelectric peak is unavoidable due to the tube-anode (in general tungsten) and elastically and Compton scattered radiation from the collimators. This peak can be reduced by filtering the secondary radiation through an element just above the photoelectric edge of W.

If an extremely pure monoenergetic radiation, composed only by the K_α peak is needed, the secondary radiation can further be filtered through an absorber with a K-absorption edge between the K_α and K_β -X-rays. In such a way, most of the K_β X-rays are removed. A good method is to employ a water solution as absorber, the thickness of which should be such as to reduce the K_β -beam to about 1/3. In such a way, a ratio $N_\alpha/N_\beta \cdot 10^2$ can be obtained (see Fig. 2.18).

(c) Radiation flux for optimal XRF-analysis

As already pointed out, direct excitation of a sample with primary bremsstrahlung radiation is less useful than excitation with secondary monoenergetic radiation, even if the latter is much less intense, for three main reasons (see Fig. 2.19):

- the most efficient photoelectric excitation is obtained with radiation with energy over (if possible just above) the absorption edge of the element to be analyzed;

- high intensity bremsstrahlung radiation (10^{11} - 10^{12} ph/s) largely saturates the electronic chain and the multichannel analyzer; it can be demonstrated (see below) that an intensity no greater than about 10^9 photons is required;
- the background, in particular that under the peak or peaks of interest, is mainly produced by inelastic scattering of incident radiation from the sample, from the sample support, from the air and so on; this effect is much more critical and less reducible for the large spectrum of bremsstrahlung radiation than for monoenergetic radiation.

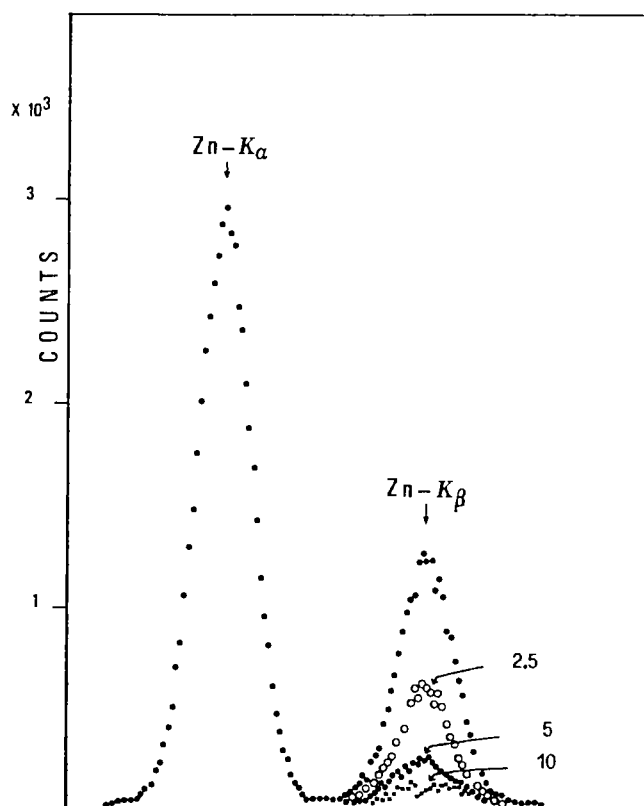


Fig. 2.18. Secondary Zn-radiation, constituted of the K_{α} and K_{β} peaks. Filtration of the radiation through a solution containing 2.5, 5, 10% of Cu strongly attenuates the K_{β} radiation.

In order to better understand these important factors, let us suppose that the aim is to excite, with monoenergetic Zn-secondary radiation, a thin sample ($m = 10^{-3}$ g/cm²) containing a small quantity of Fe ($m_{Fe} = 1\mu\text{g/cm}^2$).

The scattered radiation in the detector is given by:

$$N_{sc} = N_o k \mu_{sc} m \quad (27)$$

where N_o is the intensity of secondary radiation from the sample (photons/cm².s) k is the solid angle between sample and detector and includes the detector efficiency at energy of N_{sc} photons, m is the mass per unit area of the sample, and $\mu_{sc} = \mu_C + \mu_{el}$ represents the total attenuation coefficient of the sample for scattering processes.

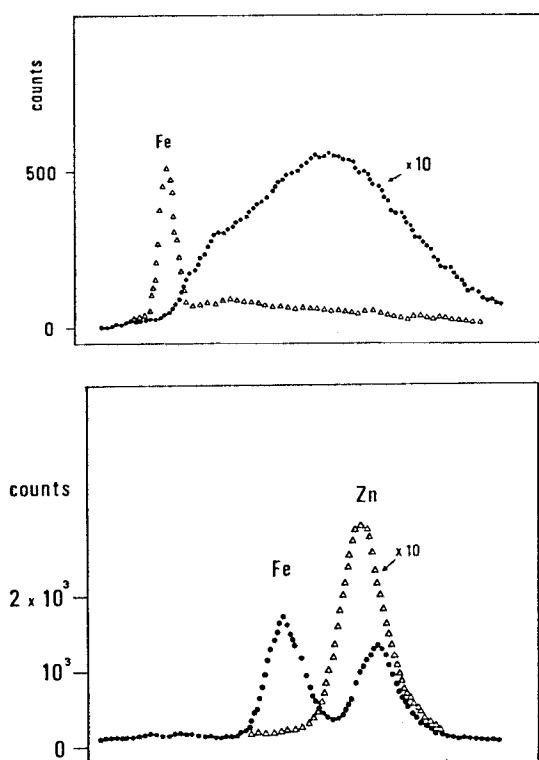


Fig. 2.19. A. Secondary radiation coming out from a Zn target and excitation of a sample containing 100 μ g Fe (triangles). B. bremsstrahlung radiation directly coming out from an X-ray tube, and excitation of the same sample as above, containing 100 μ g Fe (after Cesareo, ref. 45).

The Fe-fluorescent counts are given by:

$$N_{Fe} = N_o k' \mu_{ph.Fe} \omega_{Fe} m_{Fe} \quad (28)$$

where k' will be different from k if the detector efficiency at energy of Fe-X-rays is different from the efficiency at energy of scattered radiation.

From Eqs. (27) and (28), when $\mu_{sc} = 0.4$ we find that :

$$N_{sc} = N_o k 0.4 10^{-3}$$

$$N_{Fe} = N_o k' 88 10^{-6}$$

Now, $N_{sc} = 10^4$ are the maximum counts in the detector without severe dead time losses and degradation of energy resolution. Putting the geometrical factors $k=k'=0.01^*$, then:

$$N_{omax} = 2.5 10^9 \text{ photons/s}$$

$$N_{Fe \text{ max}} = 2.2 10^3 \text{ ph/s}$$

Similar conclusions can be reached by analyzing other elements with the secondary targets. The general conclusion is that the intensity of radiation irradiating the thin sample should not exceed $N_o = 5.10^9 \text{ ph/s}$, due to the inability of the detector and electronics to process signal pulses faster than a certain rate.

For thick samples, it can be demonstrated, by similar calculations, that intensity values no larger than 5.10^7 are required on the sample.

There is no advantage in utilizing greater intensities, since this only results in larger peaks and increasing dead times in the electronic chain.

(d) Synchrotron radiation

In the last ten years, synchrotron radiation has been used for excitation of X-Ray Fluorescence (refs. 15-18).

Synchrotron radiation (SR) is generated when electrons with typically several billion electron volts (GeV) of kinetic energy orbit in an ultrahigh vacuum tube between the poles of strong magnets. A vertical magnetic field deflects the electrons horizontally, causing the emission of SR. The SR spectrum is characterized by the critical photon energy (E_c), which is the energy above and below which one-half of the total emitted SR power falls. E_c

* The geometrical factor $k=k'=S/(4\pi d^2)$, where S is the surface of the irradiated sample, and d the distance between source and detector. When a central geometry is employed, with a radioactive source and a proportional gas counter, then $k=0.1$; when the X-ray tube is employed, with source and detector in a 90° geometry, then $k=0.01-0.02$.

and the energy range of the spectrum are dependent on the electron energy (E) and the orbital radius (R):

$$E_c = 2.218 E^3/R$$

where E_c is in keV, E is in GeV and R is in meters.

A typical spectrum of SR with the storage ring operating at 3 GeV, compared with a W-target X-ray tube is shown in Figure 2.20 (ref. 18).

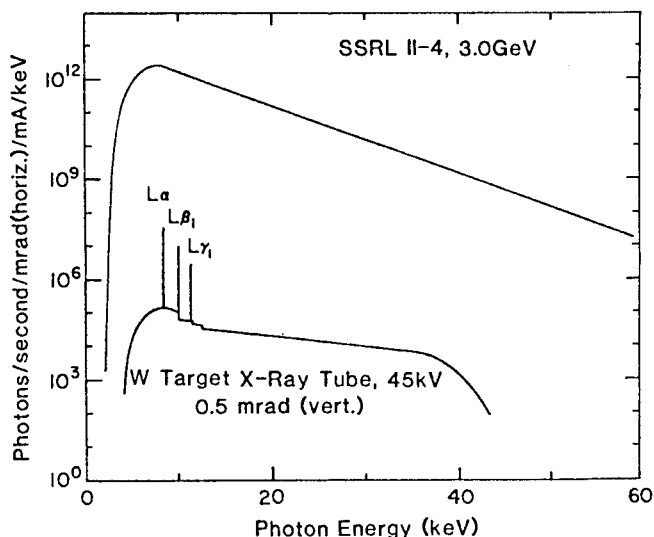


Fig. 2.20. Synchrotron radiation from SPEAR at Stanford (upper curve) compared with a W- X-ray tube (after ref. 18).

The availability of SR sources provides some advantages in comparison with conventional X-ray tube sources presently used for XRF. The advantages are:

1. high photon flux is available to irradiate the sample (several orders of magnitude greater than for most tube sources) therefore the beam can be monochromatized and, if necessary, highly collimated. A beam of submillimeter dimensions can be obtained, so that it is already possible to think of making relatively detailed elemental maps.
2. the radiation is highly polarized in the plan of the electron orbit, which reduces Rayleigh and Compton scattering by the sample.
3. the radiation varies in energy from zero to about 50 keV in energy.

Exploratory experiments by Sparks and Hardings (ref. 16) at the Stanford

Synchrotron Radiation Laboratory in 1975 assessed the application of the continuum spectrum of SR for fluorescence excitation. In 1977 and later, Sparks et al. (ref. 17) reported the use of monochromatic SR for the fluorescence analysis of small particles.

Successively, several groups of researchers all over the world started to use SR for XRF-analysis; the minimum detectable limits of SR-XRF analysis are, in general, not very different (in terms of g/cm^2 or in ppm) from the results obtained with an X-ray tube with secondary targets; the difference lies in the possibility of concentrating the very high intense SR in very small areas (refs. 17 and 18). Therefore the absolute detection limit (in ng) could be some orders of magnitude better. A fluorescent microprobe that utilizes synchrotron radiation rather than charged particles as an excitation source is provided by the improved fluorescence signal over background and the reduction in the amount of energy deposited to achieve the same MDL.

2.6.3 X-ray detectors

Different kinds of detectors can be employed in X-ray spectrometry, the choice depending upon the element or elements to be analyzed, the sensitivity required, the method of analysis (in situ, in vivo, in vitro) and the cost.

The most important characteristics of detectors for X-ray analysis are listed in Table 2.10. Energy resolution FWHM of different detectors vs energy is shown in Figure 2.21, and Ag-K-spectrum in Figure 2.22.

(a) Proportional gas detectors

Proportional gas counters are generally cylinders (typically: length 15-20 cm, diameter 6-10 cm) filled with a mixture of noble gases (neon, krypton, argon, xenon) generally at atmospheric pressure and a low percentage of quench gases (CH_4 , CO_2 and so on) (ref. 19). These detectors have a thin beryllium window for the entrance of radiation (thickness 10-100 μm) and can be employed, depending upon the filling gas, from a few keV to about 50 keV; proportional gas counters offer significant advantages over other types of X-ray detectors, including:

- high efficiency;
- simplicity of installation and operation;
- low cost.

The energy resolution of these detectors is not very good (see Fig. 2.21) and, therefore, they can be usefully employed when only a few elements are to be analyzed which are sufficiently far in energy, in order to avoid superimposition of X-rays. Gas proportional counters are very suitable for "single element analysis" and for "in situ" analysis, when extremely high sensitivity

TABLE 2.10
Detectors for X-Ray Fluorescence Analysis.

Detector	useful energy interval (keV)*	FWHM (eV)		Price ₃ (\$ x 10 ³)
		at 6.4 keV	at 60 keV	
Gas proportional counters				
Xe + 10% CH ₄	3 - 50	1200	4000	3
Kr + 10% CH ₄	3 - 20	1200	--	3
Scintillation detectors				
NaI(Tl)	>5	3000	25000	2
CsI(Na)	>5	4000	30000	2
Semiconductor detectors				
Si(Li)**	1 - 60	200	400	15
Si-ion implanted	5 - 100	--	2000	5
HPGe**	>3	200	400	12
GaAs	>5	--	1000	-
CdTe	>5	1200	3000	-
HgI ₂	>2	300	500	5
BGO ²	>50	--	40000	-

* The detector efficiency at low energy depends mainly on the Be-window.

**These detectors work at liquid nitrogen temperature.

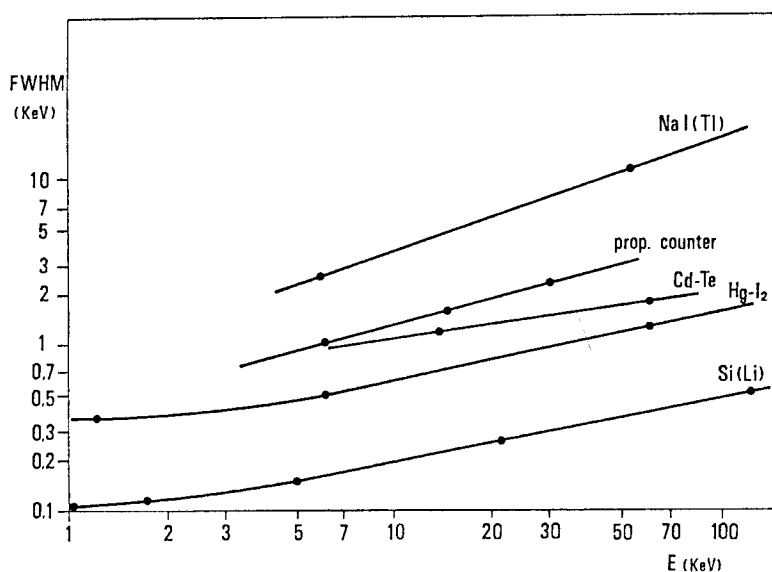


Fig. 2.21. Energy resolution (FWHM in keV) vs energy for different kinds of detectors (after Cesareo, ref. 45).

is not required.

Gas absorption characteristic of a Xe+3% CO₂ proportional detector at one atmosphere pressure is shown in Figure 2.23 (ref. 19).

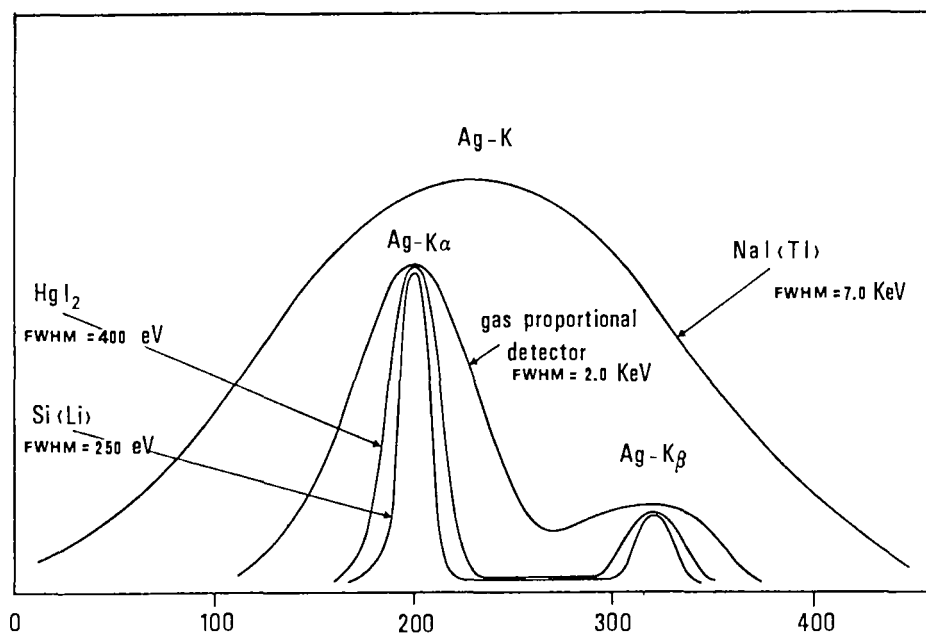


Fig. 2.22. Ag-X-rays spectra collected with different detectors (after Cesareo, ref. 45).

(b) Scintillation detectors

Scintillation detectors are employed in XRF-analysis only in single-element analysis, in which no energy discrimination is required. They present very poor energy resolution (see Fig. 2.21) and the gain of the photomultiplier shifts vs temperature. None the less, scintillation detectors have been widely employed for "in situ" analysis, because they are strong and cheap.

(c) Semiconductor detectors

Semiconductor detectors such as Si(Li), Ge(Li), HPGe and more recently Cd-Te and HgI₂, are the most widely employed detectors for high-sensitivity multielement XRF-analysis (ref. 20). They present very good energy resolution which allows us to discriminate X-rays of all elements and are very stable vs temperature. For X-Ray Spectrometry the most used are Si(Li) from about 1 to

60 keV, and coaxial or high-purity Ge-detectors above 5 keV. These detectors are very expensive and work at liquid nitrogen temperature.

Over the last few years, interest has been increasing in room-temperature mercuric iodide (HgI_2) semiconductor detectors in X-ray spectrometry because

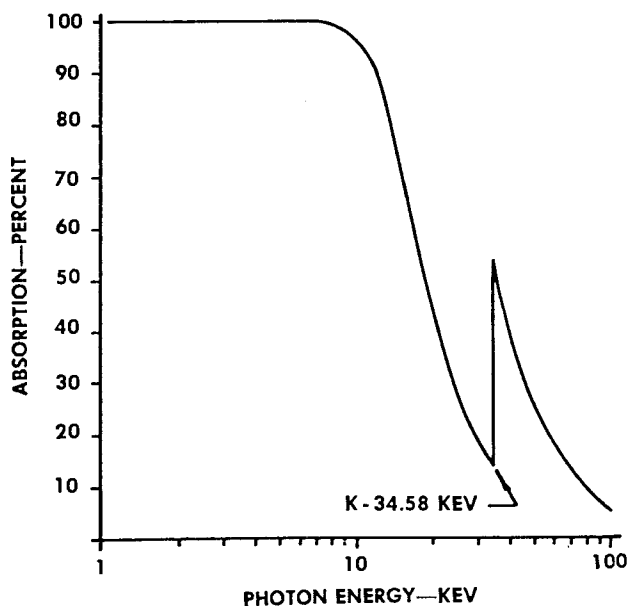


Fig. 2.23. Gas absorption of a typical proportional detector, containing Xe+3% CO_2 at atmospheric pressure (after ref. 19).

no vacuum plumbing or cryogenic cooling is required (refs. 21-26). They present an energy resolution of about 300 keV for the 5.9 keV Fe-55 line and the most recent design consists of coupling a detector directly to the first stage FET in a common preamplifier. This detector can be miniaturized and in the near future a detector-pre-amplifier package with a volume of only a few cubic centimetres is foreseen.

If certain problems can be overcome, such as sensitivity to mechanical damage, lack of purity as well as nonstoichiometry of the crystals and structural and chemical defects, HgI_2 - detectors could possibly be the best solution in the future for X-Ray Spectrometry. GaAs and CdTe detectors could also find, in the future, some interesting application in the same field.

Other kinds of semiconductor detectors are also available, which can be employed at room temperature. For example, passivated ion implanted silicon junction detectors with an Si-thickness of 300-500 μm , which present an energy

resolution of about 1.5-3 keV and a good photoelectric efficiency below 30 keV (refs. 27 and 28). Also avalanche diodes have been realized and tested which are sensitive enough to detect low energy X-rays. They operate at room temperature and have a FWHM of 10%. An array of such detectors would allow us to construct a map of elemental concentration of an irradiated sample (ref. 29).

2.6.4 Electronic chain

(a) Preamplifiers and amplifiers

The detector absorbs the energy of the incident photons (by absorbing, for example, the electrons generated via the photoelectric effect) and converts the energy to an electronic pulse. The amplitude of the pulse is proportional to the energy of the photon. Further, the pulse is electronically processed. When gas proportional detectors or semiconductor detectors are employed, the electronics following the detector is composed of a preamplifier and a main amplifier. The preamplifier usually contains a first stage, which employs field-effect transistors (FET's) placed near the detector inside the cryostat (when semiconductor detectors are employed), which exhibit very low noise when operating at an optimum temperature near 140 °K. X-ray spectrometers all employ a feed-back operational amplifier to produce an output signal the amplitude of which is proportional to the charge (charge-preamplifiers).

Pulses from the preamplifiers are characterized by a rise time of fractions of μ s, a decaying time of the order of ms and an amplitude of some mV. These are then put into a linear amplifier, which contains a gain to increase the preamplifier pulses to voltage levels compatible with analog to digital conversion. It also performs the operation of shaping pulses to permit best energy resolution of X-rays. The shaping system consists in integrators and differentiators for converting the "quasi" voltage step from the preamplifier into a pulse of limited rise time and duration approaching a Gaussian shape. Typical values of integration and differentiation time are 1-10 μ s, with an amplitude of some volts (see Fig. 2.24).

(b) Multi-channel analyzers and single-channels analyzers

The output of the main amplifier consists, therefore, of a sequence of quasi Gaussian pulses of varying amplitude which reflect the energy distribution of photons in the fluorescence spectrum.

In order to display and interpret this information, the amplitude of each pulse is measured, converted to a digital number and stored in histogram form in a suitable memory array. The histogram pulse height spectrum is then available for subsequent examination, interpretation and analysis. This operation is carried out with the so-called "multi-channel analyzer", which is

composed, schematically, of an analog to digital converter (ADC) and a memory with display and peripherals (printer, typewriter, magnetic tape and so on). There are a large number of commercial multichannel analyzers suitable for this operation. For typical XRF-analysis, a total of 1024 channels should be adequate to encode XRF-pulses.

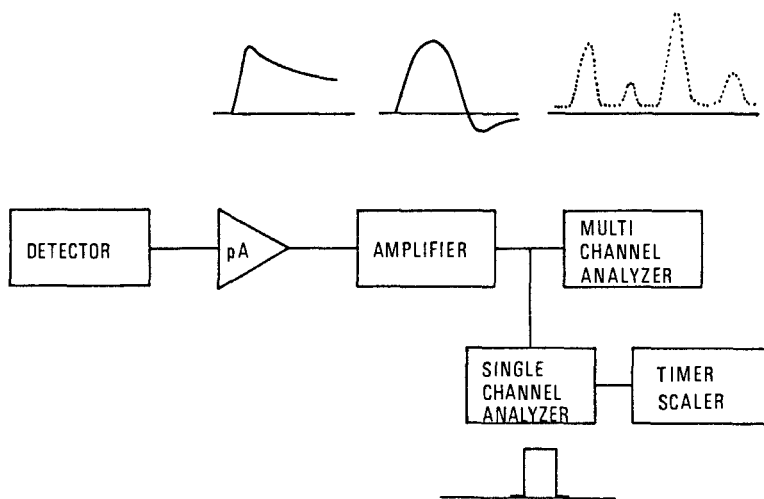


Fig. 2.24. Typical electronic chain of a XRF-analysis, pulse shapes at the output of the preamplifier and amplifier, and typical spectrum given by the multichannel analyzer.

Calibration of the analyzer energy scale is accomplished by obtaining line positions from known elements. Adjustment of the main amplifier gain determines the energy span recorded by the analyzer. The measurement of resolution and energy calibration is demonstrated in Figure 2.25. Energy calibration, in volts per channel, is obtained by dividing the known energy that separates two lines of two known elements by the number of channels separating the peaks.

Energy resolution of the system (in eV or in keV) for a given X-ray peak, is measured by the FULL WIDTH AT HALF MAXIMUM (FWHM) of the quasi Gaussian peak (ref. 30).

Recently, plug-in cards have been developed to convert the most common Personal Computers to a multichannel analyzer, eliminating the need for an external buffer and for lengthy data transfers (ref. 31).

When only one element or a few elements have to be analyzed, then a simpler and cheaper single-channel analyzer can be employed instead of a

multi-channel analyzer. A single channel analyzer, or "window" selectively tuned to the appropriate energy band, through a lower energy level E and an energy window ΔE , detects the amplified and shaped signals, converting them into fixed squared 5 Volt pulses, the intensity of which is proportional to the intensity of X-rays of the selected element. Sometimes, for standardization purposes, there is a "bank" of channel analyzers or "windows" for selective discrimination of X-rays emitted by the elements of interest, together

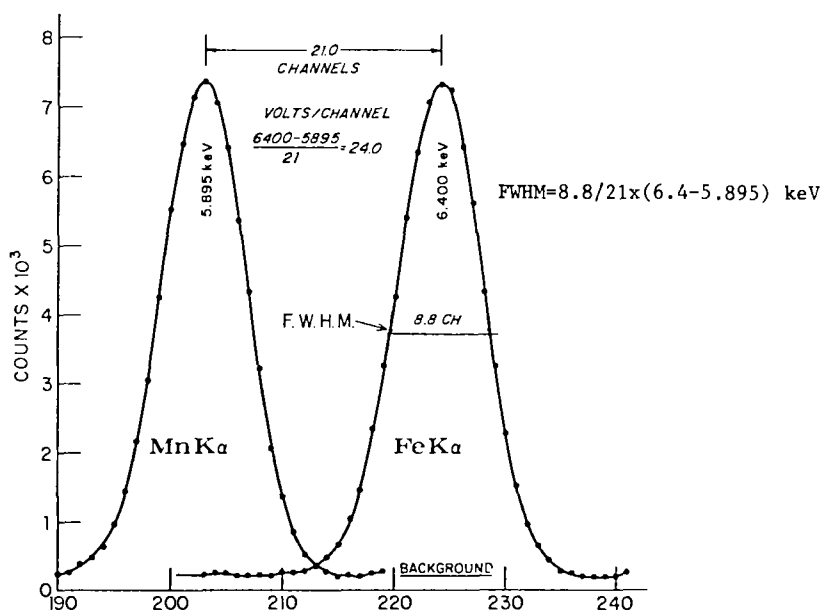


Fig. 2.25. Typical X-ray spectrum showing Mn and Fe K α -peaks, and calculation of the energy resolution in F.W.H.M.

with the inseparable background of the same energy, and of the scattered peak. In more sophisticated systems, composed of single channel analyzers and digital counter-scalers, automatic subtraction of background is possible.

(c) X-ray spectrum

When a specimen is irradiated with monoenergetic X- or gamma rays of energy E_0 , an X-ray spectrum is obtained which includes, besides X-ray fluorescence peaks, other peaks due to elastic and inelastic scattering not only in the sample, but also in the substrate, the collimators and the air. In addition further peaks due to the photoelectric effect of secondary and tertiary

radiation in interfering trace elements present in the air, the substrate of the specimen, the collimators, or in the material constituting the detector or its filling gas are also present.

An elastic scattered peak is easy to identify, because its energy is E_0 . An inelastic scattered peak has an energy value which depends on the scattering angle of the secondary radiation (when an X-ray tube with secondary target is employed). For a scattering angle ϑ , the mean energy of the Compton peak, the width of which (greater than the photoelectric peak) depends on the sample-detector solid-angle, is given by the Equation (3):

$$E_C = E_0 \left\{ \frac{1}{1 + E_0/511(1 - \cos\theta)} \right\}$$

The energy values of the Compton peak, at scattering angles of 90° (typical for production of secondary and tertiary radiation in X-ray tubes) and of 180° (typical for excitation with radioactive sources), are shown in Table 2.11 vs incident energy E_0 .

TABLE 2.11

Energy of Compton peak vs incident energy E_0 , at scattering angles of 90° and 180° .

E_0 (keV)	$E_C(90^\circ)$	$E_C(180^\circ)$
4.5	4.46	4.42
7.5	7.4	7.3
9.8	9.6	9.44
15.0	14.6	14.2
17.4	16.8	16.3
22.0	21.1	20.2
25.0	23.9	22.8
32.0	30.2	28.4
40.0	37.3	34.6
50.0	45.9	41.8
60.0	54.3	48.6

Other peaks may be present in the X-ray spectrum, due to the photoelectric effect of the different radiation from the elements constituting the detector or the filling gas. Depending upon the detectors employed and the threshold energy of the photoelectric effect from the elements of the detector (1.8 keV for Si; 11 keV for Ge; 14.3 keV for Kr; 34.6 keV for Xe and 33 keV for I) a photoelectric effect can also occur with escape of the X-ray and detection of the electron having an energy $E_0 - E_K$ or $E_0 - E_L$ when electrons of the K or L shells are involved. For example, in a mercuric iodide detec-

tor, escape peaks result from production and subsequent escape of K and L-X-rays of iodine ($K_{ab} = 33.2$ keV, $L_{IIIab} = 4.56$ keV, $L_{IIab} = 4.85$ keV, $L_{Iab} = 5.19$ keV) and K and L-X-rays of mercury ($K_{ab} = 83.1$, $L_{IIIab} = 12.3$ keV, $L_{IIab} = 14.2$ keV, $L_{Iab} = 14.8$ keV).

Finally, when radiation of low-energy is involved, the Ar-X-rays of the air, with an energy of 2.9 keV, will appear in the X-spectrum.

(d) Automatic analysis of X-Ray Spectra

Many commercial X-ray spectrometers are now equipped with dedicated computers which provide automated data collection and perform quantitative analysis to derive concentration of a given element from the intensities of the X-ray lines.

It is not the purpose of this paper to discuss the various programs which have been written in the field of quantitative XRF-analysis. To this end, refs. 32 and 33 can be consulted. In general, these programs include simple aids to the user (peak identification markers for K and L lines), spectrum deconvolution (to reveal hidden peaks), as well as spectrum scanning algorithms that attempt to report the entire list of elements present in the sample.

(i) Peak identification

Peaks detection by visual examination are subjected to selection based on considerations of shape and size relative to background statistics. In X-ray spectra, the presence of other peaks of the same element, and the peak position, can be added as criteria in the identification process. The same criteria can be employed for automated data analysis.

Detection of trace, isolated peaks above background is properly related to counting statistics, and whether the peak rises above mean background by a statistically significant amount (for example 3 standard deviations). Small peaks are much more difficult to detect when they lie adjacent to or partly under larger ones. This goes beyond the simple increase in background level and the consequent increase in peak height needed for statistical confidence, and involves the need to judge peak shape. Even with the symmetric Gaussian shapes which are used as representative of X-ray spectra, the ability of human visual processes and XRF-automatic programs to detect the peak is poor.

(ii) Quantitative analysis of thin samples

Following Eq. (19), the unknown content of a given element a in an infinitely thin sample can be determined if the geometrical coefficient k and the physical parameters ω_a and $\mu_{ph,a}$ are known, such as the incident flux N_o . In practice, as observed in par. 2.4.2, it is easier to deduce the product $N_o k$ by analyzing in the same geometrical arrangement as the unknown sample, a

standard sample containing one or more elements with a known and fixed content. The content of an element b is therefore determined, if N_b is measured, and ω_b and $\mu_{ph.a}$ are known and tabulated in the automated program.

Finally, a list of elements and relative concentration is in general given by the XRF-program.

2.7 BIOMEDICAL APPLICATIONS

2.7.1 Trace elements in water samples

The large amount of information required for studies of natural waters and for monitoring industrial process water and effluents, all result in the need for sensitive, multielement, simple, rapid, cheap and versatile analytical techniques for aqueous solutions.

Energy dispersive X-ray fluorescence may satisfy this need to a large extent. However, it is rarely applied to aqueous samples directly, because of its limited sensitivity for bulk samples, which requires enrichment steps before the analysis.

In fact, the concentrations of dissolved trace elements in water are generally so low that multi-element analytical techniques usually require a pre-concentration step, which ideally enriches the metal ions exclusively and efficiently while leaving the abundant alkali and alkaline earth ions in solution.

As an example of how low concentration trace elements are to be analyzed, Table 2.12 gives the maximum admissible concentration of trace elements in drinking water according to the Italian Public Health Law.

Considering the limits of sensitivity of XRF-analysis for bulk liquid samples it can be deduced that no information can be derived from direct XRF-analysis of waters, but some enrichment is required.

TABLE 2.12

Limiting concentrations (in ppm) of some metals in drinking water according to the Italian Public Health Law.

Element	Concentration	Element	Concentration
Ag	0.1	Fe	0.3
As	0.05	Hg	0.005
Ba	1	Mn	0.05
Cd	0.05	Ni	1
Cr ^{III}	1	Pb	0.05
Cr ^{IV}	0.05	Se	0.01
Cu	0.5	Zn	1

A very large amount of work on the combination of XRF-analysis and enrichment procedures has been carried out by Van Grieken and co-workers at the University of Antwerp (Belgium), employing several pre-enrichment techniques (refs. 34-37).

The simplest enrichment method consists of impregnating filter paper with the solution to be analyzed and then drying it. Several authors have employed this method to solve various problems, but the sensitivity, which is limited by the very small sample volumes that can be used, is no better than some tenths of ppm. Detection limits of this method, reported by Van Grieken, are listed in Table 2.13.

TABLE 2.13.

Detection limits when 1.5 ml water are spotted within a hydrophobic ring (29 mm diameter) on Whatman filter paper and analyzed for 2000 s.

Element	Detection limit (ppb) and secondary targets with X-ray tube			
	Ge	Mo	Sn	Nd
Ca	124	563		
Ti	45	219		
V	39	148		
Cr	37	112		
Mn	28	88		
Fe	35	72		
Ni	38	39	110	
Cu	65	40	93	
Zn	49	31	77	
As		30	65	
Se		29	54	
Br		30	56	
Rb		31	53	
Sr		35	57	
Zr			64	
Mo			69	
Ag			91	1165
Cd				1430
Sb-L		4850		3690
Cs-L		980		13000
La-L		550		
Eu-L		250		
Ta-L		87	255	
Hg-L		66	127	
Td-L		73	140	
Pb-L		67	130	

Better results are obtained when ion-exchange resin loaded papers are

employed for preenrichment of waters (refs. 34 and 38). For example, SA-2 (strong-acid) ion exchange resin loaded filter paper is widely employed, because it is very advantageous in XRF-analysis to analyze thin samples such as a filter (see Par. 2.4).

These filter papers are supplied by H. Reeve Angel, now Whatman Inc. The SA-2 paper is 45-50% Amberlite IR 120 A sulfonic acid type resin in alpha cellulose and is quite uniform in contamination, containing S and Ca, and traces of Cr, Fe and Cu. This paper is very useful for XRF-multielement quantitative analysis requiring minimum sample preparation and small sample volumes. In the investigations carried out by Smith & Masi (ref. 39), ten milliliters of the acidified water samples (optimum pH is 2) were passed through 2 dots of resin loaded filter paper in a microconcentrator. The microconcentrator was designed to minimize edge effects and to maximize the concentration of removed cations in the centre of the paper for the minimum sample volumes. The small sample area permits use of a collimated detector for optimum peak to background ratios. A Finnigan Model X-ray Spectrometer was employed for XRF analysis. The measuring time was 300 s. Calculated minimum detection limits were:

Cu	0.02 ppm
Pb	0.01 ppm
Cd	0.03 ppm

A detailed study of preconcentration with ion-exchange resin loaded papers for XRF-analysis was carried out by Cesareo and Gigante (ref. 40).

The authors employed SA-2 filters (exchange capacity: 0.2 mEq) which act approximately as "thin samples" for elements with an atomic number larger than 28 (copper); for lower Z elements some correction factors should be introduced. The extraction technique was previously tested (time of filtration, number of filtrations to collect almost 90% of the cations, optimal filtration volume, pH of the solution and so on). As far as concerns, for example, the filtration volume, the Sr (0.14 ppm) and Zn (0.04 ppm) counts vs the filtered volume for a mineral water are shown in Figure 2.26. The linear relation between concentration of the analyzed ions and the relative counts has been verified for various ionic forms. An example of the calibration curve for Cu^{2+} ions is shown in Figure 2.27.

Different experimental arrangements have been used for XRF-analysis of the sample. For measuring the amount of major ions in water, for example Ca^{2+} in natural waters or ions in industrial effluents, a single element apparatus has been developed. It consists of a gas proportional counter coupled to a

sealed-off radioisotopic source, a linear amplification chain, a single channel analyzer and a scaler timer. For multielement analysis of liquids containing a large variety of ions, it is necessary to analyze the filter with a semiconductor detector for X-rays and a multichannel analyzer. For light elements ($Z < 35$, analysis of K-rays) and for heavy elements ($Z > 75$, analysis of L-rays) a 3.7×10^8 Bq Pu-238 source and a Si(Li) detector having 3 mm thickness are employed. For the analysis of medium elements ($30 < Z < 60$) a 1.8×10^9 Bq Am-241 source and a Ge(Li) detector 12 mm diameter x 3 mm thickness are employed. For elements with an atomic number $Z < 22$, a $7.4 \times$

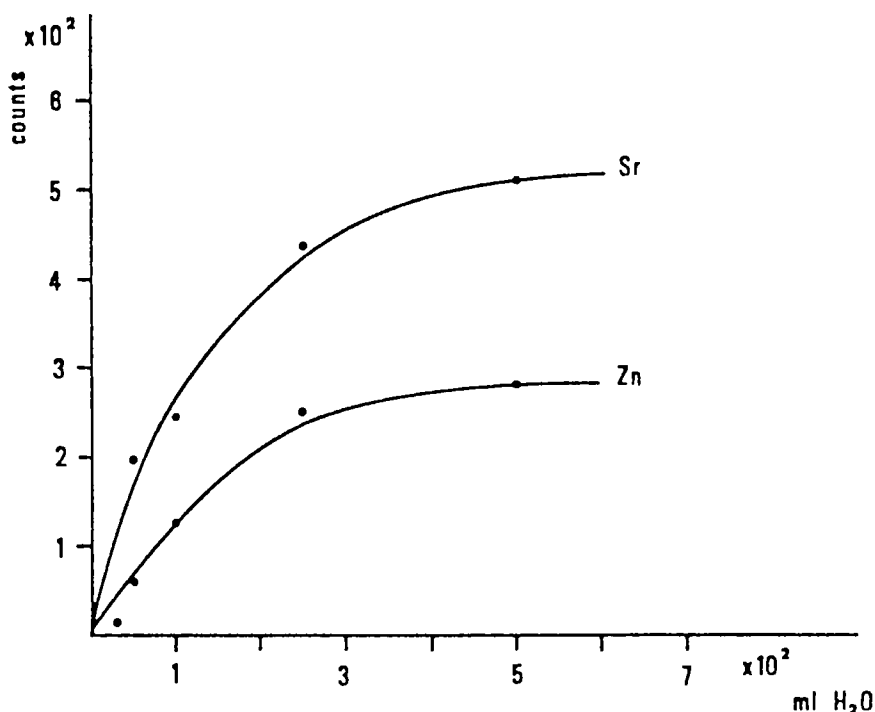


Fig. 2.26. Strontium and zinc XRF-counts vs volume of water filtered through a SA-2 ion-exchange resin loaded filter paper. Sr and Zn concentration in water is 0.14 ppm and 0.04 ppm respectively (after Cesareo and Gigante, ref. 40).

10^{10} Bq H-3/Zr is employed. The MDL (in ppb) in a measuring time of 4000 s are reported in Table 2.14.

A typical XRF- spectrum of tap water is shown in Figure 2.28. Various types of Italian mineral waters have been analyzed. Some selected results are reported in Table 2.15.

TABLE 2.14

MDL (in ppb) for analysis of waters preenriched with resin loaded filters.
Measuring time 4000 s

Element	MDL	Element	MDL
Ca	200 - 500	Br	1.5 - 5
Ti	50 - 200	Sr	30 - 100
Mn	7 - 30	Cd	15 - 50
Fe	5 - 15	Ba	10 - 30
Cu	3 - 10	Pb	20 - 60
Zn	2 - 6		

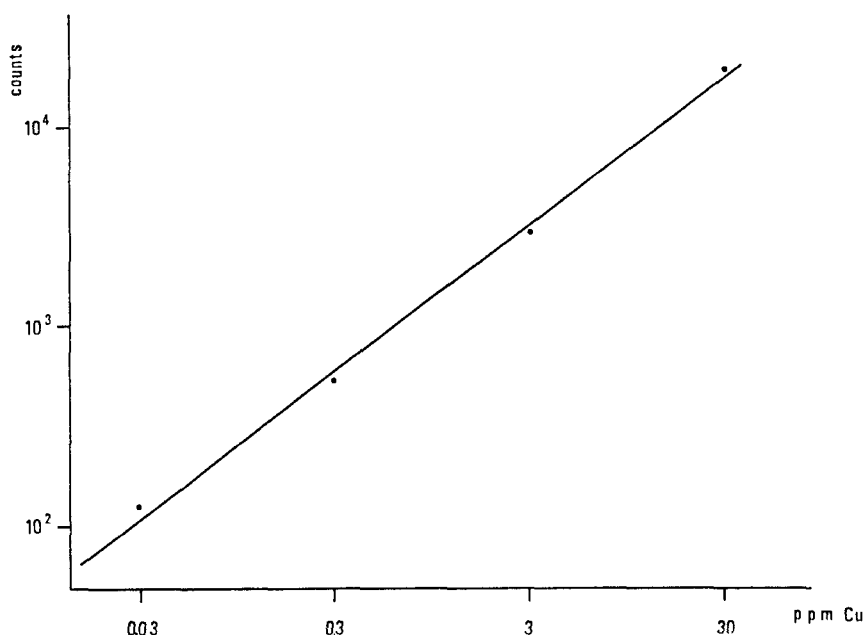


Fig. 2.27. Calibration curve for the determination of the Cu^{2+} ions content in water solution collected on SA-2 resin loaded filters (after Cesareo and Gigante ref. 40).

An interesting evaluation of seven typical commercial X-ray Analyzers for water pollution was carried out by Birks & Gilfrich (ref. 41).

2.7.2 Trace elements in air particulate matter

The application of energy dispersive X-ray analysis to the problem of atmospheric aerosols, using either proportional gas counters for single element analysis or semiconductor detectors for automatic multi-element

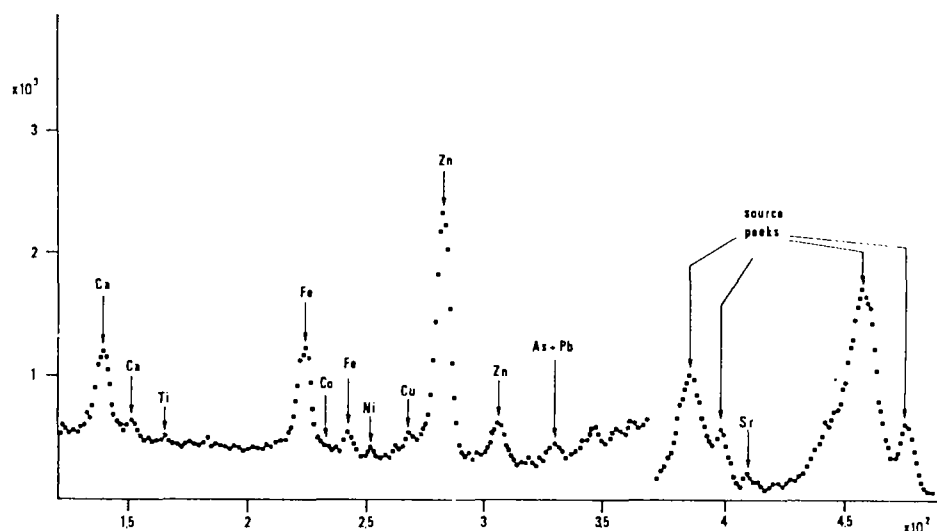


Fig. 2.28. XRF spectrum of 50 ml of tap water collected on a SA-2 filter. A radioisotopic source of Pu-238 (0.36 GBq) was employed. Measuring time: 4000 s. (after Cesareo, ref. 40).

TABLE 2.15

Quantitative results for different water samples by XRF analysis and by traditional methods (in parentheses). Concentration in ppm.

Water					
Element	Nepi*	Egeria*	Fiuggi*	Appia*	Peschiera**
K	43	65(73)	2.2(3)	55(68)	--
Ca	75(75)	95(100)	14(13)	130(140)	140
Mn	0.6(0.5)	0.3	0.04	0.07	--
Fe	0.2(0.18)	0.1	0.05	--	0.9
Co	--	0.05	--	--	0.05
Ni	0.08	0.06	0.015	0.03	0.03
Cu	0.03(0.03)	--	0.007	--	0.06
Zn	0.03	--	0.04	--	1.0
As	--	--	--	--	0.03
Sr	0.6(0.5)	1.1	0.1(0.1)	1.3(2)	0.4
Cd	--	--	0.15	--	0.03
Sn	--	0.07	0.1	0.06	0.06
Sb	--	--	--	--	0.01
Ba	0.05	0.4	0.08	0.4	0.9
Pb	--	--	--	--	0.03

* Mineral water

**Tap water

analysis has been widely discussed in the literature.

Several laboratories are currently applying this technique to the analysis of airborne particulate matter. The samples typically consist of uniform deposits of particulate matter collected on a thin clean substrate, making them ideally suited for non-destructive XRF-analysis. Rhodes (ref. 6) first has employed an automated XRF system for multi-element analysis of air pollutants.

The system was characterized by radioisotope sources, (Cd^{109} , Pu^{238} and others) an amplifier chain, and a multichannel analyzer coupled to a PDP-21 computer. At 3 S.D. level, detection limits of about $0.01 - 0.1 \mu\text{g}/\text{cm}^2$, have been measured in one 10-min count. A typical XRF spectrum of air particulates excited by Cd^{109} source is shown in Figure 2.29.

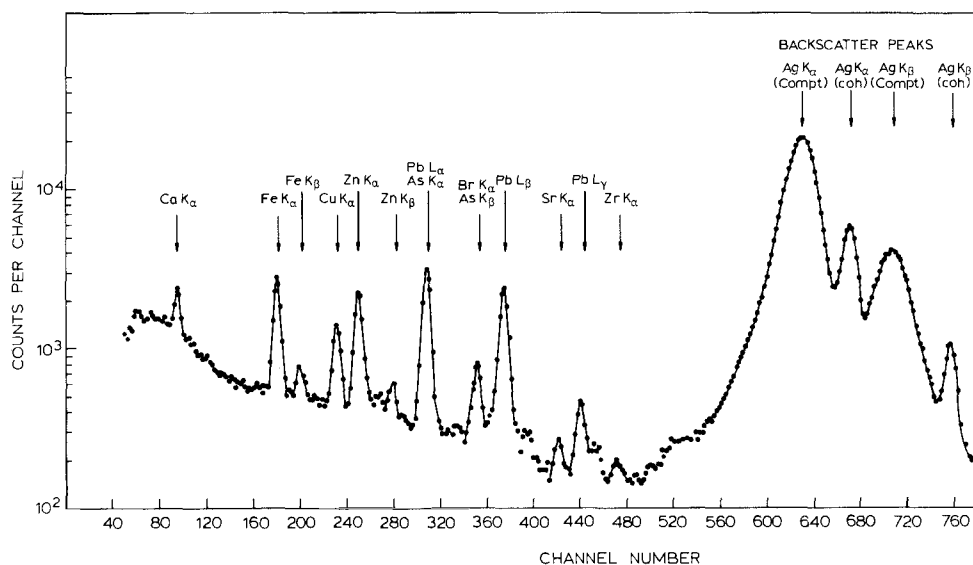


Fig. 2.29. Typical XRF spectrum of air particulates excited by a Cd^{109} source (activity: 0.1 GBq) showing characteristic X-rays and backscattered X-rays (after Rhodes, ref. 6).

Generally, an X-ray tube has been chosen as the primary excitation source because of its higher output compared to generally available radioisotope sources. The need to analyze 100 or more samples per day requires the highest possible counting rate. The high number of elements present in a typical sample of particulate matter, and the fact that the probability of producing fluorescent excitation of an element is greatest when the exciting X-ray energy just exceeds the binding energy of the electrons in the appropriate shells and falls off rapidly with increasing excitation energy, implies

that, further, very low energy characteristic X-rays are not efficiently produced by monochromatic radiation of high energy, thus limiting the range of elements that can be sensitively measured with a single exciting energy. To cover a broad range of elements with optimum excitation, several measurements are carried out on each sample, using different X-ray excitation energies, and, therefore, several secondary targets.

A wide study of the method has been, for example, carried out by Jaklevic et al. (ref. 42), who employed following secondary targets:

Ti (energy: 4.5 keV) for analyzing elements with atomic number between 13 and 20;

Mo (energy: 17.4 keV) for analyzing elements with atomic number between 20 and 38 (K-rays) and for heavy elements Hs and Pb (L-rays);

Sm (energy: 40 keV) for analyzing elements with atomic number between 38 and 56.

The sample fluorescence-detector geometry employed by Jaklevic is shown in Figure 2.30. The system has been designed to accommodate air-particulate samples collected by filtration. These samples are thin, uniform deposit of

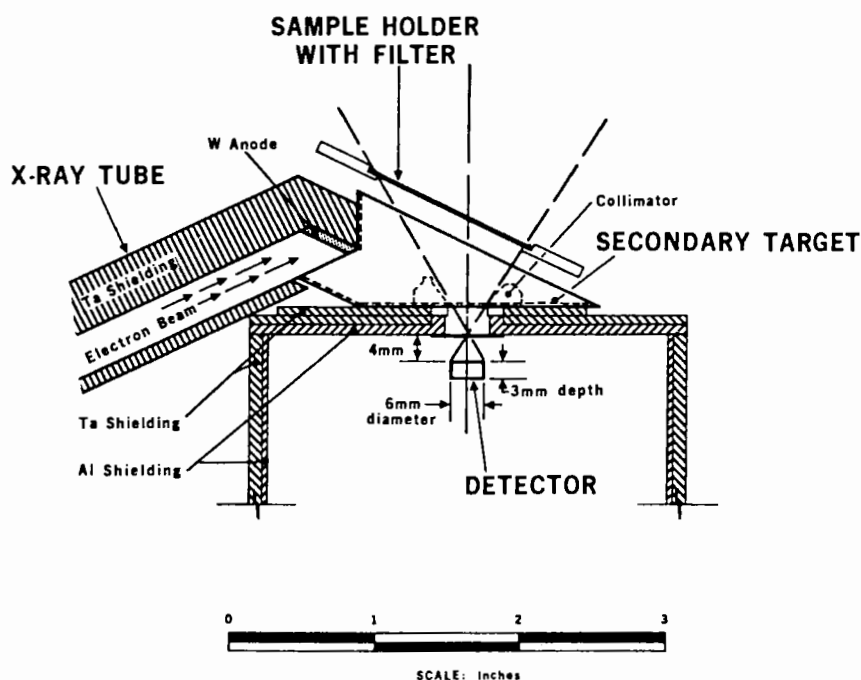


Fig. 2.30. Sample-fluorescer-detector geometry employed by Jaklevic for analysis of aerosols (after Jaklevic, ref. 42).

particles collected on clean membrane filters consisting of cellulose, polycarbonate or other hydrocarbons. The calibration of the X-ray analyzer consists of converting the observed characteristic X-ray counting rates to concentrations of elements expressed in ng/cm^2 of the filter. For samples in which the attenuation of fluorescent X-rays can be neglected, the counting rate for a given element a can be expressed as shown in Eq. (19). Counts for element a are directly proportional to its concentration.

In cases when the X-ray energies are low enough that absorption within the matrix becomes important, an attenuation correction must be included. The magnitude of this correction and the ability to estimate it accurately constitutes the major limitation of the XRF technique in the case of light elements.

Minimum detectable limits obtained by Jaklevic are shown in Table 2.16.

TABLE 2.16.

Minimum detectable limits and sensitivity for energy-dispersive X-ray fluorescence analysis (after Jaklevic and Walter, ref. 42).

Element	MDL ₂ (ng/cm^2)	S (counts/s per $\mu\text{g/cm}^2$)
Al ^a	200	7.4
Si	58.9	25.3
P	32.9	48.0
S	29.4	83.8
Cl	26.6	125.0
K	9.14	272.0
Ca _b	7.7	411
Ti ^b	31.3	28.8
V	22.2	37.8
Cr	16.6	49.3
Mn	13.5	59.8
Fe	11.8	76.4
Ni	6.2	112.0
Cu	6.5	128.0
Zn	5.3	148.0
Ga	3.8	166.0
As	3.1	209.0
Se	2.6	234.0
Br	2.7	258.0
Rb	2.8	304.0
Sr	3.8	320.0
Hg	6.0	109.0
Pb	9.1	109.0
Cd ^c	5.9	75.5
Sn	7.8	75.7
Sb	8.1	76.7
Ba	31.0	62.1

a: Ti-secondary target; b: Mo-secondary target; c: Sm-secondary target.

The expression used for the MDL, derived by Currie by assuming that the standard deviation at the minimum detectable limit is determined solely by the Poisson distributed counting statistics in the background under the X-ray peak, is:

$$MDL = \frac{3.29}{S} \sqrt{\frac{R_b}{t}}$$

where R_b is the background counting rate in counts/s under the X-ray peak, t is the time interval of the measurement, and S is the sensitivity of the instruments for that specific element expressed as counts/s per $\mu\text{g}/\text{cm}^2$ of concentration.

The following substrates have been employed: 5 mg/cm^2 Millipore filters, 1 mg/cm^2 Nucleopore polycarbonate filters, 0.5 mg/cm^2 Mylar films and ultra-thin Formvar films. Comparison of the MDL values with ambient levels of these elements in the atmosphere show that the method is more than adequate for routine measurement (see Fig. 2.31). A typical XRF-spectrum of a membrane filter containing the coarse particle fraction of aerosols ($>2\mu$) is shown in

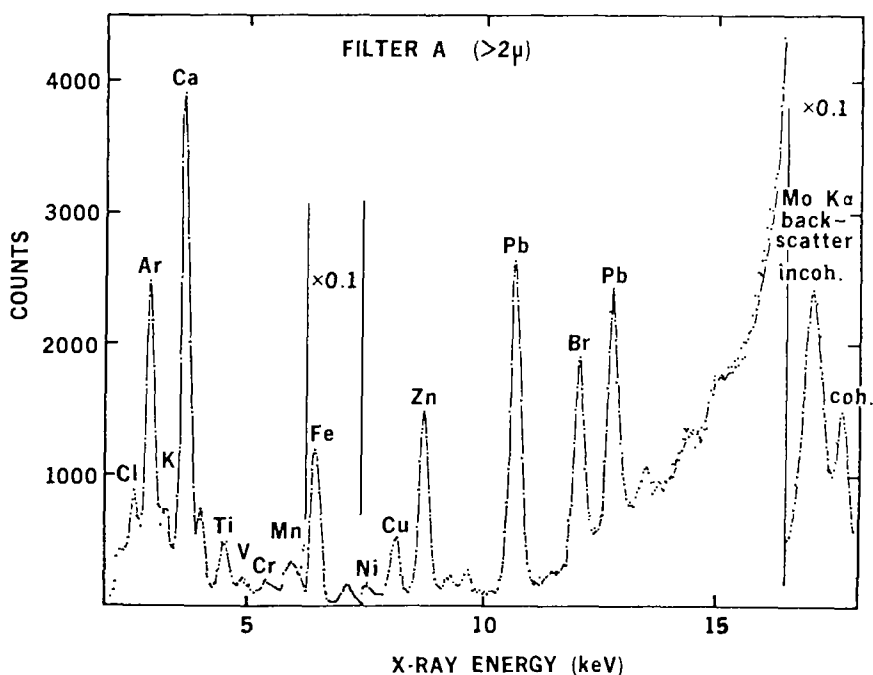


Fig. 2.31. Typical XRF spectrum of aerosols (after Jaklevic, ref. 42).

Figure 2.31. Other instruments developed by various authors for multi-element XRF analysis of aerosols are not very different from the apparatus developed by Jaklevic et al.

Very different are the portable, generally mono-elemental systems for XRF-analysis. These are characterized by a radioisotope source and by a gas-filled proportional detector.

An interesting example of such applications is found in the work of Schneider and Hill (ref. 43), who have evaluated the performance of a portable instrument for the analysis of lead on air-filter samples. The instrument used a Cd-109 radionuclide excitation source (see Par. 2.6.2a) a Xe-filled proportional detector with a 50 μm thick Be-window, a high voltage power supply, a preamplifier, a combination amplifier single channel analyzer and a timer counter readout system. The distance from the source to the sample was 5 mm, while the distance from the sample to the detector was 13 mm. The method was applied to air-filter samples, but could be applied to other types of samples, including clothing and wipe tests. The results obtained by XRF were compared to subsequent analyses of the same samples by atomic absorption. The minimum detection limit is assumed as the value of the net counts of the sample equal or greater than $2.33 \sqrt{B}$, where B is the background counts obtained from a blank sample for the same counting time. The MDL, measured in a 695 s counting time with a 1.1×10^8 Bq Cd-109 source, is found to be approximately 5 μg Pb.

Systematic errors in XRF analysis can arise from differences in Pb distribution between samples and standards and the presence of unknown quantities of interfering elements, the X-rays of which are close to those of Pb. Fe, Cu and Zn are likely to be present in the samples; an amount of these elements equal to the amount of Pb gives rise to an overestimation of Pb by factors of 3, 8 and 31% respectively.

Finally, 186 filter samples were evaluated with a portable XRF instrument using 1.1×10^8 Bq point source. This type of portable instrument appears ideally suited for in-plant measurements intended to monitor lead, and evaluate new control measures.

2.7.3 Trace elements in body fluids

(a) Analysis of Fe in blood

A very simple apparatus for XRF-analysis of Fe in blood has been developed by Cesareo and Del Principe (ref. 44), characterized by a 3.7×10^8 Bq Pu^{238} annular source, a Xe-gas proportional counter and a single-channel analyzer coupled to a counter-timer (see Fig. 2.32).

The concentration of Fe in blood ranges between approximately 400 and 600 ppm in normal adults. Iron deficiency in blood is common, especially in

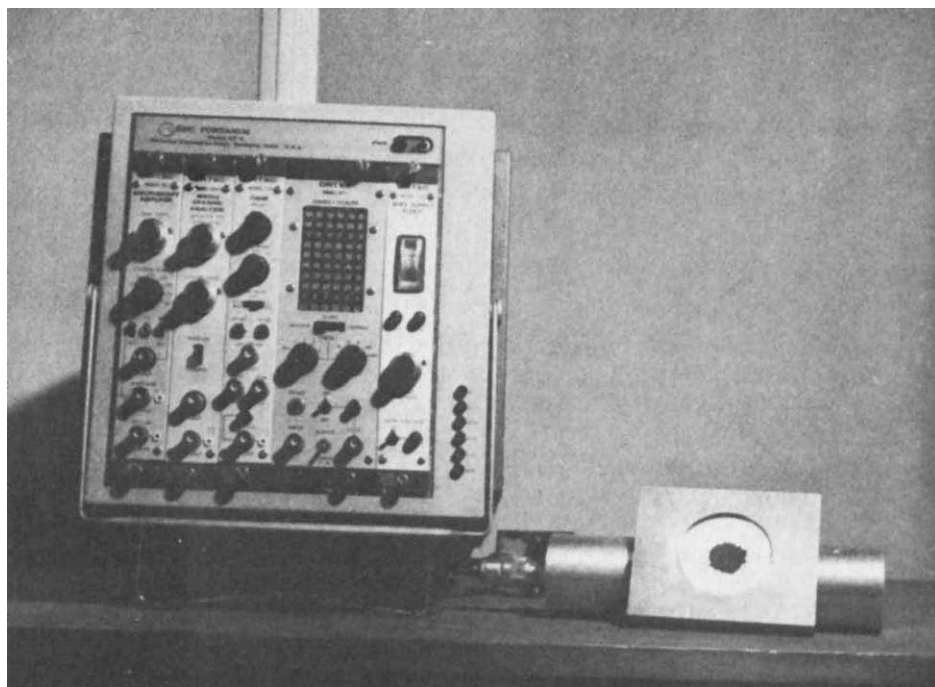


Fig. 2.32. Portable radionuclide XRF unit for analysis of Fe in blood. On the right the Xe-gas proportional counter with the Pu-238 source (intensity: 0.36 GBq) placed on the Be-window and the filter containing the blood spot (after Cesareo and Del Principe, ref. 44).

children.

The measurement requires 0.1 ml of venous blood, deposited on filter paper and allowed to dry. XRF-spectrum collected on a multi-channel-analyzer contains, besides fluorescent Fe-X-rays (20 ± 30 counts/s), $U-X_L$ -rays due to elastic scattering by the filter of the source radiation. The M.C.A. is used only in the initial system calibration for the adjustment of the amplifier gain, the single-channel analyzer threshold, and the window. The single-channel analyzer (S.C.A.) is positioned with its threshold on energy value just below the Fe-peak. Two counts are then measured. The first count, C_1 , has the S.C.A. in differential mode operation and a ΔE window width which fully includes the Fe-peak. The second count, C_2 , has the S.C.A. in integral mode operation. The number of counts $C_2 - C_1$ (which essentially include the scattered peak) is representative of the quantity of blood deposited on the filter paper. The number C_1 is proportional to the Fe-content in the blood. Therefore, $C_1 / (C_2 - C_1)$ is a measure of the quantity of Fe in a constant blood quantity.

Typical blood samples have been analyzed by the XRF-method and by chemical analysis. Results are shown in Table 2.17.

TABLE 2.17

Comparison of X-ray fluorescence analysis and chemical analysis of iron content in blood.

XRF analysis (in ppm)	Chemical analysis* (in ppm)
188 \pm 6	185 \pm 10
199 \pm 6	202 \pm 10
210 \pm 6	204 \pm 10
239 \pm 7	248 \pm 10
381 \pm 8	367 \pm 10
385 \pm 8	378 \pm 10
427 \pm 10	420 \pm 10
474 \pm 11	477 \pm 10
532 \pm 12	546 \pm 10
702 \pm 13	700 \pm 10

* The error has been determined from a series of measurements on the same blood sample

(b) Analysis of Iron in serum

Analysis of human blood serum has gained great interest over the last few years, due to the increase in knowledge on the role of some elements and the possible correlations between abnormal concentrations and pathological conditions.

Table 2.18 shows the interval of concentration of the most important trace elements in normal adult human blood serum. Concentrations are reported in $\mu\text{g/ml}$ fresh material.

X-ray spectrometry is well suited to qualitative and quantitative analysis of thin blood samples (ref. 45). It is convenient, rapid and non-destructive, and it determines the presence of major, minor and trace constituents. It is applicable to all elements down to phosphorus ($Z = 15$) although the sensitivity falls off for elements below calcium ($Z = 20$). Two different

TABLE 2.18

Mean concentration of trace elements in normal adult human blood serum (in $\mu\text{g/l}$).

Element	Mean concentration
Barium	0.06
Bromine	3.95
Calcium	98.1
Cobalt	0.006
Chromium	0.01
Copper	1.22
Iron	1.25
Iodine	0.069
Potassium	179
Manganese	0.015
Nickel	0.033
Lead	0.1
Rubidium	0.23
Selenium	0.15
Zinc	1.13

procedures have been employed for preparing thin serum samples. The first consists of directly depositing 50 μl of serum on a thin substrate of filter paper (diameter: 14 mm), drying the sample and analyzing it. The second consists in ashing 0.5 ml of serum at 450-500 $^{\circ}\text{C}$ and depositing the ash (about 3-5 mg) on a thin substrate. Iron will be present in the first sample in a quantity of about 50 ng, and in the ashed sample in a quantity ten times greater (assuming a mean concentration of 1000 ng/ml Fe in serum). Many measurements have been carried out in order to optimize the XRF-technique for Fe. Fe-solutions were prepared, and a small quantity (0.1 ml) deposited on filters and dried in order to obtain standard samples. A calibration curve was then deduced, and the linearity of the curve of Fe-content vs concentration measured. A typical sample was then excited and analyzed with different secondary targets (Cu, Ga, Au). The emitted spectra were analyzed with a Xe-proportional detector and with a HPGe detector (see Fig. 2.33). Following Par. 2.4,

the best excitation of Fe is obtained with a Ni-secondary target; therefore, the overlap of the much more intense elastic and inelastic scattered line to the Fe-X-rays should be avoided. The same can be observed for a Cu secondary target, and the "efficiency" of the Au-L-lines are too low, due to the low fluorescent yield. The best solution is obtained when a Zn-secondary target is employed (see Fig. 2.34). As observed in Par. 2.4, along the direction of the radiation beam from the X-ray tube to the detector, all the collimators were also covered by high purity Zn, to avoid fluorescence X-rays from the impuri-

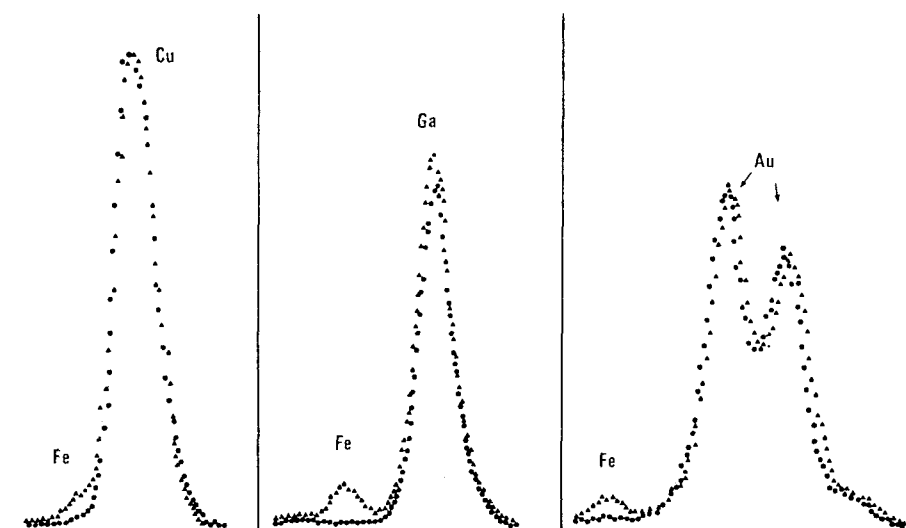


Fig. 2.33. XRF-spectrum of 0.5 ml ashed serum sample containing 0.91 μg Fe, excited by Cu, Ga and Au secondary targets, and detected with a Xe- proportional detector. Dotted curves refer to the substrate spectrum (after Cesareo, ref. 45).

ties. Nevertheless, a very small Fe-peak is always present in the X-ray spectrum, due to very low Fe-traces in Zn-foils and in the substrates.

The spectrum of a 50 μl serum sample containing 70 ng and analyzed with a HPGe detector is shown in Figure 2.35. The contribution of the substrate has been subtracted. It can be observed that 3 S.D. from the background corresponds to 1.4 ng Fe; therefore, a relative error of about 2% - 4% could be expected. Additional errors due to the inhomogeneity of the sample and of the beam can be expected.

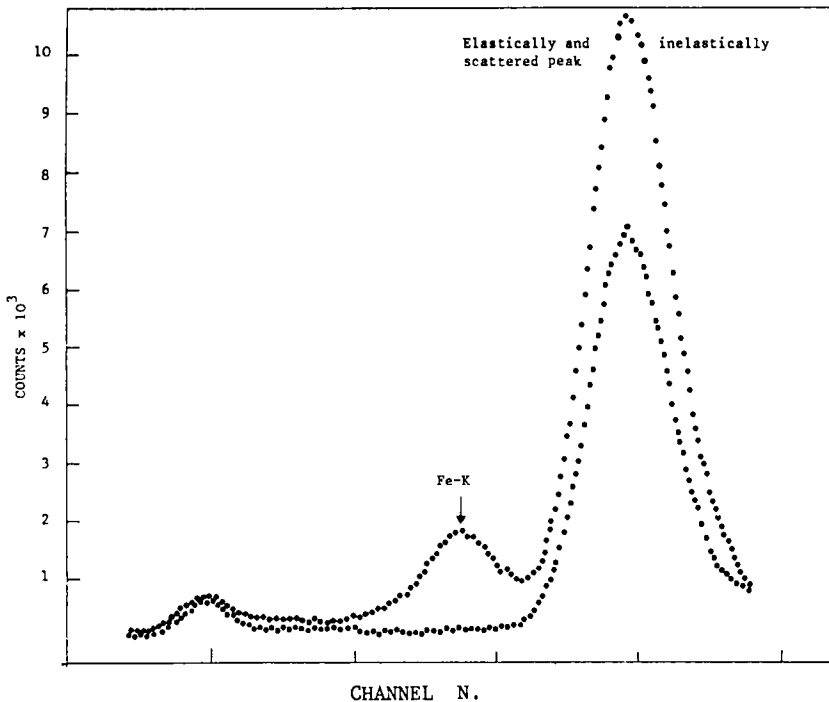


Fig. 2.34. XRF spectrum of 0.5 ml ashed serum containing $0.91 \mu\text{g Fe}$, excited by a Zn secondary target and detected with a Xe-proportional detector. Dotted curves refer to the substrate (after Cesareo, ref. 45). It is interesting to observe how scattered radiation depends on the sample.

(c) Analysis of trace elements in serum

Analysis of trace elements in serum, such as Cu, Zn, Pb, Br, Rb and others, can be carried out on the same serum samples employed for Fe-analysis, by using different secondary targets, as for example Ge (for analysis of Cu and Zn), Sr (for analysis of Se and Br) and Mo (for analysis of Pb, Br, Rb).

A typical spectrum of elements from Mn to Ni are shown in Figure 2.36. A MDL of about $1.5 \text{ ng/cm}^2 \text{ Fe}$ was obtained in 10^3 s measuring time. Approximately 250 Fe-counts/ $\mu\text{g Fe}$ s have been obtained and 2800 scattered counts/s by employing a Xe-gas proportional counter and by employing a HPGe-detector. For analysis of trace elements from Cu to Rb a Mo-secondary target has been employed (ref. 46). The "output" spectrum with such a target contains small L-lines of W (8.4, 9.8 and 11.3 keV) constituting the anode of the X-ray tube. Good results may be obtained by subtracting the substrate sample in order to reduce both the W-L-peaks and the Mo-scattered peak.

A typical XRF-spectrum of a serum sample excited by a Mo-secondary target is shown in Figure 2.37.

Analysis of trace elements in human serum by XRF-analysis has been carried out by many authors. For example, Ong and coworkers (ref. 47) have employed monochromatic radiation which was obtained with a secondary Se-target with a purity of 99.999%. With the Se-radiator (energy: 11.2 keV) Fe, Cu and Zn are analyzed in serum in about 20 min. Ni was added as internal standard. The serum sample was prepared as follows:

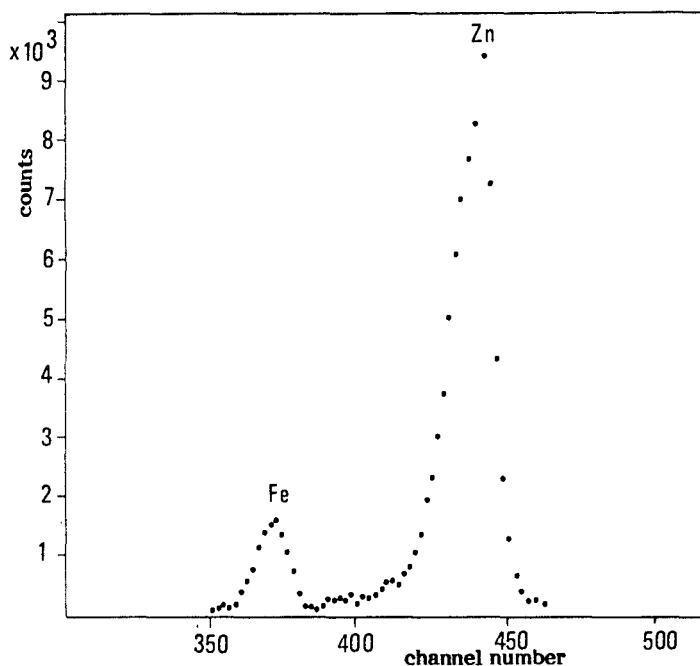


Fig. 2.35. XRF-spectrum of a 50 μ l serum sample deposited on a paper filter and dried, and containing 70 ng Fe, analyzed with a HPGe detector. The background has been subtracted.

- 2 ml serum is placed in a 10 ml pyrex glass beaker;
- an amount of Ni, corresponding to a 2 ppm of the original serum is added. This will be used as a reference for quantitative analysis;
- serum and reference material are ultrasonically mixed;
- sample is heated at 60 °C at reduced pressure to remove dissolved gases;
- the sample is hoted and dried by the use of steam, resulting in discs, about 1 cm in diameter;
- the serum discs are removed from the beaker, flattened and dried;
- the discs are placed in the asher. The ashing time is about 4 hours.

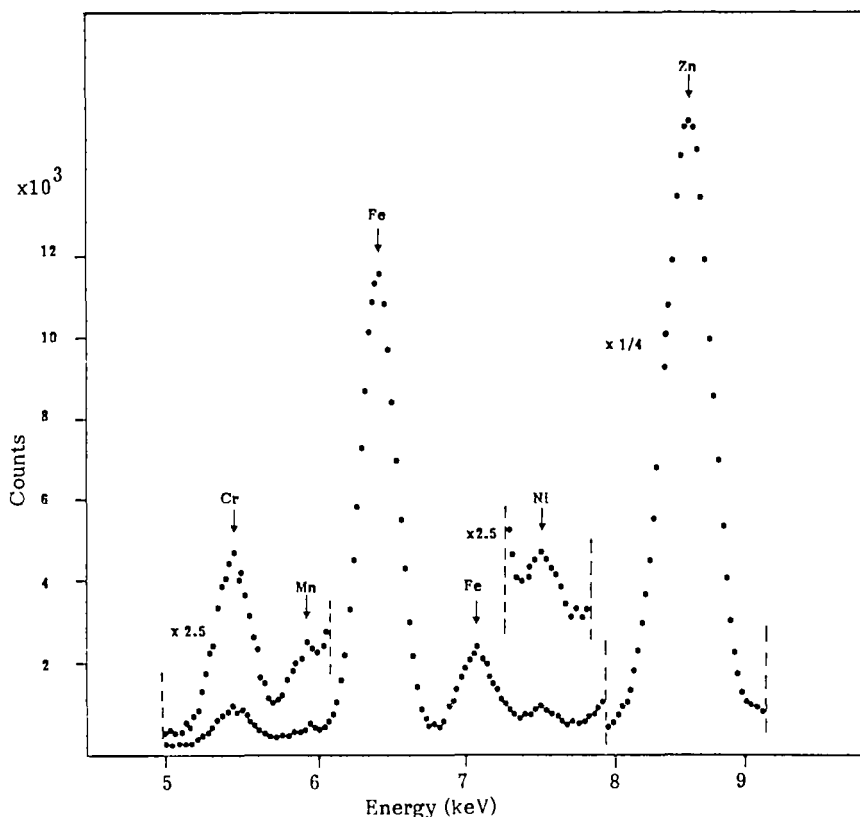


Fig. 2.36. XRF-spectrum of 0.5 ml ashed serum sample excited by a Zn secondary target and detected with a HPGe detector. Concentration values ($\mu\text{g/l}$) are: Cr = 0.15; Mn = 0.022; Fe = 1.9; Ni = 0.02 (after Cesareo, ref. 46).

Detection limits of about $10\text{--}15 \text{ ng/cm}^2$ in 1200 s measuring time have been obtained.

Sky-Peck and Joseph (ref. 48) have analyzed 5 μl of dried serum irradiated with an Ag-X-ray source at 15 mAmpere and 35 kV for 500 s. A measured amount of an aqueous Y standard (5 $\mu\text{g/ml}$ of serum) was added to each sample, prior to the drying step. Five microliters of serum were pipetted on Formvar films and allowed to air dry in a laminar flow hood. A typical spectrum is shown in Figure 2.38. MDL values are not reported in the work of Sky-Peck.

The results obtained on the concentrations of trace elements in serum for a group of 110 normal healthy adult females and 102 normal healthy adult males between the ages of 19 and 62 are presented in Table 2.19.

TABLE 2.19

Distribution of trace elements in normal human serum (after Sky-Peck and Joseph, ref. 48).

Element	Number of individual determinations	Mean value concentration(g/ml)	Range
Fe - M	102	1.337 ± 0.417	0.65 - 1.85
Fe - F	110	1.198 ± 0.497	0.50 - 1.60
Cu - M	102	1.022 ± 0.147	0.7 - 1.40
Cu - F	110	1.226 ± 0.236	0.8 - 1.6
Zn - M	102	0.896 ± 0.127	0.55 - 1.25
Zn - F	110	0.825 ± 0.119	0.6 - 1.10
Br	212	3.86 ± 0.98	2.0 - 6.0
Se	212	0.131 ± 0.022	0.07 - 0.19
As	212	0.019 ± 0.009	0.002 - 0.04

M, male; F, female.

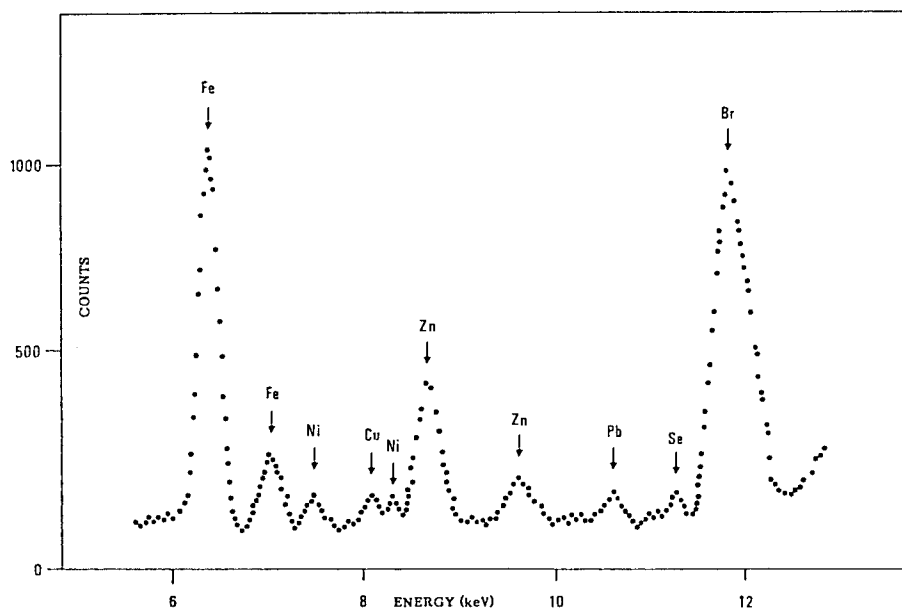


Fig. 2.37. XRF-spectrum of 0.5 ml ashed serum sample excited by a Mo secondary target and detected with a HPGe detector. Concentration values ($\mu\text{g/ml}$) are: Fe = 1.82; Ni = 0.18; Cu = 0.2; Zn = 0.65; Pb = 0.09; Se = 0.09; Br = 1.18 (after Cesareo, ref. 46).

Several authors have carried out analysis of specific elements in serum. Rapaport et al. (ref. 49) have developed a radioisotope excited XRF method for determination of Br in blood serum samples.

The rapid and accurate determination of Br in blood serum is important in medicine in the diagnosis and follow-up of Br poisoning and in the diagnosis of certain diseases. Br-poisoning may be the result of overdoses of Br-containing drugs or of over exposure to Br components. An overdose of Br containing sedatives was found to be responsible for many sedative intoxications and about 20% of lethal intoxications.

The experimental set up for Br-analysis consists mainly of a 5 I^{125} ($3.7 \times 10^8 \text{ Bq}$) point sources and in a Si(Li) detector.

Blood serum was prepared by centrifugation and 50 μl transferred to the sample cells; the drop was then dried in air. The sample obtained was very thin, and no corrections for matrix effect is required. About 20 cts/s Br were obtained and a MDL of 50 ng Br was obtained in 100 s measuring time, at 2 S.D. level. The method was applied to analyze serum samples of subjects from the Dead Sea (exposed to high Br levels in air) and of persons from Soreq Nuclear Research Centre (S.N.R.C.).

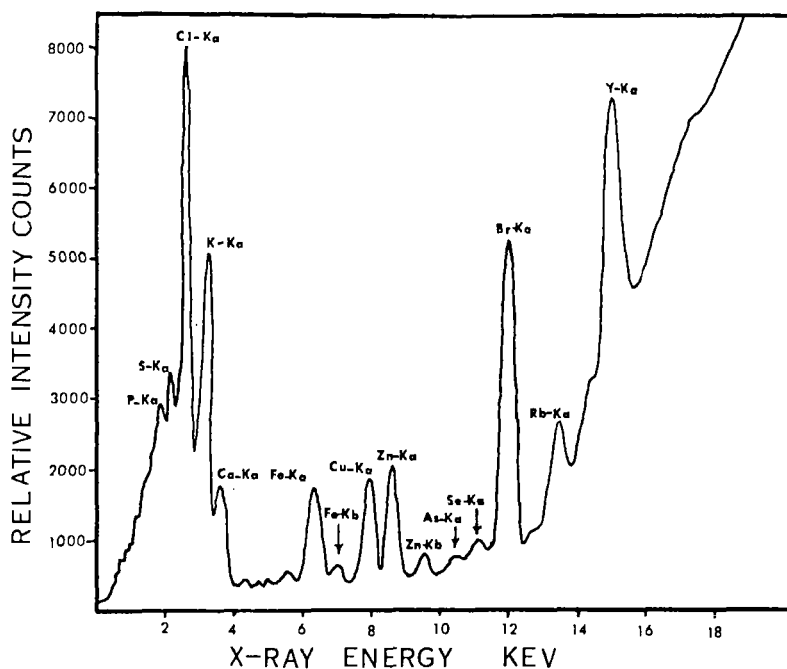


Fig. 2.38. XRF-spectrum of human serum with the addition of Y-standard. The counting time was 500 s, with a anode voltage of 35 kV and a current of 15 mA (after Sky-Peck et al., ref. 48).

Following values have been obtained

6.38 ± 0.25	$\mu\text{g Br/ml}$	for females from S.N.R.C.
7.78 ± 0.29	$\mu\text{g Br/ml}$	for males from S.N.R.C.
9.14 ± 0.12	$\mu\text{g Br/ml}$	for males from Dead Sea

A method for the XRF-analysis of selenium in blood was studied by Holinska and Markowicz (ref. 50), who have developed an enrichment method for the analysis of this element.

The measuring system consisted of a Si(Li) semiconductor detector and of exciting sources of 3.7×10^9 Bq of Pu-238 and X-ray tube with Mo and As secondary targets.

Ten grams of blood were decomposed by wet acid digestion and then Se, together with Te as co-precipitant, was reduced to its elemental form. The precipitate obtained was filtered through a membrane filter of $0.6 \mu\text{m}$ pore size. The deposit was then air dried and measured. The unit area of the deposit did not exceed $1 \mu\text{g/cm}^2$, and, therefore, matrix absorption effects were negligible and the calibration curve linear. Minimum Detectable Limits of Sr at 3 S.D. level and for 200 s measuring time are as follows:

Source	M.D.L (ng/cm ²)
Pu ²³⁸	111
Ag-target	21
Mo-target	14

The precision of the method, which depends on the statistical error, instrumental error and errors connected with the chemical preparation of the sample, amounts (expressed as 1 S.D) to about 4% for $0.4 \mu\text{g/cm}^2$ Se.

(d) Analysis of stable tracers in blood

The method usually employed to measure blood cell life span (see Fig. 2.39) or to evaluate body water compartments use radioisotope tracers with the disadvantages of high cost, the need for employing specialized personnel and the risk of radiation exposures, which limits their applications, particularly in infants and pregnant women.

The possibility of labelling blood cells or body compartments with stable tracers, and of assaying these with XRF-analysis seems to be very attractive, since the problems associated with radioactivity would be eliminated.

Choice of the stable tracer is based upon the following main selection criteria:

- the quantity added should be small enough not to be toxic;
- it should have the capacity to selectively aggregate to the cell under study;

the sensitivity of the XRF-analysis should be adequate for the tracer element.

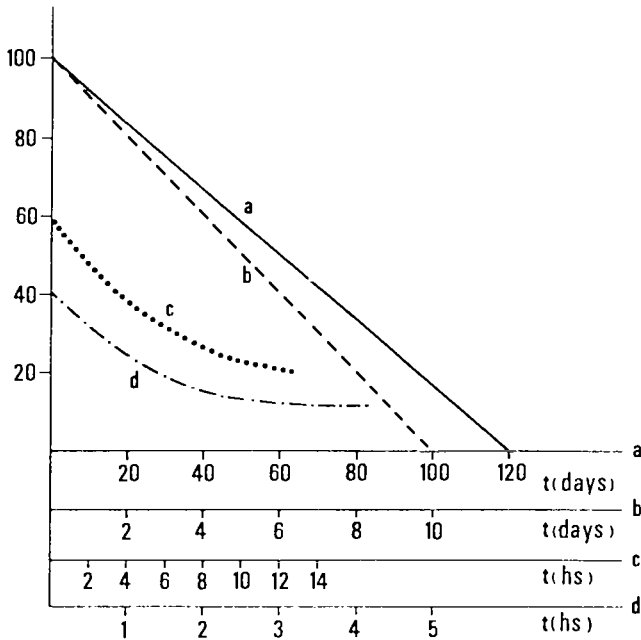


Fig. 2.39. Disappearance curve of erythrocytes (a), platelets (b), granulocytes (c) and leukocytes (d).

The following studies have been carried out:

- platelet survival with stable rubidium;
- red cell survival with stable rubidium and cesium;
- granulocytes survival with stable rubidium;
- extracellular fluid space determination with stable bromine;
- red cell volume determination with stable cesium;
- plasma volume measurement by stable iodinated serum albumin;
- glomerular filtration rate by stable iodine.

(i) Platelet survival

The study of platelet survival is useful in clinical medicine for the approach to the pathogenesis of the arterial disease thromboembolism thrombocytopenias and thrombopathies.

Recently, the half time-values of platelets labelled with stable rubidium have been measured and compared to those of platelets labelled with Cr-51

(ref. 51). Two types of experiments were carried out: a study in vitro with human platelets stored at 22 °C and a study in vivo with rabbit platelets.

Human blood was collected from healthy subjects by venepuncture with disposable plastic syringes; 20 ml aliquots were transferred to siliconized centrifuge tubes containing 2 ml EDTA at 2%. Platelet rich plasma was prepared by centrifugation at 250 g for 10 min and platelets separated from the plasma at 1000 g for 10 min. Four ml 0.154 M NaCl were added to the platelet concentrate and 1 ml of the platelet suspension was labelled at different times by incubation with 5 ml saline solution containing 35 mg RbCl. The incubation process was carried out for 30 min, permitting a good uptake of the Rb, without platelet damage. The platelet suspension was successively filtered through millipore filters with pore size of 0.65 μm permitting the retention of platelets and the passage of free RbCl molecules. The filters were then washed several times in order to remove free RbCl ions. The filters were then directly analyzed.

In the labelling of rabbit platelets, 8 ml of blood were withdrawn from a marginal vein of the ear, and transferred in a glass tube containing 1 ml trisodium citrate dihydrate at pH = 6.7. Platelet rich plasma was obtained by two centrifugation steps. In such a way about 1 ml of platelet concentrate was separated, transferred in a plastic tube and added to an equivalent volume of 0.154 M NaCl containing 0.9 mg of RbCl. The suspension was then incubated for 60 min and the labelled platelets were reinjected into the marginal ear vein of the rabbit. At successive times about 4 ml blood were withdrawn and mixed with 0.5 ml of 3.7% trisodium citrate. About 0.5 ml of the platelet concentrate was then filtered through millipore filters with pore size 0.22 μm . The filters were then analyzed.

Rubidium was analyzed with a single element version of the radioisotope induced XRF-analysis, characterized by a 3.7×10^7 Bq Cd-109 source coupled to a Xe-gas proportional counter, an amplification chain, a single channel analyzer and a timer-scaler (see Par. 2.6.3). In a successive more sensitive version, developed in order to analyze Rb in vivo, the X-ray tube with a Mo-secondary target was employed. A MDL of about 2 ng/cm² was deduced in 10³ s measuring time. A typical XRF-spectrum is shown in Figure 2.40.

Analysis of platelets labelled with Rb and deposited on thin filters is equivalent to the analysis of "thin specimens" (see Par. 2.4.2) for which the fluorescent counts depend upon the mass of Rb per unit area of the filter.

Survival curves of platelets "in vitro" labelled with stable Rb and, for comparison, with radioactive Cr-51, are shown in Figure 2.41. Half time-values $T_{1/2}$ are, respectively, 41.2 h and 44.8 h. Considering the measurements on rabbits, a great dispersion of half-time values was measured in ten expe-

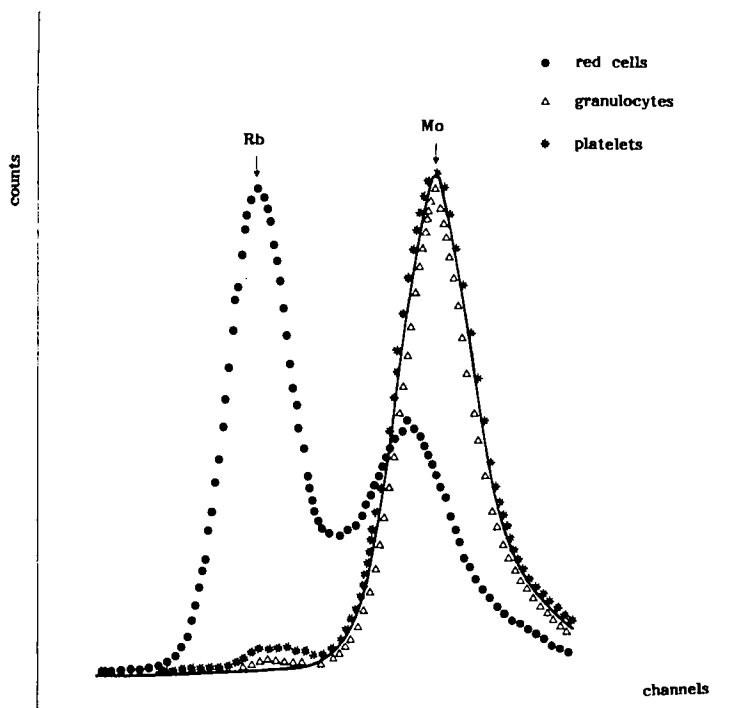


Fig. 2.40. XRF-spectrum of human red cells, platelets and granulocytes labelled with stable RbCl . The continuous curve refers to a background sample. Detector: Xe-proportional counter; Measuring time: 50 s. (after Cesareo et al., ref. 55). A Mo-secondary target was employed.

riments. The following half-time values were deduced: $T_{1/2} = 22 \pm 3$ h with stable Rb and $T_{1/2} = 18 \pm 3$ h with Cr-51 . These values can be compared with the values $T_{1/2} = 16\text{--}28$ h reported in the literature for platelets labelled with Cr-51 .

(ii) Red cell survival studies

Red cell survival of rabbits *in vivo* was measured (ref. 52). In this case, a 20 ml sample of blood was collected, transferred to a plastic tube containing 2 ml of trisodium citrate dihydrate and centrifuged at room temperature at 2500–3000 rpm. About 8 ml of concentrated erythrocytes, thus obtained, were transferred to a plastic tube to which an equivalent volume of saline solution containing 2.5 mg/ml RbCl and 10 mg/ml glucose was added. The suspension was incubated for 15 h. The erythrocytes were then washed twice, resuspended in normal saline and reinjected. About every seven days, 4 ml of blood were collected and the concentrated erythrocytes deposited on filter paper disks. For comparative purposes, red cells were labelled with Cr-51 . The red cell Rb

disappearance curves are shown in Figure 2.42.

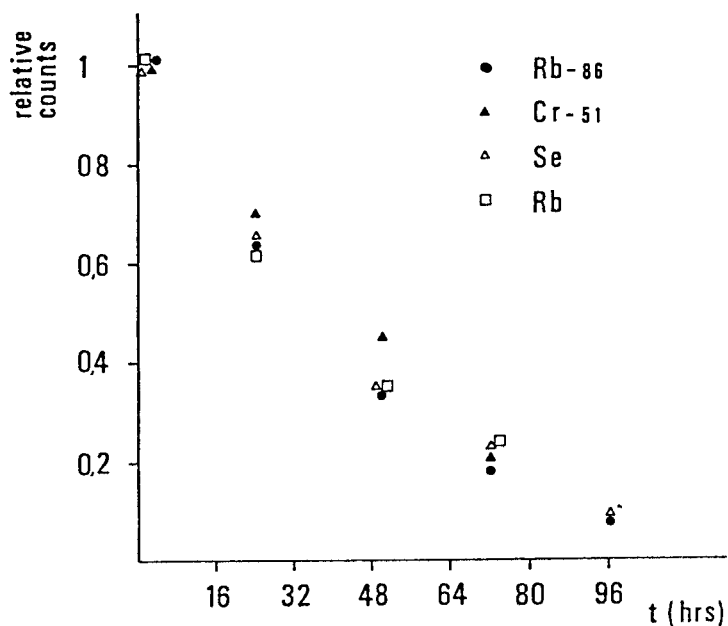


Fig. 2.41. Disappearance curve of human platelets labelled "in vitro" with Rb-86, Cr-51, stable Se-cystine, and stable Rb (after Cesareo et al., ref. 51).

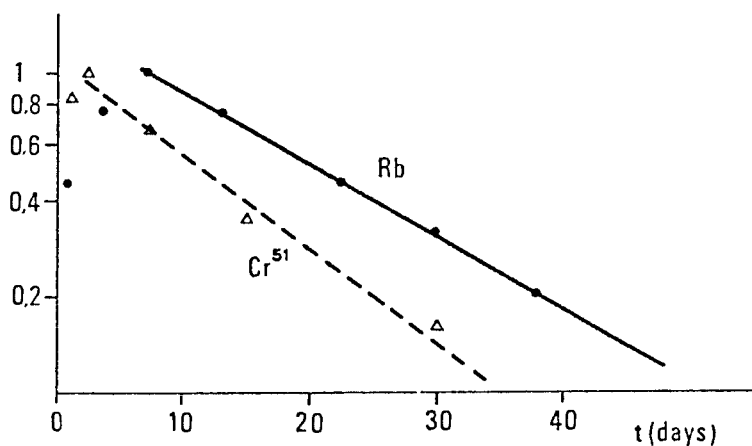


Fig. 2.42. Disappearance curve of rabbit red cells, labelled "in vivo" with stable Rb and Cr-51 (after Cesareo et al., ref. 52).

Measurements of in vivo survival of human red cells labelled with stable Cesium and measured with a XRF-method have been reported by Price et al. (ref. 54). It was noted that red cell cesium disappeared with a relatively rapid half-time of 2.4 days compared to the Cr-51 red cell half-time of 25.2 days. This accelerated cesium disappearance may be due to leakage of cesium from the labelled cells, since damage to the cells by the labelling process itself was excluded by double labelling of the same cell preparation.

(iii) Granulocyte survival with stable Rb

In this study, 20 ml of human venous blood were obtained in heparin. Red cell sedimentation by gravity at 37 °C was carried out for 90 min after adding 5 ml of 3.5% Haemacel Plasmaexpander in 0.9% saline. The supernatant, containing granulocytes and platelets was centrifuged at 250 g for 10 min, the cell bottom resuspended in 2 ml of Hank's balanced salt solution and in 6 ml of an ice bath 0.87% NH₄Cl for 5 min. The granulocytes recovered by centrifugation were labelled with 8 ml of a 0.9% RbCl solution for 60 min at room temperature. The suspension was filtered through millipore filters (pore size 3 µm). The filters were washed three times with a 0.154 M NaCl solution in order to remove residual Rb ions. For comparative purposes, granulocytes were also labelled with Tc-99m. The disappearance curve for human granulocytes from 5 normal subjects labelled in vitro with stable Rb and radioactive Tc-99m has been measured. A mean half-time value of $T_{1/2} = 8 \pm 1$ h was deduced, which can be compared with the value $T_{1/2} = 5.5 \pm 1$ h of granulocytes labelled with Tc-99m (ref. 55).

(iv) Extracellular fluid space

Measurements of extracellular fluid space were carried out by Price et al. (ref. 56) who employed stable bromine. As a standardized procedure, 40 mEq of sodium bromide is administered orally or intravenously, in the resting state, after an overnight fast. Two anticoagulated blood samples of 3 to 5 cc are drawn at 6 and 6 $\frac{1}{4}$ hr, the plasma separated, and the bromine concentrations assayed in 1 to 2 cc plasma aliquots. Cadmium-109 is used as the excitation source, resulting in the production of 11.91 and 13.30 keV characteristic X-rays of bromine. An aliquot of the same dose is retained and assayed at the same time. It is necessary to introduce mathematical correction for the Gibbs-Donnan effect and plasma protein content (0.93) as well as correction for 5.7% average tracer diffusion into red blood cells.

Table 2.20 summarizes the data obtained in a comparative study of ECFV in 11 patients using the stable-tracer method and the Br-82 method. The validity of the method is evident.

TABLE 2.20

Comparative extracellular fluid spaces in adults (after Price et al., ref. 56).

Patient	Diagnosis	stable Br		Br-80	
		ECF(1)	% body weight	ECF(1)	% body weight
1	urticaria	17.3	24	18.3	25.5
2	asthma	19.7	31.8	22.2	35.8
3	obesity	21.8	25.1	20.1	23.1
4	liver disease	19.1	32.4	18.8	31.8
5	obesity	14.5	21.3	14.0	20.5
6	myocardial infarction	13.9	26.7	13.8	26.5
7	hypertension	18.2	35.1	15.3	29.4
8	cirrhosis	22.1	39.4	21.1	37.7
9	hypertension	20.0	30.3	18.9	28.7
10	pneumonia	19.5	26.3	17.7	23.9
11	sickle cell disease	19.3	39.4	16.2	33.0

(v) Red cell volume

Measurements of in vivo red cell volume in man have been carried out by Price et al. by employing stable cesium. The technique for the determination of red cell volume by XRF of cesium-labelled autologous erythrocytes is as follows (ref. 53):

- a. draw 15 ml blood into a heparinized syringe. Transfer to a sterile sealed tube;
- b. centrifuge for 15 min and remove the supernatant plasma;
- c. to packed red blood cells, add an equal volume of 2.6% cesium chloride at pH 7.4 containing Nystatin at a concentration of 50 g/ml;
- d. incubate for 30 min at room temperature;
- e. centrifuge, remove the supernatant and wash once with 2.6% cesium chloride solution;
- f. wash 5-6 times further with normal saline, and reconstitute with normal saline to approximately 50% hematocrit;
- g. inject intravenously a weighed amount of the labelled red cells, retaining a 2 ml aliquot as a standard;
- h. draw 2 to 3 ml anticoagulated blood samples at 10 min and at 40 min for hematocrit determination and for XRF measurement of cesium;
- i. the 40 min sample is routinely used for calculation. If there has been a significant drop in cesium concentration from 10 to 40 min, this may

reflect unusual leakage of cesium out of the erythrocytes.

A comparative study on 11 humans in which red cell volume has been measured by stable cesium and by Cr-51 is shown in Table 2.21.

TABLE 2.21.
Human red cell volumes (1) (after Price et al., ref. 53).

Time after injection	10 min		40 min	
Tracer	Cr ⁵¹	Cs	Cr ⁵¹	Cs
1	2.30	2.44	2.24	2.15
2	1.69	1.64	1.71	1.73
3	0.75	0.71	0.76	0.78
4	1.39	1.45	1.41	1.46
5	1.10	1.16	1.08	1.33
6	1.35	1.38	1.35	1.35
7	1.01	0.98	1.01	1.00
8	3.46	3.26	3.56	3.41
9	2.29	2.22	2.22	2.24
10	1.24	1.29	1.28	1.36
11	2.91	2.93	2.99	2.96

(vi) Glomerular filtration rate

Estimation of the glomerular filtration rate by employing stable iodine was made by Guesry et al (ref. 57).

One of the traditional methods for measurement of the glomerular filtration rate has been determination of the blood clearance of labelled iothalamate by the kidneys. It would seem logical that the clearance of nonradioactive iothalamate would give an equally valid estimate of GFR.

Guesry et al. compared XRF of iothalamate both with insulin clearance in constant infusion studies and with I-125 iothalamate in single injection studies, as well as the evaluation of two exponential and single-exponential model for the derivation of GFR. As a result, their simple and accurate technique requires only three blood sample at 2, 3 and 4 hr after injection of a single dose of nonradioactive iothalamate intravenously. The standardized method for GFR determination by XRF-analysis is as follows:

- a. draw a preinjection blood sample into EDTA and centrifuge to obtain the background plasma sample;
- b. inject 0.15 ml/kg of Conray 60 intravenously; (282 mg/ml);
- c. anticoagulated blood samples (4 to 5 ml) are drawn at 2, 3 and 4 hr into EDTA. Plasma is separated by centrifugation;
- d. Iodine concentrations are measured by XRF on an aliquot of the injectate as well as the background and 2, 3 and 4 hr samples;

- e. the half-time clearance of plasma iodine, after background subtraction, is calculated by single exponential analysis of the three data points, and the GFR is calculated as follows:

$$\text{GFR (ml/min)} = \frac{W \times 282/1.312 \times 0.693}{T_o \times T_{1/2} \times 1.030}$$

where:

W is the weight of injectate

1.312 is the density of Conray-60

T_o is the intercept of the decay curve with t-axis (in min.)

1.030 is the density of serum.

2.7.4 XRF-analysis in forensic science

(a) Gunshot residue analysis

Gunshot residue contains several trace elements, from cartridges, gunpowder, bullets or primer powder, and also from the bullet jacket or from the barrel of the weapon.

Unjacketed bullets contain, besides large quantities of Pb, also Sb (which is the main constituent in Pb-alloy, and sometimes reaches a concentration of 3%), Ag and Cu, found at a concentration level of ng/g.

Besides copper and zinc, silver and selenium are present at concentrations of ng/g in the brass jacket of the bullet.

Primers contain Ba, Sb and Pb. Further, traces of Fe, Zn and Cu may originate from the friction between the bullet and gun's barrel. In conclusion in gunshot residues can be found traces of all following elements: Fe, Cu, Zn, Se, Ag, Sb, Ba, Pb. The determination of some of these elements allows the identification of the shooter or/and of the gunshot.

The search for a reliable method of detecting gunshot residue led to the introduction of neutron activation analysis (NAA) in this area (ref. 58). With this method, which is now routinely employed, microgram or submicrogram quantities of Sb and Ba were determined by activation of material removed from the hand of a suspect by a paraffin casting procedure followed by radiochemical isolation from the irradiated material. With NAA, analysis of gunshot residues transferred from the weapon to a victim, and determination of the distance of the firearm from a collecting surface have been carried out.

Recently, proton induced X-ray emission (PIXE; see Chapter 3 in this volume) was employed in forensic science for the analysis of gunshot residues (ref. 59). With this technique, which requires a proton accelerator, the

elements iron, copper and lead were detected in larger amounts, and Ba in very small amounts, due to the difficulty of the PIXE technique in the low-energy region (L-lines of Ba, with energy 4.6 keV).

XRF-analysis has also been employed by Cesareo et al. (ref. 60) for the identification of firearm residues, and this technique seems to be very suitable for this purpose. It gives the possibility of carrying out multielement nondestructive analysis; this is very important especially when it is essential to have the sample at one's disposal for further analysis.

The typical amount of trace elements in gunshot residue is on the order of 100 ng - 1 µg.

In a first series of experiments, elements Fe, Cu, Zn and Pb have been analyzed. For this purpose an X-ray tube with a Mo-secondary target was employed. In a second series of experiments, a Ba-target was employed for excitation of Sb, and a Fe-secondary target for excitation of Ba-L-X-rays.

The XRF method was applied to:

- direct analysis of primer components and gunpowder;
- analysis of gunpowder residues removed from the hand of the person who had discharged the weapon.

As observed many times, the sample preparation for optimal XRF analysis is a consequence of the "thin sample" criterion (see Par. 2.4.2). In this case, the sample consists of about 5-20 mg of powder collected on a surface of paper or tissue, or by a few mg of gunshot residue on a filter paper disk when analysis is carried out of ballistic residues removed from the hand of the person who has discharged the weapon. The sample is thin for all elements, except for Ba, when L-X-rays are analyzed.

In the case of analysis of primer components and gunpowder, the analyzed sample is about 10-20 mg of thick grains, and is, therefore, not exactly a thin sample, because granulometric effects occur. Several corrections are necessary with respect to the "thin sample" hypothesis, and results are affected by larger errors. On the other hand, accurate quantitative analysis of primer components and gunpowder is not so important.

Shots were fired with the following weapons: semi-automatic pistol Beretta 7.65 mod. 81; revolver Smith & Wesson 38 spec. mod. 36; revolver Smith & Wesson 44 magnum, mod. 29. The bullets employed are listed in Table 2.22.

Gunshot residues were collected from the hand of the shooter by cleaning the hand with a filter imbibed with a solution containing CH_3COOH and $\text{C}_2\text{H}_5\text{OH}$. As an alternative, the hand was washed with the above solution and the washing liquid filtered through a SA-2 Whatman ion-exchange resin loaded filter.

In another experiment, gunshot residue was collected at various distances on surfaces of cotton, wool and synthetic tissue. The following weapons and

TABLE 2.22

Composition of primer and gunpowder (columns 4 and 5); Pb-content in gunshot residues collected on filter paper target at 20 cm from weapon's tip (column 6); Pb content in gunshot residues taken from the hand of the shooter (column 7 and 8)

N.	make	Bullet calibre and type	Trace elements in gunpowder	Pb content (μg)			
				in primer ($\mu\text{g}/\text{mg}$ powder)	at 20 cm from weapon's tip	in gunshot residues	
						in paper filters	in resins
1	Fiocchi	7.65 mm FMC	Fe (traces)	2	8	0.15	3.3
2	Geco	7.65 mm FMC	-	12	33	1.2	0.8
3	Winchester	7.65 mm FMC	Pb (traces)	13	5	0.3	1.1
4	Hirtenberg	7.65 mm FMC	Fe (traces)	11	6	0.2	1.0
5	Winchester	7.65 mm SHP	Pb (traces)	12	20	3.6	3.0
6	Speer	38 Spec. LRN	Pb (traces)	15	43	0.6	1.0
7	Speer	38 Spec. SWC	Pb	13	80	1.2	3.0
8	Winchester	38 Spec. LRN	-	14	30	0.4	1.8
9	Speer	38 Spec. JHP	Fe (traces)	10	25	2.1	2.3
10	Winchester	38 Spec. LHP	Fe (traces)	12	55	2.4	5.9
11	Lapua	38 Spec. WC	Pb	13	60	0.8	3.4
12	Norma	38 Spec. LRN	-	13	60	1.0	2.8
13	Lapua	38 Spec. LRN	Fe (traces), Pb	14	77	0.8	2.3
14	Winchester	44 Magn. SWC	-	8	10	0.8	8.0
15	Federal	44 Magn. JSP	-	11	25	1.2	2.2
16	Federal	44 Magn. JHP	-	9	12	0.3	3.6

Shots were fired with the following weapons: semi-automatic pistol Beretta cal. 7.65 mm Mod. 70; revolver Smith & Wesson cal. 38 Spec. Mod. 36; revolver Smith & Wesson cal. 44 Magn., Mod. 29.

FMC: full metal case; SHP: silvertip hollow point; LRN: lead round nose; SWC: semi wadcutter; JHP: jacketed hollow point; LHP: lead hollow point; WC: wadcutter; JSP: jacketed soft point.

ammunition were employed: a semi-automatic pistol Beretta 7.65 with Browning G.F.L.; a semi-automatic pistol 9 with Parabellum G.F.L.; a revolver Smith & Wesson 38 spec with Winchester Western ammunitions.

Figure 2.43 shows the XRF-spectra of gunpowder, primer and gunshot residues from a Winchester 7.65 S.H.P. fired with the Beretta 7.65 pistol. Two additional representative XRF-spectra of gunshot residue are shown in Figure 2.44.

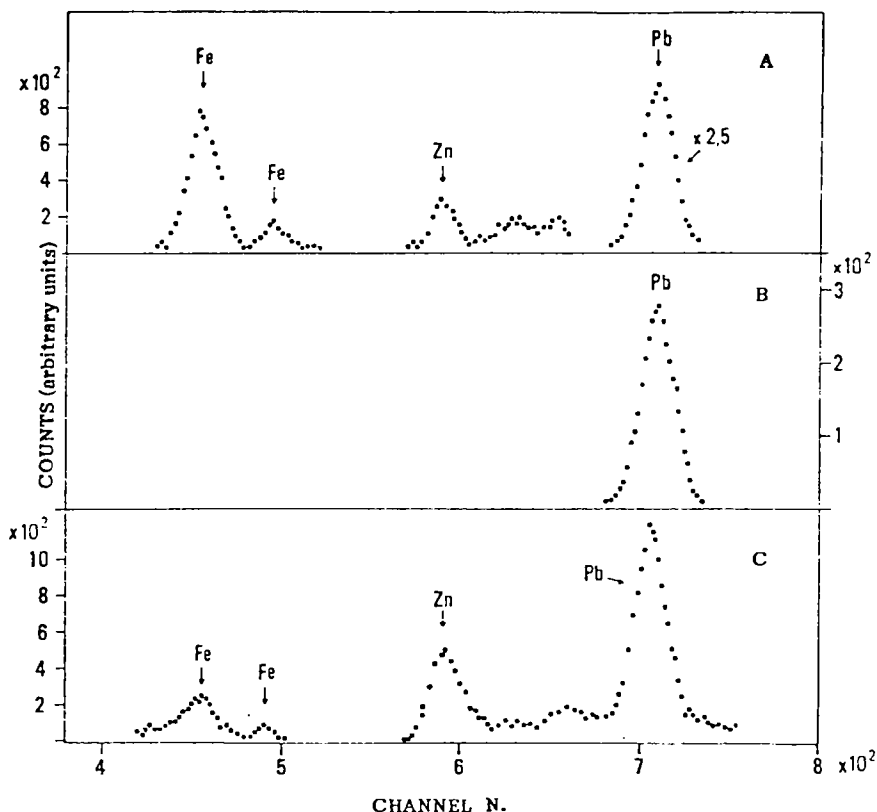


Fig. 2.43. XRF spectra of gunpowder (A), primer (B) and gunshot residue (C) removed from the hand of the shooter (gunshot N. 5 of Table 2.22). Ammunitions Winchester 7.65 mm silvertip hollow point; semi-automatic pistol Beretta 7.65 mm mod. 70. Only about 1/20 of the primer powder was analyzed. A secondary target of Mo and a HPGc detector were employed (after Cesareo et al., ref. 60).

XRF-spectra of gunshot residue collected at various distance from the firearm on targets of paper disks are shown in Figure 2.45.

Analyses have been carried out with Fe, Mo and Ba secondary targets.

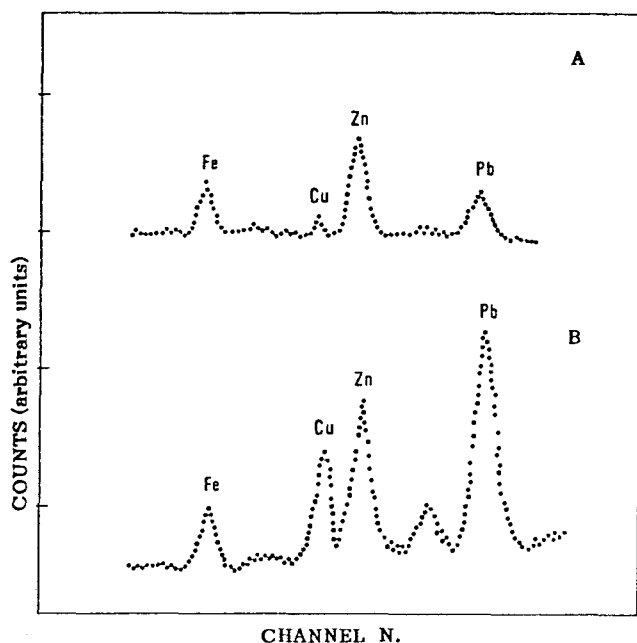


Fig. 2.44. XRF-spectra of gunshot residue collected from the hand of the shooter. A: Beretta pistol 7.65 mm mod. 92 S with ammunitions GFL; B: Smith & Wesson revolver 38 Spec. mod. 36 with ammunitions Winchester Western. A secondary target of Mo and a HPGe detector were employed. (after Cesareo et al., ref. 60).

The XRF spectrum referring to a piece of cotton, taken around the hole of a shot, in a death event is shown in Fig. 2.46. Except for bromine, which comes from the tissue, the composition is qualitatively similar to that of previously analyzed gunshot residue.

Finally, evidence indicating the presence of antimony and barium in gunshot residue can be deduced from the XRF spectra shown in Figures 2.47 and 2.48.

(b) Analysis of skin metallization

The passage of electric current through the body can give rise to burns resulting from the action of the electric current on the contact skin area. This phenomenon is called electrocution and often produces skin metallization resulting in trace elements of the metallic electrode on the contact area. That is of great importance in forensic medicine in cases of fatal electric

shocks. The detection of typical trace elements on the area of the skin in contact with the electric cable could therefore be of great importance for the diagnosis of electrocution.

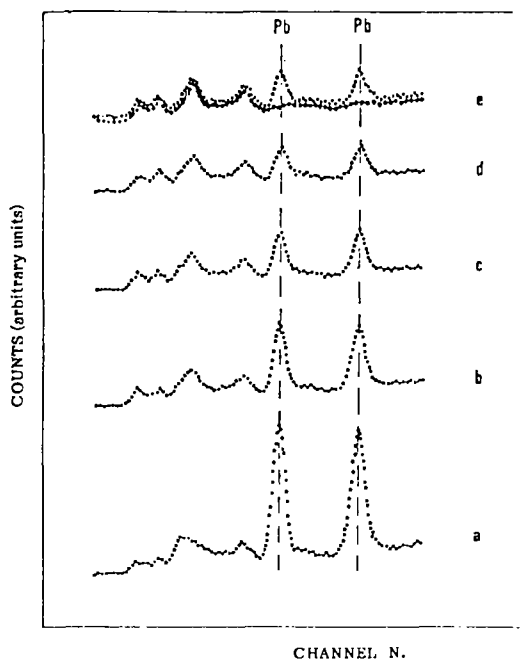


Fig. 2.45. XRF-spectra of gunshot residues, collected at various distances from weapon's tip on filter paper disks. a: 20 cm; b: 40 cm; c: 60 cm; d: 80 cm; e: 100 cm. The lower curve in Figure e refers to background. A secondary target of Mo and a HPGe detector were employed. (after Cesareo et al., ref. 60).

An interesting investigation in this field was carried out by Marcinkowski and Pankowski (ref. 61), who employed radioactive electrodes of Co^{60} and treated the skin of corpses with alternating and direct current of 10 to 250 V for 0.3 to 60 s. It was shown that the radioactivity of the skin at the site of electrode contact increases with the elevation of the voltage and its duration. In the case of alternating current the rise was about 20 fold in the range 0.3-60 s exposure time.

Using electrodes of copper, aluminium and iron (non-radioactive), it was shown by the same authors (by electrographic method) that metallization intensifies under the same conditions of time and voltage.

In our Centre, "in vitro" experiments were carried out by applying alternating current at 220 V for a period of 1 to 30 s to the skin of dead men (ref. 62). The skin was successively directly XRF-analyzed by using the

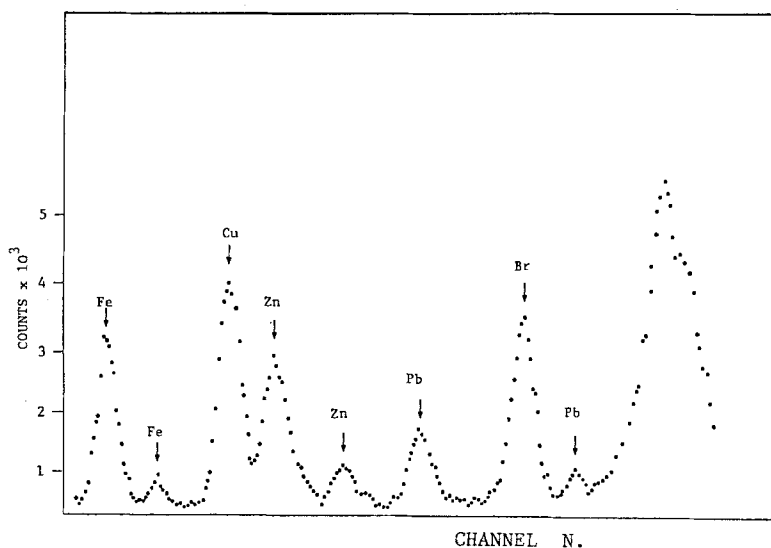


Fig. 2.46. XRF-spectrum of gunshot residue relative to a piece of cotton taken around the hole of a shoot (after Cesareo et al., ref. 60).

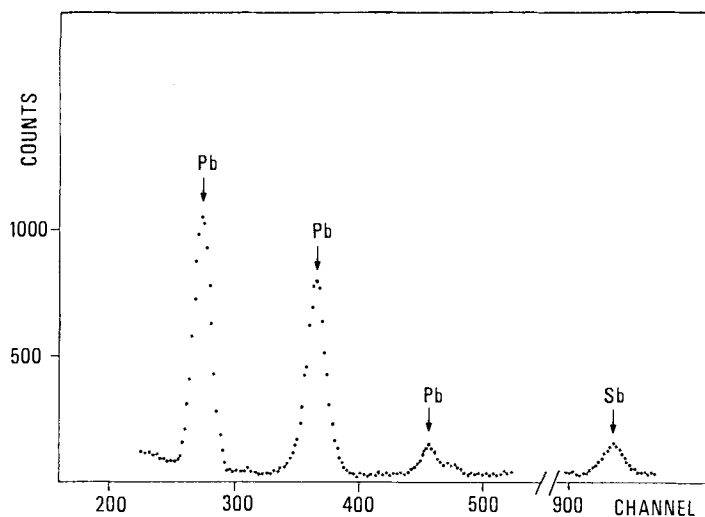


Fig. 2.47. XRF-spectrum of gunshot residue for analysis of Sb-content. A secondary target of Ba and a HPGe detector were employed.

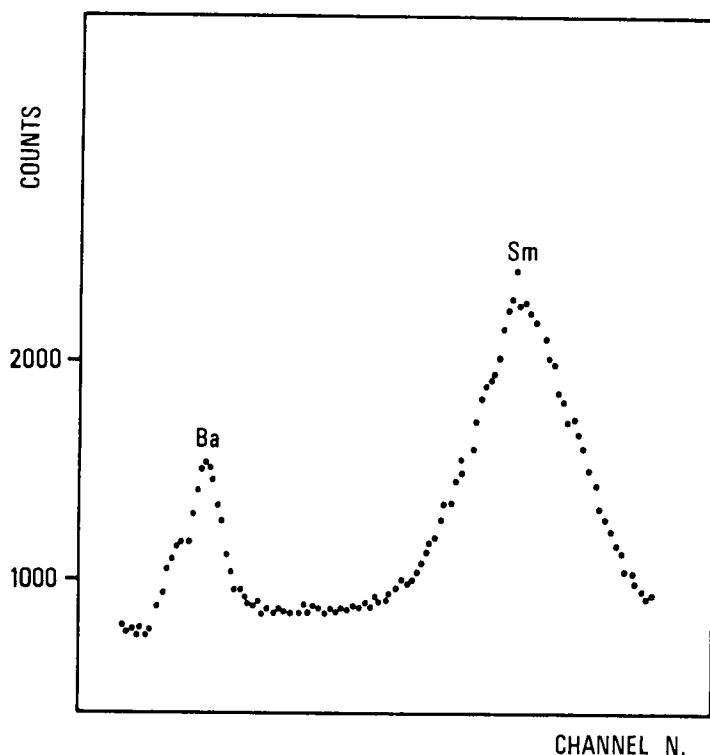


Fig. 2.48. XRF-spectrum of gunshot residue for analysis of Ba (X-K lines have been analyzed). A secondary target of Sm and a HPGe detector have been used.

XRF-tube with a Zn-secondary target for the detection of the elements Mn, Fe, and Cu constituting the employed electrodes. Traces of these elements were detected, in an amount approximately proportional to the exposure time.

Later analyses were carried out on the skin of a man who had died through electrocution. The XRF-spectrum of the burned skin is shown in Figure 2.49.

2.7.5 Analysis of urinary calculi

More information is required regarding the pathology of the disease which gives rise to kidney and bladder stones. A study of the composition and structure of stones and their correlation with diet and the composition of urine is of great importance both for treatment and prophylaxis. The homogeneity of the stone structure will provide additional information, which could lead to an understanding of the original formation.

Preparation of the specimen for XRF analysis is critical, because of the

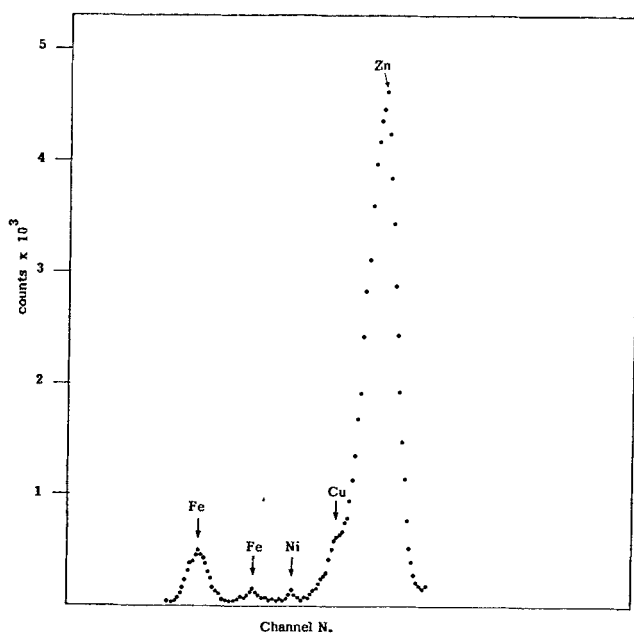


Fig. 2.49. XRF spectrum of skin metallization through electrocution in the case of a dead event.

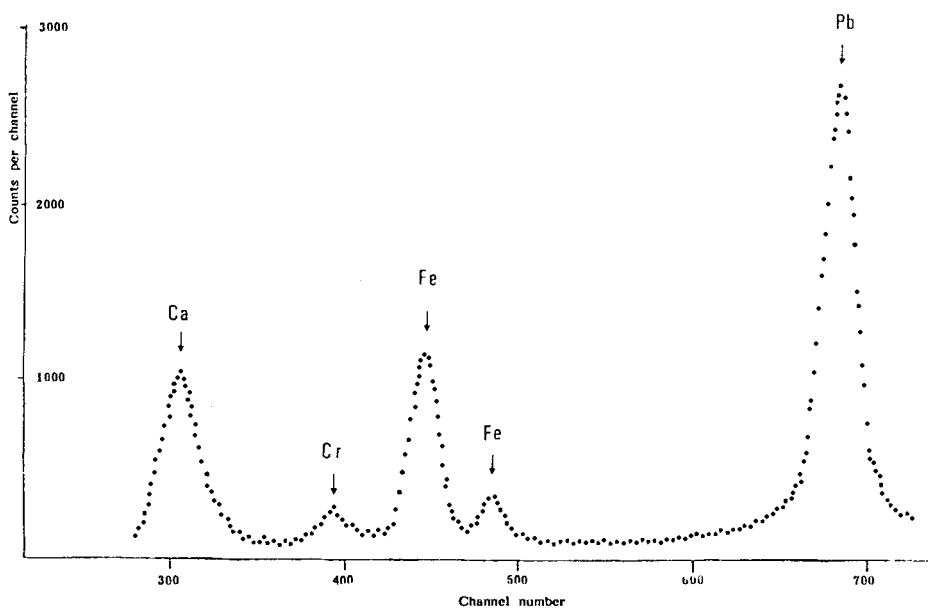


Fig. 2.50. XRF-spectrum of a kidney stone (after Cesareo et al., ref. 63).

thin sample requirement. Urinary stones of variable origin, mass and form were grated in different areas with a carbonrundum file until about 10 to 20 mg of powder were obtained. The powder, mixed with a neutral glue, was deposited on a thin plastic support. The sample was then directly analyzed (ref. 63).

Twenty-one kidney and bladder stones have been analyzed (ref. 63). Only stones with a pure composition were selected for XRF analysis. A typical XRF spectrum of a cystine stone is reported in Figure 2.50. Elements Fe and Zn were systematically detected, Cr, Mn, and Pb occasionally.

2.7.6 In vivo XRF analysis

The "in vivo" analysis of chemical elements in organs of the human body constitutes a completely different problem from the "in vitro" analysis of thin samples.

As shown in the previous paragraphs, when thin biological samples are analyzed, no matrix effects occur, and the quantitative analysis of each element is independent from the presence of other elements in the sample. The main problem in that case is to have a high intensity source of adequate energy and a good geometrical arrangement.

On the contrary, when thick samples are analyzed, one of the main problems is the very high ratio between scattered peaks (mainly Compton), which determines the background under the fluorescent peak, and fluorescent peaks.

From a general point of view, there are three main factors which affect the choice of the photon source used to estimate X-ray emission. The first is the need to maximize the photoelectric effect for the element to be analyzed, by selecting the source with an energy just above the K- edge of the element. This requirement is often in conflict with the presence of a very intense Compton scattered peak.

Considering Equations (12) and (15), valid for thick samples, the following could be written:

$$\frac{N_C}{N_a} = \frac{\mu_C(E_o) \{ \mu_t(E_o) + \mu_t(E_a) \}}{\{ \mu_t(E_o) + \mu_t(E_C) \} \omega_a \mu_{ph.a} c_a} \approx \frac{\mu_C(E_o)}{\omega_a \mu_{ph.a} c_a} \gg 1 \quad \text{when } E_a \approx E_C \approx E_o$$

where symbols have been explained in par. 2.4.

Considering for example 100 ppm Pb in solution excited by $E_o = 100$ keV incident radiation, the ratio N_C/N_{Pb} is given by:

$$N_C/N_{Pb} \approx 2.4 \times 10^2$$

if: $\mu_C(100 \text{ keV}) = 0.165 \text{ cm}^2/\text{g}$, $\mu_{ph.Pb} = 7.5 \text{ cm}^2/\text{g}$ and $\omega_{Pb} = 0.9$. Therefore,

one of the main problems encountered in in vivo XRF analysis which limits the sensitivity of the method is that the fluorescent peaks of the element of interest are superimposed to a very high background due to the scattering process in the sample, which gives rise to a large Compton peak the effect of which is propagating under the photoelectric peak of the element to be analyzed. The second factor is the need to have adequate penetration into the organ in which the element is present, in order to have a measurement over a large volume of the organ. The attenuation of incident and fluorescent radiation in the body prevents the analysis of low-Z elements and the analysis of elements in deep organs.

In order to give an idea of the attenuation effect, Figure 2.51 shows the flux of characteristic X-rays originating from a small volume located at a

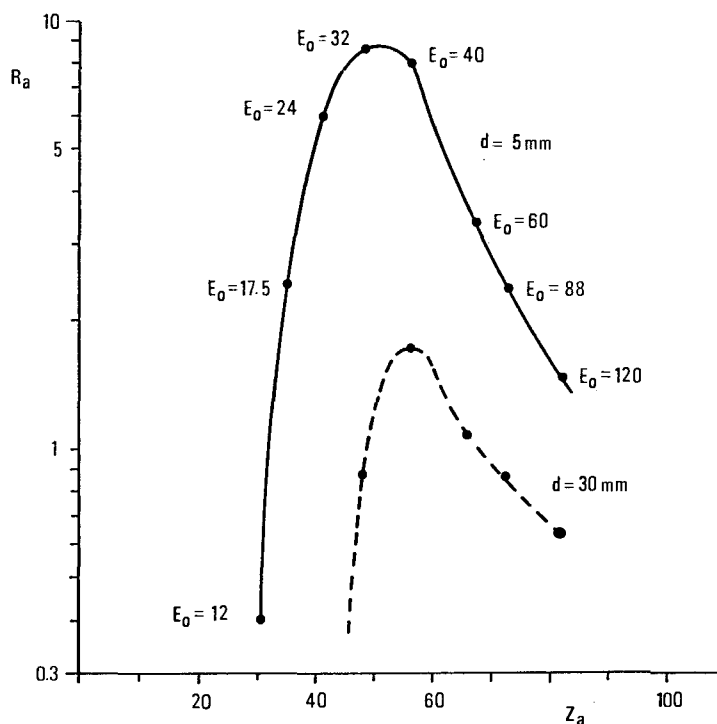


Fig. 2.51. Relative number R_a of K-X-rays emerging from a small volume of element Z at depth d in soft tissue irradiated by photons of various energies.

depth d and irradiated by photons of energy E_0 . This is proportional to:

$$R_a = \exp - \{ \mu_t(E_o) d \} \sigma_{ph.a} \omega_a \exp - \{ - \mu_t(E_a) d \} \quad (29)$$

when irradiation is made by photons with energies above the binding energy of the K-electrons; there is no great advantage in employing larger incident energies because the principal attenuation is given by output fluorescent photons. Figure 2.51 shows the calculated value of R_a for analysis of various elements at various depths. From this Figure it can be observed that in vivo XRF analysis is limited to elements with medium and high atomic number (ref. 64).

As pointed out by Ahlgren (ref. 64), a decreasing atomic number means decreasing energy of involved radiation and therefore increased absorption, which is not compensated by the higher photoelectric cross section. On the other hand, for high atomic number, the factor R decreases because photoelectric cross section decreases. The best region is around atomic number $Z=50-60$, and is function of the depth.

The third factor is concerned with minimizing the background under the peak. In problems of in vivo XRF-analysis, the resulting spectrum is constituted by a very high and large Compton peak with energy depending upon the source-subject-detector angle, by a lower intensity Rayleigh peak and by low intensity fluorescent peaks from the elements under analysis. It is of course important to have the Compton peak as far as possible from the X-ray peaks of interest in order to minimize the background. Separation of the Compton scatter and fluorescent peaks is not, however, the only criterion to be used since the detector response function has a significant low-energy component. This means that, for a given separation from the fluorescent peaks, a Compton peak below, rather than above the fluorescent peaks produces less background.

Another important point is that high incident radiation flux is, in general, not required; due to the very high Compton flux, saturation is easily achieved with low intensity sources. Radioactive sources are adequate for "in vivo" XRF analysis.

For all these reasons, no general criteria can be given for "in vivo" XRF-analysis; each problem has to be treated and optimized separately, taking into account:

- the element to be analyzed and its concentration;
- the energy and intensity of the incident radiation;
- the depth, volume and form of the organ to be irradiated;
- the detector;
- the radiation dose.

So far, the following elements have been studied (see also Table 2.23):

- a. lead in bone

TABLE 2.23.

Summary of the organs examined by "in vivo" XRF-analysis, or feasibility studies in phantoms

Examined organ	Analyzed element and emitted X-rays (keV)	Source and emitted radiation (keV)	Detector and geometry	M.D.L. ($\mu\text{g/g}$)	Absorbed dose (mGy)	N. of analyzed subjects
bone (tibia) ¹	Pb-X _K (74,85,87)	Cd-109 (88)	Ge 180°	15	0.1 bone	44
(calcaneus) ¹					0.45 skin	22
bone (forefinger) ²	Pb-X _K (74,85,87)	Co-57 (122)	Ge 90°	20	2.5	140
bone (tooth) ³	Pb-X _K (74,85,87)	Co-57 (122)	Ge 180°	15	0.8	30
bone (tibia) ⁴	Pb-X _L (10.5,12.7)	Cd-109 (22)	Si(Li) 100°	20	0.6 bone 10 skin	45
bone (tooth) ⁵	Sr-X _K (14,16)	Cd-109 (22)	Si(Li) 90°	6.6		
bone (tibia) ⁶	Sr-X _K (14,16)	Cd-109 (22) I-125 (32)	Si(Li) 90°	15	0.5 bone 10 skin	7
kidney ⁷	Cd-X _K (23,26)	Am-241 (60)	Ge 110°	20-40	0.6	12
kidney ⁸	Pt-X _K (66,77)	Co-57 (122)	Ge 90°	37		4
kidney ⁹	Hg-X _K (70,80,83)	Co-57 (122)	Ge 85°	2.5	4	phantom
thyroid ¹⁰	I-X _K (28,33)	Am-241 (60)	Kr-gas counter 150°	40	0.2-0.5 neck	3
thyroid ¹¹	I-X _K (28,33)	Am-241 (60)	Si(Li) 100°		0.15	phantom

¹ Somervaille et al. (refs. 67 and 68)² Ahlgren and Mattsson (ref. 65)³ Bloch and al. (refs. 76 and 78)⁴ Wielopolski et al. (refs. 66 and 79)⁵ Wielopolski et al. (ref. 80)⁶ Wielopolski et al. (ref. 69)⁷ Ahlgren and Mattsson (ref.70)⁸ El-Sharkawi et al. (ref.77)⁹ Smith et al. (ref. 71)¹⁰ Magrini et al. (ref. 73)¹¹ Gollnick et al. (ref. 81).

- b. strontium in bone
- c. cadmium in kidney
- d. mercury in kidney
- e. iodine in the thyroid
- f. lead in teeth
- g. platinum in kidney

A. Lead in bone

In vivo analysis of lead in bone has been carried out by Ahlgren et al. (ref. 65), Wielopolski et al. (ref. 66) and Somervaille et al. (refs. 67 and 68).

Lead is a very important element, and its toxicological effects have been appreciated for a considerable time. On account of its toxicological importance, lead uptake in occupationally exposed workers is monitored, normally through blood, serum or hair lead levels. However it is known that these levels are related to recent exposure, and that the organ of accumulation of lead is bone, which is estimated to contain over 90% of the body lead burden. This implies that measurement of bone lead levels could be expected to reflect cumulative exposure and that these levels could be an important parameter in the understanding of the long-term health effects of lead.

A detailed study of physical factors affecting the measurements of lead content in bone was carried out by Somervaille et al. (ref. 67). They stressed the advantage of employing Pb-K-rays rather than L-X-rays for the larger mean free paths. In fact, the half value bone layer for Pb-L-X-rays (mean energy values: 11.5 keV) and for lead K-X-rays (mean energy value: 80 keV) are 0.3 and 2.5 cm respectively. The long mean free path increases the range of bones which are accessible to measurement and ensure that the measurement is over as large a bone volume as possible.

The experimental arrangement employed by Somervaille et al. is shown in Figure 2.52. A typical XRF spectrum, in 20 min. measuring time, is shown in Figure 2.53.

It should be pointed out that Pb-counts depend critically upon the depth of tissue overlaying the bone, the position of the lead within the bone, upon the source-subject distance, upon the bone shape and size and the position of any marrow space. To relate a given in vivo measurement of Pb-X-rays to an absolute bone lead concentration would require knowledge of and correction for all these factors.

Somervaille has shown that the use of coherently scattered gamma-rays provides a normalization parameter for measurements using Cd-109 which obviates the need for all these corrections. Measurements of Pb content have

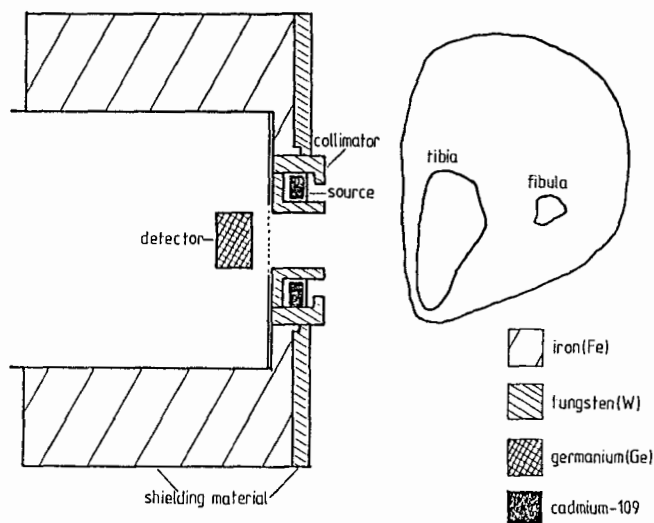


Fig. 2.52. Experimental arrangement for "in vivo" analysis of Pb in bone (tibia) showing Fe and W shielding added to prevent cross-talk between systems. Pb-excitation is performed by means of a Cd-109 source (7.4 GBq of intensity) emitting 88 keV gamma radiation (after Somervaille, ref. 67).

been carried out by the authors on phantoms and on about 100 subjects (ref. 68).

The lower limit of detection (at 2 S.D. level) was found to be 10 $\mu\text{g/g}$, which is in the lower limits of the range for non occupationally exposed adults (which is from 5 to 30 $\mu\text{g/g}$). This sensitivity is adequate for measurements on occupationally exposed subjects and for the majority of normals. The results on 38 subjects are summarized in Figure 2.54.

The mean absorbed dose to a 20 cm^2 leg section is less than 0.1 mGy and the maximum skin dose is 0.45 mGy.

A different method for "in vivo" analysis of Pb in bone was employed by Ahlgren et al. (ref. 65), who irradiated for 30 minutes with two collimated Co-57 sources having a total activity of 0.8 GBq, the left forefinger (see Fig. 2.55).

The MDL was 20 $\mu\text{g/g}$. The method has been used for in vivo measurements on about 140 persons occupationally exposed to lead for 1-30 years. A Pb concentration in the range 20-140 $\mu\text{g/g}$ has been detected. The mean absorbed dose was 2.5 mGy.

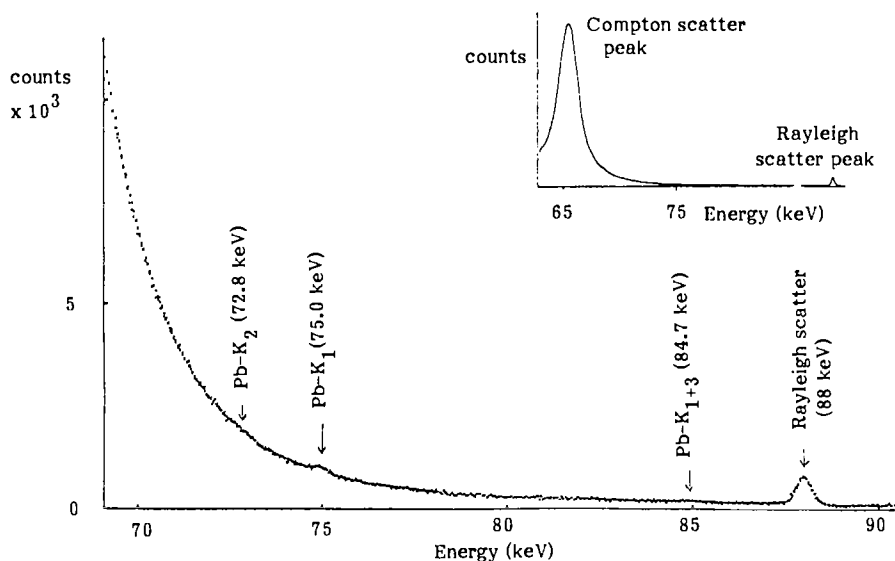


Fig. 2.53. "In vivo" XRF-spectrum of Pb in tibia (after Somervaille, ref. 67).

B. Strontium in bone

Strontium is known to occur naturally in human bone in concentrations of 20-60 µg/g. The exact role of Sr in the human body remains ambiguous even though Sr has been extensively studied with reference to the radiation hazard from Sr-90. Metabolic behaviour of Sr is, in some aspects, similar to that of Ca. It has been suggested that Sr stimulates the formation of bone matrix. At higher concentrations however, it interferes with the calcification mechanism of the bone.

Sr has occasionally been used for therapeutic purposes, in the treatment of osteoporosis and as an anticarcinogenic agent in man.

A study on Sr in human bone "in vivo" by XRF-analysis has been carried out by Wielopolski et al. (ref. 69). They utilized, for the measurements, either Te-X-rays emitted by a I-125 source or Ag-X-rays emitted by a Cd-109 source.

The half-value bone layer for Sr-X-rays (14.1 keV) is approximately 1 mm, and, therefore, only superficial bones could be considered for the measurement

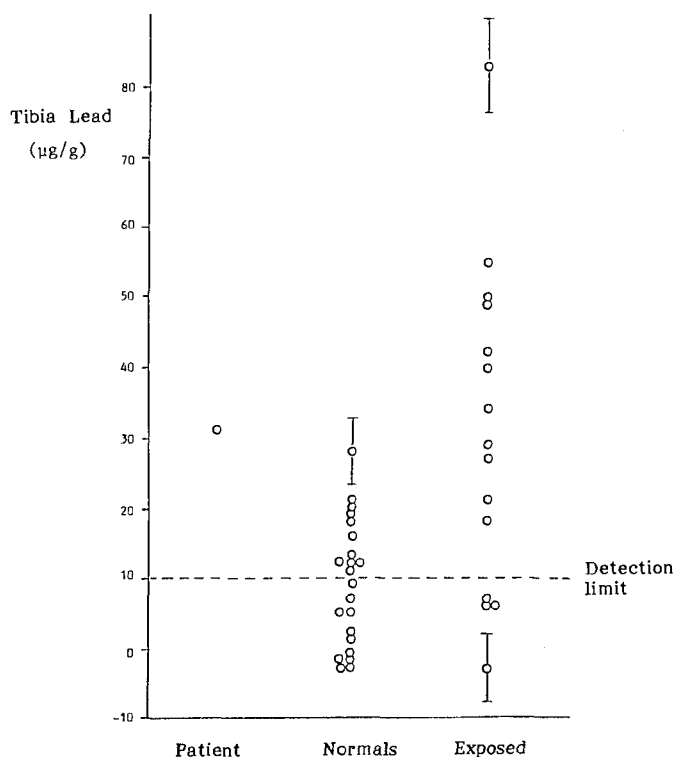


Fig. 2.54. Results on "in vivo" Pb measurements in the tibia of 38 subjects (after Somervaille, ref. 67).

of Sr. The tibial shaft was selected for XRF-measurement (see Fig. 2.56), which is covered by approximately 3-5 mm of skin. A typical spectrum, taken from a dry bone, induced by I-125 source, is shown in Figure 2.57. The Sr-peak is evident, as the well as Zn and Ca peaks, the main constituent of bone. The Fe-peak originates from the collimator.

Quantitative calibration of the Sr measurement was performed by assaying the bone specimen by atomic absorption.

The results of all the measurements are summarized in Table 2.24. The net number of counts were normalized to an exposure rate of 10^{-2} Gy. The lower detection limit of Sr (at the level of 3 S.D. above the background) is about 15 μg/g. The radiation dose delivered to the bone marrow subjacent to the exposed surface of the tibia is about 0.5 mGy.

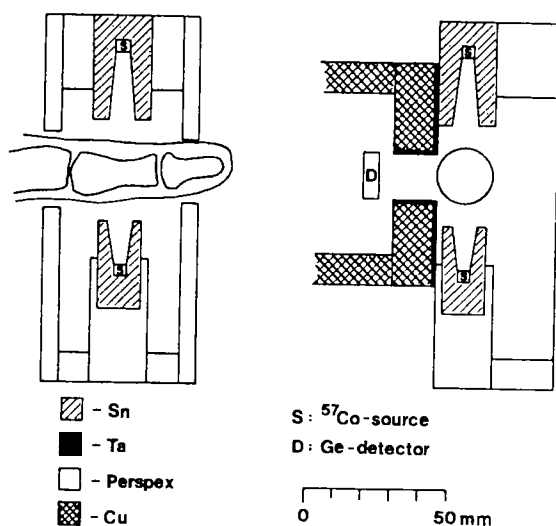


Fig. 2.55. Experimental set-up for "in vivo" XRF analysis of Pb in the finger (after Ahlgren and Mattsson, ref. 65).

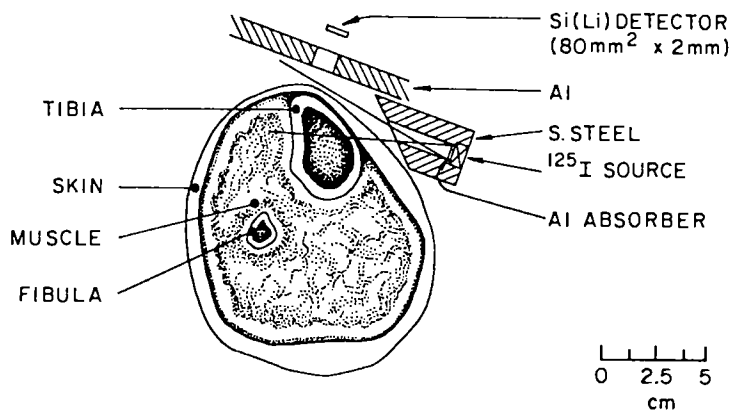


Fig. 2.56. Experimental set-up for "in vivo" measurement of Sr in tibia (after Wielopolski et al., ref. 69).

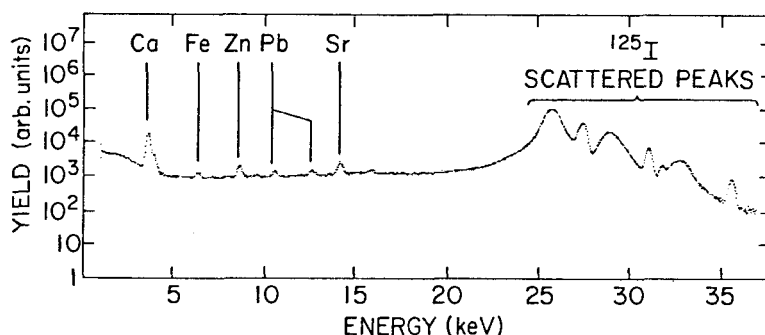


Fig. 2.57. Typical XRF spectrum of the tibia irradiated by I-125. Besides Sr, Ca, Fe and Zn peaks are evident (after Wielopolski et al., ref. 69).

TABLE 2.24

Strontium measurements on intact tibial shafts; exposure 10^{-2} Gy (after Wielopolski et al., ref. 69).

Sample	Source	Net counts* \pm SD	$\sigma_{s^{**}}$ Above Bkg
P.M. (1)			
59	I-125	1481 \pm 128	17.1
60	"	1895 \pm 133	21.3
61	"	1124 \pm 175	12.1
64	"	1274 \pm 170	14.4
65	"	1497 \pm 139	15.3
67	Cd-109	2986 \pm 151	29.7
A.L. (2)			
1610	Cd-109	1004 \pm 155	9.0
1610	I-125	1363 \pm 175	11.3
2109	Cd-109	888 \pm 193	6.7
3188	"	1363 \pm 202	9.7
4442	"	2363 \pm 191	19.3
N. (3)			
H.S.	"	1784 \pm 179	13.5
M.S.	"	840 \pm 176	6.4
S.M.	"	607 \pm 170	5.1
K.E.	"	2089 \pm 180	16.8
S.H.C.	"	1497 \pm 170	12.7
R.S.	"	1609 \pm 187	13.1
D.V.	"	1660 \pm 170	13.3

(1) P.M. - Postmortem measurement

(2) A.L. - Amputated leg measurement

(3) N. - Normal volunteers

* Uncorrected for overlying tissue

** = Background

C. Cadmium in kidney

Cadmium is an important toxic environmental pollutant and represents an increasing hazard to man. In industrialized countries, Cd is present in food, water and air. For subjects not exposed occupationally, inputs from food and cigarettes are the most important. Furthermore, for subjects not exposed occupationally, the liver and the kidney contain about 50% of the total body burden. In Sweden, the Cd concentration in the kidney cortex is about 20 $\mu\text{g/g}$ for smokers and 10 $\mu\text{g/g}$ for non-smokers, and about 1 $\mu\text{g/g}$ in the liver. For persons who have been heavily exposed to Cd, concentrations of up to about 500 $\mu\text{g/g}$ have been reported in the liver and in the kidney cortex.

A detailed study of Cd in kidney by XRF-analysis "in vivo" was carried out by Ahlgren et al. (ref. 70), who employed Am-241 sources (disc shaped 11 GBq source or annular shaped 11 GBq source). The secondary radiation from the irradiated volume was studied using a Ge(Li) detector (Fig. 2.58). The relative sensitivity for Cd detection was studied with a Cd Cl_2 (25 mm³) placed at different positions in water-filled phantoms. The minimum detectable limit, at 3 S.D. above the background, varies between 20 and 40 $\mu\text{g/g}$ for distances between the skin and the kidney of 30 to 40 mm. For kidneys located deeper than 4 cm, the absolute sensitivity is often too low even for occupationally exposed subjects. Using polarized photons the MDL was improved, respectively, to 9 $\mu\text{g/g}$ at a kidney depth of 3 cm and 28 $\mu\text{g/g}$ at 5 cm.

The XRF-technique has been applied to subjects exposed to Cd for periods varying between 6 and 36 years. Table 2.25 shows the results in 12 persons with known occupational exposure to Cd.

The mean absorbed dose to the kidney during the measurements is about 0.6 mGy (60 mrad), which is comparable to with the value of 3.3 mGy of a typical urography.

D. Mercury in kidney

Mercury is normally present in the body in small amounts (total body content 13 mg) the toxicity of which has long been recognized. The kidney is a major accumulator of mercury.

Recent exposure to the population at large refer in two main groups. The first, (in Japan) was comprised of people who ate fish contaminated with methylmercury, whilst the second was of people who ate grain treated with methylmercurial fungicide. Current monitoring methods for mercury involve the use of blood and urine, even though the normal levels are very low (30 and 20 ppb, respectively). In addition hair may also be used for analysis.

Since the kidney is the principal organ for accumulation (the range of Hg in kidney is wide, but 1 $\mu\text{g/g}$ is a representative figure) it would be of

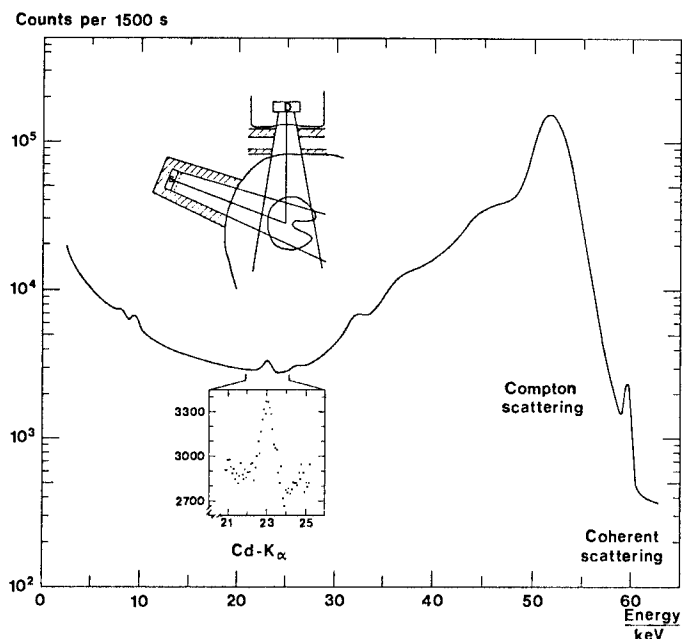


Fig. 2.58. Experimental set-up for "in vivo" XRF-analysis of Cd in kidney and typical XRF-spectrum, containing Cd- K_{α} -peaks and elastic and inelastic scattered source peaks. An 11 GBq Am-241 source and a Ge-detector were used (after Ahlgren and Mattsson, ref. 70).

TABLE 2.25

Measured cadmium concentration in the kidney cortex of occupationally exposed persons (N. 1-6) of persons working at a battery production unit (7-12) and of controls (13-15) (after Ahlgren and Mattsson, ref. 70).

Person number	Age(y)	exposure period (y)	Cadmium concentration in kidney cortex ($\mu\text{g/g}$)
1	33	6	30 ± 22
2	64	30	36 ± 13
3	35	10	47 ± 17
4	62	?	135 ± 42
5	54	25	137 ± 42
6	35	14	143 ± 45
7	51	7	$15 \pm 5^{\circ}$
8	45	13	$45 \pm 11^{\circ}$
9	51	16	$64 \pm 17^{\circ}$
10	56	26	$82 \pm 18^{\circ}$
11	52	36	$150 \pm 30^{\circ}$
12	51	36	$170 \pm 40^{\circ}$
13	36	--	$30 \pm 8^{\circ}$
14	56	--	$17 \pm 6^{\circ}$
15	37	--	30°

^o Measurements carried out with polarized photons.

interest to analyze in vivo Hg in kidney.

An explorative study on the possibility of detecting Hg in kidney in vivo using the XRF technique was performed by Smith et al. on kidney phantoms (ref. 71).

The apparatus consists of a collimated Co-source and a HPGe detector. The detection angle was taken at 85° , in order to move the Hg-peaks toward the tail of the multiple scattered photon distribution.

The measured detection limit was established to be 44 ± 9 ppm for a dose of 45 μ Gy. Assuming an irradiation dose of 4 mGy a theoretical lower detection limit of 2.5 ± 0.5 ppm was deduced.

E. Iodine in thyroid

Because of its small mass and superficial location, as well as its high iodine content, the thyroid represents an ideal subject for "in vivo" XRF-analysis and, for this reason, was the first and perhaps the most studied organ using this method.

Three main directions of research have been followed in this field:

- imaging of the intrathyroidal distribution of natural iodine, which led to the development of the fluorescent scanners of the thyroid;
- quantitation of the thyroidal natural iodine;
- dynamic uptake study of orally administered stable iodine.

The first direction is based on the detection of spatial variations in iodine concentration; this type of measurement is relative and does not require calibration.

Many XRF-iodine scanners have been developed and commercialized; they employ semiconductor-detectors and, all except one, Am-241 sources, which should be very strong to keep the scanning time within reasonable limits as the source must be strongly collimated to obtain good spatial resolution. Sources up to 7.4×10^{11} Bq have been employed. Absolute dose of $10^{-4} - 5 \times 10^{-4}$ Gy on the neck have been measured. A discussion on XRF-scanners can be found in ref. 72.

The "XRF-quantitation" is an absolute measurement, the accuracy of which depends upon how the variability in size, shape and displacement of the thyroid is taken into account in calibrating the measuring system.

From the XRF-scanners the following quantitative values have been deduced for Iodine:

- an approximate mean value of thyroidal Iodine of 10.0 ± 3.5 mg in a groups of normal subjects;
- in case of hyperthyroid Graves' disease, the total thyroidal stable iodine is increased in proportion to the size of the patient's goiter,

implying a concentration of stable Iodine which is not greatly different from normal values; values from 9 to 33 mg I have been measured;

- non-functioning nodules, benign and malignant, invariably contain no detectable stable iodine by the fluorescent technique;
- functioning nodules contain stable iodine in almost all cases, and this content is generally in proportion to the amount of tissue mass present;
- total thyroidal stable iodine content is decreased in many cases of Hashimoto's thyroiditis and undetectable in some of these (values of 2 to 5 mg I have been measured).

For "XRF-quantitation" semiconductor detectors or gas-proportional counters and relatively low activity Am-241 sources have been employed.

An interesting solution of source-detector combination has been developed by Magrini et al. (ref. 73), who analyzed the resulting X-spectrum with a Kr-gas-proportional detector. In this case, a strong "escape-peak" of energy $E_e = E_1 - E_{K-Kr} = 28.5 - 12.6 \text{ keV} = 15.9 \text{ keV}$ for Kr-K -rays is obtained from the interaction of Iodine peaks with Kr-atoms. A typical spectrum is shown in Figure 2.59. The favourable position of the "escape-peak" respect to the back-

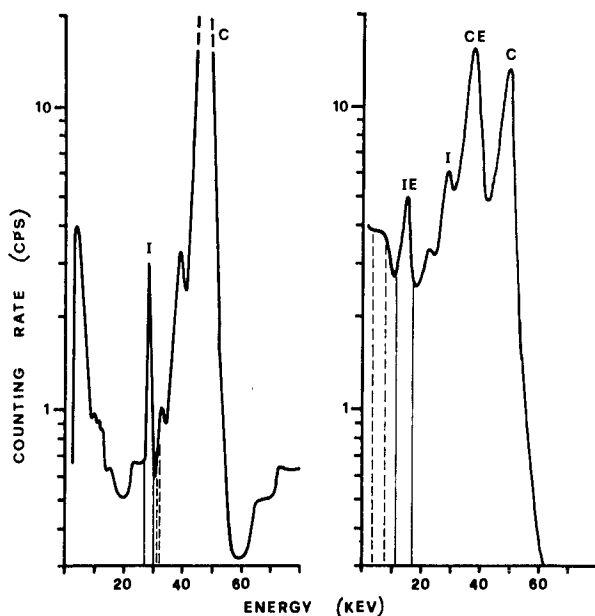


Fig. 2.59. Energy spectra collected by means of a HPGe detector (left; adapted from ref. 74) and a Kr-gas counter (right; adapted from ref. 73) on neck-thyroid phantoms at iodine concentrations comparable with that in normal thyroid. C= Compton scatter peak; I= iodine K_{α} peak; CE= Compton escape peak (Compton energy minus Kr-K fluorescence energy); IE= iodine escape peak (iodine K_{α} minus Kr- K_{α}). Possible choices of the K_{α} window (continuous vertical lines) and the background window (dashed lines) are indicated.

ground is evident. Further, the useful detection area of a gas proportional counter is very large enabling a good detector efficiency. A MDL of about 40 $\mu\text{g/g}$ Iodine was deduced, in 100 s measuring time, which is comparable with the values obtained with semiconductor detectors.

An "XRF-dynamic study" has been performed by the same author (ref. 75). The results obtained in one normal volunteer after administration of 6.2 mg I (0.08 mg I/kg body wt) are shown in Figure 2.60. Successive administration of increasing quantities of stable iodine to the same subject enabled further

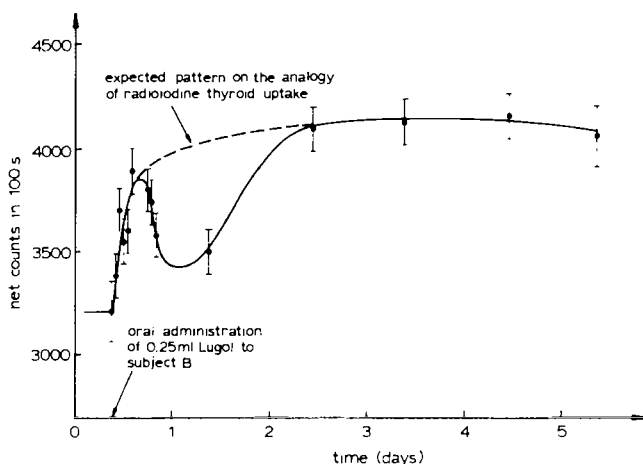


Fig. 2.60. XRF dynamic study in a normal volunteer (P.P., age 53, wt 85 kg) after oral administration of 6.2 mg of stable iodine (after Pavoni et al., ref. 75).

slight increases of intrathyroidal iodine to be detected (see Fig. 2.61). The discharge phenomenon, occurring after the 5th hour, was confirmed in two other normal subjects and is known as the Wolff-Chaikoff effect. The absorbed dose with this method is about 10^{-2} Gy for each measurement.

F. Lead in teeth

An interesting "in situ" application of XRF-analysis was carried out by Bloch et al. (ref. 78), who measured the Pb-concentration in children's teeth in situ. It should be pointed out that excessive Pb exposure to the developing central nervous system of young children may result in permanent neurological damage.

The blood Pb levels decline once exposure to Pb ceases, and hence cannot be considered indicative of the total Pb exposure. The Pb content of primary and permanent teeth of primates was shown to be dependent on the Pb-exposure

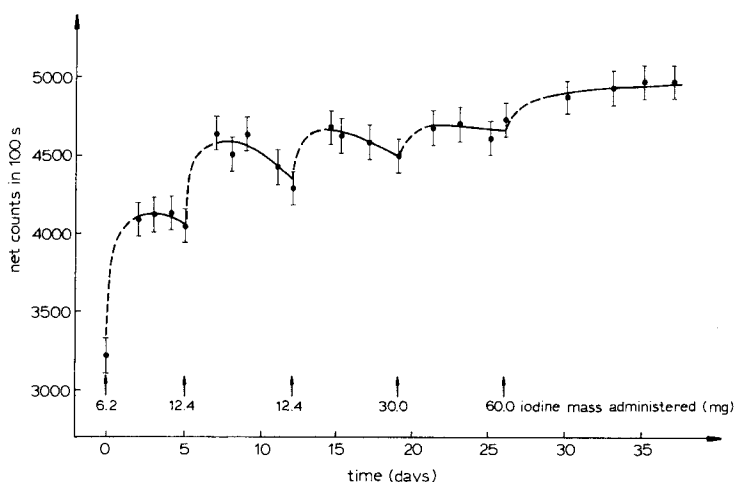


Fig. 2.61. Effect of periodic administrations of increasing quantities of stable iodine in subject P.P. (after Pavoni et al., ref. 75).

and was not reduced by chelation. Both direct chemical analysis of isolated portions of the tooth and electron microprobe microanalysis demonstrated that Pb is concentrated in a circumpulped secondary dentine zone.

In the investigation of Bloch et al., a sealed 2.2×10^8 Bq Co-57 point source was employed to irradiate the teeth and was shielded from the detector with a cylindrical Ta collimator, 1.27 cm in diameter 2.59 cm long. A bone hole 1.11 cm in diameter perpendicular to the cylinder defined the radiation beam.

The fluorescent X-rays of Pb (72.8 keV and 75.0 keV) were detected with an intrinsic Ge-planar detector, having a cross sectional area of 110 m^2 and a thickness of 7 mm.

The number of scattered X-rays was estimated by recording the number of events in the energy interval between the two Pb-X-ray peaks (73.3 to 74.3 keV).

The number of Pb-counts was estimated by recording the number of events in the energy interval 74.5 to 75.5 keV. The ratio between the latter counts and the scattered counts represents, obviously, the number of Pb-fluorescent-X-rays (N_{Pb}) to the number of Compton scattered X-rays N_{C} .

The accuracy of the tooth Pb determination is limited by counting statistics ($N_{\text{Pb}} + N_{\text{C}}$ counts). An approximate sensitivity of about 5 ppm Pb was deduced.

The X-ray exposure to the tooth from the Co-57 sources was calculated to be 0.78 mGy in 100 s, at 1.5 cm from the source. This is approximately the same exposure as from a routine dental examination. Thirty children from the Children's Hospital of Philadelphia suspected of having elevated Pb exposure had tooth Pb levels measured in situ using X-ray fluorescence (see Table 2.26).

TABLE 2.26

Range of the Pb concentration in teeth in a series of 30 children in Philadelphia (after Bloch et al., ref. 78).

Tooth Pb-levels	N _o of children
0 - 9	0
10 - 19	2
20 - 29	8
30 - 39	12
40 - 49	5
50 - 59	3

It should be observed that in a previous report (ref. 82) it was shown that the Pb levels of teeth of Indians living in a remote non industrialized jungle area was 4.3 ± 6.8 ppm, compared to the value 92.3 ± 69.8 ppm measured in Philadelphia. The report of Bloch et al. (ref. 78) shows that XRF-analysis for tooth Pb levels in children presents adequate sensitivity and low radiation exposure. Further, the method has the advantage of being rapid and non invasive.

G. Platinum in kidney

El-Sharkawi et al. (ref. 77) measured the platinum content in the kidney of four cisplatin-treated patients. Platinum, in the form of cisplatin, is used for the treatment of various tumours. One side effect of this treatment is kidney damage.

In the measurements of El-Sharkawi, Pt was detected by using a 259 MBq Co-57 source and a Ge detector in a 90° geometry. The minimum detectable limit for a measuring time of 2000 s was 37 µg/g. In one of the patients, Pt was detected at a level of 30 µg/g.

2.8 CONCLUSIONS

Photon induced X-ray Spectrometry (XRF) is, intrinsically, one of the simplest techniques for analyzing a sample, and gives information over a continuous range of elements and concentrations.

The analytical capacity of the method is determined by the choice of the source (energy and intensity of the exciting radiation, the nature of the sample, and the energy resolution of the detector.

Radioisotope sources, when used with low resolution detectors, operate to

only relatively high limits of detection, but equipments based on these sources are very simple and portable.

At the other extreme, the use of high intensity monoenergetic radiation from an X-ray tube and a high resolution semiconductor detector gives the ultimate in analytical performance and allows elemental concentrations of a few parts per million to be measured.

A further improvement in intensity of exciting radiation, for example using synchrotron radiation, would be useful only for irradiating very small areas, due to the inability of the detector and electronics to process signal pulses faster than a certain rate.

For "in vitro" XRF analysis of biological and environmental samples, the optimum specimen is prepared by deposition of the sample on, or by filtering the sample through, a thin filter. Thin samples give rise to lower limits of detection, and to a linear dependence of fluorescent counts on concentration. Minimum detectable limits of 2-10 ng/cm² have been determined in 10³ s measuring time, for elements with atomic number ranging from about 25 to about 50.

As far as concerns "in vivo" XRF-analysis, no general criteria of optimization can be given and each problem has to be treated separately, taking into account the element to be analyzed and its concentration, and the depth, volume and form of the organ to be irradiated.

Minimum detectable limits of 10-50 µg/g have been determined in a 10² s measuring time, for the following elements and organs: Pb in bone, Cd in kidney, Sr in bone, I in the thyroid, Pb in teeth, Hg in kidney, Pt in kidney.

In XRF-analysis, there is no theoretical limit of detection, for both "in vitro" and "in vivo" analysis, and the limit of detection is due to the ratio between the peak of the element to be analyzed and the underlying background, and to the present inability of the detectors and electronics to process more than 10⁴ - 10⁵ signal pulses per second without losses.

ACKNOWLEDGMENTS

The author expresses his gratitude for their cooperation to the following colleagues:

D. Del Principe, Istituto di Clinica Pediatrica, Università di Roma "La Sapienza";

G.E. Gigante, Dipartimento di Scienze Biomediche, Università di L'Aquila;

G. Mancuso, Istituto di Clinica Pediatrica, Università di Roma "La Sapienza";

B.M. Tallarida, Istituto di Clinica Pediatrica, Università di Roma "La Sapienza";

M. Ricci, Ospedale S. Giovanni, Roma;

M.G. Ciancarelli, Dipartimento di Scienze Biomediche, Università di L'Aquila;

E. Scarnati, Dipartimento di Scienze Biomediche, Università di L'Aquila;

G. Tallarida, Dipartimento di Medicina Interna, II Università di Roma;

E. Alexiu, Istituto di Medicina Legale, Università di Roma "La Sapienza";

S. Merli, Istituto di Medicina Legale, Università di Roma "La Sapienza";

G. Sacchetti, Istituto di Medicina Legale, Università di Roma "La Sapienza";

M. Sgarbazzini, Istituto di Medicina Legale, Università di Roma "La Sapienza";

G. Viezzoli, E.N.E.A., Casaccia, Roma;

A. Magrini, Dipartimento di Medicina Interna, II Università di Roma;

M. Gallucci, Istituto di Urologia, Università di Roma "La Sapienza".

The author also thanks B. Gonsior, Ruhr Universität, Bochum (FRG) for useful discussion and N.D. Pugh, of the University Hospital of Wales, for revision of the text.

Thanks are, also, due to D. Tarsitano for his expert technical assistance and for preparing the illustrative material, S. Ceccarelli for typing the manuscripts and M. Shields for the very careful revision of the English style.

The research was carried out under the auspices of the Centro per l'Ingegneria Biomedica, Università di Roma "La Sapienza". The author expresses his gratitude to the Director of the Centre, C. Bruni.

The research was supported in part by the University of Rome "La Sapienza" and in part by the National Research Council, Contract N. 83.01834.11.

REFERENCES

- 1 W. Bambynek, B. Cravemann, A.W. Fink, H. Mark, C.D. Swift, R.E. Price and P.V. Rao, *Rev. Mod. Phys.*, 44 (1972) 716.
- 2 R.W. Fink and P.V. Rao, *Handbook of Spectroscopy*, Vol. III, CRC Press, Boca Raton, 1981, 125.
- 3 E.C. Mc Cullough, *Med. Phys.* 2 (1975) 307.
- 4 J.H. Hubbell, Wm. J. Veigele, E.A. Briggs, R.T. Brown, D.T. Cromer and R.J. Howerton, *J. Phys. Chem. Ref. Data* 4 (1975) 471.
- 5 K.M. Bisgård, J. Laursen, B. Schmidt Nielsen, *X-Ray Spectrometry*, 10 (1981) 1.
- 6 J.R. Rhodes, *IEEE Trans. Nucl. Sci.*, NS-21 (1974) 608.
- 7 J.H. Hubbell, U.S. Dept. of Commerce, Nat. Bureau of Standards, NSRDS-NBS 29, 1969.
- 8 L.A. Currie, *Anal. Chem.* 40 (1968) 586.
- 9 J.M. Jaklevic in L. Kaufman and D.C. Price (Eds.), *Medical applications of fluorescent excitation analysis*, CRC Press, Boca Raton, 1979, 49.
- 10 J.R. Rhodes in *Energy Dispersion X-Ray Analysis*, ASTM Special Techn. Publ. 485, Am. Soc. for Testing and Materials, Philadelphia, 1971, 243.
- 11 The Radiochemical Centre, Amersham, Radiation sources for laboratory and industrial use, Amersham, Buckinghamshire, England.
- 12 B. Skillicorn, in J.C. Russ, C.S. Barrett, P.K. Predecki, D.E. Leyden (Eds.) *Advances in X-Ray Analysis*, Vol. 25, Plenum Press, New York, 1981, 49.
- 13 R. Vane and B. Skillicorn, in J.B. Cohen, J.C. Russ, D.E. Leyden, C.S. Barrett, P.K. Predecki (Eds.), *Advances in X-Ray Analysis*, Vol. 27, Plenum Press, New York, 1983, 415.
- 14 R. Cesareo and G. Viezzoli, *Phys. Med. Biol.*, 28 (1983) 1209.
- 15 C.J. Sparks, Jr. in H. Winich and S. Doniach (Eds.), *Synchrotron Radiation Research*, Plenum Press, New York, 1980, Ch. 14, 459.
- 16 C.J. Sparks, Jr., and J.B. Hastings, Oak-Ridge National Laboratory, Rep. ORNL-5089, 1975, 8.
- 17 C.J. Sparks, Jr., E. Ricci, S. Raman, M.O. Krause, R.V. Gentry, H.L. Yakel, and J.B. Hastings, *Anal. Chem.*, 52 (1980).
- 18 D.B. Brown, J.V. Gilfrich and M.C. Peckerar, *J. Appl. Phys.* 46 (1975) 4537.
- 19 Reuter-Stokes, X-ray proportional counters, Cleveland, Ohio, USA.
- 20 M. Cuzin, *Nucl. Instr. & Methods*, A 253 (1987) 407.
- 21 M. Singh, A.J. Dabrowski, G.C. Huth, J.S. Iwanczyk, B.C. Clark, A.K. Baird in J.R. Rhodes (Ed.), *Advances in X-Ray Analysis*, Vol. 23, Plenum Co., New York, 1980, 248.
- 22 A.K. Baird in D.K. Smith, C. Barrett, D.E. Leyden and P.K. Predecki (Eds.), *Advances in X-Ray Analysis*, Vol. 24, Plenum Publ. Co., 1981, 337.
- 23 J.S. Iwanczyk, A.J. Dabrowski, G.C. Huth and W. Drummond in J.B. Cohen, J.C. Russ, D.E. Leyden, C.S. Barrett, P.K. Predecki (Eds.), *Advances in X-Ray Analysis*, Vol. 27, Plenum Press, New York, 1983, 405.
- 24 L. Ames and W. Drummond in R. Hubbard, C.S. Barrett, P.K. Predecki, D.E. Leyden, (Eds.), *Advances in X-Ray Analysis*, Vol. 26, Plenum Press, New York, 1982, 325.
- 25 A.J. Dabrowski, in J.C. Russ, C.S. Barrett, P.K. Predecki, D.E. Leyden, (Eds.), *Advances in X-Ray Analysis*, Vol. 25, Plenum Press, New York, 1981, 1.
- 26 J.S. Iwanczyk, A.J. Dabrowski, G.C. Huth, J.G. Bradley, J.M. Conley, A.L. Alber, *IEEE Trans. Nucl. Sci.*, 33 (1986) 355.
- 27 ENERTEC, Charged particles and X-Ray Silicon detectors, Enertec- Schlumberger, Lingolsheim, France.
- 28 M.R. Squillante, R. Farrell, J.C. Lund, F. Sinclair, G. Entine and K.R. Keller, *IEEE Trans. Nucl. Sci.*, 33 (1986) 336.
- 29 G. Riepe and D. Protic, *Nucl. Instr. Methods*, 226 (1984) 103.

- 30 R. Fitzgerald and P. Gantzel, in *Energy Dispersion X-Ray Analysis*, Am. Soc. Testing and Materials, 1971, 3.
- 31 The Nucleus Inc., *The Personal Computer Analyzer*, Oak Ridge, Tennessee, USA.
- 32 T.C. Huang, *X-Ray Spectrom.*, 10 (1981) 28.
- 33 C.E. Feather and J.P. Willis, *X-Ray Spectrom.*, 5 (1976) 41.
- 34 R. Van Grieken, K. Bresselaers, J. Smits, B. Vanderborght and M. Vanderstappen, in R.W. Gould, C.S. Barrett, J.B. Newkirk and C.O. Ruud (Eds.), *Advances in X-Ray Analysis*, Vol. 19, Kendall-Hunt Publ. Co., Dubuque, Iowa, 1976, 235.
- 35 J. Smits, J. Nelissen and R. Van Grieken, *Anal. Chim. Acta* 111 (1979) 215.
- 36 J. Smits and R. Van Grieken, *Anal. Chim. Acta*, 88 (1977) 97.
- 37 R. Van Grieken, H. Robberecht, J. Shani, P. Van Dyck and L. Vos in R. Cesareo (Ed.), *X-Ray Fluorescence in Medicine*, Field Ed. Italia, Roma, 1982, 159.
- 38 D.E. Leyden, in C.L. Grant, C.S. Barrett, J.B. Newkirk and C.O. Ruud (Eds.), *Advances in X-Ray Analysis*, Vol. 17, Plenum Press, New York, 1974, 279.
- 39 F.C. Smith, Jr., and O.H. Masi, in R.W. Gould, C.S. Barrett, J.B. Newkirk and C.O. Ruud (Eds.), *Advances in X-Ray Analysis*, Vol. 19, Kendall-Hunt Publ. Co., Dubuque, Iowa, 1976, 449.
- 40 R. Cesareo and G.E. Gigante, *Water, air and soil pollution*, 9 (1978) 99.
- 41 L.S. Birks and J.V. Gilfrich, *Appl. Spectroscopy*, 32 (1978) 204.
- 42 J.M. Jaklevic and R.L. Walter, in T.G. Dzubay (Ed.), *X-Ray Fluorescence Analysis of environmental samples*, Ann Arbor Sci., 1977, 63.
- 43 E.W. Schneider and R.F. Hill, *Nucl. Instrum. Methods*, 193 (1982) 303.
- 44 R. Cesareo and D. Del Principe, *Med. Phys.* 1 (1974) 163.
- 45 R. Cesareo in R. Cesareo (Ed.), *X-Ray Fluorescence in Medicine*, Field Ed. Italia, Roma, 1982, 1.
- 46 R. Cesareo, *TrAC, Trends in anal. Chem.*, 4 (1985) 65.
- 47 P.S. Ong, P.K. Lund, C.E. Litton and B.A. Mitchell in C.L. Grant, C.S. Barrett, J.B. Newkirk and C.O. Ruud (Eds.), *Advances in X-Ray Analysis*, Vol. 16, Plenum Press, New York, 1973,
- 48 H.H. Sky-Peck and B.J. Joseph, *Clin. Biochem.*, 19 (1981) 126.
- 49 M.S. Rapaport, M. Mantel and C. Shenberg, *Phys. Med. Biol.*, 9 (1982) 194.
- 50 B. Holinska, A. Markowicz, *Int. Report* 130, Krakow, 1978.
- 51 D. Del Principe, R. Cesareo, M.G. Ciancarelli, M. Ricci, B.M. Tallarida, G. Mancuso, *Thrombosis and Haemostasis* 44 (1980) 30.
- 52 R. Cesareo, M.G. Ciancarelli, E. Scarnati, *Med. Phys.*, 7 (1980) 97.
- 53 D.C. Price in L. Kaufman and D. C. Price (Eds.), *Medical applications of fluorescent excitation analysis*, CRC Press, Boca Raton, 1979, Ch. 6, 115.
- 54 D.C. Price, S.J. Swann, S.T. Hung, L. Kaufman, J.P. Huberty, S.B. Shohet, *J. Lab. Clin. Med.*, 87 (1976) 535.
- 55 R. Cesareo, M.G. Ciancarelli, D. Del Principe, M. Ricci, B.M. Tallarida, *Intern. Symposium on Applications and Technology of ionizing radiation*, id, Riyadh, Saudi Arabia, 12-17 March 1982, 495.
- 56 D.C. Price, L. Kaufman, R.N. Pierson, *J. Nucl. Med.* 16 (1975) 814.
- 57 P. Guesry, L. Kaufman, S. Orloff, J.A. Nelson, S. Swann, M. Holliday, *Clin. Nephrol.*, 3 (1975) 134.
- 58 R. E. Jervis, *Isotope Radiation Techn.*, 6 (1968) 57.
- 59 P. Sen, G.K. Mehta, *IEEE Trans. Nucl. Sci.*, 30 (1983) 1302.
- 60 R. Cesareo, E. Alexiu, G. Sacchetti, S. Merli, *Fisica in Medicina*, 2 (1986) 71.
- 61 T. Marcinkowski and M. Pankowski, *Forensic Sci. Int.*, 16 (1980) 1.
- 62 R. Cesareo, S. Merli, G. Sacchetti, E. Alexiu, M. Sgarbazzini, C. Colesanti, G. Cave-Bondi, G. Elena, 6th Mediterranean Conf. of Legal Medicine, Halkidiki, Greece, 24-27 May 1984, 89.
- 63 R. Cesareo, V. Bisceglie, L.J. Pedraza, M. Gallucci, G. Alpi and F. Di Silverio, *Br. J. Urology*, 58 (1986) 253.

- 64 L. Ahlgren, In vivo X-Ray fluorescence analysis, Thesis, Lund. Univ. (Sweden) 1980.
- 65 L. Ahlgren, S. Mattsson, Phys. Med. Biol., 14 (1979) 136.
- 66 L. Wielopolski, K.J. Ellis, A.N. Vaswani, S.H. Cohn, A. Greenberg, J.B. Puschett, D.K. Parkinson, D.E. Fetterolf and P.J. Landrigan, Am. J. Ind. Med., 9 (1986) 221.
- 67 L.J. Somervaille, D.R. Chettle, M.C. Scott, Phys. Med. Biol. 30 (1985) 929.
- 68 L.J. Somervaille, D.R. Chettle, M.C. Scott, A.C. Aufderheide, J.E. Wallgren, L.E. Wittmers Jr., G.R. Rapp Jr., Phys. Med. Biol. 31 (1986) 1267.
- 69 L. Wielopolski, D. Vartsky, S. Yasumura and S.H. Cohn, in C.R. Hubbard, C.S. Barrett, P.K. Predecki and D.E. Leyden (Eds.), Advances in X-Ray Analysis, Vol. 26, Plenum Publ. Co., New York, 1983, 415.
- 70 L. Ahlgren, S. Mattsson, Phys. Med. Biol., 26 (1981) 19.
- 71 J.R.H. Smith, S.S. Athwal, D.R. Chettle, M.C. Scott, Int. J. Appl. Radiat. Isotopes, 33 (1982) 557.
- 72 L. Kaufman, in L. Kaufman and D.C. Price (Eds.), Medical applications of fluorescent excitation analysis, CRC Press, Boca Raton, 1979, Ch. 5, 91.
- 73 A. Magrini, S. Di Luzio, G. Izzo, L. Raganella, in R. Cesareo (Ed.), X-Ray Fluorescence in Medicine, Field Ed. Italia, Roma 1982, 87.
- 74 J.A. Patton and A.B. Brill, J. Nucl. Med., 19 (1978) 464.
- 75 P. Pavoni, F.V. Frazzoli and A. Magrini, Eur. J. Nucl. Med., 1 (1976) 464.
- 76 P. Bloch, G. Garavaglia, G. Mitchell, I.M. Shapiro, Phys. Med. Biol., 20 (1976) 56.
- 77 A.M. El-Sharkawi, W.D. Morgan, S. Cobbald, M.B.M. Jaib, C.J. Evans, L.J. Somervaille, D.R. Chettle and M.C. Scott, The Lancet (1986) 249.
- 78 P. Bloch, G. Mitchell, J.M. Shapiro, G. Garavaglia, IEEE Trans. Nucl. Sci. NS-24 (1977) 577.
- 79 L. Wielopolski, J.F. Rosen, D.N. Slatkin, D. Vartsky, K.J. Ellis and S.H. Cohn, Med. Phys. 10 (1983) 248.
- 80 L. Wielopolski, J.D.B. Featherstone, S.H. Cohn, Proc. V Conf. on Nuclear Methods in environm. and energy research, Puerto Rico, April 2-6, 1984, 742.
- 81 D.A. Gollnick and M.A. Greenfield, Radiology 126 (1978) 197.
- 82 I.M. Shapiro, G. Mitchell, I. Davidson and S.H. Katz, Arch. Environm. Health 30 (1975) 483.

Chapter 3

PARTICLE INDUCED X-RAY EMISSION (PIXE)

BERNHARD GONSIOR

Ruhr Universität Bochum

Institut für Experimentalphysik III

Postfach 102148, D-4630 BOCHUM (Federal Republic of Germany)

3.1 INTRODUCTION

The analytical use of particle induced X-ray emission (PIXE) spectroscopy has become an important tool in the biomedical field, especially in those cases, where only small amounts of sample matter are available.

Since it became obvious that trace elements, especially trace metals, play an important role in biological systems, the application of this method in the fields of medicine and biology turned out to be of high importance. The assumption is, that the distribution of trace elements in the biological organism is correlated to metabolic processes. Therefore the investigation of biological materials plays a decisive role in bioengineering research. Even one can conclude, that investigations in the biological microstructure should be done, because it is obvious, that the spatial distribution of trace elements has to be connected to cooperative cellular colonies.

The application of atomic and nuclear physics methods using small accelerators on biological and medical problems is a fast growing field during the last years. Many analytical techniques, e.g. based on characteristic X-ray emission have been developed. In 1970 the first measurements were published on the application of spectroscopy to trace analytical problems (ref. 1).

In different review articles (refs. 2-5) the physical principles of induced X-ray emission and examples of application have been described. Conferences have been currently devoted to this topic (refs. 6-7). Other conferences took place where particle beam analytical work in a broader scope or trace element analysis under the aspect of special applications have been discussed (refs. 8, 9, 10, 11). The principal aim of this chapter is a concise review of the physical basis and of all facts of importance using PIXE for quantitative analytical purposes. The main field of interest will be restricted to low concentrations i.e. to trace elements. In many fields of applied analysis a deep knowledge of physics is not necessary though; but during the

last years, certain analytical problems especially in the fields of biology, medicine and environmental research turned out to be highly interesting. In those cases the utmost power of detection, where at the same time only small amounts of material were available, was asked for; this in turn is connected to a delicate optimization of all physical parameters like conditions of inducing X-rays, background considerations, sample properties and preparation, calibration, accuracy and precision etc.. Here a consideration of all functional relationship relevant to high detection limits is of essential importance. This will be demonstrated. Illustrating examples will be given.

To this end we first recall in form of an outline the basic physical considerations of particle induced X-ray emission (see Section 3.2). The analytical technique bases on the detection of characteristic X-rays. So we start with a short description of the emission process, whereas later the excitation of the atom by incident ions is discussed. The details of the analytical procedure are in most cases tightly connected to the analytical problem under investigation. Therefore the principles of application are discussed referring to the decisive parameters like background, yield of characteristic X-rays and detection limits (see Section 3.3). As incident ions one can use protons, deuterons, α -particles or heavy ions. After having considered the general principles, we will concentrate on protons as impinging particles since in most cases these ions are used. In addition we compare in this section the two different modes of excitation, i.e. X-ray fluorescence (XRF) and PIXE regarding detection limits, precision and accuracy.

Reflecting the above discussion, the experimental set-up will be described (see Section 3.4). This will include PIXE, as the conventional analysis under vacuum conditions (Section 3.4.1.(a)), PIXE-E, the analysis with an external ion beam (Section 3.4.1.(b)) and the proton microprobe as well. A short subsection on PIGE will be appended. Also the detection of X-rays and target preparation techniques will be discussed in corresponding subsections.

Finally we present main topics of biomedical applications (see Section 3.5) observing two different aspects; mean elemental composition of a piece of biological tissue as a whole and microstructural properties of matter where the local property cannot be extrapolated from the one in bulk material. Besides we summarize a wide variety of analytical work grouped under various aspects in table form. We conclude reflecting potentialities and limits of the method and perspecting future developments.

3.2 PHYSICAL PRINCIPLES OF PIXE

In this section the basic principles of exciting atoms by ion impact and

the subsequent relaxation by emission of X-rays is described. Knowledge of these principles is important for optimizing the sensitivity in a given problem of analysis. Even in those cases of routine work where requirements in power of detection are moderate and where calibration by standards is feasible this detailed description will be of importance.

The ionization or excitation of atoms, i.e. the creation of vacancies in the electronic cloud, is considered to arise by the electromagnetic interaction between the bound electron and the incident particle. The basis for the analysing procedure is the registration of characteristic X-rays. Therefore in Section 3.2.1. we start with describing the emission of characteristic X-rays by filling vacancies in inner atomic shells. The production of these inner shell vacancies depending on type and energy of the exciting ions is described in Section 3.2.2.

3.2.1 The emission of characteristic X-rays

Whenever vacancies in the atomic shells are created they become refilled by electrons from outer shells. Thereby electromagnetic radiation with well-defined energy will be emitted. The energy of the radiation equals the difference in binding energy of the electronic shells participating in the transition and is therefore characteristic in energy for each emitting atom. The corresponding law (Moseley, 1913) relates the wavelength, i.e. the energy, of the emitted radiation to the atomic number Z of the respecting element. In all cases of interest the energy of the impinging ions is high enough, so that inner shell ionization occurs and the emitted radiation belongs to the X-ray regime. Characteristic X-rays are emitted.

In Figure 3.1 an atomic level scheme is given, which represents the electronic shells and shows the main X-ray transitions. The labelling we use is that given by Bearden (ref. 12). Details of the transition processes are described in Section 3.3.2.

Not all electron vacancies created result in emission of characteristic X-rays when being refilled. There are other kinds of transitions of less importance for analytical purposes; therefore the probability of X-ray emission following the transition to lower shells is reduced.

The ratio of vacancies filled by emission of X-ray quanta to the total number of vacancies in a shell is called fluorescence yield ω , with $\omega < 1$. Reference is given to Section 3.3.3 and to a review paper by Bambynek (ref. 13).

3.2.2 Inner shell ionization by incident ions

In order to detect an atom due to its characteristic X-ray quanta an

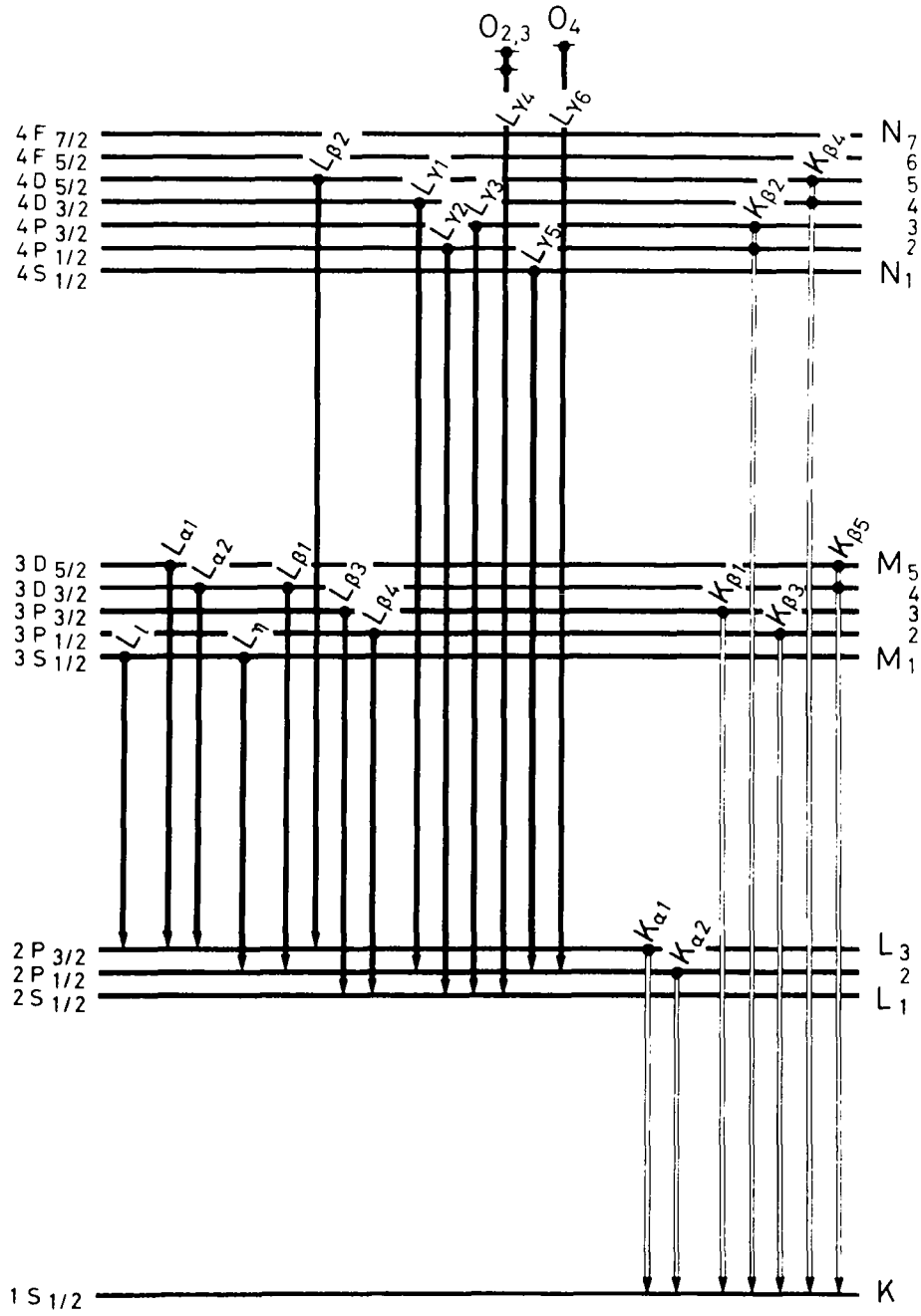


Fig. 3.1. Level scheme with the most intense X-ray transitions.

electron from an inner atomic shell must have been ejected, so that a vacancy has been created. In this chapter we consider the impact of atomic electrons with incident ions initiating this process.

In the previous Section 3.2.1 we have started with the description of the emission of characteristic X-rays as the direct link to analysis. But, from the physical point of view, the first step is the ionization, whereas emission of X-rays and ionization of the corresponding atoms are intimately connected. This will be considered in the present section.

The probability of producing a vacancy by an incoming ion is described by the ionization cross section σ_i , whereas the probability of emission of characteristic X-ray quanta is given by the cross section for production of X-rays σ_x . This cross section is defined in the following way:

$$\sigma_x = \frac{\text{number of X-ray emitting reactions/target particle} \cdot \text{second}}{\text{number of incident particles/second} \cdot \text{cm}^2}$$

Obviously the cross section is given in cm^2 , and the unit is $[\sigma_x] = 10^{-24} \text{ cm}^2$ which is called 1 barn.

The concept of cross section is demonstrated in Figure 3.2. For conve-

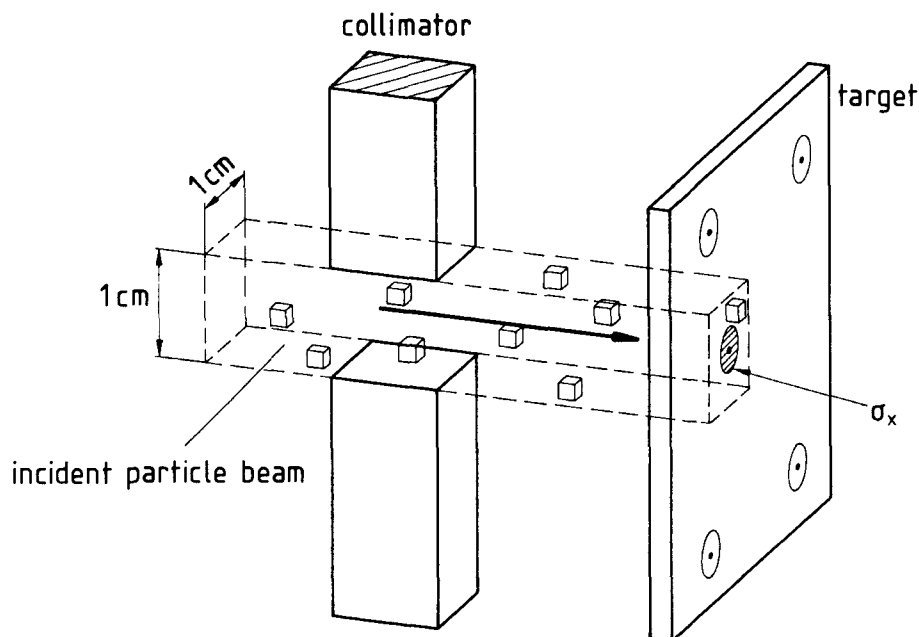


Fig. 3.2. Concept of cross section

nience we collimate the incident particle beam, so that it irradiates the finite area of 1 cm^2 . Then in 1 second, as illustrate in Figure 3.2, the particle content of a cylinder will impinge on the target. This is the number of incident particles/(second $\cdot\text{cm}^2$) given in the denominator of the equation for σ_x . We assume that in the target area the impinging beam of particles can "see" in depth just one target particle.

We count the number of reactions under consideration per each target particle and per number of incident particles, normalized to unit area and to unit time. So, the cross section can be visualized as the hypothetical area surrounding each target particle, through which those incident particles must pass to undergo the specified reaction.

Every emitted X-ray quantum requires a previous ionization, but - as outlined in Section 3.2.1 - not every ionization is followed by the emission of an X-ray quantum because there are also radiationless transitions. So, the cross section σ_x is proportional to the ionization cross section σ_I with the fluorescence yield $\omega < 1$ mentioned above, and we have

$$\sigma_x = \omega \cdot \sigma_I \quad (1)$$

describing the link between the X-ray quanta emitted and the corresponding atoms ionized.

In Section 3.3.2. we use σ_x to discuss the relationship between the actual number of X-ray quanta detected, the actual number of particles in the primary beam and the X-ray emitting target atoms under consideration. The analytical aim is to find this number of atoms. Actually this number of atoms can be given as a mass per cm^2 crossed by the beam. This is so called thickness of the target in terms of mass per unit area. One considers the area of the sample, which is transversed by the particle beam. The mass layer is given in units of $\text{g}\cdot\text{cm}^{-2}$. On the basis of the area irradiated we can directly speak of the mass of a substance given in g. E.g. we get a measure for the amount of a certain element under investigation in relation to the target specimen as a whole. We arrive at concentrations.

In this section we put our emphasis onto the excitation or ionization of inner shells. This process has been investigated for many years (refs. 14, 15) and is well understood now; cross sections can be predicted with a high degree of confidence (refs. 16, 17). In the following we give a comprehensive description of the excitation mechanism and the dependence of the ionization cross section upon the conditions of excitation.

Generally ionization by accelerated ions can be described by the Coulomb interaction of the projectile assumed to be a point charge with one electron

in the target atom.

To get quantitative analytical results one has to start from the rate of the experimentally detected X-rays, the so-called X-ray yield

$$Y_x = f(\sigma_x) \quad (2)$$

which depends on the X-ray production cross section. One can write while observing Eq. 1

$$Y_x = a \cdot \sigma_x = a \cdot \omega \cdot \sigma_I \quad (3)$$

where a includes quantities representing the analysing procedure to be outlined in Section 3.3.2. Especially the number of X-ray emitting atoms i.e. the quantity to be analysed is contained in a . Therefore, to arrive at a quantitative result after having obtained experimentally the X-ray yield Y_x from Eq. 3 one can see that the ionization cross section σ_I must be known. This cross section can be measured or theoretical predictions be applied. Also, standard samples can be used in analytical work. In any of these cases, at least an inspection of the ionization cross section for the electron shell under consideration as a function of the projectile energy, mass and charge and of the atomic number of the atom to be ionized is useful to estimate the obtainable detection limit and the optimum experimental conditions.

The cross section increases with the projectile energy E_p reaching a maximum where the projectile velocity equals the orbital velocity of the electron, which means, that under this condition the passing ion is especially apt to transfer energy to the orbiting electron. With further increasing projectile velocity the ionization cross section decreases roughly proportional to $1/E_p$.

This relationship between cross section and energy of the projectile is represented in Figure 3.3, where the energy is given in units of $(m_p/m_e)E_B$, thus normalizing the energy of the projectile to the energy of the orbiting electron. Clearly the maximum of the ionization cross section shows up where the abscissa value equals unity.

On the other hand the ionization cross section, as far as the dependence upon the atomic number Z of the trace element is concerned, drastically decreases due to the increasing binding energy of the electrons. This is represented for the cases of the K- and L-shell ionization respectively in Figure 3.4. In this figure also the ionization cross sections for impinging α -particles are given. As a rough estimate one can describe the relationship between ionization cross sections arising from projectiles with differing

atomic numbers by the scaling law

$$\sigma_I(\text{projectile } p, E_p) = Z_p^2 \cdot \sigma_I(\text{proton}, E_p \cdot A_p^{-1}) \quad (4)$$

connecting σ_I of any projectile p with mass number A_p and atomic number Z_p to the σ_I of a proton with energy $E_p \cdot A_p^{-1}$.

To give an example: We ask for the ionization cross section for α -particles ($Z_p = 2$, $A_p = 4$) at an α -particle energy $E_p = 10$ MeV. Assuming the

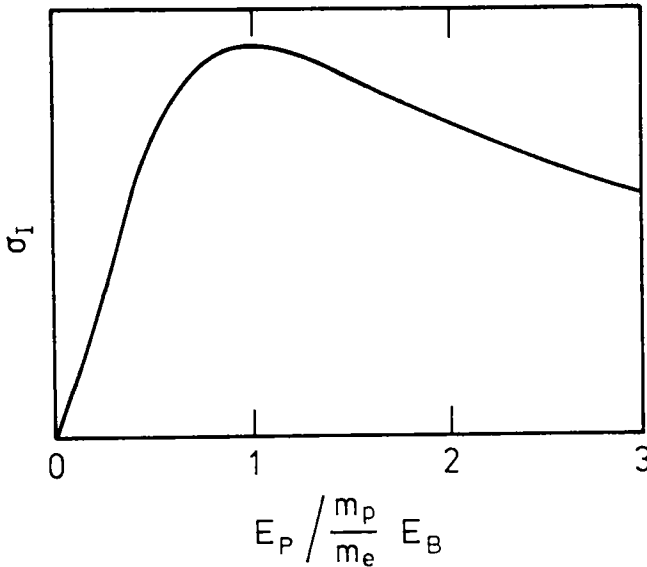


Fig. 3.3 Schematic diagram of the ionization cross section as a function of the projectile energy (in units of $(m_p/m_e) \cdot E_B$).

ionization cross section is well known for protons with a proton energy $E_p \cdot A_p^{-1} = 10 \text{ MeV} \cdot 4^{-1} = 2.5 \text{ MeV}$, than multiply this cross section by $Z_p^2 = 4$ to get the ionization cross section for α -particles asked for. Using this prescription ionization cross sections unknown for heavier particles can be calculated from the well known ionization cross sections for protons, at least in the energy regime of PIXE.

3.3 PRINCIPLES OF THE USE OF PIXE FOR TRACE ELEMENT ANALYSIS

For the detection of X-rays wavelength-and energy-dispersive techniques can be used. In wavelength-dispersive spectrometers the X-rays are diffracted

by a crystal according to the Bragg law and then counted at an angle corresponding to the characteristic wavelength. These spectrometers are in use only up to a few keV of X-ray energy, e.g. K-X rays of atoms with small atomic numbers. The apparatus is expensive, mostly used in research where highest resolution is necessary, and we are not going to discuss it in connection with applicational purposes.

In energy-dispersive X-ray spectrometry the gas proportional counter can be used if the interest is concentrated on the investigation of a small number of distinct elements. The usefulness is limited due to its poor energy resolu-

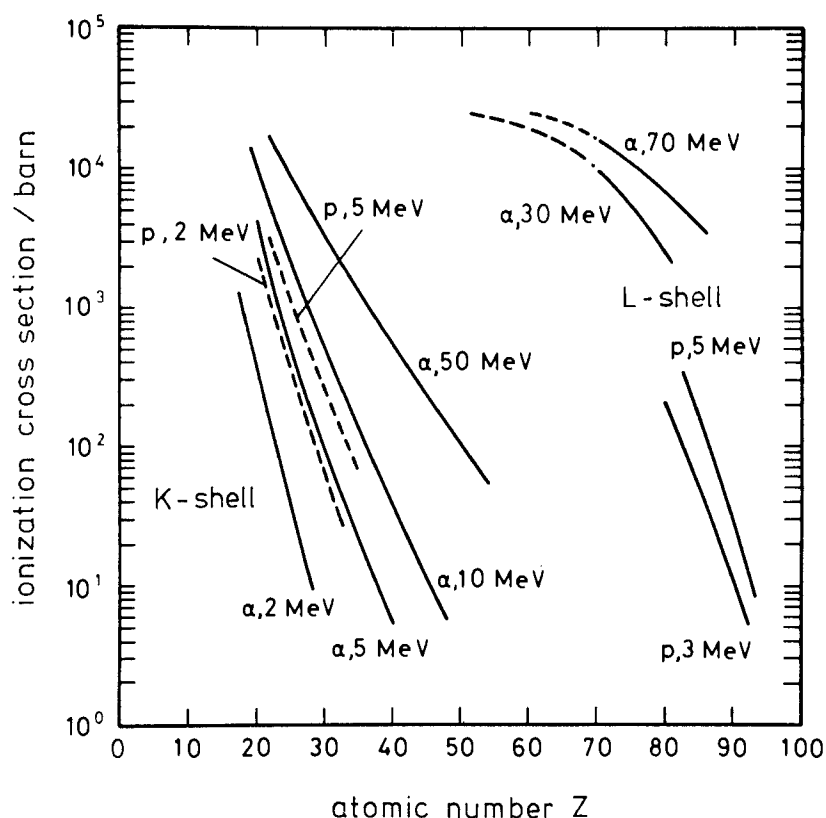


Fig. 3.4 K- and L-shell ionization cross section vs the atomic number for protons and α -particles of different energies.

tion, but it is a relatively inexpensive instrument.

On the other hand, the fast growing development of semiconductor detec-

tors brought these instruments widely in use as X-ray spectrometers for trace element analysis. Since in 1970 PIXE analysis (ref. 1) was introduced into analytical chemistry, numerous publications demonstrated the successful application of this technique (refs. 6, 7, 8, 9, 10, 11, 19) to the determination of trace elements in various types of samples. A careful description of wavelength-dispersive in comparison with energy-dispersive spectroscopy has been given recently (ref. 18).

The principle of analysis is the same in all cases. Incoming charged particles, in most cases protons of 2...3 million electron volt (MeV), interact with the electrons in the atomic shell. If the energy transferred to the electron is sufficient to ionize the atom under consideration a vacancy is created that can be filled by an electron from outer shells. Characteristic X-rays will be emitted and are detected by energy- or wavelength-dispersive spectroscopy. The physical details have been described in Section 3.2.

The resulting spectrum contains the lines of different transitions (Fig. 3.1) corresponding to the elements present in the sample. In this way identification of trace elements is possible. A typical spectrum is given in Figure 3.5. It represents a measurement on a sample of human liver.

As can be seen from Figure 3.4 and from Figure 3.5 K- as well as L-radiation can be used for analysis of elements. In the regime of low atomic numbers the K-X ray yield turns out to be higher, whereas in the regime of high atomic numbers L-radiation should be detected with advantage.

The energy resolving capability of a semiconductor detector is sufficient to resolve K_{α} - or L_{α} -lines of elements with adjoining atomic numbers Z rendering possible the simultaneous determination of these elements. The possibility of the simultaneous determination of many elements in trace amounts in one sample is one of the great advantages of this method.

In spite of the good energy resolution of semiconductor detector spectroscopy there may, however, arise problems in certain cases. This is possible e.g. when one tries to determine a trace element in the presence of large amounts of elements with adjacent Z . There are also problems associated with interferences where the K-line of one element falls close to the L-line of another element with a higher atomic number.

To arrive at a quantitative analysis, one has to use a relation between the integral under the characteristic X-ray line i.e. the X-ray yield and the amount of the trace element under investigation. This is already given in Eq. (3) and will be outlined in Section 3.3.2.

Applicability and detection limit of the method depend on the ratio of the characteristic X-ray yield to the amount of background radiation present in the energy region of the X-ray line. The term "detection limit" has to be

used with much care, especially if comparison of different excitation methods in X-ray spectrometry and their analytical results should be done. A detailed discussion, therefore, is necessary and will be performed in the following subsections. An estimation of detection limits achievable requires not only a knowledge of the ionization cross section and the fluorescence yield to evaluate the intensities of the analyte lines but also a consideration of the spectral background or blank intensities.

The background spectrum one would obtain for a blank sample using 10 MeV protons as incident ions to induce X-rays appears schematically as in

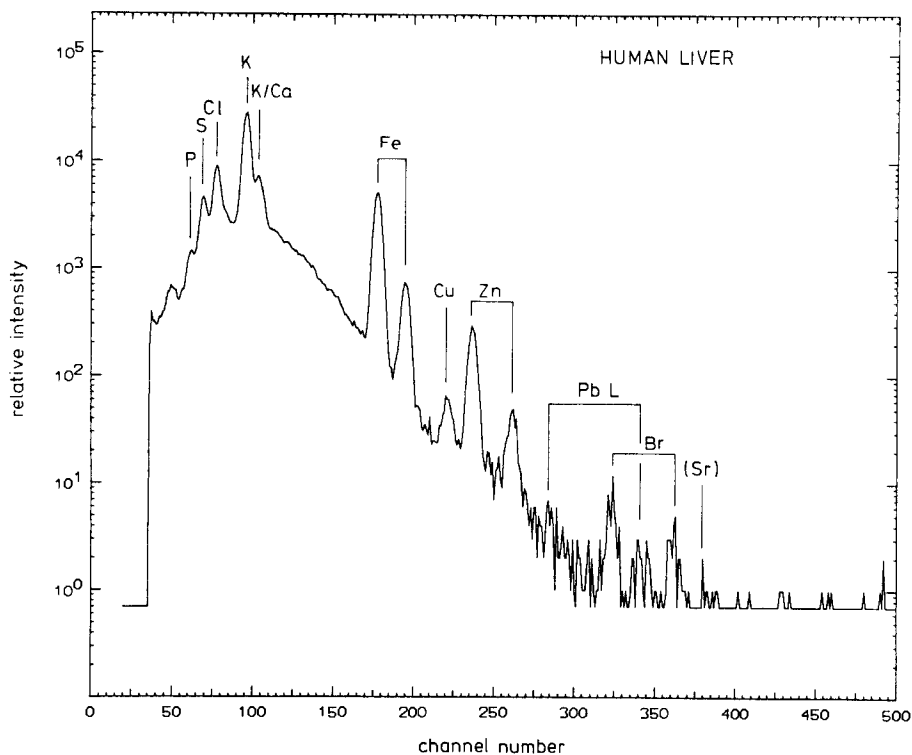


Fig. 3.5 Typical X-ray spectrum of a human liver sample.

Figure 3.6. The relative intensity of X-rays vs. their energy E_x given in keV is shown. The background in PIXE is dominated by bremsstrahlung created by the slowing down of energetic secondary electrons produced by the ion beam in the target. The result is a continuous spectrum. In the case of electron

excitation like in the scanning-electron microscope the resulting detection limit is inferior by about two orders of magnitude due to the higher background, which is mainly produced by the slowing down of the primary electrons.

The background contribution depends strongly on the experimental conditions. Therefore a detailed estimation of the detection limit connects only to a given experiment. This is the more true since the matrix of the sample under investigation is the main source of background. On the other hand having proper insight into a certain analytical problem the conditions for the best experiment can be found. It is the very goal of this section to furnish the

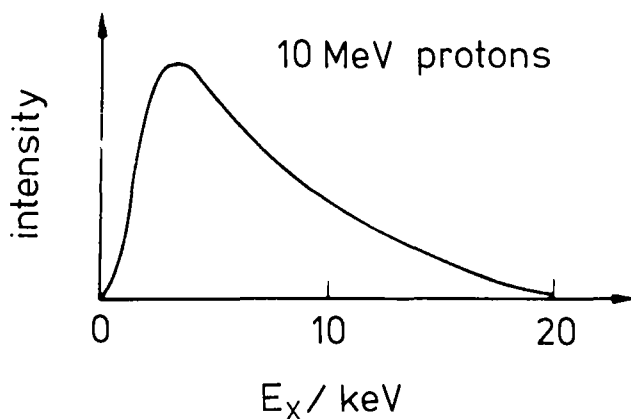


Fig. 3.6 Schematic background spectrum produced by protons of 10 MeV impinging on a sample target. The relative intensity is depicted vs the X-ray energy in keV.

criteria to this end. In case of PIXE analysis generally detection limits in the ppm region can be achieved if optimum experimental conditions are observed. Small amounts of material are sufficient. Experiments have been done with amounts of less than 1 mg. The detection limits obtained as far as the absolute amount of trace elements is concerned depend on the sample area irradiated. Using a beam of 2 mm diameter a sample thickness of $10 \mu\text{g}/\text{cm}^2$ and a detection limit of $10^{-5} \mu\text{g}/\text{g}$ quantities of $5 \cdot 10^{-12} \text{ g}$ can be detected. Collimating the impinging beam to a smaller diameter one can detect lower quantities. Taking a beam diameter of $10 \mu\text{m}$ and a beam current of 1 nA quantities of 10^{-16} g become detectable. It has been demonstrated that well collimated ion beams and PIXE can be used to investigate lateral trace element distributions with high spatial resolution and detection limits comparable to those with the broad beam technique (refs. 20, 21, 22, 23, 24, 25, 26).

In the following subsections details of the analysis will be outlined: the problem of the background radiation (3.3.1), the evaluation of the characteristic X-ray yield (3.3.2); the data analysis itself with the consideration of the calibration, the detection limits and the evaluation of accuracy and precision (3.3.3). A comparison between XRF and PIXE under optimized conditions is given in the final subsection (3.3.4).

3.3.1 Background radiation

Since trace elements are to be detected background corrections are necessary. The ion-induced X-ray spectra contain the characteristic spectral lines due to the elements under investigation superimposed on a continuous background in the same energy region as seen in Figure 3.5. It is essential for trace element analysis to minimize this background. Mainly two processes contribute to the background:

1. Production of bremsstrahlung by secondary electrons or projectiles in the Coulomb field mainly from the matrix atoms in the target.
2. Background due to Compton scattering (inelastic scattering) of γ -quanta in the detector or in its environment; those γ -quanta are produced mainly through nuclear reactions by the projectiles with the nuclei of the matrix atoms. Figure 3.7 shows the bremsstrahlung background vs. the X-ray energy normalized to an X-ray energy interval, for the case of 3 MeV protons impinging on a carbon foil. Carbon is typical for many matrix materials of biological origin.

Secondary electron bremsstrahlung (SEB) dominates in the energy region below and around E_m , the highest amount of energy transferable to a free electron at rest by a projectile of mass m_p and energy E_p ,

$$E_m \approx 4 \cdot m_e \cdot m_p^{-1} E_p,$$

where m_e is the electron mass.

Up to E_m the cross section for the production of bremsstrahlung decreases slowly with rising X-ray energy. Above E_m the cross section decreases strongly. Through the higher energy region the projectile bremsstrahlung (PB) dominates. This contribution is proportional to $1/E_x$. As far as the projectile energy is concerned the cross section of SEB is growing whereas the PB contribution falls off with rising projectile energy.

The second important contribution to the background arises through Compton scattering of γ -quanta in the detector and its environment. An accurate identification of this background contribution is difficult, though experiments could show that it is larger for α -particles and heavy ion projec-

tiles than for protons with equal velocity (ref. 27), and is increasing with the projectile energy. To suppress this background contribution nuclei with low energy nuclear levels like ^{19}F and ^{23}Na should be avoided in the target and its environment.

Above all, fluctuations in these background contributions can hide real lines from trace elements. In order to determine background fluctuations, which are decisive for the detection limits (3.3.3.b), measurements of the background radiation must be repeated many times.

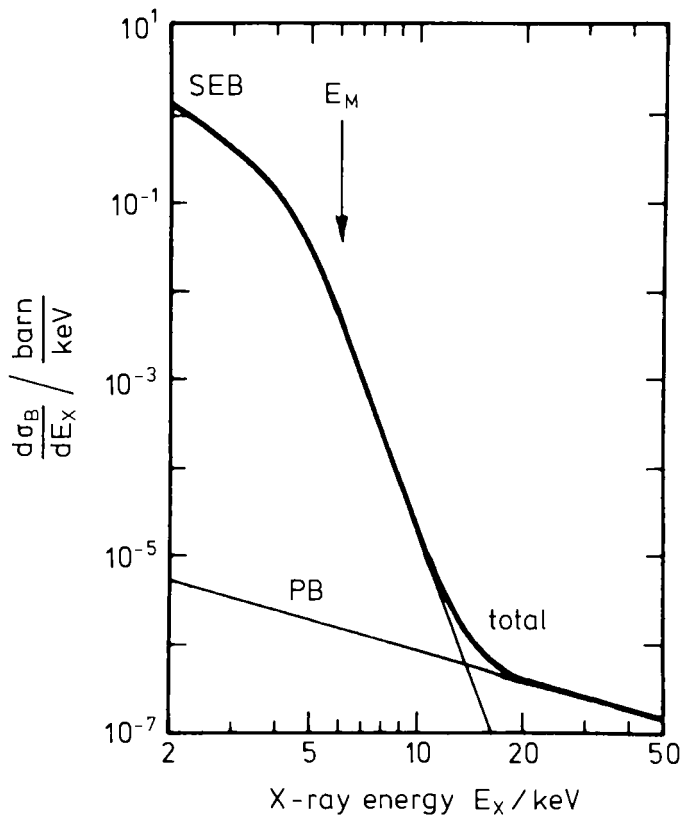


Fig. 3.7. Differential bremsstrahlung cross section for the irradiation of a carbon matrix by 3-MeV protons. The experimental background mainly consists of the secondary electron bremsstrahlung (SEB) for lower energies and of the proton bremsstrahlung (PB) for higher energies.

3.3.2 Characteristic X-rays

In a previous Section (3.2) we have given the outline of the physical

basis regarding the relation between the X-ray yield to achieve and the parameters of the excitation process i.e. kind and energy of the ions. By X-ray yield we mean the number of X-ray quanta of interest detected. In order to get this number one has to integrate the corresponding line area in the X-ray spectrum subtracting the background in the same energy region. This number is related to the amount of a certain element in the sample taking into account the total number of projectiles per cm^2 passing through the sample and exciting X-rays. On the other hand the measured X-ray yield is determined by physical quantities like the X-ray emission cross section (projectile energy and atomic number dependent), the fluorescence yield, the efficiency of the X-ray detector, the absorption in any material between sample and X-ray detector and the X-ray accepting solid angle of the detector. Using these physical quantities the relationship between the measured X-ray yield for a certain K or L spectral line and the mass of a specific element is given by the following formular (compare Eq. (3))

$$Y_x = \sigma_I \cdot \omega \cdot T_M \cdot N_A \cdot A^{-1} \cdot \Delta\Omega (4\pi)^{-1} \cdot \epsilon \cdot n \cdot (\sin\theta)^{-1} \quad (5)$$

with the following quantities:

Y_x	measured X-ray yield
σ_i	ionization cross section
ω	fluorescence yield
T_M	mass layer $/\text{g}/\text{cm}^2/$ (cfr. Section 3.3)
N_A	Avogadro's constant
A	molar mass
$\Delta\Omega$	solid angle of the detector
ϵ	efficiency (including all absorbing components of the set-up)
n	total number of the projectiles
θ	target angle with respect to the beam axis

From this formula one can isolate the physical and instrumental quantities to arrange the so-called "yield factor" for characteristic X-rays ϱ_x , which is defined as

$$\varrho_x = \sigma_I \cdot \omega \cdot N_A \cdot A^{-1} \cdot \Delta\Omega \cdot (4\pi)^{-1} \cdot (\sin\theta)^{-1} \cdot \epsilon \quad (6)$$

This yield factor can be determined experimentally and depends on the atomic number Z , since σ_I and ω are a function of Z . Doing this and using Eq. (5) the experimentally determined thickness is given as follows

$$T_M = Y_x \cdot (\varrho_x \cdot n)^{-1}$$

Using the previous equations and the measured characteristic X-ray yield the mass layer of the trace element under investigation, i.e. the mass per unit of area can be determined in principle observing one of the following prescriptions:

- 1) Using theoretical ionization cross sections (refs. 16, 17), tabulated values of the fluorescence yield (c.f. 3.2.3) and the measured X-ray yield the mass layer can be determined. Thereby the detector efficiency as well as experimental numbers like detector solid angle, corrections for absorption and total number of projectiles must be known. Generally this is difficult in practical work and correspondingly represents a source of error. To avoid these problems one can use
- 2) the method of X-ray yield curves. This method is recommended in those cases where a large number of analyses is to be performed using a fixed apparatus. For such analytical work the yield factors ϱ_x can be determined for a set of different elements using pure targets of known thickness. Since the yield factors include the properties of the detector system they are only valid for the same system and form the calibration basis in order to get the absolute amount of trace elements. The smooth dependence on Z allows for fitting the experimental yield factors of different elements and for interpolating the yield factors for all elements, which results in the so-called yield curves. The determination of the yield factors and the resulting yield curves has been described elsewhere (ref. 28). Similar to this method is
- 3), where in cases of routine application to a few certain trace elements standard samples are available. A quantitative analysis of the sample under consideration then is possible by direct comparison with the standard sample. A prerequisite consists in the fact, that the sample to be analysed and the standard sample are comparable as far as chemical composition, material properties like thickness, magnitude of concentration etc. are concerned. Standards of this kind can be ordered e.g. at the National Bureau of Standards (NBS) and at the International Atomic Energy Agency (IAEA).

3.3.3 Data analysis

In the two preceding subsections the background radiation and the yield of characteristic X-rays have been described. This is the basis for the data analysis. Since traces are to be detected, - the corrected line intensities, i.e. the net counts after subtraction of the background values must be evaluated -, a careful procedure is obligatory. This is the more necessary, if comparison of the results from PIXE and those obtained from other methods e.g.

XRF has to be done. Measuring procedures must be repeated so that mean values can be calculated. Also the blank-value fluctuations are to be determined, which are decisive for the detection limits. Details of this procedure are given elsewhere (ref. 29).

(a) Calibration

There is always the influence of systematic errors which has to be reduced to improve the accuracy of the analysis. After the m -fold measurement of the corrected line intensities, mentioned above, to get the mean values \bar{I}_L , these values are normalized either to the background ($I_N = \bar{I}_L/I_U$, i.e. the intensity ratio of the analyte line and the background in the same energy region) or better to some line of an internal standard ($I_N = \bar{I}_L/I_S$). This is well known in spectrochemistry (refs. 30, 31). To determine the three characteristic figures of merit: detection limit, accuracy and precision, a calibration by means of regression is required. For the following discussion we will assume, that the calibration range of the element content is smaller than one order of magnitude, so that the precision of intensity measurements is nearly uniform. A simple regression between the intensity ratio I_N and the independent variable, the concentration c , may be carried out. If the assumption of uniform precision is not valid, which is true if the range of content covers more than one order of magnitude, a transformation of the variables has to be performed before the linear regression (ref. 32) is done.

A linear regression, the calibration function,

$$I(c) = a + b \cdot c \quad (7)$$

yields the ordinate intercept a and the slope b of the regression straight line. The fit to this line is characterized by the standard deviation S_R of the measured values, also called the standard deviation of residuals

$$S_R = \sqrt{m \cdot (n-2)^{-1} \cdot \sum_i (\bar{I}_i - I_i)^2} \quad (8)$$

with the following quantities:

- \bar{I}_i mean value of the m -fold measurements
- I_i the calculated values of the regression line belonging to c_i
- n number of calibration samples with running index i

In Figure 3.8 a linear regression, i.e. calibration with the number of calibration samples $n = 5$ and with ($m = 4$)-fold measurements is given.

The quantities a , b and S_R have to be determined for each element separately. They describe the characteristic figures of merit: detection limit,

accuracy and precision.

(b) Detection limits

In preceding sections the background radiation and the yield of characteristic X-rays have been described. Determination of the detection limits depends on both of them. The achievable X-ray yield from trace elements as well as the background radiation resulting from the matrix material depend on kind and energy of the projectile. Hence also the detection limits are a function of these parameters; a suitable choice of them on the other hand results in best conditions for the analysis of elements under consideration. We limit the following inspection of the detection limits to the investigation of the sample targets already prepared. In this sense we refrain from including certain important possibilities to improve detection limits during the target preparation. There are various kinds of definitions of the detection

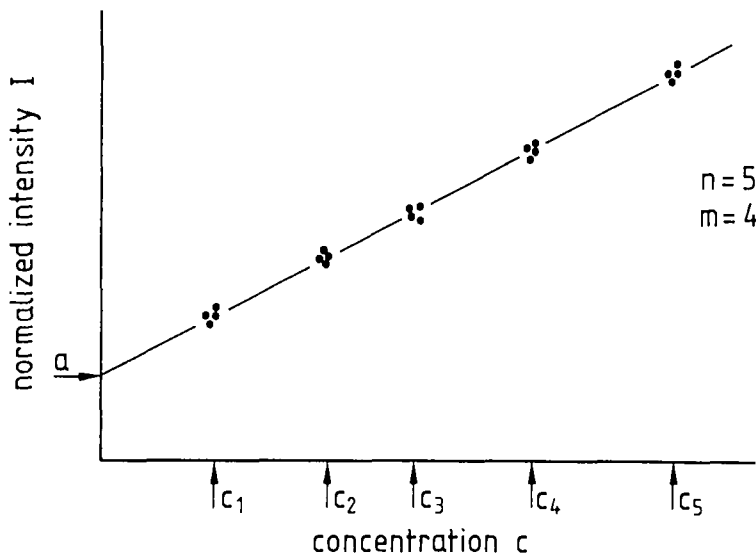


Fig. 3.8. Calibration by linear regression.

limit. In a simple way the detection limit can be defined as the ratio of the X-ray peak to the background radiation yield both taken in the energy region of the double full width half maximum (FWHM) of the peak. This ratio should be at least equal to one. The "blank equivalent" (ref. 29) as detection limit is independent of the experimental conditions like measuring time or intensity of the exciting beam.

As a more valuable criterion IUPAC derives the detection limit from the smallest value I_{\min} which can be detected with reasonable certainty (ref. 33):

$$I_{\min} = \bar{I}_{bl} + k \cdot S_{bl} \quad (9)$$

with the following quantities:

- \bar{I}_{bl} mean value of the blank measurements
- S_{bl} standard deviation of the blank measurements
- k a numerical factor depending on the desired confidence level

IUPAC recommends $k = 3$ with a confidence level of 99.86% for a normal distribution.

The detection limit c_{\min} is derived from I_{\min} by means of the calibration function $I(c)$, Eq. (7), i.e.

$$I = \bar{I}_{bl} + b \cdot c \quad (10)$$

where the ordinate intercept a equals the mean value of the blank. The slope b of the calibration function is called the analytical sensitivity; (nota bene: the "sensitivity" is not to be mixed up with the "detection limit").

For $I = I_{\min}$ Eq. (10) becomes

$$I_{\min} = \bar{I}_{bl} + b \cdot c_{\min} \quad (11)$$

Eqs. (9) and (11) lead with $k = 3$ to

$$c_{\min} = 3 \cdot b^{-1} \cdot S_{bl} \quad (12)$$

A certain detection limit can be stated as a minimum detectable concentration $c_{\min} = T^{\text{trace}} / T^{\text{matrix}}$ where T is the respective mass layer given in g/cm^2 .

Important for the achievable limit of detection is the material of the substratum chosen. In cases where only deposits on surfaces are to be analysed the substratum foil should be taken as thin as possible in order to keep the background due to bremsstrahlung small. The intensity of the bremsstrahlung due to the secondary electrons as well as the one due to the projectiles is proportional Z^2 . Therefore it is appropriate to choose matrix materials of low atomic number. Other requirements are high thermal and electrical conductivity of the material in order to dissipate heat energy and charge deposited by the ion beam in the target. Also high purity of the substratum material is to be guaranteed.

In Figure 3.9 minimum detectable concentrations are given as a function of the atomic number of the trace element under investigation for protons of several energies and ^{16}O -ions as projectiles. Similar curves have been published by many authors, e.g. (refs. 2,3, 34) and they demonstrate the following important points:

1. Using appropriate experimental conditions concentrations of less than $1\text{ }\mu\text{g/g}$ can be detected in thin samples.
2. Clearly the use of protons compares favorably with heavy ions. This is because of the background due to Compton scattered gamma quanta from nuclear reactions, which more probably originate in the case of heavy ions.
3. For elements with $Z \leq 50$ the spectroscopy of the K-X rays results in lowest detection limits whereas for heavier elements ($Z \geq 50$) lower

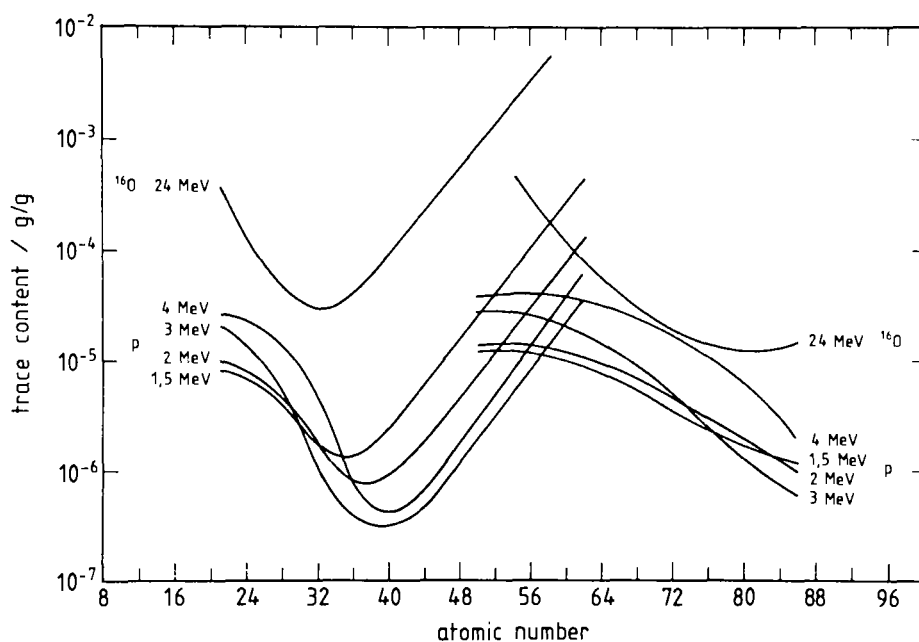


Fig. 3.9. Detection limits vs the atomic number for protons of four different energies between 1.5 MeV and 4 MeV and for ^{16}O ions of 24 MeV, i.e. 1.5 MeV/u.

detection limits are obtained by making use of the L-X rays. It must be mentioned though that the larger multiplicity of the L spectra has not been taken into consideration, thereby neglecting the problem of peak interferences.

4. Another important feature of the curves is a minimum. With rising atomic number the detectable concentration gets smaller because the background due to secondary electron bremsstrahlung falls off much more dramatic than the one of the emission probability of the characteristic X-rays. At larger Z the detectable concentration gets larger again because of the decreasing emission probability of the characteristic X-rays alone, whereas the background due to bremsstrahlung - now from the projectiles only - is relatively constant. This is of practical importance since the position of the minimum depends on the projectile energy, so that by appropriate selection of the energy one can find regions of Z with best limit of detection.
5. It is obvious, that just for elements with Z between 20 and 30, which are of high importance in life processes, the best limit of detection can be obtained.

(c) Accuracy and Precision

If a series of measurement is performed with a certain apparatus and a specific method, a range of measured values for the quantity being sought, the true value, will result. To demonstrate the quality of a method and the apparatus, used for trace element analytical purposes, besides of the detection limit also the accuracy and the precision of the method are to be determined as characteristic figures of merit.

To demonstrate the significance of these quantities we refer to Figure 3.10 (and also to Fig. 3.8). In this schematic representation is shown in which way the measurements (the small points) might scatter around the true value (the circle in the center of each subfigure). The accuracy of the mean of a measurement is defined by how close the results of the series of measurements come to the true value. The precision, on the other hand, is defined by how exactly the result is determined, irrespective of how close it is to the true value. The accuracy is determined by systematic errors of the method and by random errors, whereas the precision is determined by random errors only. Looking at the subfigures in Figure 3.10, we realize in subfigure a a measurement of low accuracy and low precision. In the other subfigures different combinations of low or high accuracy with low or high precision are shown as given in the figure caption. Quantitatively the accuracy of an analysis by a

certain method may be defined by the standard deviation of residuals, as given by Eq. (8) for the calibration measurements. This equation is equally valid for the determination of element concentrations of unknown samples. Using Eq. (8), the accuracy of the analyses is given relative to the concentration c as

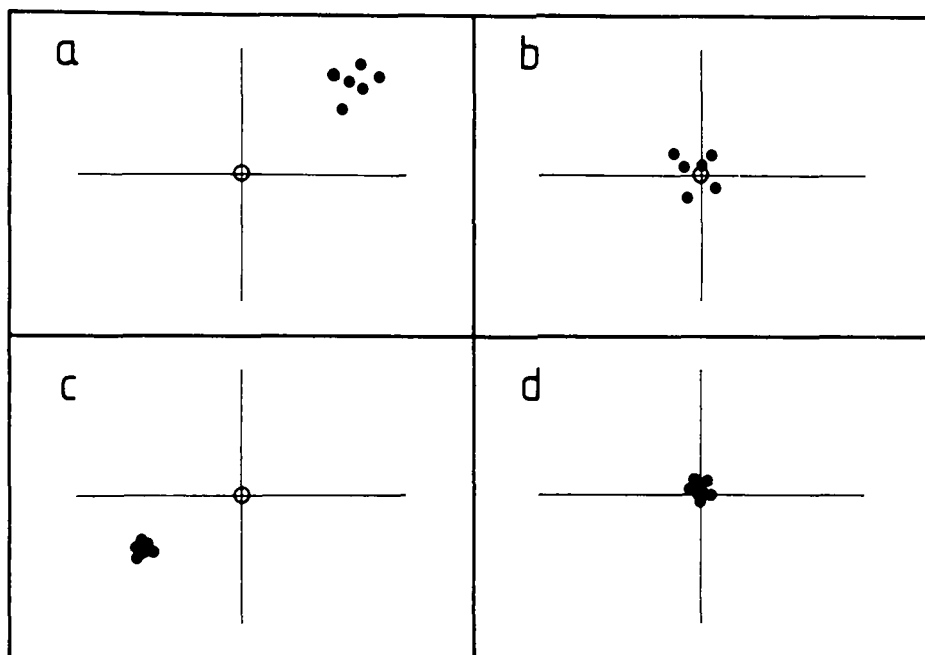


Fig. 3.10. Accuracy and precision of a measurement: case a: low accuracy, low precision; case b: high accuracy, low precision; case c: low accuracy, high precision; case d: high accuracy, high precision.

$$S_{r,R} = S_R \cdot (c \cdot b \cdot \sqrt{m})^{-1} \quad (13)$$

where

r stands for "relative"

b is the slope of regression straight line, Eq. (7) and

m the number of repeated determinations of the samples, possibly an arithmetic mean, if this number differs for different samples

\bar{I}_i is the mean value of the m -fold measurement of sample i , like in Eq. (8) and

j is the running index for the m -fold measurement, $j = 1 \dots m$.

In this way the precision represents the statistical errors only, containing

the deviations of the m-fold measurements of the different samples around their mean. Further details are given by Klockenkämper et al. (ref. 29).

Eq. (13) reflects statistical errors, to be seen as deviations of the measurements of a single sample around its mean, as well as systematic errors, e.g. the one-sided deviation from the regression line.

The precision of an analysis is determined in a similar way, i.e.

$$S_{r,P} = S_P \cdot (c \cdot b \cdot \sqrt{m})^{-1} \quad (14)$$

where

$$S_P = \sqrt{\{n^{-1} \cdot (m-1)^{-1} \cdot \sum_i \sum_j (I_{ij} - \bar{I}_i)^2\}} \quad (15)$$

is the so-called common deviation of the single deviation determined for the I_{ij} . Here i characterizes the sample as a running index, $i = 1 \dots n$ (n samples).

3.3.4 Comparison between XRF and PIXE

Comparing different techniques of excitation requires the optimization of the methods. Only then general conclusions can be drawn. Under these conditions comparison of detection limits, precision and accuracy, the three figures of merit, can be performed.

The evaluation of this kind of comparison - including also electrons as mode of excitation - has been done in detail recently, resulting from solving actual analytical problems (ref. 29). So, here only the outline will be given.

The experimental conditions to be observed in a systematic comparison are also described in the paper given above. The matrices analysed were thick samples of aluminium (low atomic number Z) and lead (high atomic number Z) and trace-concentrate targets prepared from aqueous model solutions and from very pure optical glass. To compare the two excitation modes Eq. (12) can be used basically. This enables not only the comparison with respect to the detection limits but also to the decisive factors b and S_{bl} . In order to be able to do this, these quantities have to be normalized to \bar{I}_{bl} (c.f. Eq. (9)). We arrive at the following quantities used in spectrochemistry: the relative standard deviation of the blank measurements

$$S_{r,bl} = S_{bl} \cdot \bar{I}_{bl}^{-1} \quad (16)$$

and the "blank equivalent"

$$c_{bl} = b^{-1} \cdot \bar{I}_{bl} \quad (17)$$

The concentration c_{bl} of a certain element corresponds to a line intensity which is equal to the mean value of the blank intensity \bar{I}_{bl} as seen from Eq. (10). Using the equations (16) and (17) we derive from Eq. (12) as another expression for the limit of detection

$$c_{min} = 3 \cdot c_{bl} \cdot S_{r,bl} \quad (18)$$

This expression is very useful for the comparison of different methods of excitation, since now c_{min} is split into these two normalized factors and it is therefore possible to track down the reasons of different values of the detection limit.

In a general evaluation Klockenkämper et al. (ref. 29) find, that the result of the comparison strongly depends on the analysed matrix. For thick homogeneous samples XRF is the best method if an instrument with a high stability is available; its values of $S_{r,bl}$ are much better than those for PIXE (c.f. Eq. 18). The c_{bl} values on the other hand are not much worse for XRF than for PIXE.

PIXE is advantageous if the thickness of the sample is very small, or if some kind of sample preparation has to be used which destroys the advantage of XRF, i.e. the small values of $S_{r,bl}$.

In the special case of hair sample analysis (ref. 35) the comparison between XRF and PIXE the result was found, that PIXE has a better minimum detection limit for lower Z elements, while XRF is better for $Z > 27$. This is in contrast to the results of Klockenkämper et al. (ref. 29). It seems that Orlić et al. (ref. 35) did not compare the two methods under optimized conditions.

3.4 EXPERIMENTAL ARRANGEMENT

Generally, a system for trace element analysis by emitted characteristic X-rays is composed of a suitable irradiation source, a containment for a sample target and an X-ray detector. Nevertheless the experimental apparatus approaching a certain analytical problem may vary appreciably, depending on the irradiation source. Especially the consideration and reduction of the background, which is due to the actual excitation mechanism requires different measures.

In the following we review the current procedure for trace element analysis by characteristic X-rays. For excitation we consider in this chapter irradiation by swift ions. Photon excitation has been treated in a preceding

chapter. Electrons can also be used for irradiation. The detection limits in the case of electron irradiation, however, are lower generally by one order of magnitude depending on the matrix material (ref. 29). This is due to the considerable background by bremsstrahlung of the primary electron beam. In the following we, therefore, describe only the apparatus for ion beam irradiation. Later in the Section 3.4.2 we give a description of the detector and electronic equipment together with the practical data analysis. There we confine ourselves to the method of energy-dispersive detection of X-rays. In the Section 3.4.3 sample-preparation techniques will be described. In order to fully utilize the abilities of the PIXE method, this preparation has to be adapted to each analytical problem. In Section 3.4.4, finally, a special preparatory method, the cryopreparation, will be treated briefly. This is to show that in some cases great demands are placed on the sample-taking and sample-preparing techniques.

3.4.1 Irradiation with ions

Many technical details of PIXE have been reviewed from a physics point of view in different papers (refs. 2, 3, 5, 36, 37, 38). Here we try to stress the analytical aspect of the problem. To perform PIXE analysis one must have an ion accelerator at one's disposal.

In this way the method was introduced into different analytical disciplines and especially into analytical medicine and biomedicine. We regard biomedicine as the scientific field where medicine interfaces with biology. We describe in the following the conventional analysis under vacuum conditions (a) as well as the analysis with an external proton beam (b), where the protons after the acceleration pass through an exit-foil, so that the analysis can be performed in air or in another gas.

In subsection (c) the features of a proton microprobe are described. Reducing the diameter of the proton beam down to the order of 1 μm a completely new type of information on the biological microstructure can be obtained (refs. 39, 40, 8, 41, 42). Investigations on the metabolic functions of cell colonies become possible in those cases where extrapolation of the properties of the biological material in bulk to the microstructure is not feasible.

In a final subsection (d) the features of PIGE are treated.

(a) PIXE; the conventional analysis under vacuum conditions

In many natural-science laboratories low-energy proton accelerators of the required kind are available. Most useful are so-called single-stage or tandem accelerators, producing proton beams of a few MeV and with beam currents ranging from 1 to 100 μA . A target chamber containing the sample under

investigation is connected to the beam line of the accelerator and is generally under vacuum like the whole beam line system of the accelerator itself is. A schematic outline of the experimental arrangement is given in Figure 3.11.

As seen close to this irradiation chamber the X-ray detector is mounted, in most cases separated from the vacuum system by a thin beryllium window. In order to achieve a high power of detection the solid angle of the detector should be large; that means the detector should be as close as possible to the target spot irradiated by the ion beam.

In many cases the detector is mounted under 90° with respect to the beam axis, whereas the target surface is inclined by 45° with respect to beam and detector axis. Other angles are possible though.

The beam is collimated to a beam spot at the target position of about a few mm^2 in most cases of application. Regarding the peculiar applicational possibilities using a highly focused microbeam with a diameter of some micrometer we refer to subsection (c).

In all cases where the elements are not homogeneously distributed in the sample target, care must be taken for a homogeneous intensity distribution of

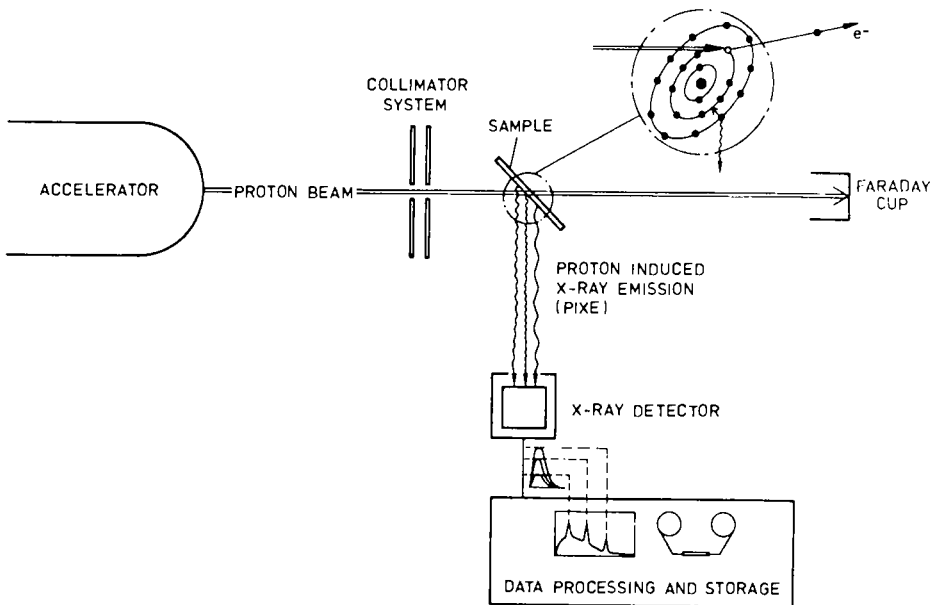


Fig. 3.11. Schematic outline of a PIXE experimental setup.

the beam across the irradiated surface. To achieve this, deflecting the beam across the entrance collimator or inserting a thin diffuser foil into the beam to get a more uniform distribution are suitable means. To get absolute concentrations the beam current must be measured; this is done by counting the protons of the beam crossing the target, i.e. measuring the integrated beam charge in a so-called Faraday cup mounted downstream behind the thin target. With thick targets special measures are necessary to determine the beam charge since the beam is stopped in the target (refs. 43, 44, 45). One must guarantee that during irradiation the charge collected in the target is carried off through the target mount. In the case of nonconducting thick targets often used as biological samples special care must be taken.

Also, under vacuum condition and under irradiation there must not be any modification of the sample due to evaporation or overheating. This limits the applicability of the method in the case of organic samples, e.g. samples of biological or medical origin because of their poor thermal conductivity.

In both respects the external beam technique represents a very interesting solution. This is discussed in the following subsection (b).

(b) PIXE-E; the analysis with an external proton beam

The difficulties mentioned in subsection (a) can be overcome if PIXE is used in a modified way (refs. 46, 47, 48, 49, 50). The accelerated protons leave the vacuum beam line through a thin vacuum-tight exit foil and impinge on the sample which is located about 10 mm downstream. A schematic outline of this experimental arrangement is shown in Figure 3.12, as used by Raith et al. (ref. 48), by way of example.

The protons are losing a part of their energy in the exit foil and in the surrounding gas; therefore the proton energy must be chosen so high that the protons have an energy of 2.3 MeV at the sample location. Different exit foils have been investigated in respect to an optimum power of detection for the elements of interest (ref. 49). The experiments are generally performed in air, but other gases like helium with a lower absorption for X-rays can be used with advantage. Performing the experiments in air a strong excitation of Ar-K X-rays arises from the air. To suppress those X-rays a 75 μm Hostaphan^(R) foil has been used in front of the X-ray detector (ref. 29).

Using this method heating-up of the sample is efficiently reduced by air cooling easing the problems mentioned in subsection (a).

Klockenkämper et al. (ref. 29) did the first explicit comparison of the two PIXE versions under "fair" conditions, using Al as a conducting matrix. They compare both versions also to XRF as described in Section 3.3.4. Regarding the two PIXE versions they arrive at the important result that no signi-

ficant difference could be found for the detection limits of PIXE and PIXE-E for atomic numbers $Z < 30$. This result cannot be extrapolated to $Z > 35$ because the background due to Compton scattering of γ -rays becomes very important for these elements in the case of PIXE-E, as Raith et al. could show (refs. 48, 49).

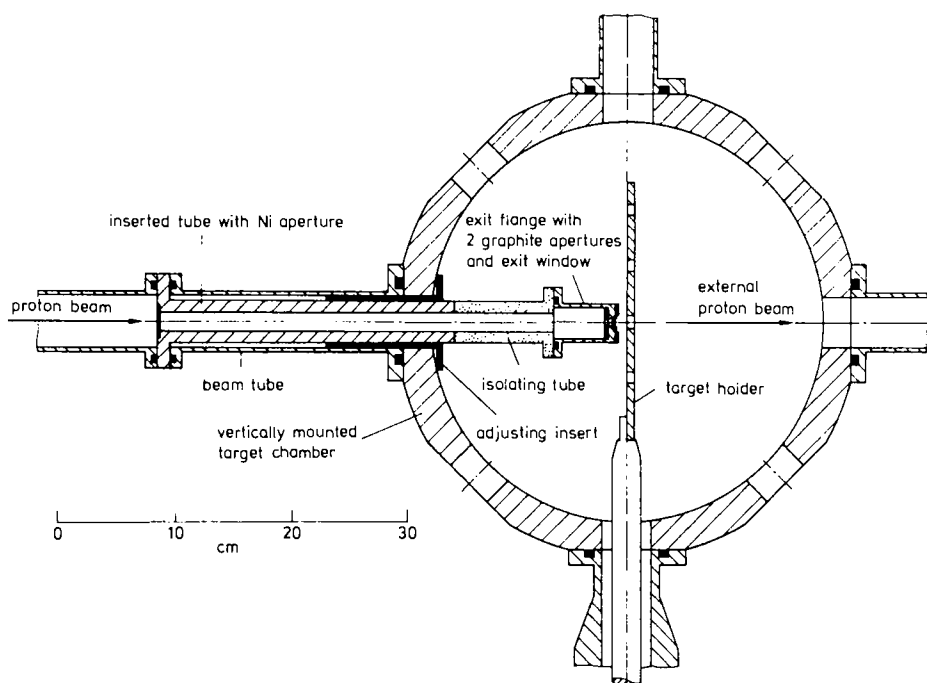


Fig. 3.12. Experimental setup for measurements with an external proton beam.

(c) The proton microprobe

An important feature of the PIXE method is that the background in the X-ray spectra that limits the power of detection is mainly produced by the interaction of the protons with the sample matrix material. Therefore the background intensity depends only on the proton beam current and on the target mass per unit area (c.f. "the concept of cross section" in Section 3.2.2) but not on the beam diameter. This feature is exploited by a proton microprobe, where the proton beam diameter is reduced down to the order of $1\ \mu\text{m}$ without loss of power of detection. One recognizes that by use of a proton microprobe

in combination with PIXE information on the biological microstructure can be obtained not available by sheer extrapolation of the properties of the biological material in bulk to the structure in small dimensions. Nowadays biology and medicine are probably the most important fields of application of this technique (refs. 7, 40).

In the following we describe in general the principles of a proton microprobe setup. Certain applications will be given in the Sections 3.5.2 and 3.5.4.

A microprobe has to be equipped with ion-optical devices which focus the beam, i.e. reduce its diameter without loss of current. In Figure 3.13 a schematic diagram of the Bochum Proton Microprobe at the University of Bochum, FRG, is shown. Its basic concept is similar to that of most of the other microprobes (refs. 39, 40).

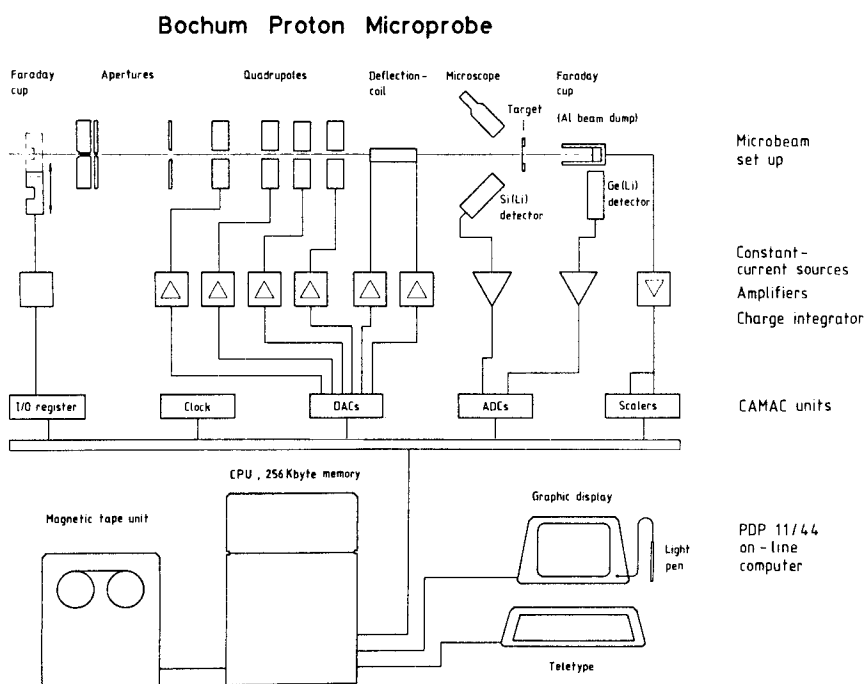


Fig. 3.13. Schematic diagram of the Bochum Proton Microprobe setup and its overall control system.

The proton beam from the accelerator is focused onto an "object"-diaphragm. The microprobe focus is generated by the lens system as a demagnified image of this aperture at the sample position. There is another diaphragm to limit the aberrations produced by the lens system. Those aberrations enlarge the focus like in every optical system. The details of the lens system which focuses the beam are given elsewhere (ref. 51).

The target chamber of the Bochum Proton Microprobe is equipped with a high-precision manipulator for sample changing that allows reproducible positioning of the samples within $\pm 5 \mu\text{m}$ with respect to the beam (not included in Figure 3.13). A microscope is provided for visual observation of the specimen and the beam spot. For the collection of the characteristic X-rays a Si(Li) detector is set up outside the vacuum chamber. Charged-particle detectors for the detection of scattered protons can be mounted inside the specimen chamber. In this way the X-ray yields can be normalized to backscattering in addition to measuring the beam current in the Faraday cup, mentioned in Section 3.4.1.(a).

Using such a setup quantitative information on element concentrations can be obtained for selected points of a sample by irradiation of these single spots with a fixed beam. For the determination of lateral element distributions of a contiguous sample area it is necessary to add to the ion-optical system a device for beam deflection in order to operate the microprobe in scanning mode.

As seen in Figure 3.13 the scanning system, an xy-deflection coil is mounted in front of the target chamber. Details are described in a paper by H8fert et al. (ref. 52).

The analysis procedure, i.e. fixed point analysis or different scanning modes, cannot be generalized. For each different analytical problem the optimum operation strategy of the microprobe has to be worked out. The final-analysis characteristics have to be determined to estimate the quality of the analysis, as outlined in Section 3.3.3. In Section 3.5.2 and 3.5.4 certain applications to biomedical research will be used to demonstrate which problems might arise for different types of analyses and to what extent they can be overcome.

(d) PIGE

Besides of PIXE also proton induced γ -ray emission (PIGE) analysis can be used to investigate biomedical samples. The use, however, has been very limited so far. With a setup very similar to the one used in PIXE analysis PIGE can be applied to the investigation of elements with an atomic number $Z < 14$ which is not possible with PIXE. Also heavier elements can be investigated by

this method. Furthermore, PIGE can even distinguish between isotopes in contrast to PIXE since nuclear effects are exploited. In Table 3.1 a few examples of application are given.

TABLE 3.1

Biomedical applications; c.f. sec. 3.5.

Sample	Elements investigated	Refs.	Sub-sect.	Comments
Human hair	Zn, Cu, Ca	99	4(a)	Correction factors for energy loss and self-absorption
Proteins, liposomes, serum broncho-alveolar lavages	Fe, Cu, Zn, Ni, Co, Br, Pb	100	4(a)	Biophysics, cancer therapy lung pathology related
Kidney, serum, NBS bovine liver	Many between K and Pb	92	4(a)	Reproducibility determination, comparison with neutron activation analysis; investigation of cancerous and normal tissue
Cells and tissue of different biological and medical specimens	Between Na and Pb	22	4(a)	Scanning proton microprobe
Serum	Ca, Fe, Cu, Zn, Br	101	3	Trace elements in pregnancy; Yttrium as internal standard; serum dried on Nuclepore polycarbonate filter membrane
Serum, cerebrospinal fluid, hair, retina of eye	$Z \geq 19$	102	3	Clinical applications
Serum	K, Ca, Fe, Cu, Zn, Br, Au	83	3	Automatic data acquisition and on-line analysis
Whole blood, liver, kidney	Fe, Cu, Zn, Pb, Cd	103	3 4(a)	Freezedried, homogenized blood pressed into pellets; tissue sections comparison with other methods
Human blood Liver tissue	Fe, Cu, Zn	104	3 4(a)	PIXE

Human blood serum	Si,Ti,Cr,Mn,Ni, Cu,Zn,Ga,Se,Br, Pb, macroelements	105	3	PIXE, external beam, correlation between geographical area and trace element composition, sample freeze-dried
Human whole blood	Fe,Cu,Zn,Br,Rb, Pb, macroelements	106	3	PIXE, external beam, freeze-dried pellets, NBS standard used
Liver	Mn,Fe,Cu,Zn,Se,Rb, Mo,Cd,Pb	107	4(a)	PIXE
Dental enamel	F	108	4(b)	PIXE and resonance reaction $^{19}\text{F}(p,\alpha\gamma)$ ^{16}O , microprobe, depth determination
Human hair	Ca,Cr,Fe,Co,Cu,Br, I,Pb relative to Zn	109	4(a)	PIXE, target prepa- ration described in detail
Human bone	Cr,Mn,Fe,Ni,Cu,Zn, Br, Sr,Pb	110	4(a)	PIXE, external beam, target preparation described in detail
Blood serum	Br	111	3	Comparison to neutron activation analysis
Organic and biological matrices	Se	112		
Blood, plasma	Cu,Zn	113	3	PIXE, neonates gestational age, zinc supplemented formula
Hair	Ca...Cd	114	4(a)	pregnant women
Water	K...Zr	115		drinking water, pre- concentration
Multielement		116		PIXE facility design in combination with PIGE, automatic con- trol, accuracy, pre- cision and detection limits reported
Hair	Cu,Zn,As,Sb,Se	117	4(b)	PIXE and NAA, hair as monitor
Blood, hair, water air		118	4(a) 4(b)	PIXE, state of the art
Hair	Na...Sr	119		sample preparation, occupationally exposed workers

Serum, hair	Zn,Cu	120	4(a)	children
—		121	4(a)	general
Hair	S,Fe,Zn,Cu	122	4(a)	pathological hairs, comparison with SEM
Blood cells	Mg...Mo	123	4(b)	metabolic disorders
Kidney	Fe,Zn,Pt,Cd	124	4(b)	cis-platin treated patients
Serum	Ca,Fe,Cu,Zn,Cr	125	4(a) 4(b)	droplets of blood, in air PIXE
Hair, blood cells liver, prostate		126	4(b)	trace element map- ping
Hair	K,Mn,Fe,Cu,Zn, Rb	127	4(a)	

3.4.2 Energy-dispersive (ED) detection of X-rays and analysis of collected data

There are two main methods to perform spectroscopy of characteristic X-rays: those with energy-dispersive and with wavelength-dispersive (WD) detectors. With the (WD) procedure crystal spectrometers especially those with curved crystals are used to detect the spectral X-ray lines. These spectrometers offer an excellent energy resolution, so that even chemical effects on the spectral lines i.e. chemical states can be determined (ref. 53). Also, besides of the spectral resolution the power of detection clearly exceeds that of an (ED) spectrometer (refs. 54, 55), if the high proton beam currents needed are tolerated by the target.

On the other hand with (ED) spectrometers a simultaneous measurement of all spectral lines detected in a sample is possible (compare Fig. 3.7). Contrary to this with crystal spectrometers the measurement of the spectral lines must be done in sequential mode and in this way turns out to be very time consuming. There are modern types of crystal spectrometers, though, where the simultaneous measurement of a few interesting spectral lines is feasible. But, there is still a small angle of acceptance of this type of spectrometer, so that there remains the time advantage for a "simultaneous" spectrometer.

Nevertheless, the comparison of ED and WD spectrometers indicates that the use of a crystal spectrometer with a curved crystal should improve the detection limits of PIXE considerably if high proton beam currents are tolerated by the target (ref. 29). So far in trace element analysis this method is almost exclusively used in combination with high power X-ray tubes and with

electron microprobes. A comparison of both detection methods has been done in the work by Klockenkämper et al. (ref. 29). In the following we will discuss the ED technique only.

Since about 20 years ED semiconductor detectors are in use and in fact triggered the break-through of PIXE as an analytical method. Nowadays mainly lithium-drifted silicon detectors (Si(Li)) are in use, but also germanium detectors (Ge(Li)) or so-called intrinsic-germanium detectors (Ge(I)) are applied.

A semiconductor detector spectrometer consists typically of the detector system proper, the registration electronics and a data handling system.

Commercially available detectors have an active detecting area of 10 to 500 mm². Silicon detectors mostly are used in the X-ray energy region below 30 keV, since the efficiency of a silicon detector decreases above 20 keV. Germanium detectors are most useful at higher X-ray energies which is due to the sufficiently high atomic number of germanium to give appreciable cross sections for X-ray absorption in this energy region. Between the target and the detector the target chamber is sealed by a Be window of 30... 200 µm thickness to prevent scattered protons from entering the detector (compare Fig. 3.11). This relatively thick window, however, strongly absorbs the low-energy X-rays, so that the efficiency of a silicon detector is limited also at low energies. Si-K X-rays are considerably suppressed, and Na-K X-rays can be detected only using a 30 µm window e.g.

The energy resolution of semiconductor detectors is limited by the statistical spread of energy losses during the detection process and is proportional to $\sqrt{E_x}$; it is typically given by $\Delta E \approx 160$ eV (FWHM) at $E_x = 5.9$ keV.

The strong absorption of low energy X-rays can be utilized to suppress interfering radiation in this energy region. This can be done by inserting other absorbers whereby problems related to the handling of high counting rates can be obviated; i.e. the so-called dead-time losses due to overloading the electronics then are avoidable.

Connected to the detector is the electronic equipment for data collection and processing. The charge carriers produced in the detector by the X-rays are collected and cause charge pulses which are converted to voltage pulses by a charge-sensitive preamplifier followed by a main amplifier. Sophisticated electronics for X-ray spectrometry including special units for pile-up rejection and dead-time correction is commercially available. In order to reduce the system dead-time there is in addition the possibility to reduce the shaping constant in the main amplifier. Typical numbers for the shaping constant are a few microseconds. Then, with modern equipment intensities up to

about 5000 counts/s can be handled. A discussion of the development under question is given by Jenkins et al. (ref. 56). As mentioned earlier normalization of the X-ray yields can be done by backscattering by means of the proton detectors, mounted inside the target chamber. Also standards can be used to arrive at absolute concentrations.

Data acquisition is computer controlled. Processing the X-ray events according to software-selected energy windows gives as a result the intensities of the X-ray spectral lines; one gets the X-ray spectrum with the energy-located lines. Computer codes are to be adapted to the spectrum evaluation. This procedure combines energy calibration, separation of interfering peaks, peak identification according to a certain element, peak integration and efficiency calibration. The final result is the amount of a definite element searched for. Many details of semiconductor spectrometers for X-ray analysis and for data acquisition are given explicitly in a number of previous review articles (refs. 2, 3, 4).

Most applications, however, require more sophisticated data analysis procedures adapted to different analytical problems. Therefore, here we refrain from more detailed discussions and come back to special data analytical procedures connected to certain applications in Section 3.5.

3.4.3 Target preparation

For each different analysis problem the appropriate sample-preparation technique has to be worked out to ensure a good quality of the analysis. Therefore it is impossible to outline a target preparation procedure of overall validity. So, we only will give a few general aspects in subsection (a), whereas in subsection (b) we will describe certain details of the cryo-preparation technique, a method which is of the utmost importance if one intends to investigate the distribution of diffusible elements in the biological microstructure. First applicational attempts are demonstrated in Section 3.5.4.

(a) General remarks

The preparation of specimen targets is one of the main problems of induced X-ray emission analysis. The requirements and limitations are even more severe in XRF analysis than in the case of PIXE. Especially the analysis of those targets is problematic which are not stable under vacuum conditions and which cannot be irradiated with particles without being destroyed by overheating. But in those situations the external beam technique (subsection 3.4.1(b)) offers an adequate solution.

Most simple is the investigation of the so-called "thin" targets, i.e.

such targets where the energy loss of the impinging particles while crossing the target is small in comparison with the energy of the particles. In certain cases one can use filters, e.g. nucleopore filters as substratum, thin in the described kind, for aerosol or solution samples or the like. Also thin carbon foils are used in those cases. They are strong but unfortunately often show too high amounts of impurities.

Biological and medical specimens can be irradiated directly if prepared as microscopic cuts. This simple preparatory technique, can, however, be applied only if the informational demand is relatively low. This is true e.g. if the mean elemental composition of biological tissue in bulk is asked for. There are other types of specimens, where by special preparation it becomes possible to improve the detection limit drastically, i.e. by orders of magnitude, applying preconcentration procedures (refs. 49, 57, 58, 59, 60). In the given references the general ideas of trace-metal enrichment for X-ray analysis are discussed. One of the most successful treatments is described by Brüggerhoff et al. (ref. 57). In this case the metal traces are enriched by coprecipitation of the traces with a few mg of a collector element which is precipitated from a solution with an organic chelating compound. The precipitate is separated from the solution by membrane filtration, directly usable as target for the X-ray spectral analysis. Applications are outlined in Section 3.5.1. In the case of enrichment clearly a large amount of material is required.

On the other hand it must be emphasized that even with extremely small amounts of material available induced X-ray emission allows for nondestructive analysis with high power of detection in comparison to other methods.

There are many different methods to produce suitable targets from a sample material depending on the material under investigation itself and on the irradiation set-up available. More details are mentioned in Section 3.5 in connection with applicational work and belonging references.

(b) Cryopreparation of samples for investigations in the biological micro-structure

Medicine and biology are probably the most important fields, where studies in the microstructure yield to a completely new type of information, which cannot be obtained just by extrapolating results from measurements of the biological material in bulk. The role of trace elements and especially trace metals in the living organism is obviously correlated with functional colonies of cells. The dimensions of those cell colonies are about 200 μm or smaller. The next smaller structure is the cell itself below 20 μm , whereas substructures of the cell are smaller than 1 μm . One is referring to the

so-called ultrastructure.

The problem, which arises if one is interested to get information on the elemental composition of microstructural parts of a larger sample in contrast to the mean composition of the biological bulk material consists in preserving the physiologically important concentrations of diffusible elements. Only in this way it will become possible to study the distribution of the elements, since the distribution in the living state is conserved until analysis is possible. As already said as a general remark biological and medical specimens to be investigated by PIXE can be irradiated directly if prepared as microscopic cuts. It is well known, that biological tissue consists to 80% of water. Therefore the preparation of microscopic cuts includes dehydration besides of chemical fixation and staining. This, however, is connected to the risk of the loss or redistribution of diffusible substances that means e.g. of trace elements. Applying cryopreparation techniques is to avoid these disadvantages and to conserve the living state of distribution of trace elements in the microstructure as far as possible for the analysis. Details of this technique applied to X-ray microanalysis are described by Zierold (ref. 61). In the following, therefore, only the outline should be given, as far as the microstructure is concerned.

As preparational steps shall be described: cryofixation and preparation of cryosections. Details of application are also discussed in the paper by Zierold mentioned above; here main aspects are illustrated by own results.

The idea of cryofixation consists of preserving the elemental distribution and composition by rapid cooling down the sample to a temperature where further diffusion of elements possibly also available as ions becomes excluded. Although there is no firm information of the characteristics of diffusion in deep frozen biological specimens, it is widely assumed, that cooling down to 190 K should be adequate according to Moor (ref. 62). This should be valid even for ultrastructural studies, whereas the demands for investigations in the biological microstructure i.e. above 1 μm certainly can be eased. In any case, however, holds the Arrhenius law: the lower the temperature the lower the diffusion.

In tissue samples the time after dissection from the organ under investigation until cryofixation is most critical for the success, since the distribution of elements will still change in this period. Therefore cooling down should proceed as fast as possible. Cooling rates as fast as 10^4 K/s are reported (ref. 63).

Due to the low thermal conductivity of water best results are obtained by cooling small biological specimens. Recently cryofixation has been reviewed by Plattner et al. (ref. 64). Again, demands for investigation in the microstruc-

ture are not that high as in the case of the ultrastructure.

Different techniques have been developed to quench-freeze biological tissues. Only two of them shall be mentioned here:

1. Rapid immersion of the specimen into liquid propane and
2. The so-called propane jet method, where liquid propane is shot onto the specimen by means of pressurized nitrogen gas (refs. 65, 66, 67, 68, 69).

Liquid propane cooled by liquid nitrogen is used as the quenching liquid since it yields the highest cooling rate (ref. 70). Rapid immersion into liquid propane is coming into use in the case of studies in the microstructure, whereas the higher demands for research in the ultrastructure has led to the use of the propane jet method.

The preparation of cryosections after the process of cryofixation seems still to be difficult as far as the ultrastructure is concerned. The phenomena are still unclear and so far are not understood from the point of view of physics. We therefore in the following will keep to discussions of the microstructure. In our investigations to preserve the original element distribution the biological material is shock-frozen in liquid nitrogen or better in liquid propane a few seconds after excision. Sections of 5 μm thickness are cut using a cryomicrotome and then freeze-dried, both at a temperature below -25°C . As the sections are relatively large and tend to rupture, they are embedded between two thin layers of Formvar^(R). The specimen can then be transferred to the target chamber for PIXE microanalysis.

3.5 BIOMEDICAL APPLICATIONS

Soon after the introduction of PIXE into the field of applications many different regions of research took advantage of this method. Fruitful interdisciplinary work began to flourish not to mention the new possibilities for research which developed. Therefore today it seems to be difficult to give a complete survey of this fast growing field. Our purpose here is to confine ourselves onto specific aspects and to outline regions of applicational interest. Above all reference is given to the International Conferences on PIXE and its Analytical Applications (refs. 6, 7, 8, 9) and to other related conferences (refs. 10, 11).

Before going into some details we prefer to give an outline of applicational work. In many applications a general survey of the multi-element content is desirable. In other cases one might be interested in certain elements only e.g. in the toxic heavy metals in the field of medical or environmental research. In such cases to get highest power of detection one can take advantage of using selected experimental conditions, like projectile

energy, as discussed earlier. In addition there are special applications where interest arises regarding aspects of spatial distribution of trace elements in the sample. This might be of concern regarding depth distribution profiles with specific consideration for surface sensitivity as well as regarding lateral distributions.

Applicational work could further be extended to new regions of interest since preconcentration techniques came into use, examples of which will be discussed regarding water samples. Meanwhile there are many fields of application which we review in Table 3.1, grouping in terms of various groups of samples where typical target preparation techniques are in use. A few typical examples we are discussing in more detail.

3.5.1 Trace elements in water samples

Water is one of the main parts of our environment and of large importance in the food chain of men. It contains essential trace elements as well as toxic elements from anthropogenic activities. The list of essential trace elements meanwhile amounts to not less than 60 elements whereas most of them seem to be toxic if they are present in too large an amount. It turns out that most of the trace element concentrations are maintained in certain limits in the biological system, i.e. above a lower one, in order to establish the role as an essential trace element and below an upper one, outside the risk of their toxic properties. It seems to be obvious that the knowledge of the trace element concentration especially of water is highly important.

Target preparation from water solutions is simple as far as only relative contents or "fingerprinting" are desirable. Most simply carbon backings, fabricated by vacuum evaporation onto glass sheets, can be floated in the water under investigation. Adding an internal standard to the solution is one prerequisite of getting approximate absolute concentrations. The carbon backing floated can be picked up using a target frame. Since in most cases the water under investigation is available in large amounts this method is very common. Also water drops can be dried on a chosen backing. Different kinds of material are in use as a backing besides of carbon, as e.g. "Nuclepore", "Formvar", "Polystyrene", "Hostaphane" etc.. Campbell (ref. 71) reviews target backing and specimen preparation techniques in detail, especially important for PIXE.

Analysing trace metals in water sometimes is performed using preconcentration techniques. One of the most successful methods (ref. 57) has been outlined in brevity in Section 3.4.3.(a) in connection with target preparations. Therefore, here only the general results of a careful study on a hydrous model solution done by Klockenkämper et al. (ref. 29) will be mentio-

ned. These are interesting in the respect of comparison between PIXE and XRF (Section 3.3.4). At the same time the quality of an analysis using preconcentration techniques, i.e. accuracy and precision as figures of merit, is quantitatively shown (c.f. Section 3.3.3 (c)).

The enrichment of the traces is done by coprecipitation with a few mg of a collector element as described in Section 3.4.3. (a). In our case Indium was chosen as a suitable collector element and at the same time could be used as internal standard. Trace metals were chosen as the elements to be investigated in the model solution (Fe, Co, Zn, Pd, Cd, Hg and Pb). Recoveries of more than 95% were obtained.

Following the outline of Section 3.3.3 especially using Eq. 18 the detection limits c_{\min} are calculated. The absolute detection limits amounted to 19 ng in the best case (Co) and 2.1 μg in the worst case (Cd). The corresponding relative numbers were 100 ng/l (Co in water) and 10.5 $\mu\text{g/l}$ (Cd in water). The analysis has been done by PIXE-E.

The detection limits of PIXE-E in this experiment are generally lower than those of XRF, on the average by a factor of 7. This is caused mainly by the values of c_{bl} (c.f. Eq. 18), which are better for PIXE-E by more than one order of magnitude. Usually the advantage of XRF regarding $S_{r,bl}$ compensates for a higher value of c_{bl} . In the case of the applied enrichment technique, however, the scatter deviation introduced by the sample preparation completely outweighs the one of XRF alone. As far as the figures of merit are concerned, no significant differences between PIXE-E and XRF could be found. This led the authors (ref. 29) to the conclusion that systematic errors are negligible for the trace concentrate targets of this water analysis.

3.5.2 Trace elements in air particulate matter

During the last years the environmental burden due to particulate matter and its effects on health has gained broad interest. These substances are present in the form of aerosols and its inhalable fraction with particle diameters below 3 μm . Emphasis is given especially to this fraction regarding the hygienic aspects. The relevant questions are connected to the relationship between the air quality, the anthropogenic sources and the biological effects. These different aspects are related through the characteristics of the particulate matter. One important part of this subject consists in the relationship between the diameter of the particles and their chemical composition. And in this respect especially the diameters of those particles are of importance which are retained by lungs. Recently Bonani et al. (ref. 75) have pointed out, that standards to protect human health should be based on respirable particulates and certain components therein.

In the following a method we applied using a proton microprobe will be described by which the chemical composition of single dust particles in dependence of the particle diameter can be directly measured. A fingerprinting in reference to industrial activities and to an immission survey becomes possible. The goal is to find out a correlation between particle diameter and elemental composition.

A seven stage cascade impactor was used for particle sampling and separation according to their size. The mass density on the sampling foils were kept low enough to separate individual particles. The size of the particles was determined by electron or light microscopy.

Before sample taking one has to decide which region of particle diameters can be analysed using the proton microprobe with reasonably good accuracy and power of detection. The reason for this is that different stages of cascade impactors deposit particles of different size (ref. 76). If the particle to be analysed is much smaller than the beam diameter then the analysed sample area consists mainly of the backing foil alone; this reduces the power of detection considerably. We therefore limited the particle size to values larger than 0.5 μm . On the other hand, if the dust particle becomes too big in the direction of the incoming beam then one has to correct the thickness determination done by thin-target calibration appreciably because of matrix effects like slowing-down of the projectiles and X-ray absorption. In order to be able to do so, however, one has to know the contents of light elements like H, C, O etc. Since one cannot get any information about these elements by PIXE no correction can be made, so that one has to limit the size of the particles to a value where the maximum error that can occur because of the neglect of matrix effects does not exceed a preset value. We chose the maximum diameter to be 5 μm ; for an iron cube of 5 μm thickness the correction would not be larger than 30% for protons of 3 MeV. This limitation is of no practical concern since the relevant diameter of respirable dust particles are anyway below this limit, as explained above.

The main question that arises refers again to the optimum microprobe-operation strategy. The first step will surely be a raster scan with a small beam diameter in order to localize the single dust particles; Figure 3.14 shows a microphoto of a dust sample with the rastered area appearing as a dark square (70 μm x 70 μm). In case one is then interested in substructures of single particles, a raster with the smallest beam diameter possible is the only reasonable choice. If one is, however, only interested in the global contents of the elements heavier than aluminium, a single-spot analysis with a beam diameter much larger than the particle diameter (for reasons of homogeneity of the beam spot) might appear to be a good and easy operation procedure. We

prefer, however, even in such a case a raster scan for the following reasons: if the beam diameter is too big one might analyse parts of neighbouring dust

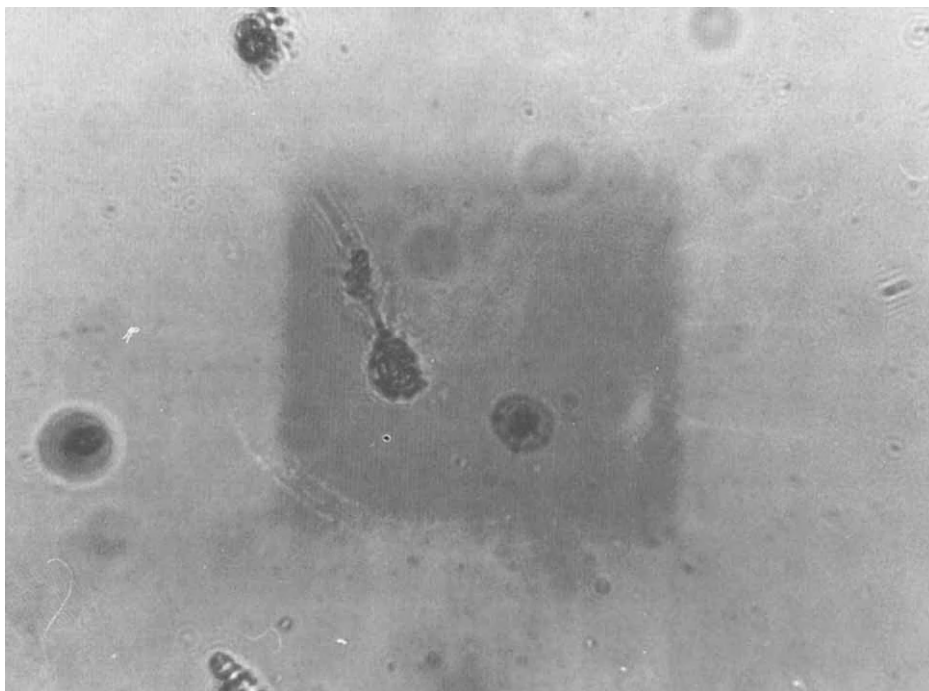


Fig. 3.14. Microphoto of a dust sample. The size of the rastered area is $70\text{ }\mu\text{m} \times 70\text{ }\mu\text{m}$.

particles simultaneously. To avoid this the beam diameter has to be diminished to about the particle size, but then the beam spot will no longer be homogeneous over the sample area, and the result of the analysis will depend on the exact position of the focus with respect to the particles; this may cause differences in the results - especially for the light elements like Si, S, Cl, K and Ca - which amount to 25% or even more. Furthermore a single-spot analysis with a fixed beam would cause distortions of the backing foil (due to heating up) which result in changes in the position of the dust particle. All these problems are avoided by rastering over the single particle with smallest beam diameter possible.

Results of this measurement are demonstrated in Figure 3.15. The intensity of the characteristic X-rays of 6 different elements is given resolved through the rastered area. This is to show that using a proton microprobe the

geometric dimension as well as the elemental composition of single dust particles can be determined. The characteristic X-ray spectrum of an indivi-

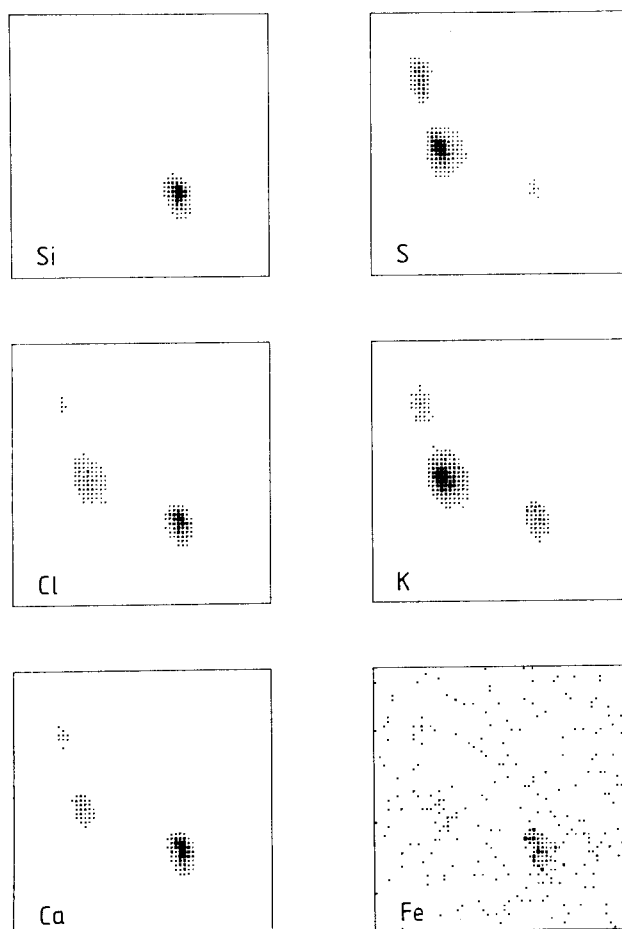


Fig. 3.15. Result of a rasterscan: intensity of the characteristic X-rays of the elements Si, S, Cl, K, Ca and Fe vs beam position ($65\ \mu\text{m} \times 65\ \mu\text{m}$).

dual particle is shown in Figure 3.16.

The results reveal interrelationship between different particles pointing to particle families of a common source. This is shown in Figure 3.17. There are groups of particles which contain a number of elements in comparable amounts. On the other hand there are particle groups where only one component could be detected. The general agreement of PIXE analysis with other methods

regarding aerosol trace element analysis has been shown recently (ref. 77). S, Cu, Br, Zn and Pb have been analysed. With certain difficulties V, Cr, Mn and Ni have been measured. Also Cd, Sb and Se have been detected.

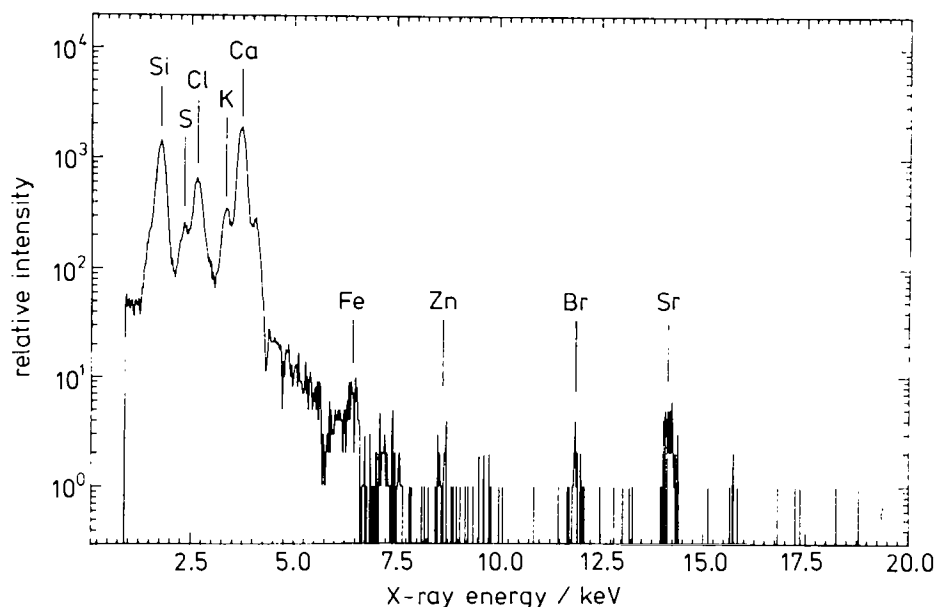


Fig. 3.16. X-ray spectrum of a single dust particle.

More work on aerosol parameters using PIXE analysis is collected in Table 3.1.

3.5.3 Trace elements in body fluids

Analysing human body samples is of rising interest since trace elements seem to play a decisive role in the metabolism. On the other hand the deleterious effects of toxic metals such as lead, mercury and cadmium are well known, the detailed mechanism of the damage is still a field of research though. As easily obtainable biological material body fluids like blood or urine are objects of investigation since many years. Much work has been done in this field (refs. 78, 79, 80, 81, 82).

The analysis of whole blood is difficult because of the high X-ray intensity due to iron. Serum on the other hand does not present this problem but cannot be regarded as representative for whole blood.

For the use in clinical work automatic systems have been developed to determine trace element concentrations (ref. 83). Kleimola et al. (ref. 84) have investigated trace elements in serum with emphasis on routine analysis of

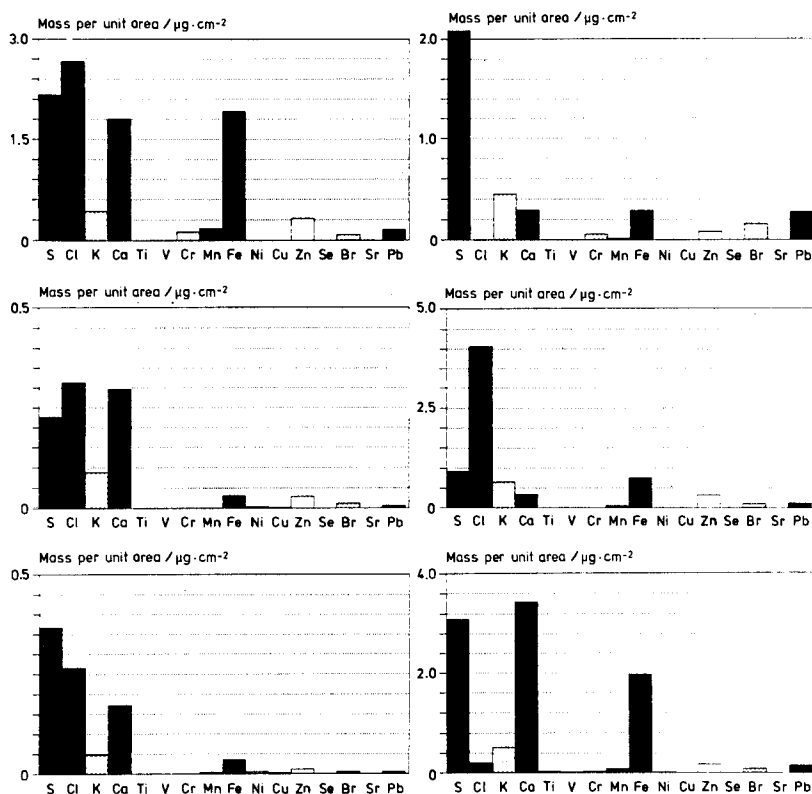


Fig. 3.17. Element composition of 6 different dust particles. Some particles (results on the left side) contain most of the detected elements in comparable amounts, other particles (right side) consist mainly of only a few elements.

healthy persons. Other examples of analytical application in this field are given in Table 3.1.

The investigation of whole blood and the problem of different trace element concentrations in the serum and in the erythrocytes offers the possibility to use the proton microprobe to distinguish between both constituents. It is a simple example to discriminate between certain points of interest with differing element composition in a sample area to be analysed. An element map

of the specimen can be produced to precisely localize the different points of interest and to measure the element composition at these points.

Using the Bochum Proton Microprobe (c.f. Section 3.4.1 (c)) such a measurement strategy was employed to obtain a spectrum from a single erythrocyte of a blood sample. Subpicture a of Figure 3.18 shows a microphoto of the

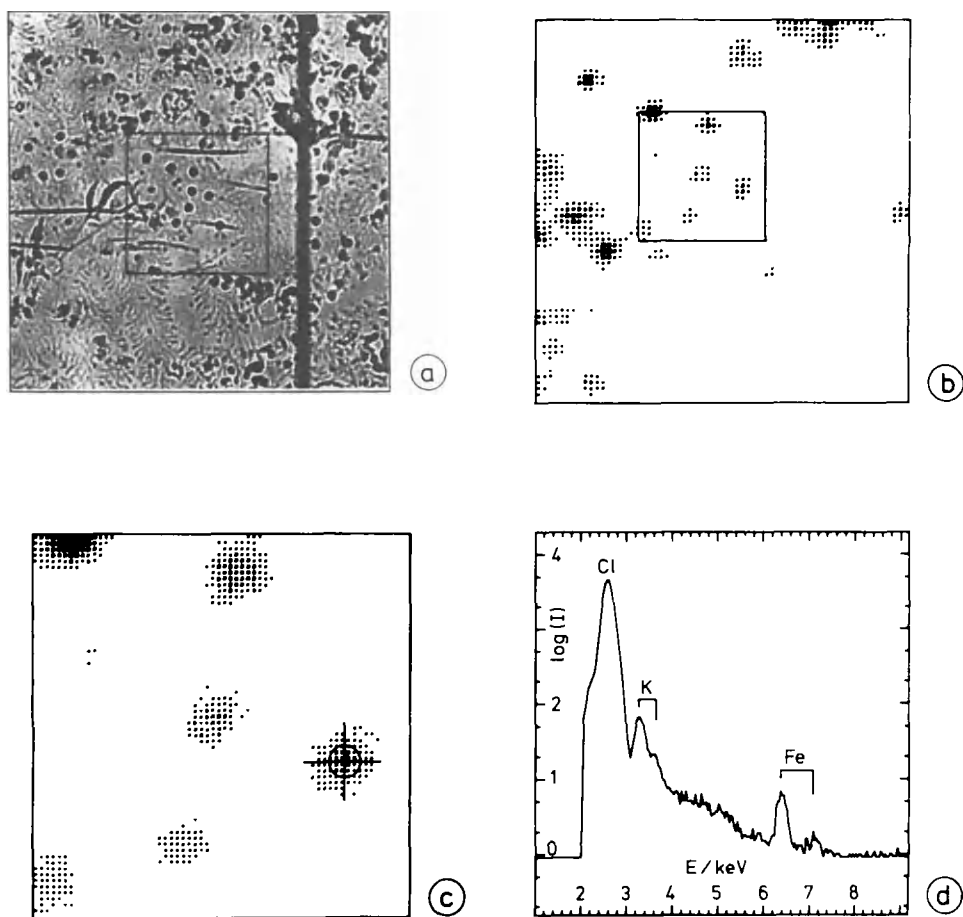


Fig. 3.18. Selection of a single erythrocyte for irradiation: a: Microphoto of the blood sample; the area of the primary scan is indicated (200 μm x 200 μm). b: Cl map of the primary scan; the area of the second scan with increased resolution is indicated. c: Cl map of the second scan; a single erythrocyte is selected for analysis. d: X-ray spectrum of the erythrocyte.

blood sample. The blood was diluted with a NaCl solution and dispersed on a thin Formvar^(R) backing ($\approx 50 \mu\text{g}/\text{cm}^2$). The erythrocytes are visible as circular structures of similar size (diameter $\approx 10 \mu\text{m}$). A primary raster scan of 64×64 points covering an area of $200 \mu\text{m} \times 200 \mu\text{m}$ was performed. The element map of Cl which was generated on-line by displaying the intensity of Cl-K-X-ray intensity vs beam position was used to determine the borders of a new scan with increased resolution (subpicture b). The Cl-distribution of the new raster scan was displayed (subpicture c) and finally a coordinate was chosen for single spot analysis (subpicture d).

In a simple way urine samples can be investigated whereas contrary to the case of blood preconcentration techniques can be applied (refs. 85, 86, 87). Examples of investigations in other body fluids are rare. Hall et al. (ref. 88) have applied PIXE to the investigation of amniotic fluid, the fluid where the child, before it is born, is submerged in, which serves to nourish and protect. The data revealed that the Ca concentration was highly correlated with Al, where Al has been determined by DCP.

3.5.4 Trace elements in biological tissues

Due to the role of trace elements in the living organism, especially in metabolic processes, there has been a drastic increase in investigating biological materials in the last years.

Normal biological behaviour relies on the absolute concentration of certain trace elements as well as on their relative amounts. Therefore by exact analytical investigation one can specify the normal concentrations in biological material and detect the deviations from the normal.

To investigate details in biomedical problems and in the metabolic behaviour related to the importance of trace elements might require research under two main different aspects: mean elemental composition in different parts of the human organism and microstructural distributions of trace elements. The subsections (a) and (b) are devoted to these points, respectively.

(a) Investigation of the mean elemental composition of biological tissues

Normally the concentration of trace elements in the biological organism remains in a relatively narrow concentration regime. To disclose the significance of certain trace elements for the metabolic processes requires the determination of these normal concentrations and of the correlation of deviations of the normal with the pathological behaviour of the organism. This introduces PIXE to interesting applications of trace element analysis on biomedical problems. There is much work on trace element concentrations in different parts of the human organism (c.f. Table 3.1). In this way those

trace element concentrations can be established which relate to the normal behaviour of a human organism. Also nutritional requirements could be documented by this analysis (ref. 89). Review on the aspects under discussion has recently been given (refs. 78, 90).

Here we are going to discuss only a few special examples. There are many diseases among industrial workers due to the hazards of abnormal environmental exposure. In some cases an environmental aggression of the lung is suspected to be the aetiological agent. Weber et al. (ref. 91) have investigated lung tissue obtained by biopsies. They report trace element concentrations and diagnosis for a number of patients.

Analysis of cancer tissue is another field of broad investigation. Mentioned should be here only one example where not only cancerous tissue has been investigated but also has been compared with normal tissue (ref. 92). Beyond that in this paper a careful study of the reproducibility of PIXE analysis and an intercomparison study in respect to instrumental neutron activation analysis is given. A major criticism which has to be made about many other analytical papers is the lack of information concerning the accuracy of the results and the precision of the methods used. Analytical results should be related to standard reference materials.

Also Maruhashi et al. (ref. 93) discuss interesting problems on the application of PIXE to cancer diagnosis. Comparison with AAS, ICP and XRF is emphasized. They prefer a combination of different methods for detection of many trace elements in biomedical samples. To their opinion it is desirable to use ICP (AAS) and XRF for screening for cancer and PIXE for confirming it. They point out advantages and disadvantages of PIXE in contrast to the other methods.

Another valuable application of PIXE regarding neurological diseases is worth to be mentioned. Van Rinsvelt et al. (ref. 94) studied indicated alterations of specific trace metals in humans and animals treated with valproic acid (VPA), an anticonvulsant. They found selenium levels to be depleted. VPA treatment also produced a significant decrease in plasma zinc levels.

Many other applications are mentioned in excellent review articles and books given in the list of references. Emphasis is given to the paper of Vis et al. (ref. 81) because they discuss Macro- and Micro-PIXE in context. This is to introduce the application of ion microbeams to the analysis of biomedical samples which is discussed in the next chapter.

(b) Investigation of the elemental distribution in the microstructure of biological tissues

In general the aim of PIXE in combination with a proton microprobe is to

get information on the elemental composition of a small particle or a small part of a larger sample. The analysis procedure, however, cannot be generalized: for each different analysis problem the optimum operation "strategy" of the microprobe and the appropriate sample-preparation technique have to be worked out, and the final-analysis characteristics have to be determined to estimate the quality of the analysis.

The interest to investigate small parts of a biomedical sample refers to the existence of functional units of cells, so-called cell colonies. Due to the role of trace elements in metabolic processes it is to be expected that the distribution of trace elements in the sample varies in correlation with these cell colonies. To investigate this distribution serves to clarify the function of the trace elements. Below the level of magnitude of the cell colonies exists the cell itself, the concentration of trace elements of which is of great interest too. We are talking of the distribution of trace elements in the biological microstructure studied by Micro-PIXE. The Bochum Proton Microprobe mentioned in chapter 3.4.1 (c) will be used as an explicit example of realization. Thereafter certain applications to biomedical problems will be used to demonstrate in detail which problems arise for different types of analyses and to what extent they can be overcome.

A certain strategy is necessary to optimize the microprobe analysis. Although a fixed beam seems to be sufficient for single-point analyses, under certain aspects scanning operations are required for these measurements as well: if a certain point of interest is to be analysed because its element composition differs from that of the surrounding sample area, an element map of the specimen has to be produced first to precisely localize this point. If, on the other hand, a point is analysed because it is assumed that its element composition is representative for a larger fraction of the sample, it must be verified by means of an element map that no contamination is present which would falsify the interpretation of the result.

To select the appropriate measurement strategy becomes crucial if element profiles of larger sample areas have to be determined. Element mapping with a raster scan of high spatial resolution may provide useful qualitative information on the distribution of major elements. The quantitative analysis of trace element concentrations, however, requires a collected beam charge of at least $1\text{ }\mu\text{C}$ for irradiation of each single spot. This means, a raster scan of e.g. 128×128 points, using a beam current of typically 1 nA , would take half a year to obtain sufficient statistics for each point.

Therefore it is inevitable for the determination of trace element profiles to reduce drastically the number of scan points, e.g. performing a well positioned line scan instead of a raster scan.

Cataracta senilis

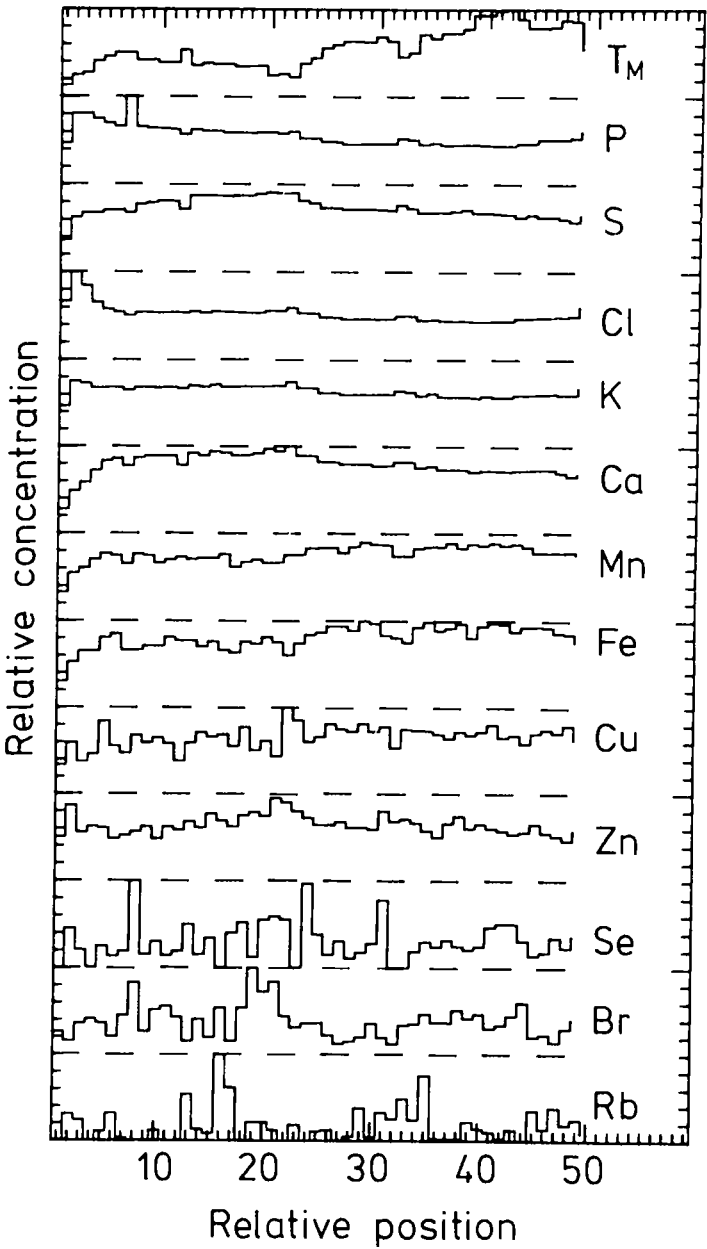


Fig. 3.19. Trace element distribution along the optical axis of a human cataract lens.

We followed this principle for the investigation of trace elements in human lenses with senile cataract. To preserve the original element distributions each lens has been shock-frozen in liquid nitrogen immediately after excision as described in Chapter 3.4.3 (b). Cryosections have been produced for the measurements. To obtain informations on the element concentrations of cataract regions as well as of non-opacified regions, line scans from anterior pole to posterior pole were performed along the optical axis of each lens. The results of one of these analyses are shown in Figure 3.19. In contrast to raster-scan measurements that were performed by another group (ref. 95) these measurements allowed quantitative analysis of trace element concentrations and revealed distinct element distributions.

It should be noted here that in this example, as in all biomedical problems where the sample to be irradiated is produced by cutting thin sections ($d < 10 \mu\text{m}$) with a microtome, trace element concentrations with respect to the actual sample thickness at the irradiated point are given instead of the actually measured mass per unit area. The reason for this is that the sample thickness - and thereby the absolute trace amounts - may vary appreciably across the sample area due to problems of cutting and drying the specimen and of course due to intrinsic density changes. The actual sample thickness, however, cannot easily be determined because for most biomedical problems the main part of the sample consists of light elements which cannot be detected at all by PIXE. So one has to find other techniques for the determination of the sample thickness.

The method we employ makes use of the fact that the elements whose X-ray lines appear in the energy region 4.2 keV and 5.2 keV usually do not occur in biological samples so that the secondary-electron bremsstrahlung (SEB) can easily be determined in this energy region of the X-ray spectrum. Since for biological material the heavier elements occur only in low concentrations they do not contribute considerably to the secondary-electron bremsstrahlung. So the relative sample thickness can be determined from the SEB intensity measured; from this the absolute thickness can be calculated by calibration using a Kapton^(R) foil of known thickness whose element composition is similar to that of biological materials.

To be able to draw conclusions concerning the role of trace elements in the living organism from microprobe measurements, it is decisive that the determined element concentrations at a certain point do represent the original element distribution before taking the sample. This places great demands on the sample-taking procedure as well as on the sample storage and preparation. In some cases these demands are actually impossible to fulfill, if samples of human beings must be taken.

The problems arising in medical diagnostic application of a proton microprobe have recently been described by the Oxford group (ref. 96). They report on an investigation into the trace element distribution of a section of diseased human liver suffering from primary biliary cirrhosis (PBC). The distribution and significance of hepatic copper in PBC could be revealed in confirmation with other results. Malmqvist et al. (ref. 97) report on studies on dermatological material and get reproducible results equivalent to those of the electron microprobe. The general shapes of the element distributions are rather similar for both modes of analysis. However, there exists a systematic difference in quantification, yielding concentrations 10 to 30% higher in the electron microprobe case. The authors discuss the probable errors.

Other examples of application are given in Table 3.1. They clearly demonstrate that the proton-microprobe technique and PIXE analysis as analytical method have been developed to a level that the combination of these two can be successfully applied to problems concerning the element composition of certain types of biomedical specimens. A versatile scanning and data acquisition system together with sophisticated computer programs for data reduction could be shown to overcome a lot of difficulties in trying to fully exploit the capabilities of the combined technique.

On the other hand, still little is known about the influence of the sample-taking procedures, sample storage and preparation on the interpretation of the analysis result especially in this case of Micro-PIXE. The same holds for effects the proton beam has on the element distribution during the sample irradiation. Detailed investigations of these questions will have to be performed to find out to what extent the mentioned sources of possible errors can be either excluded or at least taken explicitly into account.

3.5.5 Trace elements in pharmaceuticals

The intake of trace elements may be of considerable importance also in the case of pharmaceutical medication. Gonsior et al. (ref. 98) have investigated trace element concentrations on two examples using PIXE-E: quinine-salicyl-lithium (Togal)^(R) together with acetyl-salicylic acid and Maffee^(R). So e.g. the important relations between the metabolism of the myocard and the mineral balance have come to light in numerous clinical investigations. The important role of the iron-neutralizing zinc in the case of pathological iron resorption is known as well. On the other hand, the essential trace element iron may be toxic if available in excess. The authors studied two substances whose gross pharmacological effects are well known in medicine and whose administration is being extended into new fields nowadays. The knowledge of the trace element content is of particular interest when the intake is of a

chronic nature.

In Togal^(R) the trace element concentration is small and of no significance for the quinine-salicyl-lithium therapy.

In Maffee^(R) the iron content amounts to more than 1000 ppm, which is mainly due to the auxiliary substances. Also titanium is included. The high iron content is to be considered e.g. in the case of pathological iron resorption. Also Mn, Cu, Zn, Br and Sr are contained in about the same concentration. Titanium is added with the auxiliary substances and is then present with the highest concentration of all trace elements, about 70 ppm.

As a result one has a reliable general view regarding the substances present in the pharmaceuticals. As far as Togal^(R) is concerned no trace elements of significance are contained. In Maffee^(R) the mineral elements, important for the clinical application are available in high concentration. The amount of trace elements is significant and may be taken under consideration in case of secondary effects. It is well known that certain laxatives may disturb appreciably the equilibrium of macro- and trace elements. For the cardiology this has been investigated clinically and experimentally. The knowledge of the trace element content allows for an estimation of possible detrimental or favourable effects.

3.6 CONCLUSIONS AND OUTLOOK

In view of the work which has been done so far in respect to the development of the technique as well as the application is concerned PIXE stands well up to the claims which should be made for a reliable trace element analytical method. It is felt this method has many desirable and advantageous properties. To be specific trace element abundances can be obtained for all elements with an atomic number $Z > 14$ simultaneously in one analysis. A disadvantage results from the fact that interferences between K- and L-X rays from light and heavy elements, respectively, might limit the number of detectable elements, at least near the detection limit of 10^{-6} to 10^{-7} g/g. Very small amounts of a sample can be analysed whereby the analysing time generally is of the order of magnitude of only 10 minutes. Using a proton microprobe with the present lower limit of resolution structures of 1 μm diameter can be investigated. This means a minimum detectable trace element amount of about 10^{-16} g. In a body this brings about a good economy for an analysis even considering the fact that in the case of PIXE a particle accelerator is a prerequisite. A very important advantage is, that this analytical method is nondestructive.

The field is still open for developments just to mention the technique of the microprobe and the possibility of preconcentration where in some cases

already a lowering of the detection limit by more than three orders of magnitude could be achieved.

Taking for granted an interdisciplinary cooperation as a necessary basis PIXE is a method of choice promising interesting successes in many areas of application.

ACKNOWLEDGEMENTS

The author wishes to acknowledge the hospitality of the Centro per l'Ingegneria Biomedica, Università degli Studi di Roma "La Sapienza" where the initial draft of this review was written.

He also has benefited from discussions with R. Cesareo and with numerous colleagues over the years, all of which are here gratefully acknowledged. In particular, thanks are due to B. Raith, M. Höfert, S. Divoux and Miss C. Gonsior for critically reading the manuscript. The author has to thank also Mrs. E. Grieger for her patience during the preparation of the manuscript.

The work has been supported in part by Minister für Wissenschaft und Forschung des Landes Nordrhein-Westfalen, D 4000 Düsseldorf and by Bundesminister für Forschung und Technologie, D 5300 Bonn, Fed. Rep. Germany.

REFERENCES

- 1 T.B. Johansson, R. Akselsson and S.A.E. Johansson, Nucl. Instrum. Methods, 84 (1970) 141-143.
- 2 S.A.E. Johansson and T.B. Johansson, *ibid.*, 137 (1976) 473-516.
- 3 F. Folkmann, J. Phys., E 8 (1975) 429-444.
- 4 F.S. Goulding and J.M. Jaklevic, Ann. Rev. Nucl. Sci., 23 (1973) 45-74.
- 5 G.L. Macdonald, Anal. Chem., 50 (1978) 135R-143R.
- 6 Proc. Intern. Conf. Particle-Induced X-ray Emission and its Analytical Applications, Nucl. Instrum. Methods, 142 (1977)
- 7 Proc. Intern. Conf. Particle-Induced X-ray Emission and its Analytical Applications, *Ibid.*, 181 (1981).
- 8 Proc. Third Intern. Conf. on PIXE and its Analytical Applications, *Ibid.* B3 (1984).
- 9 P. Brätter and P. Schramel (Eds.), Trace Element Analytical Chemistry in Medicine and Biology, Vol. 1, de Gruyter, Berlin, 1980.
- 10 P. Brätter and P. Schramel (Eds.), Trace Element Analytical Chemistry in Medicine and Biology, Vol. 2, de Gruyter, Berlin, 1983.
- 11 Proc. of the II Intern. Conf. on Chemical Analysis, Nuc. Instrum. Methods, 197 (1982).
- 12 J.A. Bearden, Rev. Mod. Phys., 39 (1967) 78-124.
- 13 W. Bambynek, B. Crasemann, R.W. Fink, H.U. Freund, H. Mark, C.D. Swift, R.E. Price and P.V. Rao, *Ibidem* 44 (1972) 716-813.
- 14 J.D. Garcia, R.J. Fortner and T.M. Kavanagh, *Ibid.*, 45 (1973) 111-177.
- 15 D.H. Madison and E. Merzbacher, in Atomic Inner-Shell Processes, Vol. 1, B. Crasemann (Ed.), Academic Press, New York, 1975, 1.
- 16 G.S. Khandelwal, B.H. Choi and E. Merzbacher, At. Data, 1 (1969) 103.
- 17 B.H. Choi, E. Merzbacher and G.S. Khandelwal, *Ibid.*, 5 (1973) 291.
- 18 E.R. Levin, Scanning Electron Microsc., 1 (1986) 65-76.
- 19 B. Gonsior and M. Roth, Talanta, 30 (1983) 385-400.

- 20 J.A. Cookson, Nucl. Instrum. Methods, 165 (1979) 477-508.
- 21 H.R. Wilde, W. Bischof, B. Raith, C.D. Uhlhorn and B. Gonsior, Ibid., 181 (1981) 165-170.
- 22 G.J.F. Legge and A.P. Mazzolini, Ibid., 168 (1980) 563-569.
- 23 G.J.F. Legge, Ibid., B3 (1984) 561-571 and other references therein.
- 24 W. Maenhaut, Ibid., 168 (1980) 557-562.
- 25 B. Gonsior, W. Bischof, M. Höffert, B. Raith, A. Stratmann and E. Rokita, Biological Trace Element Research, in press.
- 26 M. Höffert, B. Raith, B. Gonsior, E. Rokita and T. Cichoki, Scanning Electron Microsc., accepted for publication.
- 27 T.A. Cahill, R.G. Flocchini, P.J. Feeney and D.J. Shadoan, Nucl. Instrum. Methods, 120 (1974) 193-195.
- 28 R.L. Walter, R.D. Willis, W.F. Gutnecht and J.M. Joyce, Anal. Chem. 46 (1974) 843-855.
- 29 R. Klockenkämper, B. Raith, S. Divoux, B. Gonsior, S. Brüggerhoff and E. Jackwerth, Fresenius Z. Anal. Chem., in press.
- 30 H. Kaiser, Spectrochim. Acta 3 (1947/49) 40-67.
- 31 R. Klockenkämper, H. Bubert, Fresenius Z. Anal. Chem., 323 (1986) 112-116.
- 32 H. Bubert, R. Klockenkämper, Fresenius Z. Anal. Chem., 316 (1983) 186-193.
- 33 Intern. Union of Pure and Applied Chemistry, Spectrochim. Acta, 33 B (1978) 241-245.
- 34 B. Raith, M. Roth, K. Güllner, B. Gonsior, H. Ostermann and C.D. Uhlhorn, Nucl. Instrum. Methods, 142 (1977) 39-44.
- 35 I. Orlić, J. Makjanić and V. Valković, Ibid. B 3 (1984) 250-252.
- 36 G.L. Macdonald, Anal. Chem. 52 (1980) 100R-106R.
- 37 T.B. Johansson, M. Ahlberg, R. Akselsson, G. Johansson and K. Malmqvist, J. Radioan. Chem. 32 (1976) 207-217.
- 38 R.D. Vis and H. Verheul, Ibid., 27 (1975) 447-456.
- 39 J.A. Cookson, Nucl. Instrum. Methods, 181 (1981) 115-124 and other references therein.
- 40 G.J.F. Legge, Nucl. Instrum. Methods, B 3 (1984) 568-571 and other references therein.
- 41 H.R. Wilde, M. Roth, C.D. Uhlhorn and B. Gonsior, Ibid., 149 (1978) 675-678.
- 42 W. Lindh; D. Brune, G. Nordberg and P.O. Wester, Sci. Total Environ., 16 (1980) 109-112.
- 43 F. Folkmann, in Ion Beam Surface Layer Analysis, Vol. 2, O. Meyer, G. Linker and F. Kämpeler (Eds.), Plenum Press, New York, 1976, p. 747.
- 44 M.S. Ahlberg, Nucl. Instrum. Methods, 142 (1977) 61-65.
- 45 P.M.A. Van der Kam, R.D. Vis and H. Verheul, Ibid., 142 (1977) 55-60.
- 46 G.G. Seaman and K.C. Shane, Ibid., 126 (1975) 473-474.
- 47 A. Katsanos, A. Xenoulis, A. Hadjiantoniou and R.W. Fink, Ibid., 137 (1976) 119-124.
- 48 B. Raith, H.R. Wilde, M. Roth, A. Stratmann, B. Gonsior, Ibid., 168 (1980) 251-257.
- 49 B. Raith, A. Stratmann, H.R. Wilde, B. Gonsior, S. Brüggerhoff and E. Jackwerth, Ibid., 181 (1981) 199-204.
- 50 E.T. Williams, Ibid., B 3 (1984) 211-219.
- 51 H.R. Wilde, W. Bischof, B. Raith, C.D. Uhlhorn and B. Gonsior, Ibid., 181 (1981) 165-170.
- 52 M. Höffert, W. Bischof, A. Stratmann, B. Raith and B. Gonsior, Ibid., B 3 (1984) 572-578.
- 53 R.L. Watson, A.K. Leeper, B.I. Sonobe, T. Chiao and F.E. Jensen, Phys. Rev., A 15 (1977) 914.
- 54 J.V. Gilfrich, P.G. Burkhalter, L.S. Birks, Anal. Chem., 45 (1973) 2002-2009.
- 55 R. Klockenkämper, Ullmanns Encyclopädie der technischen Chemie, Bd. 5, Verlag Chemie, Weinheim, 4. Auflage (1980), 501.
- 56 R. Jenkins, R.W. Gould and D. Gedcke, Quantitative X-Ray Spectrometry, Dekker Inc., New York and Basel, 1981, 101 ff.
- 57 S. Brüggerhoff, E. Jackwerth, S. Salewski, B. Raith, S. Divoux, B. Gonsior,

- 58 R. Cesareo and G.E. Gigante, *Water, Air and Soil Pollut.*, 9 (1978) 99-111.
- 59 D.E. Leyden and G.H. Luttrell, *Anal. Chem.*, 47 (1975) 1612-1617.
- 60 K. Wundt, H. Duscher and K. Starke, *Ibid.*, 51 (1979) 1487-1492.
- 61 K. Zierold, *Scanning Electron Microsc.*, 2 (1983) 809-826.
- 62 H. Moor, *Freeze Etching, Techniques and Applications*, E.L. Benedetti, P. Favard (Eds.), *Société Française de Microscopie Electronique*, Paris, 1973, 11.
- 63 H. Moor, *Z. Zellforschung*, 62 (1964) 546-580.
- 64 H. Plattner, *Int. Rev. Cytol.*, 79 (1982) 237-304.
- 65 N.L. Burstein and D.M. Maurice, *Micron*, 9 (1978) 191-198.
- 66 M. Müller, N. Meister and H. Moor, *Mikroskopie*, 36 (1980) 129-140.
- 67 P. Pscheid, C. Schudt and H. Plattner, *J. Microsc.*, 121 (1981) 149-167.
- 68 T. Epsevik and A. Elgsaeter, *Ibid.*, 123 (1981) 105-110.
- 69 G. Knoll, G. Oebel and H. Plattner, *Protoplasma*, 111 (1982) 161-176.
- 70 K. Zierold, *Microsc. Acta*, 83 (1) (1980) 25-32.
- 71 J.L. Campbell, *Nucl. Instrum. Methods*, 142 (1977) 263-273.
- 72 E.M. Johansson and S.A.E. Johansson, *Ibid.*, B 3 (1984) 154-157.
- 73 H.C. Hansson, E.M. Johansson and A.K. Ekholm, *Ibid.*, B 3 (1984) 158-162.
- 74 R. Cecchi, G. Ghermandi, G. Calvelli and P. Mittner, *Ibid.* B 15 (1986) 605-607.
- 75 G. Bonani, J. Satish, H.U. Wanner and W. Wölfl, *Ibid.*, B 3 (1984) 493-497.
- 76 K.R. Akselsson, *Ibid.*, B 3 (1984) 425-430.
- 77 E. Bombelka, F.W. Richter, H. Ries and U. Wältjen, *Ibid.*, B 3 (1984) 296-300.
- 78 V. Valković, *Analysis of Biological Material for Trace Elements Using X-ray Spectroscopy*, CRC Press, Boca Raton, Florida (USA), 1980.
- 79 L. Kaufman, D.C. Price, M.A. Holliday, B. Payne, D.C. Camp, J.A. Nelson and F. Deconinck, *J. Radioan. Chem.*, 43 (1978) 321-346.
- 80 M. Berti, G. Buso, P. Colautti, G. Moschini, B.M. Stievano and C. Tregnagli, *Anal. Chem.*, 49 (1977) 1313-1315.
- 81 R.D. Vis, C.C.A.H. Van der Stap and A.J.J. Bos, *Nucl. Instrum. Methods*, B 3 (1984) 319-325.
- 82 A.S. Lodhi and M.D. Rashiduzzaman Khan, *J. Radioan. Chem.* 49 (1979) 89-92.
- 83 R. Lecomte, P. Paradis, S. Monaro, M. Barrette, G. Lamoureux and H.A. Menard, *Nucl. Instrum. Methods*, 150 (1978) 289-299.
- 84 V. Kleimola, J. Dahlbacka, P. Pakarinen, T.T. Salmi and V. Nõntõ in *Trace Element Analytical Chemistry in Medicine and Biology*, P. Brätter and P. Schramel (Eds.), de Gruyter, Berlin, 1980, 331.
- 85 M. Agarwal, R.B. Bennett, I.G. Stump and J.M. D'Auria, *Anal. Chem.*, 47 (1975) 924-927.
- 86 S. Brüggerhoff, E. Jackwerth, B. Raith, S. Divoux and B. Gonsior, *Fresenius Z. Anal. Chem.*, 316 (1983) 221-226.
- 87 P. Pakarinen, J. Pallon and R. Akselsson, *Nucl. Instrum. Methods*, B 3 (1984) 168-171.
- 88 G.S. Hall, N. Roach, M. Naumann and U. Simmons, *Ibid.*, B 3 (1984) 332-336.
- 89 E.J. Underwood, *Trace Elements in Human and Animal Nutrition*, 4th Ed., Academic Press, New York, 1977.
- 90 P. Brätter and P. Schramel (Eds.), *Trace Element Analytical Chemistry in Medicine and Biology*, Vol. 3, de Gruyter, Berlin, 1984.
- 91 G. Weber, G. Robaye, P. Bartsch, A. Collignon, Y. Beguin, J. Roelandts and J.M. Delbrouck, *Nucl. Instrum. Methods*, B 3 (1984) 326-331.
- 92 W. Maenhaut, L. de Reu, H.A. van Rinsvelt, J. Cafmeyer and P. van Espen, *Ibid.*, 168 (1980) 557-562.
- 93 A. Maruhashi, K. Kobayashi, K. Shima, T. Ishihara, T. Kusumoto, T. Inada and M. Akisada, *Ibid.*, B 3 (1984) 382-384.
- 94 H.A. Rinsvelt, R.W. Hurd, J.W.A. Kondoro, J.M. Andres and J.P. Mickle, B.J. Wilder, W. Maenhaut and L. De Reu, *Ibid.* B 3 (1984) 611-617.
- 95 H. Koyama-Ito, E. Wada, T. Tsumita, M. Horiuchi and S. Iwata, *Ibid.* B 3 (1984) 625-630.
- 96 F. Watt, G.W. Grime, J. Takacs and D.J.T. Vaux, *Ibid.*, B 3 (1984) 599-605.

- 97 K.G. Malmqvist, L.E. Carlsson, B. Forslind, G.M. Roomans and K.R. Akselsson, *Ibid.*, B 3 (1984) 611-61.
- 98 B. Gonsior and E. Szirmai, *Agressologie*, 22 (1981) 143-145.
- 99 E.C. Montenegro, G.B. Baptista, L.V. De Castro Faria and A.S. Paschoa, *Nucl. Instrum. Methods*, 168 (1980) 479-483.
- 100 G. Weber, G. Robaye, J.M. Delbrouck, J. Roelandts, O. Diberers, P. Bartsch and M.C. de Pauw, *Ibid.*, 168 (1980) 551-556.
- 101 P. Kiilholma, M. Grönroos, V. Kleimola, P. Pakarinen, J. Dahlbacka and V. Nääntö, *Mineral Elements '80, Proc. Nordic Symp. Helsinki, 1980*, 259-261.
- 102 V. Nääntö, J. Dahlbacka, P. Pakarinen, T. Markkanen, V. Kleimola, L. Salminen and H. Frey, *Ibid.*, 1980, 2, 439-443.
- 103 A.E. Simpson and N.A. Dyson, *Nucl. Instrum. Methods*, 146 (1977) 473-476.
- 104 N.A. Dyson, A.E. Simpson and J.T. Dabek, *J. Radioan. Chem.*, 46 (1978) 309-319.
- 105 G.J. Bouille, M. Peisach, W.S. Dempster and H. de V. Heese, *Ibid.*, 52 (1979) 153-165.
- 106 A.H. Khan, M. Khaliqzaman, M.B. Zaman, M. Husain, M. Abdullah and S. Akhter, *Ibid.*, 57 (1980) 157-167.
- 107 W. Koenig, F.W. Richter, J.Ch. Bode and B. Meinel, *Ibid.*, 58 (1980) 327-339.
- 108 U. Lindh and A.B. Tveit, *Ibid.*, 59 (1980) 167-191.
- 109 A.E. Pillay and M. Peisach, *Ibid.*, 63 (1981) 85-95.
- 110 M. Hyvärinen-Dabek, J. Räsänen and J.T. Dabek, *Ibid.*, 63 (1981) 163-175.
- 111 M.S. Rapaport, M. Mantel and R. Nothmann, *Anal. Chem.*, 51 (1979) 1356-1358.
- 112 S.E. Raptis, W. Wegscheider, G. Knapp and G. Tölg, *Ibid.*, 52 (1980) 1292-1296.
- 113 R. Di Toro, C. Moro, L. Perrone, G. Gialanella, G.F. Grossi and R. Moro, *J. Pediatr. Gastroenterol. Nutr.*, 4 (1985) 1-6.
- 114 G.S. Hall, N. Roach, U. Simmons, H. Cong, M.I. Lee, E. Cummings, *J. Radioan. Chem.*, 82 (1984) 329-339.
- 115 N. Saleh, *Ibid.*, 74 (1982) 257-262.
- 116 K.G. Malmqvist, G.I. Johansson, K.R. Akselsson, *Ibid.*, 74 (1982) 125-147.
- 117 J.P.W. Houtman, A. Bos, R. Vis, J.A. Cookson, P.S. Tjioe, *Ibid.*, 70 (1982) 191-208.
- 118 S.A.E. Johansson, *Fresenius Z. Anal. Chem.*, 324 (1986) 635-641.
- 119 E. Clayton and K.K. Wooller, *Anal. Chem.*, 57 (1985) 1075-1079.
- 120 R. Moro and G. Gialanella, *Proc. Intern. Symp. on Three-Day in Depth-Review on the Nuclear Accelerator Impact in the Interdisciplinary Field*, P. Mazzoldi and G. Moschini (Eds.), Padova, 1984, 101-105.
- 121 G.S. Hall and E. Navon, *Nucl. Instrum. Methods*, B 15 (1986) 629-631.
- 122 B. Forslind, K. Wiren and K.G. Malmqvist, *Scanning Electron Microsc.*, in press.
- 123 E. Johansson and U. Lindh, *Nucl. Instrum. Methods*, B 12 (1985) 170-172.
- 124 T.G.M.H. Dikhoff, J.A. Van der Heide and J.G. McVie, *Ibid.*, B 10/11 (1985) 639-642.
- 125 C.M. Fou, *Ibid.*, B 10/11 (1985) 643-644.
- 126 R.D. Vis, W.J.M. Lenglet and C.C.A.H. v.d. Stap, *Ibid.*, B 10/11 (1985) 683-692.
- 127 M.F. Mahrok, D. Crumpton and P.E. Francois, *Ibid.*, B 4 (1984) 120-126.

Chapter 4

ANALYSIS OF BIOLOGICAL SAMPLES BY X-RAY ATTENUATION MEASUREMENTS

ROBERTO CESAREO

Centro per l'Ingegneria Biomedica e
Cattedra di Fisica, Facoltà di Farmacia
Università di Roma "La Sapienza"
Corso Vittorio Emanuele II, 244, 00186 Roma (Italy)

4.1 INTRODUCTION

Over the last few years there has been an increasing interest in X-Ray attenuation measurements, mainly due to the enormous development of computer assisted tomography (CAT).

With CAT, analytical information concerning the density and the mean atomic number distributions in a sample is deduced from a large number of attenuation measurements (refs. 1, 2).

Unfortunately, in CAT, bremsstrahlung radiation is employed, and therefore, it is difficult to convert the qualitative analytical information into quantitative data.

Other equipment, based on the attenuation of X-or low-energy gamma radiation, are employed, in the medical field, for the measurement of bone mineral content (refs. 3,4), for the determination of fat content in tissues and other samples (refs. 5,6) and for the measurement of single elements in solution (ref. 7).

In addition, particular transmission methods have been developed, based on the "differential attenuation" method. When a sample containing a given element \underline{a} is crossed by a pair of X or gamma-rays that bracket, as close as possible, the K or L discontinuity in the attenuation coefficient of the element, then the ratio of the two rays transmitted through the sample depends only on the concentration c_a of the element \underline{a} (refs. 8-10).

In particular, in radiology, energy-dependent techniques for removing non iodinated structures from angiographic images have emerged over the last 20-30 years. The discontinuity in the attenuation coefficient is used to isolate iodinated from non-iodinated structures, and this method is known as K-edge dichromography (refs. 11-15).

In Sections 4.2 and 4.3 the theoretical background for attenuation of radiation and for differential attenuation of radiation will be given. In Section 4.3 details about the generation of monoenergetic X-rays will be discussed.

Applications of attenuation measurements in the field of Medicine will be discussed in Section 4.4.

4.2 Attenuation of radiation

When a monoenergetic beam of X or γ rays of energy E_0 and incident flux N_0 crosses a sample of density δ (g/cm³) and thickness x (cm), then the emerging flux from the sample will be given by:

$$N = N_0 \exp - (\mu/\delta) \delta x \quad (1)$$

where μ (cm²/g) represents the mass attenuation coefficient of the sample at energy E_0 .

If the sample is composed of n elements 1,2,3..... N with concentration values $c_1, c_2, c_3 \dots c_N$, then the composition of the sample can be determined, theoretically, if not less than $(N-1)$ attenuation measurements are carried out at different energies.

For example, if a water solution is considered, containing an element a at c_a parts per million concentration, then the attenuation coefficient of the sample will be:

$$\mu = \mu_w(1-c_a) + c_a \mu_a \quad (2)$$

where μ_w and μ_a are the attenuation coefficients of water and of element a , respectively.

If the element a is present only in traces, so that $c_a \ll 1$, then:

$$\mu \approx \mu_w + \mu_a c_a \quad (2')$$

The attenuated flux from a water sample and from a water sample with a trace element a at concentration c_a is respectively given by:

$$\begin{aligned} N_1 &= N_0 \exp -(\mu_w x) \\ N_2 &= N_0 \exp -(\mu_w + c_a \mu_a) x \end{aligned} \quad (3)$$

The minimum detectable limit (MDL) of transmission methods, at 3 standard deviations from the background, is given, in general, by:

$$MDL = 3\sqrt{N_1} c_a / (N_2 - N_1) \quad (4)$$

and in the case described by Eqs.(3):

$$MDL = 3 c_a / \{ \sqrt{N_0} \exp -(\mu_w x/2) (1 - \exp -(c_a \mu_a x)) \} \quad (4')$$

Considering the optimum thickness condition: $\mu x_{opt.} \approx 2$ (ref. 16):

$$MDL = 4.1 \mu_w / \sqrt{N_0} \mu_a \quad (5)$$

The MDL values of different elements in solution at 20, 40 and 60 keV incident energy, which can be deduced from Eq. (5), are reported in Table 4.1.

TABLE 4.1

Minimum detectable limits (ppm) at 3 S.D. level, for Ca, Fe, I and Pb in solution at 20, 40 and 60 keV, for $N_0 = 10^7$ photons.

Element	20 keV	40 keV	60 keV
Ca	80	195	400
Fe	40	95	215
I	40	16	35
Pb	12	25	50

For a more general approach (ref. 17) of N X-ray energies and N substances to be detected, Eq. (3) can be written in the form:

$$N_i = N_{i0} \exp\left\{-\sum_j \mu_{ij} x_j\right\} \quad i=1,2,\dots,N \quad (6)$$

where, now, μ_{ij} is the mass attenuation coefficient of the i -th substance at the i -th energy (cm^2/g) and x_j is the amount of substance j (g/cm^2). From Eq. (6) it can be deduced:

$$\ln N_{i0}/N_i = \alpha_i = \sum_j \mu_{ij} x_j \quad (7)$$

which can be written in the matrix form:

$$\begin{bmatrix} \mu_{11} & \mu_{12} & \dots & \mu_{1N} \\ \mu_{21} & \mu_{22} & \dots & \mu_{2N} \\ \dots & \dots & \dots & \dots \\ \mu_{N1} & \mu_{N2} & \dots & \mu_{NN} \end{bmatrix} \begin{bmatrix} x_1 \\ x_2 \\ \dots \\ x_N \end{bmatrix} = \begin{bmatrix} \alpha_1 \\ \alpha_2 \\ \dots \\ \alpha_N \end{bmatrix} \quad (8)$$

The solution of this set of Equations can be written:

$$x_i = \sum_j \mu_{ij}^{-1} \alpha_i \quad (9)$$

This set of Equations has no solution if any column of the matrix (8) is a linear multiple of each other; this means that if any two substances in the sample have mass attenuation coefficients with the same energy dependence, then the amount of the two different substances cannot be measured.

The determination of N different substances using N X-ray lines of different energy is difficult to realize since most substances tend to have mass attenuation coefficients of similar dependence versus energy (see Fig. 4.1).

This cannot be true when a substance or an element is considered which has an absorption edge in the region of interest.

Returning to the specific case of two elements (e.g. element a in water solution), Eq. (8) gives rise to the solution:

$$x_a = \{ \alpha_1 - (\mu_1/\mu_2)_w \alpha_2 \} / \{ \mu_{1a} - \mu_{2a} (\mu_1/\mu_2)_w \} \quad (10)$$

The standard deviation Δx_i of the amount of substance x will, therefore, be given, from Eq.(3), by:

$$(\Delta x_i)^2 = \sum_j (\mu_{ij}^{-1})^2 (\Delta \alpha_i)^2$$

But $\Delta \alpha_j = 1/\sqrt{N_j}$, thus:

$$(\Delta x_i)^2 = \sum_j (\mu_{ij}^{-1})^2 N_j^{-1} = \sum_j (\mu_{ij}^{-1})^2 N_{j0}^{-1} \exp \left(\sum_k \mu_{ik} x_k \right) \quad (11)$$

and, if $N_{j0} = N_0$ for all j :

$$(\Delta x_i)^2 = 1/N_0 \sum_j (\mu_{ij}^{-1})^2 \exp \sum_k (\mu_{ik} x_k) \quad (11')$$

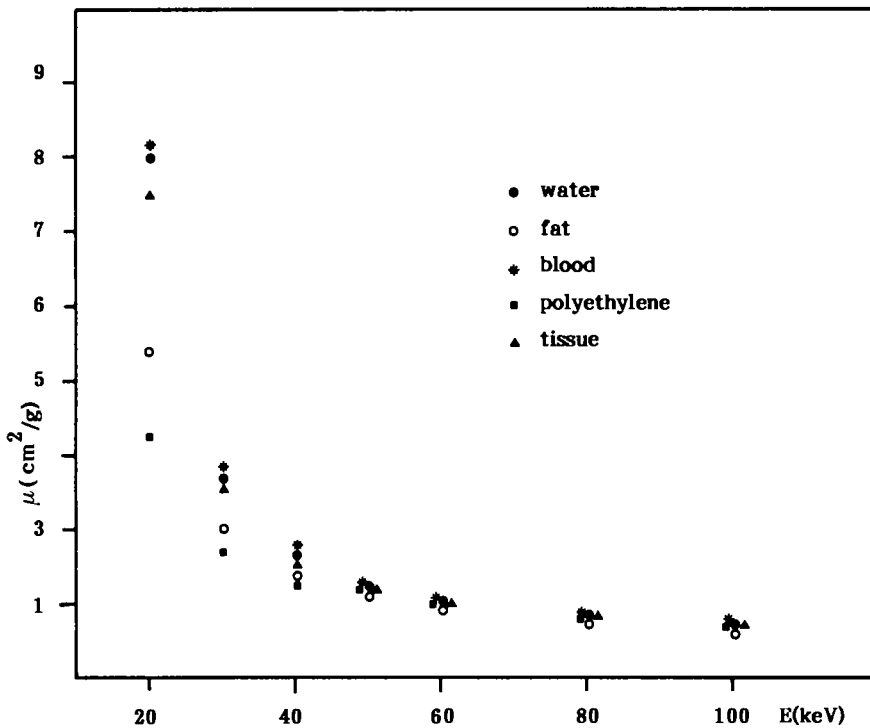


Fig. 4.1. Attenuation coefficient of water, fat, blood, polyethylene and tissue versus energy, in the range 20-100 keV.

4.2.1 Differential attenuation

By considering, for example, a sample of thickness x containing an element \underline{a} , having a concentration c_a , the attenuation of an incident radiation composed of a pair of X-rays of energies E_1 and E_2 respectively, is given, if the sample is a water solution, by:

$$N_1 = N_{10} \exp \{-\mu_w(1-c_a) + \mu_a c_a\} x \quad (12)$$

$$N_2 = N_{20} \exp \{-\mu'_w(1-c_a) + \mu'_a c_a\} x \quad (12')$$

in which N_{10} , N_{20} , N_1 and N_2 represent the intensity of incident and transmitted radiation at energies E_1 and E_2 , respectively; μ_w and μ'_w and μ_a , μ'_a represent the attenuation coefficients of water and of element \underline{a} at energies E_1 and E_2 , respectively.

The ratio $R = N_2/N_1$ can be defined, which can be written, from Eqs. (12):

$$R = R_0 \exp \{-\Delta\mu_w + \Delta\mu_a c_a\} x \quad (13)$$

where:

$$R_0 = \{N_{20} \exp(-\mu'_w x)\} / \{N_{10} \exp(-\mu_w x)\} \quad (13')$$

is the value of R for $c_a = 0$ (only water).

In Eq. (13), $\Delta\mu_a = (\mu'_a - \mu_a)$; $\Delta\mu_w = (\mu'_w - \mu_w)$. If the pair of X-rays of energies E_1 and E_2 closely bracket the photoelectric discontinuity of element \underline{a} , then, for a small difference between E_1 and E_2 , $\Delta\mu_w \ll \Delta\mu_a$, and, therefore:

$$\ln(R_0/R) = \Delta\mu_a x c_a \quad (14)$$

showing a linear relationship between $\ln(R_0/R)$ and the concentration c_a (ref. 18).

To "amplify" the effect of element \underline{a} it is necessary to select a pair of X-rays of energy E_1 and E_2 very close to each other, in order to minimize the difference, in the attenuation coefficient, of all other elements present in the sample (see Fig. 4.2).

The relative precision in the measurement of concentration c_a , i.e. σ_{c_a}/c_a can be derived from Eq. (13), and is given by:

$$\sigma_{c_a}/c_a = \{\exp(\bar{\mu}_w x/2)\} / \{N_0 \mu_a c_a x\} \cdot \{\exp(\mu_a c_a x) + \exp(\mu'_a c_a x)\}^{\frac{1}{2}} \quad (15)$$

if $N_{01} = N_{02} = N_0$ and $\mu_w = \mu'_w = \bar{\mu}_w$.

It is thus seen that the relative precision reaches a minimum value at a given value of the sample thickness and for an optimal c_a^* value satisfying the following condition:

$$\{\exp(\mu_a c_a^* x)\} (\mu_a c_a^* x - 2) = \{\exp(\mu'_a c_a^* x)\} (2 - \mu'_a c_a^* x) \quad (16)$$

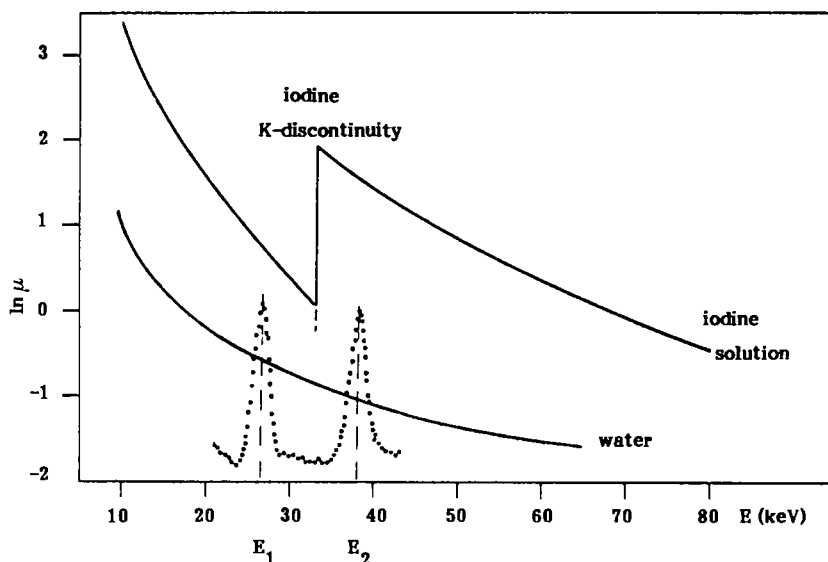


Fig. 4.2. Attenuation coefficient of a solution containing about 20% iodine, and principle of differential attenuation. Radiation of energies E_1 and E_2 which bracket the energy of the K-discontinuity of iodine is attenuated in a very different manner by a sample containing iodine and in a very similar manner by water or tissue.

4.3 EXCITATION SOURCES

For accurate transmission measurements, monoenergetic radiation, or at least quasi monoenergetic radiation is needed.

To this end, radioactive sources or X-ray tubes with secondary targets or synchrotron radiation can be employed. The intensity and tunability of synchrotron X-ray beams are highly suitable, in particular for "differential" transmission measurements. The properties of synchrotron radiation make it highly attractive as an X-ray source for use in a relatively safe and inexpensive K-edge dichromography (refs. 19 and 20).

Besides synchrotron radiation, radioactive sources can be employed. A list of useful radioactive sources is shown in Table 2.8.

When an X-ray tube is employed, coupled with appropriate secondary targets, then quasi monoenergetic radiation can be obtained in a range depending on the maximum voltage of the tube (ref. 21). A scheme of the X-ray system for monochromatizing the bremsstrahlung beam is shown in Figure 4.3, and is explained in Chapter 2, Section 2.2. The output radiation is constituted mainly by the K_α and K_β rays emitted by the secondary target.

When a completely monoenergetic beam is needed, then the output radiation has to be "filtered" through an absorber, constituted by a solution containing a filter element F in a given concentration. The element F is selected in such a manner that the energy of its K or L photoelectric absorption edge lies bet-

ween the energies of K_α and K_β rays (see Fig. 4.3). The absorber removes most of the K_β radiation as well as part of the K_α radiation (refs. 22 and 23).

It can be demonstrated (ref. 22) that the ratio of the intensities of K_α to K_β lines is given by:

$$N_\alpha / N_\beta = (N_{\alpha 0} / N_{\beta 0}) \exp (\Delta \mu_F c_F x_F) \quad (17)$$

if $\mu_w = \mu'_w$, and putting $\Delta \mu_F = (\mu'_F - \mu_F)$. The terms c_F and x_F are, respectively, the concentration of the filter element and the thickness of the solution.

From Eq. (17) it can be deduced that the value of N_α / N_β indefinitely increases with c_F and x_F . Unfortunately, the intensity of the α -line decreases in a similar manner, following the Equation:

$$\ln (N_{\alpha 0} / N_\alpha) = (\mu_w + \mu_F c_F) x_F \quad (18)$$

A compromise must be found between the opposite requirement of having a high N_α / N_β value and a low $N_{\alpha 0} / N_\alpha$ value.

Values of solution thickness x_F and concentration giving rise to attenuation values of $N_\alpha / N_{\alpha 0} = 0.33$ and $N_\alpha / N_\beta = 100$ are shown in Table 4.2.

As an example, X-ray spectra of Indium are reported in Figure 4.4, versus concentration of the filter element (silver) in water solution.

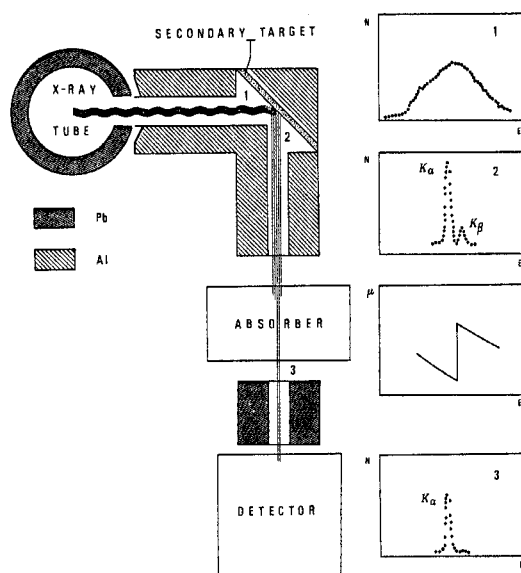


Fig. 4.3. Schema of the monoenergetic X-ray source. The collimated X-ray output, constituted by bremsstrahlung radiation (1), irradiates a fluorescent secondary target, placed at 45° . The output from the target (X-rays of the target element (2)) is collimated and crosses an absorber which selectively absorbs the K_β -X rays (attenuation coefficient μ of the absorbed is also reported). The radiation coming out from the absorber is therefore constituted by the K_α -peak mainly (3).

TABLE 4.2
Thickness x_F and concentration c_F of filter F for obtaining a ratio $N_\alpha/N_\beta = 100$ and $N_{\alpha 0}/N_\beta = 3$ for a secondary target.

Target	K_α and K_β energy values (keV)	Filter	Filter K-edge energy (keV)	x_F (cm.)	c_F (%)
Zinc	8.6 - 9.6	Cu	8.9	0.12	9
Strontium	14.1 -15.9	Rb	14.9	0.7	4
Indium	24.1 -27.6	Ag	25.5	2.4	2.3
Barium	32.0 -36.8	Cs	36.0	3.6	2.7

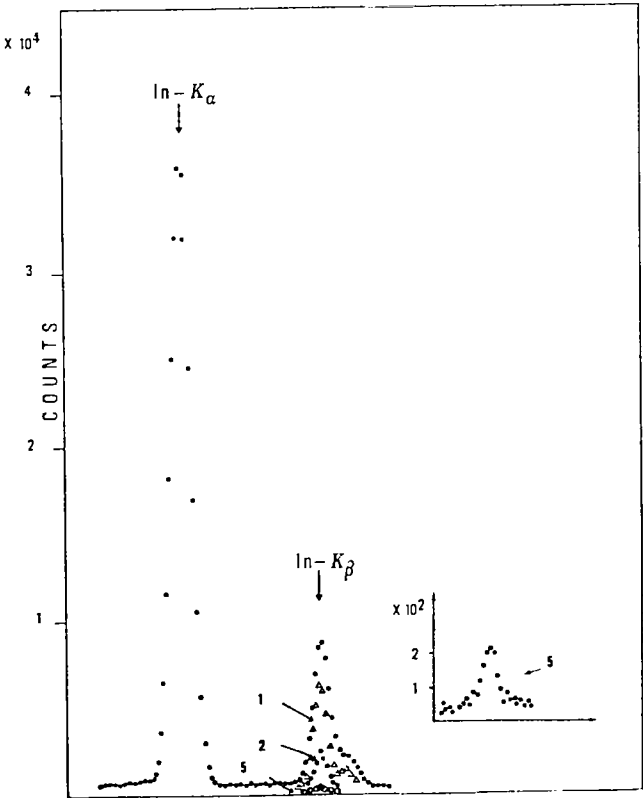


Fig. 4.4. Fluorescent X-rays from a Indium secondary target crossing a silver solution 3 cm thick at various concentration values (in %). The attenuation of K_β -peaks versus increasing Ag-concentration is shown. The K_α -peak is kept constant.

4.4 APPLICATIONS OF ATTENUATION MEASUREMENTS IN MEDICINE.

4.4.1 General considerations

The general problem, described in Section 4.2, of a set of N equations and N-transmission measurements, for determining the concentration of N elements or substances (see Eq.(9)) is very difficult to resolve since most substances or elements have mass attenuation coefficients of similar dependence versus energy.

Mass attenuation coefficients of many biological materials can be approximated as a linear combination of the coefficients of two so-called "basis" materials, and therefore, at incident energy E:

$$\mu/\delta(E) = \alpha_1 (\mu/\delta)_1 + \alpha_2 (\mu/\delta)_2 \quad (19)$$

where the subscripts 1 and 2 refer to the two basis materials, which should be sufficiently different in their atomic number Z and thereby also in their Compton and photoelectric attenuation characteristics.

The two basis materials hypothesis can be usefully applied for evaluating the attenuation of a water solution (water + one element in solution), in bone (tissue + $\text{Ca}_{10}(\text{PO}_4)_6 \cdot (\text{OH})_2$), in tissue containing fat (tissue without fat + fat), in tissue containing a contrast agent (iodine, barium and so on). In some cases, attenuation measurements are carried out at one or two incident energies without any regard to the photoelectric discontinuity of the elements in the sample (bone mineral content, fat content in tissue and so on), in other cases attenuation measurements are carried out at two energies above and below the photoelectric discontinuity of the contrast agent or of any element present in the sample.

4.4.2 Bone mineral content

This method was first suggested by Cameron and Sorenson (ref. 3) and then mainly developed by Cameron and coworkers (refs. 24-26).

Many instruments have been developed by Cameron and others for the determination of bone mineral content (see for example Fig. 4.5).

The most simple equipment is characterized by a radioactive I-125 source (half-life: 60 days; emitted radiation: 27.2 keV and 31.4 keV X-rays of Te), by a NaI(Tl) detector and by an electronic chain for the acquisition and analysis of the data. In general, the forearm attenuation is measured.

In more sophisticated equipment, a second radioactive source of Am-241 is used (half life: 468 years; emitted radiation: 59.6 keV), allowing the measurement in larger bones.

Attenuation of radiation by bone is given by the Equations:

$$\ln(N_0/N) = \mu x \quad \text{or} \quad \Delta y \Delta z \ln(N_0/N) = \mu \Delta V \quad (20)$$

in which $(x\Delta y\Delta z) = \Delta V$ is the irradiated volume. By assuming the bone as constituted by soft tissue, which is a combination of skin, fat, flesh, collagen and body fluids, having an absorption coefficient nearly the same as water, plus mineral (hydroxyapatite = $\text{Ca}_{10}(\text{PO}_4)_6(\text{OH})_2$), the following Eqs. can be written

$$\mu\Delta V = \mu_m \Delta V_m + \mu_w (\Delta V - \Delta V_m) \quad \text{or}$$

$$(\mu_m - \mu_w) \Delta V_m = \mu\Delta V - \mu_w \Delta V$$

and from Eq. (20 b):

$$(\mu_m - \mu_w) \Delta V_m = \Delta y \Delta z (\ln N_w - \ln N) \quad (21)$$

in which N_w refers to the intensity of radiation crossing a sample of water of the same volume of the bone. Since $\Delta V_m = \Delta m_m / \delta_m$, where $\delta_m = 3 \text{ g/cm}^3$ is the density of mineral in bone, then:

$$\Delta m_m = \{\Delta z \Delta y (\ln N_w - \ln N)\} / (\delta_m (\mu_m - \mu_w)) \quad (22)$$

In Eq. (22) all parameters are known or can be measured. Therefore the mineral content in bone can be deduced from Eq. (22). By scanning the entire bone, the total mineral content can be measured:

$$m_m = \{\delta_m / (\mu_m - \mu_w)\} \Delta y \Delta z \sum_i (\ln N_w - \ln N) \quad (22')$$

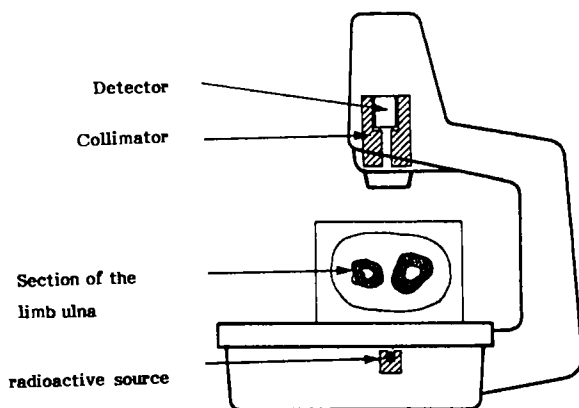


Fig. 4.5. Schema of a typical "Cameron" instrument for the measurement of the bone mineral content. X-rays from a radioactive source, crossing the limb ulna are attenuated from the bone in a manner depending on the mineral content.

Results of typical measurements are shown in Fig. 4.6.

Measurements of bone mineral content are carried out on the limb ulna (about 6 cm from the wrist), as there is a good correlation with the total body mineral content. The attenuation measurement is first carried out on the limb placed in a muff containing water. In such a manner, a reference volume is obtained (see Eq.(21)). A complete scanning of the limb is then carried out (see Fig. 4.6). With equipment for mineral content measurement, early diagnosis of osteoporosis and other diseases producing modifications in the bone mineral content is possible, as well as the monitoring of therapy for reproducing normal conditions.

4.4.3 Fat content in tissues

Determination of fat content in tissues can be considered a two basis materials problem, which are:

- tissue without fat (mean composition: 77.4% O, 10% H, 9% C, 2.7% N, 0.31% K, 0.24% S, 0.19% P);
- fat (mean composition: 77% C, 11.5% O, 11.5% H).

By considering the attenuation of monoenergetic radiation of energy E_1 and E_2 by a sample, the following Equations can be written:

$$N_1 = N_{10} \exp -\{\mu(E_1)x\} \quad N_2 = N_{20} \exp -\{\mu(E_2)x\} \quad (23)$$

From Equations (23), the ratio R can be defined as:

$$R = \ln(N_{10}/N_1) / \ln(N_{20}/N_2) = \mu(E_1)/\mu(E_2) \quad (24)$$

and for a two component sample:

$$R = \{c_a \mu_a(E_1) + c_b \mu_b(E_1)\} / \{c_a \mu_a(E_2) + c_b \mu_b(E_2)\} \quad (25)$$

By observing Fig 4.1, the attenuation coefficients of fat and tissue have approximately the same value for $E > 80$ keV. Then, for $E_2 > 80$ keV:

$$\mu_f(E_2) = \mu_t(E_2)$$

where μ_f and μ_t indicate the attenuation coefficient of fat and tissue, respectively. Eq. (25) can therefore be written in the form:

$$R = c_f \{\mu_f(E_1)/\mu_f(E_2)\} + c_t \{\mu_t(E_1)/\mu_t(E_2)\} \quad (26)$$

Further, since $c_f + c_t = 1$:

$$R = c_f \{\mu_f(E_1)/\mu_f(E_2) - \mu_t(E_1)/\mu_f(E_2)\} + \{\mu_t(E_1)/\mu_f(E_2)\} \quad (27)$$

showing a linear relationship between fat content c_f and ratio R (ref. 5).

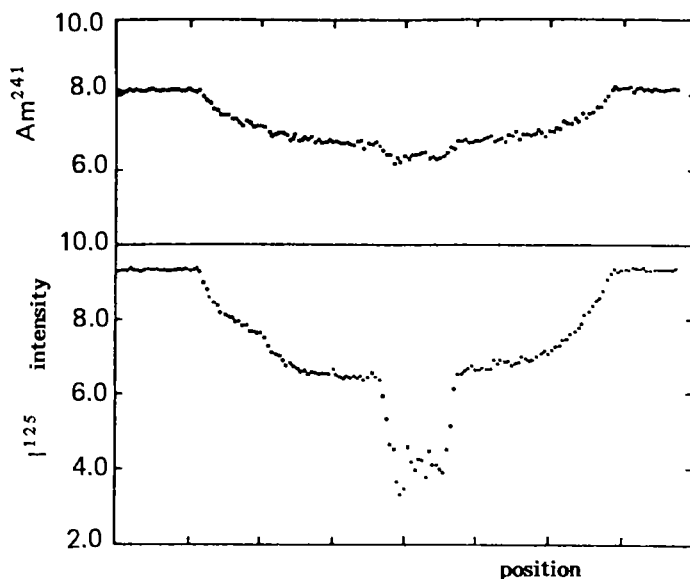


Fig. 4.6. Counts versus position in a limb-scan carried out with the instrument shown in Figure 4.5 for bone mineral content measurement. Upper curve: Am-241 radioactive source emitting 59.6 keV γ rays; lower curve: I-125 radioactive source emitting 27.3 and 31.3 keV X-rays.

4.4.4 Differential attenuation measurements and medical images

As described in Section 4.1, and theoretically discussed in Section 4.2.1, the method of employing, in attenuation measurements, a pair of monoenergetic X-rays which energies bracket the energy of the photoelectric discontinuity of a given element provides selective isolation of the element.

Applications of this method require, ideally, to work with monoenergetic X-rays, which can be obtained from an X-ray tube by filtering the continuous bremsstrahlung radiation or by using secondary targets. However, these processes considerably reduce the intensity of the radiation making exposure times much too long for medical use. Monoenergetic X-rays of sufficient intensity can be obtained with a synchrotron, but a synchrotron is large and expensive.

Applications have been performed on test objects, or in fields where measuring time is not critical, such as:

- (1) human thyroid scans (ref. 17).

For analysis of iodine in thyroid, Ba-K _{α} (32.06 keV) and Ce-K _{α} (34.56 keV) X-rays have been employed, which energy bracket the energy of I-photoelectric discontinuity (33.16 keV).

Thyroid scans have been carried out in both lateral and anterior position on euthyroid patients.

(2) in vitro bone scanning (ref. 17).

Calcium distribution in thin sections of rat femur have been investigated, by utilizing the K-discontinuity of calcium, at 4.04 keV.

(3) differential CT-images on test objects (ref. 27).

Differential CT-images have been carried out by employing monoenergetic radiation from an X-ray tube with secondary targets. For example, in Figure 4.7 are reported the tomograms of a plexiglas test object with 4 holes filled with a water solution containing 4,2,1 and 0.5% I, measured at 35.4 keV (A: Ce-K lines) and at 32.8 keV (B: Ba-K lines). The difference between the attenuation coefficient of the two images is shown in Figure 4.7.C.

The same effect was studied on lead, employing the L_{II} - discontinuity at 15.2 keV. Tomograms carried out at 15.7 keV (A: K-lines of Zr) and 14.9 keV (B: K-lines of Y), and their difference (Figure 4.8.C) are shown in Figure 4.8.

The same method can be extended to other elements which have an useful energy value of K-or L discontinuity.

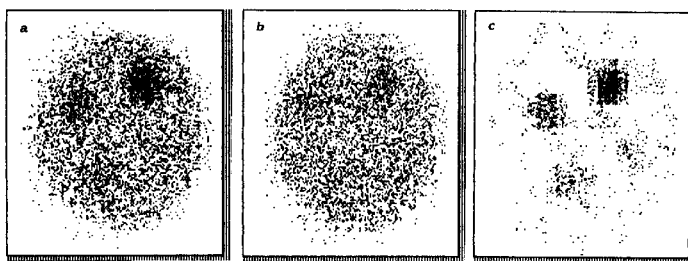


Fig. 4.7. CT-images of a plexiglas cylinder of diameter $\phi = 4$ cm with 4 holes with diameter $\phi = 0.8$ cm filled with water solutions containing 4,2,1 and 0.5% I, carried out at 35.4 keV (Ce-X-K lines) and at 32.8 keV (Ba-X-K lines). The difference between tomograms A and B is shown in Fig. 4.7.C.

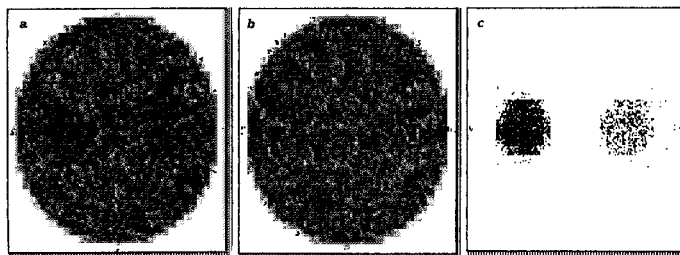


Fig. 4.8. CT-images of a plexiglas cylinder of diameter $\phi = 2$ cm with 2 holes with diameter $\phi = 0.6$ cm filled with water solutions containing 1 and 0.5% Pb respectively, carried out at 15.7 keV (Zr-X-K lines) and at 14.9 keV (Y-X-K lines). The difference between tomograms A and B is shown in Fig. 4.8.C.

REFERENCES

- 1 E.C. Mc Cullough, *Med. Phys.*, 2 (1975) 307.
- 2 W.R. Hendee, *The physical principles of computed tomography*, by Little, Brown and Co., Boston, Toronto, 1983.
- 3 J.R. Cameron, J.A. Sorenson, *Science*, 142 (1963) 230.
- 4 R.B. Mazess, J.R. Cameron, J.A. Sorenson, *Nature*, 228 (1970) 771.
- 5 L.E. Preuss, E.P. Bolin, *Isot. Radiation Techn.*, 9 (1972) 501.
- 6 L.E. Preuss, E.P. Bolin, *Isot.*
- 7 R. Cesareo, *Tecniche nucleari di analisi in medicina*, La Goliardica, Roma 1984.
- 8 W.H. Oldendorf, M.E. Phelps, P.B. Hoffer, H. Tanaka, *Am. J. Roentgenol.*, 120 (1974) 583.
- 9 R. Cesareo, L.J. Pedraza, *Nucl. Instrum. Methods*, A 239 (1985) 367.
- 10 B.K. Rutt, I.A. Cunningham, A. Fenster, *Med. Phys.*, 10 (1983) 801.
- 11 B. Jacobson, *Acta Radiol.*, 39 (1953) 437.
- 12 H.L. Atkins, W. Hauser, H.W. Kraner, *Am. J. Roentgenol.* 114 (1972) 176.
- 13 J.A. Sorenson, *J. Nucl. Med.*, 20 (1979) 1286.
- 14 C.A. Mistretta, M.G. Ort, F. Kelez, J.R. Cameron, M.P. Siedband, A.B. Crummy, *Invest. Radiol.*, 8 (1973) 402.
- 15 F. Kelez, C.A. Mistretta, *Med. Phys.*, 3 (1976) 159.
- 16 W.B. Gilboy, *Nucl. Instrum. Methods*, 221 (1984) 193.
- 17 J.L. Alberi, H.W. Kraner, *IEEE Trans. Nucl. Sci.*, NS-34 (1987) 635.
- 18 R. Cesareo in Z. Bajzer, P. Baxa, C. Franconi (Eds.), *II Intern. Conf. on Applications of Physics to Medicine and Biology*, World Sci. Publ. Co., Singapore (1983) 219.
- 19 J.N. Otis, H.D. Zeman, E.B. Hughes, L. Campbell Finman, R. Hofstadter, A. Hudson, J. Rolfe, E. Rubenstein, D.C. Harrison, R.S. Kernoff, A.C. Thompson, G.S. Brown, *IEEE Trans. Nucl. Sci.*, NS-31 (1984) 581.
- 20 E. Rubenstein, *1st Frascati Meeting on SR applications to digital subtraction angiography*, Frascati(Italy) 6-8 may 1987.
- 21 K. Doi, C.J. Vyborny, G. Holje, *Radiology*, 142 (1982) 233.
- 22 R. Cesareo, work in preparation.
- 23 R. Cesareo, G. Viezzoli, E. Alexiu, G. Sacchetti, M. Sgarbazzini, S. Merli, in S. Onori and E. Tabet (Eds.), *Physics in Environmental and Biomedical Research*, World Sci. Publ. Co., Singapore (1986) 179.
- 24 J.A. Sorenson and J.R. Cameron, *J. Bone Jt. Surg.*, 49-A (1967) 481.
- 25 J.R. Cameron (Ed.), *Proc. Bone Measurement Conference*, CONF-700515 (USAEC Techn. Information div., Springfield, VA 22151).
- 26 C. Colbert, R.B. Mazess, P.B. Schmidt, *Invest. Radiol.*, 6 (1971) 432.
- 27 R. Cesareo, submitted to *Nucl. Instrum. Methods* (1987).

Chapter 5

SCATTERING OF LOW ENERGY X- OR GAMMA MONOENERGETIC RADIATION

GIOVANNI E. GIGANTE

Centro per l'Ingegneria Biomedica

Università di Roma "La Sapienza" e

Dipartimento di Scienze Biomediche

Facoltà di Medicina e Chirurgia, 67100 L'Aquila (Italy)

5.1 INTRODUCTION

Many researchers concerned in transmission techniques have wondered whether scattered photons, produced simultaneously in the sample, could be used to obtain analytical information complementary or of better quality than that obtained by the transmitted photons.

They know that the Compton scattering is directly related to the electron density and that the coherent scattering strongly depends upon the atomic number of the target. However, they also know that the intensity of the scattered radiation is low compared to transmitted radiation.

It is worthwhile pointing out (see Fig. 5.1) that the volume from which the scattered photons emerge, is only a small portion of the total volume crossed by the primary photon beam. Moreover, the fluence of photons through an angle is proportional to the differential scattering cross-section, which is only a small fraction of the total collision cross-section.

However, this kind of technique is not frequently used for several reasons, and mainly because of the extraordinary analytical power of absorptiometric techniques that in many cases lead to satisfactory results with the adjustment of few physical parameters and the use of suitable methods of measurement.

Nevertheless, after an early enthusiasm, the normal attitude of most research workers is of skepticism regarding the use of scattered radiation in solving analytical problems. This attitude is mainly due to the number of physical and geometrical parameters to be studied and optimized in a technique using scattered photons. Actually, the use of these techniques is hardly ever immediate, on account of a series of experimental obstacles.

However, during the last decade many analytical techniques using the detection of scattered photons have been suggested,. They have been proposed

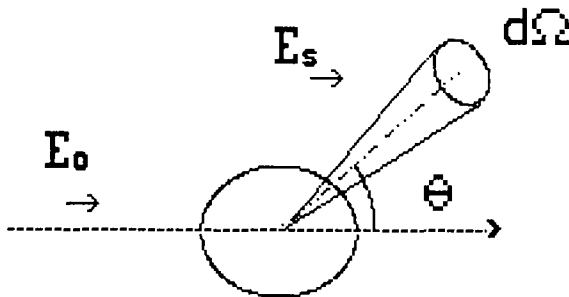


Fig. 5.1. Scattering of a narrow primary photon beam from a monoelemental target. The scattered photons into a solid angle ($d\Omega$) can be calculated through the differential cross-section ($d\sigma/d\Omega$) for the scattering processes.

for the "in vitro" and "in vivo" measurement of physical parameters such as the effective atomic number (Z_e), mass (ρ) (or the electronic (ρ_e)) density of the sample and the sample mass or thickness.

The most interesting medical application of scattering techniques is that of tissue characterization. This is a typical analytical problem in which one or more physical parameters have been considered as representative of the tissue state. To give an example, if a parameter assumes a value in a certain range the tissue is healthy, while if it falls in another range, the tissue is affected by a particular disease. Unfortunately, as already observed in the case of bone disease the definition of the interval of values corresponding to a particular state, is not easy. In fact, a large amount of accurate data is needed to establish a good statistical significance of the different interval limits.

This topic was introduced in connection with the computed tomography techniques (CT); then it was extensively studied by means of other imaging techniques, with a special effort for ultrasounds. It should be stressed that in tissue characterization an absolute measurement is required. Therefore, only analytical techniques having good performance, especially "in vivo", in terms of sensitivity, precision, and accuracy may be used.

The photon scattering techniques, referred to below as P.S.T., can be subdivided into two main classes according to the energy resolution of the detector used. One class includes the techniques in which the reduced resolution of the detector (usually a scintillator) is not sufficient to separate the coherent and Compton scattering peaks. In these techniques usually is used the approximation to consider the scattered photons only due to the Compton scattering. Therefore, these are employed mainly in the determination of the electron density of the tissues, using single- and dual-source configurations (refs. 1-6).

The imaging techniques using Compton scattering can be considered as belonging to this class. Attempts have been made to produce an image of internal tissue density by using an external source of gamma rays and scintillator or semiconductor detectors placed at an angle to the incident beam. Tomographic systems, using one or more scintillator scanning detectors, semiconductor detectors, and gamma camera, have been described (refs. 7-11). These were initially proposed in planning the radiation therapy and later for certain diagnostic purposes. These techniques are less precise and accurate than fixed point systems, but their capacity to produce an image is very important for many applications. Only the analytical aspects of these techniques are discussed in the present chapter.

To the other class belong those techniques that use both coherent and Compton scattering. These may be performed only with the use of high energy resolution detectors, i.e. with a FWHM of a few hundred eV, such as hyperpure Germanium detectors. The most important technique of this class uses the coherent to Compton scattering ratio, referred to here as the Rayleigh/Compton technique (R/C.T.). It was proposed about 10 years ago to measure the effective atomic number (refs. 12-14) and later to evaluate the trabecular bone mineral concentration (refs. 15-17). This technique uses the scattering intensity ratio to reduce the influence on the accuracy of the geometrical and attenuation effects.

Further, the scattering theory and the limitations of the use of these techniques "in vivo" is briefly discussed. Finally, in the last two sections the main characteristics of P.S.T. and their analytical performances are discussed.

5.2 INCOHERENT (COMPTON) AND COHERENT SCATTERING OF LOW ENERGY X- AND GAMMA MONOCHROMATIC RADIATION

In the energy range of photons of biomedical interest (i.e., in the 30 to 100 keV range), the only scattering processes to be taken into account are

(i) the incoherent (Compton) scattering and (ii) the coherent scattering, that, in this energy range is almost entirely due to Rayleigh scattering.

A better understanding of the behaviour of scattering differential cross-sections, as a function of energy (E_0), the scattering angle (θ) and the atomic number (Z), enables us to establish the capacity of P.S.T. to solve analytical problems. Moreover, the simple study of the cross-sections behaviour and the knowledge of the detection efficiency and the source strength, enable a first evaluation to be made regarding the possibility of carrying out a measurement.

5.2.1 Compton scattering

According to the classic theory of inelastic scattering of a photon with a free electron (using the conservation of energy and momentum), the energy of the scattered photon is related to the scattering angle by the following relation:

$$E_c = E_0 \left(1 + \left(\frac{E_0}{mc^2} (1 - \cos \theta) \right) \right)^{-1} \quad (1)$$

It is well known that the energy distribution of the scattered photons is broadened around the E_c value because of the electron motion in the target (ref. 18). This broadening effect gives rise to the characteristic Compton profile; an example of this is shown in Figure 5.2, where scattering spectra produced by a monochromatic radiation (60 keV) in a low Z target detected at

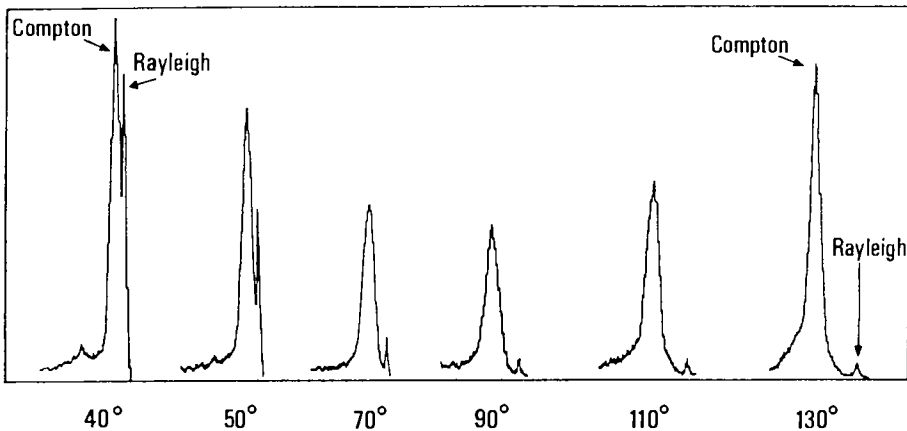


Fig. 5.2. Scattered spectrum produced in a low atomic number target by monochromatic radiation ($E = 60$ keV) detected at different scattering angles.

different scattering angles, are represented. This figure shows two important facts: the shift towards lower energies of the maximum of the Compton band that increases with the scattering angle and the minimum of the Compton intensity at ninety degrees.

It is worth noting that, in a configuration with finite size of the source and detector, the shape of the Compton band is partially due to geometrical effects. Figure 5.3 shows a change of the scattering angle in a sample of finite size. An imaging technique using the consequent energy shift of the Compton band maximum has been proposed by Farmer and Collins (ref. 9). This kind of effect must be taken carefully into account, especially when working with a low energy resolution detector, such as a scintillator.

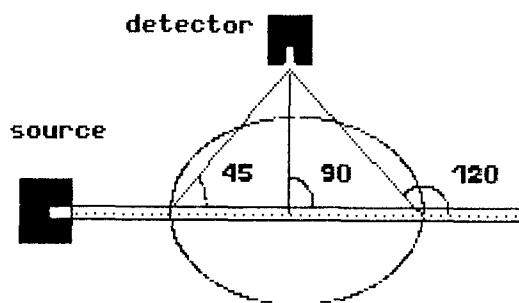


Fig. 5.3. Change of the scattering angle within a finite geometry. When the sample size is not negligible the scattering angle is not univocally defined.

An illustration of what might occur is given in Figure 5.4 showing a scattering spectrum from an ancient painting, obtained using a well collimated assembly of two americium-241 point sources and a hyperpure germanium detector. The double peak of the Compton scattering is due to the wood support behind the canvas.

Multiple scattering events also contribute to the enlargement of the Compton profile, sometimes producing characteristic small humps at the left, i.e. at lower energies of the Compton band.

The Compton scattering differential cross-section, that represents the scattering for unit solid angle ($d\Omega$) in a certain direction (see Fig. 5.1), can be expressed by

$$\frac{d\sigma_I}{d\Omega} = \frac{d\sigma_{KN}}{d\Omega} S(x, Z) \quad (2)$$

where $d\sigma_{KN}/d\Omega$ is the Klein-Nishina cross-section for a single free electron that, using the definition of E_c given in Eq. (1), can be written as

$$\frac{d\sigma_{KN}}{d\Omega} = \frac{r^2}{2} \left(\frac{E_0}{E_c} \right)^2 \left(\frac{E_0}{E_c} + \frac{E_c}{E_0} - \sin^2 \theta \right) \quad (3)$$

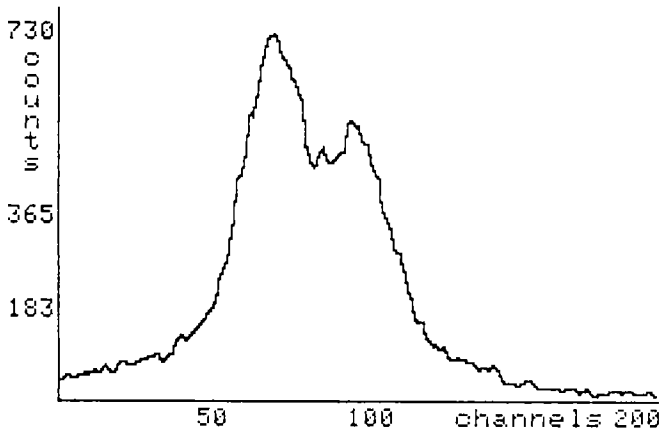


Fig. 5.4. A scattering spectrum from an old painting. The woody support behind the canvas has produced the doubling of the Compton peak.

where r is the classic electron radius (e^2/mc^2); $S(x, Z)$ is the incoherent scattering function whose deviation from Z is a measure of the effect of electron binding, and

$$x = \frac{\sin \frac{\theta}{2}}{\lambda} = \frac{E_0}{12.4} \sin \frac{\theta}{2} \quad (4)$$

is the momentum transfer variable. In Eq. (4), the wavelength (λ), and the energy (E_0) are expressed in Angstrom and keV, respectively.

The binding effects are important for small x values, i.e., small scattering angle and low energy, and they are stronger for high Z elements. For example for very low Z elements these effects are negligible for energy E_0 greater than 50 keV while in calcium binding effects are not negligible even for energies up to 300 keV. However, the function $S(x, Z)$ assumes the asymptotic value of Z for high x values. A good tabulation of the $S(x, Z)$ function has been reported by Hubbell et al. (ref. 19).

The angular distribution of the Compton scattering photons is of particular interest for some P.S.T.'s. Figure 5.5 shows the characteristic behav-

four of the Compton cross-section as a function of the scattering angle at different energies E_0 . It can be seen that the characteristic minimum near ninety degrees is less pronounced at lower energies, due to the electron binding effects. At higher energies and with large scattering angles, the shape of the curves is similar to that of the Klein-Nishina function. At small scattering angles, the electron binding effects are evident. At these angles, the reduced intensity of the Compton scattering is characterized by a corresponding increase in the coherent scattering (see next section).

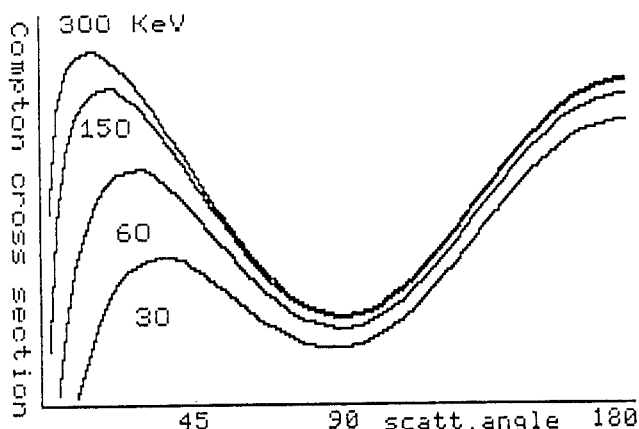


Fig. 5.5. Compton differential cross-section as function of photon scattering angle and energy. The strong reduction at very small angles (< 45 degrees) is due to the electron binding effects.

The Compton scattering intensity decreases with energy; an example of this behaviour is shown in Figure 5.6 for soft tissue. This Figure shows the characteristic decrease of the interaction cross-sections with energy; is evident the more rapid reduction of the coherent scattering and photoelectric cross-sections.

From an analytical point of view, it is more interesting the decrease of the Compton scattering intensity with Z . In particular, to study this behaviour in a multielemental target it is necessary to introduce the differential mass absorption coefficient for Compton scattering

$$\frac{\mu_I}{\rho} = N_A \left(\frac{d\sigma_{KN}}{d\Omega} \left(\sum_Z \left(w_Z \frac{S(x, Z)}{A_Z} \right) \right) \right) \quad (5)$$

where A_z and w_z are the atomic weight and the weight fraction respectively, of each element (Z) of the sample, ρ is the mass density, and N_a is the Avogadro number. The sum must be calculated upon all the elements contained in the sample.

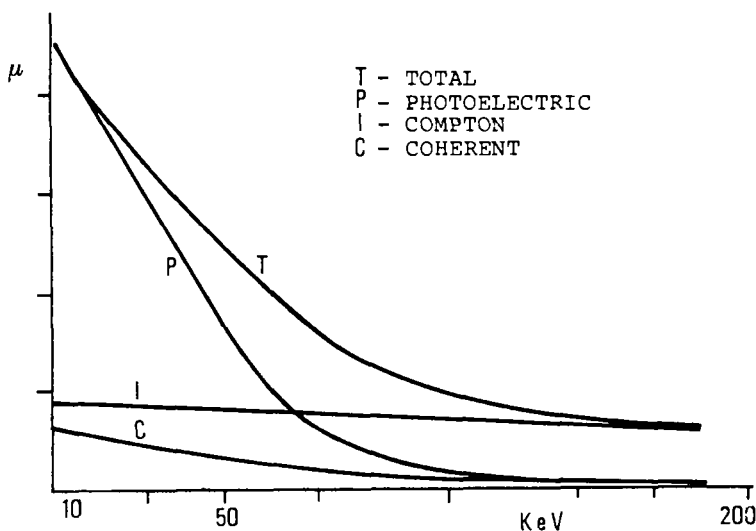


Fig. 5.6. Attenuation coefficients vs photon energy for soft tissue. The photoelectric and coherent coefficients decrease as $E^{-3.28}$ and $E^{-2.02}$, respectively.

As $S(x, Z)$ is always lower than Z , the Compton scattering intensity decreases with Z more rapidly, than the (Z/A) ratio. In fact, for high atomic numbers, the function $S(x, Z)$ approaches slowly its asymptotic value. This behaviour is clearly shown in Figures 5.7 and 5.8, where the Compton scattering cross-section over Z vs atomic number is reported for two energies.

However, we can expect that for high x values (i.e. energies higher than one hundred keV and not very small angles), the commonly used assumption of a direct proportionality between Compton scattering and the electron density is true. In fact, the electron density is defined as follows

$$\rho_e = \rho \sum_Z w_Z \frac{Z}{A_Z} \quad (6)$$

where the sum is performed upon the elements compounding the material.

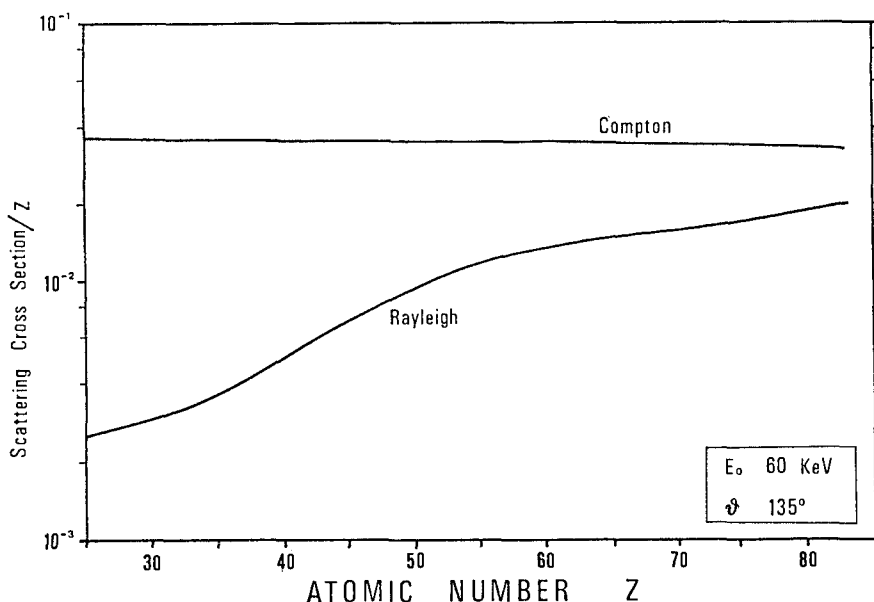


Fig. 5.7. Compton and Rayleigh scattering cross-section over Z , as a function of Z for 60 keV photons and at an angle of 135 degrees.

5.2.2 Coherent scattering

Coherent scattering, i.e. the emission in all directions of scattered photons with energy equal to that of the incident photons, is a consequence of some processes taking place in the photon interaction with bound electrons (known as Rayleigh scattering), and the nuclei (Thompson scattering). However, in the photon energy range considered here, coherent scattering is almost entirely due to Rayleigh scattering.

Coherent scattering is of increasing interest for medical physics, as recently pointed out by several authors (refs. 20-23). Much effort has been devoted, in recent years, to obtain a better theoretical evaluation of the coherent scattering cross-sections (refs. 22-24).

Coherent scattering, at first approximation, can be well explained in terms of the classic theory of the electron. When an electromagnetic wave is incident on an electron, a periodic force is exerted which sets the electron into vibration at the forcing frequency. The electron then radiates electromagnetic energy, the intensity and angular distribution of it being determined by its behaviour as an electric dipole. This radiation appears as

scattered photons of the same energy of the incident photons.

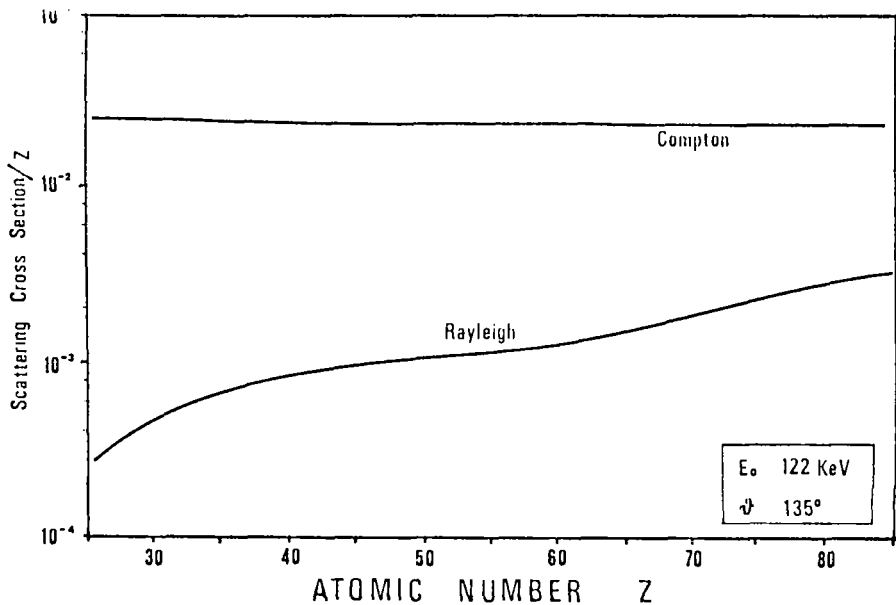


Fig. 5.8. Compton and Rayleigh scattering cross-sections over Z, as a function of Z, for 120 keV photons and at an angle of 135 degrees.

This theory seems to be in contrast with that proposed in the previous section for the Compton scattering. This is indeed true, but part of the electrons involved in the scattering processes may be considered loosely bound to their parent atoms, which in turn are bound to the crystal lattice. The theory states that the momentum of the incident photon is taken up by the parent atom, or the lattice, or the molecule. However, the coherent scattering is in competition with the incoherent scattering.

From the classic theory of the electron, it is possible to deduce the Thomson differential cross-section, given here by

$$\frac{d\sigma_T}{d\Omega} = \frac{r^2}{2}(1 + \cos^2 \theta) \quad (7)$$

This classic approach clearly shows how the coherent scattering strongly depends upon the primary photon polarization. In particular, the cross-section given in Eq. (7) (commonly known as Thomson cross-section) is that for unpolarized photons. According to the classic theory for polarized radiation, the

coherent scattering cross-section is null at ninety degrees. The strong dependence of coherent scattering on polarization has been recently observed in the experiments with synchrotron radiation, which is linearly polarized in the orbit plane of the accelerated electrons (ref. 25).

The dependence upon the scattering angle of the coherent scattering is strongly peaked in the forward direction, as a consequence of the process known as Rayleigh scattering. Therefore, more accurate theoretical deductions have led in the description of the coherent scattering to the introduction of a new formalism, i.e. the form factor formalism. The latter is believed to be accurate for small momentum transfer, i.e., for x values up to about 10 \AA^{-1} when the photon energy is large compared to the binding energy of all the atomic electrons (ref. 23).

In the form factor formalism, the coherent scattering cross-section is given by

$$\frac{d\sigma_c}{d\Omega} = \frac{d\sigma_T}{d\Omega} F^2(x, Z) \quad (8)$$

where $F^2(x, Z)$ is the atomic form factor which accounts for the wave interference of scattering from different electrons. It is useful to remember that the two scattering functions $F(x, Z)$ and $S(x, Z)$ are related to the atomic number by the following equation

$$Z = F^2(x, Z) + S(x, Z) \quad (9)$$

Several tabulations of the $F(x, Z)$ factor have been reported in the literature; the most recent being that of Shaupp et al. (ref. 24).

As shown in Figure 5.6, the decrease of coherent scattering cross-section with energy is more rapid than that of the Compton scattering. Taking into consideration the relation between the momentum transfer variable and the energy, we may observe that, for a given element, the function $S(x, Z)$ increases for increasing energies. Consequently, for Compton scattering the reduction of cross-section with the energy is due entirely to the Klein-Nishina cross-section. Conversely in the case of coherent scattering the rapid decrease of $F(x, Z)$ function with energy determines the behaviour of coherent scattering cross-section.

To understand the behaviour of the coherent scattering cross-section with the scattering angle, analogous considerations should be made. Although, in this case we must take into account: (i) the Thompson cross-section depends on scattering angle and (ii) the relationship between x and ϑ is not linear. As a consequence, the reduction of the coherent scattering cross-section with the

scattering angle is very strong, as shown in Figure 5.9 where the coherent scattering cross-section is shown as a function of the scattering angle.

The most striking characteristic of coherent scattering is that it is strongly dependent upon the Z of the target. This suggested some analytical techniques to determine a higher Z element (for example calcium) in a matrix of lower Z elements.

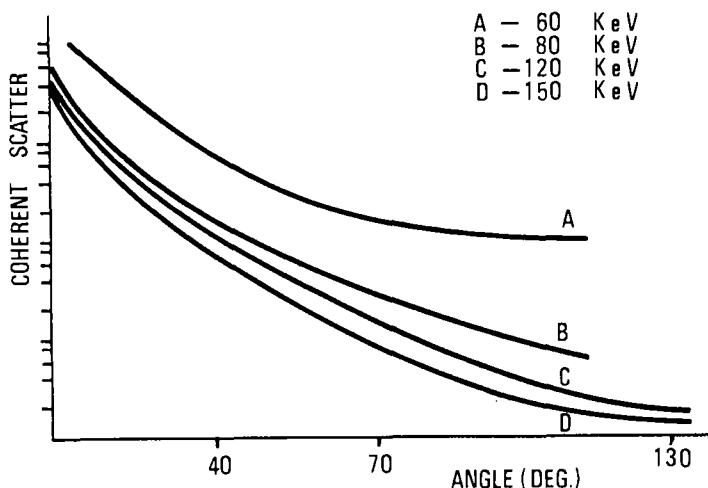


Fig. 5.9. Coherent scattering cross-section as a function of scattering angle at different energy values.

In a first theoretical approach to the coherent scattering, using a Thomas-Fermi approximation for the electron distribution, it can be deduced that the coherent scattering is proportional to about Z^3 .

Later experimental and theoretical results have shown that the situation is more complex. However, the power law dependence of the coherent scattering cross-section on Z is well established

$$\frac{d\sigma_c}{d\Omega} = K Z^n \quad (10)$$

even if the value of the power index (n) changes markedly in the different atomic number intervals. The problem has been reviewed recently (refs. 20, 26) showing that the power index may assume values in the 1.5-7 range; in particular, it has been demonstrated that the power index becomes higher with increasing values of momentum transfer variable (x).

To have an idea of the behaviour of the coherent scattering cross-section vs the atomic number, the coherent scattering cross-section over Z , as a function of Z , is reported in Figures 5.7 and 5.8, for two energies of incident photons at 135° scattering angle. For comparison, the same relation for the Compton scattering is given. It can be seen that, in the low Z range, the coherent scattering is very strongly ($n \approx 4$) dependent upon Z .

It is worth noting that for increasing x value (i.e., when the dependence on Z becomes stronger), the coherent scattering cross-section unfortunately quickly falls-off. This occurs in a more accentuated way for low Z elements that are of prevalent biological interest. Therefore the problem of finding the best working conditions with a technique using coherent scattering turns out to be complicated. At small angles, i.e. small x values, the intensity of elastic peak is great, but its dependence upon the atomic number is weaker and the overlapping of the Compton band with the elastic peak is stronger. At a large angle the intensity quickly decreases, but the dependence upon Z is more marked, and the overlapping problem is reduced. The question is how to find the optimal working conditions. Much efforts have been made to find criteria of general agreement (refs. 15-17, 27, 28). In the next section this problem will be discussed in relation to the R/C.T..

Finally, the increasing interest in the coherent scattering is fully justified despite the fact that the correct evaluation of the elastic peak intensity is not easy due to the marked overlap of the coherent peak with the Compton broad band. This is more evident for low scattering angles and/or low energies of incident photons (see Fig. 5.2). Some authors have pointed out marked discrepancies between the theoretical and experimental values. These occur in all cases in which a finite geometry must be used. Manninen et al. (ref. 29) have discussed the precautions that should be taken to avoid errors in the determination of the elastic peak intensity.

5.2.3 The coherent to Compton scattering ratio and the effective atomic number

The simultaneous detection of the coherent and Compton scattering intensities, which is possible with a solid state detector, has led in the last decade to the measurement of the coherent to Compton scattering intensity ratio (R/C). If one assumes that the detection efficiency and the attenuation effects are the same for the two scattered radiations (hence, they can be neglected), the R/C ratio for a given sample can be written as

$$R/C = \frac{\mu_c}{\rho} / \frac{\mu_I}{\rho} \quad (11)$$

where μ_c/ρ is the differential mass absorption coefficient for the coherent scattering in the sample, defined in a similar manner as μ_T/ρ in Eq. (5).

As can be deduced from the two previous sections, for energies greater than fifty keV and with a quite large scattering angle (i.e., for x values not very low) the dependence of R/C upon Z is almost completely due to the coherent scattering (see Figs. 5.7 and 5.8). In Figure 5.10 the R/C ratio as a function of Z is reported, for the same values of the incident photon energies and of the scattering angle as in Figures 5.7 and 5.8. From a direct comparison of these two curves, i.e. that of the coherent scatter and that of the R/C ratio, it can be seen that their shape is very similar.

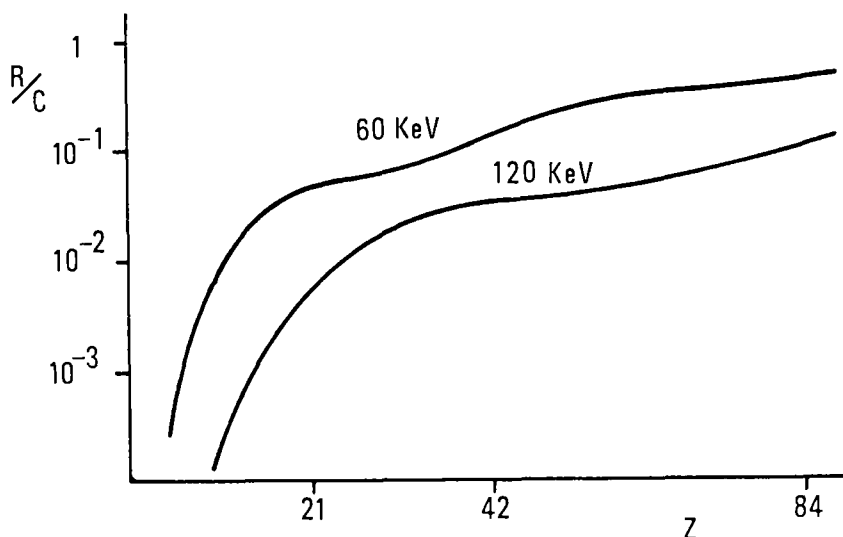


Fig. 5.10. Coherent to Compton scattering ratio R/C vs atomic number, for 60 and 120 keV photons and at 135 degrees angle.

However, for low values of the momentum transfer variable the Compton scattering also shows a stronger dependence upon Z . In these cases the approximation of the behaviour of R/C as a function of Z is complicated. Fortunately, for "in vivo" measurements (and also for field applications), where the advantages of $R/C.T.$ are more evident, the best experimental conditions are obtained at values of x for which the Compton scattering dependence upon Z is negligible compared with the very strong dependence of the coherent scattering.

Also the behaviour of the R/C ratio as a function of the scattering

angle, is fully dominated by the coherent scattering. This is shown in Figure 5.9, where the coherent scattering cross-section as a function of scattering angle, for various energies of the incident photons are reported. It should be noted that the fall-off at increasing angles is more rapid at higher energy values.

A very interesting characteristic of the R/C ratio is its independence on the variables having the same value in both the ratio terms. In particular, this is true for (i) the density, (ii) the incident photon beam intensity and (iii) the detector efficiency and in time fluctuations of the electronic chain. The complete independence of the R/C ratio on the density, justifies the assumption that there is a direct relationship between effective atomic number (Z_e) and R/C, i.e. it is possible to determine Z_e directly from the R/C measurement.

The use of the effective atomic number is usually accepted. This parameter has a physical meaning and allows many characteristics of a material (or a tissue) to be visualized with a number. Unfortunately, its value depends strictly upon the technique used for its measure, i.e. for the same tissue the Z_e values obtained by the use of absorptiometric and scattering techniques are not equal. Obviously, for analogous techniques an expression that relates the different Z_e values for the same sample may be obtained. This problem has been well studied for dual energy X-ray transmission methods (refs. 30-32).

For transmission techniques the definition of Z_e is not easy due to the different Z dependence of absorption processes such as photoelectric, coherent and Compton. In R/C.T. this definition is not even more difficult. In this case the complex energy and the Z dependence of the scattering processes must be taken into account. As shown in the previous section, the power law dependence of the coherent scatter upon Z is quite complex since the value of the power index depends upon the energy and the angle, and also upon Z. In fact, in many cases, the power law dependence for the low Z element range differs considerably from that for the high Z range.

However, many attempts have been made to find a rule to calculate Z_e . Some formulas empirically deduced, have been reported in the literature (ref. 14) but their validity is limited to the experimental conditions used in that particular work. Other authors refer to a hypothetical effective atomic number without giving the rule for its calculation. More recently, Manninen and Koikkalainen (ref. 33) attempted to solve the problem for a energy of 60 keV and large angles, by assuming the coherent scattering intensity proportional to Z^3 and the Compton intensity to Z. The proposed formula is the following

$$Z_e = \left(\frac{\sum_Z w_Z Z^3}{\sum_Z w_Z Z} \right)^{\frac{1}{2}} \quad (12)$$

They have shown that this equation gives good results for low Z materials and high scattering angles, i.e. $\theta > 120^\circ$. A more general approach could be to substitute in Eq. (12) the correct n value given by the power function approximation for the energy, angle and Z range under study. Moreover, the correct dependence of Compton scattering upon Z which is not always linear could be considered. The Compton scattering dependence upon Z is weak compared to the very strong dependence for coherent scattering, especially at higher x values. Now, if we consider the dependence of Compton scattering upon Z as negligible, a possible approximated formula for the calculation of the effective atomic number could be (refs. 28, 31)

$$Z_e = \left(\sum_Z w_Z Z^n \right)^{\frac{1}{n}} \quad (13)$$

where n can be determined experimentally or calculated from the power function approximation of the theoretical R/C values.

Finally, it must be underlined that the use of the effective atomic number requires great care. In particular, for techniques using coherent scattering, a definition useful for a particular experimental situation can not be immediately generalized to other cases. In addition, it should be remembered that a Z_e definition good for all Z values does not exist because of the different power law dependence of light and heavy elements. These limitations considerably restrict the use of Z_e .

Apart the use of the effective atomic number, one can consider the sample under study as a two- or three-phase system. This method is extensively used in connection with the dual-photon absorptiometric, in which the bone tissue is considered as a mixture of bone mineral and soft tissue (refs. 34).

In the assessment of bone mineral with R/C.T., the bone is taken as a two phase system (ref. 15). The mineral fraction is usually referred to as Bone Mineral Density (BMD)*. The meaning of this term may be misunderstood because the R/C.T. is unable to measure directly density change.

A two-phase model may simplify the relation between weight fraction of one of the two phases and the measured R/C ratio. Under the hypothesis of small variations of the Compton scattering coefficients, Eq. (10) can be approximated with a linear relation

$$R/C = \frac{\frac{\mu_{c,A}}{\rho} w_A + \frac{\mu_{c,B}}{\rho} w_B}{\frac{\mu_{t,A}}{\rho} w_A + \frac{\mu_{t,B}}{\rho} w_B} \approx R_B w_B + R_A w_A \quad (14)$$

where w's are the weight fractions of the two components and μ_c/d 's and μ_t/d 's

* in the case of the trabecular bone measurements only, it becomes TBMD.

are the differential absorption coefficients for coherent and Compton scattering, respectively. In the linear approximation R_A and R_B are the coherent to Compton scattering ratios for the two components. Obviously, the sum of the two weight fractions is one in Eq. (14).

The advantage of having a linear relationship between the measured quantity and the parameter to determine is evident. In this case, in fact, it is easier to define some important figures, such as for example sensitivity and precision. As can be deduced from Eq. (14), sensitivity is given by the difference between the R/C ratio for the two components, i.e. $R_A - R_B$.

Also the statistical precision, i.e. the precision under the assumption of only statistical uncertainty, may be expressed in a very simple way

$$\Delta w = \frac{\Delta R}{R_A + R_B} = \frac{R/C}{(I_R)^{\frac{1}{2}}(R_A + R_B)} \quad (15)$$

where I_R are the total counts detected in the elastic peak.

Moreover, using the above-mentioned approximation, it is easier to answer the question concerning the choice of the best working conditions. By expressing the net signal as the product of the sensitivity and the weight fraction, and by assuming a noise due only to statistical fluctuations, it can be deduced that the signal to noise ratio can be written

$$\frac{S}{N} = (I_0 q f)^{\frac{1}{2}} \frac{\left(\frac{\mu_{C,A}}{\rho} - \frac{\mu_{C,B}}{\rho} \right) w_A}{\left(\frac{\mu_{C,A}}{\rho} w_A + \frac{\mu_{C,B}}{\rho} w_B \right)^{\frac{1}{2}}} = (I_0 q f)^{\frac{1}{2}} G(x, Z_A, Z_B) \quad (16)$$

where I_0 is the intensity of the primary beam, q is the total efficiency of the measuring system and f is a correcting factor that accounts of attenuation and multiple scattering effects. If we consider a two-element mixture Z_A, Z_B , for example carbon and calcium, it is possible to study the behaviour of the S/N ratio. To do this, let us introduce the function $G(x, Z_A, Z_B)$, defined above, as a figure of merit. In Figure 5.11, a plot of $G(x, Z_A, Z_B)$ as a function of the scattering angle at several energies, is shown. It is possible to see that for a given energy the S/N ratio is high at small ($\vartheta < 45$ degrees) scattering angles (where the overlapping of the two scattering peaks is greater), but it decreases rapidly reaching a fairly constant value. This ratio also decreases, at a given angle, with the energy. However, for a given energy the variations of this figure for an angle greater than seventy degree, are small. This explains the controversial results obtained experimentally by various authors. In the region of a scattering angle of about ninety degrees and for an energy of the primary beam below one hundred keV, the efficiency

and perhaps the attenuation effects play a more important role than any other variables. In fact, looking for an angle that allows a reduction of the paths inside the sample or requires a less tight collimation, one may obtain better S/N ratios at larger rather than at smaller angles.

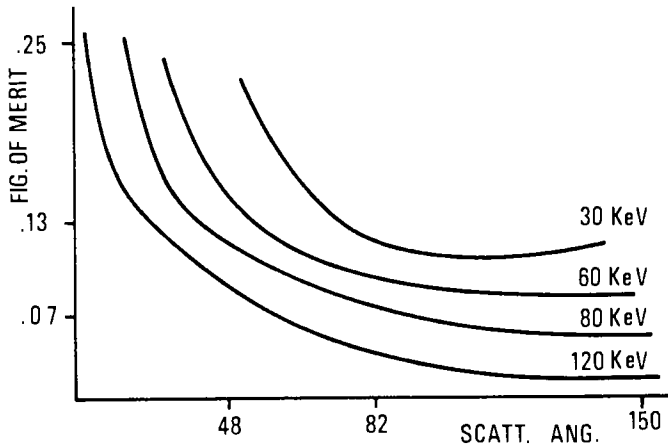


Fig. 5.11. The figure of merit $G(x, Z_A, Z_B)$, as defined in Eq. (16), as a function of the scattering angle for several energies. The calculation has been done assuming a mixture of 25% Ca and 75% C.

5.3 THE INHERENT SOURCES OF ERROR IN PHOTON SCATTERING TECHNIQUES

In this section, problems concerning the photon scattering techniques (P.S.T.) and their use especially "in vivo", will be discussed.

One of the most attractive characteristic of the P.S.T. is the possibility to perform measurements on internal samples, i.e. samples surrounded by materials not involved in the measurement. This can be done by using suitable collimators for the source and the detector (*). As pointed out by several authors, this possibility is limited by problems affecting the accuracy of measurements (refs. 5, 15, 35, 36). Therefore, one of the major drawbacks in developing new applications of P.S.T., is the evaluation of useful correction factors to reduce the main sources of error. These may be regrouped in the

(*) in the following one source and one detector geometry will be considered. Extension to multisources (or detectors) assembly can be easily done.

following categories:

- a) finite geometry effects;
- b) absorption and selfabsorption effects in surrounding materials and in the sample, respectively;
- c) multiple scattering effects;
- d) nonhomogeneity of the sample and variability of its matrix.

The study of these effects cannot be made separately because of the mutual influence of one kind of error upon the others. However, to understand the peculiarities of each source of errors the influence of each will be studied separately. The interconnections will be underlined in each paragraph.

5.3.1 Problems arising with a finite geometry

The common statement that the measurements are always influenced by the geometrical arrangement used, is more severe for P.S.T.. In this case, it is necessary to use a source-detector set-up characterized by a finite geometry (ref. 37). Poorer efficiency of the measuring system must be carefully avoided especially for R/C.T., in which the counting rate in the coherent peak is the limiting factor. Therefore, the need to improve the measuring system response requires the use of a finite geometry.

In a finite geometry, the measured parameter is evaluated within a volume defined by the source and detector collimators. This volume is referred to as the scattering volume (s.v.). Its size and shape are defined only by geometrical factors such as the scattering angle and the distances of detector and source from the sample. Further, the s.v. depends also upon the collimator characteristics. A good knowledge of s.v. is needed in order to position this imaginary volume within the sample (i.e., in the case of "in vivo" measurement, within the studied tissue).

The s.v. may be easily visualized as the intersection volume of the two cones, the primary photon beam cone and the field of view of the detector. It has been pointed out (ref. 17) that shape and size are strongly dependent on the scattering angle. Figure 5.12 shows how a ninety degrees scattering angle produces a smaller s.v. compared with the larger (and elongated) ones at larger and smaller angles. Moreover, at ninety degrees the s.v. seems to be characterized by a more regular shape. However, the total size of the s.v. alone, is not enough to evaluate its usefulness for the measure. The system response is, in fact (see Fig. 5.13) dependent on the path length of incoming and outgoing photons in the sample (a and b) and in the materials surrounding the sample (c and d). For example in Figure 5.13, it can be seen how in an ellipsoidal object containing in the center a circular sample, small (forward-scattering) and very high (back-scattering) scattering angle minimize the

above mentioned distances. Obviously, in a sample not placed in the center, a back-scattering geometry is, in principle, the most convenient.

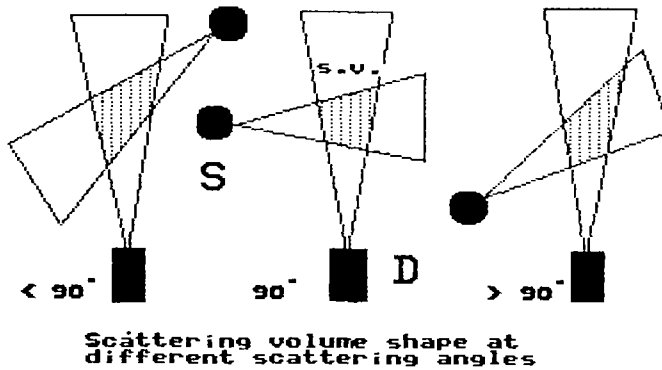


Fig. 5.12. Variations of the size of the effective scattering volume (s.v.) as a function of the angle. The size of the s.v. is smaller at an angle of ninety degrees than at larger and smaller angles.

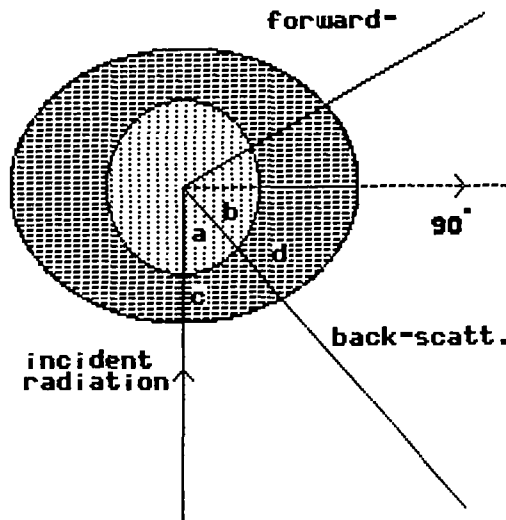


Fig. 5.13. Schematic drawing showing that with an ellipsoidal object containing in the centre a circular sample, the forward- and back-scattering geometries increase the performances of the measuring system.

In addition, it should not be forgotten that the s.v. presents an intrinsic internal non-uniformity of the response. In fact, the scattered photon

fluences coming from each elemental volume in the s.v., are not equal. For example the flow from the penumbra regions at the border of the s.v. is very small in comparison to the one coming from the central part of the s.v.. Therefore, a study of the internal structure of the s.v. must be done, i.e. the knowledge of the contribution to the detected spectrum coming from each part of s.v. because it is very useful in the evaluation of system performance and accuracy.

The experimental determination of the internal structure of the s.v. is not easy; one way is to explore it by using an object of small size, in comparison to that of the s.v.. In these measurements, a long measuring time is needed in order to obtain good counting statistics. This procedure is time consuming and unpractical. In many investigation, the evaluation of s.v. has been carried out using different size objects (refs. 5, 35, 37). This method allows one to evaluate the influence on the measuring system response of a group of effects, such as selfabsorption, multiple scattering, and finite geometry effects.

In many cases, the study of system response using objects of increasing size, is useful to validate a measuring system but is unable to give sufficient information on the internal structure of the s.v..

Recently, Wolf and Munro (ref. 38) studied how in a finite (backscattering) geometry sample positioning is critical, and there is a strong interaction between attenuation and multiple scattering effects. They have shown that the results of the measurements can also be influenced by the presence of objects outside the s.v..

The best way to study the internal structure of the s.v. is to calculate by means of numerical approximations the contributions to the detected spectrum coming from each point of the s.v.. This can be done by evaluating for each point the solid angle subtended by the source and the detector respectively, taking into account the presence of the collimator as shown in Figure 5.14. Referring to this Figure, the product of these two solid angles ($\Omega(x, y, h)$) is proportional to the fluence from an infinitesimal volume identified by the point P. The results of these calculations are profiles of the $\Omega(x, y, h)$ function in one direction or more precisely, integrals of this function along particular axes or planes as shown in Figures 5.15 and 5.16. This method allows immediate visualization of the internal structure of the s.v.. Obviously, the integral of $\Omega(x, y, h)$ on the whole s.v. gives the geometrical efficiency of the measuring system. A preliminary simulation of the s.v. structure by means of a computer, is very useful; it allows both the choice of the most favourable source-detector collimation and optimization of the performances of the system. The last point is extremely important for R/C.T.'s

where, as seen in section 5.2.3, the efficiency of the measuring system sometimes plays a fundamental role. In addition, in evaluating the accuracy of measurements on objects of variable shape and size (for instance "in vivo" measurements), knowledge of the internal structure of the s.v. is necessary. In this case the anatomy of the chosen site must be taken into account.

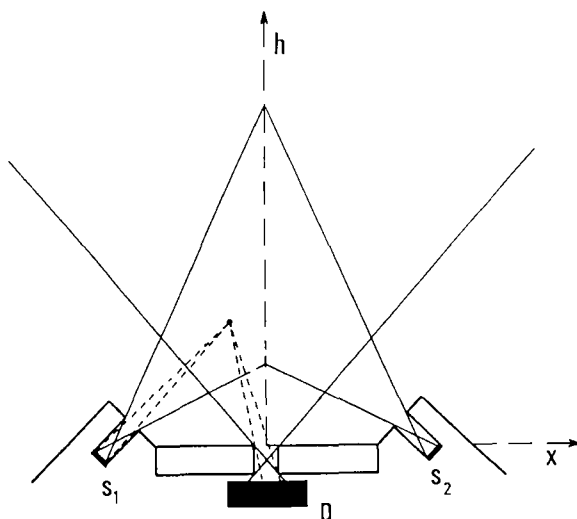


Fig. 5.14. Schematic drawing of a two-source-detector geometry. The contribution to the detected spectrum from each point of the scattering volume can be calculated by considering the solid angles subtended by the source(s) and detector.

5.3.2 Attenuation effects

There are two kinds of attenuation effects:

- a) absorption of primary and scattered photons in the material surrounding the s.v.;
- b) selfabsorption of the same radiation in the s.v..

The two effects behave differently. The first gives always rise to an attenuation of the signal whereas the second may determine either an increase or a decrease of the signal. To understand the nature of these two effects, let us consider the simple model depicted in Figure 5.17. In this model, a scattering layer of thickness T is surrounded by an absorbing layer H . In other words the first layer represents the s.v. whereas the second represents the surrounding materials.

Taking at first a scattering angle of more than ninety degrees, the Compton scattering intensity can be calculated integrating the absorption factors for incoming and outgoing radiation over the layer thickness (T). After the integration, regrouping the homogeneous terms, it is possible to

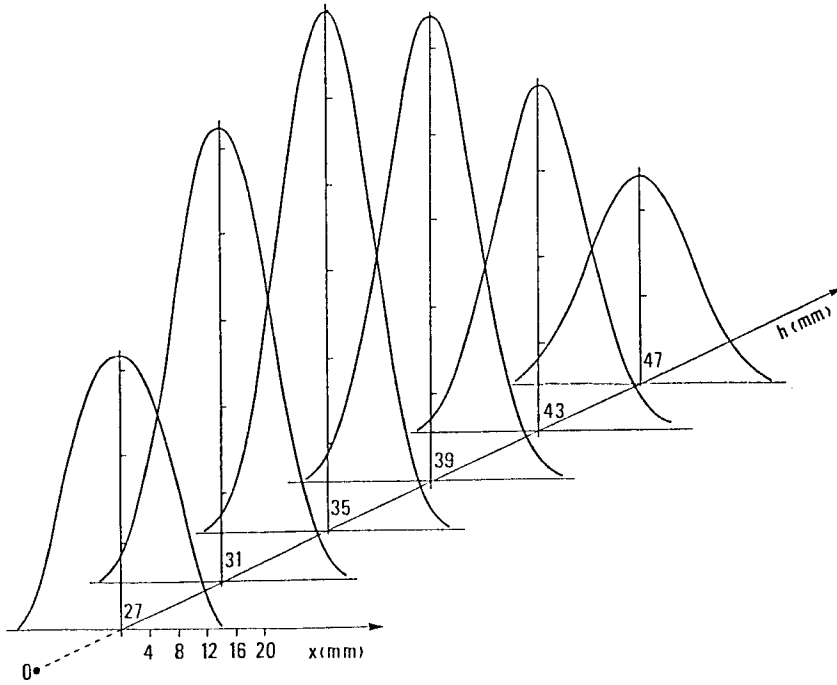


Fig. 5.15. Computer simulation of the scattering volume shape for the geometry of Figure 5.14. The profiles along the principal axes (x and h) are shown.

write the Compton scattering intensity as follows

$$I_I = \left(I_0 \frac{\mu_I}{\rho} \right) \left(\frac{1 - \exp(-kT)}{k} \right) \left(\exp(-k'H) \right) \quad (17)$$

where $k = \mu(E_c) - (\mu(E_o)/\cos(\vartheta))$, $k' = \mu'(E_c) + (\mu'(E_o)/\cos(\vartheta))$ and $\mu(E)$'s and $\mu'(E)$'s are the mass absorption coefficients for the scattering and absorbing layers, respectively. In the above equation the efficiency is assumed equal to one.

The term in the second pair of brackets in Eq. (17) represents the selfabsorption contribution whereas that in the third pair, the absorption contribution. For a backscattered geometry the cosine is always negative,

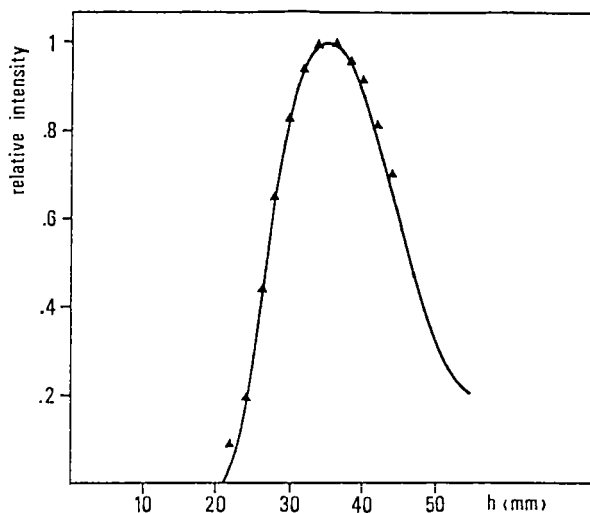


Fig. 5.16. Calculated profile along the h axis that gives in depth the system response. For comparison some experimental points, i.e. Compton scattering relative intensity, are reported. The measurements were performed with a thin sheet of absorbing material.

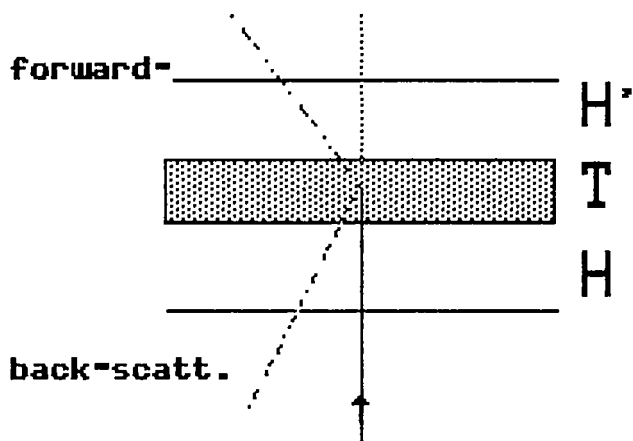


Fig. 5.17. Schematic drawing of a scattering sample composed of three sheets. The internal sheet (T) represents the scattering volume, whereas the other two (H) represent the surrounding materials.

therefore, the selfabsorption term is always positive. For this kind of geometry, the selfabsorption always produces an increment of the detected signal. This increment becomes smaller and smaller with increasing T values. In particular, one can define a thick sample approximation, i.e. the values of T for which the increment of selfabsorption function is less than one percent. Values of thick sample approximation for bone tissue as a function of energy, are reported in Figure 5.18.

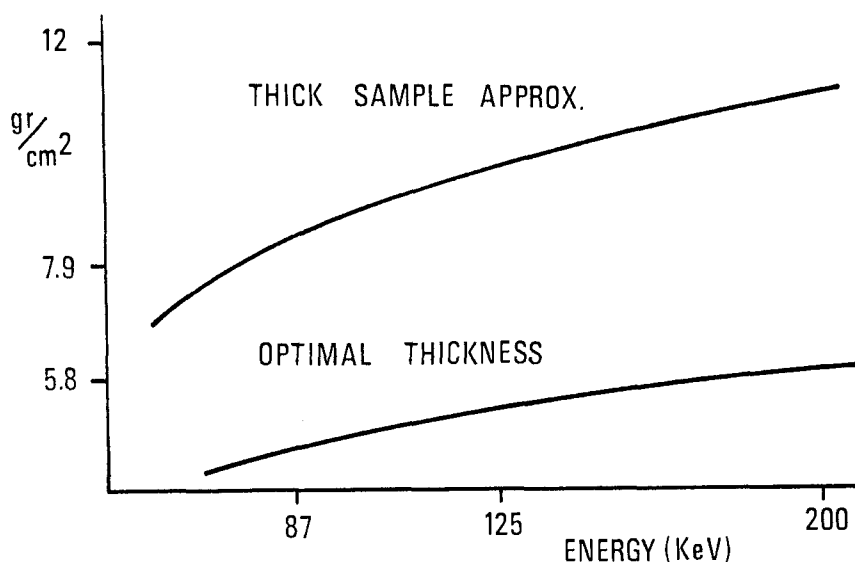


Fig. 5.18. Lower curve: optimal thickness values (Eq. (19)), for bone sample and an angle of 45 degrees, as a function of energy; upper curve: thick sample approximation in a backscattering (135 degrees) geometry (see text).

Another interesting aspect of the selfabsorption function is its behaviour at increasing Z values of the sample. In weakly absorbing samples such as biological samples, this function assumes values greater than one while in strongly absorbing samples it can be much lower than one. This explains the drastic reduction of the backscattered radiation intensity when the primary radiation impinges on an highly absorbing object (see Fig. 5.19). Further, it must be stressed that in a two component mixture when the weight fraction of the higher Z sample component increases the detected signal becomes higher, reducing the corresponding decrease due to selfabsorption.

In the case of a scattering angle smaller than ninety degrees (forward scattering), the selfabsorption function behaviour is more complicated because the incoming photons have the same direction of the detected ones. However, also in this case it is possible to study the selfabsorption according to a

model analogous to that used in backscattered geometry as shown in Figure 5.17 where another absorbing layer of the same thickness is placed on the other side of the scattering layer. With an integration over it, it is possible to obtain a relation similar to Eq. (14) with a multiplying factor. Then the

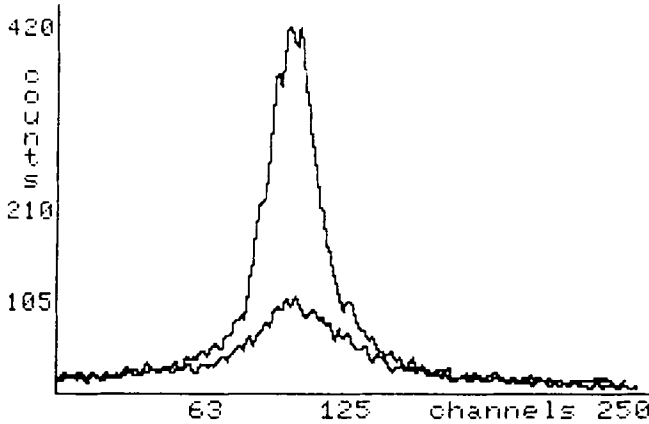


Fig. 5.19. Scatter spectra of a bone sample (upper curve) and a bronze object (lower curve) detected with the same measuring system and with equal measuring times. The marked reduction of the Compton scattering intensity in the high Z object is almost entirely due to selfabsorption.

selfabsorption term becomes:

$$G = \frac{1 - \exp(-kT)}{k} \exp\left(-\frac{\mu(E_0)}{\cos \theta} T\right) \quad (18)$$

where G has a maximum at:

$$T = \frac{\log\left(\frac{\mu(E_c) \cos \theta}{\mu(E_0)}\right)}{\frac{\mu(E_0)}{\cos \theta} - \mu(E_c)} \quad (19)$$

This behaviour can be easily understood considering that the scattered intensity in a particular direction increases with T until its marginal increment (due to selfabsorption) is greater than its marginal reduction (due to the absorption). Therefore, G is symmetrical around the maximum which assumes the meaning of an optimal sample thickness. In fact, around this thickness the function is smooth, i.e. the first derivative is near zero and the detected signal is maximum. Thus, working with a sample having this optimal thickness, better precision and sensitivity will be obtained. To give an example, the optimal T values for bone tissue are reported in Figure 5.18,

as a function of the energy. It can be observed that these values are of a few grams per square centimeter (i.e., 3 ÷ 4 centimeters) for tissues while for higher Z material (for example metal alloys) are less than one millimeter. The risk of working with thicknesses greater than the optimal value is greatly reduced in "in vivo" measurements. However, if the thickness of the sample is known, it is possible to use an energy for which this value is near to the optimal.

Whilst the selfabsorption effects cannot be immediately understood, the absorption effects in the surroundings materials can be more easily explained. They give rise to an attenuation of both the incoming and the outgoing beams proportional to the absorption coefficients of the crossed materials. This relationship is clearly shown in the third term of Eq. (17). The absorption effects cannot be neglected. If one considers, for example, a bone sample localized three centimeters inside the body, the decrease in the detected signal due to the presence of the surrounding soft tissues is of sixty-nine percent at 60 keV and of sixty-three percent at one hundred keV.

Fortunately, using the ratio of two intensities the absorption effects in the material outside the s.v. can be easily corrected. Obviously, the presence of absorption cannot be completely neglected. To do this, it would be necessary to use two beams of the same energy crossing the same piece of material.

Several procedures to correct absorption in surrounding materials have been proposed for various Compton scattering techniques. These techniques and the methods used to correct the absorption of primary and scattered radiation will be described in section 5.4.

5.3.3 The problem of Multiple Scattering

In a finite size s.v. the probability that a detected photon comes from a secondary or tertiary interaction (i.e. results from two or three successive scattering events), is not negligible. Obviously, the probability of a multiple scattering event decreases rapidly with the order of the interaction. Moreover, the probability of a secondary scattering process due to two successive coherent scattering interactions is much less than that of two successive Compton scattering events or of mixed events, i.e. a coherent scattering event followed by a Compton scattering event. From these simple considerations it may be deduced that the influence of multiple scattering on the coherent peak intensity is very little (with the exception of the interactions at small angles). Therefore, the following considerations will be restricted to the multiple Compton scattering, which is by far the most probable event.

The spectral distribution of multiple scattered photons is different from that of the single scattered photons. This can be understood observing that

first order scattered photons are produced in the sample by collisions from a well-known direction, while the scattered photons of a higher order are produced in processes involving photons with complex angular distribution.

This problem is not easy to solve, and since it is highly geometry dependent, it can be treated only using crude approximations. Indeed, Kennet and Webber (ref. 35) have shown that the form of the relation between the fraction of the n-order to the first-order scattered photons which falls within a particular spectral window, and the order of multiple interaction is gaussian in nature. For the calculations they use the Klein-Nishina formula and a simple deconvolution method. They show that it is possible to find a link between the first order and the higher order spectra.

To obtain the spectral distribution of the multiple scattered photons under more realistic approximations the only way is a simulation by means of a Monte Carlo method (ref. 39). The experimental and theoretical results reported by various authors on multiple scattering spectra show that there are both an enlargement of the Compton profile and the appearance of a continuum spectrum towards lower energies. Further, the spectral distribution of the multiple scattering photons is characteristic of the particular geometry under study. In fact, it can be easily demonstrated that many effects such as attenuation and the geometry used, contribute to the spectral distribution of multiple scattering photons (see sections 5.3.1 and 5.3.2).

As pointed out by Battista et al. (ref. 10), multiple scattering plays a more important role in imaging techniques than in single point techniques. For imaging techniques, careful theoretical studies of the problem have been performed (refs. 10, 40-42); the presence of the multiple scattering strongly reduces the contrast that can be obtained. Multiple scattering is still a major problem for those techniques using low energy resolution detectors (refs. 35, 36) while becomes a minor problem in the R/C.T.'s, in which solid state detectors are used.

It is well known that the probability of a collision within a particular object is proportional to the mass per unit surface $\mu = d/l$, where l is a characteristic length of the object multiplied by the mass absorption coefficient. If one wants to consider only the collision that produces a coherent or Compton scattering photon, it is necessary to multiply the above-mentioned probability by the ratio (k) of the scattering to the total absorption coefficient. As a matter of fact, if the photoelectric contribution to the total coefficient is negligible the value k is equal to about one. This happens for low Z materials and for photon energies higher than one hundred keV. In conclusion, the probability (P) of a photon being scattered in a single event is proportional to

$$p_1 \approx k\mu(E_0)a \quad (20)$$

Therefore, the probability of a photon being Compton scattered in a secondary event at a fixed angle is proportional to

$$p_2 \approx k\mu(E_0)\frac{\mu_I}{\rho}a^2 \quad (21)$$

where (μ_I/ρ) is the differential mass attenuation coefficient of Compton scattering. The probabilities of tertiary and higher order events can be similarly deduced. However, they rapidly fall-off due to the presence of a higher order power of the attenuation coefficient.

From the above two equations, it can easily be deduced that the importance of the multiple scattering is greater for big objects and for large solid angles. Moreover, if the other mechanism of interaction can be neglected the ratio of double to single scattering is directly related to the absorption coefficient (ref. 35).

The multiple scattering gives rise to an enhancement of the scattered radiation and so it behaves as an antagonist of the selfabsorption. For example, from Eq. (21) it can be deduced that in strongly absorbent media the multiple scattering contribution is more evident; however, this is not completely true. In fact, the simultaneous presence of selfabsorption strongly reduces the effective s.v. size, and consequently the probability of the multiple scattering events.

Finally, it is worth noting that multiple scattering is responsible for some curious effects described by various authors, working with objects of increasing size. They observed that the scattered radiation intensity continues to increase, also using objects of greater size than the s.v. size. This phenomenon can be explained in terms of a multiple scattering effect due to the object parts surrounding the s.v..

5.3.4 Nonhomogeneity of the sample and variability of its matrix

The use of finite size s.v. introduces in the presence of a nonhomogeneity of the sample, an additional error. The detected scattered radiation is the sum of the scattered photon fluences from each elemental volume in the s.v.. Therefore, the nonhomogeneity of the sample under study directly influences the measured quantity(-ies). It follows that the determined parameter (e.g., the electronic density, the weight fraction of a particular sample component, etc.) is a weighted mean on the s.v..

It is necessary to distinguish between the presence of a nonuniformity in

the sample, i.e. a change in the sample density and the variation of the matrix composition, for example of the amount of fat in bone tissue. These two sources of error affect the detected signal in a different way. The first affects considerably the measurements of electron density, the second affects the R/C.T. measurements of TBMD. Of course, these two changes may occur simultaneously.

The presence of a nonuniformity in the sample, known before the measurement, can be minimized by placing the s.v. in such a way as to reduce the amount of fluence coming from the nonuniformity region. The use of standard samples and phantoms, can make the study of the correction procedure easier.

The situation is more complex in cases of nonhomogeneities that occur casually, as shown by Coates for fractional content of air in the lung (ref. 36). The only way to treat this error is to consider it as a change of matrix composition. For example, if it is possible to measure the amount of air in the lung, this error can be corrected taking into account the decrease in the scattered radiation with increasing air content. Generally, the correction of the measured intensity both scattered and transmitted, can be expressed as a linear function of the change of matrix composition.

The variability of the sample matrix is a source of error almost ever present in the P.S.T.'s. The method to correct this kind of error is to consider the sample as a ternary mixture. In particular, one component represents the parameter under study while the other two simulate the matrix. An example of this model is bone tissue (refs. 17, 43), which can be considered as a mixture of bone mineral (hydroxiapatite), soft tissue, and fat (the last two components can simulate the non mineralized matrix of the bone). The problem is to foresee the amount of fat in the bone; actually, this cannot be easily done. The study of the behaviour of the scattered radiation intensity with increasing fat content can provide only an estimation of the accuracy error.

The intensity ratio at two different energies is often used to correct absorption in materials surrounding the s.v.. This method is also used to correct variations of sample matrix. Obviously, the best correction is when the two intensities are simultaneously recorded with the same detector. This is always true for R/C.T. while for Compton scattering techniques the situation must be considered for each individual case.

The sample matrix variability changes the effective value of the atomic number and/or electron density of the sample simulating a variation of the component under study. This reveals another ambiguity in the use of effective parameters such as Z_{eff} .

5.4 COMPTON SCATTERING TECHNIQUES

Several Compton scattering methods have been proposed using Compton scattered radiation (or scattered and transmitted radiation), to measure the electron density within a particular internal part of the object. Medical applications of these methods have been reported in two main areas: a) bone and lung densitometry (refs. 1-6, 44, 45), and b) whole body tomographic imaging (refs. 7-11). These techniques can be subdivided into three groups a) dual and single energy Compton scattering densitometry (refs. 1-2); b) dual energy Compton scattering densitometry, using only scattered radiation according to a method proposed by Huddleston and Weaver (ref. 6); c) Compton scattering imaging (refs. 7-11).

These methods will be described in the next three sections and the principal results obtained will also be reported.

Another analytical use of the Compton scattered radiation concerns the measurement of sample mass. This application is based upon the relationship existing between the intensity of the Compton scattered radiation and the sample mass involved in the scattering processes (ref. 46). Obviously, the Compton scattered intensity is also a function of the sample composition. This is a very strong limitation for samples of variable composition at small values of momentum transfer (see par. 5.2.1), especially for high Z materials. So far, this measurement is used only for correcting sample mass variations in energy dispersive X-ray fluorescence techniques (XRF).

5.4.1 Techniques using the transmitted and Compton scattered photons

In the early seventies two different Canadian groups described the basic method for Compton densitometry and used transmitted radiation to correct the attenuation effects (refs. 1-2). In this method a single or dual source configuration can be used according to the primary photon energies and scattering angle.

The simple idea on which these methods are based, is that of measuring the attenuation of the primary and scattered beams, through transmission measurements using sources of appropriate energy (see Fig. 20). In particular, the Compton scattered photons in a given direction have an energy distribution around the value given in Eq. (1) (see par. 5.2.1). Therefore, by using a second source having this lower energy, one can correct for the attenuation of the Compton scattered beam. A set of matched pairs of low energy monoenergetic gamma sources may be proposed for this kind of measurement.

The basic idea is to perform two scattering measurements by rotating the sample of an angle of 180 degrees and simultaneously two transmission measurements, using a second detector. The paths in the transmission and scattered

measurements are the same. In this method, the sample should be of very small size. The four equations for attenuation and scattered processes are given as follows:

$$\begin{aligned}
 S_1 &= I_1 \frac{\mu_1}{\rho} \rho C_a \exp(\mu(E_0)e) \exp(\mu(E_c)h) \\
 S_2 &= I_1 \frac{\mu_1}{\rho} \rho C_a \exp(\mu(E_0)g) \exp(\mu(E_c)f) \\
 T_1 &= I_1 \rho C_b \exp(\mu(E_0)(e+g)) \\
 T_2 &= I_2 \rho C_a \exp(\mu(E_c)(f+h))
 \end{aligned} \tag{22}$$

where C_a , C_b are the detector efficiencies at the two energies E_0 and E_c , respectively.

Now, dividing the product of the two scattered intensities (S_1 , S_2) to that of the two transmitted (T_1 , T_2) ones, we obtain

$$\rho_e \propto \rho \frac{\mu_1}{\rho} \left(\frac{C_b I_2 S_1 S_2}{C_a I_1 T_1 T_2} \right)^{\frac{1}{2}} \tag{23}$$

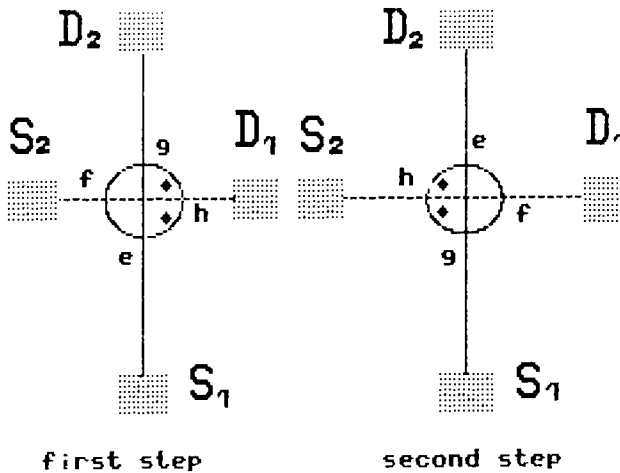


Fig. 5.20. Schematic drawing of the sources (S_1 , S_2) and detectors (D_1 , D_2) for electron density measurements using both transmitted and scattered photons.

From Eqs. (6) and (22) it can be deduced that the electron density is proportional to the ratio of the scattered to the transmitted intensities. Therefore, this method can be used to determine the electron density of the

sample but not its density. The latter can be deduced knowing the value of the effective (Z/A) ratio (see below) of the sample under study.

It is worth noting that at the energy and scattering angle used in these techniques only a proportionality relation between the electron density and Compton scattering intensity can be obtained. The proportionality constant is determined by performing the same set of measurements on a water sample. This step only partly resolves the problem. In fact, the influence due to the different elemental composition of the standard sample, i.e. water, and the unknown sample, for example bone sample, still remains.

Another severe limitation of the described method is the assumption that the effective path lengths of a transmitted and a scattered beam in the sample are the same. As clearly shown in Figure 5.21, the dimension of the transmitted photon beam is only determined by the collimator of the detector used while the shape of the scattered photon beam is defined by the combination of both source and detector collimators.

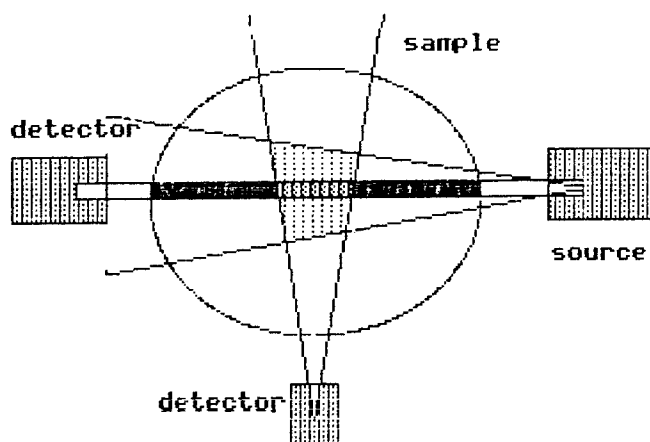


Fig. 5.21. Plan view of the measuring system showing the geometry of scattered and transmitted beams. The average attenuation for the scattered beam is less than that for the transmitted beam.

The assumption that the sample size is very small implies that the selfabsorption effects can be neglected. Good results are thus obtained only for small variations of the sample size. Huddleston and Bhaduri (ref. 5) have shown that measurements with this photon scattering technique are strongly dependent on the sample size. They have attributed the observed bias in the electron density determination to the concomitant action of the multiple

scattering and the selfabsorption effects.

Many changes in the original method have been proposed by various authors. In particular, Olkkonen and Karijalainen (ref. 4) described a single-source low energy, small scattering angle, method; this method has later been extensively used by Huddleston (refs. 5, 37). Webber and Coates (ref. 45) constructed a three source densitometer for measurement of lung density. This system avoids the rotation of the object under study.

In their original work Garnett et al. (ref. 2) demonstrated how the use of an energy close to ninety keV improves the overall performances of a Compton scattering technique for the measurement of bone density. To reach this conclusion they studied the energy behaviour of: a) the Compton scattering differential mass absorption coefficient; b) the total mass absorption coefficient of soft tissue and bone; c) the detector efficiency and d) the time required in order to attain a given dose from a fixed source strength.

It is well known that Compton scattered radiation decreases with increasing energy, just as the absorption coefficient and the detector efficiency; the smaller attenuation of the beams with increasing energy, is fully compensated by the simultaneous reduction of detector efficiency and Compton scattering intensity. Then, the optimum energy can be found looking at the energy dependence of the Compton scattering intensity for unit dose; this curve has a maximum at about ninety keV.

Apart from the first system proposed by Clarke (ref. 1) using a pair of high energy sources, almost all the single point Compton scattering systems work with radioisotopic sources with an energy in the 80-130 keV range. Preuss et al. (ref. 47) studied the problem of the monochromatic sources available for these measurements. They give a list of possible pairs of sources and the corresponding scattering angle to be used. Table 5.1 shows the most interesting sources available for single and dual source techniques.

TABLE 5.1

Sources available for single and dual source techniques.

Isotope	energy (keV)	half life	second source	angle (degrees)
Ba-133	80 (36%)	8.9 y		
Tm-170	84 (3.3%)	129 d	Ba-133	44
Gd-153	99 (54%)	239 d	Tm-170	86
Eu-155	87(32%),105(20%)	1.8 y		
Co-57	122 (87%)	269 d	Gd-153	86
Se-75	134 (57%)	122 d	Co-57	51
Ce-144	134 (11%)	282 d	Co-57	51

The analytical performances of P.S.T.'s both in laboratory and "in vivo" measurements are well established. In the assessment of bone density, Webber and Kennett (ref. 3) found that with 3-minute measuring time it is possible to obtain a statistical precision of 1%. Moreover, assessing the overall precision they found values of 1.5%. Finally, they studied the accuracy of the technique in relation to the major sources of error, i.e. finite geometry, non-identical geometry, and multiple scattering. After a careful study, they found that the bias in the measurements is usually positive and that the accuracy is of 10%.

Huddleston et al. (refs. 5, 37), using the Compton scattering densitometry studied how the relative electron density is strongly influenced by both the density and the size of the sample. They used cylindrical samples with a diameter in the range 4-8 cm filled with compounds having a density range of 0.9-1.8 g/cm³. They found that the positive bias is particularly evident in the larger samples filled with compounds of higher density. Furthermore, they found variations in the measured electron densities in the range between 2-9% and observed that the density bias increased for higher density and for greater samples. These authors showed that corrections can be introduced using a linear approximation (ref. 37).

Shrimpton (ref. 48) studied the analytical performances of these methods in the determination of the electron density of different low Z liquids. Performing "in vitro" measurements on thirteen different liquids, he demonstrated that a very good linear correlation can be achieved between measured and theoretical electron density values (see Fig. 5.22). This result clearly reveals the analytical capabilities of this method. Similar conclusions can be attained from the results reported by Huddleston et al. (refs. 5, 37).

Shrimpton (ref. 48) evaluated the performances of these methods in measurements on the electron density of human tissues. The results obtained (see Table 5.2) are very encouraging as far as the tissue characterization is concerned. The precision exceeded 1.5% for laboratory measurements, while for "in vivo" measurements the situation is more critical, for the reasons already mentioned.

It is particularly interesting to determine of the effective ratio (Z/A) of materials as discussed by various authors (refs. 5, 48). From the definition of the electron density (see Eq. (6)) it is possible to deduce the density of a given material knowing only the effective (Z/A) ratio defined as below

$$\left(\frac{Z}{A}\right)_{eff} = \sum_Z w_Z \frac{Z}{A_Z} \quad (24)$$

Unfortunately, the value of $(Z/A)_{\text{eff}}$ cannot be measured independently but only deduced from the composition of the sample. The $(Z/A)_{\text{eff}}$ must be determined before the measurements if the goal of them is to determine the sample

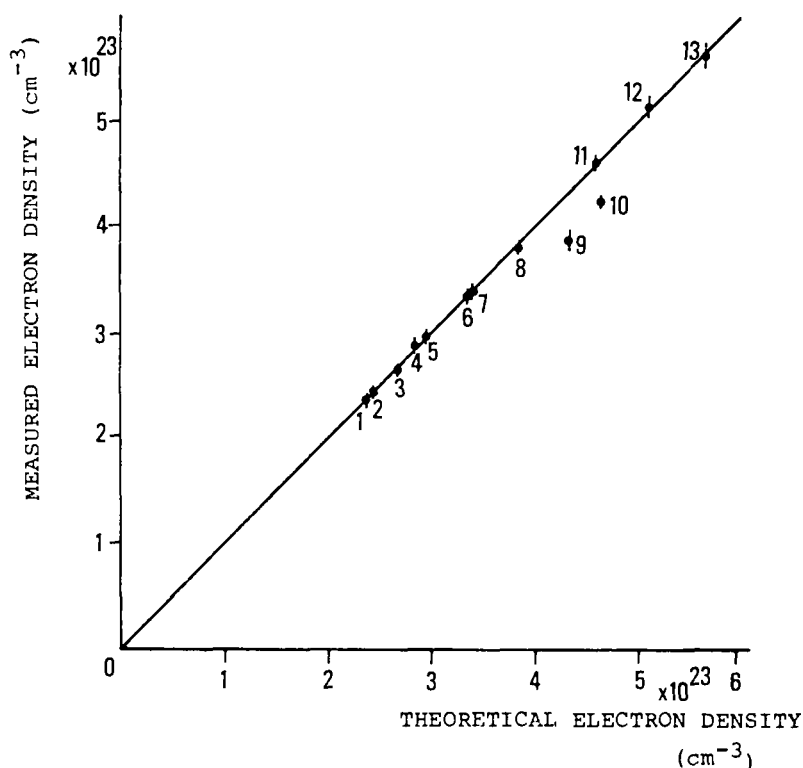


Fig. 5.22. Comparative plot of measured vs calculated electron density for the following liquid samples: 1) n-heptane, 2) Diethyl ether, 3) Isopropyl alcohol, 4) Xylene, 5) Ethyl acetate, 6) Water, 7) Glacial acetic acid, 8) Formic acid, 9) Chloroform, 10) Carbon tetrachloride, 11) Fuming nitric acid, 12) Perchloric acid, 13) Conc. sulphuric acid. (after Shrimpton, ref. 48).

density.

One of the uses of the methods described in the present paragraph is the "in vivo" determination of lung density. The wide range of values for lung density, 0.26-1.06 g/cm³, encourages this application. These density variations are only in part to be attributed to the state of the lung. However, Webber and Coates (refs. 36, 45) using a three sources densitometer optimized for this application, have obtained good results in terms of statistical precision (2.2%), total precision (\approx 5%), and accuracy. The accuracy of the

method has been extensively studied by these authors using wood phantoms. They conclude that no relevant contribution is to be expected from the effects discussed in section 5.3.3 with the exception of the influence on the measurement of the value of the fractional air content of the lung. The only way to reduce the influence of this effect is to perform measurements at fixed lung volume. In this case the accuracy error turns out to be acceptable.

TABLE 5.2

Calculated and measured electron densities of some selected tissues.

Sample	density g/cm ³	elect.density range* (calculated)	elect.density* (measured)
Adipose tiss.	0.92-0.93	3.08-3.13	3.10 + 0.02
Brain	1.03-1.04	3.41-3.47	3.47 + 0.03
Breast	0.97-1.05	3.21-3.46	3.40 + 0.03
Kidney	1.05	3.41-3.48	3.43 + 0.05
Liver	1.05-1.07	3.49-3.57	3.50 + 0.05
Lung	0.26-1.06	0.86-3.48	2.29 + 0.03
Muscle	1.04-1.06	3.41-3.50	3.51 + 0.04
Pancreas	1.02-1.05	3.38-3.51	3.48 + 0.02
Spleen	1.05-1.06	3.47-3.52	3.46 + 0.02
Thyroid	1.04-1.07	3.45-3.55	3.61 + 0.04

* $\rho \times 10^{23}$ (e/cm³)

5.4.2 Dual-energy Compton scattering method

Huddleston and Weaver (ref. 6) recently introduced a new Compton scattering method using a dichromatic source. This method has the advantage of avoiding the rotation of detectors and sources around the sample under examination.

A schematic drawing describing the dual-energy Compton scattering method, is shown in Figure 5.23 which also defines some of the symbols used below. This method starts with the assumption that the measuring system involves a s.v. small compared to the sample size. It is to be noted that the Compton scattering intensity produced in samples of increasing size decreases with the increasing of the sample size. This phenomenon is due to the absorption of both the primary and scattered photons by the sample parts not involved in the scattering processes. In this case, if there is further material surrounding the sample, the scattering intensity decreases exponentially with the increasing of the path lengths of the two beams in the sample and in the surrounding material. If we now introduce the two total path lengths for the sample S_s and for the external materials s_E and correspondingly define the effective attenuation coefficients k_s and $k_E(E)$, the Compton scattering intensity for a given

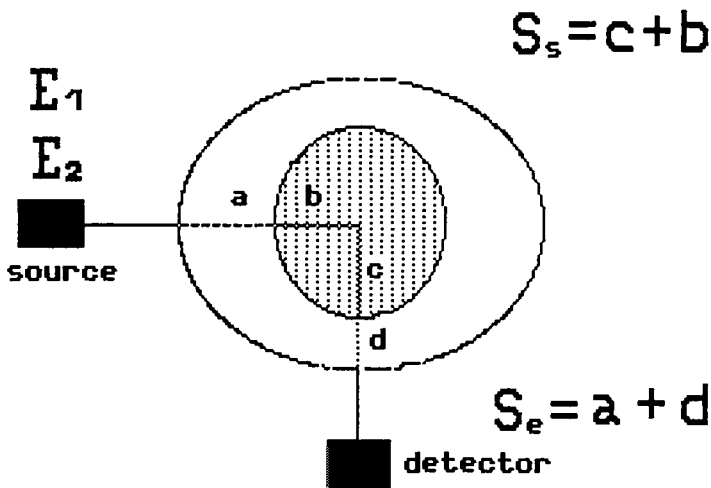


Fig. 5.23. Schematic drawing of the geometry of the source-detector system in dual-energy Compton densitometry.

energy of the primary beam, may be written as

$$S_i = K_i \rho_e \exp\left(-k_S(E)S_S\right) \exp\left(-k_E(E)S_E\right) \quad (25)$$

where $K_i \rho_e = I_i C_i \frac{\mu_i^1}{\rho} \rho$

Provided that the total path length $D = S_S + S_E$ may be estimated and the effective attenuation coefficients may be independently determined, a system of three equations and three unknowns may be written

$$\begin{aligned} S_1 &= K_1 \rho_e \exp\left(-k_S(E_1)S_S\right) \exp\left(-k_E(E_1)S_E\right) \\ S_2 &= K_2 \rho_e \exp\left(-k_S(E_2)S_S\right) \exp\left(-k_E(E_2)S_E\right) \\ D &= S_S + S_E \end{aligned} \quad (26)$$

where the two scattering intensity relations concern two different energies. In this method it is necessary to simultaneously detect the two scattering intensities, using the same detector.

Resolving the system of Eqs.(26) for ρ_e one finds the following Equations

$$\rho_e = \frac{S_1}{K_1} \exp(k_S(E_1)S_S) + (k_E(E_1)(D - S_S))$$

$$S_S = \frac{J_E D - \ln \frac{S_2 K_1}{S_1 K_2}}{J_E - J_S} \quad (27)$$

$$J_E = k_E(E_2) - k_E(E_1)$$

$$J_S = k_S(E_2) - k_S(E_1)$$

The effective attenuation coefficients may be evaluated using samples of increasing size and known composition; during these measurements no surrounding substance should be used. The coefficients at each energy are determined by curve-fitting of logs vs. S_b (see Eq. (25)) according to Huddleston and Weaver (ref. 6). From a direct comparison of measured and theoretical attenuation coefficients concerning substances of known composition, it was possible to validate the efficacy of the method.

From the few results published so far, the characteristics of this method seem very promising. In the first paper by Huddleston and Weaver (ref. 6) a table comparing the theoretical and measured electron densities of different materials is reported. Their apparatus was equipped with a gadolinium-153 sealed source and a scintillator, both tightly collimated in a 90 degree geometry. The estimated precision always exceeded 3% and the accuracy, evaluated by direct comparison of theoretical and experimental values, exceeded 3.5%.

In a later investigation, Huddleston and Sackler (ref. 49) used iridium-192 source (emitting 317 and 468 keV photons) in order to obtain a better separation between the two scattered peaks, detected simultaneously by a scintillator detector. Also in this case, a ninety degree scattering angle was used. The results obtained in both the two works are very encouraging as shown in Table 5.3. The precision exceeds 2% and the accuracy 4%.

TABLE 5.3
Calculated and measured electron densities of some substances.

Substance	density g/cm ³	elect.density* (calculated)	elect.density* (measured)	% diff.
H ₂ O	1.00	3.344	3.233	-0.63
NaCl	1.013	3.032	3.044	+0.40
KBr	1.133	3.188	3.249	+1.91
CuSO ₄	1.183	3.647	3.711	+1.75
K ₂ HPO ₄	1.458	4.386	4.381	-0.11
K ₂ HPO ₄	1.699	5.110	5.081	-0.57

* $\rho \times 10^{23}$ (e/cm³)

The use of higher energy photons reduces the influence of some major sources of error, such as multiple scattering, finite geometry, and attenuation, and qualifies this new method as a valid alternative to that described in section 5.4.1. In addition, this method is promising for in "in vivo" measurements in relation to radiotherapy treatment planning and skeletal bone densitometry, provided that a very small s.v. can be used.

5.4.3 Imaging Techniques using Compton Scattering

The measurement of the photons fluence which a small volume of a sample scatters by Compton effect from a narrow incident beam of monoenergetic X- or gamma-radiation, provides a direct method for determining the electron density of a volume inside the sample. This simple principle in conjunction with various imaging techniques, has been used to image transverse and longitudinal sections of the body. In particular, the imaging techniques so far proposed are able to reconstruct an internal section: (i) transversal using point-by-point imaging (refs. 7, 8, 10) or line-by-line imaging (ref. 9), or (ii) longitudinal using a planar beam of gamma-radiation and a gamma-camera (ref. 11).

In this subsection the main characteristics of these techniques are briefly outlined, the aim being to allow the reader to make an initial comparison between the analytical capacity of single point and imaging techniques.

Compton tomography was developed initially by Lale (ref. 7) using a narrow photon beam (3 mm diameter) which passed through the patient. In this system, the rays scattered from a small volume of tissue are accepted by a large focusing collimator behind the patient and reach a scintillator. The direct beam and the rays scattered by the tissues surrounding the small volume are absorbed by this collimator. By scanning both the beam and the detector along the patient, the Compton scattering intensities can be used for constructing an electron density image.

Lale initially used an iridium-192 source emitting photons in the energy range 300-600 keV, and later X-rays from a linear accelerator (5.6 MeV X-rays). The results obtained by Lale were not completely satisfactory either in the spatial resolutions (1 cm) or in tissue electron density resolution (5%). Modifications of the Lale tomograph have been described by Clarke et al. (ref. 8) who used cobalt-60 and caesium-137 sources.

The technique used by Lale (see Fig. 5.24) consists in a large detector and a multi-hole collimator for recording possibly only the singly scattered radiation from a small volume. The size of s.v. limited the obtainable spatial resolution.

Conversely, Farmer and Collins (ref. 9) used a completely different

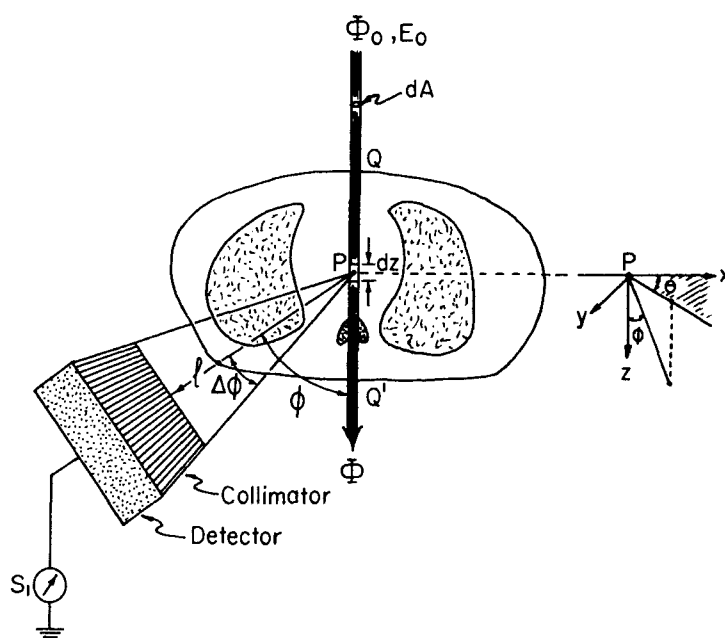


Fig. 5.24. Basic principles of tomography with Compton scattered radiation using a multihole collimator and a single scintillator detector. (after Battista and Bronskill, ref. 41).

strategy, recording with a small detector the scattered photons from all parts of the primary beam (see Fig. 5.25). The energy of the Compton scattered photons determines the interaction point along the primary beam. In this technique a highly monoenergetic primary beam is needed as well as a detector with very good energy resolution, i.e. a solid state detector. In other words in the Farmer and Collins' method the spatial resolution along a line is limited by the detector resolution. The relationship between the energy shift and the scattering angle is non linear, so the length of the segment usefully recorded in a single measurement must be negligible. Since the energy shift increases with increasing photon energy, in this technique it is advisable to use high energy radiation (compatible with the reduction of the detector efficiency). Until now, this technique even if very interesting has not produced good quality analytical results.

Later, Battista and al. (refs. 10, 41) developed several new methods to correct for multiple scattering and attenuation. They built a Compton scanner characterized by a cesium-137 source and a scintillator detector; the system was later used "in vivo" with satisfactory results. Battista and Bronskill (ref. 50) employed the Compton tomography as an aid for planning radiotherapy.

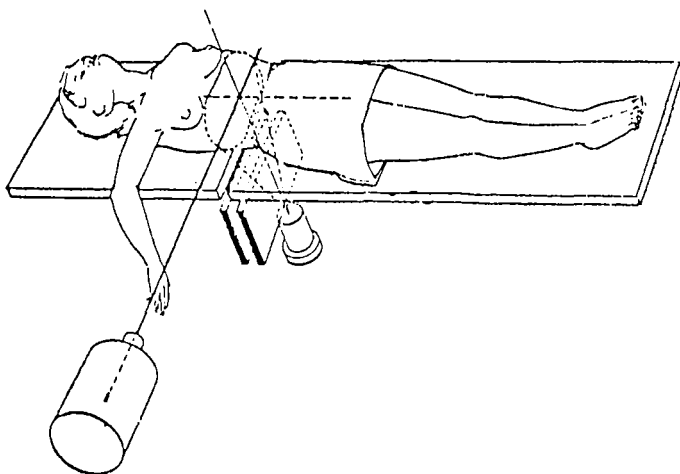


Fig. 5.25. The tomographic system proposed by Farmer and Collins (ref. 9) using a germanium detector.

To this aim, they made a thorough analysis of the analytical performances of their device; results of a direct comparison of Compton-measured and true electron density are reported in Figure 5.26. Linear regression analysis shows that the maximum deviation from linearity is 0.038, in terms of relative electron density. Moreover, Battista and Bronskill compared the results that can be obtained by using Compton and CT scanners. They concluded that the Compton scattering technique is able to image tranverse sections with a spatial resolution of 0.5 cm and a relative electron density accuracy of 4% at a maximum radiation dose for the patient of 11 rad. They stressed that this standard of performance approaches the theoretical optimum for Compton imaging but falls short of the capability of commercial X-ray CT scanners. The only advantages of the Compton technique are the more easily imaging of the patient under radioterapy treatment and measurement of the direct electron density distribution.

The imaging technique developed by Guzzardi et al. (refs. 11, 51) uses a collimated fan beam of monochromatic gamma rays produced by a linear source of mercury-203 (279 keV gamma rays) and a gamma camera placed at 90° , equipped with a parallel hole collimator (see Fig. 5.27). This technique allows an ideal tomography insofar the image plane (slab) is irradiated. The dose necessary for a single measurement is lower than that required by analogous techniques. Guzzardi et al. (ref. 11) used this technique to visualize density

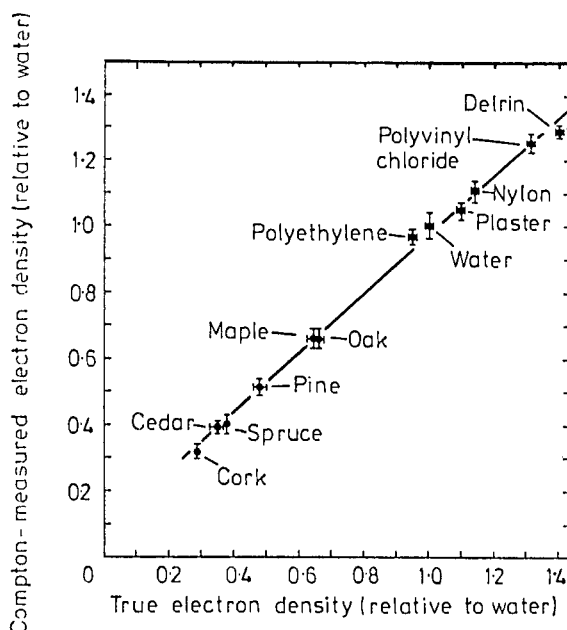


Fig. 5.26. Calibration of the Compton scanner designed by Battista and Bronskill (ref. 50) in terms of electron density relative to water. The average deviation from linearity (full line) is 0.015, and the maximum deviation is 0.038.

gradients in the chest; in lung pathology marked changes in density (see Table 5.2) have been observed by the authors. They pointed out that due to the attenuation and multiple scattering effects, results are limited. In experimental evaluation, a 14% precision in the determination of electron density was reached without correcting attenuation.

In conclusion the imaging techniques, despite the fact that they offer a tomographic image, are characterized by limited analytical performances compared to the single point techniques. The use of more efficient correction methods for attenuation and multiple scattering effects, would only partially compensate this disadvantage. Furthermore, there is strong competition between these and the CT techniques. Recently, a mixed system that used transmitted and Compton backscattered radiation has been proposed by Brateman et al. (ref. 42); results show that complementary information can be obtained from the Compton scattering and CT images. Moreover, Harding and Fischler (ref. 52) have developed a new tomographic system in which a high intensity X-ray tube (160 kVp, 3 KW) and two multidetector arrays (sixty-four BGO detectors). The

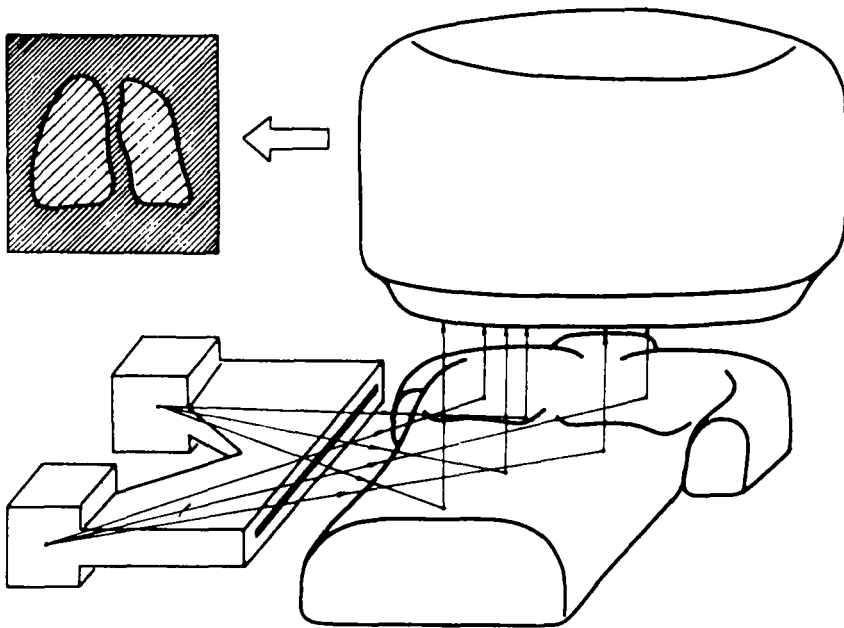


Fig. 5.27. Schematic illustration of 90 degrees Compton tomography of the lung with the technique proposed by Guzzardi et al. (ref. 11).

analytical performances of this system, using a dual energy method, have been assessed with a phantom finding encouraging results. Probably, in the near future, following these new proposals we might expect to see CT systems endowed with additional detectors in order to record scattered radiation; these new systems could produce two complementary images.

5.5 THE COHERENT (RAYLEIGH) TO COMPTON SCATTERING RATIO TECHNIQUE (R/C.T.).

The first proposal to use the ratio of the two scattered peak intensities was made by Kunzendorf in 1972 (ref. 12). This first work immediately showed the potentialities of the method despite the primitive (uncollimated) set-up used. Kunzendorf results were obtained with a backscattering geometry, using a Si(Li) detector (FWHM=250 eV) and plutonium-238 (emitting 13.5, 17.2 and 20.2 keV photons), cadmium-109 (22.1 and 24.9 keV) and americium-241 (59.4 keV) radioisotopic sources. The results reported demonstrated that the value of the power index of the R/C ratio vs Z relation was greater for higher energies of

primary photons.

Later, Puumalainen et al. (ref. 13) started extensive studies on this method; they proposed the use of the R/C ratio in the measurement of TBMD using an americium-241 source and a ninety degrees scattering angle. The coherent to Compton scattering ratio technique became more interesting with the introduction of solid state detectors and in particular of planar germanium detectors, which have a very good energy resolution (FWHM 200-400 eV) and a high counting efficiency also in the hundred keV ranges. With this type of detector it is possible to resolve the elastic peak from the Compton band. Clearly the counters used are solid state detectors.

In 1979 Schätzler (ref. 14) described the first analytical applications of the R/C.T. using an americium-241 source and scattering angles of 48 and 68 degrees. Analysing twenty-six organic compounds, he found a relationship between the R/C ratios and an empirically defined effective parameter, the effective atomic number; his aim was to demonstrate that it is possible to identify a compound only by measuring its R/C ratio. Figure 5.28 shows the plot of the R/C ratios relative to water as a function of the effective atomic number. Schätzler approximated these values with a power function of Z , introducing an index of 3.5 which agrees with the strong dependence of coherent scattering coefficient on Z discussed in section 5.2.2. This author also

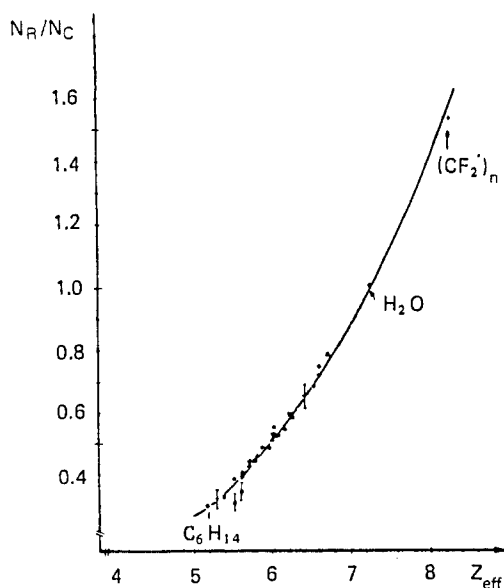


Fig. 5.28. The coherent to Compton scattering ratios relative to water, for 26 organic compounds. The primary beam energy was 60 keV and the scattering angle 68 degrees. (after Schätzler, ref. 14).

also gave examples of the analysis of binary mixtures; he attempted to determine the percentage of fat content in milk and in meat using R/C.T.. From the results reported, it can be seen that a precision of 3.4 % can be reached with a measuring time of a few hundred seconds. Similar results have been obtained by Puumalainen et al. (ref. 53) in the determination of iodine in tissues. The results reported showed a precision of about one milligram per cubic centimeter. It can be observed that the typical sensitivity of the R/C.T. in measurements of concentration of a particular element in a sample, is very low as compared with that of other analytical techniques such as X-ray fluorescence and neutron activation analysis. These latter two techniques can be also employed in "in vivo" measurements. The above-mentioned results in the very early attempts already, characterized R/C.T. as an analytic technique able to perform bulk analysis rather than the determination of a single element present in a sample at low concentrations.

Almost simultaneously in the 1980's some groups proposed the use of R/C.T. to the determination of TBMD, using a small scattering angle and energies around one hundred keV (refs. 15, 16). In particular, Stalp and Mazess (ref. 16) carried out experimental studies on the behaviour of the R/C ratio using radioisotopic sources of americium-241 and gadolinium-153 and a scattering angle of less than sixty degrees. Their conclusions were that with a 103 keV energy of the primary beam and at a scattering angle of thirty degrees (i.e. at a value of momentum transfer variable of 2.15 Å) better results can be obtained than at ninety degrees using an americium-241 source ($x = 3.42$). Stalp's conclusions can be explained considering that at 103 keV with a scattering angle of 30 degrees there is both a lower x value and a lower attenuation of the primary and scattered beam. However, it should be pointed out that in this work the authors did not attempt to optimise the geometry at different angles but used the same collimation condition at 30 and 60 degrees. No larger scattering angle was investigated.

Kerr et al. (ref. 15) using a very tightly collimated experimental set-up introduced a procedure to optimise the performance of the measuring system with respect to primary beam energy and scattering angle. Using this procedure they found that the best conditions are attained at an energy of 80 keV and a scattering angle of 25 degrees. The procedure was as follows. For a given energy and scattering angle, the FWHM of the Compton band was determined by assuming a given spread of the scattering angle and introducing the detector resolution. The coherent peak and the Compton band are considered to be resolved when the full-width at tenth maximum (FWTM) of the Compton band coincides with the lower limit of the FWTM of the elastic peak. Having determined the minimum acceptable coherent-Compton separation in this way, the

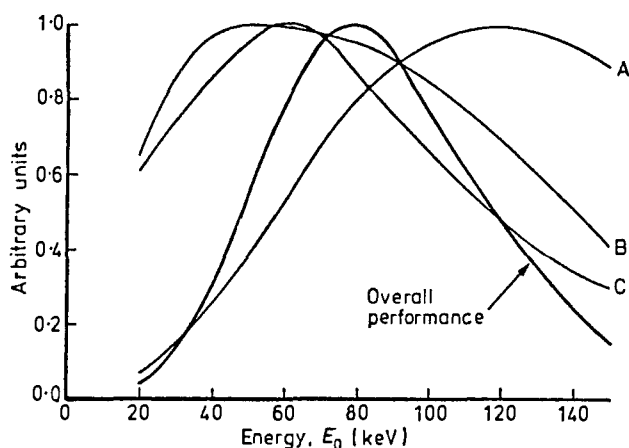


Fig. 5.30. The energy dependence of the performance of a system (Kerr et al. (ref. 15)) for the measurement of TBMD based upon the R/C.T.. Energy dependence of: A the number of coherently scattered photons per unit dose; B the detector counting efficiency; C the mass absorption coefficient for bone.

showed that the principal parameter to be optimized is the precision (see Eq. (15)) that simultaneously includes the counting rate and the sensitivity. Their conclusions were that the optimising procedure proposed by Kerr et al. must be completed by taking into account the changes in sensitivity and precision observed at higher momentum transfer values. Many of the theoretical results of these works have been reported in section 5.2.3. Finally, these authors clearly pointed out the importance of the geometrical counting efficiency that changes considerably at different scattering angles. So far this group is the only one to have published results on the clinical use of the R/C.T. in the measurement of TBMD. Using a 71 degrees angle and a 1.2 Ci americium-241 source they obtained an accuracy of 5% and a precision of 3% with a counting time of 15 minutes. The dose to the patient is about 300 mRad. Figure 5.31 shows a comparison between bone mineral density determined by R/C.T. and that measured directly (ref. 55).

Gigante and Sciuti (ref. 43) extended the analysis of the above mentioned group (refs. 28, 54) showing that a backscattering geometry can optimize the system performance in term of precision at a given counting statistic. Studies on the s.v. shape and on the behaviour of the selfabsorption function in a backscattering geometry, were also carried out.

An interesting development from an instrumentation point of view is that illustrated by Puumalainen et al. (ref. 56) with the use of a X-ray tube in substitution of the less intense radiosotopic sources. The aim of these

corresponding Compton energy shift was then calculated (see E. (1)). With this procedure it is possible to find for a given energy (and known values of the collimation parameters) the minimum scattering angle that can be usefully employed. Figure 5.29 shows the spectrum of photons scattered from a foot using a primary beam energy of 103 keV and a scattering angle of 22.5 degrees. To find the optimal range of primary photon energies the authors studied the energy dependence of: (i) the number of coherently scattered photons per unit dose, (ii) the detector (an intrinsic planar germanium of 400 mm² active area) counting efficiency, (iii) differential coherent scattering mass absorption

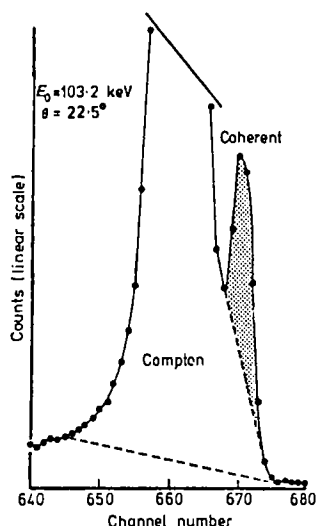


Fig. 5.29. Scattered spectrum from a cadaver foot. (after Kerr et al., ref. 15).

coefficient. From Figure 5.30 that shows the plot of the functions studied by Kerr et al., turns out that an energy around 80 keV is the most favourable.

In 1982 Greenfield et al. (refs. 17, 27, 28, 54) published the results obtained in the measurement of TBMD using americium-241 sources and a larger scattering angle. The authors (ref. 17) discussed the experimental obstacles encountered in the development of a measuring system for clinical use. They showed the advantages of using a 90° geometry in order to obtain a s.v. of more regular shape compared to the elongated forms obtained at smaller angles. These authors, depicted the methodology for studying the different sources of error in an "in vivo" system. In two later reports (refs. 28, 54), they pointed out that the best sensitivities can be obtained either at larger scattering angle for a 60 keV primary beam energy, or generally at higher momentum transfer values (see sections 5.2.2 and 5.2.3). In particular, they

authors was to obtain a more intense primary beam possibly with a tunable energy. The monochromatic beam was obtained using a CsCl filter and a tube tension of 59 Kv_p. They thus obtained a 38.9 keV energy beam useful only for "in vitro" studies. Recently, Timms et al. (ref. 57) with a X-ray tube and the technique of balanced filters obtained a sixty keV beam. They used this to determine the R/C ratios of standard samples obtaining very good results. The availability of more intense X-ray sources as for example the Synchrotron radiation sources (characterized by a high degree of polarization, characteristic that may be usefully used), will certainly give a new impulse to these techniques.

Besides the very interesting application in the determination of TBMD, R/C.T. can be used in other analytical applications for the identification of

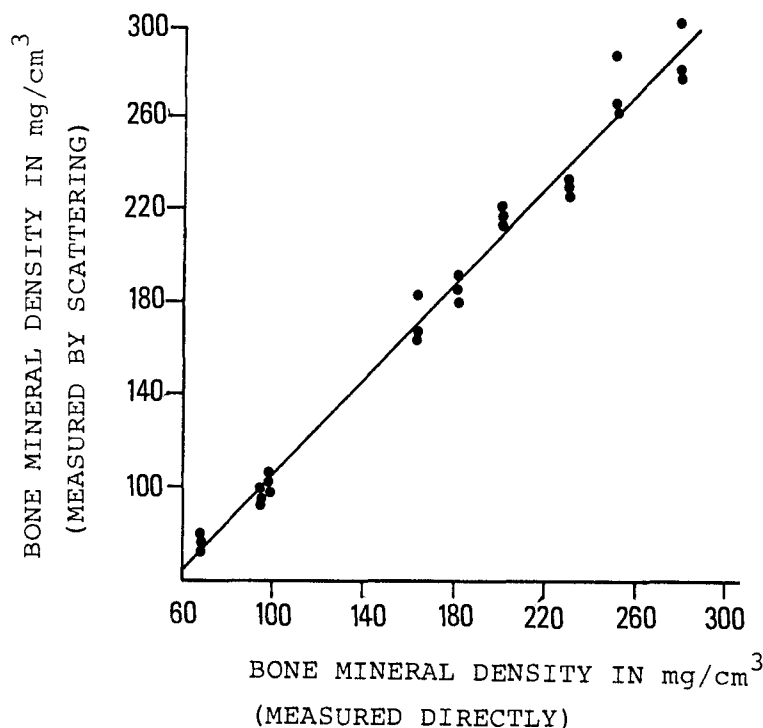


Fig. 5.31. Comparison between the bone mineral density determined by R/C.T. and that measured directly. The regression line is also shown. (After Greenfield et al., ref. 55).

unknown materials and/or in the characterization of tissues. The latter was studied by Holt et al. (ref. 58) using a spectrometer devoted to Compton profile analysis (ref. 59). This spectrometer uses a 5 Ci americium-241

source and a 171 degrees scattering angle. The results demonstrated that accurate characterization of the tissues through the determination of their R/C ratios, can be obtained. Table 5.4 shows the R/C values reported in this work, as measured in different tissues and low Z samples.

TABLE 5.4

The R/C values measured in different tissues and low Z samples.

Sample	R/C $\times 10^{-3}$
De-ionized water	1.023 + 0.017
0.9% saline solution	1.210 + 0.017
Breast cyst fluid	1.163 + 0.017
In-tissues liver*	1.246 + 0.017
In-tissue liver+	1.277 + 0.017
Homogenised liver*	1.180 + 0.031
Homogenised liver+	1.197 + 0.031

* Taken from rats treated with saline solution

+ Taken from rats treated with phenobarbitol (80 mg/kg solution)

Other measurements carried out with saline solutions up to 20% have shown that R/C.T. has a good sensitivity, in fact a change of 0.2% in concentration gives a measurable 2.5% change in the intensity ratio. Holt et al. (ref. 58) underlined that in order to obtain such good results, a careful study of the Compton profiles is necessary to minimize the errors in the R/C ratio measurements.

Several investigations have been carried out on the analytical power of R/C.T. in the identification of low Z compounds and in the analysis of metal alloys.

Cesareo (ref. 60) demonstrated the potentialities of this technique in the analysis of binary silver alloys. Later, Gigante and Sciuti (ref. 27) used simultaneously both the informations coming from the scattering and fluorescence components. The XRF spectrum is available only if some elements in the sample emit fluorescence photons of sufficiently high energy, i.e. comparable to that of the scattered photons. The two components are in many cases complementary. This strategy is particularly useful in the analysis of tertiary and quaternary alloys, possibly using scattering intensities from the same material at different primary beam energies (ref. 61). Furthermore, some authors have shown that identification of low-Z material is possible using only the R/C ratio (ref. 27). The calculated values of the scattering intensity ratio are compared in Figure 5.32 with those measured with a spectrometer, using a backscattering geometry and two americium-241 sources as depicted in Figure

5.14. The theoretical values were calculated from the data of Hubbell et al. (ref. 19). Gigante and Sciuti (ref. 27) have shown that identification of a sample is possible using the theoretical R/C ratio values for the single element and a specific computer programme. Corrections for the attenuation effects can be introduced using the tabulated values of the attenuation coefficients.

Manninen et al. (ref. 29) first, and later Manninen and Koikkalainen (ref. 33) offered an alternative, namely the possibility to define an effective atomic number. They carefully studied the behaviour of the R/C ratio as a function of Z , both for pure elements and low- Z compounds. Using the Equation (12) they found that a good agreement between calculated and measured R/C values can be obtained for an energy of 60 keV and large scattering angles.

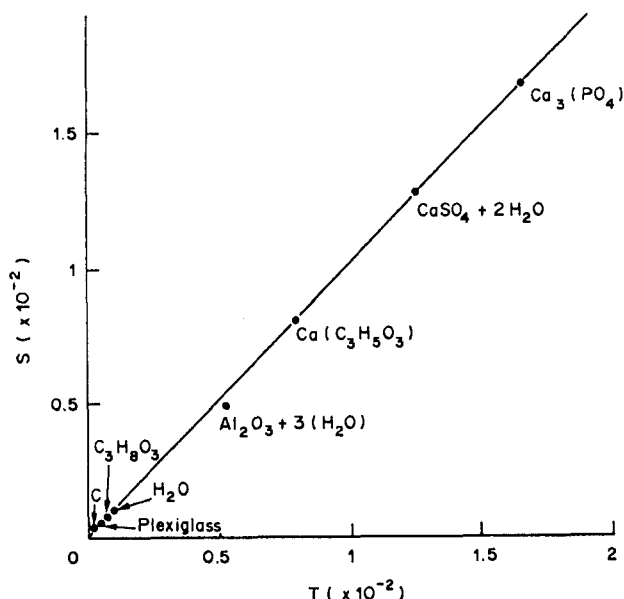


Fig. 5.32. Measured vs calculated R/C ratios for different compounds. (After Gigante e Sciuti, ref. 27).

These results show that for such energy and large angles, there is a dependence of the coherent scattering on Z^3 and of the Compton scattering on Z . Figure 5.33 shows the results obtained by these authors at different scattering angles. The measured Ze values differ from the calculated ones (using Eq. (12)) by less than 0.5%.

The analytical potentialities of R/C.T. are clearly shown by the above reported results. The sensitivity of this technique is very good both in the determination of the TBMD "in vivo" and in the identification of tissues and materials. Further improvements are possible using more intense monochromatic sources and faster counting chains. In the near future, R/C.T. will surely become one of the most used techniques of tissue characterization and bulk analyses.

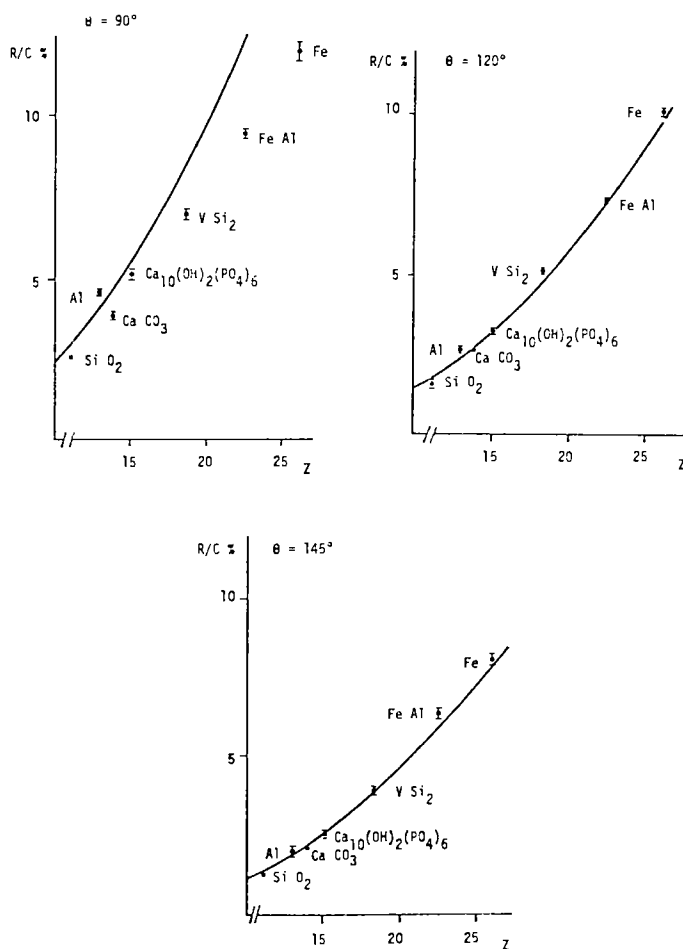


Fig. 5.33. The measured R/C ratios for various compounds, for a primary beam energy of 60 keV and different scattering angles.

ACKNOWLEDGMENTS

The author is deeply grateful to Prof. S. Sciuti for his continuous support and advice in research on PST, and his critical reading of the text and Mr. D. Tarsitano for his technical assistance.

REFERENCES

- 1 R.L. Clarke and G. Van Dyk, *Phys. Med. Biol.*, 18 (1973) 532.
- 2 E.S. Garnett, T.J. Kennett, D.B. Kenyon and C.E. Webber, *Radiology*, 10 g (1973) 209.
- 3 C.E. Webber and T.J. Kennett, *Phys. Med. Biol.*, 21 (1976) 760.
- 4 H. Olkkonen and P. Karjalainen, *Br. J. Radiol.*, 48 (1975) 594.
- 5 A.L. Huddleston and D. Bhaduri, *Phys. Med. Biol.*, 24 (1979) 310.
- 6 A.L. Huddleston and J.B. Weaver, *Int. J. Appl. Radiat. Isotopes*, 34 (1983) 997.
- 7 P.G. Lale, *Phys. Med. Biol.*, 4 (1959) 159 and *Radiology*,
- 8 R.L. Clarke, E.N.C. Milne and G. Van Dyk, *Med. Phys.*, 3 (1976) 225.
- 9 F.T. Farmer and M.P. Collins, *Phys. Med. Biol.*, 16 (1977), 229.
- 10 J.J. Battista, L.W. Santon and M.J. Bronskill, *Phys. Med. Biol.*, 22 (1977) 229.
- 11 R. Guzzardi, M. Mey, M. Pistolesi, S. Solfanelli and C. Giuntini, *J. Nucl. Med. Allied Sci.*, 22 (1978) 11.
- 12 H. Kunzendorf, *Nucl. Instrum. Methods*, 99 (1972) 611.
- 13 P. Puumalainen, A. Uimairihusta, E.M. Alhva and H. Olkkonen, *Radiology*, 120 (1976) 723 and P. Puumalainen, H. Olkkonen and P. Sikanen, *Int. J. Appl. Radiat. Isotopes*, 28 (1977) 785.
- 14 H.P. Schützler, *Int. J. Appl. Radiat. Isotopes*, 28 (1979) 115.
- 15 S.A. Kerr, K. Kouris, C.E. Webber and T.J. Kennett, *Phys. Med. Biol.*, 25 (1980) 1037.
- 16 J.T. Stalp and B. Mazess, *Med. Phys.*, 7 (1980) 723.
- 17 S.S. Ling, S. Rustgi, A. Karellas, J.D. Craven, J.S. Whiting, M.A. Greenfield and R. Stern, *Med. Phys.*, 9 (1982) 208.
- 18 G.A. Carlsson, C.A. Carlsson, K.F. Berggren and R. Ribberfors, *Med. Phys.*, 9 (1982) 868.
- 19 J.H. Hubbell, W.J. Weigle, E.A. Briggs, R.T. Brown, D.T. Cromer and R.J. Howerton, *J. Phys. Chem. Ref. Data*, 4 (1975) 471.
- 20 D.A. Bradley and A.M. Ghose, *Phys. Med. Biol.*, 29 (1984) 1385.
- 21 P.C. Johns and M.J. Yaffe, *Med. Phys.*, 10 (1983) 40.
- 22 L. Kissel, R.H. Pratt and J.S.C. Roy, *Phys. Rev. A*, 22 (1980) 1970.
- 23 S.C. Roy, L. Kissel and R.H. Pratt, *Phys. Rev. A*, 27 (1983) 285.
- 24 D. Schuapp, M. Schumacher, F. Smend, P. Rullhusen and J.H. Hubbell, *J. Phys. Chem. Ref. Data*, 12 (1983) 467.
- 25 A.L. Hanson, *Nucl. Instrum. Methods*, 243 A (1986) 583.
- 26 S.C. Roy, *Nucl. Instrum. Methods*, 150 (1978) 283.
- 27 G.E. Gigante and S. Sciuti, *Int. J. Appl. Radiat. Isotopes*, 35 (1984) 481.
- 28 I. Leichter, A. Karellas, J.D. Craven and M.A. Greenfield, *Med. Phys.*, 11 (1984) 31.
- 29 S. Manninen, T. Pitkanen, S. Koikkalainen and T. Paakkari, *Int. J. Appl. Radiat. Isotopes*, 35 (1984) 93.
- 30 R.A. Rutherford, B.R. Pullan and I. Isherwood, *Neuroradiology*, 11 (1976) 15.
- 31 D.R. White, *Phys. Med. Biol.*, 22 (1977) 219.
- 32 D.F. Jackson and D.J. Hawkes, *Phys. Rep.*, 70 (1981) 169.
- 33 S. Manninen and S. Koikkalainen, *Int. J. Appl. Radiat. Isotopes*, 35 (1984) 965.
- 34 R.B. Mazess, J.R. Cameron and J.A. Sorenson, *Nature*, 228 (1970) 771.
- 35 T.J. Kennett and C.E. Webber, *Phys. Med. Biol.*, 21 (1976) 770.
- 36 G. Coates and C.E. Webber, *Med. Phys.*, 9 (1982) 478.
- 37 A.L. Huddleston, D. Bhaduri and J. Weaver, *Med. Phys.*, 6 (1979) 519.
- 38 E.A. Wolf and T.R. Munro, *Int. J. Appl. Radiat. Isotopes*, 36 (1985) 97.
- 39 F. Arinc and R.P. Gardner, *J. Radioan. Chem.*, 54 (1979) 221.
- 40 F.T. Farmer and M.P. Collins, *Phys. Med. Biol.*, 19 (1974) 808.
- 41 J.J. Battista and M.J. Bronskill, *Phys. Med. Biol.*, 23 (1978) 23.
- 42 L. Brateman, A.M. Jacobs and L.T. Fitzgerald, *Phys. Med. Biol.*, 29 (1984) 1353.
- 43 G.E. Gigante and S. Sciuti, *Med. Phys.*, 12 (1985) 321.

- 44 K. Reiss, D. Ing, W. Schuster, *Radiology*, 102 (1972) 613.
- 45 C.E. Webber, G. Coates, *Med. Phys.*, 9 (1982) 473.
- 46 H.L. Cox, P.S. Ong, *Med. Phys.*, 4 (1977) 99.
- 47 L.F. Preuss, D.G. Piper, C. Bugenis, in C.L. Grant, C.S. Barrett, J.B. Newkirk and C.O. Ruud (Eds.), *Advances in X-Ray Analysis*, Vol. 18, Plenum Press, New York, 1975, 545.
- 48 P.C. Shrimpton, *Phys. Med. Biol.*, 26 (1981) 907.
- 49 A.L. Huddleston and J.P. Sackler, *Med. Phys.*, 12 (1985) 13.
- 50 J.J. Battista and M.J. Bronskill, *Phys. Med. Biol.*, 26 (1981) 81.
- 51 R. Guzzardi, M. Mey, *Phys. Med. Biol.*, 26 (1981) 155.
- 52 G. Harding and R. Tischler, *Phys. Med. Biol.*, 31 (1986) 477.
- 53 P. Puumalainen, H. Olkkonen and P. Sikanen, *Nucl. Instrum. Methods*, 163 (1979) 261.
- 54 A. Karellas, I. Leichter, J.D. Craven and M.A. Greenfield, *Med. Phys.*, 10 (1983) 605.
- 55 M.A. Greenfield, J.D. Craven, S.S. Shukla, A. Karellas and I. Leichter, *Medical and Biological Engineering and Computing*, 23 (Suppl.) (1985) 1074.
- 56 P. Puumalainen, A. Uimairihuhta, H. Olkkonen and E.M. Alhva, *Phys. Med. Biol.*, 27 (1982) 425.
- 57 D.N. Timms, M.J. Cooper and R.S. Holt, *J. Phys. E: Sci. Instrum.*, 20 (1987) 76.
- 58 R.S. Holt, K. Kouris, M.J. Cooper and D.F. Jackson, *Phys. Med. Biol.*, 28 (1983) 1435.
- 59 M.J. Cooper, *Contemp. Phys.*, 18 (1977) 4896.
- 60 R. Cesareo, *Nucl. Instrum. Methods*, 179 (1981) 545.
- 61 G.F. Gigante, L.J. Pedraza and S. Sciuti, *Nucl. Instrum. Methods*, 12 B (1985) 229.

Chapter 6

"IN VITRO" ACTIVATION ANALYSIS

NIKY MOLHO

Dipartimento di Fisica - Sezione di Fisica Medica

Università di Milano

Via Celoria 16, 20122 Milano (Italy)

6.1 INTRODUCTION

Activation analysis has been a very powerful tool for quantitative analytical research since 1936 (ref. 1). Many technical developments have improved the quality of the results so that nowadays this technique is one of the most sensitive and reliable, especially in the domain of trace element determination. This fact has a strong impact in biomedical sciences because the role of trace elements in human metabolism can be studied only if quantitative measurements are feasible and reliable.

The basic principle of activation analysis is the following: a sample is exposed to a particle flux so that nuclear reactions can take place. If the element of interest, by means of a nuclear reaction, gives rise to a radioactive nucleus, the subsequent delayed decay may cause the emission of a radiation that identifies the parent nucleus. By measuring its intensity it is then possible to go back to the quantitative determination of the element of interest.

In the following paragraphs details on the procedures will be given.

6.2 NUCLEAR REACTIONS

A nucleus is constituted by nucleons: neutrons and protons. In a very simplified picture a nuclear reaction may be defined as the rearrangement that occurs in a system of nuclear particles when they mutually interact. The rearrangement may be produced in many different ways that are called with different names (scattering, direct reactions, fission, fusion etc.) but in activation analysis the most significant reactions are produced via the compound nucleus (CN) formation; (neutron radiative capture may be considered a particular case of CN reaction).

The compound nucleus reaction model is depicted as the formation and subsequent decay of a compound system created in a highly excited state by the capture of an incident nuclear particle i into a target nucleus T (see Fig. 6.1).

The compound nucleus cools down evaporating particles (or clusters) if the excitation energy is sufficiently high and at least emitting electromagnetic radiations (γ cascades): what remains of the compound nucleus is called the residual nucleus R and may be considered the final product of the reaction process.

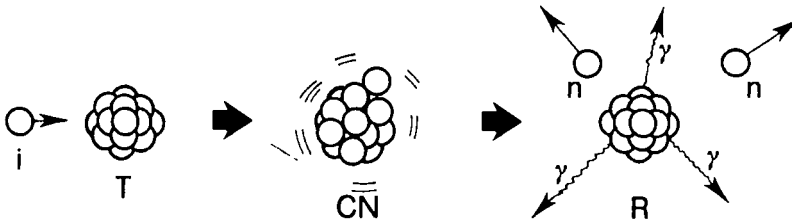


Fig. 6.1. Schematic representation of a CN reaction: the incident particle i hits the target nucleus T fusing with it and giving rise to an excited compound nucleus CN in which energy is partitioned among the nucleons.

The energy of the incident particle is one of the most significant parameters of the reaction. Total energy is conserved in a nuclear reaction and for this reason one has also to take into account the binding energies of protons and neutrons in all the interacting nuclei.

The total energy balance, in the sense of rest and kinetic energy, may be written as:

$$\sum_k (m_{ok}^i c^2 + E_k^i) = \sum_j (m_{oj}^f c^2 + E_j^f) \quad (1)$$

where m_{ok}^i and E_k^i are the initial rest masses, and kinetic energies, m_{oj}^f and E_j^f are the final rest masses and kinetic energies. The difference between final and initial kinetic energies is specific of every nuclear reaction and is usually indicated as Q .

$$\sum_j E_j^f - \sum_k E_k^i = \sum_j m_{oj}^f c^2 - \sum_k m_{ok}^i c^2 = Q \quad (2)$$

This Q energy specifies the modification of the binding energies of the partners involved in the reaction and may be positive or negative: if the Q

value is negative the reaction can occur only if the incoming particle energy is greater than a threshold energy equivalent to $|Q|$.

To specify the probability of occurrence of a particular nuclear reaction one introduces the concept of cross section σ . This physical quantity has the dimension of a surface and is an index of the effective section of the nuclei involved in the specific reaction.

If one has a beam of N_0 nuclear particles per second impinging on a target constituted by a thin foil of thickness x and density n nuclei per unit volume, the number N_R of specific nuclear reactions per unit time may be written as:

$$N_R = N_0 \sigma_R n x \quad (3)$$

where σ_R is the reaction cross section (see Table 6.1).

The relation (3) is equivalent to:

$$N_R = N_0 \sigma_R (N_A / A) \delta x \quad (4)$$

where N_A is the Avogadro number, A the mass number and δx the thickness of the target measured in unit of mass/surface (g/cm^2).

The cross sections are usually measured in barn units, that is 10^{-24} cm^2 , and are usually strongly dependent upon the type and the energy of the incident particle.

TABLE 6.1

Typical magnitudes of some nuclear reaction cross sections.

Reaction	Typical cross section (millibarn)
(n, th, γ)	$10 - 10^8$
(n, p)	$1 - 100$
$(n, 2n)$	$1 - 1000$
(p, n)	$10 - 1000$
$(p, 2n)$	$100 - 1000$
(p, α)	$1 - 100$
(d, n)	$1 - 100$
$(d, 2n)$	$100 - 1000$
(α, n)	$10 - 1000$
(α, pn)	$1 - 1000$

6.3 NUCLEAR DECAY

Usually the residual nucleus produced during the reaction is unstable, that is after a more or less long delay it decays spontaneously by emission of nuclear particles.

The daughter nucleus so produced is generally left in an excited state from which it decays to the ground state emitting a well specified series of γ rays that make possible the identification of the nucleus itself.

The decay of a radioactive nucleus on a macroscopic time scale is regulated by a well known law that is essentially statistic: if there are N radioactive nuclei at a certain time, the probability that in the subsequent interval dt occurs a decrease $-dN$ because of nuclear decay is given by:

$$dN = -\lambda N dt \quad (5)$$

where λ is a constant characteristic of the specific radioactive nucleus and called "decay constant".

By integration and assuming N_0 as the number of radioactive nuclei existing at $t = 0$, one gets:

$$N = N_0 e^{-\lambda t} \quad (6)$$

The quantity $\tau = 1/\lambda$ is called "mean life" of the radioactive nucleus and the quantity $T_{1/2} = \ln 2/\lambda = \tau \ln 2$ is called "half life" and represents the time required for any number of the specific nuclei to reduce to half the initial value (see Table 6.2).

A brief outline of different nuclear decays will be useful for the detailed understanding of the arguments that will follow.

6.3.1 Alpha decay

This decay was historically the first investigated and it consists in the emission of a cluster of 2 protons and 2 neutrons (one ${}^4\text{He}$ nucleus).

The energy spectrum of the emitted particles is discrete and it spans the region of a few MeV.

Nuclei decaying α are usually the heaviest ($Z > 85$), but there is some exception.

The α decay of the nucleus ${}^A_Z\text{X}$

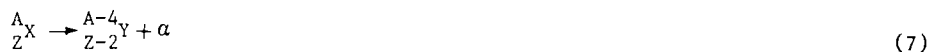


TABLE 6.2

Typical examples of nuclear half lives.

Element	Half lives
^{235}U	$7.04 \cdot 10^8 \text{ y}$
^{244}Pu	$8.3 \cdot 10^7 \text{ y}$
^{226}Ra	1600 y
^{90}Sr	29 y
^{152}Eu	13 y
^{131}I	8.04 d
^{24}Na	15.02 h
^{123}I	13.1 h
^{11}C	20.4 m
	10.6 m
^{13}N	9.97 m
^{15}O	122 s
^{16}N	7.11 s
^{12}N	11 ms

decreases the mass number A of 4 units and the atomic number Z of 2 units. In the nuclid chart the α decay is represented like in Figure 6.2.

The α decay is schematically interpreted as if the α particle, preformed in the nucleus, is confined by a potential barrier through which the particle can escape quantummechanically.

6.3.2 Beta decay

The decays in which the atomic number Z is modified by 1 unit and the mass number A is left inalterate are classified as β decays.

If a negative electron is emitted (β^- decay) the atomic number Z is increased by 1 unit.

In β^+ decay a positron is emitted and the atomic number is decreased by 1 unit.

In electron capture (EC) an atomic electron from the inner shells is absorbed in the nucleus so that the nuclear charge is decreased of 1 unit as in β^+ decay.

The energy spectrum of β decay is essentially continuous, terminating at an end energy determined by the total energy balance between parent and daughter nuclei.

In the nuclid chart β decays are represented as in Figure 6.3.

88	^{221}Ra 29 s	^{222}Ra 38 s	^{223}Ra 11.43 d	^{224}Ra 3.64 d	^{225}Ra 14.8 d	^{226}Ra 1600 y	^{227}Ra 41.3 m	^{228}Ra 5.75 y	^{229}Ra 10 m	^{230}Ra 1 h
Z	^{220}Fr 28 s	^{221}Fr 4.8 m	^{222}Fr 15 m	^{223}Fr 22 m	^{224}Fr 27 m	^{225}Fr 3.9 m	^{226}Fr 1.4 m			
86	^{219}Rn 3.96 s	^{220}Rn 55.6 s	^{221}Rn 25 m	^{222}Rn 3.824 d	^{223}Rn 43 m	^{224}Rn 1.9 h	^{225}Rn 4.5 m	^{226}Rn 6 m	142	
	^{218}At 2 s	^{219}At 0.9 m					140			
84	^{217}Po < 10 s	^{218}Po 3.05 m			138					
134 N 136										

Fig. 6.2. Part of the nuclid chart is represented in a simplified version: only mean life is given for radioactive nuclei and isotope abundance for stable nuclei. The arrow indicates the α decay in the sense that if ^{226}Ra decays by α emission, the daughter nucleus will be ^{222}Rn .

22	^{41}Ti 89 ms	^{42}Ti 0.20 s	^{43}Ti 0.49 s	^{44}Ti 47 y	^{45}Ti 3.078 h	^{46}Ti 8.0	^{47}Ti 7.5
Z	^{40}Sc 0.162 s	^{41}Sc 0.60 s	^{42}Sc 61 s	^{43}Sc 0.60 s	^{44}Sc 0.44 ms	^{45}Sc 3.89 h	^{46}Sc 58.6 h
20	^{39}Ca 0.07 s	^{40}Ca 96.94	^{41}Ca $1.3 \cdot 10^5$ y	^{42}Ca 0.65	^{43}Ca 0.14	^{44}Ca 2.08	^{45}Ca 163 d
	^{38}K 9.95 s	^{39}K 7.63 m	^{40}K 93.3	^{41}K $1.28 \cdot 10^9$ y	^{42}K 6.7	^{43}K 12.36 h	^{44}K 22.2 h
18	^{37}Ar 34.3 d	^{38}Ar 0.07	^{39}Ar 269 y	^{40}Ar 99.59	^{41}Ar 1.83 h	^{42}Ar 33 y	^{43}Ar 5.4 m
20 22 24 N							

Fig. 6.3. Same as Fig. 6.2 but for β decays. The arrow directed downward, decreasing the proton number, indicates the emission of a β^- or an EC process. The upward directed arrow indicates a β^+ process with an increase of the proton number.

6.3.3 Gamma decay

Very few radioactive nuclei decay emitting only electromagnetic radiation. Nevertheless, gamma decay is fundamental in activation analysis because it is the dominant process by which trace elements are identified. In fact, when a radioactive nucleus decays emitting an α or β particle, the daughter nucleus is usually left in an excited state from which the ground state is reached by emission of a series of γ rays.

In Figure 6.4 a typical process is represented.

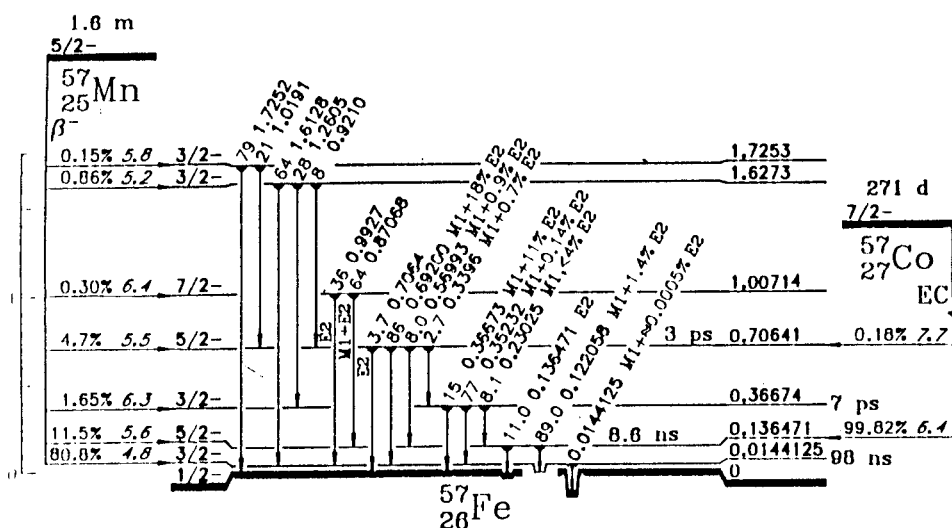


Fig. 6.4. Levels and decay scheme of ^{57}Fe (ref.2). The most important data one can draw from it for activation studies are: a) production (in this example by means of β^- decay of ^{57}Mn or EC process of ^{57}Co); b) population of the levels (in this case 80.8% of the decays from ^{57}Mn populate the 0.0144 MeV level or 99.82% of the decays from ^{57}Co populate the 0.0144 MeV level); c) decay and branching (89% of the ^{57}Fe nuclei excited at the 0.1364 MeV level decay to the 0.0144 MeV level emitting a 0.1220 MeV γ ray and only 11% decay directly to the ground state emitting a 0.1364 MeV γ ray).

The γ rays are electromagnetic radiations of nuclear origin ranging from a few keV to a few MeV.

Obviously the emission does not modify neither the mass number A nor the atomic number Z of the decaying nucleus.

6.4 BASIC EQUATIONS

The number n_x of radioactive nuclei of isotope x produced per unit time and per gram of target is:

$$n_x = \sigma_x N_A / A \varphi \quad (8)$$

where σ_x is the cross-section for the specified induced reaction; N_A is the Avogadro's number, A is the target mass number and φ is the flux of incident particles, that is the number of particles incident on target per cm^2 per second.

During the irradiation time t_i there is a certain decay of the isotope x already produced. If

$$dn_x = \sigma_x (N_A / A) \varphi dt \quad (9)$$

is the number of radioactive nuclei produced during the interval dt at a time t , the number dN_x of these radioactive nuclei left over at the end of irradiation is:

$$dN_x = dn_x e^{-(t_i - t) / \tau} \quad (10)$$

By integration, the total number N_x of radioactive nuclei left over after irradiation of one gram of sample is obtained:

$$N_x(t_i) = \sigma_x (N_A / A) \varphi \int_0^{t_i} e^{-(t_i - t) / \tau_x} dt = \sigma_x (N_A / A) \varphi \tau_x (1 - e^{-t_i / \tau_x}) \quad (11)$$

where τ_x is the mean life of the radioactive isotope.

After irradiation, usually a time t_w must elapse before spectra are collected, and during this interval a decay occurs; the number of radioactive nuclei remaining after the interval $t_i + t_w$ from the beginning of irradiation is thus:

$$N_x(t_i + t_w) = N_x(t_i) e^{-t_w / \tau_x} = \sigma_x (N_A / A) \varphi \tau_x (1 - e^{-t_i / \tau_x}) e^{-t_w / \tau_x} \quad (12)$$

What is particularly interesting is the produced activity, that is the instantaneous disintegration rate of the isotope just after irradiation. To obtain this quantity the relation (12) must be differentiated with respect to t_w at the time $t_w = 0$ changing the sign because activity is opposite to the

time rate decrease of the radioactive isotope:

$$A_o = - \left(\frac{dN_x \{t_i + t_w\}}{dt_w} \right)_{t_w=0} = \sigma_x \left(\frac{N_A}{A} \right) \varphi \left[1 - e^{-t_i/\tau_x} \right] \quad (13)$$

The expression in square brackets is called the saturation factor S and is a term approaching a unity value in the case of $t_i \gg \tau_x$.

Assuming for $t_i \gg \tau_x$ a limit value of $S = 1$, one gets for activity:

$$A_\infty = \lim_{t_i \rightarrow \infty} A_o = \sigma_x \left(\frac{N_A}{A} \right) \varphi \quad (14)$$

This saturation activity A_∞ is independent of the mean life of the isotope and represents the maximum value of activity attainable for one gram of sample with a definite incident flux φ .

The activity reaches a saturation value with increasing t_i because a steady situation is set up in which the decaying process has the same intensity of the production process.

The saturation factor S is a very meaningful term in planning an activation analysis measure. It is not remunerative to protract the irradiation time for more than 3-4 times the mean life of the produced radioisotope because saturation is attained.

After the waiting time t_w the γ decay spectrum is collected during a time t_m . The total decay number I_x of the isotope x per one gram of target during this interval is:

$$\begin{aligned} I &= N_x(t_i + t_w) - N_x(t_i + t_w + t_m) = \\ &= \sigma_x \left(\frac{N_A}{A} \right) \varphi \tau_x \left(1 - e^{-t_i/\tau_x} \right) \left(1 - e^{-t_m/\tau_x} \right) e^{-t_w/\tau_x} \end{aligned} \quad (15)$$

What one is interested in is the number of events registered by the detector for the chosen transition.

This number is proportional to I_x , and is also proportional to:

- a) α , the percentage of the particular γ transition for every decay;
- b) ϵ , the efficiency of the detector for the particular energy;
- c) $\Omega/4\pi$, the relative solid angle the detector subtends on the sample.

The number of counts registered for the particular γ ray is so:

$$I'_x = \alpha \epsilon \left(\frac{\Omega}{4\pi} \right) I_x = \alpha \epsilon \left(\frac{\Omega}{4\pi} \right) \sigma_x \left(\frac{N_A}{A} \right) \varphi \tau_x \left(1 - e^{-t_i/\tau_x} \right) \left(1 - e^{-t_m/\tau_x} \right) e^{-t_w/\tau_x} \quad (16)$$

6.5 INSTRUMENTATION FOR ACTIVATION ANALYSIS

Many projectiles can be used to induce nuclear reactions for activation analysis, but this discussion will be restricted only to thermal neutrons and light ions.

6.5.1 Reactors as neutron sources

By far the most used particles for activation analysis are slow neutrons produced in research reactors.

The physical mechanism on which the most part of nuclear reactors is based is fission of ^{235}U . In this process, the ^{235}U nucleus is splitted in two intermediate mass nuclei with a release of energy of about 200 MeV and with the emission of 2-3 neutrons.

The fission process is asymmetric in the sense that generally one light mass and one complementary heavy mass fragment are produced.

A typical mass spectrum is shown in Figure 6.5.

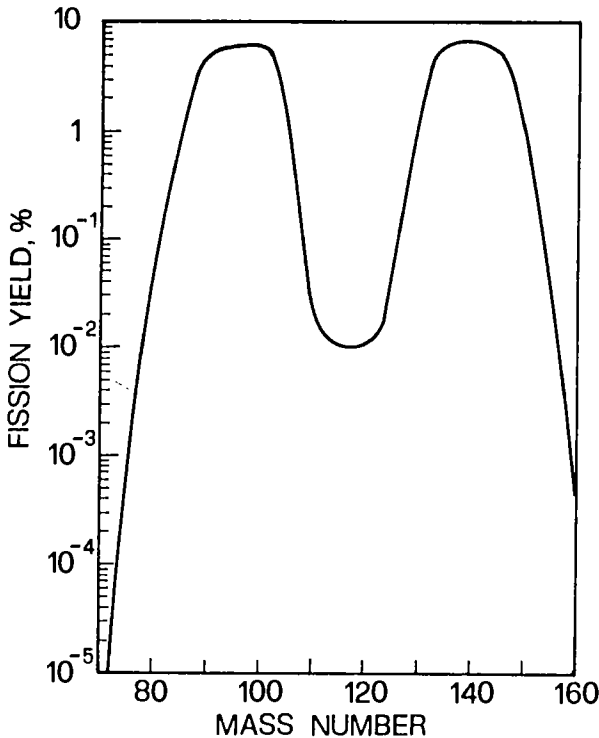


Fig. 6.5. Relative fission yield in ^{235}U : the masses of the produced fragments have a relative distribution that is nearly symmetric, and the probability of symmetric fission is much lower than the probability of fragmentation with two different masses.

The neutrons emitted during the fissioning process have an average energy of 2 MeV and their energy spectrum is very broad as can be seen in Figure 6.6.

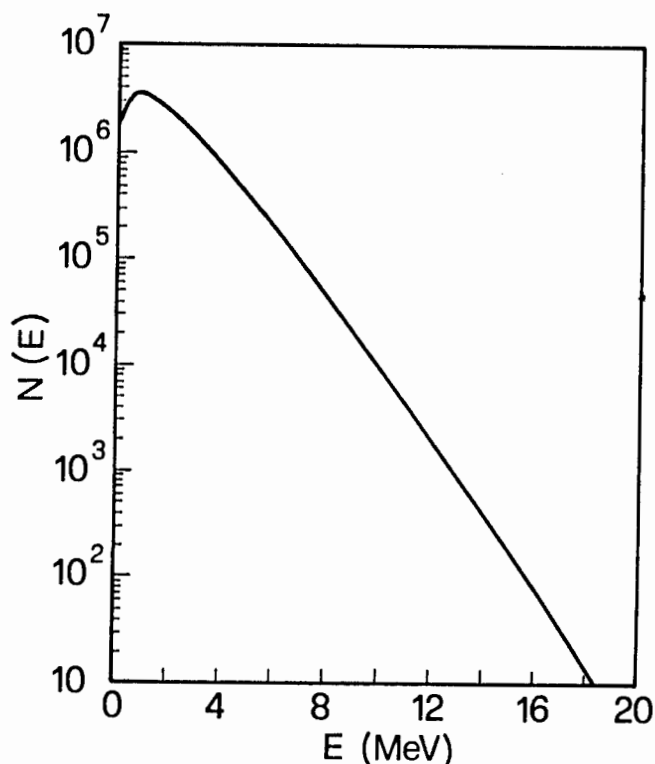


Fig. 6.6. Energy spectrum of fission neutrons. The energies of the prompt neutrons emitted in fission of ^{235}U cover a range of more than 17 MeV: the average value of the neutrons energy is 2.0 MeV.

The fission of ^{235}U is induced by neutrons and the cross section for the process is strongly dependent on the neutron energies: at the thermal energy of 0.025 eV σ is about 580 barns, at 1 eV is about 60 barns and at 10 keV is about 4 barns.

If the fission process has to be self-sustained the energy of the neutrons emitted during the fissioning must be reduced so that part of them can induce with high cross section a new fission event on ^{235}U .

For this purpose "moderators" are used, that is light elements whose nuclei have a mass comparable with that of the neutrons in order to absorb energy in elastic scattering.

A fundamental condition that must be fulfilled by a moderator is that its neutron absorption cross section must be very little. Good moderators are H_2O , D_2O , Be and C and among them H_2O is the most widely used in research reactors because of low cost, optical transparency that allows the direct observation of the reactor core, and efficiency as cooler and as shield.

To improve the efficiency of confinement of the thermalized neutrons into the fissile materials, a graphite "reflector" shield may be used because carbon, with respect to H_2O , has a lower absorption cross section and allows a greater part of the escaping thermal neutrons to be scattered back to the core.

The fuel of a research reactor is constituted by some kg of uranium enriched with about 20% of ^{235}U : the fuel elements are usually in the form of plates or rods. The fuel mass must be supercritical, that is if assembled in compact form must develop a disruptive chain reaction.

To control the reaction rate, a number of movable control rods, made of materials like cadmium, that have a very high neutron absorption cross section, must be interposed among the fuel elements. The greater or lesser insertion of the control rods within the fuel elements allows to modify the power developed into the core and, consequently, the neutron flux.

Essentially one can say that a research nuclear reactor is constituted by a core of fissile material (uranium enriched in ^{235}U) with a series of control rods, the whole immersed into a moderator (H_2O).

The same water may be used as a shield against damaging radiation so that the core for a 250 kw reactor is situated in an underground pool of water, 2 m. in diameter and 6 m. deep.

For activation analysis one would like to have the highest flux of thermal neutrons without contamination of fast neutrons, but this result is impossible to achieve. At the irradiation positions, the thermal neutron flux may be of the order of some $10^{12} \text{ n cm}^{-2} \text{ s}^{-1}$, but the flux of higher energy neutrons is not negligible.

The accurate measurement of the neutron flux and of the neutron energy spectrum is a difficult task: many methods may be useful and, generally, they are based on "threshold" properties, but their routine application is not feasible. During normal operation the use of indirect monitors previously calibrated is preferred.

From the general description of a nuclear reactor one can immediately deduce one of the most interesting advantages of this neutron source for activation analysis: the possibility of contemporary irradiation of many different samples.

In fact, by means of mechanical or pneumatic systems many different

locations of the reactor can be reached by the samples. Sometimes, the locations have different characteristics and, sometimes, with a rotating rack, for example, many samples can receive the same averaged neutron flux.

For very short lived isotopes, the so-called "rabbit", a pneumatic device, allows a very rapid positioning and recovery of samples.

A very brief comment must also be dedicated to the reactor pulsing technique (refs. 5, 6). By pneumatic ejection of a control rod, a research reactor can safely generate high power pulses (some 1000 MW at peak) during short periods (some 10 ms).

For very short lived isotopes this operation is an advantage because in steady conditions saturation activity at normal flux is reached very rapidly, so that the total number of neutrons that can contribute to the activity is relatively limited. If a larger number of neutrons can be injected onto the sample in a short burst, they all contribute to activation and a net gain in activation of the sample is attained.

6.5.2 Cyclotrons as charged particle sources

Charged particles, in comparison with neutrons, need a much higher energy to induce nuclear reactions because of the Coulomb repulsion between nuclei: protons, for example, need an average energy of some MeV to have significant interactions with medium mass nuclei.

For activation analysis the best suitable machine for light ions acceleration is the cyclotron.

This is essentially constituted by an electro-magnet that generates a cylindrical symmetric magnetic field in the volume where a vacuum box contains the central injector and the accelerating electrodes.

The accelerating electrodes called "dees" are connected to a radio frequency generator so that an alternative electric field is established in the narrow gap between the dees (see Fig. 6.7).

A positive charged particle of mass m , charge q and velocity v moving in a magnetic field B will follow a circular trajectory determined by the balance between the centrifugal and the Lorentz forces:

$$mv^2/r = qvB \quad (17)$$

The revolution frequency $f = v/2\pi r$ is so

$$f = qB/2\pi m \quad (18)$$

and if the magnetic field is taken constant one sees that f is independent

from velocity and radius.

If the radiofrequency generator works at a frequency f , a particle crossing the electrodes gap when the electric field is directed so to

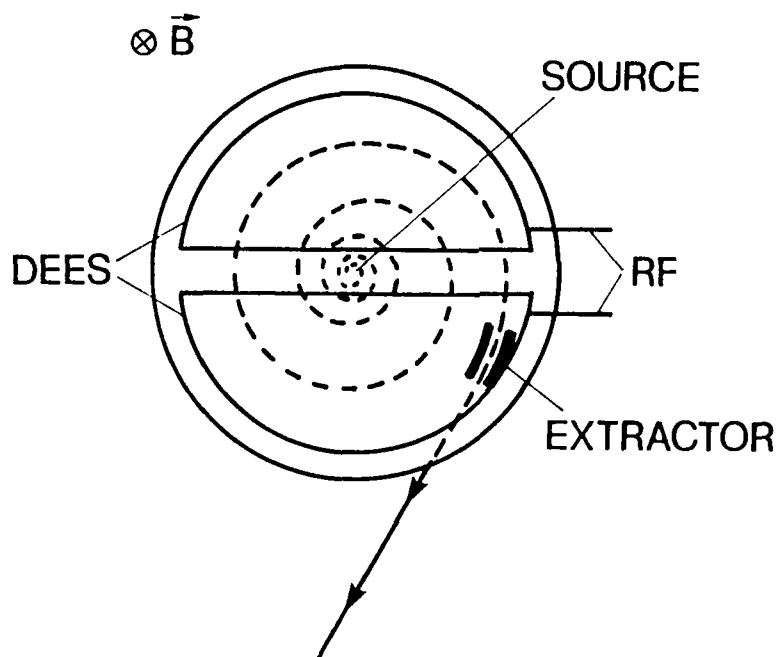


Fig. 6.7. Schematic drawing of a cyclotron: the induction magnetic field B is perpendicular to the foil.

increases the particle velocity will consequently increase the trajectory radius, but will cross the other electrodes gap after a semiperiod when in the gap the reversed electric field will again accelerate the charged particle.

At each crossing the particle will therefore raise its energy and its trajectory radius starting from the central source up to a point where a strong electric field ("extractor") is applied to guide the particle outside.

The modern compact cyclotrons have many features that make them very different from the above simplified description, but the general physical principle of "isochronism" is maintained.

One must observe that the particles accelerated in a cyclotron are not emitted isotropically but are concentrated in a beam whose cross section has an area of the order of about 1 cm^2 . So, instead of using the flux to define the capability of irradiation, one prefers to use the "beam current", that is the total particle charge that each second flows through a section of the

beam.

For activation analysis is good to have different particles to induce specific reactions, and modern commercial cyclotrons accelerate protons, deuterons, alphas and ^3He at variable energies.

Reasonable maximum values for energies are about 40 MeV for protons and alphas, about 20 MeV for deuterons and about 50 MeV for ^3He .

The beam currents obtainable are of the order of 50-100 μA . For comparison, a beam current of 50 μA of protons over a 1 cm^2 area corresponds to a flux of about 3×10^{14} protons $\text{cm}^{-2}\text{s}^{-1}$.

6.6 DETECTORS

The decay spectra registered nowadays for activation analysis are almost only spectra of γ radiation.

The most suitable detector of γ rays is the semiconductor Ge crystal: it consists of a high purity Ge monocrystal through which a strong electric field is applied at liquid nitrogen temperature.

The electron-hole pairs produced during the interaction of the γ rays rapidly migrate to the electrodes giving rise to a current pulse proportional to the number of charges collected.

As in the average 3 eV are necessary to create an electron-hole pair in Ge, a large number of charges is generated during the interactions of γ rays. The statistical fluctuations in the output pulses are so reduced and the energy resolution of the detector is greatly increased in comparison, for example, with a NaI scintillator detector that needs about 300 eV to produce one photoelectron.

The geometrical shapes of the detectors are essentially:

- a) planar
- b) coaxial
- c) well-shaped

The planar type has a very good resolution but a poor efficiency, especially for energies greater than 200-300 keV.

The coaxial one may be grown in greater volume and so the efficiency is sufficient also at some MeV energies but the resolution is a little degraded.

The well type is particularly apt to activation analysis because it allows to position active samples in the inner part of the detector, so increasing the solid angle.

To exploit the characteristics of a Ge detector one must associate very high standard electronics.

The preamplifier is usually supplied with the detector, the amplifier

must be of research type with the possibility to adjust gain, shaping time, pole zero cancellation, DC level, and pile-up rejection.

The HV bias supply must be highly stabilized in order to avoid long term fluctuations and ripple.

Also the analog to digital converter (ADC) must be a high class one because a high resolution spectrum is needed on a wide energy range, and this implies a conversion of 1-2 mV/channel for at least 4 K channels.

The ADC output is sent to a Multi Channel Analyser (MCA) that will increment by one the channel corresponding to the input: in this way, the energy spectrum is constructed and is usually shown onto a display.

The MCA must have at least 4096 channels to fulfil the requirements of dynamic range and resolution used in activation analysis; moreover, many features are very useful: memory splitting, coupled timer, dead time correction etc. Many modern MCA are coupled to microprocessors that allows a pre-analysis also on line.

As spectra are often collected during very long times (some days), particular attention must be devoted to the overall stability of the system, especially with regard to temperature effects.

To understand some of the problems that will be discussed later, it is necessary to know the microscopic interaction mechanisms of γ rays with matter.

Three mechanisms are dominant:

a) photoelectric effect

The γ ray interacts with one of the innermost electrons of the Ge atom disappearing and transferring all the energy to the electron that is ejected with an energy

$$1/2 mv^2 = E_\gamma - B \quad (19)$$

where B is the binding energy of the electron.

The cross section for photoelectric effect in Ge is shown in Figure 6.8.

b) Compton effect

The γ ray interacts with an electron whose binding energy is negligible in comparison with the energy E_γ . The incoming photon is deflected losing part of its energy and the electron is ejected.

The wavelength λ' of the deflected photon is increased of the quantity:

$$\Delta \lambda = \lambda' - \lambda = h/mc (1 - \cos \theta) \quad (20)$$

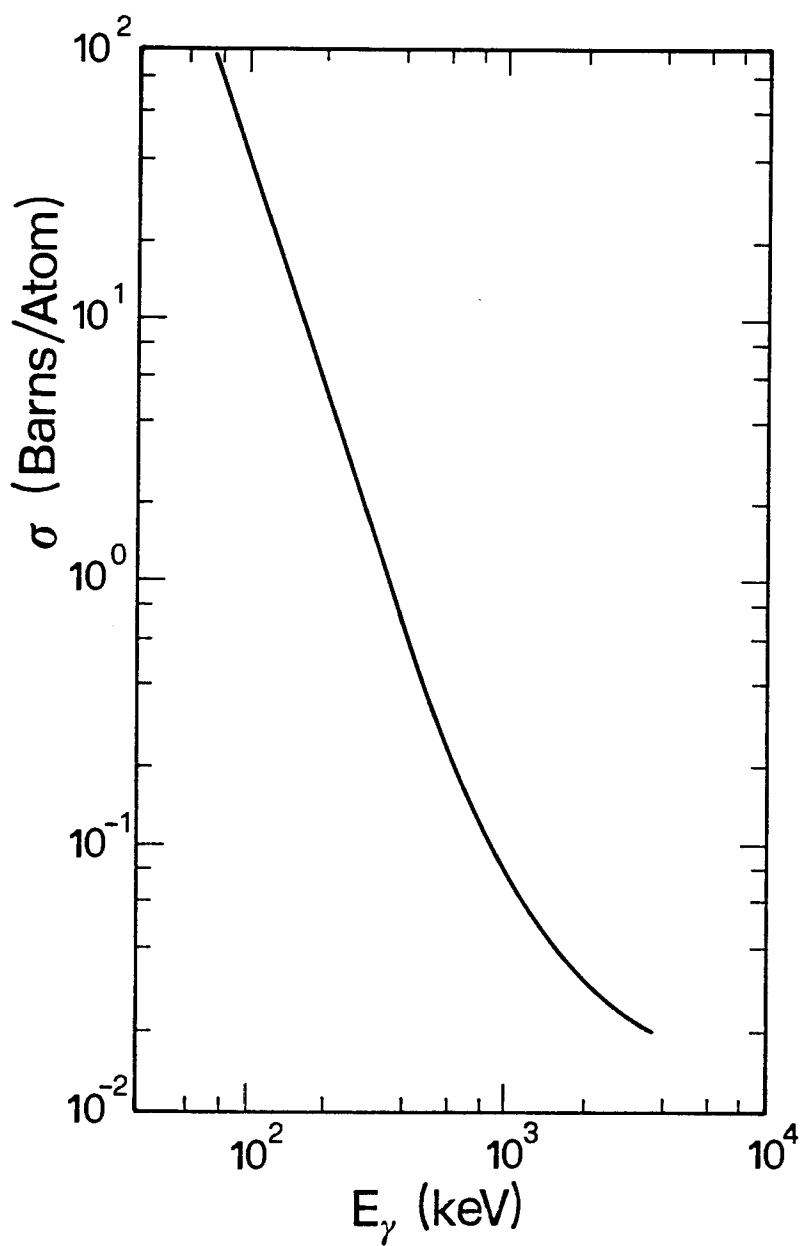


Fig. 6.8. Cross section for photoelectric effect in germanium. This effect is dominant for γ energies below 150 keV.

depending on the γ -ray deflection angle θ . The kinetic energy of the outgoing electron is

$$\frac{1}{2} m v^2 = h\nu - h\nu' \quad (21)$$

The cross section for Compton effect in Ge is shown in Figure 6.9.

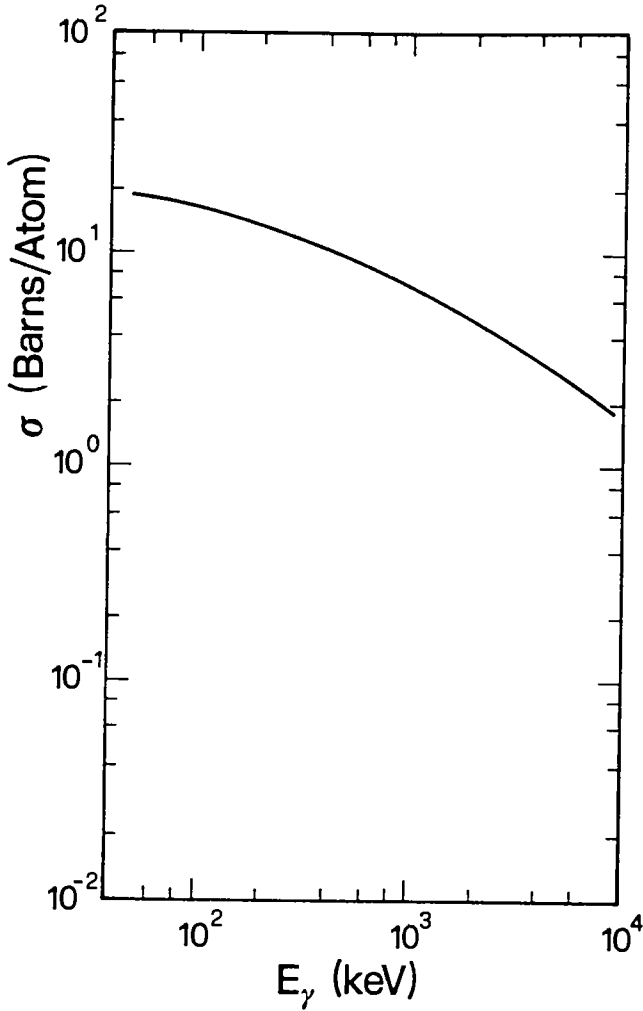


Fig. 6.9. Cross section for Compton effect in germanium. This effect is dominant for γ energies between 150 keV and 7 MeV.

c) Pair production

If the γ ray has an energy greater than 1.022 MeV, the interaction with a nucleus may transform its energy into mass with the creation of an electron-positron pair.

After slowing down, the positron, interacting with another electron, annihilates with the emission in opposite directions of two 511 keV photons.

The cross section for pair production in Ge is shown in Figure 6.10.

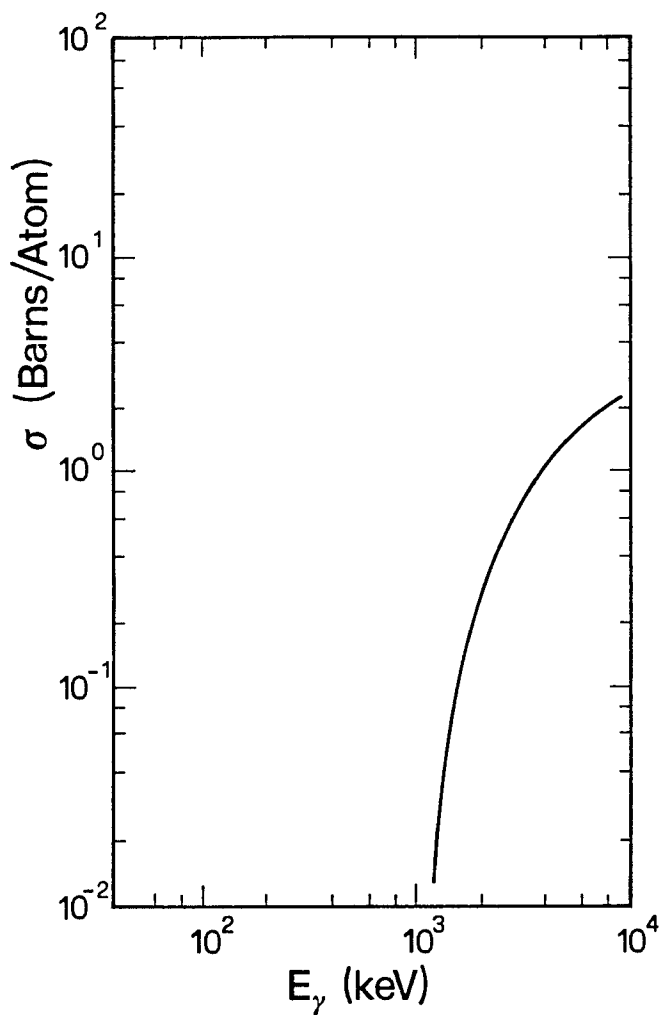


Fig. 6.10. Cross section for pair production in germanium. This effect is dominant for γ energies above 7 MeV.

Charged particles loose their energy by ionization in a very short path in comparison with electromagnetic radiation, so that only in photoelectric effect can one say that all the incoming γ ray energy is used for ionizing Ge.

In Compton and pair production events only part of the incoming energy is used for Ge ionization: the remaining part is associated with new γ radiation that has a large probability to escape from the detector.

The above discussion explains the shape of the response of a Ge detector when exposed to a monochromatic γ radiation beam (see Fig. 6.11).

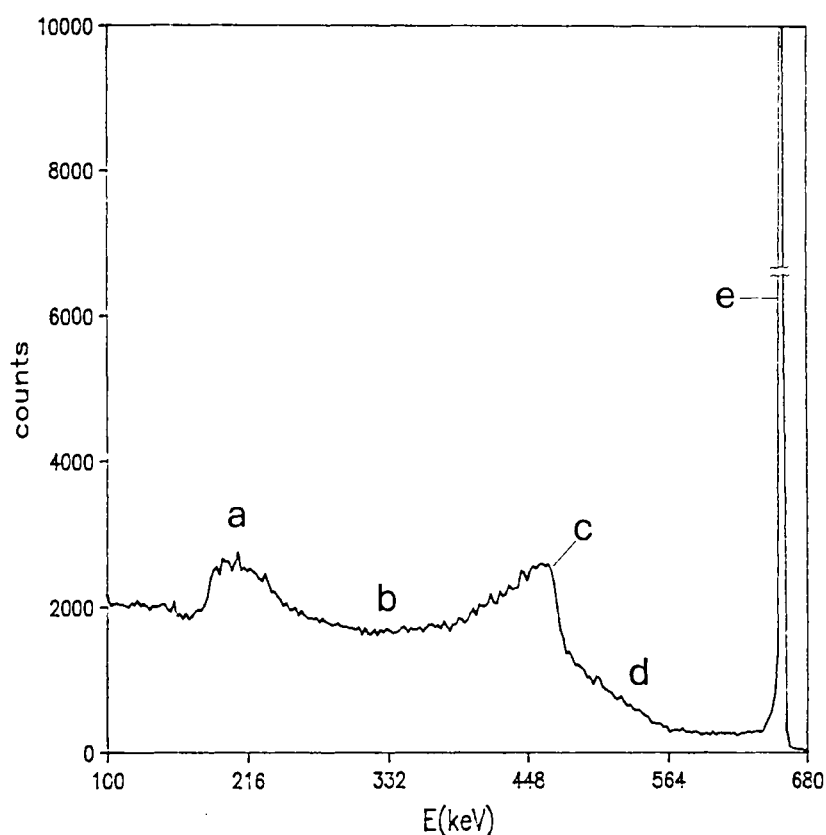


Fig. 6.11. Typical response function of a Ge detector to a monochromatic radiation. a) is the backscattering contribution due to the materials surrounding the crystal; b) is the Compton contribution; c) is the Compton edge corresponding to the maximum energy transfer to an electron in a single event; d) is the contribution from multiple Compton events; e) is the photoelectric (or full energy) contribution.

This point is important in activation analysis because it is the main contribution to the background in γ spectra collected from the samples.

For a correct analysis of the γ spectra one must know for each detector the energy calibration, the energy resolution and the relative efficiency. All these data can be acquired using, for example, a standard ^{152}Eu source: in fact, one knows with great precision the energies and the intensities of the transitions produced in this source (ref. 2).

The energy calibration is nearly linear, but a slight contribution of a higher order terms allows a better determination of the relation channel-energy that defines the energy of the peaks within about 0.1 keV.

The resolution R may be measured as FWHM of different peaks: there is a small dependence from energy E that may be parametrized as:

$$R = k_1\sqrt{E} + k_2 \quad (22)$$

The relative photopeaks efficiency may be obtained by comparison between the peak areas and the relative intensities reported in ref. 2. A log-log plot shows for a wide energy range a nearly linear shape (see Fig. 6.12) of relative efficiency.

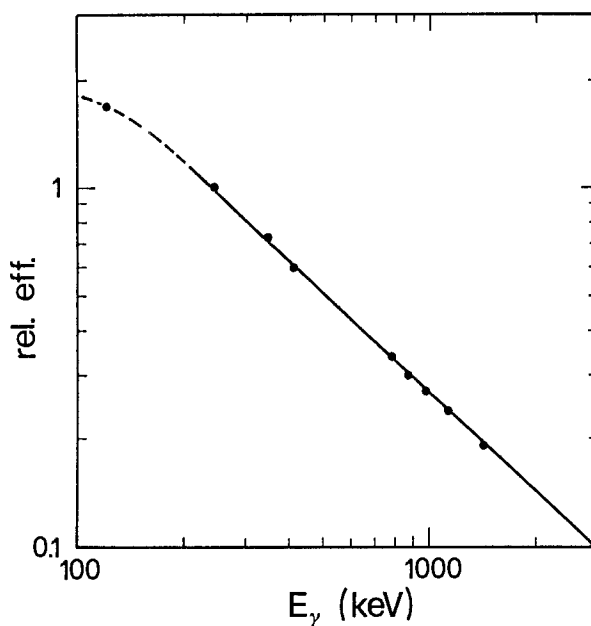


Fig. 6.12. Relative efficiency of a Ge detector. The experimental points were obtained with a ^{152}Eu source. The intensity of the 244.7 keV transition was used as normalised unit value.

6.7 DATA ANALYSIS

Usually the data collected with a MCA are registered on a permanent or semipermanent support (magnetic tape, floppy disk etc.) so that a careful analysis may be performed off-line. The aim of the analysis is to determine with the greatest possible precision the position and the area of the interesting peaks.

Two main philosophies may be followed: one can assume that the peaks have a definite geometrical shape (for example gaussian), or, on the contrary, one may disregard completely the shape of the peaks.

The former assumption is useful when the number of channels involved in one peak is greater than 15-20 in order to allow a significant best fitting procedure.

If the γ transition is a weak one, it is worth to compact the spectrum into a smaller number of channels in order to put in evidence the peak over the statistical fluctuations. In this case the best fitting procedure is therefore a nonsense.

To evaluate the peak position, in one case the gaussian center, in the other case the center of mass of the channels involved are assumed.

Preliminary to the position determination is an estimate of the peak width. In fact, if an interference peak is so near the one of interest that cannot be resolved, the overall effect will be a deformation of the peak associated with an incorrect position and area determination.

To check this possibility, a comparison between the peak width and the detector resolution at the same energy must be performed: if there is a significant difference, the hypothesis of an interference must be carefully considered.

In many cases, the best fitting procedure allows to disentangle a multiplet of peaks but the results must be examined with great attention.

One of the most delicate problems in spectra analysis is the background subtraction. There are two kinds of background important for our purposes: the so-called natural background and the Compton background.

The first one is due to the radiation emitted by the natural radioactive elements present in the materials surrounding the detector: air, walls, shields, the germanium itself, etc. and by cosmic rays.

Its contribution is not very great, a part the case of very long measures, and it may be easily subtracted from the useful spectra. In fact, in a fixed geometry, this background is constant in time and it is possible to measure it, removing all the artificial sources and samples from the detector.

The Compton background is one of the factors limiting the sensitivity of activation analysis. In fact, taking into consideration the Ge response

function of Figure 6.11, one can deduce that at each energy there is a contribution of Compton scattering from all the γ rays at greater energy.

The contribution is additive and especially at the lowest energies may reach very high values (see Fig. 6.13) that may conceal some important little peak.

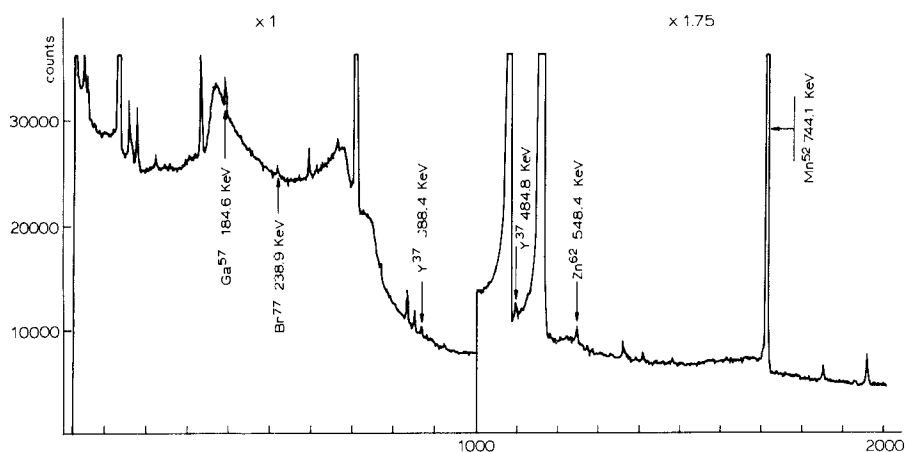


Fig. 6.13. A γ spectrum obtained with a Ge detector. The high background essentially due to Compton contribution prevents to determine with good precision the peak areas, in particular for 184.6 and 238.9 keV transitions.

Compton background can be reduced either electronically with active shields, or by means of radiochemistry.

In any case when one has to evaluate a peak area there is always to subtract some background whose shape is not known "a priori".

As a first approach a linear shape below the peak is acceptable, but the choice of the extreme points of the segment is very questionable. Usually, to smooth statistical fluctuations, one chooses some points besides the peak and considers the average values as extreme points for background subtraction. If on one side of the peak there is a perturbation, this procedure may introduce significant errors as shown in Figure 6.14.

The random character of the decay process introduces errors in the evaluation of the related quantities. Usually, these statistical errors give the largest contribution to the total non systematic error in a measurement so

that often only these are reported.

To evaluate statistical errors Poisson's statistics are needed and if an event like a peak area is represented by a number N of counts, its statistical estimated error is given by $\sigma = \sqrt{N}$.

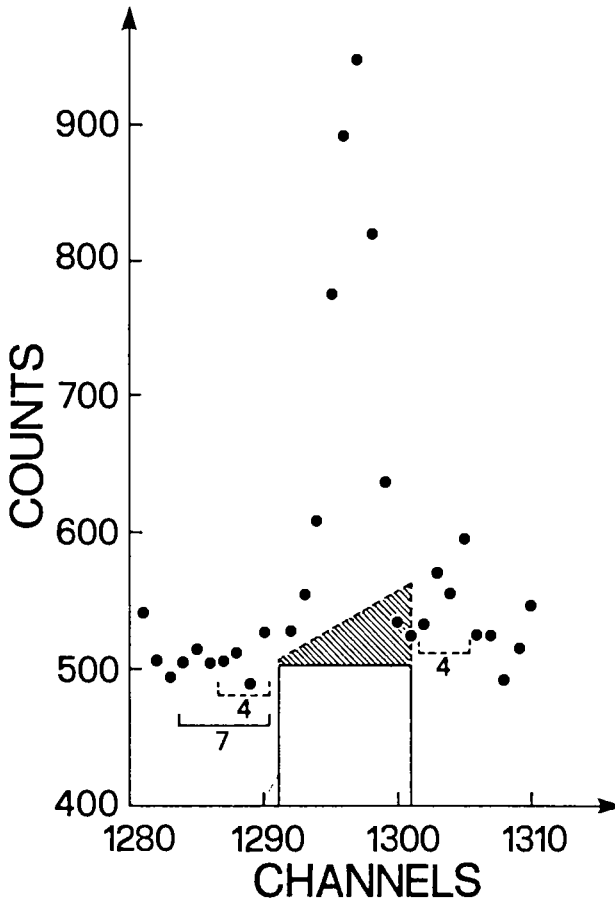


Fig. 6.14. Example of background subtraction. The dotted line is the estimated background considering for its calculation the average content of 4 channels on both sides of the peak. The continuous line is the estimated constant background considering for its calculation only the average value of 7 channels on the left side of the peak. The shadowed area indicates the difference between the two estimations.

One deduces that if an accuracy of 10% is wanted it is sufficient to have $N = 100$, but if an accuracy of 1% is wanted, N must rise to a value of 10.000.

The background too has a statistical error, and the total error in the peak area determination is given by the square sum law: for this reason a high background may deteriorate the quality of a measurement.

Nowadays many software programs have been developed for automatic analysis of spectra: there are refined algorithms to recognize peaks, to determine their corresponding energies, to evaluate their areas with associated statistical errors, to individuate the radioactive isotopes from which are generated and so on.

In my opinion, these automatic procedures are very useful and time saving, but I think that, especially for crucial points, the analyst has to work, step by step, with a continuous control of the situation and with a global sight of the problem.

6.8 ABSOLUTE MEASUREMENTS AND COMPARATORS

To obtain the absolute value of the amount of the trace element x contained in the sample, the number I'_x of the decays registered by the detector for a chosen transition of the corresponding radioactive nucleus must be measured.

This number is expressed by the relation (16) multiplied by the mass m of the sought element: four quantities are usually known with inadequate accuracy: the efficiency ϵ of the detector for the particular γ ray energy, the solid angle Ω subtended by the detector, the cross section σ_x for the induced nuclear reaction, the flux φ of incident particles.

To overcome this difficulty an internal or external reference method may be used.

If the biological sample to be analysed is doped with a suitable known amount M_{ref} of an external reference element, the spectrum collected is like that shown in Figure 6.15a where ref and x indicate the γ lines coming from the reference element and from the element of interest respectively.

The ratio R between the measured intensities I'_x and I'_{ref} of these lines is proportional to the ratio of the contents of the two elements

$$R = I'_x / I'_{\text{ref}} = k m_x / M_{\text{ref}} \quad (23)$$

where k is a quantity independent of φ and Ω as can be seen from Equation (16).

To determine the value of k , a standard sample of the same biological material doped with the same amount M_{ref} of the reference element and with an accurately measured quantity M_x of the element under study, large with

respect to its natural content, is prepared.

The spectrum collected from the standard sample is like that of Figure 6.15b. A relation analogous to Equation (23) between the contents M_x and M_{ref} and the ratio R_s of the measured intensities of the γ lines can be written

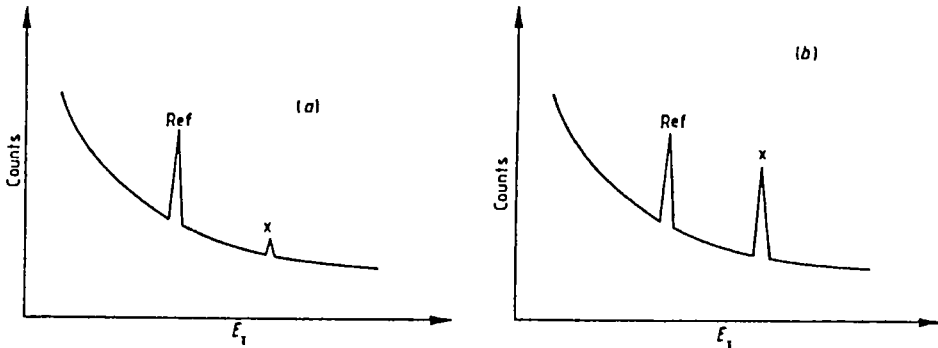


Fig. 6.15. Schematic representation of the γ spectra: a) of the sample with an unknown amount m_x of the searched element and with a quantity M_{ref} of the reference element; b) of the standard with a known amount M_x of the searched element and with a quantity M_{ref} of the reference element.

$$R_s = k' M_x / M_{ref} \quad (24)$$

If t_i , t_w , and t_m are the same for the standard sample and for the sample to be analysed and if the detector is the same then $k = k'$.

In any case, if the characteristic times are different, the equivalence $k = k'$ is obtainable by simple normalization of the intensities of the γ lines to the same values of t_i , t_w and t_m through Equation (16).

From Equations (23) and (24) one obtains

$$m_x = (R/R_s) M_x. \quad (25)$$

It is therefore possible to evaluate the quantitative amount of the trace element from the measurement of the ratios R and R_s independently of the knowledge of the above mentioned parameters: ϵ , Ω , σ and φ .

If, as it is the case of a rotating multi sample rack, one can assume that for two different samples the flux φ is the same, a simplified and more

clean procedure can be followed provided the geometry of measurement of the two samples is exactly the same: the above assumption implies that ϵ and Ω are also identical for the two samples.

One can then get rid of the reference element; it is sufficient to have a comparator, that is a sample doped with a known amount M_x of the isotope of interest.

The ratio of the intensities of the corresponding lines obtained from the two samples is equal to the ratio of the corresponding masses: as one mass (M_x) is known, the unknown mass m_x may be immediately determined. In the choice of the reference element one has to observe that its introduction into the sample may be the cause of contaminations and may significantly increase the background because of Compton scattering contribution.

6.9 MAJOR PARAMETERS AFFECTING SENSITIVITY

Sensitivity may be defined as the capability of an instrument or a methodology to discern small variations of the quantity under measurement.

In spectral analysis this is equivalent to say that sensitivity is an index of the capability to measure a peak area with a given precision. Obviously, the background plays a fundamental role in the definition of sensitivity because of its contribution to the total error in the peak measurement.

Strictly bound to this subject is the definition of detection limit: usually, in a somewhat arbitrary manner, this quantity is defined as the amount of a given isotope in a given matrix or tissue that gives a peak whose height is 3 times the square root of the average background, that is 3 times the statistical error of the background.

It is worth noting that the detection limit is significant only if the matrix is specified because of its contribution to the background.

Many parameters affect sensitivity and in the following a brief discussion will be made about the most important.

a) Mean life of the produced radioisotope

A relatively short value of τ implies an easily reached saturation, a high activity of the isotope of interest and this means a high flux of useful γ rays.

In contrast with this positive point, one must observe that a small τ implies also a short cooling time t_w that brings to a high background.

A compromise must be made in the t_w choice in order to decrease the background at the expense of the useful γ rays intensity until the best signal to noise ratio is reached.

The waiting time problem is not so pressing if τ is very long, but in this case the intrinsic activity does not reach saturation and the associated γ rays flux is very low.

From the sensitivity point of view, the best results may be obtained with values far from the extremes.

b) Cross section σ

The cross section for the production of the radioisotope of interest is a fundamental quantity in the definition of sensitivity.

If all the other parameters are taken equal or at least similar, the relevant peak area is proportional to σ .

As the precision in the peak area determination is associated with the square root of the area itself, the sensitivity may be considered proportional to the square root of σ .

c) Isotopic abundance

The above argument is valid also for the abundance of the isotope of interest because what is seen in activation analysis is the amount of a given isotope, but what one is really interested in is the amount of the chemical element, independently of its isotopic composition.

d) Branching of the decay

Same argument as above but turned to the decay scheme.

e) Detector efficiency

The total efficiency of a detector may vary over a wide range depending upon the crystal volume and the geometry.

The peak area is proportional to the total efficiency, provided the other conditions stay constant: the larger is the total efficiency, the larger is the number of counts in the peak and the smaller the relative error in the peak area evaluation.

Moreover if the efficiency is high, the probability of escape for Compton scattered γ 's is low and this means that the total energy peak to Compton ratio is high. This implies a relative reduction of the background with respect to the peak area with an increase in the precision of the measurement.

As sensitivity is associated with precision in the measurement, it follows that sensitivity increases with detector efficiency.

f) Energy of the γ -ray

If E_γ is very near the energy of a transition coming from another

isotope, the resolution of the detector may not be sufficient to separate the two peaks so decreasing the precision of the peak area evaluation: as a consequence the sensitivity decreases too.

A second point to be emphasized is associated with the detector relative efficiency. As shown in Figure 6.12 the relative efficiency is rapidly decreasing with energy: under the same other conditions a peak at low energy has an area much larger than a peak at high energy, so that the measurement precision decreases with energy and the sensitivity too (if the background does not play a major role).

6.10 PRECISION AND ACCURACY

Accuracy refers to the closeness of the measurements to the "actual" value or the "real" value of the quantity of interest, whereas the term precision is used to indicate the closeness with which the measurements agree with one another quite independently of any systematic error involved (ref. 11). In trace elements determination in biological materials the difference between precision and accuracy may be quite significant.

Actually it is not rare the case in which many measurements, repeated on a series of samples of identical material agree within some percent, but some unknown systematic error, intrinsically bound to the methodology, may not be a priori excluded.

For example the analysis performed by Kosta (ref. 12) on the correlations existing between the mean values of some trace elements in reference materials and the employed analytical techniques is very significant.

In sea plant homogenate SP-M-1 cobalt, determined by neutron activation in many different laboratories, has a mean concentration of 220 mg/kg, but when determined by atomic absorption spectroscopy has a mean concentration of 39 mg/kg.

It is realistic to think that one of the techniques has an unrevealed systematic error so that also if the precision of the measurements may be very good, nevertheless the accuracy is poor.

6.11 SAMPLING

A very delicate step in biological material trace element analysis is the collection, transport and storage of samples.

The sample to be analyzed must be representative of the tissue from which it has been extracted (ref. 13): for urine, for example, one must collect the 24 hours excretion, mix and homogenize, and only then draw out the sample to

be measured (ref. 14).

Contamination problems may arise already at the collection moment; environment may contribute with dust and volatile components in air: personnel (ref. 15) with sweat, cosmetics, tobacco etc: instruments (ref. 16) with abrasions.

One must be very careful when operating for sampling and in particular only non contaminant (or little contaminant) instruments like titanium or quartz scalpels can be utilized.

All the containers have preferably to be made of teflon or high purity polyethylene (ref. 15): for instance blood withdrawn must be done by means of teflon catheters instead of metallic needles.

Transport too may give some problem: for example powdered samples with vibrations may distribute with a density gradient, so loosing homogeneity.

Two main problems must be faced during biological sample storage: first, how to preserve the material from degeneration that might produce modifications in elemental composition (e.g. fermentation, oxidation, microbial attacks etc.), second, how to reduce the contamination from containers, especially for long term storage. Usually a convenient mode of preservation of biological material is provided by freeze drying: the maximum storage time depends on the tissue, but with temperature $< -15^{\circ}\text{C}$ the preservation may be quite long.

Teflon and polyethylene containers are normally used for long term storage: moreover, to reduce contamination from the container surface, samples must be stored in the most compact form in order to minimize the surface over volume ratio.

6.12 RADIOCHEMISTRY

The radiochemistry field is very wide and specific so that only a general outline will be given in this section.

The main purpose of radiochemistry is to separate, by chemical methods, one radioisotope (or a group of radioisotopes) from the irradiated samples: in this way a drastic reduction of the background can be obtained and one can reach an increase of sensitivity which is, in some cases, of some orders of magnitude. The main advantage of post irradiation chemistry is that contamination problems are dropped off because all the instruments (reagents, vessels, etc.) are not radioactive, in contrast with the object of the analysis that is determined by means of its radioactivity.

Many and specific processes have been developed to separate the elements of interest, but here only the general procedure will be discussed. The first

step is generally the dissolution of the irradiated sample: this can be done, for example, with a mixture of sulphuric and nitric acid paying attention not to loose some sought element if it is volatile like iodine.

In some cases, one has to add some "carrier": this term indicates a small amount, of the order of some milligram, of the same element of the radioisotope of interest.

The purpose of this addition is to bring the concentration of the chemical element corresponding to the radioisotope produced by means of nuclear activation to a level where the chemical behaviour is more stable and absorption problems may be disregarded because of the negligible percentage of the radioactive isotope in comparison with the stable element. A first separation may be done by distillation of the dissolved sample: the subsequent separation techniques may be precipitation, ion-exchange chromatography, solvent extraction etc.

At the end a solution is usually obtained in which nearly all the radioisotopes of interest are concentrated, and nearly all the other radioactive elements are left out.

Two main problems are connected to radiochemistry: the reproducibility of the procedures and the time necessary to operate. The first point may be controlled preliminarily by adding to some blank samples a large amount of the radioisotope of interest as tracer and checking by means of a γ detector the losses occurring at the different steps of the procedure. By operating with good laboratory practice the losses can be reduced to some percent: moreover, repeating the check for different samples, one can make sure of the repetibility of the results, so that if the losses are known with sufficient precision, the final estimation of the radioactivity of the sample may be done with good accuracy.

The time necessary to operate has influence on the applicability of radiochemistry whether the mean life of the radioisotope of interest is too short or the manpower necessary for the treatment is too high.

6.13 APPLICATIONS OF ACTIVATION ANALYSIS TO BIOMEDICAL SAMPLES

The role of trace elements in living systems is not yet well understood and in particular the study of their behaviour in human metabolism is only a commencement.

A lot of works is in progress on this subject, but more must be done in future.

One of the main difficulties that arises in the measurement of trace elements in living tissues is the presence of a large quantity of interfering

elements that decreases the specific sensitivity. Actually the bulk of living matter is constituted by H, C, N, O, Na, Mg, P, S, Cl, K, Ca and the trace elements considered essential for warmblooded animals are F, Si, V, Cr, Mn, Fe, Co, Ni, Cu, Zn, As, Se, Mo, Sn and I.

Moreover, there are contaminant elements depending on the environment, like Cd and Pb.

At the moment very little is known about the detailed metabolism of trace elements: only for few metals the biochemical and physiopathological behaviour is partially understood. For the most part of the essential trace elements the only quantitative data collected regards the percentage amount in different tissues (blood, urine, muscle, bone, etc.).

Also at this level there are problems in defining the "normal" ranges of variability of trace elements and the eventual correlations with pathological states.

6.13.1 Neutron activation analysis (NAA)

a) Cross sections

In Table 6.3 the radioactive capture cross sections for neutrons on different elements are listed. One can observe a large variability of values that is related to a wide range in neutron activation specific sensitivity.

b) Sample preparation

A part the general precautions (see par. 6.11) one must take in order to avoid contamination before irradiation, some particular care is necessary in treating biological samples. Usually polyethylene vials are used as containers for the irradiation process and they are normally sealed to prevent reactor contamination by leakage of the sample.

If the neutron flux is high some problems may arise from the heating and the radiation decomposition due to capture recoils, fast neutron collisions and γ rays radiolysis: in particular there may be a release of gases especially from liquid samples. In these cases it is advisable to use quartz vials and preferably to dry the samples before irradiation.

If the neutron flux is very high the decomposition of organic matter must be expected and is hence useful to ash the sample before irradiation: in this case, however, the risks of volatilization must be taken in due consideration.

c) Irradiation and measurement

The choice of the irradiation technique is strictly bound to the physical properties of the trace elements of interest. If short lived isotopes are measured, a fast loading system (rabbit) is necessary. Automatic and precise

TABLE 6.3
Thermal neutrons cross sections.

Element	Isotopic Abundance	Cross Section (barn)
^1H	99.985	0.33
^6Li	7.5	950
^9Be	100	0.01
^{10}B	18.8	4020
^{12}C	98.89	0.0032
^{14}N	99.63	1.8
^{17}O	0.037	0.5
^{19}F	100	0.009
^{23}Na	100	0.53
^{25}Mg	10.1	0.27
^{27}Al	100	0.23
^{28}Si	92.17	0.1
^{31}P	100	0.2
^{36}S	0.017	0.14
^{35}Cl	75.53	44
^{39}K	93.2	1.9
^{42}Ca	0.64	40
^{45}Sc	100	23
^{48}Ti	73.8	7.8
^{51}V	99.75	4.5
^{53}Cr	9.5	18
^{55}Mn	100	13.3
^{54}Fe	5.9	2.2
^{59}Co	100	37
^{58}Ni	68	4.3
^{63}Cu	69	4.4
^{64}Zn	48.9	0.5
^{71}Ga	39.9	4.6
^{73}Ge	7.8	14
^{75}As	100	4.3
^{76}Se	9.1	85
^{79}Br	50.6	2.9
^{85}Rb	72.2	0.85
^{86}Sr	9.8	1.3
^{89}Y	100	1.3
^{91}Zr	11.2	1

⁹³ Nb	100	1
⁹⁵ Mo	15.7	14
¹⁰² Ru	31.5	1.2
¹⁰³ Rh	100	150
¹⁰⁸ Pd	26.7	11
¹⁰⁹ Ag	48.6	84
¹¹³ Cd	12.3	27000
¹¹⁵ In	95.8	197
¹¹² Sn	1.02	1.3
¹²¹ Sb	57	7
¹²³ Te	0.88	400
¹²⁷ I	100	6.3
¹³³ Cs	100	31
¹³⁸ Ba	71.7	0.55
¹³⁹ La	99.91	8.9
¹⁴⁰ Ce	88.47	0.6
¹⁴¹ Pr	100	11
¹⁴³ Nd	12.2	320
¹⁴⁹ Sm	13.8	66000
¹⁵¹ Eu	47.8	8600
¹⁵⁷ Gd	15.7	180000
¹⁵⁹ Tb	100	45
¹⁶⁴ Dy	28.2	2700
¹⁶⁵ Ho	100	64
¹⁷⁰ Er	14.9	9
¹⁶⁹ Tm	100	125
¹⁶⁸ Yb	0.14	11000
¹⁷⁶ Lu	2.6	3200
¹⁷⁷ Hf	18.5	370
¹⁸¹ Ta	99.99	22
¹⁸⁶ W	28.7	36
¹⁸⁵ Re	37.1	105
¹⁹⁰ Os	26.4	8
¹⁹¹ Ir	38.5	1000
¹⁹⁵ Pt	33.7	27
¹⁹⁷ Au	100	98
¹⁹⁹ Hg	16.9	2000
²⁰³ Tl	29.5	11
²⁰⁷ Pb	21	0.73
²⁰⁹ Bi	100	0.033

^{232}Th	100	7.5
^{238}U	99.27	2.8

clock signals must allow an accurate measure of irradiation and post-irradiation times. A rabbit device usually does not allow the irradiation of more than one sample at a time, and this set some difficulty for example when a comparator must be irradiated at exactly the same neutron flux. If the mean lives of the isotopes of interest are longer, the loading times does not become an important factor and the use of a rotating rack allows a multisample irradiation with identical geometries and fluxes.

Another opportunity is the use of filters (ref. 17) to absorb thermal neutrons so that epithermal neutrons dominate in the flux impinging onto the samples. Cadmium and boron are normally used as filter materials because of their large absorption cross section for thermal neutrons. The advantage of the filtering technique is based on the fact that some elements like, for example, Br, Ag, Mn have some isotopes that show large cross section resonances in the region of epithermal energies: many of the biological matrices constituents do not have such property and as a final result there is a relative activation enhancement of some selected elements.

The measurement of the γ spectra is also bound to the mean life of the isotope of interest. If τ is short, it is not possible to have an adequate interval between irradiation and measurement and this implies a high contribution to the background from the short lived isotopes of the biological matrices. Moreover, in such cases also a radichemical treatment is very difficult due to the fast decay of the measured isotopes.

Another problem that may involve the γ spectra detection is the activation of the sample container.

If very high purity polyethylene is used for irradiated vials, the contribution to the background is very limited because of the very short mean life of the radioactivity deriving from the basic constituents of the plastic material; therefore it is possible to collect the spectra without changing the sample container.

If impurities are present in the container, they are activated during irradiation and their contribution to the spectrum can conceal the useful data.

To avoid this problem it is simply necessary to change the sample container before the τ spectrum detection.

d) Controls

To evaluate the reliability of the measurements, many specific controls must be performed: a brief discussion about the most significant checks is given in the following.

The energy spectrum of the neutron flux in a reactor is sufficiently wide to allow different reactions to occur apart from radioactive capture: $(n, 2n)$, (n, p) (n, α) etc. It is so possible that the same radioactive isotope is produced by means of different reactions starting from different parent nuclei. For example if the element of interest is manganese and the detection is accomplished by measuring the decay of ^{56}Mn , one must be very careful to avoid interferences from ^{59}Co (n, α) , ^{56}Mn and $^{56}\text{Fe}(n, p)$ ^{56}Mn reactions: the cross sections for these reactions may be very little in comparison with (n, γ) reactions, but the abundance of the target isotope may be so high to compensate, and the final result may be the complete loss of validity of the measurement.

Another non infrequent interference is due to the accidental near coincidence of the relevant γ rays energies from the decay of the radiosotope of interest and from the deexcitation of some other radioisotope produced in the sample.

A good check to verify the purity of a γ transition, that is the absence of competing transitions at the same energy, is the control of the decay constant. By measuring the sample with fixed geometry at different waiting times, the decrease with time of the intensity of specific γ lines can be followed: the slope of the semilogarithmic plot of the intensity versus time is a measure of the decay constant, and any significant deviation from linearity is a signal of some contribution from γ transitions coming from radioactive nuclei with different mean life (see Fig. 6.16).

e) Some recent results obtained with neutron activation analysis (NAA) in biomedical materials

i) Characterization of macromolecules

Many biologically significant macromolecules have been found to have trace elements essential to their function and structure.

A new type of detection technique for metalloproteins separated by electrophoresis, using a trace element to determine a protein location, has been developed (ref. 18). A group of protein samples (human serum, phosvitin, bovin albumin, carbonic anydrase) has been analysed by means of polyacrylamide gel electrophoresis.

All the reagents were previously analysed in order to control the relevant elements contaminations.

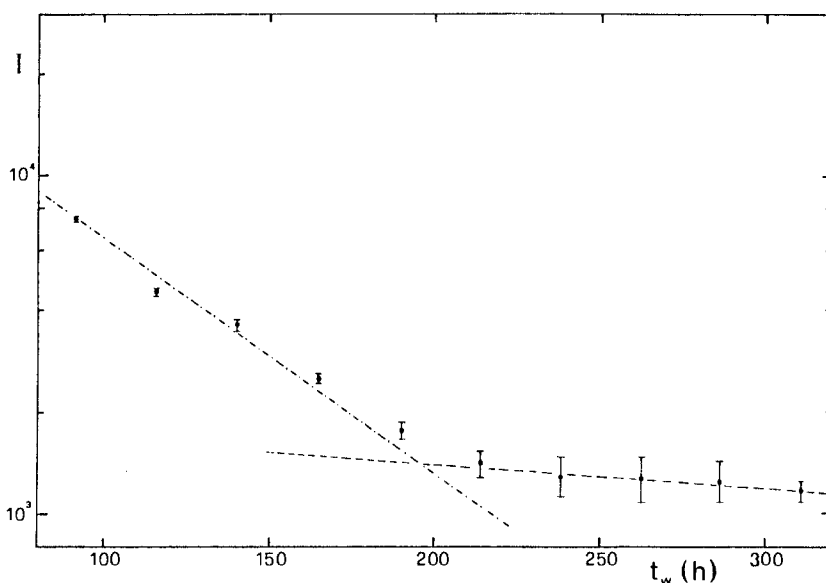


Fig. 6.16. Time decay of the 983.5 keV line. The transition at this energy may originate from two different nuclei, ^{48}V and ^{48}Sc : the former has a half life of 23.04 d and the latter a half life of 2.64 d. From the analysis of the shown time decay one deduces immediately that both nuclei are produced in the reaction and till 200 h the contribution from ^{48}Sc is predominant, beyond 200 h the contribution from ^{48}V is the dominant one. The dotted lines correspond to decays with 2.64 d and 23.04 d half lives.

Gel sections (5 mm by 10 mm) were removed from protein bands and after lyophilisation were irradiated with a flux of the order of $10^{13} \text{ n/cm}^2 \text{ s}$. The zinc content of the samples was then determined and significant elevations of zinc concentrations above the background were detected only for serum, phosphovitin and carbonic anhydrase protein bands. This results is in agreement with the known missing association of zinc with bovine albumin.

Quantitative determinations have not yet been performed, but with increasing knowledge and experience it should become possible to understand the mechanisms of changes in the structure and composition of the molecules during the polyacrylamide gel electrophoresis.

ii) Determination of protein concentration

The quantitative determination of very small amounts of protein is

usually carried out by measuring the intensity of the silver stain induced in the bands produced in polyacrylamide gel electrophoresis.

The mechanism of silver staining is not well understood, yet the intensity of the stain has been used as a measure of the abundance of proteins because it was the only procedure available that could detect such small amounts of protein. A simple check of optical absorbance versus protein concentration shows however the lack of linearity between the two quantities.

A method for the quantitative determination of small amounts of protein samples was developed employing neutron activation analysis (ref. 19).

With a suitable procedure silver-protein complexes were produced in which the metal was proportional to the amount of protein present in each sample.

The determination of silver content by means of instrumental neutron activation analysis (INAA) was performed and by simple calibration it was possible to measure the protein content of the sample.

iii) Interaction of orthopaedic implants with patients organism

Metal implants are widely used in orthopaedic surgery and the impact of corrosion by body fluids was analysed measuring in blood, serum and a variety of tissues the concentration of a critical element like Co (ref. 20).

The concentration of this element in normal persons is very low (of the order of some tenths of ng/g) so that a high sensitivity technique like neutron activation analysis was necessary, with a particular care to avoid external contaminations.

In Figure 6.17 distributions of Co in patients with and without implants are shown.

The mean values are significantly different:

$0,33 \pm 0,16$ ng/ml without implants and $1,13 \pm 0,43$ ng/ml with totalendoprostheses of the hip joint made of Co - Cr alloy.

Another important feature that was determined regards the time dependence of Co concentration in serum: in one patient there was an increase of a factor three during a period of 20 days after implantation.

The data collected for two deceased implant bearers show a significant burdening by Co and Cr for some tissues and organs: the prostheses corrosion is not only an occurrence of local importance. In liver, for example, Co can be found at a level more than 100 times the normal one.

iv) Trace elements in neurological disorders

The importance of lithium in many forms of mental diseases is well known from a long time.

An increasing interest is demanded on the role played by other elements,

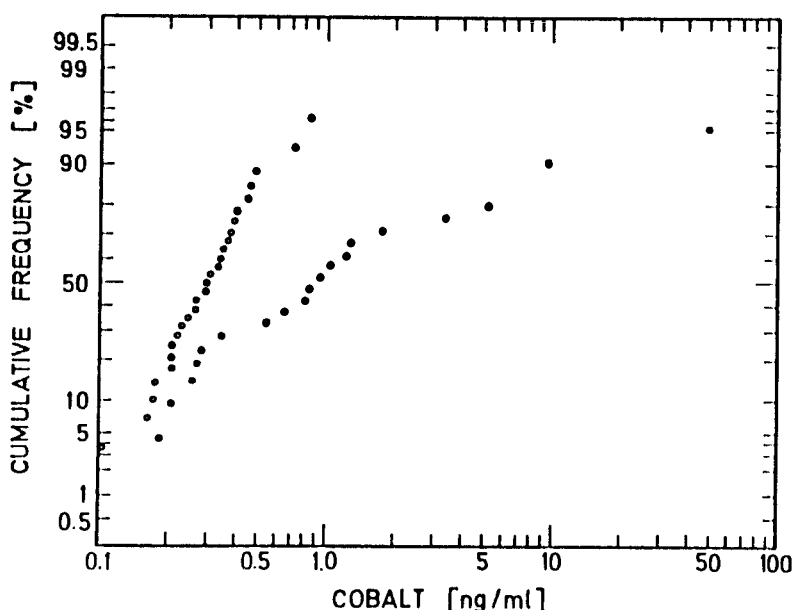


Fig. 6.17. Distribution of Co in serum from patients a) with and b) without implants.

in particular vanadium and aluminium.

The V content in serum of 26 depressive patients was measured (ref. 21) and compared with the results of a healthy control group. The irradiation was performed with a flux of $2 \times 10^{14} \text{ n cm}^{-2} \text{ s}^{-1}$ and the reaction was $^{51}\text{V}(\text{n}, \gamma) ^{52}\text{V}$ giving rise to a radioisotope with a half life of 3.76 minutes decaying with emission of a 1.434 MeV γ ray.

The mean value obtained for the control group was: $0.67 \pm 0.33 \text{ ng/ml}$ without apparent correlation with sex and age. Part of this group was also controlled one year and half later with a result of $0.65 \pm 0.17 \text{ ng/ml}$.

The depressive patients showed a much higher concentration of vanadium in serum ranging from 0.678 to 5.6 ng/ml with a mean value of $2.97 \pm 1.4 \text{ ng/ml}$.

A very significant point is that a group of 12 patients were controlled after 6 months therapy showing a decrease of vanadium concentration in serum from a mean value of $3.37 \pm 1.30 \text{ ng/ml}$ to $0.23 \pm 0.13 \text{ ng/ml}$.

Another very important study (ref. 22) was performed on brain tissue from Alzheimer's disease individuals.

By comparison with the results obtained for the same tissues in a control

group a significant difference in concentration of different elements was detected.

In particular for Al and V the data obtained (in ng/g) were:

	<u>Alzheimer disease</u>		<u>Controls</u>	
	Hippocampus	Cortex	Hippocampus	Cortex
Al	7.46	9.14	2.68	2.83
V	0.016	0.013	0.027	0.027

In this case vanadium concentration in brain tissues is decreased in Alzheimer's disease individuals: at the moment the data are inadequate to try to find a link between the concentration in brain tissues and in plasma.

v) Platinum determination in antineoplastic treatment

Antitumor efficiency of Cisplatin (CDDP) is well established, but little is known about the mechanism of action and cytotoxicity of this drug.

A study (ref. 23) was performed to investigate the distribution of platinum in selected foetal and maternal tissues following administration of CDDP to pregnant mice.

In another work (ref. 24) the effects of 1,2-diarylethylene-diamine-platinum (II) complex were considered.

Two points were investigated: i) the absorption of drug in tumor tissue and in different organs; ii) the change of concentration of biologically essential trace elements in tissues of therapied compared to non therapied mice.

6.13.2 Activation analysis with charged particles

Many general points have already been discussed in the paragraphs referring to NAA: here only the specific topics will be reported.

a) Cross sections

The induction of a nuclear reaction by charged particles implies the getting over the Coulomb repulsive barrier between the target nucleus and the incoming projectile and this requires an amount of energy well above the thermal energy of neutrons. Moreover the accelerators, like cyclotrons, employed to reach the low limit energies are usually able to reach also higher energies so that a wide variety of nuclear reactions must be considered when the incident projectiles are charged particles.

For incident light particles like protons, deuterons, helium-3, and alphas the most probable reactions are evaporations of neutrons and protons from the compound nucleus.

The cross sections for such reactions are strongly dependent from the incident energy and the specific target used, but there is an average smooth relationship among the cross sections and the incident energies and the target mass number that is shown in Figure 6.18.

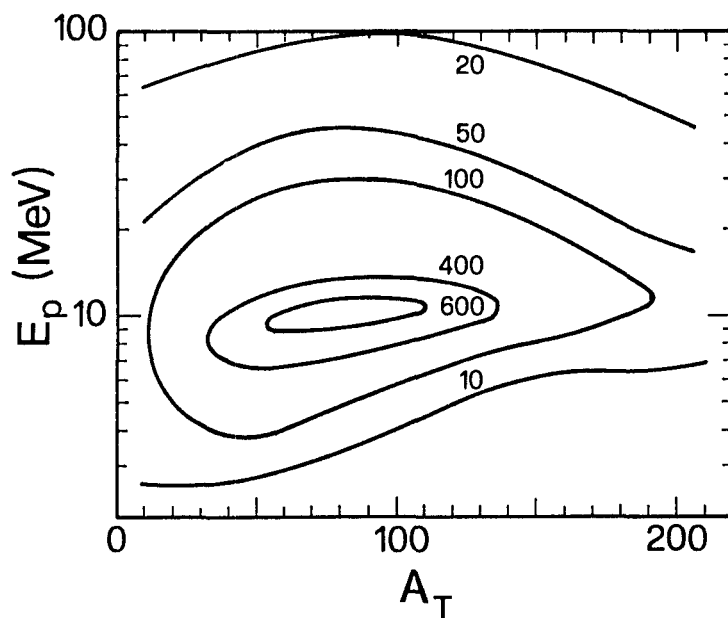


Fig. 6.18. Approximate three-dimensional plot of cross sections for (p, n) reactions as functions of incident energy E_p and target mass A_T . The isovalued lines are given in millibarns.

It must be clear that the isocrosssection lines in the drawings are only very rough approximations of the experimental data, but nevertheless they give an order of magnitude of the cross sections for the reactions involved.

It is important to observe that, for nuclei not too heavy, (p, n) reactions are considerably induced at energies around 10 MeV where the other reactions like $(p, 2n)$, (p, pn) or (p, α) are strongly hindered.

This means that (p, n) reactions are usually very clean in the sense that the contribution from the other kinds of reaction is very low: because of this reason (p, n) reactions must be preferred when possible, also if there is some disadvantage in the yield.

b) Excitation functions

Once defined the target and the kind of reaction of interest it is

necessary to get more precise informations on the needed incident projectile energy. The data shown in the former paragraph are too approximate to be taken into consideration on a quantitative basis: the knowledge of sufficiently precise excitation functions is essential.

Excitation functions represent the cross section of a given reaction on a given target as dependent on the incident particle energy: referring to the figures shown in the previous paragraph they may be interpreted as cuts of the threedimensional plots parallel to the incident energy axis.

There are many data published on this subject, but due to the wide possibility of combinations of reactions and targets there is often a lack of information in literature.

It is therefore often necessary to measure preliminarily the excitation functions for the nuclei of interest: in reality what is needed in activation analysis is simply the relative yield of the different γ rays of concern.

The classical way to perform these measurements is to prepare a series of identical targets of the element to be studied, to expose them to beams at different energies with an accurate measure of the incident fluxes. The subsequent determinations of the relevant peaks areas, suitably normalized for different fluxes and times, give the relative excitation functions corresponding to the specific transitions. A critical point in this kind of measure is the determination of the integral flux of the beam: the charge collection is easily affected by large errors due for example to secondary electron emission. This problem can simply be overcome if a pile of identical foils of the element is irradiated: if the thickness of the foils is suitably chosen, the energy degradation of the incident beam in each foil is sufficient to cover the energy range to be analysed (see Fig. 6.19). Each foil is therefore irradiated with the same flux, but at different energies that can be evaluated by means of the specific energy loss relationship (ref. 25).

c) Sample preparation

A major problem in sample preparation is due to the ionizing properties of energetic charged particles: the energy loss per unit path is very high so that a compulsory requirement for the sample is a very limited thickness, of the order of some tenths of millimeter. A high energy degradation in the sample gives rise to a large spread of the incident particle energies contributing to the reactions so reducing the useful yield and the purity of the reaction. Moreover the energy lost by the beam is transformed into heat that must be removed in order to avoid a dangerous increase in temperature that may deteriorate the sample.

Nearly all the biological materials can be reduced in the form of powder

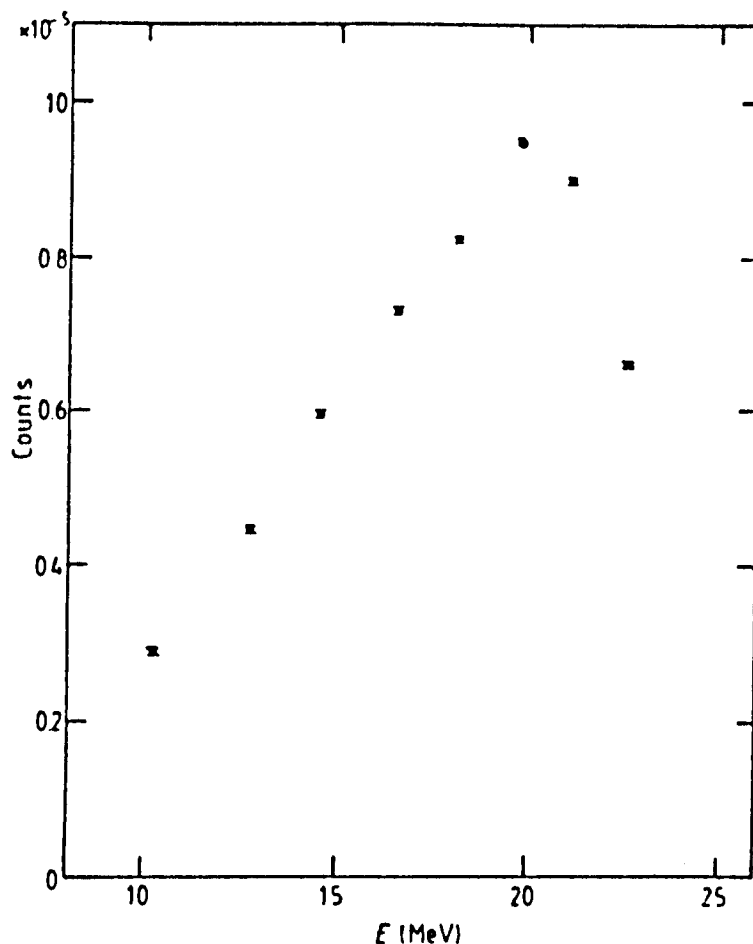


Fig. 6.19. Relative yield of the reaction $^{78}\text{Se}(p, 2n)^{77}\text{Br}$ as a function of the incident proton energy. The data were obtained irradiating with a 25 MeV proton beam a pile of 8 identical SeO_2 pressed powder discs, each one 80 mg cm^{-2} thick.

that can be compressed and pelleted as a disc with a diameter of about 1 cm and an adequate thickness. To reduce external contamination this pellet can be sealed between two very thin non contaminating mylar foils: after irradiation the foils can be removed.

d) Irradiation

Some points are worth noting in irradiation with charged particles beams

especially in comparison with thermal neutrons. The beams are collimated, and this allows high fluxes concentrated in a small region of the order of some cm^2 .

To give an order of magnitude of the beam intensities used to activate biological samples one may report that for protons at an energy of 12-15 MeV a beam current of 300-500 nA is well suitable.

The energy definition of the incident beams is good either in absolute value either in resolution: for both items 1% of the particles energy is a quite typical dispersion value.

Charged particle beams can be handled by electromagnetic lenses, and can be guided also at considerable distance from the accelerator, but this requires high vacuum pipes in order to avoid degradation in energy and collimation because of the strong ionizing interactions also with gases. The penetration in air of a proton beam of some MeV is of the order of one meter: for practical reasons it is often useful to irradiate in air, but this is possible only if the beam is extracted from the vacuum pipe through a very thin window (for example 0.1 mm of tungsten) and if the path to the target in air is short, of the order of some centimeters.

To reduce the effects of heating of the sample, in which the charged particle beam may loose several watts, a suitable cooling system must be set up in order to maintain the sample temperature below 40-50 °C.

The irradiation in air has two main advantages: from one part it allows an easy access to the target and facilitates the cooling, from the other point it reduces the danger of losses due to volatilization of sample elements.

In contrast there is a disadvantage in the degradation of energy and angular resolution of the incident beam and usually, because of cooling, there is also some problem with condensation onto the sample holder, with possibility of contamination of the sample itself.

e) Specific controls

Apart the controls already described in paragraph 6.13.1d on neutron activation analysis, two points require some comment in charged particle activation analysis of biological samples.

The already mentioned relatively high energy of the projectiles allows the opening of many reaction channels that can interfere with the measurement in course. Also if the dominant reaction is the evaporation of one neutron, the emission for example of an alpha particle is often energetically allowed. Moreover the energy degradation in the sample spreads the incident energy over a few MeV so increasing the possibility of interfering reactions. The control on the production of the radioisotopes of interest by means of spurious reactions

on different parent nuclei is very important and delicate: the evaluation of threshold energies, cross sections, isotope abundances must always be performed, and if possible also an experimental check is highly advisable.

Powderized biological materials are normally bad heat conductors: it is not easy to transfer outside the power dissipated by the incident beam into the sample. On the other hand, to avoid degradation and decomposition of the biological material the temperature must not rise above 50 °C. It is difficult to foresee the thermal behaviour of the samples, but a control must be set up in order to determine the maximum beam current that can be injected into the target. An estimate of the bulk temperature may be obtained embedding a very little NRC thermistor into one sample: in a test with a proton beam of 300 nA the temperature was about 40 °C and with 400 nA it rised to about 80 °C (ref. 27).

f) Some recent results obtained with charged particles activation analysis in biomedical materials

i) Ferrokinetic studies with stable isotopes as tracers

Disturbances of iron metabolism are frequently observed. Radioactive tracers are routinely used for the determination of plasma iron clearance and for iron absorption studies: to avoid the inherent radiation damage the use of stable isotopes as tracers was studied.

An investigation on iron metabolism in rabbits using a double tracer technique with stable iron isotopes (^{57}Fe and ^{58}Fe) is presented in ref. 28.

For comparison a simultaneous study with radioactive ^{55}Fe and ^{59}Fe was performed in the same subjects. After intravenous injection of ^{55}Fe and ^{58}Fe and oral administration of ^{59}Fe and ^{57}Fe , plasma samples were withdrawn at different times. The measurement of the specific activity of each sample together with the determination of the content of ^{57}Fe and ^{58}Fe by means of proton activation analysis allowed the intercomparison of the results.

An example for iron clearance is shown in Figure 6.20 and is completely satisfactory.

It is worth noting that the use of stable tracers implies the use of nuclear techniques for the measurement and in the case of iron isotopes neither neutron activation analysis nor mass spectroscopy analysis show sufficient sensitivity.

ii) Determination of Cadmium, Thallium and Lead by proton activation analysis

The considered elements are poisonous for human beings. Their control in body and environment is therefore very important, for the study of contamina-

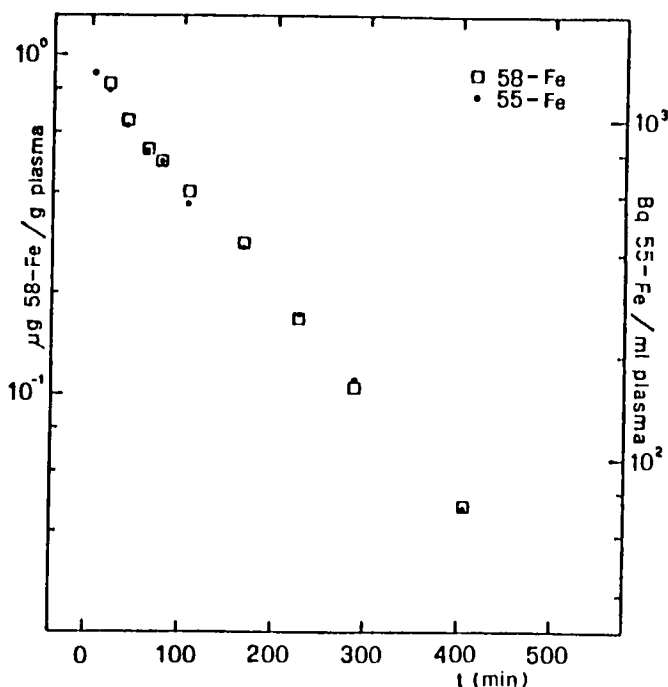


Fig. 6.20 Comparison of the clearance data obtained for the same subject by means of ^{58}Fe content and ^{55}Fe activity measurements.

tion, but their determination by means of techniques like atomic absorption spectroscopy, or mass spectrometry is quite critical in particular in presence of a complex matrix like that of biological samples. Moreover Tl and Pb are not conveniently determinable by means of neutron activation analysis.

In ref. 29 the results obtained with proton beams on certified materials like NBS-SRM 1633 a (Coal fly ash) and BRC-CRM 176 (City waste incineration ash) are presented.

Tests were performed at different energies inducing different reactions. The data obtained are shown in Table 6.4 and are in good agreement with the certified values, with a precision ranging from 1.6 to 6%.

In ref. 30 the determination of cadmium (together with titanium) content in human serum is reported. The measurement was performed with a 13.5 MeV proton beam of the AVF cyclotron of the University of Milan. A preliminary comparison with NBS 1577 Bovine liver gave for cadmium a value of 0.28 ± 0.07

TABLE 6.4

Summary of the results for NBS-SRM 1633a and BCR-CRM 176 together with the certified values. For Cd and Pb in BCR-CRM 176 results of instrumental determinations are also reported.

		x	s	n	Certified values
<u>NBS-SRM 1633a</u>					
Cd ($\mu\text{g/g}$)	15 MeV	0.890	0.030	3	1.00 ± 0.15
	23 MeV	0.943	0.056	4	
Tl ($\mu\text{g/g}$)	23 MeV	5.73	0.28	3	5.7 ± 0.2
Pb ($\mu\text{g/g}$)	23 MeV	73.8	1.2	4	72.4 ± 0.4
<u>BCR-CRM 176</u>					
Cd ($\mu\text{g/g}$)	12 MeV ^a	477	11	3	470 ± 9
	15 MeV	474	13	3	
	23 MeV	485	20		
Tl ($\mu\text{g/g}$)	23 MeV	2.72	0.11	4	2.85 ± 0.19
Pb ($\mu\text{g/g}$)	23 MeV	11.04	0.26	4	10.87 ± 0.17
	23 MeV ^a	11.20	0.40	4	

^ainstrumental determination.

$\mu\text{g/g}$ whereas the certified value is $0.27 \pm 0.04 \mu\text{g/g}$.

The data obtained for human serum were $0.025 \pm 0.005 \mu\text{g/ml}$ of Cd (and $0.09 \pm 0.01 \mu\text{g/ml}$ of Tl).

iii) Trace elements analysis by means of prompt γ emission

Strictly speaking prompt γ emission is not related to an activation process in the sense that there is not the production of a radioactive nucleus with a well defined mean life. Nevertheless the basic physics is the same either in prompt emission either in γ emission following a radioactive decay: in both cases there is the production of a nucleus in an excited state and the main difference from the point of view of the measurement resides in the different time scale.

Fluorine is a very typical element that can be measured by means of prompt γ emission induced by proton beams. To determine the fluorine concentration in dental and tissue matrices the absolute cross-section for $^{19}\text{F}(p, p'\gamma)^{19}\text{F}$ reaction was measured (ref. 31). It was then possible to assess the sensitivity of detection that allows also depth-profiling.

In ref. 32 another example of proton induced prompt γ rays emission is given for the analysis of major elements in serum in pregnant women and new born babies.

The serum samples were dried, pelleted and bombarded with the 4.1 MeV

proton beam generated by the SMV EGP-10-II tandem accelerator of the University of Helsinki.

C, Cl, N, Na, O and P were determined by means of $(p, p'\gamma)$ reactions: with 15 minutes irradiation time sufficient sensitivity was reached in the measurements to detect significant differences for some elements in early pregnant, late pregnant and new born babies groups.

6.14 CONCLUSIONS

In this brief chapter I tried to give an overview of the role played by in vitro activation analysis in biomedical sciences, giving also some details on general principles and technical aspects.

My aim was not to write a review for experts in the field, but to describe some in vitro activation analysis procedures and results for researchers involved in trace elements determination in biological samples. I hope that this work could be of some help in the choice of the most useful approach to their problems.

Activation analysis is not the only mean to measure elements at very low concentrations but the fact of being based on nuclear properties of the elements of interest make it very different from atomic based measures like for instance atomic absorption spectroscopy. This difference may play an important role when complex matrices are involved in the measurement and interferences from other elements may disturb the quantification of the searched element.

Neutron activation analysis (NAA) is a very powerful tool in trace elements determination and its cost, disregarding the reactor purchase, is not too high.

If a research reactor is easily accessible, NAA may be considered as a routinely usable technique for the determination of specific elements.

The sensitivity of NAA is not the same for all the elements, depending essentially on the very variable neutron capture cross sections: for very light and very heavy elements and for some specific substance like for instance iron, sensitivity is usually insufficient.

Charged particles activation analysis in many cases is complementary to NAA. In former paragraphs some examples are reported where good sensitivity is reached with proton beams in seeking for elements which do not fit for NAA.

Certainly the costs of charged particle activation analysis are high but nevertheless for some specific application this kind of analysis is the only suitable one.

Moreover research on new developments and applications must not be too much conditioned by costs: in particular for intercomparison studies charged

articles activation analysis, due to the wide degrees of freedom in the choice of projectiles and energies, allow a good check of possible systematic errors.

REFERENCES

- 1 G.V. Hevesy, H. Levi, Kgl. Danske Videnskab Mat.-fys. Medd., 14 (1936) 3.
- 2 C.M. Lederer, V.S. Shirley, Table of Isotopes, 7th edn., by J. Wiley, New York, 1978.
- 3 I. Kaplan, Nuclear Physics, by Addison Wasley Publ. Co., Reading, Mass., 1956.
- 4 J.M.A. Lenihan and S.J. Thompson (Eds.), Advances in activation analysis, Vol. 1, Academic press, New York, 1969.
- 5 F. Grass, 7th International Conference on Modern Trends in Activation Analysis, Copenhagen, 1986, 255.
- 6 W.D. James, Ibidem, 267.
- 7 P. Kruger, Principles of activation analysis, Wiley Interscience, New York, 1971.
- 8 Experiments in Nuclear Science, AN 34, Ortec Publ., Oak Ridge, Tenn., 1976.
- 9 F. Groppi, N. Molho, L. Pirola, INFN/TC, 14/85, Frascati, Italy, 1985.
- 10 M.C. Cantone, N. Molho, L. Pirola, INFN/TC, 79/18, Frascati, Italy, 1979.
- 11 J. Topping, Errors of observation and their treatment, Chapman and Hall Ltd., London, 1966.
- 12 L. Kosta, Technical Report 197 STI/DOC/10/197, IAEA, Vienna (1980) 317.
- 13 G.V. Iyengar, 7th International Conference on Modern Trends in Activation Analysis, Copenhagen, 1986, 107.
- 14 R. Cornelis, Ibidem, 93.
- 15 B. Sansoni, G.V. Iyengar, Technical Report 197/STI/DOC/10/197, IAEA, Vienna (1980) 57.
- 16 F. Lux, 7th International Conference on Modern Trends in Activation Analysis, Copenhagen, 1986, 117.
- 17 F. Chisela, D. Gawlik, P. Brätter, Ibidem, 235.
- 18 S.F. Stone, R. Zeisler, Ibidem, 65.
- 19 W.D. Frasch, J. Larson, N. Bowlby, I. Apel, J.D. Jones, Ibidem, 33.
- 20 R. Michel, F. Loer, M. Nolte, M. Reich, J. Zilkens, Ibidem, 495.
- 21 M. Simonoff, Y. Llabador, C. Hamon, B. Berdeu, G. Simonoff, C. Conri, B. Fleury, P. Couzigou, A. Lucena, Ibidem, 517.
- 22 N.J. Ward, J.A. Mason, Ibidem, 925.
- 23 M. Esposito, P. Collecchi, M. Oddone, S. Meloni, Ibidem, 829.
- 24 S. Trebert Haeberlin, F. Lux, J. Karl, T. Spruss, H. Schönnenberger, Ibidem, 859.
- 25 C.F. Williamson, J.P. Boujot and J. Picard, Rapport CEA, K3042, Paris, 1966.
- 26 M.C. Cantone, N. Molho, L. Pirola, INFN/TC, 82/3, Frascati, Italy, 1982.
- 27 M.C. Cantone, N. Molho, L. Pirola, Fisica in Medicina, 4 (1984) 63.
- 28 M.C. Cantone, N. Molho, L. Pirola, Ch. Hansen, P. Roth, E. Werner, Med. Phys. 14 (1987)
- 29 G. Wauters, C. Vandecasteele, K. Strijckmans, J. Hoste, 7th International Conference on Modern Trends in Activation Analysis, Copenhagen, 1986, 81.
- 30 M.C. Cantone, N. Molho, L. Pirola, J. Radioan. Nucl. Chem., 91 (1985) 197.
- 31 M.A. Chaudhri, VII Intern. Conf. on Medical Physics, Espoo, Finland, 1985, 1076.
- 32 M. Hyvonen-Dabek, J.T. Dabek, P. Nikkinen, J. Raisanen, R. Hanninen, Ibidem, 1078.

Chapter 7

IN VIVO NUCLEAR ACTIVATION ANALYSIS

KAMIL VICTOR ETTINGER

Department of Internal Medicine
University of Rome "Tor Vergata"
Via O. Raimondo - 00173 Roma
ITALY

7.1 INTRODUCTION

The nuclear activation analysis in vivo has been considerably developed during the last two and half decades and at present has established itself as a flexible research tool as well as a clinical technique and an aid to medical diagnosis. It has greatly increased our knowledge of the physiological processes in health and disease, which are affecting the elemental composition of the body. It has also provided a quantitative information on the composition of human body, with regard to sex, age, race, body size and even life style. As a result of accumulated information an improvement became possible in diagnosis, staging and management of patient with disorders of metabolism, with wasting diseases and with certain cancers.

The "prehistory" of IVNAA is linked to involuntary irradiation by fast neutron flux and gamma rays of personnel involved in a radiation accident on a reactor in 1957 (ref. 1).

The received doses were reconstructed from the activity of Na induced in their blood (ref. 2). The variation of radiation dose delivered by beams of neutrons of energies ranging from 25 keV to 14 MeV in a tissue equivalent phantom was investigated in 1962 by Smith and Boot (ref. 3). The 1962 paper on activation of sodium in man phantoms was already half way between the provision of reliable data for health physicists facing another reactor accident and the preparation for intentional IVNAA for medical purposes (ref. 4).

At the same time a group at MIT was suggesting the use of neutron beams for measurement of calcium in vivo (refs. 5,6). In 1964 a team from the King's College Hospital in London (ref. 7) reported the first determination of chlorine and sodium in vivo, indicating a possibility of measuring calcium and other elements. The same group in 1967 presented a paper with more advanced results, particularly in respect of calcium in vivo determination (ref. 8).

Accurate whole body measurements of calcium and sodium were reported by the Birmingham group in 1968 (refs. 9,10), even though Chamberlain in his one-page review of the state-of-the art (ref. 11) doubted if IVNAA will ever become a diagnostic tool for routine use. Both Boddy (ref. 12) and Lenihan et al. (ref. 13) have described the measurements of iodine in thyroid in vivo. When Comar (CEA, Orsay) in 1969 wrote his survey of IVNAA, his list of activable elements contained eight entries (ref. 14,15). The first period of development of IVNAA was culminated by conferences in Orsay (1968) and East Kilbride (1969).

The history of development of IVNAA will not be continued further as a separate paragraph. Instead, the reader will find in individual chapters references to important developments in this field.

The number of elements which can be measured by in vivo nuclear activation analysis is very large and includes all the principal components of the body together with a substantial fraction of the minor elements. Furthermore IVNAA has been successful in detection of elements which are not naturally present in the tissues but which accumulate as a result of contamination,

ingestion or inhalation of toxic substances released into the environment. The list of elements detectable in vivo at the present stage of technology is given in Table 7.1.1.

TABLE 7.1.1. ELEMENTS DETECTABLE IN VIVO BY NUCLEAR ACTIVATION ANALYSIS.

<u>Major elements</u>		
Hydrogen	Oxygen	Nitrogen
Carbon	Calcium	Phosphorus
Sodium	Potassium	Chlorine
<u>Minor elements</u>		
Iron	Magnesium	Iodine
<u>Trace elements and contaminants</u>		
Cadmium	Lithium	Boron
Silicon	Mercury	

There is also a number of elements for which feasibility studies have been initiated, like beryllium, or for which the analysis of relevant cross sections, abundances, branching schemes etc. indicates that they should be measurable, even in very small quantities, in vivo in man. Examples of such elements are: sulphur, titanium, manganese, nickel, zinc, gadolinium*, dysprosium, erbium and gold.

Until very recently most of the work in this field was concerned with the use of neutron beams. There is currently a growing interest in the use of high energy photons as means of nuclear activation analysis. The choice of the technique depends upon the nuclear reactions and processes available for the determination of nuclides of interest, upon the interferences and errors inherent in each method and upon the availability of equipment.

It is likely that fast and slow neutrons will remain most commonly used probes for the determination of elemental body composition, because the majority of elements can be determined with neutron beams and also because neutron sources are easily available.

A recently developed technique of Nuclear Resonance Fluorescence is likely to become more widespread with the growing number of quasi-monoenergetic X-ray high energy sources, associated with electron linacs and with synchrotron light sources.

A number of excellent reviews of the field of IVNAA is available, e.g. those by Cohn (refs. 16,1), Chettle and Fremlin (ref. 17), Cohn and Parr (ref. 18) as well as a compilation of reports published by IAEA (ref. 19). A 1973 review by Cohn and Palmer (ref. 20) of whole body counters, which are widely used in IVNAA, is still one of the best sources of information on the subject.

* Inclusion of gadolinium in potentially activable elements is not a joke; Gd in a chelated form is at present widely used as paramagnetic tracer in NMR investigations and any possible retention of the element may require a check by IVNAA because of toxicity of Gd. The same applies to Dy and Er.

7.2 PRINCIPAL TECHNIQUES OF IVNAA

7.2.1 General

The use of term "activation analysis" refers to the fact that in order to detect any element we must "activate" it, by rendering it radioactive, or by inducing it to emit a photon or some nuclear particle.

So far there are five principal methods of activation analysis in vivo:

1. Method of induced radioactivity
2. Method of prompt capture gamma rays
3. Method of inelastic scattering of neutrons
4. Photoneutron method
5. Method of nuclear resonance fluorescence (resonance scattering)

These methods will be discussed separately in the following paragraphs.

7.2.2 Method of induced radioactivity

This is an application of a well known technique to in vivo methodology. The patient (or animal) is exposed to a neutron flux and various radioactive species are formed in situ. The induced radioactivity is then counted, either by a whole or partial body counter or in exhaled gas or even in sweat or excreta. This technique is applicable to many elements of the human body e.g. nitrogen, oxygen, sodium, chlorine, calcium, phosphorus, magnesium, copper, iodine and others. This technique may be based either on slow or fast neutron reactions or on photoreactions. If radioactivity is measured in an irradiated patient it is important that the transfer to a detection facility is done sufficiently fast, in order not to lose a substantial amount of induced activity following end of bombardment, particularly with short lived activities of phosphorus ($T_{1/2} = 2.24$ min), calcium ($T_{1/2} = 8.72$ min), nitrogen ($T_{1/2} = 9.96$ min). An even shorter activity of ^{16}N ($T_{1/2} = 7.2$ s) encountered in measurements of oxygen requires that the counting is done in the same place as irradiation, which raises problems of high background, inherent in the irradiation facility.

The initial activity following irradiation (ref. 1) is given by

$$I_0 = \frac{W N \phi \sigma m}{A} (1 - \exp(-\lambda t))$$

where I_0 - activity in Bq

W - mass of target element

N - Avogadro number 6.023×10^{23} atoms per gram atom

A - atomic weight of target nuclide

ϕ - average neutron flux density neutron $\text{cm}^{-2} \text{sec}^{-1}$

σ - absorption cross section (b)

m - fractional isotopic abundance of target nuclide

λ - decay constant (sec^{-1})

t - duration of irradiation (sec)

For $t = 0.693/\lambda$ a half-value of maximum achievable activity is reached. It is important to remember that, neglecting certain types of interference, it is better from the point of view of reducing the dose to the patient to perform irradiation as rapidly as possible. For duration of irradiation less than the half life of induced activity the absorbed dose and the activity are nearly proportional to each other, which is not the case for longer periods of exposure. If there is a delay between the end of bombardment and the beginning of counting, activity at the beginning of counting period will be $I_0 \exp(-t_{\text{del}}\lambda)$.

The transfer of the patient to the counting facility in purpose designed laboratories is swift and may be reduced to sliding the couch along the rails

TABLE 7.2.1 MEASUREMENT OF ELEMENTAL BODY COMPOSITION BY MEANS OF INDUCED RADIOACTIVITY

Element	Amount in ICRP reference man per 70 kg (g)	Activation reaction	Reaction threshold (MeV)	Half-life of induced activity	Energies of emitted photons	Comments
Oxygen	43 000	$^{16}\text{O}(\text{n},\text{p})\ ^{16}\text{N}$	10.24	7.2 s	6.134	
Oxygen	43 000	$^{16}\text{O}(\gamma,\text{n})\ ^{15}\text{O}$	15.67	1.23 s	0.511	
Nitrogen	18 000	$^{14}\text{N}(\text{n},2\text{n})\ ^{13}\text{N}$	11.31	9.96 m	0.511	
Nitrogen	18 000	$^{14}\text{N}(\gamma,\text{n})\ ^{13}\text{N}$	10.55	9.96 m	0.511	
Nitrogen	18 000	$^{14}\text{N}(\text{p},\alpha)\ ^{11}\text{C}$	3.13	20.34 m	0.511	(*) Reaction induced by recoil proton flux
Calcium	1 000	$^{48}\text{Ca}(\text{n},\gamma)\ ^{48}\text{Ca}$	0	8.72 m	3.08	
Calcium	1 000	$^{40}\text{Ca}(\text{n},\alpha)\ ^{37}\text{Ar}$	0	35.2 d	0.0026	(*) X-rays and Auger electrons
Phosphorus	780	$^{31}\text{P}(\text{n},\alpha)\ ^{28}\text{Al}$	2.01	2.24 m	1.779	
Carbon	16 000	$^{12}\text{C}(\gamma,\text{n})\ ^{11}\text{C}$	18.72	20.34 m	0.511	
Potassium	140			1.177 $\times 10^3$ y	1.460	Naturally occurring activity of ^{40}K
Sodium	100	$^{23}\text{Na}(\text{n},\gamma)\ ^{24}\text{Na}$	0	15.02 h	2.754;1.369	
Chlorine	95	$^{37}\text{Cl}(\text{n},\text{p})\ ^{37}\text{S}$	0	5.07 m	3.10	
Chlorine	95	$^{37}\text{Cl}(\text{n},\gamma)\ ^{38}\text{Cl}$	0	37.3 m	2.168;1.642	
Magnesium	19	$^{26}\text{Mg}(\text{n},\gamma)\ ^{27}\text{Mg}$	0	9.46 m	1.013;0.84	
Iodine	0.013	$^{127}\text{I}(\text{n},\gamma)\ ^{128}\text{I}$	0	25.0 m	0.443	Almost all in the thyroid
Iron	4.2	$^{56}\text{Fe}(\text{n},\text{p})\ ^{56}\text{Mn}$	2.96	2.58 h	0.847;1.811	
Copper	0.072	$^{63}\text{Cu}(\text{n},\gamma)\ ^{64}\text{Cu}$	0	12.7 h	1.346;0.511	Mostly liver
Copper	0.072	$^{65}\text{Cu}(\text{n},\gamma)\ ^{66}\text{Cu}$	0	5.1 m	1.039	" "

In addition, some elements which are present naturally in trace amounts, when introduced into the body for purpose of therapy, like lithium, are detectable by this method.

(*) Measurement of the radioactivity in exhaled gas.

from one facility to another. On the other hand the author recalls the rush accompanying hurried up transfer of a patient to an ambulance and a very fast ride to the nearby hospital for whole body counting, with lights flashing, siren sounding etc., as was happening in Birmingham in the sixties.

The regimen of irradiation and counting depends on the facilities. If the uniform activation throughout the body is to be achieved with one neutron source, the patient must be rotated standing on a turntable (ref. 21) or turned over lying on a couch (ref. 22). Simultaneous, bilateral irradiation have been employed in some centres (refs. 23-25). If the whole body has been irradiated simultaneously, the induced activity is best counted simultaneously for all parts of the body. If however the detection facility is a scanning device a proper correction must be introduced to account for different time delays and consequent decay. This can be done automatically by varying exponentially the couch speed. Various arrangements in which a scanning neutron source (one or two neutron generators) and a scanning shadow shield monitor can be coupled together to provide satisfactorily uniform whole body IVNAA are described by Boddy et al. (ref. 26) and by Haywood et al. (ref. 27).

Premoderation of neutron sources and prefiltering has been developed to provide a desired penetration of neutron flux and to compensate for the varying thickness of moderation tissues. The devices employed range from polystyrene chips to plastic armour to water filled containers in which the extremities are immersed. Cohn (ref. 16) gives a well illustrated survey of these appliances.

A gamma ray spectrum from an irradiated patient obtained with an array of NaI(Tl) scintillation detectors in a whole body counter is shown in Figure 7.2.1 (ref. 28). For a part body counter fitted with germanium detectors the corresponding spectrum will consist of much narrower spectral lines, with much higher contrast between the spectral lines and the continuum. As it can be seen from Figure 7.2.1 the shape of the spectrum depends on the energy of incident neutrons. The spectrum changes during the counting as various components are decaying with different rates. It also depends on the resolution of detector crystals and on their peak to total ratios.

Measurements of the induced activity includes a group of techniques based on collection of exhaled gases. Palmer (ref. 29) described a technique for measurement of total body calcium by means of a reaction $^{40}\text{Ca}(n,\alpha)^{37}\text{Ar}$. Argon diffuses from bones to blood and eventually is exhaled. The exhaled gases are collected and purified until only argon is fed to a proportional gas counter. In another paper Palmer et al. (ref. 30) proposed to use the exhalation technique to measure nitrogen in vivo, utilizing the fast proton recoil flux which accompanies neutron irradiation of soft tissues. These secondary protons produce hot atoms of C in vivo by reaction $^{14}\text{N}(p,\alpha)^{11}\text{C}$. The hot atoms acquire other atoms or parts of molecules in the slowing down process and eventually are exhaled as ^{11}CO , $^{11}\text{CO}_2$, $^{11}\text{CH}_4$ etc. Carbon oxides are easy to trap chemically (e.g. an alkaline solution for CO_2 , haemoglobin suspension for CO) and owing to the positron emission by ^{11}C a simple coincidence set up of two large scintillation detectors provides an almost 100% efficiency of detection and very little background (refs. 31,32). The method of exhaled gas counting is highly sensitive in that it requires a radiation dose less than other methods for Ca involving radiation, only $600\text{ }\mu\text{Sv}$ for the whole body (ref. 33). This technique was independently developed in other laboratories as well (ref. 34) and in conjunction with very sensitive detectors and, perhaps, mass spectrometric selection, may be useful for measurement of iodine in thyroid by measurement of exhaled xenon produced in reaction $^{127}\text{I}(p,n)^{127}\text{Xe}$. There is also a fascinating possibility of determination of ^{239}Pu in lungs in vivo by observation of exhaled gaseous fission products (xenon and krypton) following an exposure to low energy neutrons. A miniature gas counter, with an exceptionally low background has been described by Kummer et al. (ref. 35). Another use of the exhaled gases for IVNAA is in measurement of lithium introduced as a therapeutic agent in psychiatry. Tritium is formed in the reaction $^6\text{Li}(n,\alpha)\text{T}$. This tritium is eventually exhaled as HT and serves as a measure of lithium concentration in the irradiated organ (usually brain). This method has been proposed by Vartsky (ref. 36) and was implemented in Brookhaven (ref. 37).

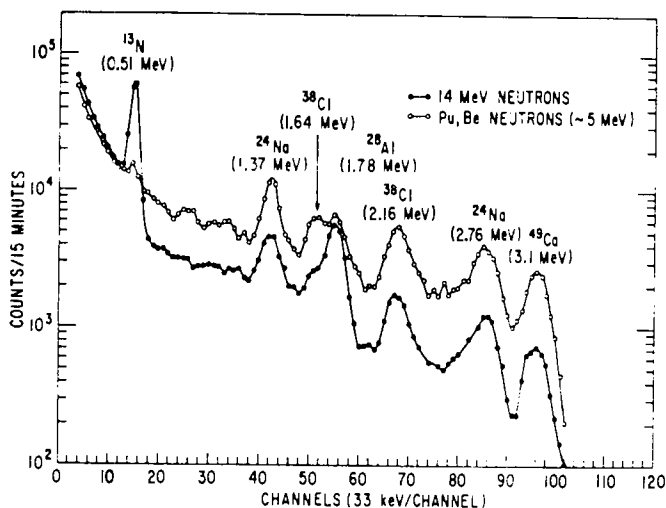


Fig. 7.2.1 The gamma ray spectra of a patient following irradiation with ^{238}Pu -Be neutrons and with 14 MeV neutrons, normalized to the same dose.

7.2.3 Method of prompt gamma rays from neutron capture

The radiative capture of neutron consists of absorption of a neutron by the nucleus which then becomes excited having absorbed the kinetic and binding energies of the projectile. The excitation energy is very quickly ($<10^{-14}$ sec) emitted in form of one or few gamma photons, thus permitting the nucleus to return to the ground state. This process is slightly slower if an isomeric level has been excited. Neutron capture is always energetically possible and available in all elements. Gamma rays from neutron capture can be used for the purpose of activation analysis if their intensity is sufficient to provide good spectral contrast. It is customary to define the intensity I of a spectral line as number of photons per 100 neutrons undergoing capture. The sensitivity of any given spectral line is then $S = \sigma I/A$ where σ —thermal capture cross section and A is atomic number. These quantities are tabulated for all elements (refs. 38-40). Whether a line can be used for prompt capture activation analysis depends whether there is no other line in the vicinity and also on the intensity of the continuum in the region of interest. This continuum originates from Compton scattering in the radiation detectors and in the source, keeping in mind that the capture gamma rays are generated at various depths of the body.

The irradiation proceeds at the same time as the detection of neutron capture gamma rays, which necessitates shielding of detectors in order to reduce the amount of activation (particularly for sodium iodine scintillators) and radiation damage. This last factor is particularly important in solid state detectors. The detectors must be out of the fast neutron beam and sheathed in thermal neutron absorber, based on ^6Li . The use of boron and cadmium would introduce a source of gamma rays in the vicinity of the detector.

The use of gamma rays from neutron capture in hydrogen was first proposed by Rundo and Bunce (ref. 41) who observed the 2.223 MeV radiation inside whole body counters. The first, and still remaining in use, purpose built installation for IVNAA with prompt gamma detection was MERMAID in Birmingham (refs. 42-44).

The source of neutrons for MERMAID was the cyclotron and three large sodium iodide detectors were used for detection. An idea of the installation can be obtained from Figures 7.2.2 and 7.2.3.

TABLE 7.2.2 MEASUREMENT OF ELEMENTAL BODY COMPOSITION BY MEANS OF NEUTRON CAPTURE GAMMA RAYS

Element	Amount in ICRP reference man (70 kg) or organs (g)	Thermal capture cross section (b) per element	Energies of emitted photons	Comments
Hydrogen	7000	0.332	2.223	
Nitrogen	1800	0.075	10.83	
Calcium	1000	0.43	6.420;4.419;1.942	
Cadmium	0.023 whole body 0.0056g / 1800 g liver 0.0032g / 143 g kidney	1.98×10^4	0.559	
Boron	therapeutically introduced	752	0.478	This not a neutron radiative capture but a (n, α) reaction with deexcitation of one of the products.
Gadolinium	diagnostically introduced	4.9×10^4	6.748;1.186; 0.944	
Mercury	0.013	376	5.966;1.694 0.368	

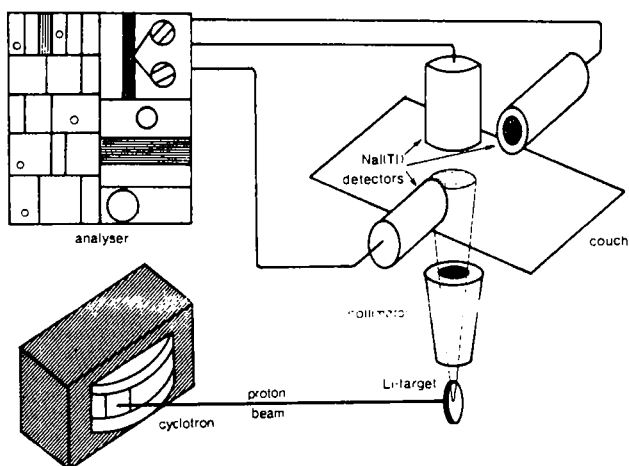


Fig. 7.2.2 MERMAID, irradiation and monitoring facility employing neutron capture gamma rays. The lateral detectors were 15.2 x 15.2 cm and the vertical 12.7 x 12.7 cm (ref. 43).

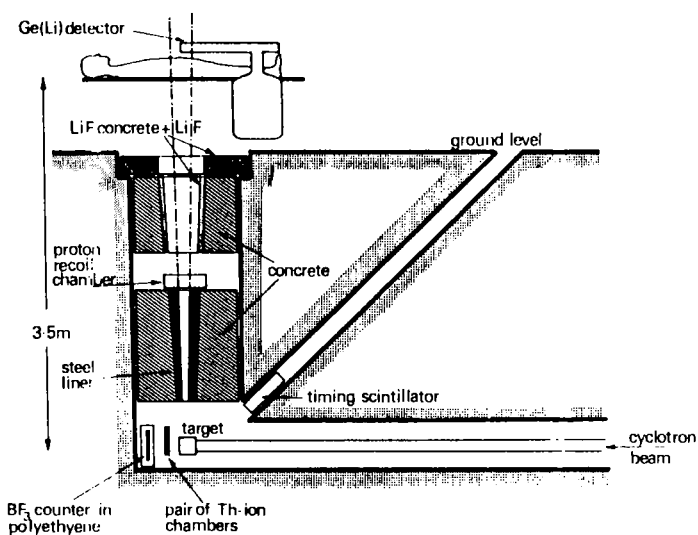


Fig. 7.2.3. The neutron collimator and beam monitoring facilities in MERMAID (Ref. 43).

As MERMAID installation became a prototype of many accelerator based installations for facilities utilizing neutron capture gamma rays, so the Brookhaven installation (see Fig. 7.2.4) became the prototype for installations based on isotopic sources.

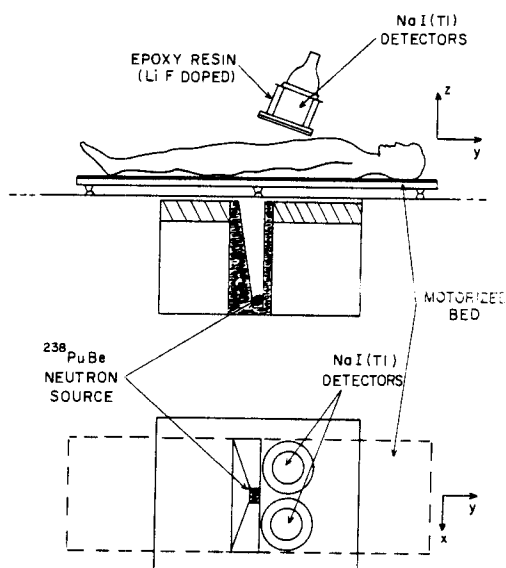


Fig. 7.2.4. Brookhaven facility for measurement of nitrogen by detection of neutron capture gamma rays (Ref. 45).

Gamma ray spectra obtained from prompt gamma ray facilities employing scintillation detectors are showing many peaks, often unresolvable, merging into a continuum. The use of this technique for nitrogen was facilitated by the presence of a peak at 10.83 MeV, the highest listed in tabulations, which effectively meant that there will be no interference from other elements. The high energy "tail" of a gamma ray spectrum from a phantom filled either with a complete tissue equivalent solution or the same solution but without nitrogen is shown in Fig. 7.2.5.

Installations utilizing semiconductor detectors for measurement of gamma rays from neutron capture are, so far, used in the region of up to about 3 MeV because of the full peak sensitivity falling with energy. This type of detector was used to detect cadmium in cadavers (refs. 46,47) and, then, *in vivo* (ref. 48). The Brookhaven facility of 1977, which later underwent further improvements, is shown in Figure 7.2.7 (refs. 49,50). Facilities for *in vivo* activation analysis with prompt gamma ray detection were built in many places (ref. 51-54). A detailed analysis of the technique was provided by Zamenhof et al. (ref. 55), where one can find the general appearance of high resolution gamma ray spectra from neutron capture in tissue equivalent material. With a continuing improvement in the resolution of germanium detectors one can expect to be able to detect in partial body analysis such elements as calcium, manganese, copper, iron, gold and others. Rare earths, like gadolinium, erbium, dysprosium which found use as paramagnetic tracers in NMR diagnostics, may undergo retention in the body or otherwise be a source of poisoning; they should be detectable by the capture method in sufficiently low concentrations.

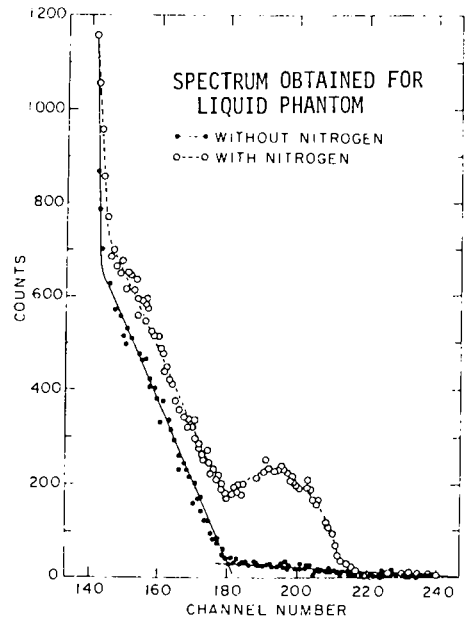


Fig. 7.2.5. High energy end of prompt gamma ray spectra obtained from a phantom filled with complete tissue equivalent liquid (open dots) or the same liquid but without nitrogen (filled dots). (Ref. 45).

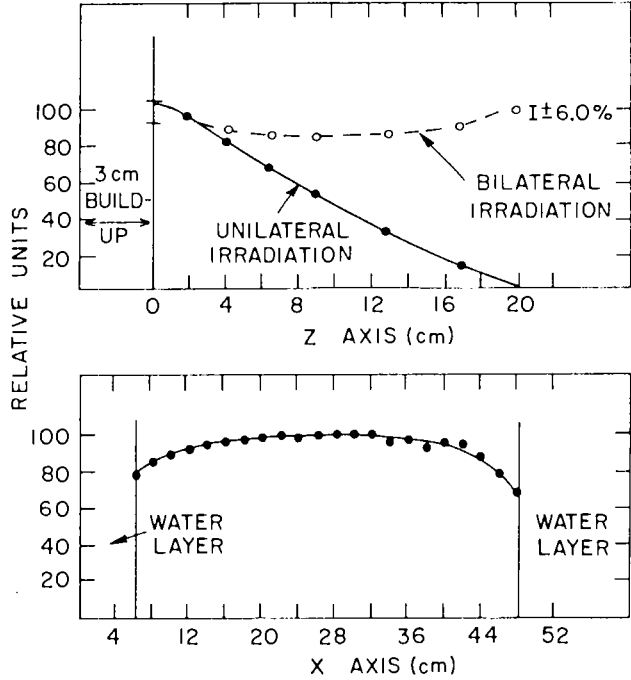


Fig. 7.2.6. The composite sensitivity (irradiation and detection) along Z and X axes, for whole body nitrogen determination (ref. 45).

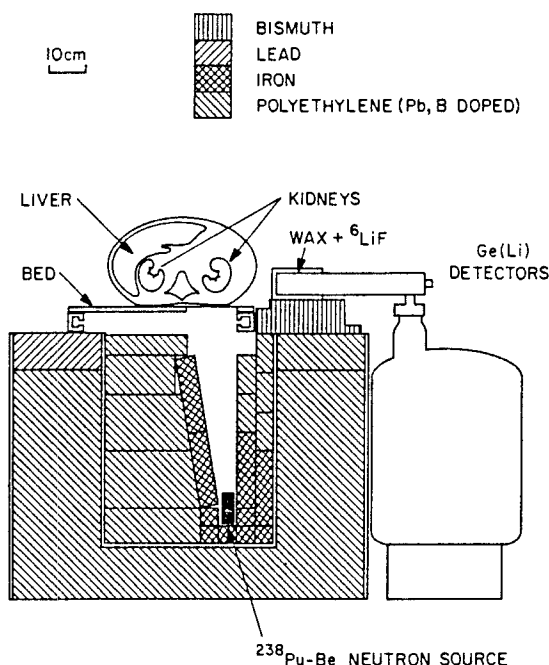


Fig. 7.2.7. Brookhaven irradiation facility for measurement of Cd in liver and kidneys. The source was later replaced by the ^{252}Cf type (ref. 50).

7.2.4 Method employing gamma rays from inelastic scattering of neutrons

In inelastic scattering the incident neutron excites one of the levels in the nucleus and a neutron is emitted with its kinetic energy reduced by the amount taken away for the excitation. The excited nucleus in a very short time deexcites emitting a photon of energy corresponding to the excitation energy. Depending upon the energy of the projectile different levels can be excited. The emitted gamma rays, having the energy depending on the level spacing, carry thus the 'signature' of nucleus which has scattered the incident neutron. The gamma rays from an inelastic scattering on carbon and oxygen in the tissues were observed first in Birmingham (ref. 44) and their use for the purpose of activation analysis in vitro was described in the works of the Leeds group (ref. 56).

Essentially, the same facility that is used for detection of prompt gamma rays from neutron capture can be used for monitoring photons from inelastic scattering of neutrons. However, an application of pulsed beams, produced by neutron generators and other accelerators, renders possible a significant improvement in the sensitivity of the method. If a short pulse of neutrons is sent into the bulk of tissue, the emission of photons takes place immediately on the arrivals of the neutrons and continues until the end of the pulse, say 1 μs . The gamma rays from capture of thermalized neutrons require some time, about 0.5 μs to appear following the neutron burst, but will continue for few hundreds of microseconds during which the thermalization still takes place. The shorter is duration of the beam burst in comparison with the period of time needed to thermalize and 'extinguish' the slow neutron flux, the lesser is the interference from thermal neutron dependent processes. In fact, during the beam

burst the main interfering factors are other gamma rays from inelastic scattering, reaction gamma rays, and gamma rays from the neutron target.

Only two major and few other elements are listed in Table 7.2.3 as being suitable for determination by the inelastic scattering technique at present but this number is likely to increase. In experiments with realistic phantoms in Brookhaven (refs. 60,61) few grams of silicon were discernible in a model of a lung. The technique of inelastic scattering appears to offer a sensitive method of detecting iron in individual organs (W.D. Morgan in ref. 19).

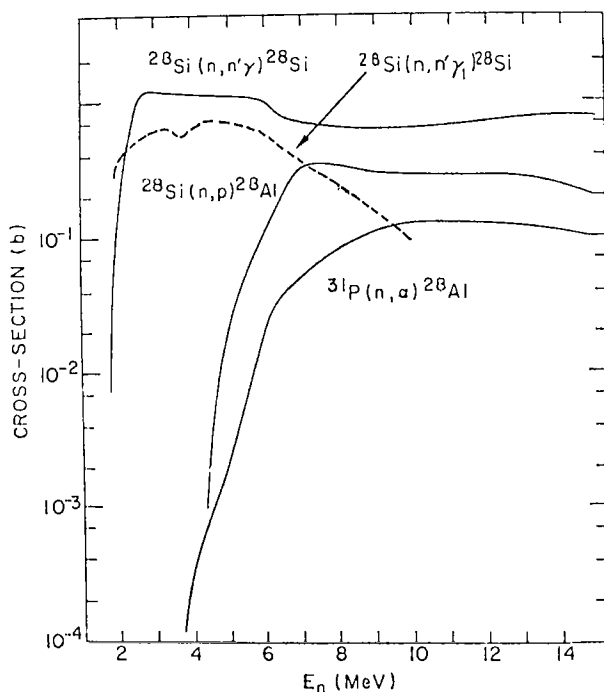


Fig. 7.2.8. Cross sections for production of 1.780 MeV gamma ray in collision of fast neutrons with nuclei of ^{28}Si and cross sections for interfering reactions plotted as a function of neutron energy (ref. 61).

The experiments with detection of silicon *in vivo* illustrate the importance of a proper choice of projectile energy, in order to maximize the sensitivity and minimize the effects of interferences. This is shown in Fig. 7.2.9, illustrating the interference from $^{31}\text{P}(n,\alpha)^{28}\text{Al}$ reaction on the detection of silicon by means of $^{28}\text{Si}(n,n'\gamma)^{28}\text{Si}$ reaction.

TABLE 7.2.3 MEASUREMENT OF BODY ELEMENTAL COMPOSITION BY MEANS OF GAMMA RAYS FROM NEUTRON INELASTIC SCATTERING

Element	Nuclide observed	Amount in ICRP man (70 kg)	Photon energy (MeV)	Gamma ray production cross section (mb/sr) at 90° per element		Comments
				14 MeV	2.8 MeV	
Carbon	¹² C	16 000	4.435	13		
Oxygen	¹⁶ O	43 000	6.131	12		
Iron	⁵⁶ Fe	4.3	0.847	58	97	
Magnesium	²⁴ Mg	19	1.369	39	35	
Silicon	¹⁸ Si	0.2 few g in silicosis	1.780	47	45	Concentrates in lungs

Cross sections taken from Engesser et al. 1964; Thompson and Engesser, 1965; Engesser and Thompson, 1965. (refs. 57-59).

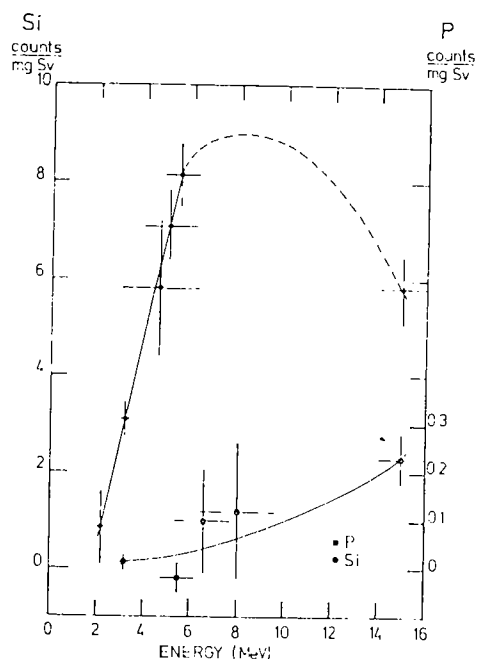


Fig. 7.2.9 Yields of 1.780 MeV gamma rays from two interfering reactions, $\text{Si}(n, n' \gamma) {}^{28}\text{Si}$ and ${}^{31}\text{P}(n, \alpha) {}^{28}\text{Al}$ in a phantom containing Si and P (ref. 61).

7.2.5 Method employing photonuclear activation

Photon activation analysis has been known for a considerable time and many excellent reviews are available on this subject (e.g. ref. 62). It has been tried to analyze samples of biological origin and an induced activity was detected in post-treatment patients undergoing therapy with high energy bremsstrahlung (ref. 63). In essence, the photonuclear activation analysis relies on stripping off the most weakly bound nucleon from the nucleus which has absorbed photon of sufficiently high energy. Thresholds of photonuclear reactions as well as their cross sections are reasonably well known (refs. 64-66). Bremsstrahlung induced activity yields for the reactions on oxygen, nitrogen and carbon in a variety of experimental conditions were measured by Piltingsrud (ref. 67).

Photonuclear activation analysis has been proposed as a method of detection of minute traces of beryllium in lungs of people occupationally exposed to beryllium metal and its compounds. Even amounts as small as $10 \mu\text{g}$ per lung appear to be associated with berylliosis (ref. 68). Nucleus of ${}^9\text{Be}$ has the smallest photonuclear threshold known, 1.665 MeV. The next higher threshold is that of deuterium, 2.223 MeV. It is possible to find natural gamma emitters which produce photons almost entirely in the energy range between these two thresholds, e.g. ${}^{124}\text{Sb}$ or ${}^{88}\text{Y}$. The apparatus for detection of beryllium *in vivo*, utilizing photoneutron production may employ radiation detectors based on ${}^{10}\text{B}$, e.g. gaseous BF_3 proportional counters. These detectors are virtually (but not entirely) insensitive to gamma rays and in practice the neutron background from cosmic rays and alpha emitter contamination of the radiation detectors are the limiting factors for the low count rates which could be observed in detection of beryllium.

A more realistic equipment for photonuclear detection of beryllium is likely to utilize an X-ray source, operating in continuous or pulsed mode.

Early experiments, with a view of establishing feasibility of the technique in humans, were performed by a group in Brookhaven (ref. 69) followed by the work of Miola (ref. 61) and Morgan (ref. 70).

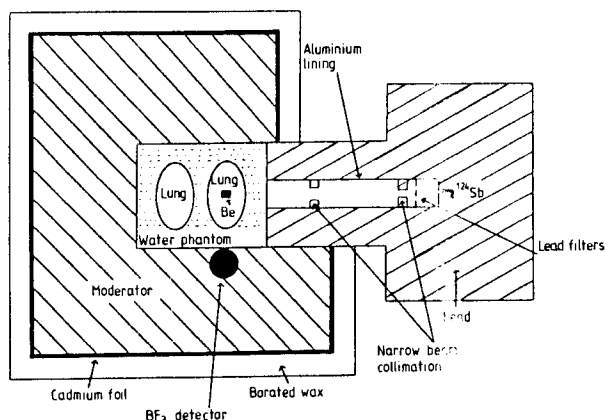


Fig. 7.2.10 Schematic diagram of lung phantom irradiation geometry in Swansea. From ref. 70.

In the feasibility experiments, scaled down to one BF detector, a reliable estimation was made by the Swansea group, indicating that with a filtered source of ^{124}Sb and 20 neutron detectors, beryllium could be measured to an accuracy of 0.33 mg per lung, which corresponds to 0.67 mg per lung if 20 detection criterion is applied (ref. 70) and the dose is 50 mGy.

Miola (ref. 61) who proposed to use an array of 150 BF_3 detectors, creating in effect a 'cage' around the man undergoing measurement, arrived, for a dose of 5 cGy, at a detection limit of 52 μg . The use of pulsing helps to reduce the effects of natural neutron background and of alpha emitters inside the detectors. In an interesting modification of this scheme Miola proposed to detect 2.223 MeV gamma rays from capture of released neutrons in a special hydrogenous radiator and in the body itself (fig. 7.2.11).

This modification, albeit less sensitive than the BF system (0.126 mg detection limit at 5 cGy), can be used as a whole body counter for other IVNAA purposes.

The use of bremsstrahlung to measure concentration of deuterium (and by implication, concentration of hydrogen, assuming ratio of $\text{D}/\text{H} = 0.0148\%$) may either rely on measurement of 2.223 MeV recapture radiation or direct observation of neutrons, which may be quite effective in small animals. Because of low sensitivity and thus high dose requirements, this technique is more suitable for animal work.

Ulin and Zamenhof (ref. 71) have analyzed the use of bremsstrahlung for *in vivo* activation analysis of major elements (Table 7.2.4). The technique, as proposed, is based on the deconvolution of the induced radioactivity decay curve.

Figure 7.2.12 shows a typical bremsstrahlung spectrum from a thin target, filtered through 1.6 cm of lead and the cross sections for photoneutron production from major elements (ref. 71).

TABLE 7.2.4 MEASUREMENT OF ELEMENTAL BODY COMPOSITION BY MEANS OF PHOTONUCLEAR REACTIONS

Element	Amount in ICRP Reference Man (70 kg) in g	Activation Reaction	Half-life min	Threshold MeV	Detected particle	Comments
Oxygen	43 000	$^{16}\text{O}(\gamma, n) ^{15}\text{O}$	2.05	15.7	0.511 MeV photons	
Oxygen	43 000	$^{16}\text{O}(\gamma, x) ^{11}\text{C}$	2.05	25.9	0.511 MeV photons	These are interfering reactions in determination of carbon and nitrogen
Oxygen	43 000	$^{16}\text{O}(\gamma, x) ^{13}\text{N}$	2.05	25.0	0.511 MeV photons	
Carbon	16 000	$^{12}\text{C}(\gamma, n) ^{11}\text{C}$	20.4	18.7	0.511 MeV photons	
Nitrogen	18 000	$^{14}\text{N}(\gamma, n) ^{13}\text{N}$	10.0	10.6	0.511 MeV photons	
Phosphorus	780	$^{31}\text{P}(\gamma, n) ^{30}\text{P}$	2.50	12.3	0.511 MeV photons	
Potassium	140	$^{39}\text{K}(\gamma, n) ^{38}\text{K}$	7.70	13.1	0.511 MeV photons	This is an interfering reaction
Chlorine	95	$^{35}\text{Cl}(\gamma, n) ^{34m}\text{Cl}$	32.5	12.7	0.511 MeV photons	This is an interfering reaction
Deuterium	1.04	$^2\text{H}(\gamma, n) ^1\text{H}$	---	2.223	neutron	This reaction is likely to find use only in animal studies
Beryllium	10^{-5} to 10^{-1} g as pulmonary toxic contaminant	$^9\text{Be}(\gamma, n) ^8\text{Be}$	---	1.665	neutron	

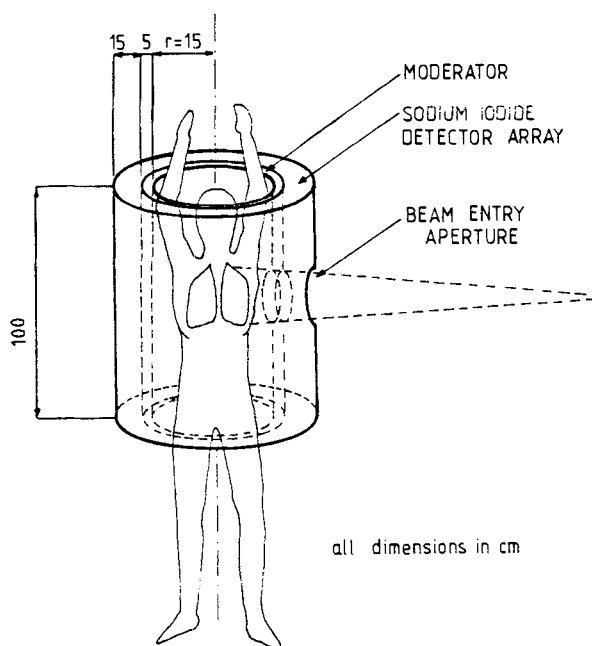


Fig. 7.2.11 Proposed beryllium detection system (ref. 61).

The use of filtering is necessary in order to reduce the intensity of lower energy part of the spectrum, which contributes only to the dose received by the patient (ref. 71).

This yields of induced isotopes as a function of energy are shown in Fig. 7.2.13 (from ref. 71) and it is clear that the optimum value of electron energy is about 35 MeV.

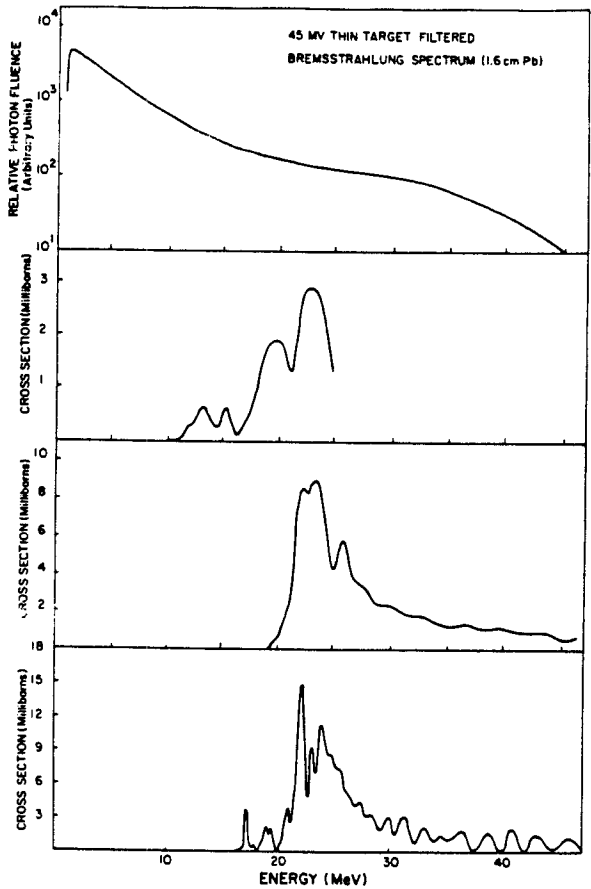


Fig. 7.2.12 Calculated 45 MV bremsstrahlung spectrum and photoneutron cross sections for nitrogen, carbon and oxygen (ref. 71).

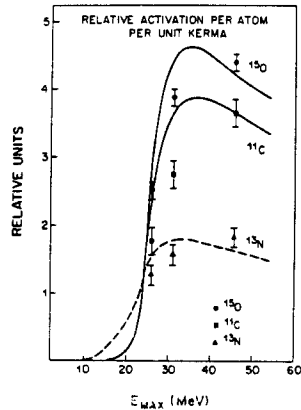


Fig. 7.2.13 Relative activation per unit kerma in muscle for major body elements (ref. 71).

Corrections are necessary for ^{13}N and ^{11}C formed in $(\gamma, 2np)$ and $(\gamma, 3n2p)$ reactions on ^{16}O . It is evident that the availability of fine energy control would make the analysis of data simpler.

Ulin and Zamenhof claim for the photonuclear method fairly small coefficients of variation, 2% for O, 7% for N and 2% for C. The radiation dose necessary to attain this precision is about 2 cGy. The photonuclear method is likely to benefit from the availability of quasi-monoenergetic intense beams of photons, such as produced from interactions between laser light and fast electron beams (reverse Compton scattering) (ref. 72).

7.2.6 Method employing nuclear resonance fluorescence (resonant scattering)

The nuclear resonance fluorescence is a process in which a nucleus absorbs a photon which raises it to its excited nuclear level, and then, after a very short time, the nucleus is deexcited by emission of a quantum of the same energy. The cross section for this process has a strongly resonant character; the so called intrinsic width of the resonance could be fraction of an electronvolt. The use of nuclear resonance fluorescence for purpose of activation analysis in vivo has been proposed by Vartsky in Birmingham (ref. 73) and further developed in Brookhaven (refs. 74-78). In order to excite the desired nuclear level one must use a source of radiation of precisely resonant energy; to excite a nuclear level E with a photon E_g the following relationship must be fulfilled

$$E_g = E + E^2/2Mc^2$$

where M is the mass of absorbing nucleus and c - speed of light.

This relationship is a consequence of a need to compensate for energy taken by the recoiling absorber. Similarly, when a nuclear level decays to the ground state (energy difference E) the emitted gamma ray has an energy E_g , and the emitter recoils:

$$E_g = E - E^2/2Mc^2$$

The excitation of the resonance level can be achieved by a broad spectrum excitation source e.g. by bremsstrahlung, but one should keep in mind that all these photons which do not contribute to the excitation of nuclear fluorescence, however, contribute to the dose absorbed by the patient. One of the methods of slight broadening of a gamma spectral line which just misses the resonance in an absorber, is to heat the source to a temperature at which the Doppler effect will shift the energy of some of emitted photons by a right amount. This may not be always practically possible. The use of centrifuges, ion beams moving in vacuum, and other methods of achieving the resonance were considered, but the most practical method so far was the use of gamma ray source employing a transition through the same levels which are sought to be involved in resonance scattering preceded immediately by a radioactive decay. The Doppler shift is thus caused by a recoil, following an emission of beta particle, neutrino or photon. Gamma rays thus emitted, will have an energy spread depending upon the recoil velocity and the angle between the two successive emissions. This broadened line width, by a large factor exceeds the intrinsic line width, even widened by the thermal motion. In order that this scheme works, the emitter nucleus must continue its recoil motion when the second (i.e. gamma) transition takes place and this is possibly only in the gas phase, far from walls of the container.

In the Brookhaven installation for determination of iron stores in man in vivo (fig. 7.2.14) the source is made of 4 mg of MnCl_2 in an evacuated quartz ampoule exposed to a high neutron flux ($\approx 10^{14} \text{ n.cm}^{-2} \text{ sec}^{-1}$) for about 4 hrs. During the activation analysis procedure the source is heated to 1030°C .

TABLE 7.2.5 MEASUREMENT OF BODY ELEMENTAL COMPOSITION BY NUCLEAR RESONANCE FLUORESCENCE (RESONANT SCATTERING)

Element	Excitation source	Half-life of source	Level excited MeV	Source temperature °C	Detection limit mg/g
Iron	MnCl ₂	2.58 h	0.847	1040	1
Copper	ZnI ₂	244 d	1.116	750	1
Chrome	VCl ₃	3.76 m	1.434	200	0.1

From ref. 76.

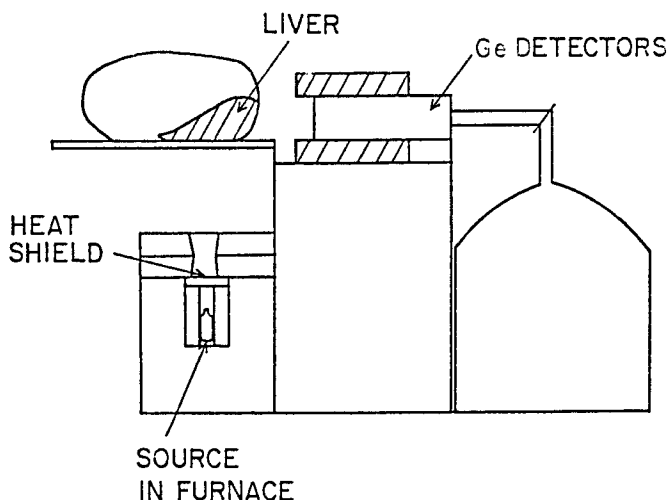


Fig. 7.2.14. Schematic illustration of the source, patient position and the detector for iron measurement by nuclear fluorescence (ref. 76).

Mn which has been formed during exposure to neutron flux, decays by beta emission to the 847 keV level in ^{56}Fe , which subsequently decays to the ground level of ^{56}Fe with a 7 psec half life. This fluorescence radiation is monitored by two large germanium detectors. The results of tests with a phantom of liver are shown in Fig. 7.2.15.

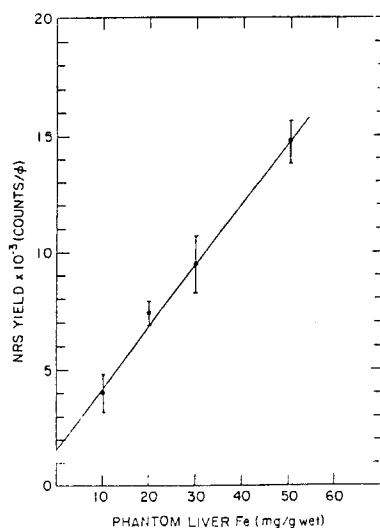


Fig. 7.2.15. Liver iron calibration in Alderson phantom. Nuclear resonance fluorescence yield is given as counts per unit of exciting flux (ref. 78).

The details of the technique of nuclear resonance fluorescence in general can be found in Metzger (ref. 79) and in the book of Deconninck (ref. 80). The latter gives a table of elements suitable for this type of activation analysis.

It is very likely that the technique of nuclear resonance fluorescence will receive a boost from the proliferation of synchrotron X-ray sources. The use of reverse Compton scattering offers a method of generation of quasi-monoenergetic photons, with energies that may overlap the nuclear levels of interest in medically important elements (ref. 72).

The most important improvement expected from the reverse Compton systems is that they are not specific for a given element, but that the energy of photons can be varied in fairly large range by a change in the system parameters.

7.3 FLUX DISTRIBUTIONS IN THE HUMAN BODY FOR FAST NEUTRON IRRADIATIONS

7.3.1 Behaviour of fast neutron beam entering tissue

When a fast neutron beam enters a volume of tissue it undergoes scattering resulting in spreading of the beam. In the collisions with the nuclei of the tissue, the neutrons will lose energy until they become thermalized, unless they are lost earlier in consequence of capture or escape. As a result "pure" fast neutron beam will acquire an admixture of slower neutrons. Furthermore a "halo" will form around the fast beam of a thickness of an order of 14 cm. This halo will contain slowed and thermalized neutrons. This generation of thermal flux from the original fast neutron beam results in the loss of intensity of the original beam. Some idea of the attenuation of the fast flux can be obtained from Figure 7.3.1 which actually shows how energy delivered to the tissue per incident neutron falls down with distance in the phantom.

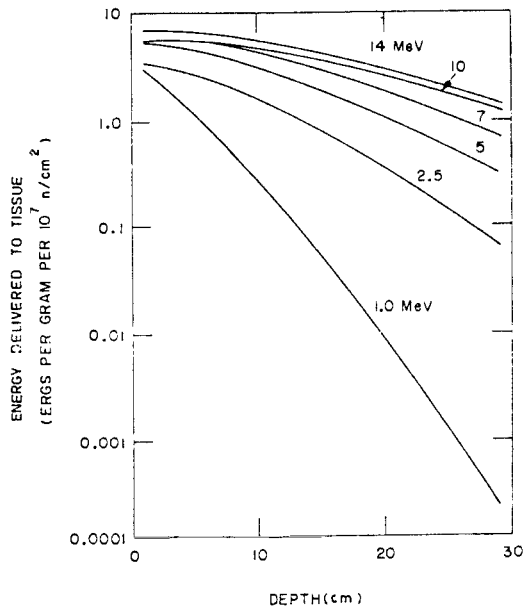


Fig. 7.3.1. Distribution of fast neutrons with depth for a cylindrical phantom (ref. 81).

It is very difficult to obtain satisfactorily uniform fast neutron activation because the spectrum of the fast beam changes with depth. This change has been calculated using neutron transport programme DOT and an example of degradation of fast flux of 14 MeV neutrons on entering a slab of soft tissue is shown in Figure 7.3.2.

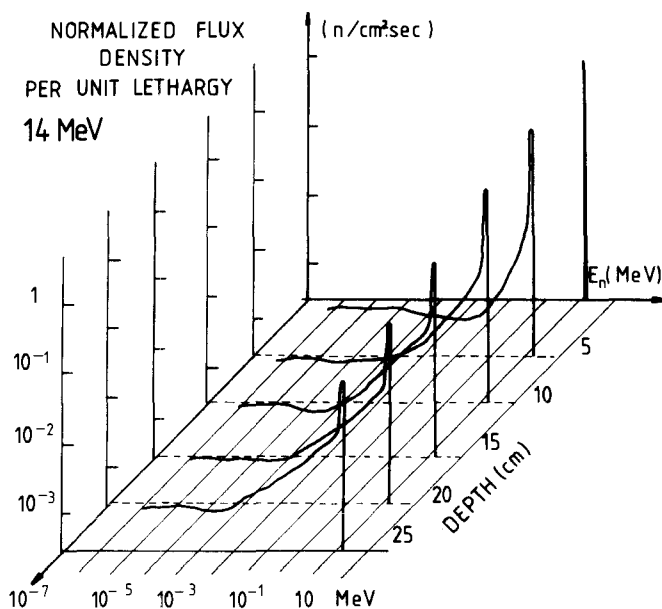


Fig. 7.3.2. DOT calculations of neutron transport in a slab phantom of a narrow cylindrical beam of initial energy 14 MeV.

The accurate determination of fast neutron profile is very difficult and for actual practical purposes often useless. The important information is however brought by the determination of an activation profile using the same reaction which is to be observed *in vivo*. With this approach details of the cross section need not to be known. Such measurements are best performed in a water tank, or even better, with an anthropomorphic phantom.

The quantity which determines the outcome of the process of analysis is the reaction rate profile. The reaction rate at a given depth is given as

$$N(x) = \int_{E_{\min}}^{E_{\max}} \Phi(E, x) \Sigma(E, x) dE$$

where Φ - neutron flux spectrum at a depth x

Σ - macroscopic cross section for the reaction in question.

The integration extends from the reaction threshold to the maximum energy present in the neutron spectrum.

While it is very difficult to obtain satisfactorily uniform fast neutron flux in human body, a large part of activation analysis procedures uses thermal neutron flux for activation.

A typical depth profile for a broad beam of fast non-monoenergetic neutrons entering the body is shown in Figure 7.3.3 (ref. 81). The position of the peak on the curve depends on the initial energy of neutrons. For neutrons in the lower energy range, such information is provided in next section. In that

energy range, for practical application in human activation analysis in vivo, position of the peak does not depend on the shape of the phantom. However, when working with small animals (mice, rats) the thermal flux distribution should be tested experimentally, e.g. with activation foils.

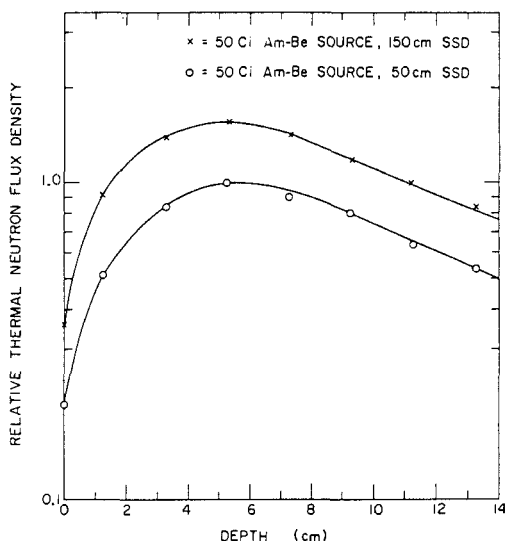


Fig. 7.3.3. Thermal neutron flux depth profile for broad beam incident upon phantom.

For incident neutron energies in the range of MeV there is a marked dependence on the phantom geometry, summarized in Figure 7.3.4.

For so called broad-beam geometry the results of Aceto and Churchill (ref. 82) lead to the following expression

$$\log x = 0.2296 \log E + 0.7263$$

where x - depth in cm

E - neutron mean energy in MeV

For a narrow beam (ref. 50) the position of the thermal peak with depth can be described by

$$\log x = 0.1168 \log E + 0.6269$$

A more uniform geometry can be obtained by bilateral irradiation or by use of premoderators placed in the path of the neutrons before they enter the body (fig. 7.3.5).

Even further improvement can be obtained with neutrons from Am-Be sources or from bombardment of Li target by 10 MeV protons, if both premoderator and cadmium filter are used bilaterally, as shown in Fig. 7.3.6 (ref. 88).

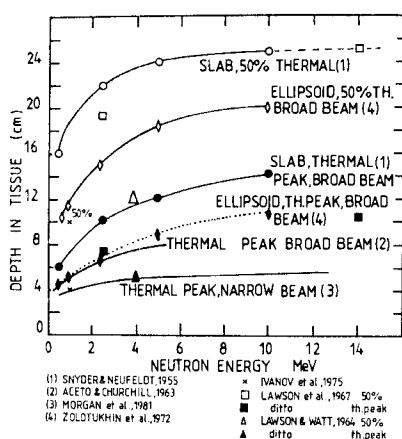


Fig. 7.3.4. Position of thermal peak in tissue as a function of incident neutron energy for different geometry of the beam and the phantom. (1) - ref. 83; (2) - ref. 82; (3) - ref. 50; (4) - ref. 84; X - ref. 85; □, ■ - ref. 86; △, ▲ - ref. 87.

In the animal studies one may face problem of uniformity of irradiation of an animal thicker and broader than 24 cm or so. Using fan shaped neutron beams and multilateral exposures such irradiations are feasible.

7.3.2 Some dosimetric considerations

The neutron kerma per unit of incident fluence can be found from relevant tables in ICRU 26 (ref. 89) and Caswell et al. (ref. 176). See also Figure 7.3.7.

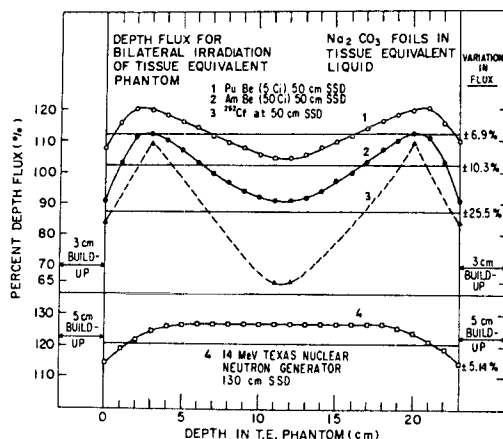


Fig. 7.3.5. Thermal flux distributions for bilateral irradiation and premoderation (build up). From Cohn et al. (ref. 81).

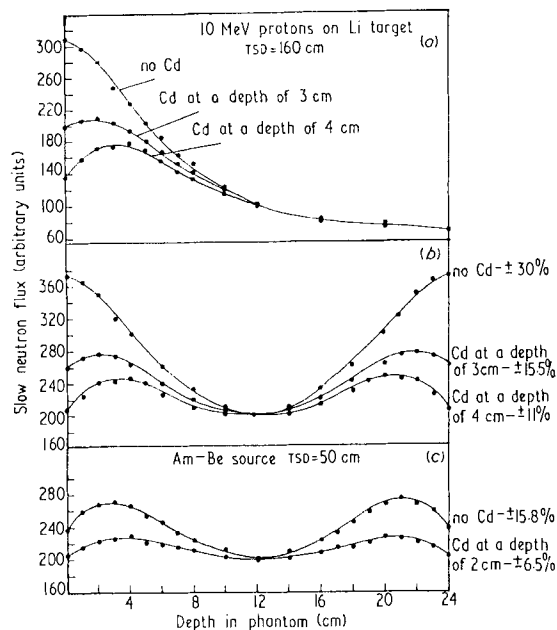


Fig. 7.3.6. Thermal neutron flux distribution produced in 24 cm deep phantom for (a) 10 MeV protons on lithium target, unilateral irradiation; (b) 10 MeV protons on lithium target, bilateral irradiation; (c) Am-Be source, bilateral irradiation. The uniformity of bilateral irradiation with and without cadmium positioned at different depth in the premoderator (4.5 cm thick polyethylene) is shown at the right hand side of the diagram (ref. 88).

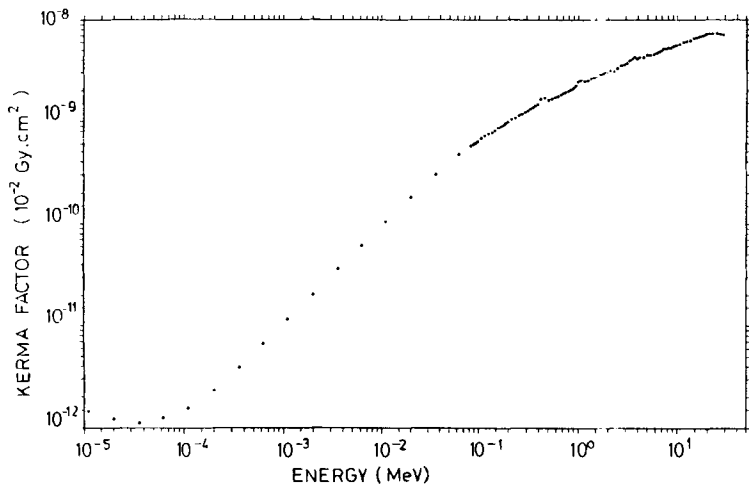


Fig. 7.3.7. Kerma per unit of incident fluence for ICRU Muscle as a function pf energy.

It is evident that the radiation dose per neutron drops rapidly with neutron energy. The average quality factor QF, obtained by dividing the maximum dose equivalent, at any depth in tissue, by the maximum absorbed dose at any depth in tissue, is shown in Fig. 7.3.8, taken from NCRP 38 (ref. 90).

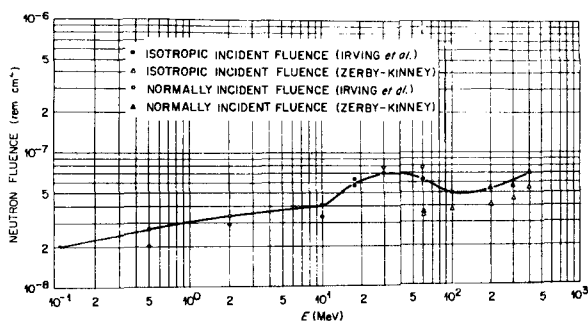


Fig. 7.3.8. Average quality factor (QF) as a function of neutron energy (NCRP 38).

Furthermore, at neutron energies below approx. 5 keV, the Quality Factor QF drops to a value of 2. The behaviour of effective quality factor which changes with the penetration of the neutron beam into the tissue is shown in Figures 7.3.9 and 7.3.10, taken from ref. 90, where a comprehensive information on the depth doses in a cylindrical phantom irradiated with neutron beams of different energies can be found.

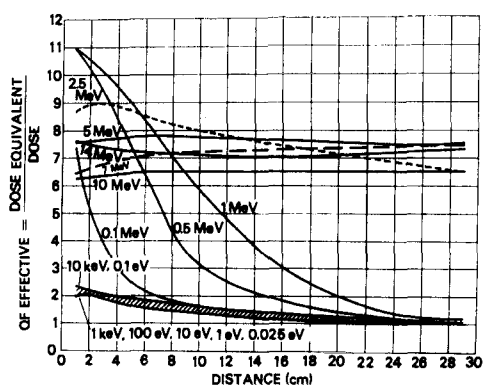


Fig. 7.3.9. Effective quality factor in the direction of the neutron beam as a function of penetration depth for various neutron energies (From ref. 90).

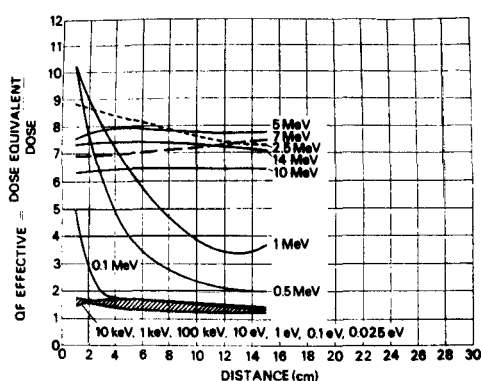


Fig. 7.3.10. Effective quality factor in the direction perpendicular to the neutron beam as a function of penetration depth for various neutron energies (From ref. 90).

Zolotukhin et al. (ref. 84) have produced an atlas with calculated and plotted dose and dose equivalent distributions in transversal sections through a homogeneous elliptical phantom. Some of these distributions are reproduced here (see Figs. 7.3.11 and 7.3.12).

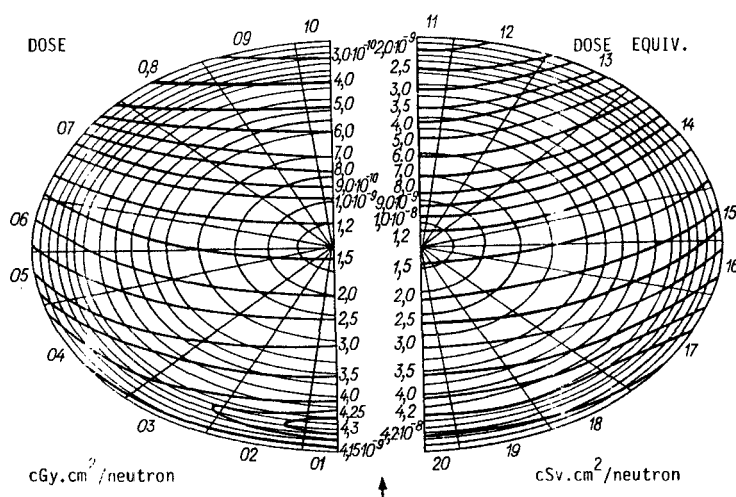


Fig. 7.3.11. Dose (D) and dose equivalent (E) distribution in the ellipsoidal torso phantom. Half-axes of the ellipse are 18 and 12 cm. From Zolotukhin et al. (ref. 84). $E_n = 2.5$ MeV.

It is important to remember that dosimetric measurements on phantoms as well as the transport calculations in cylindrical and ellipsoidal phantoms are only rough approximations to the real distributions in non-homogeneous and irregularly shaped human bodies.

Radiation doses in the practice of IVNAA are, as a rule, expressed in terms of the dose equivalent with the help of quality factor prescribed for

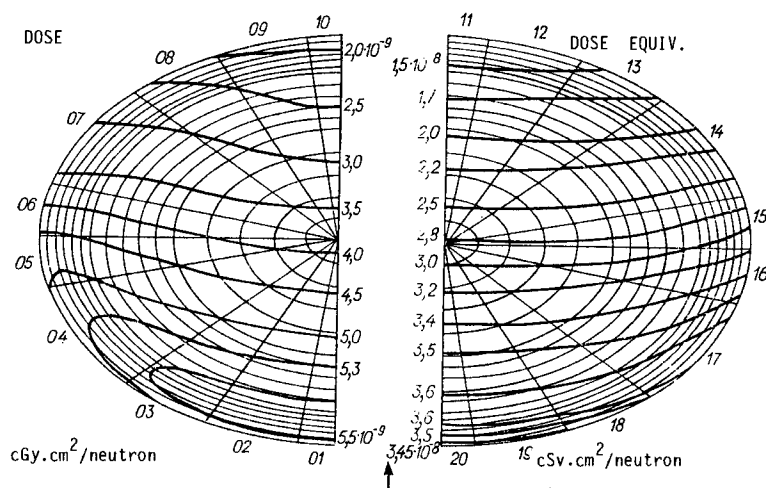


Fig. 7.3.12 As for Fig. 7.3.11 but neutron energy $E_n = 10$ MeV.

neutrons of energy used in the experiments. This is a common practice in activation analysis and makes possible comparison between various implementation of this technique. It is, however, important to remember that in the dose range relevant to the applications of IVNAA, an increase in the Relative Biological Effectiveness, defined for such end-points as lens opacification or induction of mammary carcinomas has been observed with the reduction of absorbed dose (refs. 91,92). This should be taken into account when evaluating benefits and risks associated with the use of IVNAA.

7.3.3 Reported dose levels

A review of radiation doses reported in available literature can be found in Cohn and Parr (ref. 18). The absorbed dose is composed of neutron dose and gamma ray dose. To obtain dose equivalents an appropriate factor must be applied to the neutron dose.

In the measurements of calcium in the whole body the neutron doses were in the range 0.3 - 2.0 mGy depending upon the type of neutron source, required precision and means at the disposal of the research team. In the partial body analysis the doses are generally higher, because there is less calcium to measure and thus for the same precision the higher level of activation is required. For the region of the trunk, the partial body calcium assay requires neutron doses in the range 1.2 - 24 mGy. For calcium in the extremities the corresponding doses are in the range 2 - 24 mGy.

For the total body nitrogen the range of neutron doses was from 0.05 mGy to 1.4 mGy, and the corresponding dose in the trunk segment analysis was about 0.5 mGy.

The activation analysis for cadmium in the liver and kidneys requires neutron doses in the range from 0.17 to 2 mGy. It is likely that the neutron doses required for *in vivo* determination of mercury would turn out to be much higher as well as the doses to lungs in the measurement of their silicon content.

The ICRP has laid the guidelines for the use of ionizing radiations in medical research and these recommendations are reflected in the individual national regulations. Those who plan research in the field of IVNAA are well advised to evaluate the dose and dose-equivalent levels beforehand.

7.3.4 Dosimetry for IVNAA

A good guideline for proper measurement and evaluation of absorbed dose components is provided by the European Protocol for Neutron Dosimetry in Radiotherapy (ref. 93). However, with regard to much lower doses delivered during IVNAA procedures, a larger volume chamber is needed, that would be required in neutron therapy. Measurement of doses produced by 14 MeV neutrons in tissue phantoms were described in detail by Makrigiorgos and Waker (ref. 94). The technique used is, essentially, based on the use of tissue equivalent ion chamber, made of Shonka plastic A-150 and filled with methane based tissue equivalent gas. The nominal sensitive volume of the chamber was 8.38 cm^3 . This chamber measures both neutron and gamma components of the radiation field. A GM detector (Philips Model ZP1300) which is virtually insensitive to neutrons and is enclosed in an energy response compensating shield was the second detector. The determination of the dose components requires solving a system of two equations with two unknowns, after all the calibration and correction factors have been taken into account, (ref. 95). The same group used also a Rossi type counter (0.5 inch., Messrs. Far West Technology Inc.) to determine the microdosimetric event-size spectra. Details of this technique in practical application can be found from Stinchcomb et al. (ref. 100) and in Makrigiorgos and Waker (ref. 94). In measurements with a phantom, the gamma ray fraction accounted for about 15% of the entrance dose and up to 40% at the exit. In the centre of the head and the trunk the gamma ray fractions were about 25%. Additional relevant material can be found in refs. 96-99.

The microdosimetric event-size spectrum (see Fig. 7.3.13) was used to determine the average quality factor QF, using method of Hartmann et al. (ref. 101). The average quality factor in the centre of the phantom was found to be 9.3.

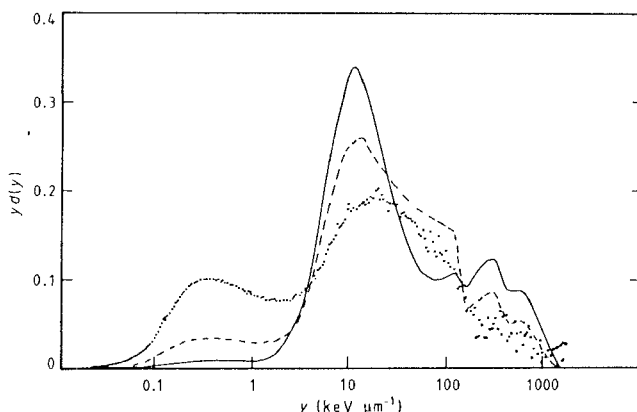


Fig. 7.3.13. Microdosimetric event-size spectra for 14 MeV neutrons (dose distribution per logarithmic interval of linear energy). — at the target; ----- at the collimator mouth; centre of phantom. The equivalent tissue volume diameter: $2 \mu\text{m}$. (ref. 94).

7.4 NEUTRON SOURCES FOR IVNAA

7.4.1 General

The type of neutron source required for IVNAA depends on the nuclear reaction employed in the activation, on the location and size of the irradiated part of the body, including whole body irradiations, and whether a continuous or pulsed source is to be used.

The following types of sources found practical applications in IVNAA:

1. Isotopic sources based on nuclear reactions caused by photons or charged particles.
2. Isotopic fission sources (^{252}Cf).
3. Accelerator sources: cyclotrons, Van de Graafs, neutron generators.
4. Nuclear reactors.

While neutrons from accelerators and certain isotopic sources (Pu-Be, Am-Be) can be used in virtually all applications, sources of low energy neutrons are suitable only for partial body IVNAA, because of limited penetration.

The spectra of neutron sources can be changed by filtration and moderation and, thus, it is in many occasions possible to adopt the source to the task required. The optimization of the neutron spectrum is needed in order to obtain maximum sensitivity of detection per given dose, to minimize interferences, to obtain proper penetration into the body.

Surveys of the neutron sources for activation analysis *in vivo*, together with dose distributions, flux profiles etc. were originally published by Cohn et al. (ref. 81) and by Boddy (ref. 102). A very comprehensive monograph on neutron sources for basic physics research and for various applications has been recently made available (ref. 103).

7.4.2 Low energy neutron sources

The use of thermal neutron reactions has the advantage of large cross sections in comparison with the activation by fast neutron flux. The use of neutron resonance reactions have not been yet proposed for IVNAA.

When reactions with thermal neutrons are employed, almost as a rule, the incident neutron beam has the average energy higher than thermal and the neutron thermal flux is created by the moderation within the body.

Reactors are sources of intense neutron fluxes and have been used in radiobiological experiments for more than three decades. The spectrum of the beam emerging from a reactor depends on the design of the device and on the area from which the beam is extracted. Very rarely the neutron spectrum outside the reactor corresponds to the primary fission spectrum. For the HPRR reactor in Oak Ridge dosimetric studies were published by Hubbel (ref. 104) and by Jones (ref. 105). The neutron depth dose drops to 50% (relative to the surface peak) at a depth of about 5 cm. The conversion factor (cGy/unit of fluence) varies from 2.1×10^{-9} in the region of sub-surface peak to 1.05×10^{-9} at a depth of 6-8 cm. The neutron beam of similar characteristics has been used by Boddy et al. (ref. 106) for the determination of iodine in the thyroid. Reactor beams are, as a rule, contaminated with gamma rays; in the measurements by Boddy et al. (ref. 106) the gamma ray contribution to the total dose was about 9%. This contribution can be reduced by a proper choice of filter, e.g. made of bismuth or lead. A comprehensive survey of information on depth dose, dose equivalent and quality factor for leakage neutron spectra from reactors can be found in a paper by Singh (ref. 107) which also gives information on various types of critical assemblies. It is remarkable that the dose equivalent at a given depth in the tissue changes by a factor of 8 between the highly degraded and "raw" neutron spectra. This is an indication of the extent to which the filtering of the primary neutron beam can change the dosimetric characteristics of radiation.

A detailed study of depth dose characteristic of neutrons from fission sources modified by filtration through low-Z and high-Z materials has been

published by the same group (refs. 108-109). Filtration by high-Z materials, which lowers the effective neutron energy, has an almost imperceptible effect on the depth dose distribution and on the distribution of the thermal flux. The absolute values of the conversion factors are, however, altered. E.g. the fission neutron spectrum filtered through 30 cm of iron has the conversion factor of 1.6×10^{-9} cGy/unit fluence while the same beam which passes through only 5 cm of Fe has the conversion factor for neutron dose of 3.2×10^{-9} cGy/unit fluence. The dose equivalent is reduced even to a larger extent owing to the "softening" of neutron spectrum. When materials with low-Z are used as neutron beam filters the effect is opposite: the spectrum hardens. This effect is almost the same whether the filter is made of water, polyethylene or materials of similar composition. As the neutron beam "hardens", its average energy increases i.e. the lower energy neutrons are being preferentially removed. The medium-Z filters (concrete and beryllium) act similarly to those made of high-Z materials.

The ability to modify the neutron spectra from critical assemblies and fission sources is of great practical importance in IVNAA because it offers a method to tailor the penetration of the neutron beam to suit the experimental conditions, with a view of minimizing the dose imparted to the body. The quality factor and RBE for degraded fission spectra have been discussed by Murthy (ref. 110). Neutron beams from a fast reactor HARMONIE are described in ref. 111. The neutron dose drops with the depth in a phantom with a halving value of about 5 cm. A block of steel (high-Z) reduces this halving thickness to about 3.4 cm. Reactor neutrons of higher energy and, thus, deeper penetration can be obtained from a U-235 converter exposed to the original reactor neutron beam. Such an arrangement is provided in JANUS reactor in Argonne (ref. 112). The neutron dose and thermal flux as a function of depth in the phantom are given in Fig. 7.4.1. The conversion factor in the irradiation facility is in the range $(1.94-1.37) \times 10^{-9}$ cGy/unit fluence.

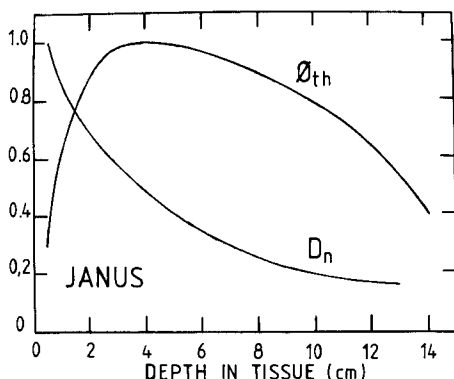


Fig. 7.4.1. Neutron dose and thermal flux from JANUS reactor as a function of depth in the phantom (ref. 112).

The thermal beam from a reactor has very poor penetration, but may still find use in the activation of Ca in bone structures located immediately beneath stretched skin. The conversion coefficient for the total dose is about 4.5×10^{-10} cGy/unit fluence and QF is about 2 (see Fig. 7.4.2).

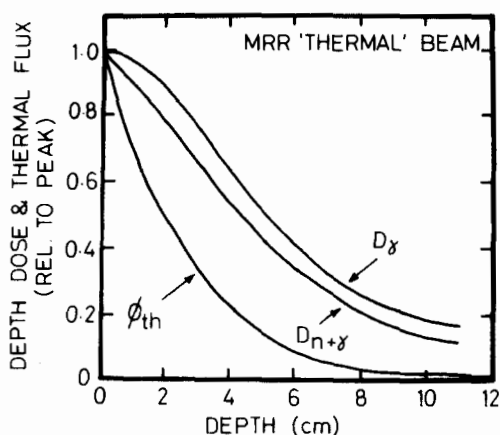


Fig. 7.4.2. Depth doses of gamma rays and neutrons in the "thermal" beam from Medical Research Reactor in Brookhaven (ref. 113).

The epithermal i.e. cadmium filtered beam from the same reactor (MRR in Brookhaven) has much better penetration properties and, effectively, the same conversion factor (ref. 114) (see Fig. 7.4.3).

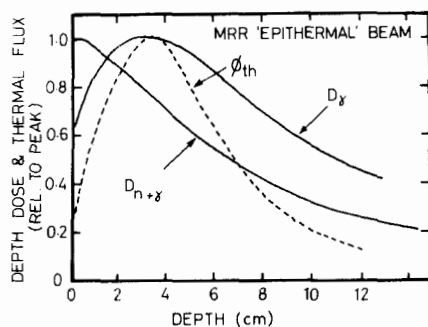


Fig. 7.4.3. Depth doses of gamma rays and neutrons in the "epithermal" beam from Medical Reactor in Brookhaven. The thermal flux distribution is also shown (ref. 114).

This type of beam can be used for Ca measurements in the skull and in the extremities. Zamenhof et al. (ref. 115) investigated properties of low neutron beams including a 37 eV beam as well as modified neutron beams produced by ^{252}Cf (moderation by a 30 cm thick layer of heavy water and further optional filtration with ^{10}B) (see Fig. 7.4.4). The rationale for this approach is that there is a minimum of kerma per unit fluence at neutron energies of about 2-60 eV. For 55 eV the conversion factor is 7.4×10^{-11} cGy/unit fluence.

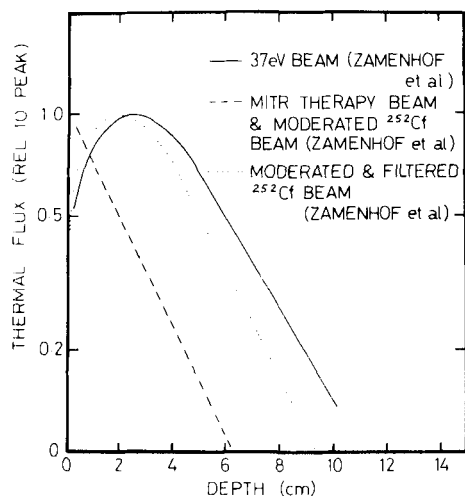


Fig. 7.4.4. Thermal flux as a function of depth in the tissue for various neutron beams considered by Zamenhof et al. (ref. 115).

TABLE 7.4.1 FILTERED NEUTRON BEAMS.

Filter material	Neutron mean energy (keV)	Dose equivalent per unit fluence (cSv)
¹⁷⁰ Er	0.060	1.16×10^{-9}
¹⁸⁴ W	0.160	1.16×10^{-9}
⁶⁸ Zn	0.40	1.16×10^{-9}
natSc	2.0	9.58×10^{-10}
⁶⁰ Ni	4.0	8.96×10^{-10}
⁵⁸ Ni	14.0	1.11×10^{-9}
natFe	24.0	1.73×10^{-9}
natS	74	4.48×10^{-9}
natSi	120	6.94×10^{-9}

A significant improvement in the properties of reactor beams is brought by the use of quasi monoenergetic neutrons obtained by filtration of primary beams. This process uses the dips and peaks in the scattering cross section of filter elements (refs. 116-120).

Figures 7.4.5 and 7.4.6 show the thermal flux distributions for 2 and 24 keV beams respectively.

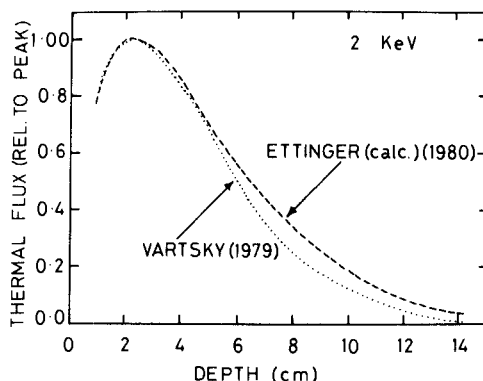


Fig. 7.4.5. Thermal flux as a function of depth in tissue. (Vartsky, priv. comm., measured in HFBR reactor, Ettinger, transport calculations).

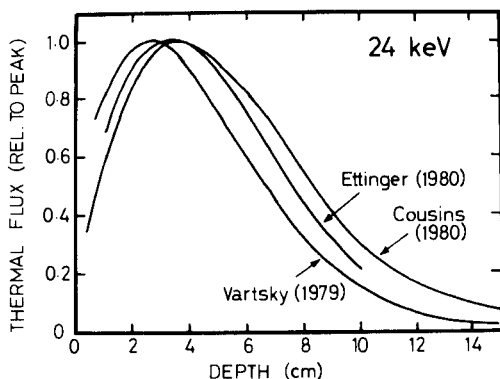


Fig. 7.4.6. Thermal flux as a function of depth in tissue for 24 keV beam. (Vartsky, priv. comm., measured in HFBR reactor, Brookhaven; Ettinger, measurements with Sb-Be source; Cousins et al., 1980, filtered reactor beam, ref. 121).

Cousins et al. (ref. 121) demonstrated that with a filtered 25 keV beam a very high detectability of Ca in spine can be achieved, with dose sparing by a very large factor in comparison with techniques using Am-Be source or cyclotron produced neutrons (fig. 7.4.7). A typical future application of a filtered low energy neutron beam is in measurements of mercury in the brain, making good use of a very high neutron capture cross section (2000 barn for ^{199}Hg). In order to attain an almost uniform detection sensitivity within the brain, a trilateral irradiation may be necessary. The skull calcium can be conveniently measured with a 2 keV beam, with a very good dose sparing to the eyes (fig. 7.4.8).

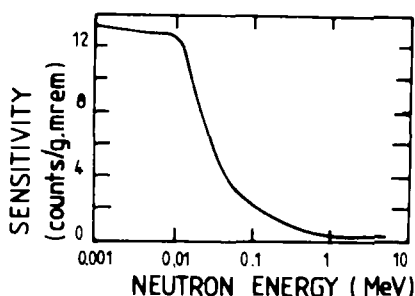


Fig. 7.4.7. Detectability of calcium in spine as a function of incident energy of neutron beam (ref. 121). Very similar relationship applies to the detection of calcium in skull.

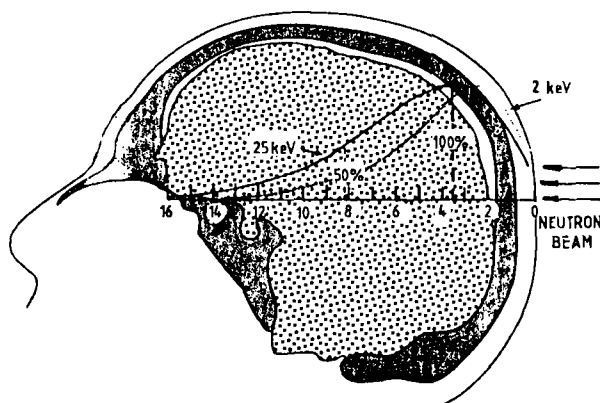


Fig. 7.4.8. Thermal flux profiles superposed on the skull cross-section for 2 keV and 24 keV neutron beams.

It is desirable to have the thermal neutron fluence peak in the region of the feature which is the object of IVNAA. The position of the thermal neutron fluence peak in the tissue, measured from the skin, is shown in Figure 7.4.9 based on observations of several authors. The theoretical calculation of the peak position for neutron energies below approx. 100 eV suffers from errors arising from lack of data on slowing down and thermalization of neutrons in real tissue.

^{252}Cf is an isotope undergoing spontaneous fission. Its neutron yield is 2.34×10^{12} n/s per gram or 0.116 n/s per Bq of total activity. Its spectrum is shown in the next section.

The half-life of ^{252}Cf is 2.65 years and the average neutron energy is 2.14 MeV. The spectrum is well described by the formula.

$$N(E) = \text{Const.} \times E^{-1/2} \exp(-E/t)$$

where t ("temperature") has a value of 1.424 MeV.

Boddy et al. (ref. 122) has used ^{252}Cf sources for partial body activation analysis by means of thermal neutron reactions. A very detailed analysis of properties of neutron beams from ^{252}Cf by Zamenhof et al. (ref. 115) and by Evans et al. (ref. 52) made possible the design of irradiators for IVNAA (see

Fig. 7.4.10). Cf. also ref. 132.

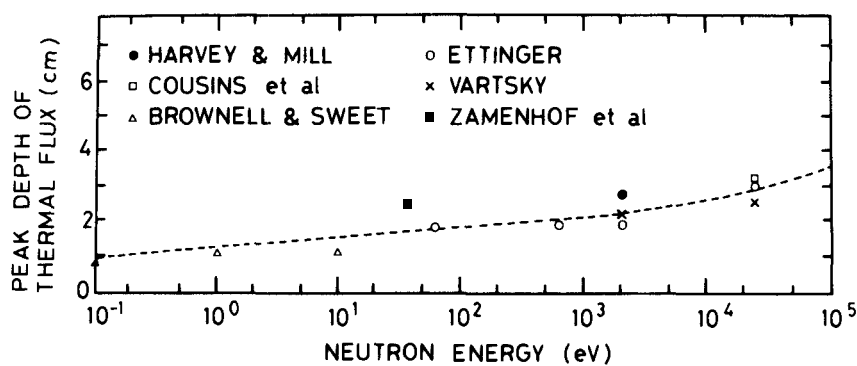


Fig. 7.4.9. Position of the thermal peak in the tissue as a function of incident neutron energy.

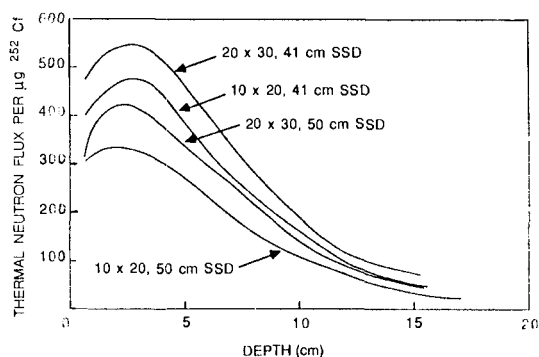


Fig. 7.4.10. The thermal neutron flux, per μg of ^{252}Cf versus the depth in the phantom for several collimator geometries (ref. 52).

Morgan et al. (ref. 50) have demonstrated that fission neutrons from ^{252}Cf sources can effectively replace Pu-Be and Am-Be sources in IVNAA systems for the detection of cadmium and, by implication, in those applications of IVNAA in which the limited penetrating power of ^{252}Cf is adequate (see Fig. 7.4.11).

Despite the differences in the average neutron energy from Pu-Be and Cf sources (3.9 MeV and 2.3 MeV correspondingly) the thermal flux profiles are very similar. A very accurate data exist on the dose distribution in the radiation field of ^{252}Cf , provided by Piesch (refs. 123,124).

7.4.3 (α , Neutron) sources utilizing radionuclides

There exists a whole variety of neutron sources based on reactions of (α , n) type. The source of alpha particles can be chosen according to their energy in a broad range of half lives (see Table 7.4.2).

At present most commonly used in neutron sources are ^{241}Am , ^{210}Po and ^{238}Pu . The commonest target material is Be, but neutron sources with boron, fluorine, and lithium targets were fabricated and their properties investigated (ref. 175) (see Table 7.4.3).

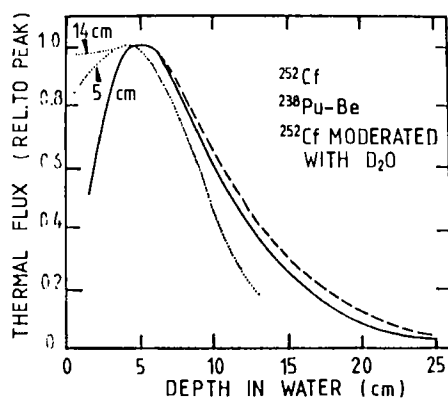


Fig. 7.4.11. Thermal flux profiles for Pu-Be and ^{252}Cf neutron sources (ref. 50). A profile for ^{252}Cf source moderated with D_2O (5 and 14 cm thick) is shown for comparison.

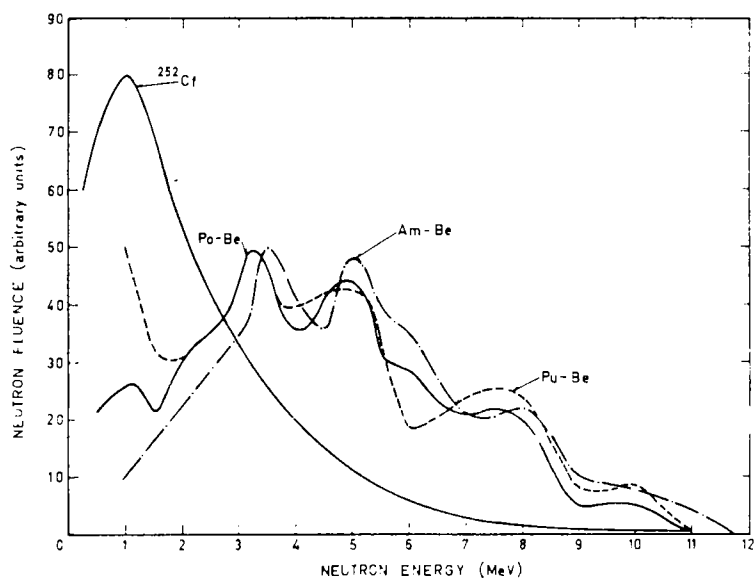


Fig. 7.4.12 Energy spectra of some neutron sources (ref. 102).

TABLE 7.4.2 SOME ALPHA EMITTERS SUITABLE FOR (α, n) SOURCES.

Nuclide	Half-life	Alpha particle energy (MeV)	Neutron yield on Be per 10^6 alphas
Plutonium-239	24 000 y	5.14	65
Plutonium-238	87.4 y	5.48	79
Polonium-208	2.93 y	5.11	62
Polonium-209	103 y	4.88	50
Polonium-210	138 d	5.31	73
Americium-241	433 y	5.48	82
Curium-244	18 y	5.79	100
Curium-242	162 d	6.10	118
Radium-226 + daughters	1602 y	multiple	502
Actinium-227 + daughters	21.6 y	multiple	702

TABLE 7.4.3 AVERAGE ENERGIES AND FLUENCE-TO-KERMA FACTORS FOR (α, n) SOURCES.

Type of neutron source	\bar{E} (MeV)	$k \times 10^7$ (Gy cm ² /n)
Pu - Be	3.9	3.52
Am - Be	4.5	3.86
Po - Be	4.3	3.85
Ra - Be	3.8	3.40
Po - ¹⁰ B	2.2	2.97
Po - ¹¹ B	2.9	3.48
Po - ¹⁸ O	2.3	3.15
Po - F	1.3	2.45
Pu - F	1.1	2.26
Po - Li	0.36	1.23

(ref. 175).

Neutron sources in which lithium is the target for alpha particles are characterized by "soft" spectrum, of particular interest to irradiations of shallow penetration depth (see Fig. 7.4.13).

7.4.4 Photoneutron sources utilizing radionuclides

The threshold for production of photoneutrons is 1.665 MeV for ⁹Be and 2.223 MeV for D. For other stable nuclei this threshold is much higher, of an order of 10-25 MeV. For practical use in activation analysis in vivo only two gamma ray sources are suitable: ¹²⁴Sb (60.2 d) and ⁸⁸Y (107 d). Y-Be source emits essentially neutrons with energies of 949 and 152 keV. Sb-Be source produces monoenergetic neutrons with energy of ≈ 24 keV.

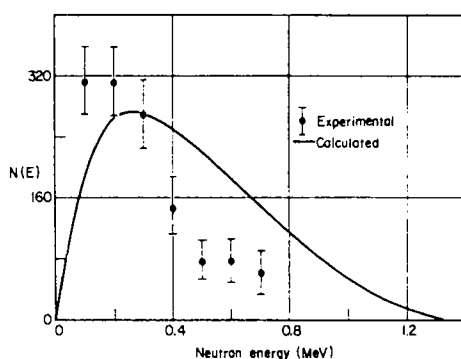


Fig. 7.4.13. ^{210}Po -Li neutron spectrum. The experimental spectrum has a maximum at about 180 keV (ref. 175).

7.4.5 ACCELERATOR NEUTRON SOURCES

A number of low threshold nuclear reactions can be used to produce neutrons in laboratories equipped with small accelerators (see Table 7.4.4)

The actual neutron energy depends both on the energy of the charged projectile and on the angle of emission in relation to the direction of the charged particle, as can be seen from Figure 7.4.14. It should be remembered

TABLE 7.4.4 THRESHOLDS OF NUCLEAR REACTIONS PRODUCING NEUTRONS IN SMALL ACCELERATORS.

Reaction	Threshold for forward production (MeV)
$^7\text{Li}(p, n)^7\text{Be}$	1.882
$^3\text{T}(p, n)^3\text{He}$	1.019
$^{12}\text{C}(d, n)^{13}\text{N}$	0.328
$^2\text{D}(d, n)^3\text{He}$	0
$^3\text{T}(d, n)^4\text{He}$	0

that the energy spread of the neutron beam depends on the thickness of the target, energy spread of the charged particle beam and on the solid angle in which emission is considered. More details can be found in De Pangher and Tochilin (ref. 175) and in Uttley (ref. 126).

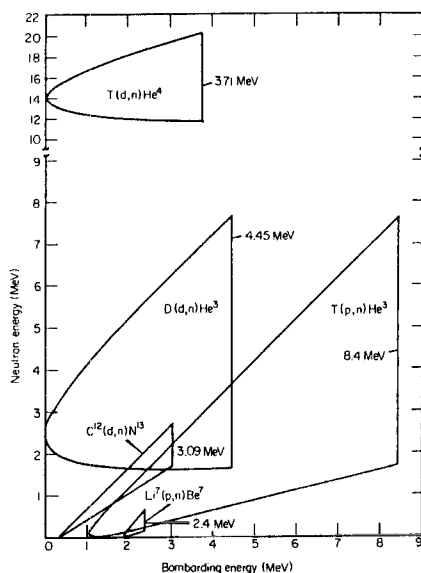


Fig. 7.4.14. Ranges of neutron energies available from the five most commonly used monoenergetic neutron reactions. The neutron energy is maximum at 0° and minimum at 180° . Vertical lines indicate bombarding particle energies at which competing neutron producing reactions become possible (ref. 125).

A particularly simple and relatively inexpensive source of neutrons is neutron generator utilizing the last two reactions in Table 7.4.4. Even though these reactions do not exhibit a threshold, the neutron yield increases with bombarding beam energy. A satisfactory operation is achieved at an accelerating potential of 150 kV. Neutron generators are essentially of two types: with sealed tube or with demountable tube assembly. The first type has an advantage of compactness, whilst in the demountable type it is possible to replenish exhausted targets. A detailed discussion of problems associated with neutron generators can be found in Barschall (ref. 127).

As it can be seen from Figure 7.4.14, small neutron generators with an accelerating potential of the order of 150–400 kV produce almost monoenergetic neutrons at 14 MeV (D-T reaction) and a slightly more diffused spectrum in the vicinity of 2.6 MeV (D-D reaction).

However, neutron sources with broad energy spectrum find very often use in IVNAA. An example of such source is a thick target bombarded with accelerated particles from a cyclotron. Both lithium and beryllium targets were used, beryllium having an advantage of robustness and higher melting point. Typical neutron spectra from Li and Be targets are shown in Figure 7.4.15.

Fig. 7.4.16 shows neutron yields in the projectile energy range up to 10 MeV. The mean energies of neutrons and the yields from beryllium targets in a broader energy range available from compact cyclotrons are shown in Figures 7.4.17 and 7.4.18.

Low energy neutrons produced by accelerators, with a possibility of an

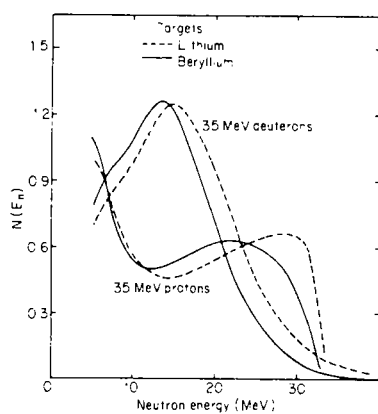


Fig. 7.4.15. Typical neutron spectra from thick targets of Li and Be. (ref. 128).

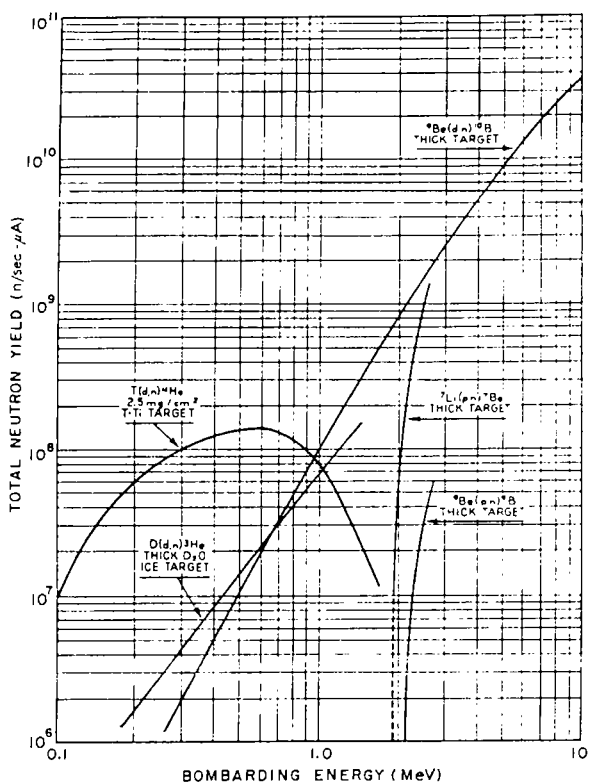


Fig. 7.4.16. Total neutron yield plotted against bombarding energy for some reactions utilized in accelerator sources (High Voltage Engineering Corp.).

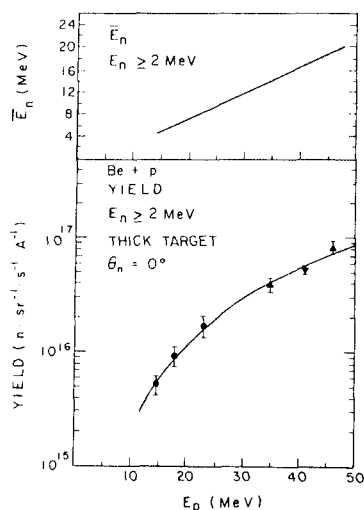


Fig. 7.4.17. Calculated thick target neutron yield and the average neutron energy at 0° from the $p + \text{Be}$ reaction (ref. 129).

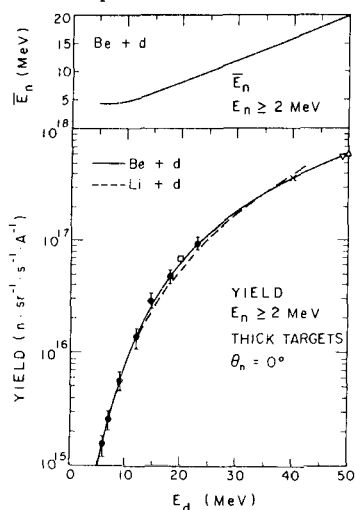


Fig. 7.4.18. Experimental thick target neutron yield and the average neutron energy at 0° from the $d + \text{Be}$ reaction (ref. 129).

electronic control of neutron beam energy, are of particular interest to partial body IVNAA, because they make possible to achieve variable depth penetration. Examples of nuclear reactions producing these low energy beams are given in Table 7.4.5. (ref. 126).

The use of (α, n) nuclear reaction for production of photoneutrons by means of electron accelerators, (linacs, betatrons) while possible in principle, is beset with difficulties because of the need to filter off the photon component. Furthermore conflicting requirements for the beam target and neutron source geometry have not been effectively reconciled so far. References to this type of source can be found in Berger (ref. 130).

TABLE 7.4.5. REACTIONS PRODUCING MONOENERGETIC NEUTRONS IN THE KEV ENERGY RANGE.

Reaction	Threshold keV	Energy range of monoenergetic neutrons keV
$^{45}\text{Sc}(p, n)^{45}\text{Ti}$	2909	5.6 - 52
$^{51}\text{V}(p, n)^{51}\text{Cr}$	1564	2.36 - 786
$^{57}\text{Fe}(p, n)^{57}\text{Co}$	1648	2 - 1425

7.4.6 Pulsing of neutron flux

Isotopic neutron sources emit neutrons continuously and, as such, they cannot be pulsed. However, it may be possible to obtain an interrupted neutron beam by mechanical means e.g. by application of a fast chopper.

Accelerator neutron sources are fairly easy to operate in a pulsed mode. There are essentially two types of pulsing: pre-acceleration and post-acceleration. Pre-acceleration variety is in effect pulsing of the ion source by commutating the supply potentials or by using electrostatic gating of the low energy ion beam. In neutron generators the ion source is often of the radio frequency type. Pulsing of the radiofrequency waveform results in a pulsed beam.

Pulsing of the ion sources is capable of producing pulses of length varying from infinity down to about $10\ \mu\text{s}$. Below that value the pulsing may become unreliable and the waveform of the beam current may deviate significantly from the rectangular shape. Post-acceleration pulsing is an interruption of the beam at its full energy. As a rule, this is done by means of an electrostatic deflector placed in the beam transport system. Post-acceleration pulsing is expensive, occupies space in the beam transport line, but it can be made very fast, with rise and cut-off times well below $1\ \mu\text{s}$. A full discussion of pulsing systems can be found in Ettinger (ref. 131). It is important to notice that the pre-acceleration system of pulsing makes possible to operate an accelerator in a regime characterized by a low average beam current, but a high peak current value, which otherwise could not be sustained in a continuous operation.

7.4.7 Neutron source intensities for IVNAA

As a result of the procedure involving an exposure of a patient to neutron flux and detection of a number of photons arising as a consequence of irradiation one expects to collect a number of counts corresponding to the species of nuclei which are being determined. The first step in the process of finding the required source intensity is to decide on the statistical error of the final result, which is admissible for the user. Making some reasonable assumptions concerning the background one can arrive at the minimum number of counts, which will produce the expected statistical accuracy of the result. Then from the overall (i.e. geometrical and intrinsic) efficiency of the detector system one can arrive at the minimum number of photons reaching the detector. A correction is needed for the absorption of photons in the body. It is necessary to have an estimate of the total amount of an element which one is aiming to determine. The knowledge of isotopic fraction of the isotope involved

in the measurement and of the effective cross section makes possible to find the total neutron fluence which is required. This neutron fluence must be then corrected for the losses due to scattering, moderation and absorption in the body in order to arrive at the incident neutron fluence. It is important to take also into account any pre-moderation or filtering. The neutron yield which is required from the source determines the duration of the exposure and, perhaps, the source to skin distance (SSD) of the source.

This approach is usually full of uncertainties because the degree of thermalization is rarely known precisely as well as the spectrum of the neutron beam at various depths in the tissue. It is therefore necessary to perform phantom measurements in a water tank to arrive at the correct values of required incident fluence.

A good guide is provided by a compilation IAEA RL/131 (ref. 19) which lists the incident neutron flux density reported for a large number of IVNAA installations. For the whole body measurements this flux density lies in the range from $3 \times 10^3 \text{ n cm}^{-2} \text{ s}^{-1}$ (determination of carbon in the whole body, University of Leeds) for the time of exposure 1800 s, to $2 \times 10^7 \text{ n cm}^{-2} \text{ s}^{-1}$ and time of exposure of 8 s (Sloan Kettering Cancer Center, NY) used for determination of Ca, Na and Cl. For part-body irradiations in determination of cadmium the total incident fluences are in the region of 10^7 n cm^{-2} . Similar values are reported for part-body measurements of calcium.

It is obvious that these values reflect the varying degrees of total counting efficiency of radiation detectors and the degree of optimization of incident beam. Probably the most sensitive whole body counter in the world, installed in the Brookhaven National Laboratory (USA) is associated with an irradiation facility using only $1.5 \times 10^7 \text{ n cm}^{-2}$ for the whole body measurement of Ca, while the installation at the University of Washington, Seattle, for identical type of measurement requires a fluence of $2.3 \times 10^8 \text{ n cm}^{-2}$.

The actual neutron yields which are required depend upon the skin-to-target distance, the solid angle of collimator and also on an optional premoderation. For the whole body irradiations with cyclotrons the source yields are in the range from $2 \times 10^{10} \text{ n s}^{-1}$ to 10^{11} n s^{-1} . For partial body irradiations a typical value is between 10^9 and $2 \times 10^7 \text{ n s}^{-1}$.

7.5 THE USE OF PULSED BEAMS

7.5.1 Phenomenological description of pulsed neutron beam behaviour

When a pulse of fast neutrons is injected into a human body the process of moderation and ultimately thermalization starts at once. In the human body, which has dimensions of the same order as characteristic lengths used to describe the process of thermalization and scattering, a very large number of neutrons will never reach thermal energies, but will escape with degraded energy. This is particularly true of the head and the extremities. During the process of slowing down the intensity of reactions produced by thermal neutrons will increase, followed by decay caused by absorption of thermal neutrons and neutrons and their escape. At the same time, the intensity of reactions produced by fast fluence will quickly drop to zero after the end of the neutron pulse. This is illustrated in Figure 7.5.1 (ref. 42) which shows the experimentally observed thermal neutron flux in a water phantom, as a function of time, following an injection of a neutron burst.

The separation of fast and slow components of the beam in time and the corresponding effect on gamma ray intensity is shown in Figure 7.5.2. This figure includes also the effect of induced radioactivity in the object, detectors etc. which has a half-life much longer than the interval between the beam pulses.

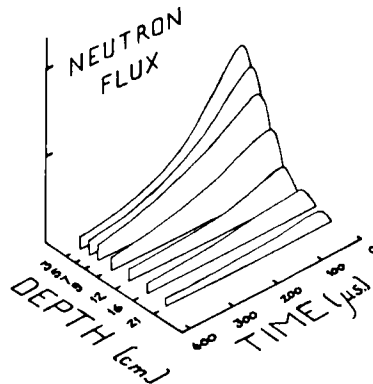


Fig. 7.5.1 The thermal neutron flux, measured with a BF_3 detector in a tissue equivalent phantoms as a function of time after a beam pulse. Neutron beam energy 2.6 MeV average, maximum energy 6.0 MeV (ref. 42).

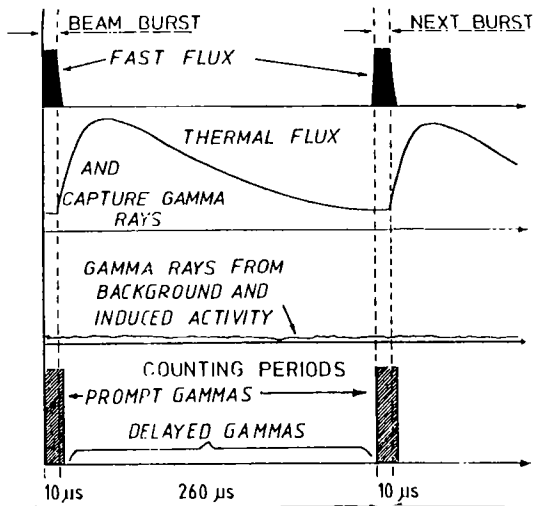


Fig. 7.5.2 Fast and slow components of the neutron flux in the body and the corresponding production of the gamma rays (modified from Miola, ref. 61).

7.5.2 Experimental investigations of beam pulsing for IVNAA

The first recorded use of neutron beam pulsing for the purpose of IVNNA is that of Birmingham group (refs. 42-44, 47). Experimental studies and Monte Carlo simulations of the use of gamma rays from neutron capture *in vivo* were reported in detail by Zamenhof et al. (ref. 55). The possibility of use of beam pulsing for the detection of oxygen and carbon *in vivo* was reported by Biggin et al. (ref. 42) and the same principle was used for detection of silicon (ref. 60-61). Miola has also performed an extensive study on the properties of small size thermalizing phantoms, in order to obtain an insight into the techniques of IVNAA based on the use of pulsed neutron beams.

The first pre-requisite for the use of pulsed beams is the presence of an adequate pulsing system in an accelerator. So far, there are no practical

pulsing systems for isotopic neutron sources. A detailed description of number of pulsing systems, for use on cyclotrons is contained in the thesis of Ettlinger (ref. 131). Neutron generators as a rule are provided with a pulsed ion source. The type of an electrostatic beam pulser, used in Brookhaven (see Figure 7.5.3), can be added to almost any existing accelerator.

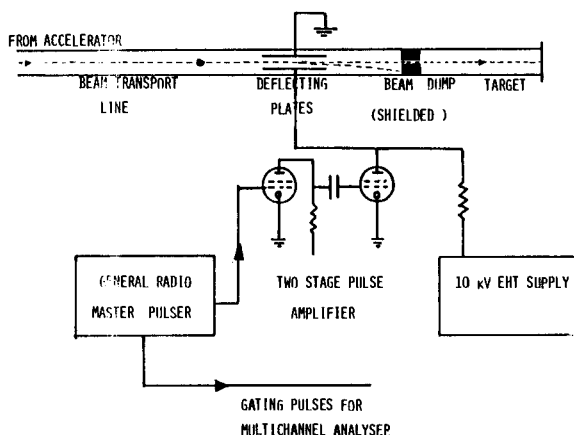


Fig. 7.5.3 The principle of the post-acceleration deflection beam pulsing used with the Brookhaven Tandem Accelerator (ref. 61).

7.5.3 Time dependent neutron flux in IVNAA

The behaviour of a neutron pulse injected into a moderating medium has been studied from the point of view of reactor physics and technology and detailed reports on various moderating systems are available (refs. 133, 144). The processes of slowing down and thermalization are well understood for materials and geometries used in nuclear engineering (refs. 134-137) but the moderating and particularly thermalizing properties of tissues and whole organs are poorly understood.

The measurements of time dependent neutron flux in reactor systems are not directly applicable to the problems of IVNAA owing to the different physical size of the media into which the neutrons are injected. In the systems which have the characteristic length comparable with the slowing down, diffusion and thermalization lengths, the phenomenon of diffusion cooling i.e. preferential escape of more energetic neutrons from the system, affects the neutron spectra and density distributions. The important physical factors for evaluation of the potential of pulsed method in vivo is the shape of the build-up curve and the duration of the thermal flux in the system (reverberation time).

The first quantity determines how well the fast flux, and the gamma rays from fast neutron processes, i.e. inelastic scattering, prompt reaction gammas, short-lived isomers, can be separated from the thermal flux and its interactions in time. The second quantity tells us what is the minimum period between the neutron bursts if we want to reap the full advantages of the neutron beam pulsing. In the first respect, the results of Zamenhof et al. (ref. 55) gave the build-up curve based on a rather small number of points in the interval 0-20 μ s from the beginning of the beam pulse. Slowing down of fast neutrons (average energy of 2 MeV) was described by Camarda (ref. 138). For slowing down in homogeneous medium from 2 to 1 MeV the interval was only 52 ns. The formulas given by Camarda for water are, for the final energy E

$$t = 38/(E)^{0.35} \quad \text{for } E \text{ larger than } 15 \text{ keV,}$$

$$t = 54/(E)^{0.5} \quad \text{below } 15 \text{ keV}$$

(E in keV, t in ns).

Miola and Ettinger (ref. 139) measured the build-up and decay of thermal fluence in moderating spheres exposed to 2.5 and 14 MeV neutrons from a neutron generator. The detector was lithium glass scintillator. A typical time dependence of the observed flux is shown in Figure 7.5.4 (ref. 139).

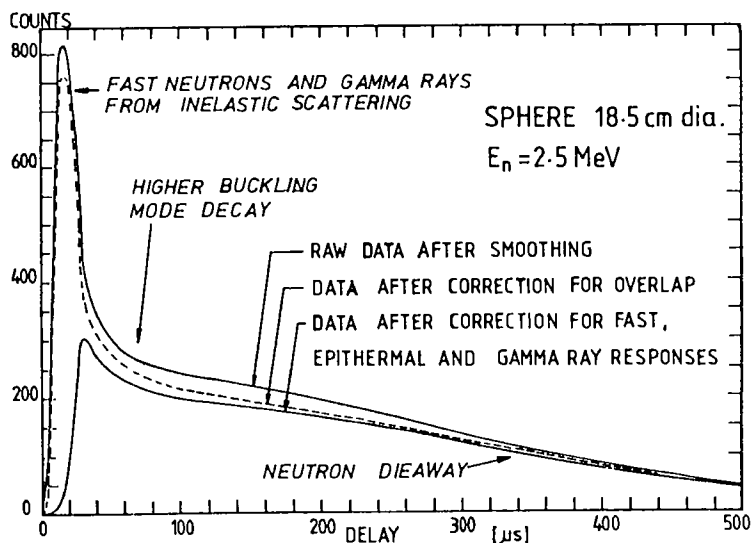


Fig. 7.5.4 Response of a ^6Li detector to a neutron beam burst when placed inside a paraffin wax sphere, 18.6 cm in diameter (ref. 139).

The time needed for a thermalization of a fast neutron has been measured by several authors. In water, placed in a container of large dimensions compared with the thermalization length, this time has been measured to be within the range of 6–10 μs (refs. 140–142). How the time of thermalization varies in various tissues is not yet known, and the theoretical calculations appear not to have been attempted. In the initial period following the injection of the pulse into the medium the fate of neutron fluence depends upon the geometry of the medium; the molecular effects on the thermalization appear only after some time has passed. Figures 7.5.5 and 7.5.6 show the decay of thermal neutron flux following a 14 MeV neutron pulse, for different diameters of moderating spheres.

Measurement of the decay times of thermal neutron flux performed by different authors gave slightly discrepant results (Figure 7.5.7).

The origin of this discrepancy may lie with the different moderating material or slightly different geometry.

The use of pulsing as means to separate prompt and delayed events requires knowledge of the thermal flux build-up during the duration of the fast pulse. This is shown in Figure 7.5.8, from which it can be seen that during the first 10 μs from the start of the fast neutron pulse, the accumulated thermal fluence is no more than about 2% of the value which will be reached in an infinite time.

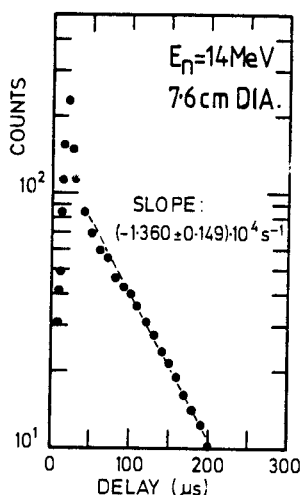


Fig. 7.5.5 Thermal neutron flux decay in a paraffin sphere 7.6 cm dia. (ref. 61).

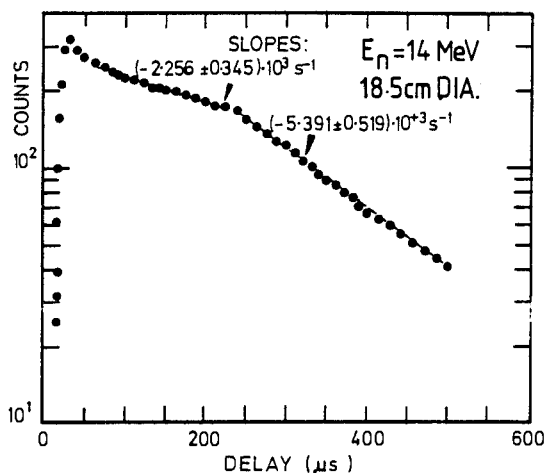


Fig. 7.5.6 Thermal neutron flux decay in a paraffin sphere 18.5 cm dia. (ref. 61).

The 'reverberation time' of neutrons within a tissue block is of an order of 200–400 μs , this time being defined as interval needed for thermal flux to drop down to $1/e$ value. If pulsing is employed to reduce the pile-up then it is sufficient to reduce the instantaneous counting rate until pile-up disappears. On the other hand, if pulsing is used to eliminate interferences in detection, then longer intervals between beam pulses may become necessary.

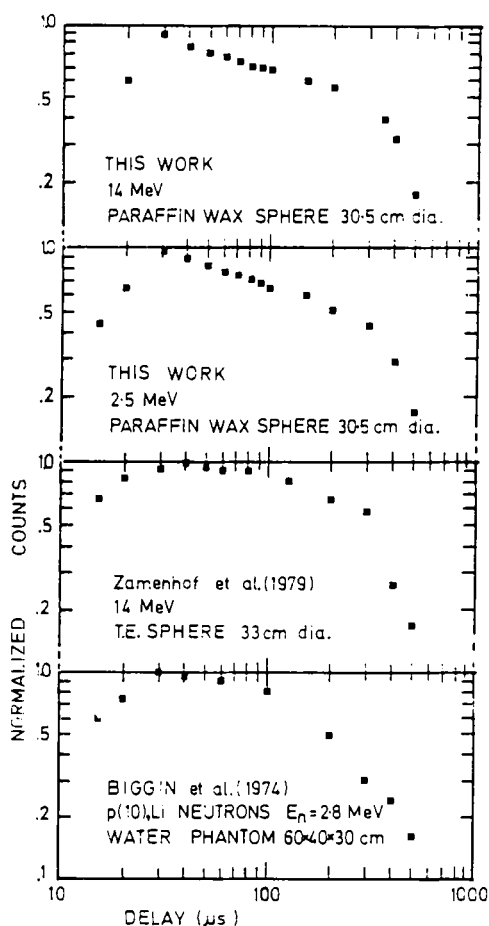


Fig. 7.5.7 Comparison of slowing down measurements of Miola (ref. 61), Zamenhof et al. (ref. 115) and Biggin et al. (ref. 47).

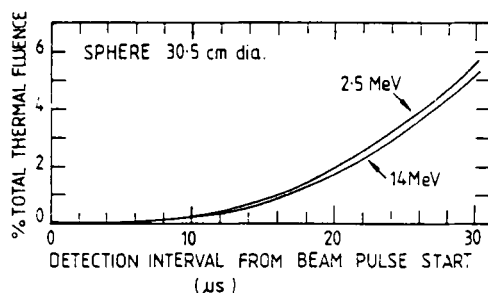


Fig. 7.5.8 Fraction of the total thermal fluence registered in an interval defined by the beginning of fast neutron burst and an arbitrary end limit. Neutron burst length: 10 μs . (Ref. 61).

7.6 DETECTION FACILITIES

7.6.1 General

The detection facilities for IVNAA are chosen according to the particular technique in use. For systems based on the use of prompt radiation (gamma rays from capture and from inelastic scattering of neutrons) the detectors must be placed next to the irradiated field and a considerable ingenuity is required to achieve good sensitivity, uniformity of detection and acceptable background. The off-line detection facilities are whole and partial body counters, built for general purposes or specifically designed for activation analysis. The design of the detection equipment determines the trade-off between the cost of the installation and the dose delivered to the patient, necessary to achieve the required precision and uniformity of analysis.

The choice of radiation detectors is very limited, it is either a scintillation detector, as a rule based on sodium iodide activated with thallium, or a solid state germanium device.

Sodium iodide detectors are easily available, either as cylinder of height approximately equal to diameter (these are still traditionally expressed in inches), or as a bar of rectangular cross section. Fairly large assemblies have been built from sodium iodide e.g. 'crystal balls', 'crystal walls' and 'crystal wells' of linear dimensions exceeding 40". On the other hand germanium detectors are relatively small in size, the record volumes being at present (1987) somewhere around 700 cm³. For this reason the solid angle subtended by the detector at the source of radiation is much lower. This disadvantage is less important in counting the emissions coming from small organs near the surface, but so far germanium based detection facilities do not include whole body counters where the solid angle would be crucial.

However, the energy resolution of solid state detectors is much superior to that of scintillation detectors with sodium iodide, as shown in Fig. 7.6.1.

The high energy resolution of solid state detectors is vital for separation of the neighbouring peaks and also makes it easier to identify accurately the baseline in the vicinity of the line of interest (fig. 7.6.2).

Scintillation detectors are used when the degree of spectral contrast is sufficient, e.g. in the measurements of ⁴⁹Ca activity (3.08 MeV) or detection of prompt gamma rays from ¹⁵N (10.83 MeV). It is also used for observation of 6.13 and 4.43 MeV gamma rays from inelastic scattering of neutrons on oxygen and carbon, respectively. At the present state of semiconductor detector technology the detection efficiencies of these detectors are so pathetically low at energies over, say 2.5 MeV, that a sodium iodide scintillator is the only means of detection.

For analysis of weak spectral lines, particularly below 2.3 MeV the germanium detectors are essential. Sodium iodide detectors are being used for 511 keV photons from the decay of positron emitters but those are from major components of the body. Neither detection of cadmium, mercury, *in vivo* would be possible without germanium detectors nor the applications of nuclear resonance fluorescence to IVNAA.

Detailed information on radiation detection can be found in the works of Knoll (ref. 145) and Tsoulfanides (ref. 146). The following sections will deal only with matters of particular relevance to IVNAA.

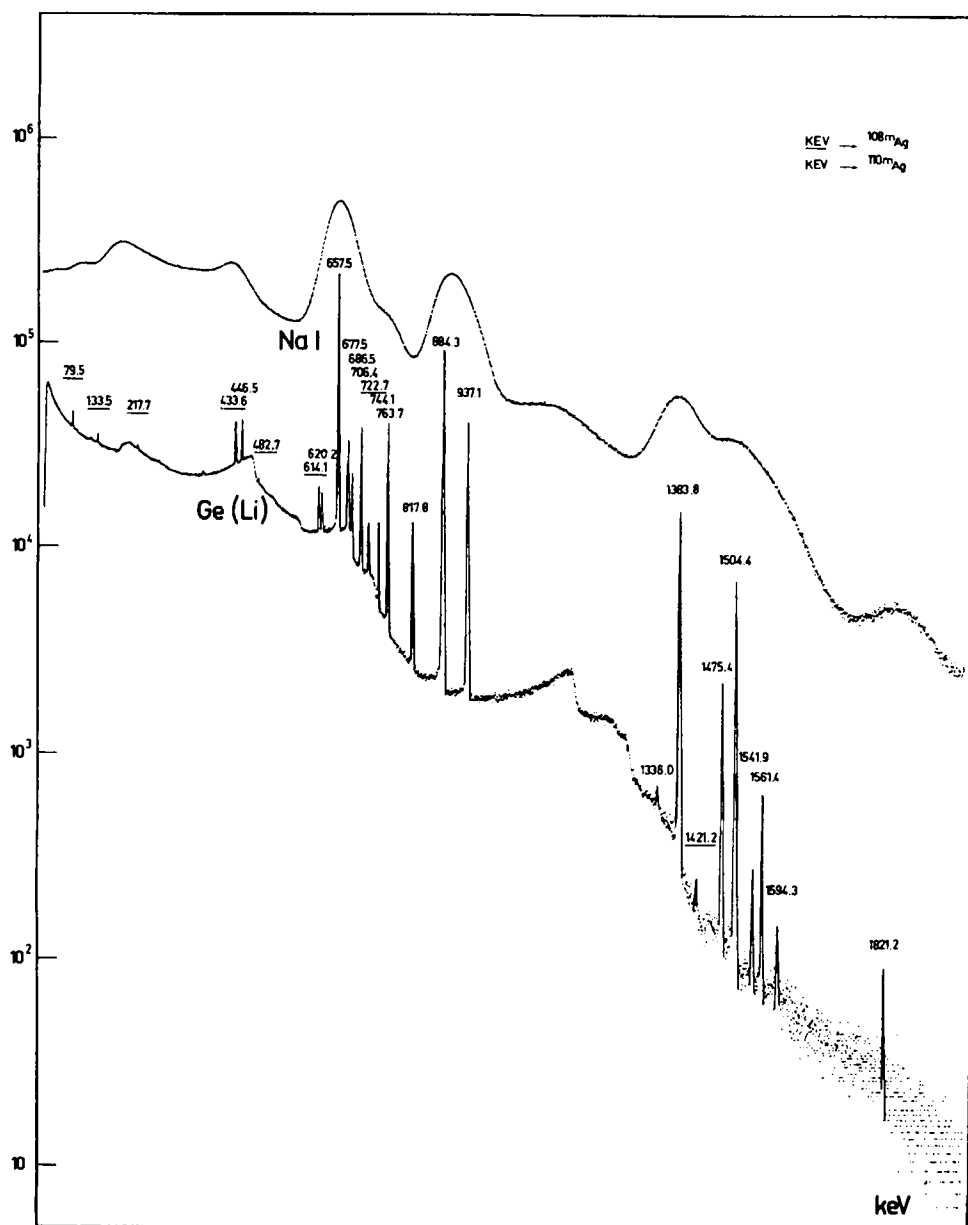


Fig. 7.6.1. Comparable energy spectra recorded using a sodium iodide scintillator and a Ge(Li) detector. The source was a mixture of ^{108}mAg and ^{110}mAg . The energies of individual peaks are indicated in keV (ref. 143).

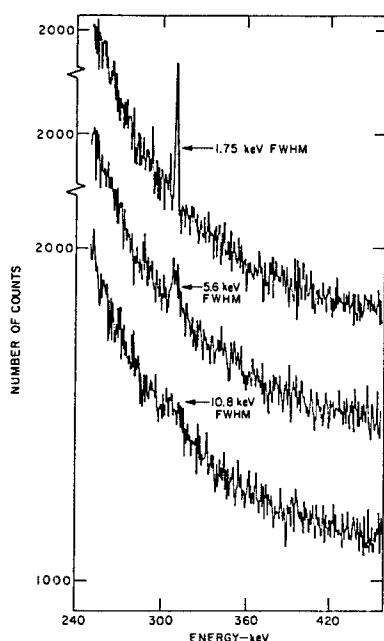


Fig. 7.6.2 The ability to identify and quantify a weak peak superposed on fluctuating baseline depends on the energy resolution of the detection system, as can be seen from the graphs corresponding to three different energy resolutions (ref. 144).

7.6.2 Scintillation detectors for IVNAA

One of the most important factors for estimation of the dose-sensitivity trade-offs in the design of IVNAA facilities are detection efficiencies. The absolute detection efficiency, ϵ_{abs} is the ratio of number of counts recorded by the recording system to the total number of photons emitted from the source in the same time. It can be shown that the absolute efficiency is a product of an intrinsic efficiency, ϵ_{in} and the relative solid angle $\omega/4\pi$ subtended by the detector at the source, presumed isotropic. The efficiencies defined in way do not take into account the spectral features of recorded events. They refer to the event energy spectrum extending from the maximum energy of the gamma quanta to the baseline noise level produced by electronics. It is the usual practice to count only the events under the photopeak i.e. total absorption peak) and in some cases under first or even second escape peaks as well, depending upon the interferences and spectral contrast. The peak-to-total ratio, also called photopeak fraction, is therefore an important parameter. These efficiencies have been measured or calculated in the past. Grosjean and Bossaert (ref. 147) (1965) have produced extensive tables of absolute detection efficiencies of cylindrical scintillation detectors, which are also reprinted in the monograph of Crouthamel, in the second edition prepared by Adams and Dams (ref. 148).

Total absolute efficiency curves for large sodium iodide detectors are shown in Fig. 7.6.3. Further curves of this type can be found in Marion and Young (ref. 149). Peak-to-total fractions were tabulated, among others, by Weitkamp (ref. 150) and by Young et al. (ref. 151). The peak-to-total ratios for some sizes of NaI crystals are shown in Fig. 7.6.4, taken from (ref. 149). The Harshaw Chemical Co. have produced a set of curves of peak-to-total ratios

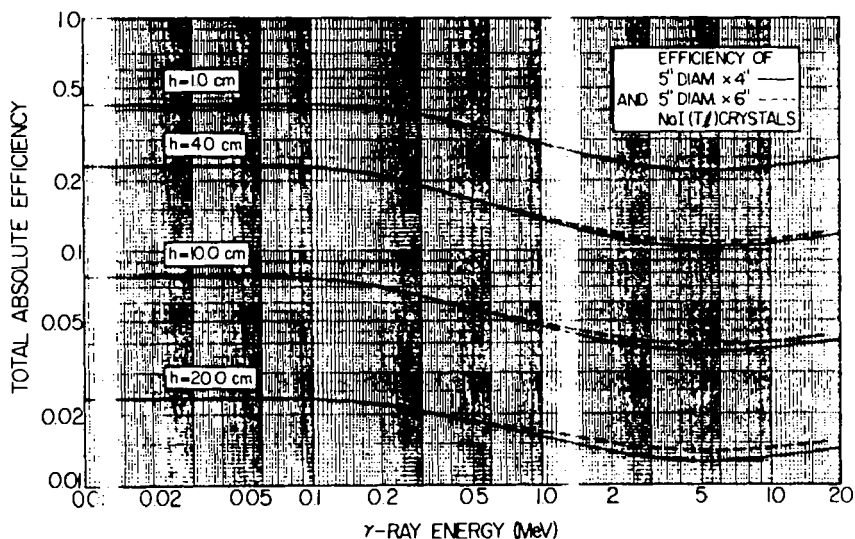


Fig. 7.6.3 Total absolute efficiency as a function of gamma ray energy for a variety of distances between the front face of detector and a radiation source (ref. 149).

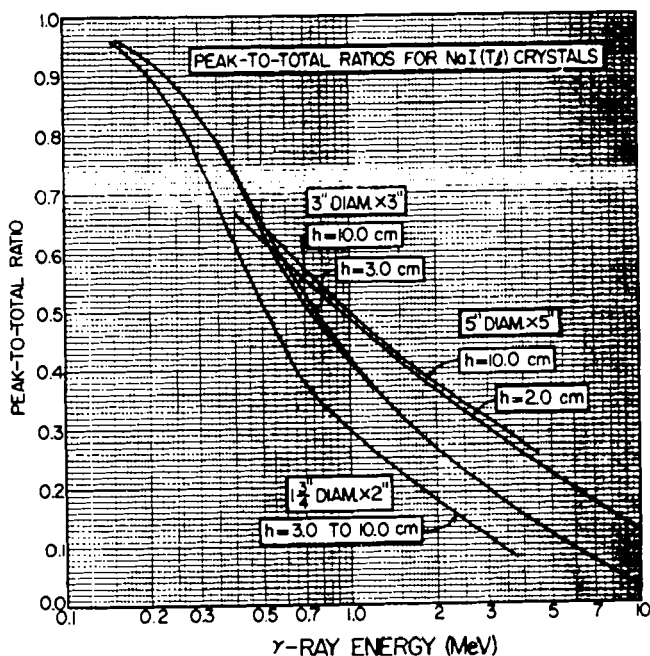


Fig. 7.6.4 Peak-to-total ratio for selected sizes of sodium iodide detectors as a function of gamma ray energy for different distances, between the front face of the detector and a radiation source (ref. 149).

for a large selection of sizes (Fig. 7.6.5) but extending only to 3 MeV. One should keep in mind using these data, that unless specifically mentioned, they are calculated not for extended but rather for point sources of radiation. The difference depends on the detector-source distance and can be practically neglected for distances over 30 cm. Useful solid angle calculations were reported by Gander et al. (ref. 152).

It has been observed that a marked directivity of sodium iodide detectors is apparent at higher energies if the detectors are of elongated shape. The maximum sensitivity coincides with the longer axis of the detector. The scintillation detectors should be shielded, not only to reduce radiations coming from unwanted directions, but also in order to reduce the amount of activation of detectors by neutrons and to reduce the radiation damage. The main consequence of exposure of NaI to a fast neutron flux is formation of defects e.g. colour centres in the lattice, leading to a loss in scintillation amplitude and degradation of timing performance. These effects are seen at accumulated fluences over 10^{12} n cm⁻². The immediate effect of slow neutron fluence is activation of ¹²⁷I, which forms a 30 min. ¹²⁸I. The decay of ¹²⁸I and the discrete gamma energies emitted in the process all contribute to the detector background. While gamma rays are effectively stopped by lead, the use of bismuth offers a lower background because there are less interfering interactions between the fast flux and bismuth. Slow neutrons are effectively absorbed by ⁶Li, but natural lithium can be used as well. In contact with moisture lithium is corrosive and dangerous. It can be used on its own inside sealed containers, and in form of LiF it is sufficiently inert to be added to epoxy resin and other fillers.

The use of lithium metal and LiF for shielding of scintillation detectors is illustrated in Fig. 7.6.6.

7.6.3 Germanium detectors

The efficiency of germanium detectors is a critical factor in the design of IVNAA facilities. The absolute photo-peak efficiency (i.e. absolute efficiency multiplied by the photopeak fraction) drops with an increase in energy of gamma rays and above energy of several MeV the photopeak efficiency is lower than the double escape peak efficiency. Furthermore, the double escape peak efficiency is higher than the efficiency for single escape. A typical energy dependence of the absolute photopeak efficiency is shown in Fig. 7.6.7 (From ref. 153). This graph is for a 38 cm³ detector and larger detectors are characterized by similar curves, though the numerical values of the efficiency are higher. In Fig. 7.6.8 are shown the escape peak ratios: R_1 is the ratio for single escape peak and photopeak; R_2 is the same for double escape peak. $R = R_2/R_1$.

Fast neutron damage shows itself in the broadening of resolution and can be observed already at fluences 10^8 to 10^9 n cm⁻² in p-type germanium and about $5 \cdot 10^8$ - 10^{10} n.cm⁻² in n-type germanium. With the advent of high purity germanium detectors in which there is no lithium to leak out, an annealing procedure usually removes almost all of the neutron damage. However, some damage remains and eventually the detector has to be replaced. Some suppliers of radiation detectors provide annealing kits for performing this procedure by the users. Bell (ref. 154) suggested that an estimate of amount of fast neutron damage can be found from a simple empirical formula:

neutrons per cm² = $300 \times (\text{counts under } 693.4 \text{ keV peak}) / \text{detector volume in cm}^3$

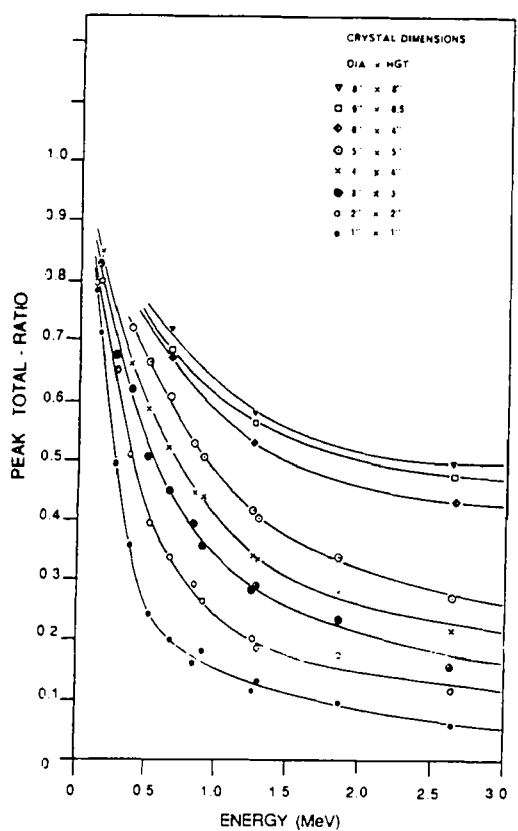


Fig. 7.6.5. Peak-to-total ratios for a number of sizes of sodium iodide detectors as a function of energy of gamma rays. The source detector distance: 50 cm. (Courtesy Harshaw Chemical Co.).

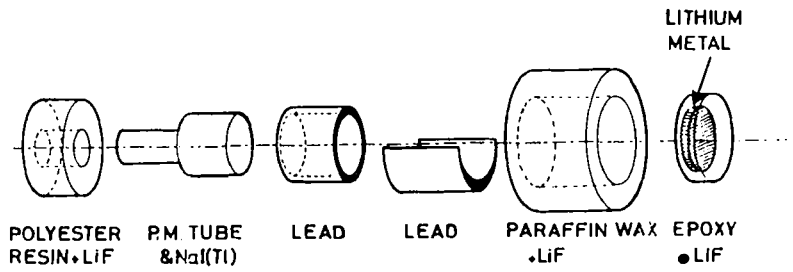


Fig. 7.6.6. Exploded view of a shield for a lateral NaI detector in the MERMAID installation in Birmingham (ref. 42).

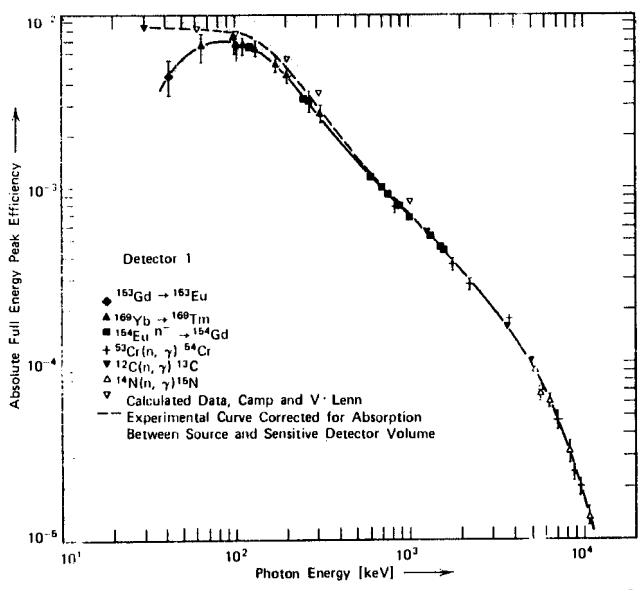


Fig. 7.6.7. Absolute full energy peak efficiency for 38 cm³ Ge(Li) detector, and a point source located 8.3 cm from the detector face. (ref. 153).

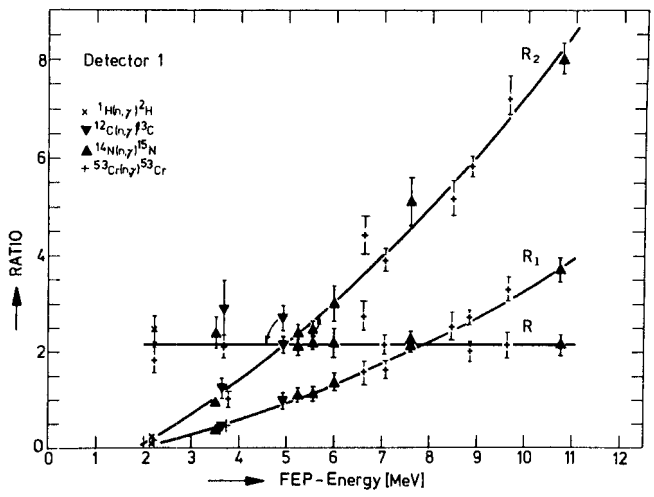


Fig. 7.6.8. Escape peak ratios (as defined in text) for the same detector (ref. 153).

Fast neutrons striking the detector during activation procedures not only cause radiation damage but are confusing the recorded spectrum and may interfere with the determination of some elements. The interference spectrum from fast neutrons in Ge(Li) detector is reported by Bunting and Kraushar (ref. 155).

To avoid problems with fast neutrons it is necessary to protect the germanium detectors from fast flux by careful positioning and by shielding. Thermal component can be easily cut off by a sleeve filled with lithium. An example of such shielding is shown in Fig. 7.6.9.

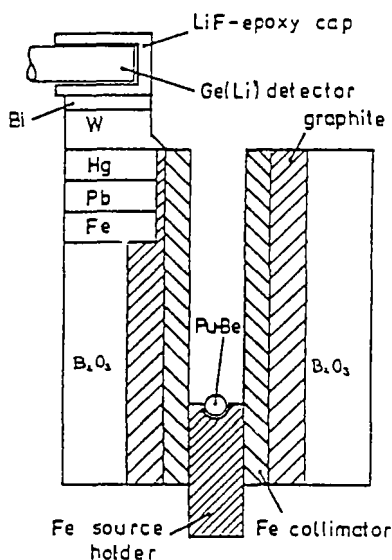


Fig. 7.6.9. Shielding of germanium detector in Birmingham in equipment used to determine cadmium *in vivo*. (From ref. 19).

7.6.4 Whole body counters

Whole body counters were built originally for purposes of health physics to monitor the radioactive internal contamination among staff employed in nuclear industry and research workers. In the Fifties and Sixties whole body counters were built for monitoring of the body burden from fall-out and for clinical studies with radioisotopes. During that period a number of publications appeared (e.g. refs. 156-158) and a number of symposia took place devoted to the subject of whole body counting. It appears that there is no scarcity of information on the whole body monitors in general (e.g. refs. 159,20) and the present section will only be concerned with these aspects which are relevant to the techniques of IVNAA.

Essentially there are two types of design which found wide spread use in IVNAA: the multi-crystal stationary bed geometry and the scanning geometry employing single, two or four crystals. So far, all the designs of whole body counters for IVNAA are based on sodium iodide scintillation detectors.

The whole body counter shown in Fig. 7.6.10 can be fitted with virtually any number of detectors. For a small number of detectors e.g. less than six it is difficult to secure uniformity of detection and at the same time maintain good sensitivity, particularly with different body sizes. The use of a larger number of detectors is exemplified by the Oak Ridge whole body counter Fig. 7.6.11. The geometrical response is very good.

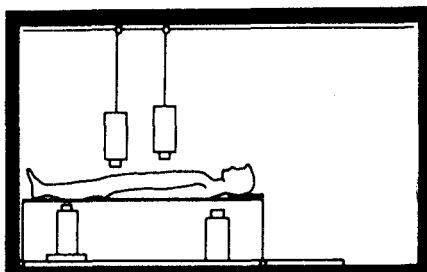


Fig. 7.6.10. A very simple four detector whole body counter (ref. 160).

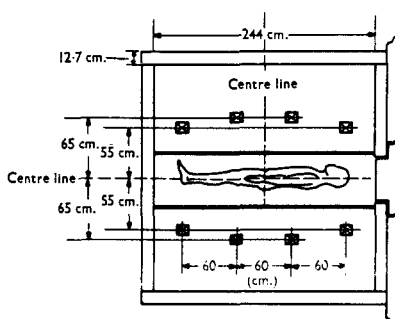


Fig. 7.6.11. Stationary bed whole body counter, built in Oak Ridge (Ref. 161).

The largest of whole body counters of this type ever built is in Brookhaven. (Fig. 7.6.12).



Fig. 7.6.12. Brookhaven whole body counter (ref. 20). The top bank of 27 detectors is visible above the patient, the other bank is underneath the couch. Both banks can be moved closer to the patient body.

The Brookhaven counter uses 54 large (6" dia. x 2" thick) sodium iodide detectors placed below and above the supine patient in 9 x 3 arrangement. (ref. 162). For a homogeneously distributed induced activity within the body the detectors in the centre are having higher geometrical efficiency than those positioned near the head or feet. The body absorption of radiation is the

largest in the centre and the two effects are partially compensating each other in overall response.

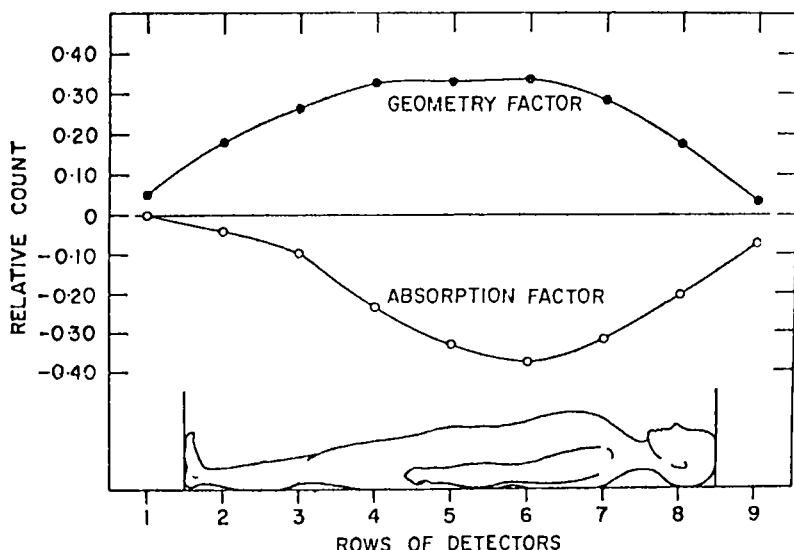


Fig. 7.6.13. The effects of geometrical efficiency of detectors and the absorption of radiation within the body thickness (From ref. 20).

Obviously the amount of absorption varies with the energy of radiation and patient thickness. It also depends on the location in the body of monitored activity (e.g. bones of the skull are close to the surface, but pelvis is deeply hidden).

Chen and Cohn (ref. 163) have devised a mathematical technique employing the response matrix of multi-detector system, which provides an elegant solution to the determination of the radioactivity in a patient, and which takes into account both the geometry of the counter and the geometry of the patient.

Some further 'sharpening' of the geometrical resolution is possible by the use of coincidence technique when counting positron emitters (^{13}C , ^{15}O and ^{13}N) which are produced in (γ, n) and ($n, 2n$) reactions, (ref. 164).

The scanning counters are used when the number of detectors at disposal could not warrant sufficiently uniform response in fixed geometry. Many early whole body counters were built on this principle (cf. Idaho Falls spiral scanner described in ref. 20; or ring scanner in ref. 165). This type of scanning counter found fairly wide use in IVNAA, where it is usually employed as a shadow-shield counter i.e. with stationary detectors and movable scanning couch. The use of a shadow shield reduces the weight and cost of the installation. An example of an economical design is the East Kilbride scanning counter utilizing two large (11.5" dia x 4 height) sodium iodide detectors, shielded by lead. The patient couch can move with the same speed as that used in the irradiation facility, so that the radioactive decay of induced activity can be automatically compensated. In some installations it is actually the same couch that moves the patient through the irradiator and through the counter afterwards. Shadow shield counters are very simple to build, permit correction for in-body absorption and can double as clinical counters for monitoring of conventionally administered activity (refs. 166-168, 24). This type of counter, when fitted with a good shadow shield, can also be used for clinical measurements of ^{40}K (refs. 169-170).

In the design of shadow shields it is possible to use in the external parts ordinary concrete, the inner parts, particularly those close to the detector should be made of aged lead or radioactivity-free steel. The couch

should also be non-activable. Wood, cotton and most plastics are satisfactory, but one should keep in mind that nylon and delrin can be activated by high energy neutrons.

A typical shadow shield whole body counter can be seen in Fig. 7.6.14..

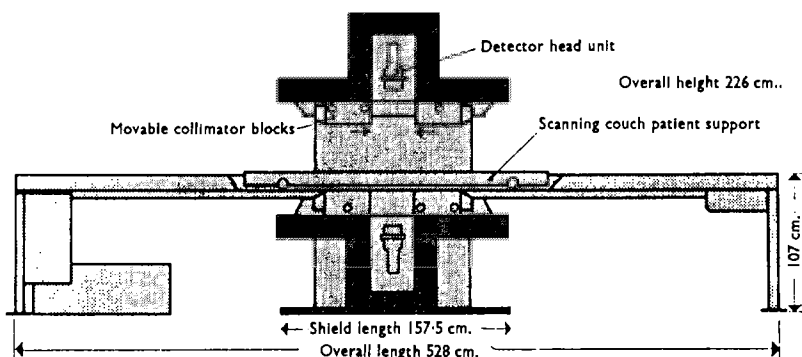


Fig. 7.6.14. Cross section through a simple shadow shield scanning counter From ref. 159. Also in Warner (ref. 171).

7.6.5 Partial body counters

Partial body counting as an off-line procedure is done either inside whole body counters of fixed geometry or, if those are provided with a scanning motion, with the scanner switched off. In some cases purpose built monitors are employed e.g. a pair of sodium iodide detectors facing each other for measurement of calcium and phosphorus in hand or a rectangular elongated scintillation detector for the spine or the foot etc. Part body monitors are as a rule used in the IVNAA of the thyroid (e.g. Boddy and Alexander, ref. 172). Processing of the data from body counters relevant to IVNAA, by means of sequential stripping is described by Cohn (ref. 173). A superior technique of least square analysis, presented by Wielopolski and Cohn (ref. 174) is based on matching a whole library of standard spectra mixed together in varying proportions until the best fit (in least square sense) to the experimental spectra is attained.

7.7 COMMENTS ON SOME APPLICATIONS OF IVNAA

7.7.1 Availability of alternative techniques

There is a considerable number of techniques in existence which provide information on the body composition, not including the technique of analysis of cadavers. An alternative to activation analysis of soft tissues is the use of Computerized Tomography employing X-rays. This technique does not give the elemental composition of the individual organs but distinguishes the electron densities of fat and muscle. The technique of nuclear magnetic resonance, in which no ionizing radiation is employed permits to identify the type of tissues by the measurement of spin-lattice and spin-spin relaxation times, in addition to the direct measurement of the concentration of protons (refs. 202 and 177). During the last few years a considerable improvement has been achieved in tissue recognition and characterization by NMR. One should note, that in many applications of IVNAA to clinical medicine it is the histological composition of the body which is sought, rather than the weights of individual elements. Bone calcium is not measured at present by NMR, but it may be possible in the near future to measure the phosphorus in bone mineral, as distinct from the phosphorus in the bone marrow and elsewhere.

The techniques for measurement of calcium in bones are many. The use of these techniques has been exhaustively discussed by many authors (e.g. refs. 178-180) and the more comprehensive are discussions contained in the works of Cohn (refs. 181-182) and in the review of Mazess (ref. 183). The techniques of absorptiometry using single or dual energy radiation sources are competing in clinical practice with the neutron activation analysis. The value of the total body calcium is obtained in much easier and, almost certainly, in more reliable way by activation analysis in vivo. Computerized tomography systems are in reality only a minor improvements over the linear scan absorptiometers and, in terms of radiation dose delivered to the patient, are most objectionable. Iodine in the thyroid can be measured without difficulty by techniques of X-ray fluorescence induced by low energy gamma rays or X-rays. The same procedure can be used for measurements of lead, mercury and cadmium in tissues accessible to the exciting beam and located not too deep so that it is possible to detect the characteristic radiation from them (see Chapter 2 in this volume).

In general, the list of non-invasive alternatives to IVNAA of trace elements is very short and for those elements which are deposited deeply, there appears to be no choice.

7.7.2 Measurement of calcium by activation of ^{48}Ca versus ^{37}Ar method

There is no doubt that the method of measurement of calcium in vivo by exhaled argon is extremely sensitive, reducing the dose requirement to values of an order of 10 Gy or even less for a whole body measurement with statistical error of counting about 1%. (ref. 186). There are many advantages of such a low dose requirement, not all of them related to the reduction of an exposure of a patient to ionizing radiation. The design of a neutron source is simpler and one may use longer source-to-skin distances, minimizing non-uniformity of neutron flux arising from geometrical conditions of irradiation. However, the process of assessment of calcium in vivo by the exhaled argon method is much more complex than the measurement in situ of induced activity of ^{48}Ca . The fate of ^{37}Ar produced from ^{48}Ca has been studied by Biggler (refs. 33,187) and it is evident that a significant and, perhaps, variable fraction of gas never reaches the blood stream: it is trapped inside crystals of the bone mineral. The kinetics of the process of elimination of argon is not sufficiently understood. Biggler et al. (op. cit.) reports that two-component analysis of the exhalation curve indicates that 82% of gas leaves the body by the way of lungs with a half-life of about 40% and the remaining 18% was exhaled with 200 min half-life. However, this leaves about 30% of estimated argon production still unaccounted for. Lewellen quotes a lower figure of 15% for the retained argon (ref. 191). Some further problems are a consequence of the technique of collecting exhaled argon involving use of a breathing circuit in which argon recirculates. The use of this type of breathing system increases the absorption of argon by fat (refs. 188,189). The number of components into which the exhalation curve can be resolved, and their half-lives are, so far, not established in a manner satisfactory for the variety of normal and pathological cases. The problems in the interpretation of the exhalation curve are arising from the fact, that the Ar method measures the eliminated product while the system is not in equilibrium. It may be that the shape of an exhalation curve and the derived half-lives are themselves indicative of the state of the bones. This is, most likely, the reason why a caution is advocated in interpretation of the results of measurement of calcium by exhaled gas method (ref. 190).

7.7.3 Principal applications of the calcium mass measurements

The measurement of bone mass and related quantities are important in the diagnosis of many diseases and in the monitoring of appropriate therapy as well as in the investigation of therapeutic agents used in the treatment of bone diseases.

A wealth of data on the relationship between the bone mineral and age, sex, weight, height, race etc. in normal individuals, have been accumulated in

the course of work of Cohn's group in Brookhaven (ref. 16 and references therein). These data provide baseline for the study and diagnosis of metabolic bone disorders. An important finding of the Cohn's group is that the decrease in bone mass, associated with the loss of bone mineral, is a part of the aging process. Data of Cohn and his co-workers were obtained from the total body analysis of calcium, (ref. 192). In addition Harrison and McNeill (ref. 193) were measuring the baseline using data on calcium in the trunk only. A simple but effective technique of measuring bone mineral in hand was employed for the same purpose by Maziere et al. (ref. 194).

In the sequential studies of calcium in man, it is important to measure reliably small changes, of an order of 1-2%, in the whole body or in selected part of the skeleton. The required precision and reproducibility of measurement are high, but the absolute value may not need to be known with high accuracy. For sequential measurements the requirements are thus relaxed, as long as the experimental conditions remain unchanged. In the case of absolute measurements of calcium the uniformity of neutron fluence and the uniformity of detection within the body must be carefully controlled and the 'raw' number of counts must be corrected for a number of factors. Kennedy et al. (ref. 195) reviews the procedures used in Edinburgh to calibrate measurements of total body calcium by activation of ^{48}Ca . A subject irradiated in a standing position between moderating walls was exposed to cyclotron produced neutrons. The absolute value of total body calcium (TBCa) was estimated from the relationship:

$$\text{TBCa} = \text{measured calcium} \times \text{height correction} \times \text{depth correction} \times \\ \times \text{fat correction} \times \text{wall correction}$$

where the correcting factors were defined as follows:

height correction = $0.5 (\text{subject height} - 1.50) + 1$, for height < 1.5 m
or height correction = 1 for those taller than 1.5 m.

depth correction = $1.6 (\text{subject depth} - \text{TST} - 0.2) + 1$

fat correction = $1.8 (\text{TST} + \text{LST}) + 1$

wall correction = wall separation - subject depth + 1

TST and LST are mean torso and mean limb skinfold thickness, respectively. The derivation of correction factors is based of fitting the experimental data and is not necessarily unique. With the help of forty volunteers the predictors were also established in which the raw, i.e. uncorrected data, were then corrected only for weight and height or span and weight. The predictors provide the 'normal' value of calcium mass as the function body weight, height and span. The predictors are not unique and e.g. Cohn et al. (ref. 192) had proposed predictors which include lean body mass obtained from potassium measurements.

The availability of normal values of calcium bone mass makes possible to diagnose early osteoporosis and indicate individuals at risk, particularly post-menopausal women (ref. 206). The study of various proposed pharmacological agents (e.g. analogues of Vitamin D) to arrest the course of osteoporosis or, at least, to slow down its progress is reported by many authors (e.g. refs. 207-208). The use of drugs to help the sufferers of osteodystrophy among the patients on renal dialysis is described in literature (e.g. refs. 209-213). Measurement of bone calcium have also been involved in the studies of osteomalacia and the treatment of its various forms. The role and importance of bone calcium measurement in a number of endocrine diseases (e.g. hyperthyroidism, hyperparathyroidism, Cushing's syndrome, acromegaly), in Paget's disease and in consequences of use of corticosteroids in the treatment of rheumatoid arthritis

are documented in the reviews of Cohn (refs. 16 and 214).

7.7.4 Total body element measurements and its uses

There are two methods currently employed in the measurement of total body nitrogen: one is based on measurement of induced activity of ^{13}N and another on the measurement of prompt capture gamma rays from thermal reaction on ^{14}N . The measurement of ^{13}N is fraught with a number of difficulties. Being a fast neutron reaction, it is difficult to estimate changes in the reaction cross section through the body. The interfering reactions e.g. production of other positron emitters are not serious because the amounts produced are very small. ^{13}N is produced not only from ^{14}N but also from ^{16}O in a (p, α) process. The error for a standard man may reach 20% and hence from the total value of detected nitrogen a number of counts must be subtracted. To estimate the 'oxygen correction' it is necessary to find the amount of nitrogen in vivo either from the total body water measurement or from direct measurement of oxygen by one of available techniques: observation of prompt gamma rays from inelastic scattering or from measurement of activity of ^{16}N (7.6 sec) produced in a (n,p) process from body oxygen, (ref. 184). Haywood et al. who measured the interferences and used phantoms of varying size, estimated the interferences from oxygen to be equal 20.3%, from phosphorus 13.7% and from sodium, chlorine and calcium altogether about 17%. The procedures described assured acceptable determination of nitrogen in vivo (ref. 27) in all categories of patients.

The technique of prompt gamma rays arising from neutron capture is free from the problems of interference. The prompt gamma ray technique also lends itself easily to absolute measurements of nitrogen. This method, introduced by Vartsky (ref. 185) utilizes hydrogen, which has almost constant concentration throughout the soft tissue, as an internal standard. In effect the ratio of N/H is determined. The technique is extremely simple in practical realisation and requires only accumulation of data on concentration of H, together with the counting of nitrogen. The hydrogen concentration is easily found from a strong gamma ray spectral line at 2.223 MeV.

Measurement of nitrogen in vivo provides direct information on the body protein and less directly on the body muscle. This information alone is valuable to the clinician but full benefit of the analytic technique based on IVNAA can be achieved by a study of body composition involving more than one element. In fact, the development of IVNAA made possible to formulate a model of body composition, different from models proposed before, which were based on specific anatomical compartments. It is possible to consider model of the body comprising of five principal compartments: fat, protein, water, ash, and carbohydrates. In vivo activation analysis, aided by other, related techniques like whole body counting, analysis of urine and blood, renders possible numerical evaluation of these compartments in a reliable and non-traumatic way. In fact, taking of blood samples (for determination of total body water) may be avoided altogether in the future. In addition to the total body protein which is derived from total body nitrogen measurements, the 'ash' is the mineral content of bones found from total body calcium measurements. The carbohydrate compartment, which is of small size, of an order of 0.5 kg, is related to the total body carbon. One can consider finding the fat as a difference between the total body weight and the already determined compartments; an alternative is an algebraic technique which involves solving a simultaneous system of equations. Ellis and Cohn (ref. 225) point out that the compartmental analysis can identify separately muscle mass, non-muscle lean tissue mass and the visceral component of the lean body mass, from the knowledge of total body potassium and total body nitrogen. Total body measurements of sodium and chlorine are indicators of the content of the intercellular and extracellular water compartments.

The information on body composition is of great clinical value. Leaving aside the importance of calcium status in patients with various bone diseases, endocrine disorders, the body composition studies are of primary importance in dietetics and nutrition, in staging and therapy of wasting diseases as well as

in management of geriatrics. Measurements of TBN seem to have implications for the understanding of diabetes (refs. 215-217).

7.7.5 Detection of heavy toxic metals

Installations for measurement of cadmium in liver and kidneys represent nowadays sophisticated pieces of nuclear engineering, particularly as far as the collimation of neutrons and gamma ray shielding of detectors is concerned. This is particularly evident from their descriptions (refs. 50,218 and 219). The tailoring of neutron spectrum has an effect of reducing the dose administered to the patient. An example of design is the Brookhaven system with the 2σ detection limit for one (left) kidney of 2.2 mg and for liver 1.5 $\mu\text{g/g}$ of wet tissue, while the dose equivalent is 4.7 mSv. Detection systems for cadmium are usually transportable because cadmium accumulates as a result of occupational exposure or as a result of high local concentrations of Cd in the environment (ref. 220). In such circumstances it is more practical and economical to bring the analytical system to the affected enterprise or locality, so that a large number of subjects can be examined without problems of absence from work and without inconvenience of travel for older subjects.

Calcium concentrates in liver and in kidneys. The conditions of measurement in both organs are not identical. Liver, a large organ compared with kidneys, in the present state of technology cannot be measured for the presence of cadmium as a whole. So far, the detection equipment illuminates a part of liver with the neutron beam and an associated gamma ray detector detects gamma rays from approximately the same region. It is possible to build a scanning system, if need arises, which may encompass in the measurement a larger part of the organ. In the existing systems the obtained data represent for liver the concentration of Cd in the 'illuminated' part. Unless a heavy pathological or degenerative damage took place, a reasonable assumption is that cadmium is distributed uniformly through the volume, which can be determined by a CAT or NMR scanner.

Detection of cadmium in the kidneys takes place in different conditions. Not only a whole kidney is in the detection volume (actually it is, usually, a significantly larger volume), but the thickness of intervening tissue between the skin and the kidney varies. The exact position and depth of kidneys have to be determined, e.g. by ultrasound, so that proper corrections have to be applied for attenuation of the neutron beam and for detection efficiency. To obtain reliable absolute values of kidney Cd burden in these circumstances a considerable amount of calibration is required.

The ability of IVNAA to measure cadmium in absolute amounts makes possible to correlate the severity of disease with the measured concentrations, the cause-effect relationship.

Cadmium has been implicated in renal and hepatic failure, has been linked to hypertension and other disorders, (refs. 221-224).

The same type of installation, as for detection of Cd, can be used for detection of mercury and it may be advisable to design systems capable of detecting and measuring both elements in vivo.

8 CONCLUDING REMARKS

This work was neither intended as a review of the state-of-the-art of IVNAA nor as a detailed manual of techniques and procedures. It was thought of as a broadly based introduction to the methodology and instrumentation in this well established area of research and clinical practice. It is thus unavoidable, that some of the more detailed and specific descriptions had to be left out, the reader being referred to the available published literature.

One of such important aspects of IVNAA is the electronic circuitry for the spectrometry of detected radiation. In addition to usual requirements of stability and reliability of operation, the electronic signal chain in IVNAA has to operate frequently at count rates corresponding to the upper regions of commer-

cially available high count rate systems, i.e. in excess of 5×10^4 events.s⁻¹. One of the solutions to the problem of spectrometry at high count rates was presented by Vartsky (ref. 196), specifically intended for IVNAA. The data processing must also cope with a high event rate and a system for spectrum elaboration used in a IVNAA installation should be able to eliminate artefacts generated by neutron flux reaching the detectors.

Delivery of the neutron or photon beam, originating from an accelerator to patients, requires that the delivered fluence is precisely integrated, because the precision of the measurement of the activating radiation dose is the main part of the total evaluated precision of measurement. One of such neutron beam integrators, based on a transmission chamber is described in ref. 197.

With the rare exceptions, the irradiating installations for IVNAA employ collimators. It is important to realize that the requirements for neutron collimators for use in IVNAA are often severe: not only the proper geometrical performance is required, but the gamma rays produced by the neutron flux in the collimator itself are likely to find way into the prompt radiation detector, (refs. 198-201). Those who wish to set up their own systems will have to learn the art of preparation of phantoms and the methods of evaluating of interferences in the detection, so that they can be accounted for in the final result.

It is important that all the procedures are well discussed in advance with the radiation protection staff before implementation. Handling of radioactive sources, use of liquid and demountable phantoms, testing and calibration of the irradiation systems require proper care and strict observation of the safety rules. Very careful planning is needed to avoid unwanted build-up of radioactivity which in turn could contaminate the low-level counting installation. It appears that nuclear activation analysis may find practical use in animal production as a convenient technique for analyzing the development of an individual animal as well as an aid in formulating the feeds and studying effects of feed additives, (refs. 202-205). In addition to activation analysis techniques implemented for the use of humans, a number of other techniques is conceivable e.g. those using nuclear reaction of secondary recoil proton flux, characterized by higher doses of radiation.

It is important to remember that the histological body composition, i.e. division into muscle, fat, bone etc. can be obtained from the measurements using nuclear magnetic resonance, which utilize different relaxation times of protons and other species in different living tissues in vivo. Similarly, the measurement of Cd and Hg can be sometimes attained by means of X-ray based techniques. The actual advantage of one technique over another changes with time and with the use to which the results are put. If IVNAA has to retain its important position in the field of in vivo determination of body composition it must continue to improve and develop.

Acknowledgements

The author was privileged to study activation analysis in vivo from two masters of the art: Professor John H. Fremlin, University of Birmingham U.K. and Dr. Stanton H. Cohn, Brookhaven National Laboratory, USA; to them he is profoundly indebted for the inspiration which lasts the lifetime.

A. APPENDIX

DESCRIPTIONS OF SYSTEMS IN USE

According to a survey in 1986 by IAEA (ref. 19) there were at least 20 centres in 8 countries actively pursuing nuclear activation analysis in vivo. They used different apparatus, as a rule fabricated to own designs, no commercial systems being available at the time of writing. This section brings a selection of proven designs, based on information presented in the IAEA survey.

1) SYSTEM FOR PARTIAL BODY ACTIVATION ANALYSIS

(Calcium in hand) (figs. A1, A2)

Service Hospitalier Frédéric Joliot,
CEA Department de Biologie,
F-91406 Orsay, France

Overall system performace

Elements measured: Ca, Na, Cl
Organ of interest: hand
Radiation dose: 24 mGy
In operation since: 1975

Irradiation Device

Source: 2 x ^{252}Cf (Optional 4 x $^{238}\text{Pu-Be}$ ($6.8 \times 10^7 \text{ n s}^{-1}$) for measurement of phosphorus).
Total activity/output at source: $9.2 \times 10^8 \text{ n.s}^{-1}$
Geometry: 1 above, 1 below the hand
Incident neutron flux density in body: $7 \times 10^5 \text{ n(th).cm}^{-2}.\text{s}^{-1}$
Exposure time: 5 min
Uniformity of irradiation for element & organ of interest: 4%
Special features: irradiation device at the centre of a 1 m^3 paraffin cube

Counting Device

Detectors: 2 x NaI(Tl), 12.7 x 12.7 cm
Geometry: 1 above, 1 below the hand
Shielding: 10 cm lead
Measurement time: 32 min

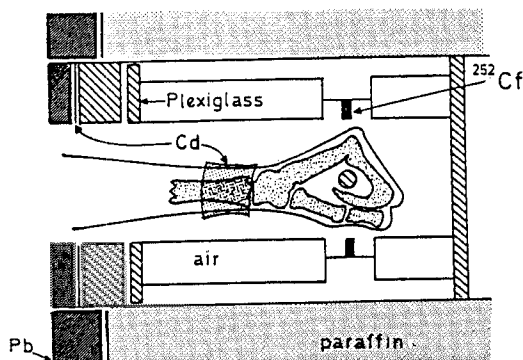


Fig. A1 - Irradiation device

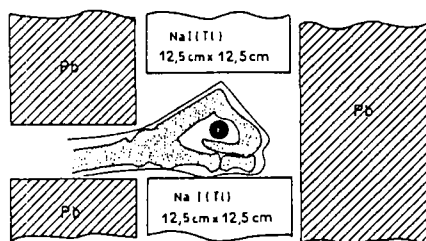


Fig. A2 - Counting device

2) SYSTEM FOR PARTIAL BODY ACTIVATION ANALYSIS

(Calcium in spine) (Fig. A3)

Department of Medical Physics and Medical Engineering,
Royal Infirmary,
Edinburgh EH3 9YW, UK.

Overall system performance

Element measured: Ca

Organ of interest: spine

Radiation dose: skin: 13 mGy; bone: 1.5 mGy

Reproducibility of measurement: 3.0%

Irradiation DeviceSource: $2 \times {}^{252}\text{Cf}$ Total activity/output at source: initially 4 GBq, $4.6 \times 10^8 \text{ n.s}^{-1}$

Geometry: partial body, spine and upper pelvis, FWHM 43 cm

Incident neutron flux density in body: $10^6 \text{ n.cm}^{-2} \text{ .s}^{-1}$

Exposure time: initially 2 min

Uniformity of irradiation for element & organ of interest: $\pm 30\%$
over depth of vertebraeCounting DeviceDetectors: $4 \times \text{NaI(Tl)}$, 15 x 10 cm

Geometry: 2 above, 2 below supine body

Shielding: steel shadow shield

Measurement time: 17 min

3) SYSTEM FOR PARTIAL BODY ACTIVATION ANALYSIS

(Cadmium in liver and kidneys) (Fig. A4)

Department of Physics,
University College of Swansea
Singleton Park
Swansea SA2 8PP, Wales, UK.

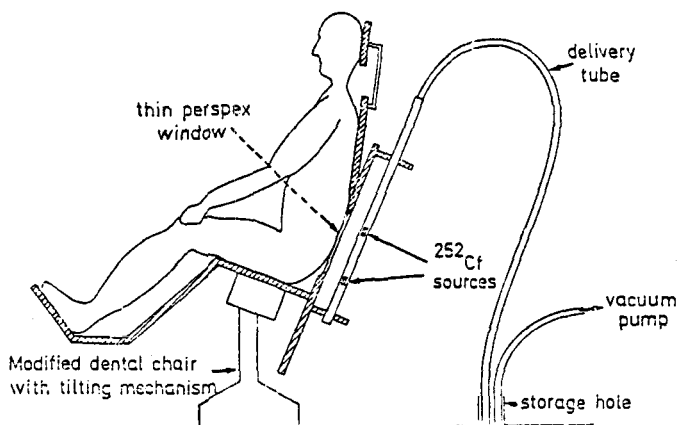


Fig. A3 - Spine irradiation apparatus

Overall system performance

Element measured: Cd
 Organ of interest: kidney, liver
 Radiation dose: skin: 0.35 mGy; organ: 0.13 mGy
 Reproducibility of measurement: 10%

Irradiation Device

Source: $1 \times {}^{252}\text{Cf}$
 Total activity/output at source: 4.0 GBq ($4.6 \times 10^8 \text{ n.s.}^{-1}$)
 Geometry: partial body
 Incident neutron flux density in body: $3 \times 10^4 \text{ n.cm}^{-2} \text{ .s}^{-1}$
 Exposure time: 33 min
 Uniformity of irradiation for element & organ of interest: $\pm 15\%$
 Special features: shutter arrangement, variable source position, interchangeable tapered iron collimators, organ localisation by ultrasound.

Counting Device

Detector: $1 \times 21\% \text{ Ge(Li)}$
 Geometry: detection at right angles to incident neutron beam
 Shielding: lead, borated wax, tungsten, ${}^6\text{LiF}$
 Measurement time: 33 min

- 4) SYSTEM FOR PARTIAL BODY ACTIVATION ANALYSIS
 (Cadmium in liver and kidneys) (For illustration see Fig. 7.2.7)
 Medical Research Center
 Brookhaven National Laboratory
 Upton, New York 11973, USA

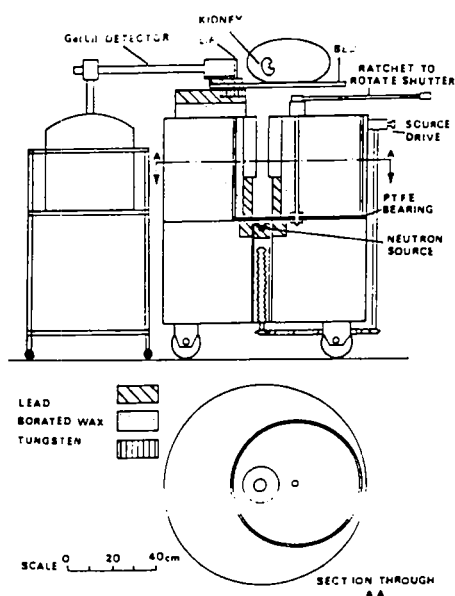


Fig. A.4

Overall system performance

Element measured: Cd
 Organ of interest: kidney, liver
 Radiation dose: max. skin dose: 0.2 mGy
 Reproducibility of measurement: 5%

Irradiation Device

Source: 100 μg ^{252}Cf
 Total activity/output at source: $2.2 \times 10^8 \text{ n.s}^{-1}$
 Geometry: partial body, 12.7 cm diameter beam size, source to skin distance = 60 cm
 Exposure time: 1000 to 2000 s
 Uniformity of irradiation for element & organ of interest: 10%
 Special features: accurate kidney and liver localisation accomplished by ultrasonic scanning; shield exceeds IAEA regulations for certification as transport container, iron collimator

Counting Device

Detectors: 2 x 25% Ge(Li), 2.5 keV FWHM at 1.33 MeV
 Geometry: 15 cm from centre of neutron beam
 Shielding: boron-doped polyethylene
 Measurement time: 1000 to 2000 s
 Special features: in vivo detection limits: 2.3 mg in kidney and 1.6 mg/kg in liver.

- 5) SYSTEM FOR PARTIAL BODY ACTIVATION ANALYSIS
 (Iron in liver and heart) (For illustration see Fig. 7.2.14)
 Medical Research Center,
 Brookhaven National Laboratory
 Upton, New York 11973, USA

Overall system performance

Element measured: Fe
 Organ of interest: liver, heart
 Radiation dose: skin, 10 mGy
 Reproducibility of measurement: 6%

Irradiation Device

Source: 1 x ^{56}Mn source in a quartz capsule
 Total activity/output: 2×10^{10} photons $\cdot \text{s}^{-1}$
 Geometry: partial body
 Incident flux density in body: 1×10^6 photons $\text{cm}^{-2} \cdot \text{s}^{-1}$
 Exposure time: 2000 s
 Special features: gaseous source kept at 1000°C

Counting Device

Detector: 2 x HPGe (25% efficiency, 2.1 KeV resolution)
 Geometry: positioned at 90° to the incident photon beam
 Shielding: Bi, annulus with 6 mm lead disc in front of detectors
 Measurement time: 2000 s

- 6) SYSTEM FOR PARTIAL BODY ACTIVATION ANALYSIS
 (Multielement) (Fig. A.5))
 Scottish Universities
 Research and Reactor Centre,
 East Kilbride, Glasgow G75 0QU, UK.

Overall system performance

Elements measured: Ca, N, Na, Cl, P, O
 Organ of interest: whole body
 Radiation dose: skin; 1.4 mGy
 Reproducibility of measurement: Ca: 2.5%, N: 1.3%, Na: 3.1%, Cl: 4.7%, P: 0.8%, O: 2.9%

Irradiation Device

Source: 2 x sealed tube 14 MeV generators (Philips type 18602)
 Total activity/output at source: $2 \times (1 \times 10^{10}) \text{ n.s}^{-1}$
 Geometry: simultaneous bilateral scanning irradiation
 Incident neutron flux density in body: $1 \times 10^5 \text{ cm}^{-2} \cdot \text{s}^{-1}$
 Exposure time: 2.75 min
 Uniformity of irradiation for element & organ of interest:
 fast: $\pm 2.1\%$, thermal: $\pm 4.5\%$
 Special features: located close (9 m) to counter enabling rapid transfer of subject (30 s), minimal premoderator used over legs only.

Counting Device

No. and type of detector: 2 x NaI(Tl), 29 x 10 cm (Scintiflex)
 Geometry: 1 above, 1 below supine body; motorised scanning bed
 Shielding: 10 cm lead shadow shield (8000 kg approx.)
 Measurement time: 60 min approx. including ^{40}K background
 Special features: scanning speed identical to irradiation, to compensate for radioactive decay along length of body.

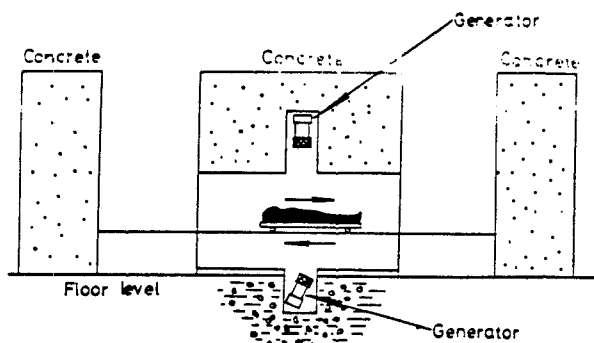


Fig. A.5 - Sectional diagram of the 14 MeV irradiation device at SURRC.

7) SYSTEM FOR TOTAL BODY ACTIVATION ANALYSIS

(Carbon) (Fig. A.6)
 Department of Medical Physics,
 The General Infirmary
 Leeds, LS1 3EX, UK.
 United Kingdom

Overall system performance

Element measured: C
 Organ of interest: whole body
 Radiation dose: skin; 0.2 mGy; whole body: 0.2 mGy
 Reproducibility of measurement: 3%

Irradiation Device

Source: one sealed tube D-T generator (Philips).
 Total activity/output at source: $2.4 \times 10^9 \text{ n.s}^{-1}$
 Geometry: horizontal beam of neutrons incident alternately on the right and left sides of the supine patient
 Incident neutron flux density in body: $3000 \text{ n.cm}^{-2}.\text{s}^{-1}$
 Exposure time: $2 \times 900 \text{ s}$
 Uniformity of irradiation for element & organ of interest: $\pm 20\%$
 (fast neutrons)

Counting Device

Detectors: 2 x NaI(Tl), 13 x 10 cm
 Geometry: 1 above, 1 below supine body
 Shielding: steel, lead and boric acid
 Measurement time: 2 x 900 s

- 8) SYSTEM FOR TOTAL BODY ACTIVATION ANALYSIS
 (Multielement system) (Figs. A.7 and A.8)
 Department of Medical Physics
 The General Infirmary
 Leeds, LS1 3EX, UK.

Overall system performance

Elements measured: Ca, N, Na, Cl, P, K,
 Organ of interest: whole body

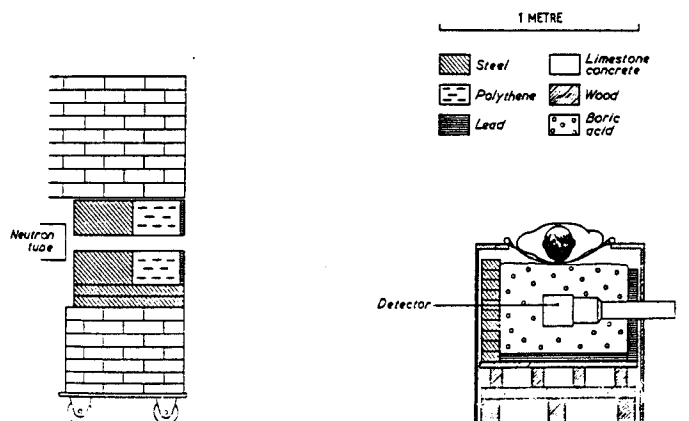


Fig. A.6

Radiation dose: skin; 0.5 mGy; whole body: 0.5 mGy
 Reproducibility of measurement : Ca: 3.6%, N: 2.8%, Na: 3.1%, Cl: 3.8%, P: 2.6%, K: 1.9%

Irradiation Device

Source: one sealed tube D-T generator (Philips).
 Total activity/output at source: $3 \times 10^{10} \text{ n.s}^{-1}$
 Geometry: horizontal beam of neutrons incident alternately on the right and left sides of the supine patient
 Incident neutron flux density in body: $4 \times 10^4 \text{ n.cm}^{-2} \text{ .s}^{-1}$
 Exposure time: 2 x 200 s
 Uniformity of irradiation for element & organ of interest: $\pm 20\%$ (fast neutrons)

Counting Device

Detectors: 8 x NaI(Tl), 15 x 10 cm

Geometry: 4 above, 4 below supine body

Shielding: lead lined steel room

Measurement time: 1800 s

Special features: induced radioactivity and natural activity of ^{40}K are measured simultaneously; corrections are applied for known interference reactions; can be used to measure critically ill patients.

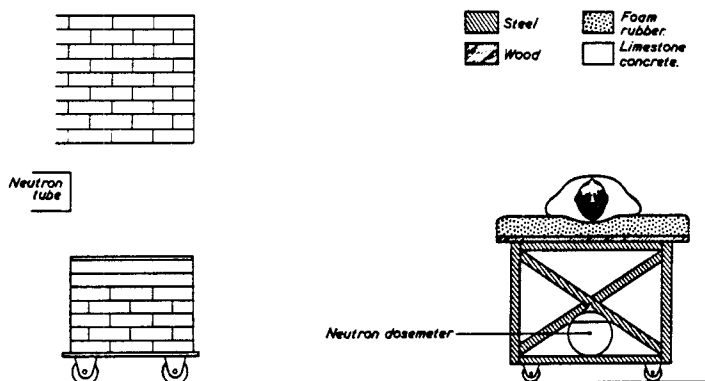


Fig. A.7

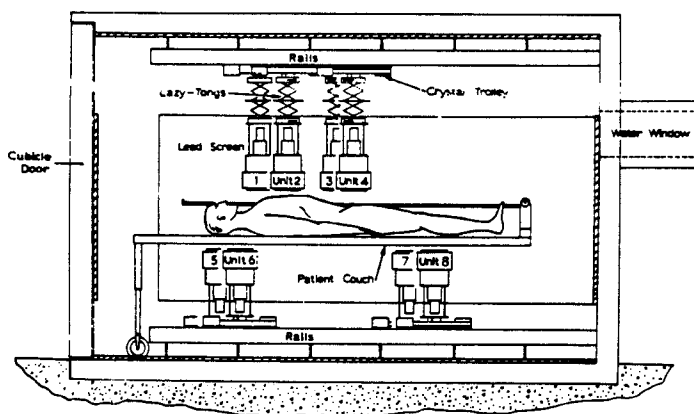


Fig. A.8

- 9) SYSTEM FOR TOTAL BODY ACTIVATION ANALYSIS
(Nitrogen) (For illustrations see Figs. 7.2.4-7.2.6)
Medical Research Center
Brookhaven National Laboratory
Upton, New York 11973, USA.

Overall system performance

Element measured: N
Organ of interest: whole body
Radiation dose: skin: 0.05 mGy;
Reproducibility of measurement: 4%

Irradiation Device

Sources: 2 x 42 Ci ^{238}Pu -Be
Total activity/output at source: $2.3 \times 10^8 \text{ n.s}^{-1}$
Geometry: whole body (scanning geometry)
Incident neutron flux density in body: $7.2 \times 10^3 \text{ n.cm}^{-2} \text{ .s}^{-1}$
Exposure time: 200 s
Uniformity of irradiation for element & organ of interest: $\pm 4\text{-}6.5\%$
Special features: heavy water premoderator

Counting Device

Detectors: 2 x NaI(Tl), 15.5 x 15.25 cm
Shielding: epoxy resin + Li
Measurement time: 2000 s

- 10) SYSTEM FOR TOTAL BODY ACTIVATION ANALYSIS
(Calcium) (Fig. A.9)
Medical Sloan-Kettering
Cancer Center,
1275 York Ave,
New York, NY 10021, USA.

Overall system performance

Element measured: bone Ca
Organ of interest: whole body
Radiation dose: skin; 0.1 mGy;

Irradiation Device

Source: cyclotron (Cyclotron Corp. CS-15) $^9\text{Be}(^3\text{He},n)$ reaction. Total
activity/output at source: $1.4 \times 10^{10} \text{ n.s}^{-1} \text{ .}\mu\text{A}^{-1}$
Geometry: open field at 200 cm source to skin distance
Exposure time: 2 min
Uniformity of irradiation for element & organ of interest: phantom
derived correction used

Counting Device

Detector: 10 cm^3 volume gas proportional counter
Measurement time: overnight
Special features: special low-background detectors and detector shielding,
procedures developed in Brookhaven National Laboratory.

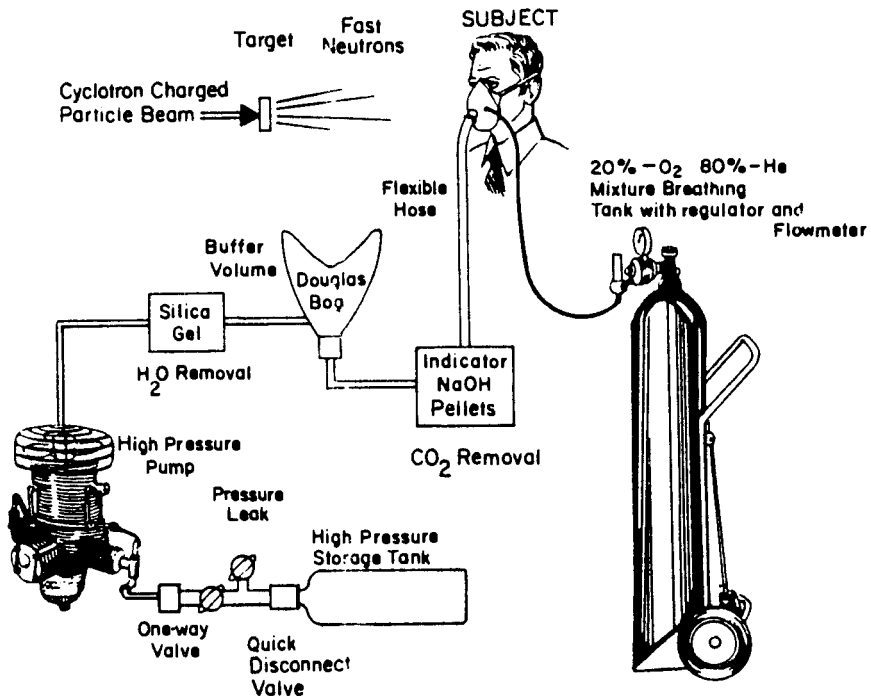


Fig. A.9. Apparatus used to store the ^{37}Ar exhaled by human subjects following fast neutron irradiation and prior to separation of the ^{37}Ar from the breath for activity measurement in a gas proportional counter.

REFERENCES

- 1 S.H. Cohn, *Med.Phys.*, 8 (1981) 145
- 2 J.G. Hoffman and L.H. Hempelmann, *Am.Journ.Radiol.*, 77 (1957) 144
- 3 J.W. Smith and S.J. Boot, *Phys.Med.Biol.*, 7 (1962) 45
- 4 J.W. Smith, *Phys.Med.Biol.*, 7 (1962) 341
- 5 C.J. Maletskos, A.T. Keane, S. Littlefields and R.A. McClatchley, MIT Radioactivity Center, Annual Progress Report Document, 952 (1961) 68
- 6 C.J. Maletskos, H.F. Osborn and A.G. Braun, MIT Radioactivity Center. Annual Progress Report Document, 9505 (1962) 47
- 7 J. Anderson, S.B. Osborn, R.W.S. Tomlinson, D. Newton, J. Rundo, L. Salmon and J.W. Smith, *Lancet* II (1964) 1201
- 8 C.K. Battye, R.W.S. Tomlinson, J. Anderson and S.B. Osborn in *Nuclear Activation Analysis in the Life Sciences*, Proc.Symp.IAEA, Amsterdam 1967, IAEA Vienna, 1967.
- 9 M.J. Chamberlain, J.H. Fremlin, D.K. Peters and H. Philip, *Brit. Med. Journ.* 2 (1968) 581
- 10 M.J. Chamberlain, J.H. Fremlin, D.K. Peters and H. Philip, *Brit. Med. Journ.* 2 (1968) 583
- 11 M.J. Chamberlain, *New Scientist* Sep.18th. (1969) 575
- 12 K. Boddy, *Radioakt.Isotopen in Klinik und Forschung*, 7 (1966) 377
- 13 J.J. Lenihan, D. Comar, R. Riviere and C. Kellersohn, *Nature* 214 (1967) 1221
- 14 D. Comar (Ed.) *Proc.Conf.On In Vivo Activation Analysis*, CEA, Orsay, July 1968 (unpubl.) .
- 15 D. Comar in J.M.A. Lenihan and S.J. Thomson (Eds.) *Advances in Activation Analysis*, Academic Press, London, 1969.
- 16 S.H. Cohn, *Atomic Energy Review*, 18 (1980) 599
- 17 D.R. Chettle and J.H. Fremlin, *Phys.Med.Biol.*, 29 (1984) 1011
- 18 S.H. Cohn and R.M. Parr, *Clin.Phys.Physiol.*, 6 (1985) 275
- 19 IAEA / RL /131 *Nuclear-based Techniques For the In-Vivo Study Of Human Body Composition*. Document IAEA, Vienna, 1986 .
- 20 S.H. Cohn and H.E. Palmer, *J.Nucl.Med.Biol.*, 1 (1974) 155
- 21 W.B. Nelp, H.E. Palmer, R. Murano, K. Palthorp, M.H. Gervas, C. Rich, J. Williams, T.G. Rudd and J.D. Denny, *J.Lab.Clin.Med.*, 76 (1970) 156
- 22 M.J. Chamberlain, J.H. Fremlin, I. Holloway and D.K. Peters, *Int.J.Appl.Radiat.Isot.*, 21 (1970) 725
- 23 S.H. Cohn, K.K. Shukla, C.S. Dombrowski and R.G. Fairchild, *J.Nucl. Med.* 13 (1972) 487
- 24 K. Boddy, I. Holloway, A. Elliott, D. Glaros, I. Robertson and B.W. East in *Nuclear Activation Analysis Techniques In the Life Sciences*, Proceedings of the Symposium in Bled, 1972. IAEA, Vienna, 1972 .
- 25 K. Boddy, I. Holloway and A. Elliott in *In-Vivo Activation Analysis*, Proceedings of a Panel, Vienna, 1972. IAEA, Vienna, 1973 .
- 26 K. Boddy, E.D. Williams, J.K. Haywood, I. Harris and I.A. Harris in *Nuclear Activation Analysis Techniques In the Life Sciences*, Proceedings of a Symposium, Vienna, 1978. IAEA, Vienna, 1979.
- 27 J.K. Haywood, E.D. Williams, F.J. McArdle and K. Boddy, *Phys.Med.Biol.*, 26 (1981) 603
- 28 S.H. Cohn, R.G. Fairchild and K.K. Shukla, *Phys.Med.Biol.*, 18 (1973) 648
- 29 H.E. Palmer, *J.Nucl.Med.*, 14 (1973) 522
- 30 H.E. Palmer, T.K. Lewellen, C.H. Chestnut and W.B. Nelp in *Proc.3rd Conf.on Applications of Small Accelerators*, Denton, Texas, 1975,
- 31 B.J. Thomas, M.S. Wright, E. Ozbas and D. Vartsky, *Proc.Analyt.Div.Chem.Society* 13 (1976) 207
- 32 K.V. Ettinger in *Proc.2nd East Kilbride Conf.on Progress and Problems in In Vivo Activation Analysis*, Scottish Univ.Research Reactor Centre Report, SURRC 57/76, Glasgow, 1976 .
- 33 R.E. Biggler, J.S. Laughlin, R. Davis and J.C. Evans, *Radiat.Res.*, 67 (1976) 266
- 34 E. Ozbas, D.R. Chettle, K.V. Ettinger, J.H. Fremlin, T.C. Harvey, W.V. Prestwich and B.J. Thomas, *Int.J.Appl.Radiat.Isot.*, 27 (1976) 227

- 35 F.H. Kummer, R.W. Stoenner and R. Davis jr., Brookhaven Natl. Laboratory Report BNL-16972 (1971)
- 36 D. Vartsky, A. LoMonte, K.J. Ellis, S. Yasumura and S.H. Cohn, *Phys. Med. Biol.*, 30 (1985) 1225
- 37 D. Glaros, A.F. LoMonte, K.J. Ellis, S. Yasumura, R.W. Stoenner and S.H. Cohn, *Med. Phys.*, 13 (1976) 45
- 38 D. Duffey, A. El-Kady and F. Senftle, *Nucl. Instr. Meth.*, 80 (1970) 149
- 39 F. Senftle, H.D. Moore and D.B. Leep, *Nucl. Instr. Meth.*, 93 (1971) 425
- 40 M.A. Lone, R.A. Leavitt and D.A. Harrison, *Atom. Nucl. Data Tables* 26 (1981) 511
- 41 J. Rundo and L.J. Bunce, *Nature* 210 (1966) 1023
- 42 H.C. Biggin, N.S. Chen, K.V. Ettinger, J.H. Fremlin, W.D. Morgan, R. Nowotny, M.J. Chamberlain, P.W. Dykes and T.C. Harvey in *Proc. 3rd Int. Conf. on Medical Physics*, Goeteborg, 1972 .
- 43 H.C. Biggin, N.S. Chen, K.V. Ettinger, J.H. Fremlin, W.D. Morgan, R. Nowotny and M.J. Chamberlain in *Nuclear Activation Techniques in the Life Sciences*, Proceedings of a Symposium, Bled 1972. IAEA, Vienna, 1972.
- 44 K.V. Ettinger, H.C. Biggin, N.S. Chen, D.R. Chettle, J.H. Fremlin, T.C. Harvey, W.D. Morgan, R. Nowotny, B.J. Thomas and D. Vartsky, *Kerntechnik*, 17 (1975) 89
- 45 K.J. Ellis, D. Vartsky and S.H. Cohn in *Nuclear Activation Techniques in the Life Sciences*, Proceedings of a Symposium, Vienna, 1978 . IAEA, Vienna, 1979.
- 46 H.C. Biggin, N.S. Chen, K.V. Ettinger, J.H. Fremlin, W.D. Morgan and R. Nowotny, in *Proc. Colloquium CNRS on Activation Analysis*, Paris, 1972.
- 47 H.C. Biggin, N.S. Chen, K.V. Ettinger, J.H. Fremlin, W.D. Morgan, R. Nowotny, M.J. Chamberlain and T.C. Harvey, *J. Radioanal. Chem.*, 19 (1974) 207
- 48 J.S. McLellan, B.J. Thomas, J.H. Fremlin and T.C. Harvey, *Phys. Med. Biol.*, 20 (1975) 88
- 49 D. Vartsky, K.J. Ellis, N.S. Chen and S.H. Cohn, *Phys. Med. Biol.*, 22 (1977) 1085
- 50 W.D. Morgan, D. Vartsky, K.J. Ellis and S.H. Cohn, *Phys. Med. Biol.*, 26 (1981) 413
- 51 B. Carlmark and P. Reizenstein in *In Vivo Neutron Activation Analysis*, Proceedings of a Panel, Vienna, 1972. IAEA, Vienna, 1973.
- 52 C.J. Evans, P. Cummins, J. Dutton, W.D. Morgan, A. Sivyer and R.R. Ghose in *Nuclear Activation Techniques in the Life Sciences*, Proceedings of a Symposium, Vienna, 1978. IAEA, Vienna, 1979 .
- 53 A. Al-Hiti, I.H. Al-Sidi and M.B. Albedri, *Int. J. Appl. Radiat. Isot.*, 31 (1980) 563
- 54 B.J. Thomas, T.C. Harvey, D.R. Chettle, J.S. McLellan and J.H. Fremlin, *Phys. Med. Biol.*, 24 (1979) 432
- 55 R.G. Zamenhof, O.L. Deutsch and B.W. Murray, *Med. Phys.*, 6 (1979) 179
- 56 K. Kyere, B. Oldroyd, C.B. Oxby, L. Burkinshaw, R.E. Ellis and G.L. Hill, *Phys. Med. Biol.*, 27 (1982) 805
- 57 F.C. Engesser, W.E. Thompson and J.M. Ferguson, Report USNRDL-TR-796 (1964).
- 58 W.E. Thompson and F.C. Engesser, Report USNRDL-TR-861 (1965) .
- 59 F.C. Engesser and W.E. Thompson, Report USNRDL-TR-916 (1965) .
- 60 K.V. Ettinger, W.D. Morgan, U.J. Miola, D. Vartsky, K.J. Ellis, L. Wielopolski and S.H. Cohn, *Med. Phys.*, 9 (1982) 550
- 61 U.J. Miola, *Studies in Medical Neutron Physics*, Ph.D. Thesis, Dept. of Biomedical Physics and Bioengineering, University of Aberdeen, Aberdeen, UK, (1982).
- 62 G.J. Lutz, *Anal. Chem.*, 43 (1971) 93
- 63 A.L. Kairento and P. Nikkinen-Vilkki, *Strahlentherapie*, 148 (1974) 155
- 64 NBS 322, *Photonuclear Data Index*. NBS Special Publication no. 322, Natl. Bur. Standards, Washington DC, 1970 .
- 65 E.G. Fuller, H.M. Gerstenberg, H. Vander Malen and T.C. Dunn, *Photonuclear Reaction Data 1973* . Natl. Bur. Standards, Washington D.C., 1973 .
- 66 R.J. Howerton, D. Braff, W.J. Cahill and N. Chazan, Lawrence Radiation Lab. Report UCRL-14006 (1964) .
- 67 H.V. Piltingsrud, *Med. Phys.*, 10 (1983) 147
- 68 J.D. Stoeckle, H.L. Hardy and A.I. Weber, *Am. J. Medicine* 46 (1969) 46
- 69 K.V. Ettinger, W.D. Morgan, U.J. Miola, D. Vartsky, K.J. Ellis, L. Wielopolski and S.H. Cohn, in *Proc. 4th Int. Conf. on Nuclear Methods in Environmental and Energy Research*, Columbia Miss., 1980, CONF 800433 (1980).

- 70 P.A. Ali, J. Dutton, C.J. Evans, W.D. Morgan and A. Sivyer, *Phys.Med.Biol.*, 30 (1985) 1277
- 71 K. Ulin and R.G. Zamenhof, *Med.Phys.*, 13 (1986) 887
- 72 A. Luccio, *Biomedical Imaging in Ettore Majorana Summer School of Physics on Medical Imaging and Related Dosimetry, Erice, 1986. (Preprint)*
- 73 D. Vartsky, B.J. Thomas, D.J. Hawkes and J.H. Fremlin, *Phys.Med.Biol.*, 21(1976) 970
- 74 D. Vartsky, L. Wielopolski, K.J. Ellis and S.H. Cohn, *Nucl.Instr.Math.*, 193 (1982) 359
- 75 D. Vartsky, K.J. Ellis, D.H. Hull and S.H. Cohn, *Phys.Med.Biol.*, 24 (1979) 689
- 76 L. Wielopolski, D. Vartsky and S.H. Cohn, *Trans.Am.Nucl.Soc.*, 44 (1983) 31
- 77 L. Wielopolski, D. Vartsky, D.C. Rorer, P.W. Levy and S.H. Cohn, *IEEE Trans. Nucl.Sci.*, 30 (1983) 591
- 78 L. Wielopolski, R.C. Ancona, R.Y. Massey, A.N. Vaswani and S.H. Cohn, *Med.Phys.*, 12 (1985) 401
- 79 F.R. Metzger, *Progr.Nucl.Phys.*, 7 (1959) 54
- 80 G. Deconninck, *Introduction to Radioanalytical Physics, Elsevier, Amsterdam, 1978 .*
- 81 S.H. Cohn, R.G. Fairchild and K.K. Shukla in *In Vivo Neutron Activation Analysis, Proceedings of a Panel, Vienna, 1978. IAEA, Vienna, 1978 .*
- 82 H. Aceto and B.W. Churchill in *Lawrence Radiation Lab. Report UCRL-10267 (1963) .*
- 83 W.S. Snyder and J. Neufeld in *Protection Against Neutron Radiation Up To 30 MeV, NBS Handbook 83, Natl. Bur. Standards, Washington DC, 1955 (reprinted 1967).*
- 84 V.G. Zolotukhin, I.B. Keirim-Markus, O.A. Kochetkov, G.M. Obaturov and V.I. Cvetkov in *Tissue Doses of Neutrons in Human Body, Atomizdat, Moscow, 1972 . (in Russian)*
- 85 V.H. Ivanov, *Atomnaya Energiya (Moscow)*, 39 (1975) 360 , (in Russian) .
- 86 R.C. Lawson, D.M. Clare and D.E. Watt, *Phys.Med.Biol.*, 12 (1967) 201
- 87 R.C. Lawson and D.E. Watt, *Phys.Med.Biol.*, 9 (1964) 487
- 88 D. Vartsky and B.J. Thomas, *Phys.Med.Biol.*, 21 (1976) 139
- 89 ICRU 26, *Neutron Dosimetry for Biology and Medicine, Int.Comm.on Radiation Units and Measurement, Report 26, Washington DC, 1977 .*
- 90 NCRP 38 , *Protection Against Neutron Radiation, Natl. Council on Radiation Protection and Measurements, Report 38, Washington DC, 1971 .*
- 91 A.M. Kellerer in H.G. Ebert and G. Burger (Eds.), *Proc. 2nd Symp. on Neutron Dosimetry in Biology and Medicine, München, 1974 . EUR 5272 (1975) .*
- 92 D. Chmelevsky in J. Booz, H.G. Ebert and H.D. Hartfiel (Eds.), *Proc. 7th Symp. on Microdosimetry, Oxford, 1980. EUR 7147 (1981) .*
- 93 J.J. Broerse, B.J. Mijneer and J.R. Williams, *Br.J.Radiol.*, 54 (1981) 882
- 94 G. Makrigiorgos and A.J. Waker, *Phys.Med.Biol.*, 30 (1985) 909
- 95 B.J. Mijneer and J.R. Williams, *Phys.Med.Biol.*, 26 (1981) 57
- 96 ICRU 36, *Microdosimetry, Int.Comm.on Radiation Protection and Measurements, Report 36, Washington DC, 1983 .*
- 97 J. Booz, A.A. Edwards and K.G. Harrison in *Proc. Workshop on Microdosimetric Counters in Radiation Protection, Rad.Prot.Dosim. , 9 (1984) 137*
- 98 A.J. Waker and G. Makrigiorgos in J. Booz and H.G. Ebert (Eds.), *Proc. 8th Symp. on Microdosimetry, Jülich, 1982 .EUR 9395 (1983) .*
- 99 A.J. Waker, *Nucl.Instr.Meth.Phys.Res.*, A 234 (1985) 354
- 100 T.G. Stinchcomb, F.T. Kuchnir and L.S. Skaggs, *Phys.Med.Biol.*, 25 (1980) 51
- 101 G. Hartmann, H.G. Menzel and H. Schumacher in G. Burger and H.G. Ebert (Eds.) *Proc. 4th Symp. on Neutron Dosimetry, München, 1981 . EUR 7448 (1982)*
- 102 K. Boddy in *In Vivo Neutron Activation Analysis, Proceedings of a Panel, Vienna, 1972. IAEA, Vienna, 1973 .*
- 103 S. Cierjacks (Ed.) *Neutron Sources For Basic Physics And Applications, Pergamon, Oxford, 1983 .*
- 104 H.H. Hubbel, *Health Phys.*, 27 (1974) 289
- 105 T.D. Jones, *Health Phys.*, 27 (1974) 87
- 106 K. Boddy, J.A. Dennis and R.C. Lawson, *Phys.Med.Biol.*, 14 (1969) 471
- 107 D. Singh, *Health Phys.*, 35 (1978) 369
- 108 D. Singh, *Nucl.Instr.Meth.*, 159 (1979) 229

- 109 D. Singh, *Health.Phys.*, 37 (1979) 751
- 110 M.S.S. Murthy, *Health Phys.*, 27 (1974) 9
- 111 A. Ricourt in G.Burger, H. Schraube and H.G. Eberte (Eds.), *Proc. 1st Symp. on Neutron Dosimetry in Biology And Medicine*, München, 1972. EUR 4896 (1972) .
- 112 F.S. Williamson and N.A. Frigerio in G.Burger, H. Schraube and H.G. Ebert (Eds.), *Proc. 1st Symp. Neutron Dosimetry in Biology And Medicine*, München, 1972. EUR 4896 (1972) .
- 113 R.G. Fairchild, *Phys.Med.Biol.* 10 (1965) 491
- 114 R.G. Fairchild and L.J. Goodman, *Phys.Med.Biol.*, 11 (1966) 15
- 115 R.G. Zamenhof, B.W. Murray, G.L. Brownell, G.R. Wellum and E.I. Tolpin, *Med. Phys.* 2 (1975) 47
- 116 B.W. Howes, Idaho Nucl. Corp. Report IN-1308 (1969) .
- 117 R.M. Brugger and O.D. Simpson in *Proc. Conf. on Irradiation Facilities For Research Reactors*, IAEA, Vienna, 1973 .
- 118 K.R. Bryant and S.R. Bull in *Proc. Conf. on Biological Effects of Neutron Irradiation*, IAEA, Vienna, 1974 .
- 119 R.C. Greenwood and R.E. Chrien, *Nucl. Instr. Meth.*, 138 (1976) 125
- 120 J.R. Harvey and A.J. Mill in G.Burger and H.G. Ebert (Eds.), *Proc. 3rd Int. Symp. Neutron Dosimetry in Medicine And Biology*, München, 1979. EUR 5848 (1979)
- 121 T. Cousins, T.J. Kennett, W.V. Prestwich and C.E. Webber, *Med. Phys.*, 7 (1980) 655
- 122 K. Boddy, I. Robertson and D. Glaros, *Phys.Med.Biol.*, 19 (1974) 853
- 123 E. Piesch in *Some Physical Dosimetry And Biological Aspects of Californium-252*, IAEA, Vienna, 1976 .
- 124 E. Piesch and E.M. Sayed in G. Burger and H.G. Ebert (Eds.), *Proc. 2nd Int. Symp. on Neutron Dosimetry in Biology and Medicine*, München, 1975. EUR 5273 (1975) .
- 125 G.F. Knoll, chapter 2 in S. Cierjacks (Ed.), *Neutron Sources For Basic Physics And Applications*, Pergamon, Oxford, 1983 .
- 126 C.A. Uttley, chapter 3 in S. Cierjacks (Ed.), *Neutron Sources for Basic Physics And Applications*, Pergamon, Oxford, 1983 .
- 127 H.H. Barschall, ch.4 in S. Cierjacks (Ed.), *Neutron Sources For Basic Physics And Applications*, Pergamon, Oxford, 1983 .
- 128 H.I. Amals, J.F. Dicello, M. Avsshalom, L. Coulson, S.W. Johnsen and R.B. Theus, *Med. Phys.*, 4 (1977) 86
- 129 M.A. Lone and C.B. Bigham, chapter 6 in S. Cierjacks (Ed.), *Neutron Sources For Basic Physics and Applications*, Pergamon, Oxford, 1983 .
- 130 H. Berger, *Neutron Radiography*, Elsevier, Amsterdam, 1965 .
- 131 K.V. Ettinger, *Pulsed Cyclotron Beams*, Ph.D. Thesis, Department of Physics, Univ. of Birmingham, Birmingham UK, 1970 .
- 132 H.J. Evans, A.D. LeBlanc and P.C. Johnson, *Med. Phys.*, 3 (1976) 145
- 133 D. Kokinos in P. Groebler and E.J. Henley, *Advances in Nuclear Science And Technology*, vol. 3, Academic Press, New York, 1966 .
- 134 J.J. Dorking, Brookhaven Natl. Lab. Report BNL-11680 (1967) .
- 135 J.H. Ferziger and P.F. Zweifel, *The Theory of Slowing Down In Nuclear Reactors*, MIT Press, Cambridge, Mass., 1966 .
- 136 P.A. Egelstaff and M.S. Poole, *Experimental Neutron Thermalization*, Pergamon, Oxford, 1969 .
- 137 M.M.R. Williams, *The Slowing Down And Thermalization of Neutrons*, North Holland, Amsterdam, 1966 .
- 138 H.S. Camarda, *Nucl. Instr. Meth.*, 106 (1973) 205
- 139 U.J. Miola and K.V. Ettinger. Unpubl. results. (1984) .
- 140 G.F. von Dardel, *Trans. Royal Inst. Technol. (Stockholm)*, 75 (1954) 345
- 141 G.F. von Dardel and N.G. Sloestrand, *Progr. Nucl. Energy, Ser. 1*, 2 (1958) 185
- 142 S.N. Purohit, *Nucl. Sci. Eng.*, 9 (1961) 157
- 143 J.C. Philippot, *IEEE Trans. Nucl. Sci.*, 17 (1970) 446
- 144 G.A. Armantrout, A.E. Bradley and P.L. Phelps, *IEEE Trans. Nucl. Sci.*, 19 (1972) 107
- 145 G.F. Knoll, *Radiation Detection And Measurement*, Wiley, New York, 1979 .
- 146 N. Tsoulfanidis, *Measurement And Detection Of Radiation*, McGraw-Hill, New York, 1983 .

- 147 C.C. Grosjean and W. Bossaert, Table of absolute detection efficiencies of cylindrical scintillation gamma-ray detectors, Computing Lab., University of Ghent, Ghent, 1985.
- 148 C.E. Crouthamel, F. Adams and R. Dams, Applied gamma ray Spectrometry, 2nd Ed., Pergamon Press, Oxford, 1965.
- 149 J.B. Marion and F.C. Young, Nuclear reaction analysis, North Holland, Amsterdam, 1968
- 150 C. Weitkamp, Report Kernforschungszentrum Karlsruhe, KFK-188 (1963)
- 151 F.C. Young, H.T. Heaton, G.W. Philips, P.D. Forsyth and J.B. Marion, Peak-to-total Ratios And Efficiencies For A 5 in. Diam x 5 in NaI Crystal, Dept. of Physics, Univ. of Maryland, Techn. Report 490 (1965) .
- 152 P. Gander, K. Verghese and H.M. Lee, Nucl. Instr. Meth., 176 (1980) 615
- 153 H. Seyfarth, A.M. Hassan, B. Hrastrnik, P. Gottel and W. Delang, Nucl. Instr. Meth. 105 (1972) 301
- 154 R.A.I. Bell, Tables For Calibration Of Radiation Detectors, Austr. Natl. Univ. Report, ANU-P/606, (1974) .
- 155 R.L. Bunting and J.J. Kraushar, Nucl. Instr. Meth., 118 (1974) 565
- 156 D.E. Watt and D.R. Ramsden, High Sensitivity Counting Techniques, Pergamon, Oxford, 1964 .
- 157 S.H. Cohn (Ed.) Proc. Conf. on Clinical Uses of Whole-Body Counting, Vienna, 1966 . IAEA, Vienna, 1966 .
- 158 A.L. Orvis, in G.J. Hine (ed.), Instrumentation in Nuclear Medicine, vol. 1, Academic Press, New York, 1967 .
- 159 P. Reizenstein, Clinical Whole Body Counting, J. Wright and Sons, Bristol, 1973 .
- 160 J. Rundo, in Proc. Conf. on Whole Body Counting, Vienna, 1962. IAEA, Vienna, 1962 .
- 161 Y. Naversten in S.H. Cohn (Ed.), Proc. Conf on Clinical Uses Of Whole Body Counting, Vienna, 1966. IAEA, Vienna, 1966 .
- 162 S.H. Cohn and C.S. Dombrowski, IEEE Trans. Nucl. Sci., 18 (1971) 73
- 163 N.S. Chen and S.H. Cohn, Int. J. Nucl. Med. Biol., 1 (1974) 169
- 164 N.S. Chen, K.J. Ellis, H.R. Pate and S.H. Cohn, Int. J. Nucl. Med. Biol., 1 (1974) 175 .
- 165 I.H. Davies, A. Jacobs and G.M. Owen, Int. J. Nucl. Med. Biol., 1 (1974) 145
- 166 G.T. Warner and R. Oliver, Phys. Med. Biol., 11 (1966) 83
- 167 K. Boddy, Br. J. Radiol., 40 (1967) 631
- 168 K. Boddy, Phys. Med. Biol., 12 (1967) 43
- 169 K. Boddy, P.C. King, P. Tothill and J.A. Strong, Phys. Med. Biol., 16 (1971) 275
- 170 D. Gvozdanovic, K.V. Ettinger, D.B. Smith, C.G. Taylor, S. Gvozdanovic and J.R. Mallard in Proc. Symp On Medical Radionuclide Imaging, Heidelberg, 1980. IAEA, Vienna, 1981 .
- 171 G.T. Warner, Shadow Shield Whole Body Counters For Clinical Investigations, Medical Monograph no. 2, Nuclear Enterprises Ltd., Edinburgh, 1969 .
- 172 K. Boddy and W.D. Alexander in Nuclear Activation Techniques In the Life Sciences, Proc. Symposium, Amsterdam, 1967 . IAEA, Vienna, 1967.
- 173 S.H. Cohn, Computer Analysis Of Gamma-Ray Spectral Data: Whole Body Counting in Handbook of Biomedical Information, Encyclopedia Britannica, 1970. Also in Brookhaven Natl. Lab. Report, BNL-14535 (1970)
- 174 L. Wielopolski and S.H. Cohn, Med. Phys., 11 (1984) 526
- 175 J. De Pangher and E. Tochilin in F.H. Attix and E. Tochilin (Eds.), Radiation Dosimetry, vol. 2, Academic Press, New York, 1969 .
- 176 R.S. Caswell, J.J. Coyne and M.L. Randolph in J.J. Broerse (Ed.), Basic Physical Data For Neutron Dosimetry, EUR 5629 (1976) .
- 177 M.F. Fuller, M.A. Foster and J.M.S. Hutchinson, Nuclear Magnetic Resonance Imaging of Pigs in D. Lister (Ed.), In Vivo Measurement of Body Composition In Meat Animals, Elsevier Appl. Science, London, 1984 .
- 178 I. Zanzi, C. Colbert, R. Backtell, K. Thompson, J. Aloia and S.H. Cohn, in Proc. 4th Int. Conf. on Bone Measurement (Abstract), Am. J. Roentgenol., 131, (1978) 551
- 179 S.M. Garn, A. Poznanski, G. Mayor and J. Pottenger, in Proc. 4th Int. Conf. on Bone Measurement (Abstract), in Am. J. Roentgenol., 131 (1978) 551

- 180 B. Maziere, D. Kuntz and D. Comar, Proc. 4th Int. Conf. on Bone Measurements (Abstract), Am.J.Roentgenol., 131 (1978) 550
- 181 S.H. Cohn, Intercomparison of Techniques For the Non-invasive Measurement of Bone Mass, in J.V. Dequeker and C.C. Johnston (Eds.), Non-Invasive Bone Measurement : Methodology And Problems, IRL Press, 1982 .
- 182 S.H. Cohn, Retrospect and Prospects, Ch.10 in S.H. Cohn (Ed.), Non-invasive Measurements of Bone Mass And Their Clinical Application, CRC Press, Boca Raton, Florida, 1981.
- 183 R.B. Mazess, Non-invasive Measurement of Bone in U.S. Barzel (Ed.), Osteoporosis II, Grune and Stratton, 1979 .
- 184 E.D. Williams, K. Boddy, I. Harvey and J.K. Haywood, Phys.Med.Biol., 23 (1978) 405
- 185 D. Vartsky, W.V. Prestwich, B.J. Thomas, J.T. Dabek, D.R. Chettle, J.H. Fremlin and K. Stammers, J.Radioanalyt.Chem., 48 (1977) 243
- 186 R.E. Bigler, J.S. Laughlin, R. Davis jr and J.C. Evans, Int.J.Nucl.Med.Biol., 3 (1976) 105
- 187 R.E. Bigler, Applied Radiology, 7 (1978) 149
- 188 M.O. Leach, C.M. Bell, B.J. Thomas, J.T. Dabek, H.M. James, D.R. Chettle and J.H. Fremlin, Phys.Med.Biol., 23 (1978) 282
- 189 C.M. Bell, M.O. Leach, J.T. Dabek, D.R. Chettle, H.M. James, B.J. Thomas and J.H. Fremlin, J.Nucl.Med., 19 (1978) 54
- 190 R.E. Bigler, in IAEA/ RL /131, Nuclear-based Techniques For the In-Vivo Study of Human Body Composition. Document IAEA, Vienna, 1986 .
- 191 T.L. Lewellen, in IAEA/ RL /131, Nuclear-based Techniques For the In-Vivo Study of Human Body Composition. Document IAEA, Vienna, 1986 .
- 192 S.H. Cohn, A. Vaswani, J. Aloia, M. Roginsky, I. Zanzi and K.J. Ellis, Metabolism 25 (1976) 89
- 193 J.E. Harrison and K.G. McNeill, Am.J.Roentgenol., 126 (1976) 1308
- 194 B. Maziere, D. Kuntz, D. Comar and A. Ryckenwaert, J.Nucl.Med., 20 (1979) 85
- 195 N.S.J. Kennedy, R. Eastell, C.M. Ferrington, J.D. Simpson, M.A. Smith, J.A. Strong and P. Tothill, Phys.Med.Biol., 27 (1982) 697
- 196 D. Vartsky, B.J. Thomas and W.V. Prestwich, Nucl.Instr.Meth., 145 (1977) 321
- 197 K.V. Ettinger, B.J. Thomas and D.J. Filkin in L. Joho (Ed.), Cyclotrons and Their Uses, Proc. 7th Int. Conf., Zürich, 1975, Birkhauser Verlag, Basel, 1975.
- 198 E.M. Lent, Lawrence Radiation Lab. Report UCRL-50857 (1968)
- 199 K.M. Jones and C.A. Kelsey, Med.Phys., 1 (1974) 215
- 200 F.H. Attix, L.S. Augst and P. Schapiro, Med.Phys. 4 (1977) 118
- 201 U.J. Miola, Development of Neutron Collimator, Internal Report, Dept. of Biomedical Physics and Bioengineering, Univ. of Aberdeen (U.K.), 1980 .
- 202 K.V. Ettinger, M.A. Foster and U.J. Miola, Future Developments In the In Vivo Measurement of Body Composition In Pigs, in D. Lister (Ed.), In Vivo Measurement of Body Composition In Meat Animals, Elsevier Appl. Science, London, 1984.
- 203 B.W. East, T. Preston and I. Robertson, The Potential of In Vivo Neutron Activation Analysis For Body Composition Measurements In the Agricultural Sciences, in D. Lister (Ed.), In Vivo Measurement of Body Composition In Meat Animals, Elsevier Appl. Science, London, 1984.
- 204 T. Preston, B.W. East and I. Robertson, Body Composition Measurement In Rats, Pigs And Humans In Neutron Activation Analysis, in D. Lister (Ed.), In Vivo Measurement of Body Composition In Meat Animals, Elsevier Appl. Science, London 1984 .
- 205 T. Preston, B.W. East and I. Robertson, Proposals For a "Portable" Facility For In Vivo Protein Determination And Carcass Quality Prediction In Farm Animals By Neutron Activation Analysis, in D. Lister (Ed.), In Vivo Measurement of Body Composition In Meat Animals, Elsevier Appl. Science, London, 1984.
- 206 S.H. Cohn, J.F. Aloia, A.N. Vaswani, Kapo Yuen, S. Yasumura and K.J. Ellis, Calcif. Tissue Int., 38 (1986) 9
- 207 C.H. Chesnut, W.B. Nelp, D. Baylink and J.D. Denny, Metab. Clin. Exp. (US), 26 (1977) 267
- 208 C.H. Chesnut, J.L. Ivey, W.B. Nelp and D.J. Baylink, Assessment of Anabolic Steroids And Calcitonin In the Treatment of Osteoporosis, in W. Barzel (Ed.), Osteoporosis, Grune and Stratton, 1981 .

- 209 G.R.D. Catto, M. MacLeod, B. Pelc and E. Kodicek, *Brit. Med. J.*, 1 (1975) 12
- 210 G.R.D. Catto, B.J.R. Junor, R.A. Fraser, F.W. Smith, K.V. Ettinger, N. Edward and M. MacLeod, *Proc. Eur. Dialysis Transplant Assoc.*, 16 (1979) 637
- 211 G.R.D. Catto, N. Muirhead, N. Edward, R.A. Fraser, J.L.H. O'Riordan, S.E. Papapoulos and S. Adami, *Proc. Eur. Dialysis Transplant Assoc.*, 17 (1980) 543
- 212 B.J.R. Junor, G.R.D. Catto, M. MacLeod, S.E. Papapoulos, J.L.H. O'Riordan and R.A. Fraser, *Proc. Eur. Dialysis Transplant Assoc.*, 13 (1976) 424
- 213 G.R.D. Catto, J.A.R. McIntosh and M. MacLeod, *Proc. Eur. Dialysis Transplant. Assoc.*, 10 (1973) 173
- 214 S.H. Cohn, Total Body Neutron Activation, in S.H. Cohn (Ed.), *Non-invasive Measurements of Bone Mass And Their Clinical Application*, CRC Press, Boca Raton, Florida, 1981.
- 215 S.H. Cohn, A. Sawitzky, D. Vartsky, S. Yasumura, I. Zanzi and K.J. Ellis, *Nutrition and Cancer*, 2 (1980) 67
- 216 C.H. Walsh, N.G. Soler, H.M. James, T.C. Harvey, J.H. Fremlin, B.J. Thomas, M.G. Fitzgerald and J.M. Melius, *Queensl. J. Med. (NS)* XLV 178 (1976) 295
- 217 J.E. Harrison, K.G. McNeill, J.B. Mernagh and K.N. Jeejeebhoy in *Nuclear Analysis Techniques In the Life Sciences*, *Proceedings of a Symposium*, Vienna 1978. IAEA, Vienna, 1979.
- 218 W.D. Morgan, C.J. Evans, P.E. Cummins, P.C. Elwood, A.C. Ames, A. Thomas, D. Cross, R.R. Ghee, A. Sivyer and J. Dutton in *Proc. Conf. on Heavy Metals In an Urban-Industrial Environment*, Amsterdam, 1981. PEP Consultants, Edinburgh, 1982.
- 219 J.G. Fletcher, D.R. Chettle and I.K. Haddad, *J. Radioanalyt. Chem.*, 71 (1982) 547
- 220 W.D. Morgan, K.J. Ellis, D. Vartsky, S. Yasumura and S.H. Cohn, *Phys. Med. Biol.*, 26 (1981) 577
- 221 W.D. Morgan, *Lancet* 77 (1976) 1361
- 222 K.J. Ellis, D. Vartsky, I. Zanzi, S.H. Cohn and S. Yasumura, *Science* 205 (1979) 323
- 223 K.J. Ellis, W.D. Morgan, S. Yasumura, D. Vartsky, I. Zanzi and S.H. Cohn, in *Proc. 4th Int. Conf. on Nuclear Methods in Environmental and Energy Research*, Columbia Miss., 1980, CONF 800433 (1980).
- 224 K.J. Ellis, W.D. Morgan, I. Zanzi, S. Yasumura, D. Vartsky and S.H. Cohn, *J. Toxicol. & Env. Health*, 7 (1981) 691
- 225 K.J. Ellis and S.H. Cohn, in *Proc. 5th Int. Conf. on Nuclear Methods in Environmental and Energy Research*, Mayaguez, Puerto Rico, 1984, CONF 840408 (1984).

AUTHOR INDEX

- Abdullah, M., see Khan, A.H. et al.
 Aceto, H. and Churchill, B.W., 321, 323, 377
 Agarwal, M. Bennett, R.B. Stump, I.G. D'Auria, J.M., 169, 178
 Ahlgren, L. and Mattsson, S., 102, 103, 104, 105, 108, 110, 111, 121
 Akselsson, K.R., 163, 178; see Johansson, T.B. et al.; see Malmqvist, K.G. et al.; see Pakarinen, P. et al.
 Albedri, M.B., see Al-Hiti, A. et al.
 Alber, A.L., see Iwanczyk, J.S. et al.
 Alberi, J.L. and Kraner, H.W., 183, 192, 194
 Alexiu, E., see Cesareo, R. et al.
 Alfrey, A.C., Hegg, A. and Craswell, P., 15, 17
 Al-Hiti, A., Al-Sidi, I.H. and Albedri, M.B., 307, 376
 Alha, E.M., see Puumalainen, P. et al.
 Ali, P.A., Dutton, J., Evans, C.J., Morgan, W.D. and Sivyver, A., 313, 377
 Aloia, J., see Cohn, S.H. et al.; see Zanzi, I. et al.
 Amals, H.I., Dicello, J.F., Avshalom, M., Coulson, L., Johnsen, S.W. and Theus, R.B., 340, 378
 Ames, L. and Drummond, W., 57, 119
 Ancizar-Sordo, 12, 16
 Anderson, J., Osborn, S.B., Tomlinson, R.W.S., Newton, D., Rundo, J., Salmon, L. and Smith, J.W., 299 375; see Battye, C.K. et al.
 Anke, M. Grappel, B. and Kronemann, H., 1, 15
 Arinc, F. and Gardner, R.P., 222, 247
 Armantrout, G.A., Bradley, A.E. and Phelps, P.L., 351, 378
 Atkins, H.L., Hauser, W. and Kraner, H.W., 181, 194
 Baird, A.K., 57, 119
 Bambynek, W., Cravemann, B., Fink, A. W., Mark, H., Swift, C.D., Price, R.E. and Rao, P.V., 25, 119; 125, 176
 Barbier, F., see Versieck, J. et al.
 Barrette, M., see Lecomte, R. et al.
 Barschall, H.H., 339, 378
 Battista, J.J., Santon, L.W. and Bronskill, M.J., 197, 222, 225, 234, 247; 235, 237, 248
 Battye, C.H., Tomlinson, R.W.S., Anderson, J. and Osborn, S.B., 299 375
 Bearden, J.A., 125, 176
 Beath, O.A., see Rosenfeld, I.
 Bell, C.M., Leach, M.O., Dabek, J.T., Chettle, D.R., James, H.M., Thomas, B.J. and Fremlin, J.H., 360, 380; see Leach, M.O. et al.
 Bell, R.A.I., 353, 379
 Berger, H., 341, 379
 Berman, E., 13, 14, 17
 Berti, M., Buso, G., Colautti, P., Moschini, G., Stievano, B.M. and Tregnaghi, C., 166, 178
 Bhaduri, D., see Huddleston, A.L. et al.
 Biggin, H.C., Chen, N.S., Ettinger, K.V. Fremlin, J.H., Morgan, W.D., Nowotny, R. and Chamberlain, M.J., 304, 307, 343, 344, 348, 376
 Biggler, R.E., Laughlin, J.S., Davis, R. and Evans, J.C., 303, 375
 Birchall, J.D., 2, 15
 Birke, G., Johnels, A.G., Plantin, I.O., Sjostrand, B., Skerfving, S. and Westermark, T., 12, 16
 Birks, L.S. and Gilfrich, J.V., 67, 120; see Gilfrich, J.V. et al.
 Bischof, W., see Gonsior, B. et al.; see Hbfert, M. et al.; see Wilde, H.R. et al.
 Bisgård, K.M., Laursen, J. and Schmitt Nielsen, B., 34, 119
 Bloch, P., Garavaglia, G., Mitchell, G. and Shapiro, I.M., 114, 116, 121
 Boddy, K., Dennis, J.A. and Lawson, R.C. 329, 377
 Boddy, K., Holloway, I. and Elliott, A., 299, 375
 Boddy, K., Williams, E.D., Haywood, J.K. 303, 375
 Boddy, K., 359, 379
 Boddy, K., see Haywood, J.K. et al.; see Williams, E.D. et al.
 Bolin, E.P., see Preuss, L.E.
 Bombelka, E., Richter, F.W., Ries, H. and Wätjen, U., 166, 178
 Bonani, G., Satish, J., Wanner, H.U. and Wölfl, W., 162, 178
 Boot, S.J., see Smith, J.W.
 Booz, J., Edwards, A.A. and Harrison, K.G., 328, 377
 Bos, A., see Houtman, J.P.W. et al.; see Vis, R.D. et al.
 Boulle, G.J., Peisach, M., Dempster, W. S., de V. Heese, H., 154, 178
 Bradley, D.A. and Ghose, A.M., 203, 206, 247
 Brasseleers, K., see Van Grieken, R. et al.
 Brateman, L., Jacobs, A.M., Fitzgerald, L.T., 222, 237, 247
 Brätter, P. and Schramel, P., 123, 132, 176; 160, 170, 178
 Brill, A.B., see Patton, J.A.

- Broerse, J.J., Mijneer, B.J. and Williams, J.R., 328, 377
- Bronskill, M.J., see Battista, J.J.; see Battista, J.J. et al.;
- Brown, D.B., Gilfrich, J.V. and Peckerrar, M.C., 52, 53, 54, 119
- Brown, G.S., see Otis, J.N. et al.
- Brown, R.T., see Hubbell, J.H. et al.
- Brownell, G.L., see Zamenhof, R.G. et al.
- Brugger, R.M. and Simpson, O.D., 332, 378
- Brüggerhoff, S., see Klockenkämper, R. et al.; see Raith, B. et al.
- Brüggerhoff, S., Jackwerth, E., Salewski, S., Raith, B., Divoux, S., Gonsior, B., 158, 177; 161, 169, 178
- Brune, D., see Lindh, W. et al.
- Bryant, K.R. and Bull, S.R., 332, 378
- Bubert, H., see Klockenkämper, R. et al.
- Buganis, C., see Preuss, L.E. et al.
- Bull, S.R., see Bryant, K.R.
- Bunce, L.J., see Rundo, J.
- Bunting, R.L., and Kraushar, J.J., 356, 379
- Burkinshaw, L., see Kyere, K. et al.
- Burkhalter, P.G., see Gilfrich, J.V. et al.
- Burnstein, N.L., and Maurice, D.M., 160, 178
- Buso, G., see Berti, M. et al.
- Buzzo, A., Biffoli, R., Chiti, F. and Pisani, B., 12, 16
- Cafmeyer, J., see Maenhaut, W. et al.
- Cahill, J.A., Flocchini, R.G., Feeney, P.J., Shadoan, D.J., 136, 177
- Cahill, W.J., see Howerton, R.J.
- Camarda, H.S., 345, 378
- Cameron, J.R. and Sorenson, J.A., 181, 189, 194; see Mazess, R.B. et al. see Mistretta, C.R. et al.
- Camp, D.C., see Kaufman, L. et al.
- Campbell Finman, L., see Otis, J.N. et al. Campbell, J.L., 161, 178
- Cantone, M.C., Molho, N. and Pirola, L., 293, 294, 297
- Carlmark, B. and Reizenstein, P., 307, 376
- Carlsson, C.A., see Carlsson, G.A. et al.
- Carlsson, G.A., Carlsson, C.A., Berggren, K.F. and Ribberfors, R., 198, 247
- Carlsson, L.E., see Malmqvist, K.G. et al.
- Cartwright, G.E., see Wintrobe, M.M. et al.
- Casey, C.E. and Hambidge, K.M., 11, 16
- Catto, G.R.D., Mac Leod, M., Pelc, B. and Kodicek, E., 361, 381
- Catto, G.R.D., Junor, B.J.R., Fraser, R. A., Smith, F.W., Ettinger, K.V., Edward, N. and Mac Leod, M., 361, 381
- Catto, G.R.D., Muirhead, N., Edward, N., Fraser, R., O' Riordan, J.L.H., Papapoulos, S.E. and Adami, S., 361, 381
- Cave-Bondi, G., see Cesareo, R. et al.
- Cesareo, R. and Viezzoli, G., 48, 119
- Cesareo, R. and Gigante, G.E., 65, 66, 67, 68, 120; 158, 178
- Cesareo, R. and Del Principe, D., 73, 74, 120
- Cesareo, R., 46, 51, 76, 77, 78, 120
- Cesareo, R., 78, 80, 81, 120
- Cesareo, R., Giancarelli, M.G. and Scarnati, E., 86, 87, 120
- Cesareo, R., Ciancarelli, M.G., Del Principe, D., Ricci, M. and Tallarida, B.M., 86, 88, 120
- Cesareo, R., Alexiu, E., Sacchetti, G. and Merli, S., 92, 94, 95, 96, 97, 120
- Cesareo, R., Merli, S., Sacchetti, G., Alexiu, E., Sgarbazzini, M., Cole-santi, C., Cave-Bondi, G., Ellena, G., 96, 120
- Cesareo, R., Bisceglie, V., Pedraza, L. J., Gallucci, M., Alpi, G. and Di Silverio, F., 99, 100, 120
- Cesareo, R., 181, 185, 187, 194
- Cesareo, R., Viezzoli, G., Alexiu, E., Sgarbazzini, M. and Merli, S., 187, 194
- Cesareo, R., 193, 194
- Cesareo, R., 244, 248
- Chamberlain, M.J., Fremlin, J.H., Peters, D.K. and Philip, H., 299, 303; see Biggin, H.C. et al.
- Chaudhri, M.A., 295, 297
- Chazan, N., see Howerton, R.J. et al.
- Chen, N.S. and Cohn, S.H., 358, 379
- Chen, N.S., Ellis, K.J., Pate, H.R. and Cohn, S.H., 358, 379
- Chestnut, C.H., see Palmer, H.E. et al.
- Chestnut, C.H., Nelp, W.B., Baylink, D. and Denny, J.D., 361, 380
- Chestnut, C.H., Ivey, J.L., Nelp, W.B. and Baylink, D.J., 361, 380

- Chettle, D.R. and Fremlin, J.R., 299, 300, 375; see Bell, C.M. et al.; see El-Sharkawi, A.M. et al.; see Ettinger, K.V. et al.; see Fletcher, J.G., et al.; see Leach, M.O. et al.; see Ozbas, E. et al.; see Smith, J.R.W., et al. see Somervaille, L.J. et al.; see Thomas, B.J. et al.
- Cheung, W.Y., 2, 15
- Chiao, T., see Watson, R.L. et al.
- Chisela, F., Gawlik, D. and Brätter, P., 283, 297
- Chiti, F., see Buzzo, A. et al.
- Chmelevsky, D., 323, 377
- Choi, B.H., Merzbacher, E. and Khandelwal, G.S., 128, 138, 176; see Khandelwal, G.S. et al.
- Chrien, R.E., see Greenwood, R.C.
- Churchill, B.W., see Aceto, H.
- Ciancarelli, M.G., see Cesareo, R. et al.; see Del Principe, D. et al.
- Cichoki, T., see Häfner, M. et al.
- Cierjacks, S., 329, 377
- Clark, B.C., see Singh, B. et al.
- Clarke, R.L. and Van Dyk, G., 197, 225, 228, 234, 247
- Clayton, B.E., 12, 16
- Clayton, E. and Wooler, K.K., 154, 179
- Cleare, M.J., and Hydes, P.C., 15, 17
- Coates, G. and Webber, C.E., 212, 224, 225, 228, 247
- Cobbold, S., see El-Sharkawi, A.M. et al.
- Cohn, S.H., 299, 300, 301, 303, 375; 356, 359, 379; 360, 380; 362, 381
- Cohn, S.H. and Parr, R.M., 300, 375
- Cohn, S.H. and Palmer, H.E., 300, 358, 375
- Cohn, S.H., Shukla, K.K., Dombrowski, C.S. and Fairchild, R.G., 303, 375
- Cohn, S.H., Fairchild, R.G. and Shukla, K.K., 303, 375; 320, 321, 377
- Cohn, S.H. and Dombrowski, C.S., 357, 379
- Cohn, S.H., Vaswani, A., Aloia, J., Roginsky, M., Zanzi, I. and Ellis, K.J., 361, 380
- Cohn, S.H., Aloia, J.F., Vaswani, A. N., Kapo Yuen, S., Yasumura, S. and Ellis, K.J., 361, 380
- Cohn, S.H., Sawitzky, A., Vartsky, D., Yasumura, S., Zanzi, I. and Ellis, K.J., 363, 381
- Cohn, S.H., see Wielopolski, L.
- Colautti, P., see Berti, M. et al.
- Colbert, C. and Mazess, R.B., 189, 194; see Zanzi, I. et al.
- Colesanti, C., see Cesareo, R. et al.
- Collecchi, P., see Esposito, M. et al.
- Collignon, A., see Weber, G. et al.
- Collins, M.P., see Farmer, F.T.
- Comar, D., 299, 375; see Lenihan, J.J. et al.; see Maziere, B. et al.
- Cong, H., see Hall, G.S. et al.
- Conley, J.M., see Iwanczyk, J.S. et al.
- Conri, C., see Simonoff, M. et al.
- Cookson, J.A., 134, 147, 177; see Houtman, J.P.W. et al.
- Cooper, M.J., 243, 248; see Holt, R.S. et al.; see Timms, D.N. et al.
- Cornelis, R., see Versieck, J. et al.
- Coulson, L., see Amals, H.I. et al.
- Cousins, T., Kennett, T.J., Prestwich, W.V., Webber, C.E., 333, 378
- Couzigou, P., see Simonoff, M. et al.
- Cox, H.L. and Ong, P.S., 225, 247
- Crappier, D.R., Krishnan, S.S. and Dalton, A.J., 15, 17
- Craswell, P., see Alfrey, A.G. et al.
- Cravemann, B., see Bambynek, W. et al.
- Craven, J.D., see Greenfield, M.A. et al. see Karellas, A. et al.; see Leichter, I., et al.; see Ling, S.S. et al.
- Cromer, D.T., see Hubbell, J.H. et al.
- Crouthamel, C.E., Adams, F. and Dams, R., 351, 379
- Crummy, A.B., see Mistretta, C.A. et al.
- Crompton, D., see Mahrok, M.F. et al.
- Cuevas, M.A., see Jaffe, W.G. et al.
- Cummings, E., see Hall, G.S. et al.
- Cummins, P., see Evans, C.J. et al.
- Cunningham, I.A., see Rutt, B.K. et al.
- Currie, L.A., 40, 119
- Cuzin, M., 56, 119
- Cvetkiv, V.I., see Zolotukhin, V.G. et al. al.
- Dabek, J.T., see Dyson, N.A.; see Hyvönen-Dabek, M., et al.; see Leach, M.O. et al.; see Bell, C.M. et al.
- Dabrowski, A.J., see Iwanczyk, J.S. et al.; see Singh, M., et al.
- Dahlbacka, J., see Kiilholma, P. et al.; see Kleimola, V. et al.; see Nuntö, V. et al.
- Dalton, A.J., see Crappen, D.R. et al.
- Dams, R., see Crouthamel, C.E. et al.
- Davidson, I., see Shapiro, I.M. et al.
- Davies, I.H., Jacobs, A. and Owen, G.M., 358, 379
- Davies, T.S., 15, 17
- Davis, R., see Biggler, R.E. et al.
- Davis, R. Jr., see Kummer, F.H. et al.
- D'Auria, J.M., see Agarwal, M. et al.

- De Castro Faria, L.V., see Montenegro, E.C., et al.
- Deconninck, F., see Kaufman, L. et al.
- Deconninck, G., 320, 377
- Deffeyes, K.S., see Gould, J.L. et al.
- Delang, W., see Seyfarth, H. et al.
- Delbrouck, J.M., see Weber, G. et al.
- Del Principe, D., Cesareo, R., Ciancarelli, G., Ricci, M., Tallarida, B.M., Mancuso, G., 73, 74, 85, 87, 120; see Cesareo, R., et al.
- Dempster, W.S., see Bouille, G.J. et al.
- Dennis, J.A., see Boddy, K., et al.
- Denny, J.D., see Chesnut, C.H. et al. see Nelp, W.B., et al.
- De Pangher, J. and Tochilin, E., 338, 379
- De Pauw, M.C., see Weber, G. et al.
- De Reu, L., see Maenhaut, W. et al.; see Rinsvelt, H.A. et al.
- De Rudder, J., see Versieck, J. et al.
- Deutsch, O.L., see Zamenhof, R.G. et al.
- Diberers, O., see Weber, G. et al.
- Dicello, J.F., see Amals, H.I. et al.
- Dikhoff, T.G.M.H., Van der Heide, J.A. and Mc Vie, J.G., 155, 179
- Di Luzio, S., see Magrini, A. et al.
- Di Silverio, F., see Cesareo, R. et al.
- Di Toro, R., Moro, C., Perrone, L., Gialanella, G., Grossi, G.F. and Moro, R., 154, 179
- Divoux, S., see Klockenkämper, R. et al.; see Brüggerhoff, S. et al.
- Doi, K., Vyborny, C.J. and Holje, G., 186, 194
- Dombrowski, C.S., see Cohn, S.H. et al.
- Dorking, J.J., 345, 378
- Drummond, W., see Iwanczyk, J.S. et al.
- Duffey, D., El-Kady, A. and Senftle, F., 304, 376
- Dunea, G., Mahurkar, S.D., Mamdani, B. and Smith, E.C., 15, 17
- Dunn, T.C., see Fuller, E.G. et al.
- Duscher, H., see Wundt, K. et al.
- Dutton, J., see Ali, P.A. et al.; see Evans, C.J. et al.
- Dykes, P.W., see Biggin, H.C. et al.
- Dyson, N.A., Simpson, A.E. and Dabek, J.T., 153, 179
- East, B.W., see Boddy, K. et al.
- Eastell, R., see Kennedy, N.S.J. et al.
- Edward, N., see Catto, G.R.D. et al.
- Edwards, A.A., see Booz, J. et al.
- Egelstaff, P.A. and Poole, M.S., 345, 378
- Ellena, G., see Cesareo, R. et al.
- Elgsacter, A., see Epsevik, T.
- Elinder, C.G., see Friberg, L. et al.
- El-Kadi, A., see Duffey, D. et al.
- Elliott, A., see Boddy, K. et al.
- Ellis, K.J. and Cohn, S.H., 14, 17;
- Ellis, K.J., Vartsky, D. and Cohn, S.H., 307, 308, 376
- Ellis, K.J., Vartsky, D., Zanzi, I., Cohn, S.H. and Yasumura, S., 362, 381
- Ellis, K.J., Morgan, W.D., Yasumura, S., Vartsky, D., Zanzi, I. and Cohn, S., 363, 381
- Ellis, K.J., see Chen, N.S. et al.; see Cohn, S.H. et al.; see Ettinger, K. V. et al.; see Glaros, D. et al.; see Kyere, K. et al.; see Morgan, W.D. et al.; see Vartsky, D. et al.; see Wielopolski, L. et al.
- El-Sharkawi, A.M., Morgan, W.D., Cobbold, S., Jaib, M.B.M., Evans, C.J., Somerville, L.J., Chettle, D.R. and Scott, M.C., 116, 121
- Engesser, F.C. and Thompson, W.E., 311, 376; see Thompson, W.E.
- Entine, G., see Squillante, M.R. et al.
- Epsevik, T. and Elgsaeter, A., 160, 178
- Epstein, S.G., 15, 17
- Esposito, M., Collecchi, P., Oddone, M., Meloni, S., 288, 297
- Ettinger, K.V., 303, 375
- Ettinger, K.V., Biggin, H.C., Chen, N.S., Chettle, D.R., Fremlin, J.H., Harvey, T.C., Morgan, W.D., Nowotny, R., Thomas, B.J. and Vartsky, D., 304, 376
- Ettinger, K.V., Morgan, W.D., Miola, U. J., Vartsky, D., Ellis, K.J., Wielopolski, L. and Cohn, S.H., 310, 313, 376
- Ettinger, K.V., see Biggin, H.C. et al.; see Catto, G.R.D. et al.; see El-Sharkawi, A.M. et al.; see Gvozdanovic, D. et al.; see Miola, U.J. et al.; see Ozbas, E. et al.
- Evans, C.J., see El-Sharkawi, A.M. et al.
- Evans, G.W., 14, 17
- Evans, J.C., Cummins, P., Dutton, J., Morgan, W.D., Sivyver, A. and Ghose, R.R., 307, 376; see Ali, P.A. et al.; see Biggler, R.E. et al.
- Fairchild, R.G., see Chamberlain, M.J. et al.; see Cohn, S.H. et al.; see Goodman, L.J.
- Fairchild, R.G., 331, 378

- Farmer, F.T. and Collins, M.P., 197, 199, 222, 225, 234, 236, 247
- Farrell, R., see Squillante, M.R. et al.
- Feather, C.E. and Willis, J.P., 62, 120
- Featherston, J.D.B., see Wielopolski, L. et al.
- Feeney, P.J., see Cahill, T.A. et al.
- Fenster, A., see Rutt, B.K. et al.
- Ferguson, J.M., see Engesser, F.C. et al.
- Ferrington, C.M., see Kennedy, N.S.J. et al.
- Ferziger, J.H. and Zweifel, P.F., 345, 378
- Fetterolf, D.E., see Wielopolski, L. et al.
- Fink, R.W., see Bambynek, W. et al.; see Katsanos, A. et al.
- Fitzgerald, L.T., see Brateman, L. et al.
- Fitzgerald, M.G., see Walsh, C.H. et al.
- Fitzgerald, R. and Gantzel, P., 59, 120
- Fletcher, J.G., Chettle, D.R. and Haddad, I.K., 363, 381
- Fleury, B., see Simonoff, M. et al.
- Flocchini, R.G., see Cahill, T.A. et al.
- Folkmann, F., 123, 142, 147, 149, 176; 149, 177
- Forslind, B., see Malmqvist, K.B. et al.
- Forslind B., Wiren, K. and Malmqvist, K.B., 155, 179
- Forsyth, P.D., see Young, F.C. et al.
- Fortner, R.J., see Garcia, J.D. et al.
- Fou, C.M., 155, 179
- Foster, M.A., see Ettinger, K.V. et al.; see Fuller, M.F. et al.
- Foulkes, E.C., 13, 17
- Francois, P.E., see Mahrok, M.F. et al.
- Frankel, R.B., Blakemore, R.P. and Wolfe, R.S., 2, 15
- Frasch, W.D., Larson, J., Bowlby, N., Apel, I. and Jones, J.D., 286, 297
- Fraser, R.A., see Catto, G.R.D. et al. see Junor, B.J.R. et al.
- Frazzoli, F.V., see Pavoni, P. et al.
- Fremlin, J.H., see Bell, C.M. et al.; see Biggin, H.C. et al.; see Chamberlain, M.J. et al.; see Ettinger, K.V. et al.; see Leach, M.O. et al.; see Mc Lellan, J.S. et al.; see Ozbas, E. et al.; see Thomas, B.J. et al.; see Vartsky, D. et al.; see Walsh, C.H. et al.
- Frey, H., see Nantø, V. et al.
- Friberg, L., Elinder, C.G., Kjellstrom, T. and Nordberg, G.F., 5, 13, 16
- Fuller, E.G., Gerstenberg, H.M., Van der Malen, H. and Dunn, T.C., 312, 376
- Fuller, M.F., Foster, M.A. and Hutchinson, J.M.S., 359, 379
- Gallucci, M., see Cesareo, R. et al.
- Gander, P., Verghese, K. and Lee, H.M., 353, 379
- Gantzel, P., see Fitzgerald, R.
- Garavaglia, G., see Bloch, P. et al.
- Garcia, J.D., Fortner, R.J. and Kavanagh, T.M., 128, 176
- Gardner, R.P., see Arinc, F.
- Garn, S.M., Poznanski, A., Mayor, G. and Pottenger, J., 360, 379
- Garnett, E.S., Kennett, T.J., Kenyon, D. B. and Webber, C.E., 197, 225, 228, 247
- Gawlik, D., see Chisela, F. et al.
- Gedcke, D., see Jenkins, R. et al.
- Geerner, W., see Wiesener, W. et al.
- Gentry, R.V., see Sparks, C.J. Jr. et al.
- Gerstenberg, H.M., see Fuller, E.G. et al.
- Gervas, M.H., see Nelp, W.B. et al.
- Ghose, A.M., see Bradley, D.A.
- Ghose, R.R., see Evans, C.J. et al.
- Gialanella, G., see Di Toro, R. et al.; see Moro, R. et al.
- Gigante, G.E., see Cesareo, R.
- Gigante, G.E. and Sciuti, S., 207, 224, 241, 247
- Gigante, G.E., Pedraza, L.J. and Sciuti, S., 244, 248
- Gilboy, W.B., 182, 194
- Gilfrich, J.V., see Birks, L.S.
- Gilfrich, J.V. and Burkhalter, P.G., 155, 177
- Giuntini, C., see Guzzardi, R. et al.
- Glaros, D., Lo Monte, A.F., Ellis, K.J., Yasumura, S., Stoenner, R.W. and Cohn, S.H., 303, 307, 376; see Boddy, K. et al.
- Göllner, K., see Raith, B. et al.
- Göllnick, D.A. and Greenfield, M.A., 103, 121
- Gonobe, B.I., see Watson, R.L. et al.
- Gonsior, B., and Roth, M., 132, 176
- Gonsior, B., Bischof, W., Höfbert, M., Raith, B., Stratmann, A. and Rokita, E., 134, 177; see Brüggerhoff, S., et al.; see Höfbert, M. et al.; see Klockenkämper, R. et al.; see

- Raith, B. et al.; see Wilde, H.R. et al.
- Goodman, L.J., see Fairchild, R.G.
- Gottel, P., see Seyfarth, H. et al.
- Gottlieb, N.L., Smith, P.M. and Smith, E.M., 15, 17
- Gould, J.L., Kirschvink, J.L. and Deffeyes, K.S., 2, 15
- Gould, R.W., see Jenkins, R. et al.
- Goulding, F.S. and Jaklevic, J.M., 123, 176
- Grappel, S., see Anke, M. et al.
- Grass, F., 261, 297
- Greenberg, A., see Wielopolski, L. et al.
- Greenfield, M.A., Craven, J.D., Shukla, S.S., Karellas, A. and Leichter, I., 241, 242, 247; see Gollnick, D.A.; see Karellas, A. et al.; see Leichter, I. et al.; see Ling, S.S. et al.
- Greenwood, R.C. and Chrien, R.E., 332, 378
- Grime, G.W., see Watt, F. et al.
- Grönroos, M., see Kiiholma, P. et al.
- Grosjean, C.C., 351, 379
- Grossi, G.F., see Di Toro, R. et al.
- Gubler, C.J., see Wintrobe, M.M. et al.
- Guesry, P., Kaufman, L., Orloff, S., Nelson, J.A., Swann, S. and Holliday, M., 90, 120
- Gutnecht, W.F., see Walter, R.L. et al.
- Guzzardi, R., Mey, M., Pistolesi, M., Solfanelli, S. and Giuntini, C., 197, 225, 236, 247
- Guzzardi, R. and Mey, M., 236, 248
- Gvozdanovic, D., Ettinger, K.V., Smith, D.B., Taylor, C.G., Gvozdanovic, S. and Mallard, J.R., 358 379
- Gvozdanovic, S., see Gvozdanovic, D. et al.
- Haddad, I.K., see Fletcher, J.G. et al.
- Hadjiantonion, A., see Katsanos, A. et al.
- Hall, G.S., Roach, N., Naumann, M. and Simmons, U., 169, 178;
- Hall, G.S., Roach, N., Simmons, U., Cong, H., Lee, M.I. and Cummings, E., 154, 155, 179
- Hambidge, K.M., see Casey, C.E.
- Hamon, C., see Simonoff, M. et al.
- Hanninen, R., see Hyvonen-Dabek, M. et al.
- Hanson, A.L., 205, 247
- Harding, G. and Tischler, R., 237, 248
- Hardy, M.L., see Stoeckle, J.D. et al.
- Harris, I.A., see Boddy, K. et al.
- Harrison, D.A., see Lone, M.A. et al.
- Harrison, D.C., see Otis, J.N. et al.
- Harrison, J.E. and McNeill, K.G., 361, 380
- Harrison, J.E., McNeill, K.G., Mernagh, J.B. and Jeejeebhoy, K.N., 363, 381
- Harrison, K.G., see Booz, J. et al.
- Hartmann, G., Menzel, H.G. and Schumacher, H., 324, 377
- Harvey, I., see Williams, E.D. et al.
- Harvey, J.R. and Mill, A.J., 332, 378
- Harvey, T.C., see Biggin, H.C. et al.; see Ettinger, K.V. et al.; see McLellan, J.S. et al.; see Ozbas, E. et al.; see Thomas, B.J. et al.; see Walsh, C.H. et al.
- Hassan, A.M., see Seyfarth, H. et al.
- Hastings, J.B., see Sparks, C.J. Jr.
- Hauser, W., see Atkins, H.L. et al.
- Hawkes, D.J., see Jackson, D.F.; see Vartsky, D. et al.
- Haywood, J.K., Williams, E.D., Mc Ardle F.J. and Boddy, K., 303, 375; see Boddy, K. et al.
- Heaton, H.T., see Young, F.C. et al.
- Heese, H. de V., see Boule, G.J. et al.
- Hegg, A., see Alfrey, A.C. et al.
- Hempelmann, L.H., see Hoffman, J.G.
- Hendee, W.R., 181, 194
- Hevesy, G.V. and Levi, H., 249, 297
- Higuchi, T., see Suzuki, H. et al.
- Hill, G.L., see Kyere, K. et al.
- Hill, R.F., see Schneider, F.W.
- Höfert, M., Raith, B., Gonsior, B., Rokita, E. and Cichoki, T., 134, 152, 177; see Gonsior, B. et al.
- Hoffer, P.B., see Oldendorf, W.H. et al.
- Hoffman, J.G. and Hempelmann, L.H., 299, 375
- Hofstadter, R., see Otis, J.N. et al.
- Holinska, B. and Markowitz, A., 83, 120
- Holje, G., see Doi, K.
- Holliday, M.A., see Kaufman, L. et al.
- Holloway, I., see Boddy, K. et al.; see Chamberlain, M.J. et al.
- Holt, R.S., Kouris, K., Cooper, M.J. and Jackson, D.F., 243, 248; see Timms, D.N. et al.
- Horiuchi, Y., see Suzuki, H. et al.
- Horiuchi, M., see Koyama-Ito, H. et al.
- Horvath, D.J., 12, 16
- Hoste, J., see Wanters, G. et al.
- Houtman, J.P.W., Bos, A., Vis, R., Cookson, J.A. and Tjioe, P.S., 154, 179
- Howerton, R.J., Braff, D., Cahill, W.J. and Chazan, N., 312, 376; see

- Hubbell, J.H. et al.
 Howes, B.W., 332, 378
 Hrastnik, B., see Seiferth, H. et al.
 Hsueh, T.C.H., see Ling, D.S. et al.
 Huang, T.C., 62, 120
 Hubbel, H.H., 329, 377
 Hubbell, J.H., Weigle, W.J., Briggs, E.A., Brown, R.T., Cromer, D.T., and Howerton, R.J., 200, 247;
 Hubbell, J.H., 31, 33, 39, 119; see Schaupp, D. et al.
 Hubert, G., Rieder, N., Schmitt, G. and Send, W., 2, 15
 Huberty, J.P., see Rice, D.C. et al.
 Huddleston, A.L., Bhaduri, D. and Weaver, J., 197, 212, 213, 225, 227, 228, 229, 231, 233, 247
 Hudson, A., see Otis, J.N. et al.
 Hughes, E.B., see Otis, J.N. et al.
 Hull, D.H., see Vartsky, D. et al.
 Hung, S.T., see Price, D.C. et al.
 Hurd, R.W., see Rinsvelt, H.A. et al.
 Husain, M., see Khan, A.H. et al.
 Hutchinson, J.M.S., see Fuller, M.F. et al.
 Huth, G.C., see Iwanczyk, J.S. et al. see Singh, M. et al.
 Hydes, P.C., see Cleare, M.J.
 Hyvönen-Dabek, M., Räsänen, J. and Dabek, J.T., 154, 179;
 Hyvönen-Dabek, Dabek, J.T., Nikkinen, P., Raisanen, J. and Hanninen, R., 295, 297
 Inada, T., see Maruhashi, A. et al.
 Ing, D., see Reiss, K. et al.
 Irukayama, K., see Tsubaki, T.
 Isherwood, I., see Rutherford, R.A. et al.
 Ishihara, T., see Maruhashi, A. et al.
 Ivanov, V.M., 323, 377
 Ivey, J.L., see Chesnut, C.H. et al.
 Iwanczyk, J.S., Dabrowski, A.J., Huth, G.C. and Drummond, W., 57, 119;
 Iwanczyk, J.S., Dabrowski, A.J., Huth, G.C., Bradley, J.G., Conley, J.M. and Alber, A.L., 57, 119
 Iwata, S., see Koyama-Ito, H. et al.
 Iyengar, G.V., Kollmer, W.E. and Bowen, H.J.M., 5, 11, 13, 16
 Iyengar, G.V., 5, 13, 16; see Sansoni, B.
 Iyengar, G.V., 277, 278, 297
 Izzo, G., see Magrini, A. et al.
 Jackson, D.F. and Hawkes, D.J., 209, 247; see Holt, R.S. et al.
 Jackson, M.L., see Lee, J.S.
 Jacobs, A., see Davies, I.H. et al.
 Jacobs, A.M., see Brateman, L. et al.
 Jacobson, B., 181, 194
 Jaffe, W.G., Raphael, D., Mondragon, M. C. and Cuevas, M.A., 12, 16
 Jaklevic, J.M., 41, 49, 119;
 Jaklevic, J.M. and Walter, R.L., 70, 71, 72, 120; see Goulding, F.S.
 James, H.M., see Bell, C.M. et al.; see Leach, M.O. et al.; see Walsh, C. H. et al.
 James, W.D., 261, 297
 Jeejeebhoy, K.N., see Harrison, J.E. et al.
 Jenkins, R., Gould, R.W. and Gedcke, D., 157, 177
 Jensen, F.E., see Watson, R.L. et al.
 Jervis, R.E., 91, 120
 Johansson, E. and Lindh, U., 155, 179
 Johansson, G.I., see Malmqvist, K.G. et al.
 Johansson, S.A.E., see Johansson, T.B. et al.
 Johansson, S.A.E. and Johansson, T.B., 142, 147, 176
 Johansson, S.A.E., 154, 179
 Johnels, A.G., see Birks, G. et al.
 Johns, P.C. and Yaffe, M.J., 203, 247
 Johnsen, S.W., see Amals, H.I. et al.
 Jones, T.D., 329, 377
 Joseph, B.J., see Sky-Peck, H.H.
 Joyce, J.M., see Walter, R.L. et al.
 Junor, B.J.R., see Catto, G.R.D. et al.; Junor, B.J.R., Catto, G.R.D., MacLeod, M., Papapoulos, S.E., O'Riordan, J.L.H. and Fraser, R.A., 361, 381
 Kagi, J.H.R. and Nordberg, M., 6, 16
 Kairento, A.I. and Nikkinen-Vilkki, P., 312, 376
 Kaiser, H., 139, 177
 Kapo Yuen, S., see Cohn, S.H. et al.
 Karellas, A., Leichter, I., Craven, J.D. and Greenfield, M.A., 241, 248 ; see Greenfield, M.P. et al.; see Leichter, I. et al.; see Ling, S.S. et al.
 Karjalainen, P., see Olkkonen, H.
 Karl, see Trebert Haerberling, S. et al.
 Katsanos, A., Xenoulis, A., Hadjiantoniou, A. and Fink, R.W., 149, 177
 Katz, S.A., 13, 17
 Katz, S.H., see Shapiro, I.M. et al.
 Kaufman, L., 112, 121
 Kaufman, L., Price, D.C., Holliday, M.A., Payne, B., Camp, D.C., Nelson, J.A. and Deconninck, F., 166, 178; see Price, D.C. et al.
 Kavanagh, T.M., see Garcia, J.D. et al.
 Kazantzis, G., 6, 16 ; see Pershagen, G. et al.

- Keane, A.T., see Maletskos, C.J. et al.
- Keirim-Markus, see Zolotukhin, V.G. et al.
- Kelez, F. and Mistretta, C.A., 181, 194; see Mistretta, C.A. et al.
- Keller, K.R., see Squillante, M.R. et al.
- Kellerer, A.M., 323, 377
- Kennedy, N.S.J., , Eastell, R., Ferrington, C.M., Simpson, J.D., Smith, M.A., Strong, J.A. and Tothill, P., 361, 380
- Kennett, J.S. and Webber, C.E., 197, 247; see Garnett, E.S. et al.; see Webber, C.E.; see Cousins, T. et al.
- Kenyon, D.B.; see Garnett, E.S. et al.
- Kernoff, R.S., see Otis, J.N. et al.
- Kerr, S.A., Kouris, K., Webber, C.E. and Kennett, T.J., 197, 207, 210, 212, 240, 241, 242, 247
- Khaliquzzaman, M., see Khan, A.H. et al.
- Khan, A.H., Khaliquzzaman, M., Zaman, M.B., Husain, M., Abdullah, M. and Akhter, S., 154, 179
- Khandelwal, G.S., Choi, B.H. and Merzbacher, E., 128, 138, 176; see Choi, B.H. et al.
- Khaw, K.T., see Kopito, L. et al.
- Kiilholma, P., Grönroos, M., Kleimola, V., Pakarinen, P., Dahlbacka, J. and Nääntö, V., 153, 179
- King, P.C., see Boddy, K. et al.
- Kirschvink, J.L., see Gould, J.L. et al.
- Kissel, L., Pratt, R.H. and Roy, J.S.C., 203, 247; see Roy, J.S.C. et al.
- Kjellstrom, T., see Friberg, L. et al.
- Kleimola, V., Dahlbacka, J., Pakarinen, P., Salmi, T.T. and Nääntö, V., 167, 178; see Kiilholma, P. et al.; see Nääntö, V. et al.
- Klein, S., see Woggon, H.
- Klockenkämper, R., Raith, B., Divoux, S., Gonsior, B., Brüggerhoff, S. and Jackwerth, E., 139, 140, 145, 146, 149, 155, 156, 177;
- Klockenkämper, R., Bubert, H., 140, 145, 146, 155, 177;
- Klockenkämper, R., 140, 146, 155, 177; see Bubert, H.
- Knapp, G., see Raptis, E. et al.
- Knoll, G., Oebel, G. and Plattner, H., 160, 178
- Knoll, G.F., 349, 378
- Kobayashi, K., see Maruhashi, A. et al.
- Kochetkov, O.A., see Zolotukhin, V.G. et al.
- Kodicek, E., see Catto, G.R.D. et al.
- Koenig, W., Richter, F.W., Bode, J. Ch., and Meinel, B., 154, 179
- Koikkalainen, S., see Manninen, S. et al.
- Kokinos, D., 345, 378
- Kollmer, W.E., see Iyengar, G.V. et al.
- Kondoro, I.W.A., see Rinsvelt, H.A. et al.
- Kopito, L., Mahmodian, A., Townley, R.R. W., Khaw, K.T. and Schwachman, H., 14, 17
- Kostan L., 277, 297
- Kouris, K., see Holt, R.S. et al.; see Kerr, S.A. et al.
- Koyama-Ito, H., Wada, E., Tsumita, T., Horiuchi, H. and Iwata, S., 173, 178
- Kraner, H.W., see Alberi, J.L.; see Atkins, H.L.
- Krause, M.O., see Sparks, C.J. Jr., et al.
- Kraushar, J.J., see Bunting, R.L.
- Krishnan, S.S., see Crapper, D.R. et al.
- Kronemann, H., see Anke, M. et al.
- Kuchnir, F.T., see Stinchcomb, T.G. et al.
- Kummer, F.H., Stoenner, F.W. and Davis, R. Jr., 303, 376
- Kuntz, D., see Maziere, B. et al.
- Kunzendorf, H., 197, 238, 247
- Kuschner, M., see Pershagen, G. et al.
- Kusumoto, T., see Maruhashi, A. et al.
- Kyere, K., Oldroyd, B., Oxby, C.B., Burkinshaw, L., Ellis, R.E. and Hill, G.L., 309, 376
- Lale, P.G., 197, 225, 234, 247
- Lamoureux, G., see Lecomte, R. et al.
- Landrigan, P.J., see Wielopolski, L. et al.
- Larson, J., see Frasc, W.D. et al.
- Laughlin, J.S., see Biggler, R.E. et al.
- Laursen, J., see Bisgård, K.M. et al.
- Lawson, R.C., Clare, D.M. and Watt, D. E., 323, 377; see Boddy, K. et al.
- Leavit, R.A., see Lone, M.A. et al.
- Leach, M.O., Bell, C.M., Thomas, B.J., Dabek, J.T., James, H.M., Chettle, D.R. and Fremlin, J.H., 360, 380; see Bell, C.M. et al.
- Lecomte, R., Paradis, P., Monaro, S., Barrette, M., Lamoureux, G. and Menard, H.A., 153, 167, 178
- Lederer, C.M., Shirley, V.S., 269, 297
- Lee, H.M., see Gander, P. et al.
- Lee, M.I., see Hall, G.S. et al.
- Leep, D.B., see Senftle, F. et al.

- Leeper, A.K., see Watson, R.L. et al.
 Legge, G.J.F., 134, 151, 177
 Legge, G.J.F. and Mazzolini, A.P., 147, 151, 153, 177
 Leichter, I., Karellas, A., Craven, J.D. and Greenfield, M.A., 207, 210, 247; see Greenfield, M.A. et al.; see Karellas, A. et al.
 Lenglet, W.J.M., see Vis, R.D. et al.
 Lenihan, J.J., Comar, D., Riviere, R. and Kellersohn, 299, 375
 Lerney, G., see Versieck, J. et al.
 Levander, O.A., 14, 17
 Levi, H., see Hevesy, G.V.
 Levin, E.R., 132, 176
 Lewellen, T.K., see Palmer, H.E. et al.
 Lewellen, T.L., 360, 380
 Leyden, D.E., 65, 120
 Li, C.S. and Jackson, M.L., 12, 16
 Li, S., see Yang, G. et al.
 Lindh, U. and Tveit, A.B., 154, 155, 179
 Lindh, W., Brune, D., Nordberg, G. and Wester, P.O., 147, 177
 Ling, D.S., Chen, Q.M. and Yu, Z.C., 12, 16
 Ling, S.S., Rustgi, S., Karellas, A., Craven, J.D., Whiting, J.S., Greenfield, M.A. and Stern R., 197, 207, 213, 224, 247
 Littlefields, S., see Maletskos, C.J. et al.
 Litton, , see Ong, P.S. et al.
 Llabador, Y., see Simonoff, M. et al.
 Lodhi, A.S. and Rashiduzzaman, M.D., 166, 178
 Loer, F., see Michel, R. et al.
 Lo Monte, A., see Glaros, D. et al., see Vartsky, D. et al.
 Lone, M.A., Leavitt, R.A. and Harrison, D.A., 304, 376; and Bigham
 Lone, M.A. and Bigham, C.B., 341, 378
 Luccio, A., 317, 319, 377
 Lucena, A., see Simonoff, M. et al.
 Lund, J.C., see Squillante, M.R. et al.
 Lund, P.K., , see Ong, P.S. et al.
 Lutz, G.J., 312, 344, 376
 Lux, F., 278, 297; see Trebert Haerberling, S. et al.
 Mac Donald, G.I., 123, 147, 176
 Mac Leod, M., see Catto, G.R.D. et al.; see Junor, B.J.R. et al.
 Maenhaut, W., 134, 177;
 Maenhaut, W., de Reu, L., van Rinsvelt, H.A., Cafmeyer, J. and van Espen, P., 170, 178 ; see
 Rinsvelt, H.A. et al.
 Magrini, A., Di Luzio, S., Izzo, G., Raganella, G., 113, 121
 Magrini, A., see Pavoni, P. et al.
 Mahmodian, A., see Kopito, L. et al.
 Mahrok, M.F., Crumpton, D. and Francois, P.E., 155, 179
 Mahurkar, S.D., see Dunea, G. et al.
 Makjanic, J., see Orlic, I. et al.
 Makrigiorgos, G. and Waker, A.J., 328, 377
 Mallard, J.R., see Grozdanovic, D. et al.
 Malmqvist, K.G., Carlsson, L.E., Forslind, B., Roomans, G.M. and Akselson, K.R., 174, 179; see Forslind, B. et al.
 Mamdani, B., see Dunea, G. et al.
 Mancuso, G., see Del Principe, D. et al.; see Cesareo, R. et al.
 Manninen, S., Pitkanen, T., Koikkalainen, S. and Paakkari, T., 207, 247
 Manninen, S. and Koikkalainen, S., 209, 247
 Mantel, M., see Rapaport, M.S. et al.
 Marcinkowski, T. and Pankowski, M., 96, 120
 Marion, J.B. and Young, F.C., 351, 352, 379; see Young, F.C. et al.
 Mark, H., see Bambynek, W. et al.
 Markkanen, T., see Nantti, V. et al.
 Markowicz, , A., see Holynska, B.
 Martoja, R. and Viale, D., 2, 15
 Maruhashi, A., Kobayashi, K., Shima, K., Ishihara, T., Kusumoto, T., Inada, T. and Akisada, M., 170, 178
 Masi, O.M., see Smith, F.C. Jr., 65, 120
 Mason, J.A., see Ward, N.J.
 Massey, R.Y., see Wielopolski, L. et al.
 Mattson, S., see Ahlgren, L.
 Maurice, D.M., see Burstein, R.L.
 Mayor, G., see Garn, S.M. et al.
 Mazess, R.B., Cameron, J.R. and Sorenson, J.A., 181, 194; 197, 210, 240, 247;
 Mazess, R.B., 360, 380
 Maziere, B., Kuntz, D. and Comar, D., 360, 361, 380
 Maziere, B., Kuntz, D. Comar, D. and Ryckenwaert, A., 361, 380
 Mazzolini, P., see Legge, G.J.F.
 Mc Ardle, F.J., see Haywood, J.K. et al.
 Mc Clatchley, R.A., see Maletskos, C.J. et al.
 Mc Cullough, E.C., 27, 119; 181, 194
 Mc Lellan, J.S., Thomas, B.J., Fremlin, J.H. and Harvey, T.C., 307, 376;
 see Thomas, B.J. et al.
 Mc Neill, K.G., , see Harrison, J.E.
 Mc Vie, J.G., see Dikkoff, T.G.M.H. et al.

- Mehta, G.K., see Sen, P.
 Meinel, B., see Koenig, W. et al.
 Meister, N., see Müller, M. et al.
 Melius, J.M., see Harrison, J.E. et al.; see Mernagh, J.B. et al.; see Walsh, C.H. et al.
 Melone, S., see Esposito, M. et al.
 Menard, H.A., see Lecomte, R. et al.
 Menzel, H.G., see Hartmann, G. et al.
 Merli, S., see Cesareo, R., et al.
 Merzbacher, E., see Choi, B.H. et al. see Khandelwal, G.S. et al.
 Metzger, F.R., 320, 377
 Mey, M., see Guzzardi, R. et al.
 Michel, R., Loer, F., Nolte, M., Reich, M., Zilkens, J., 286, 297
 Mickle, J.P., see Rinsvelt, H.A. et al.
 Mijnheer, B.J. and Williams, J.R., 328, 377; see Boerse, J.J. et al.
 Mill, A.J., see Harvey, J.R.
 Milne, E.N.C., see Clarke, R.G. et al.
 Miola, U.I., and Ettinger, K.V., 344, 346, 347, 348, 378; see Ettinger, K.V. et al.
 Mistretta, C.A., Ort, M.G., Kelez, F., Cameron, J.R., Siedband, M.P. and Crummy, A.B., 181, 194
 Molho, N., see Cantone, M.C. et al.
 Monaro, S., see Lecomte, R. et al.
 Mondragon, M.C., see Jaffe, W.G. et al.
 Monseu, G., 15, 17
 Montenegro, E.C., Baptista, G.B., De Castro Faria, L.V. and Paschoa, A.S., 153, 179
 Moor, H., 159, 178; see Müller, M. et al.
 Moore, H.D., see Senftle, F. et al.
 Morgan, W.D., Vartsky, D., Ellis, K. J. and Cohn, S.H., 309, 310, 376
 Morgan, W.D., Evans, C.J., Cummins, P.E., Elwood, P.C., Ames, A.C., Thomas, A., Cross, D., Ghee, R. R., Sivyer, A. and Dutton, J., 363, 381
 Morgan, W.D., see Ali, P.A. et al.; see Biggin, H.C. et al.; see El-Sharkawi, A.M. et al.; see Ettinger, K.V. et al.; see Evans, C.J. et al.
 Moro, R., see Di Toro, R. et al.;
 Moro, R., and Gialanella, G., 155, 179
 Muirhead, N., see Catto, G.R.D. et al.
 Müller, M., Meister, N. and Moor, H., 160, 178
 Munro, T.R., see Wolf, E.A.
 Murano, R., see Nelp, W.B. et al.
 Murray, B.W., see Zamenhof, R.G. et al.
 Murthy, M.S.S., 330, 378
 Näntö, V., Dahlbacka, J., Pakarinen, P., Markkanen, T., Kleimola, V., Salmi-nen, L. and Frey, H., 153, 179; see Kiilholma, P. et al.; see Klei-mola, V. et al.
 Naumann, M., see Hall, G.S. et al.
 Navon, E., see Hall, G.S.
 Nelissen, J., see Smits, J. et al.
 Nelp, W.B., Palmer, H.E., Murano, R., Palthorp, K., Gervas, M.H., Rich, C., Williams, J., Rudd, T.G. and Denny, J.D., 303, 375; see Chesnut, C.H. et al.; see Palmer, H.E. et al.
 Nelson, J.A., see Kaufman, L. et al.
 Neufeld, J., see Snyder, W.S.
 Newton, J., see Anderson, J. et al.
 Niese, S., see Wiesener, W. et al.
 Nikkinen, P., see Hyvonen-Dabek, M. et al.
 Nikkinen-Vilkkki, P., see Kairento, A.L. et al.
 Nolte, M., see Michel, R. et al.
 Nordberg, G., see Lindh, W. et al.
 Nordberg, G.F., see Friberg, L.
 Nordberg, M., see Kagi, J.H.R.
 Norseth, T., see Pershagen, G. et al.
 Nothmann, R., see Rapaport, M.S. et al.
 Nowotny, R., see Biggin, H.C. et al.; see Ettinger, K.V. et al.
 Obaturov, G.M., see Zelotukhin, V.G. et al.
 Oddone, M., see Esposito, M. et al.
 Oebel, G., see Knoll, G. et al.
 Ohtaki, S., see Suzuki, H. et al.
 Oldendorf, W.H., Phelps, M.E., Hoffer, P.B. and Tanaka, H., 181, 194
 Oldroyd, B., see Kyere, K. et al.
 Olkkonen, H. and Karjalainen, P., 197, 225, 228, 247; see Puumalainen, P. et al.
 Ong, P.S., Lund, P.K., Litton, C.E. and Mitchell, B.A., 79, 120; see Cox, H.L.
 O'Riordan, J.L.H., see Catto, G.R.D. et al.; see Junor, B.J.R. et al.
 Orlic, I., Makjanic, J. and Valkovic, V., 146, 177
 Ort, M.G., see Mistretta, C.A. et al.
 Orvis, A.L., 356, 379
 Osborn, H.F., see Anderson, J. et al.; see Battye, C.K. et al.; see Malet-skos, C.J. et al.
 Ostermann, H., see Raith, B. et al.
 Otis, J.N., Zeman, H.D., Hughes, E.B., Campbell Finman, L., Hofstadter, R., Hudson, A., Rolfe, J., Rubenstein,

- E., Harrison, D.C., Kernoff, R. S., Thompson, A.C. and Brown, G. S., 186, 194
- Owen, G.M., see Davies, I.H. et al.
- Oxby, C.B., see Kyere, K. et al.
- Ozbas, E., Chettle, D.R., Ettinger, K.V., Fremlin, J.H., Harvey, T. C., Prestwich, W.V. and Thomas, B.J., 303, 375; see Thomas, B.J. et al.
- Paakkari, T., see Manninen, S. et al.
- Pakarinen, P., Pallon, J. and Akselson, R., 169, 178; see Kiilholma P. et al.; see Kleimola, V. et al.
- Paliwal, K.V., 12, 16
- Pallon, J., see Pakarinen, J. et al.
- Palmer, H.E.; 300, 375;
- Palmer, H.E., Lewellen, T.K., Chestnut, C.H. and Nelp, W.B., 300, 303, 375; see Cohn, S.H. et al.; see Nelp, W.B. et al.; see Palthomp, K. et al.
- Palthomp, K., see Nelp, W.B. et al.
- Pankowski, M., see Marcinkowski, T.
- Papapoulos, S.E., see Catto G.R.D. et al.; see Junor, B.J.R. et al.
- Paradis, P., see Lecomte, R. et al.
- Parkinson, D.K., see Wielopolski, L. et al.
- Parr, R.M., 4, 16
- Pate, H.R., see Chen, N.S. et al.
- Patton, J.A. and Brill, A.B., 113, 121
- Pavoni, P., Frazzoli, F.V. and Magrini, A., 114, 115, 121
- Payne, B., see Kaufman, I. et al.
- Peckerar, M.C., see Brown, D.B. et al.
- Pedraza, L.J., see Cesareo, R. et al.; see Gigante, G.E. et al.
- Peet, M., 15, 17
- Peisach, M., see Bouille, G.J. et al.
- Pelc, B., see Catto, G.R.D. et al.
- Perrone, L., see Di Toro, R. et al.
- Pershagn, G., Kuschner, M., Piscator, M., Nordseth, T., Sunderman, F.W. and Kazantzis, G., 15, 17
- Peters, D.K., see Chamberlain, M.J. et al.
- Pfeiffer, C.C., Siegert, E. and Sohl-er, A.H., 12, 16
- Phelps, M.E., see Oldendorf, W.H. et al.
- Phelps, P.L., see Armantrout, G.A. et al.
- Philip, H., see Chamberlain, M.J. et al.
- Philippot, J.C., 350, 378
- Philips, G.W., see Young, F.C. et al.
- Picard, J., see Williamson, C.F. et al.
- Pierson, R.N., see Price, D.C. et al.
- Piesch, E., 335, 378
- Piesch, E. and Sayed, E.M., 335, 378
- Pillay, A.E. and Peisach, M., 154, 179
- Piltingsrud, H.V., 312, 376
- Piper, D.G., see Preuss, L.E. et al.
- Pirola, L., see Cantone, M.C. et al.
- Piscator, M., see Pershagen, G. et al.
- Pistolesi, M., see Guzzardi, R. et al.
- Pitkanen, T., see Manninen, S. et al.
- Plattner, H., 159, 178; see Pscheid, P. et al.; see Knoll, G. et al.
- Poole, M.S., see Egelstaff, P.A.
- Pottenger, J., see Garn, S.M. et al.
- Poznanski, A., see Garn, S.M. et al.
- Prasad, A.S., 12, 16
- Pratt, R.H., see Kissel, L. et al.; see Roy, J.S.C. et al.
- Prestwich, W.V., see Cousins, T. et al.; see Ozbas, E. et al.
- Preuss, L.E. and Bolin, E.P., 181, 191, 194
- Preuss, L.E., Piper, D.G., Bugenis, C., 228, 248
- Price, D.C., Kaufman, L. and Pierson, R.N., 88, 89, 120; see Kaufman, L. et al.
- Price, R.E., see Bambynek, W. et al.
- Protic, D., see Riepe, G.
- Pscheid, P., Schudt, C. and Plattner, H., 160, 178
- Pullan, B.R., see Rutherford, R.A. et al.
- Purohit, S.N., 346, 378
- Puschett, J.B., see Wielopolski, I. et al.
- Puumalainen, P., Uimairihuhta, A., Alhva, E.M. and Olkkonen, H., 197, 239, 240, 247
- Puumalainen, P., Olkkonen, H. and Sikanen, P., 239, 240, 247; 241, 248
- Raganella, L., see Magrini, A. et al.
- Räsänen, J., see Hyvärinen-Dabek, M. et al.
- Raith, B., Roth, M., Gölner, K., Gonsior, B., Ostermann, H. and Uhlhorn, C.D., 142, 149, 177
- Raith, B., Stratmann, A., Wilde, H.R., Gonsior, B., Brüggerhoff, S. and Jackwerth, E., 149, 150, 177; see Brüggerhoff, S. et al.; see Gonsior, B. et al.; see Hüfner, M. et al.; see Klockenkämper, R. et al.; see Wilde, H.R. et al.
- Raman, S., see Sparks, C.J. Jr. et al.
- Ramsden, D.R., see Watt, D.E.
- Rao, P.V., see Bambynek, W. et al.
- Rapaport, M.S., Mantel, M. and Shenberg,

- C., 82, 120
 Rapaport, M.S., Mantel, M. and Nothmann, R., 154, 179
 Raphael, D., see Yaffe, W.G. et al.
 Raptis, S.E., Wegscheider, W., Knapp, G. and Tblg, G., 154, 179
 Rashiduzzaman Khan, M.D., see Lodhi, A.S. et al.
 Reich, see Michel, R. et al.
 Reiss, K., Ing, D. and Schuster, W., 225, 248
 Reizenstein, P., see Carlmark, B., 307, 376;
 Reizenstein, P., 356, 379
 Rhodes, J.R., 43, 69, 119
 Ribberfors, R., see Carlsson, G.A. et al.
 Ricci, E., see Sparks, C.J. Jr. et al.
 Ricci, M., see Cesareo, R. et al. see Del Principe, D. et al.
 Rich, C., see Nelp, W.B. et al.
 Richter, F.W., see Bombelka, E. et al.; see Koenig, W. et al.
 Ricourt, A., 330, 378
 Rieder, N., see Hubert, G. et al.
 Riepe, G. and Protic, D., 58, 119
 Ries, H., see Bombelka, E. et al.
 Riviere, R., see Lenihan, J.J. et al.
 Roach, N., see Hall, G.S. et al.
 Robaye, G., see Weber, G. et al.
 Robberecht, H., see Van Grieken, R. et al.
 Robertson, I., see Boddy, K. et al.
 Roelandts, J., see Weber, G. et al.
 Roginsky, M., see Cohn, S.H. et al.
 Rokita, E., see Gonsior, B. et al.; see H8fert, M. et al.
 Roland, M., see Monsen, G. et al.
 Rolfe, I., see Otis, J.N. et al.
 Rosenfeld, I. and Beath, O.A., 12, 16
 Roth, M., see Gonsior, B. et al.; see Raith, B. et al., see Wilde, H.R. et al.
 Roy, J.S.C., Kissel, L. and Pratt, R. H., 203, 247;
 Roy, J.S.C., 205, 206, 247; see Kissel, L. et al.
 Rubenstein, E., 186, 194; see Otis, J.N. et al.
 Rudd, T.C., see Nelp, W.B. et al.
 Rullhusen, P., see Schaupp, D. et al.
 Rundo, J. and Bunce, L.J., 304, 376;
 Rundo, J., 357, 379
 Rupp, H. and Weser, U., 14, 17
 Rustgi, S., see Ling, S.S. et al.
 Rutherford, R.A., Pullan, B.R. and Isherwood, I., 209, 247
 Rutt, B.K., Cunningham, I.A. and Fenster, A., 181, 194
 Ryckenwaert, A., see Maziere, B. et al.
 Sacchetti, G., see Cesareo, R. et al.
 Sackler, J.P., see Huddleston, A.L.
 Saleh, N., 154, 179
 Salewski, S., see Brüggerhoff, S. et al.
 Salmi, T.T., see Kleimola, V. et al.
 Salminen, L., see N8nt8, V. et al.
 Salmon, L., see Anderson, J. et al.
 Sansoni, B. and Iyengar, G.V., 278, 297
 Santon, L.W., see Battista, J.J. et al.
 Satish, J., see Bonani, G. et al.
 Sayed, E.M., see Piesch, F.
 Sawa, K., see Suzuki, H. et al.
 Sawitzky, A., see Cohn, S.H. et al.
 Scarnati, E., see Cesareo, R. et al.
 Sch8tzler, M.P., 197, 239, 247
 Schaupp, D., Schumacher, M., Smend, F., Rullhusen, P. and Hubbell, J.H., 203, 205, 247
 Schmidt, P.B., see Colbert, C. et al.
 Schmidt Nielsen, B., see Bisgård, K. M. et al.
 Schmitt, G., see Hubert, G. et al.
 Schneider, E.W. and Hill, R.F., 73, 120
 Sch8nenberger, M., see Trebert Haeberling, S. et al.
 Schramel, P., see Br8tter, P., 123, 132, 176; 160, 170, 178
 Schudt, C., see Pscheid, P. et al.
 Schumacher, H., see Hartmann, G. et al.
 Schumacher, M., see Schaupp, D. et al.
 Schuster, W., see Reiss, K. et al.
 Schwachman, H., see Kopito, L. et al.
 Sciuti, S., see Gigante, G.E.
 Scott, M.C.; see El-Sharkawi, A.M. et al.; see Smith, J.R.N. et al.; see Somervaille, L.J. et al.
 Seaman, G.G. and Shane, K.C., 149, 177
 Sen, P. and Mehta, G.K., 91, 120
 Send, W., see Hubert, G. et al.
 Senftle, F., see Duffey, D. et al.
 Seyfarth, H., Hassan, A.M., Hrastnik, B., Gattel, P. and Delang, W., 353, 355, 379
 Sgarbazzini, M., see Cesareo, R. et al.
 Shadoan, D.J., see Cahill, J.A. et al.
 Shane, K.C., see Seaman, G.G.
 Shani, J., see Van Grieken, R. et al.
 Shapiro, I.M., see Bloch, P.
 Shenberg, C., see Rapaport, M.S. et al.
 Shima, K., see Maruhashi, A. et al.
 Shirley, V.S., see Lederer, C.M.
 Shohet, S.B., see Price, D.C. et al.
 Shrimpton, P.C., 229, 230, 248
 Shukla, K.K., see Cohn, S.H. et al.
 Shukla, S.S., see Greenfield, M.R. et al.

- Siedband, M.P., see Mistretta, C.A. et al.
- Siebert, E., see Pfeiffer, C.C. et al.
- Sikanen, P., see Puumalainen, P. et al.
- Simkiss, K., see Taylor, M.G.
- Simmons, U., see Hall, G.S. et al.
- Simonoff, G., see Simonoff, M. et al.
- Simonoff, M., Llabador, Y., Hamon, C., Berdeu, B., Simonoff, G., Conri, C., Fleury, B., Couzigou, P. and Lucena, A., 287, 297
- Simpson, A.E. and Dyson, N.A., 153, 179
- Simpson, J.D., see Kennedy, N.S.J. et al.
- Simpson, O.D., see Brugger, R.M.
- Sinclair, F., see Squillante, M.R. et al.
- Singh, D., 329, 330, 377; 330, 378
- Singh, M., Dabrowski, A.J., Huth, G. C., Iwanczyk, J.S., Clark, B.C., and Baird, A.K., 57, 119
- Sivyer, A., see Ali, P.A. et al.; see Evans, C.J. et al.
- Sjostrand, B., see Birks, G. et al.
- Skaggs, L.S., see Stinchcomb, T.G. et al.
- Skerfving, S., see Birks, G. et al.
- Skillicorn, B., 47, 119
- Sky-Peck, H.H. and Joseph, B.J., 80, 81, 82, 120
- Sloestrand, N.G., see von Dardel, G. F.
- Smend, F., see Schaupp, D. et al.
- Smith, D.B., see Gvozdanovic, D. et al.
- Smith, E.C., see Dunea, G. et al.
- Smith, E.M., see Gottlieb, N.L. et al.
- Smith, F.C. Jr. and Masi, O.H., 65, 120
- Smith, F.W., see Catto, G.R.D. et al.
- Smith, J.W., 299, 375
- Smith, J.W. and Boot, S.J., 299, 375; see Anderson, J. et al.
- Smith, M.A., see Kennedy, N.S.J., et al.
- Smith, P.M., see Gottlieb, N.L. et al.
- Smith, R.J.H., Athwal, S.S., Chettle, D.R., Scott, M.C., 112, 121
- Smits, J., Nelissen, J. and Van Grieken, R., 64, 120
- Smits, J. and Van Grieken, R., 64, 120; see Van Grieken, R. et al.
- Snyder, W.S. and Neufeld, J., 323, 377
- Snyder, W.S., 5, 16
- Sohler, A.H., see Pfeiffer, C.C. et al.
- Soler, N.G., see Walsh, C.H. et al.
- Solfanelli, S., see Guzzardi, R. et al.
- Somervaille, L.J., Chettle, D.R. and Scott, M.C., 103, 104, 121;
- Somervaille, L.J., Chettle, D.R., Scott, M.C., Aufderheide, A.C., Wallgren, Wittmers, L.E. Jr., Rapp, G.R., 104, 105, 106; see El-Sharkawi, A.M. et al.
- Sorenson, J.A. and J.R. Cameron, 181, 194; see Cameron, J.R.; see Mazzess, R.B. et al.
- Sparks, C.J. Jr., 52, 119;
- Sparks, C.J. Jr. and J.B. Hastings, 52, 119
- Sparks, C.J. Jr., Ricci, E., Raman, S., Krause, M.O., Gentry, R.V., Yakel, H.L. and Hastings, J.B., 52, 119
- Squillante, M.R., Farrell, R., Lund, J.C., Sinclair, F., Entine, G. and Keller, K.R., 58, 119
- Stalp, J.T. and Mazess, B., 197, 207, 240, 247
- Starke, K., see Wundt, K. et al.
- Stern, R., see Ling, S.S. et al.
- Stievano, B.M., see Berti, M. et al.
- Stinchcomb, T.G., Kuchnir, F.T. and Skaggs, L.S., 324, 377
- Stoeckle, J.D., Hardy, H.L. and Weber, A.I., 312, 376
- Stoenner, R.W., see Glaros, D. et al.; see Krummer, F.H. et al.
- Stone, S.F. and Zeisler, R., 284, 297
- Stratmann, see Gonsior, B. et al.; see Höffert, M. et al.; see Raith, B. et al.
- Strijckmans, K., see Wanters, G. et al.
- Strochkova, L.S., see Zavoronkov, A.A.
- Strong, J.A., see Boddy, K. et al.; see Kennedy, N.S.J. et al.
- Struelens, M., see Monsen, G. et al.
- Stump, I.G., see Agarwal, M. et al.
- Sun, S., see Yang, G. et al.
- Sunderman, see Pershagen, G. et al.
- Suzuki, , Higuchi, T., Sawa, K., Ohtaki, S. and Horiuchi, Y., 12, 16
- Swann, S.J., see Price, D.C. et al.
- Swift, C.D., see Bambynek, W. et al.
- Szirmai, E., see Gonsior, B.
- Takacs, J., see Watt, F. et al.
- Tallarida, B.M., see Cesareo, R. et al.; see Del Principe, D. et al.
- Taylor, C.G., see Gvozdanovic, D. et al.
- Taylor, M.G. and Simkiss, K., 2, 15
- Teraoka, H., 13, 17
- Theus, R.B., see Amals, H.I. et al.
- Thomas, B.J., Wright, M.S., Ozbaz, E. and Vartsky, D., 303, 375

- Thomas, B.J., Harvey, T.C., Chettle, D.R., Mc Lellan, J.S. and Fremlin, J.H., 307, 376; see Bell, C. M. et al.; see Ettinger, K.V. et al.; see Leach, M.O. et al.; see Mc Lellan, J.S. et al.; see Ozbass, E. et al.; see Vartsky, D. et al.; see Walsh, C.M. et al.
- Thompson, K., see Zanzi, I. et al.
- Thompson, W.E. and Engesser, W.E., 311, 376; see Engesser, F.C. et al.
- Thompson, R.H., 2, 15
- Timms, D.N., Cooper, M.J. and Holt, R.S., 243, 248
- Tipton, I.H., Johns, J.C. and Boyd, M., 14, 17
- Tischler, R., see Harding, G.
- Tochilin, E., see De pangher, J.
- Tölg, G., see Raptis, E. et al.
- Tolpin, E.I., see Zamenhof, R.G. et al.
- Tomlinson, R.W.S., see Anderson, J. et al.; see Battyl, C.K. et al.
- Topping, J., 277, 297
- Tothill, P., see Boddy, K. et al.; see Kennedy, N.S.J. et al.
- Trebert Haerberlin, , Lux, F., Karl, J., Spruss, T. and Schönenberger 288, 297
- Tregnaghi, C., see Berti, M. et al.
- Tsoufanidis, N., 349, 378
- Tsubaki, T. and Irukayama, K., 13, 17
- Tsumita, T., see Koyama-Ito, H. et al.
- Tveit, A.B., see Lindh, U.
- Uhlhorn, C.D., see Raith, B. et al.; see Wilde, H.R. et al.
- Uimairihuhta, A., see Puumalainen, P. et al.
- Ulin, K. and Zamenhof, R.G., 313, 315 316, 377
- Underwood, E.J., 11, 16; 170, 178
- Uttley, C.A., 338, 378
- Valkovic, V., 8, 13, 16; 166, 170, 178; see Orlic, I. et al.
- Vanballenberghe, L., see Versieck, J. et al.
- Vanderborcht, B., see Van Grieken, R. et al.
- Vandercastele, C., see Wauters, G. et al.
- Van der Heide, I.A., see Dikoff, T. G.M.H. et al.
- Van der Kam, P.M.A., Vis, R.D. and Verheul, H., 149, 177
- Van der Malen, H., see Fuller, E.G. et al.
- Van der Stap, C.C.A.P., see Vis, R.D. et al.
- Vanderstappen, M., see Van Grieken, R. et al.
- Van Dyck, P., see Van Grieken, R. et al.
- Van Dyk, G., see Clarke, R.L.
- Vane, R. and Skillicorn, B., 47, 119
- Van Espen, P., see Maenhaut, W. et al.
- Van Grieken, R., Bresseleers, K., Smits, J., Vanderborcht, B. and Vanderstappen, M., 64, 120
- Van Grieken, R., Robberecht, H., Shanni, J., Van Dyck, P. and Vos, L. 65, 120; see Smits, J.
- Van Rinsvelt, H.A., Hurd, R.W., Kondoro, J.W.A., Andres, J.M. and Mickle, J.P., 170, 178; see Maenhaut, W. et al.
- Vartsky, D., Lo Monte, A., Ellis, K.J., Yasumura, S. and Cohn, S.H., 303, 307, 376
- Vartsky, D., Thomas, B.J., Hawkes, D.J., and Fremlin, J.H., 317, 322, 377
- Vartsky, D., Wielopolski, L., Ellis, K. J. and Cohn, S.H., 322, 377
- Vartsky, D., Ellis, K.J., Hull, D.H. and Cohn, S.H., 324, 377; see Ellis, K.J. et al.; see Ettinger, K.V. et al.; see Morgan, W.D. et al.; see Thomas, B.J. et al.; see Wielopolski, L. et al.
- Vasvani, A.N., see Cohn, S.H. et al.; see Wielopolski, L. et al.
- Vaux, D.J.T., see Watt, F. et al.
- Veigle, Wm.J., see Hubbell, J.H. et al.
- Verghese, K., see Gander, P. et al.
- Verheul, H., see Vis, R.D.; see Van der Kam, P.M.A. et al.
- Vernon-Roberts, B., 15, 17
- Versieck, J., 3, 4, 8, 15, 16; Versieck, J., Vanballenberghe, L., Lerne, G., Barbier, F., Cornelis, R. and De Rudder, J., 15, 17
- Viale, D., see Martoja, R.
- Viezzoli, G., see Cesareo, R.
- Vis, R., see Houtman, J.P.W. et al.
- Vis, R.D., Van der Stap, C.C.A.H. and Bos, A.J.J., 166, 178
- Vis, R.D. and Verheul, H., 147, 177
- Vis, R.D., Lenglet, W.J.M. and Van der Stap, C.C.A.H., 155, 179; see Van der Kam, P.M.A. et al.
- Von Dardel, G.F., 346, 378
- Von Dardel, G.F. and Sloestrand, N.G., 346, 378
- Vos, L., see Van Grieken, R. et al.
- Vyborny, C.J., see Doi, K. et al.
- Waker, A.J., see Makrigiorgios, G.
- Walsh, C.H., Soler, N.G., James, H.M., Harvey, T.C., Fremlin, J.H., Thomas, B.J., Fitzgerald, M.G. and

- Melius, J.M., 363, 381
 Walter, R.L., see Jaklevic, J.M.;
 Wang, M. and Yingyang Xuebao, 12, 16
 Wang, S., see Yang, G. et al.
 Wanner, H.U., see Bonani, G. et al.
 Ward, N.J. and Mason, J.A., 287, 297
 Warner, G.T., 359, 379
 Waslien, C.I., 12, 16
 Watermark, T., see Birks, G. et al.
 Wätjen, U., see Bombelka, E. et al.
 Watt, D.E., see Lawson, R.C. et al.
 Watt, D.E. and Ramsden, D.R., 356, 379
 Wauters, G., Vandecasteele, C., Strijckmans, K. and Hoste, J., 294, 297
 Weaver, J.B., see Huddleston, A.L.
 Webb, M., 8, 16
 Webber, C.E. and Kennett, T.J., 197, 212, 223, 224, 225, 228, 229, 247; see Cousins, T. et al.; see Garnett, E.S. et al.; see Kerr, S.A. et al.
 Weber, A.I., see Stoeckle, J.D. et al.
 Weber, G., Robaye, G., Bartsch, P., Collignon, A., Beguin, Y., Roelandts and Delbruck, J.M., 170, 178;
 Weber, G., Robaye, G., Delbrouck, J. M., Roelandts, J., Diberers, O., Bartsch, P. and De Pauw, M.C., 153, 179
 Wegscheider, W., see Raptis, S.E. et al.
 Weigele, W.J., see Hubbell, J.H. et al.
 Wellum, G.R., see Zamenhof, R.G. et al.
 Weser, U., see Rupp, H.
 Wester, P.O., see Lindh, W. et al.
 White, D.R., 209, 210, 247
 Whiting, J.S., see Ling, C.S. et al.
 Wielopolski, L., Ellis, K.J., Vaswani, A.N., Cohn, S.H., Greenberg, A., Puschett, J.B., Parkinson, D.K., Fetterolf, D.E. and Landrigan, P.J., 103, 104, 121
 Wielopolski, L., Vartski, D., Yasumura, S. and Cohn, S.H., 106, 108, 109, 121
 Wielopolski, L., Vartski, D. and Cohn, S.H., 317, 318, 377
 Wielopolski, L., Vartski, D., Rorer, D.C., Levy, P.W. and Cohn, S.H., 318, 322, 377
 Wielopolski, L., Ancona, R.C., Masey, R.Y., Vaswani, A.N. and Cohn, S.H., 322, 377
 Wielopolski, L. and Cohn, S.H., 359, 379; see Ettinger, K.V. et al.; see Vartski, D. et al.
 Wiesener, W., Geerner, W. and Niese, S., 13, 15, 17
 Wilde, H.R., Bischof, W., Raith, B., Uhlhorn, C.D. and Gonsior, B., 134, 147, 177; see Raith, B. et al.
 Wilder, B.J., see Rinsvelt, H.A. et al.
 Williams, E.D., Boddy, K., Harvey, I., and Haywood, J.K., 360, 362, 380
 Williams, E.T., 149, 177
 Williams, J., see Nelp, W.B. et al.
 Williams, J.R., see Mijneer, B.J.; see Broerse, J.J. et al.; see Williams, J.R. et al.
 Williams, M.M.R., 345, 378
 Williamson, C.F., Boujot, J.P. and Picard, J., 290, 297
 Williamson, F.S. and Frigerio, M.A., 330, 378
 Willis, J.P., see Feather, C.E.
 Willis, R.D., see Walter, R.L. et al.
 Wintrobe, M.M., Cartwright, G.E. and Gubler, C.J., 14, 17
 Wiren, K., see Forslind, B. et al.
 Woggon, H. and Klein, S., 3, 16
 Wolf, E.A. and Munro, T.R., 215, 247
 Wolf, W.R., 4, 16
 Wolfe, R.S., see Frankel, R.B. et al.
 Wölfl, W., see Bonani, G. et al.
 Wooler, K.K., see Clayton, E.
 Wright, M.S., see Thomas, B.J. et al.
 Wundt, K., Duscher, H. and Starke, K., 158, 178
 Xenoulis, A., see Katsanos, A. et al.
 Yaffe, M.J., see Johns, P.C.
 Yakel, H.L., see Sparks, C.J. Jr. et al.
 Yang, G., Zhou, R., Sun, S., Wang, S., and Li, S., 12, 16
 Yasumura, S., see Cohn, S.H. et al.; see Ellis, K.J. et al.; see Glaros, D. et al.; see Morgan, W.D. et al.; see Vartsky, D. et al.; see Wielopolski, L. et al.
 Young, see Marion, J.B.
 Yu, Z.C., see Ling, D.S. et al.
 Zaman, M.B., see Khan, A.H. et al.
 Zamenhof, R.G., Deutsch, O.L. and Murray, B.W., 307, 315, 316, 348, 376
 Zamenhof, R.G., Murray, B.W., Brownell, G.L., Wellum, G.R. and Tolpin, E.I., 331, 334, 377, 378
 Zamenhof, R.G., see Cohn, S.H. et al.; see Ellis, K.J. et al.; see Ulin, K. et al., see Z
 Zanzi, I., Colbert, C., Backtell, R., Thompson, K., Aloia, J. and Cohn, S.H., 360, 379; see Cohn, S.H. et al.; see Ellis, K.J. et al.
 Zavoronkov, A.A. and Strkhova, L.S., 12, 16

- Zeisler, R., see Stone, S.F.
Zeman, H.D., see Otis, J.N. et al.
Zhou, R., see Yang, G. et al.
Zierold, K., 159, 160, 178
Zolotukhin, V.G., Keirim-Markus, I.B.,
 Kochetkov, O.A., Obaturov, G.M.
 and Cvetkov, V.I., 322, 323, 326,
 327, 377
Zweifel, P.F., see Ferziger, J.H.

SUBJECT INDEX

- accuracy and precision (PIXE-analysis) 67
- activation analysis
 - applications to biomedical samples 279,296
 - basic Equations 256
 - characterization of macromolecules 284
 - description of systems for in vivo A.A. 365
 - detection of heavy toxic metals 363
 - detector facilities for in vivo NAA 348
 - determination of protein concentration 285
 - fast neutron irradiation 320
 - ferrokinetic studies 293
 - gamma-rays from inelastic scattering of neutrons 309
 - induced radioactivity 301
 - in vitro A.A. 249-297
 - in vivo A.A. 299-380
 - neurological disorders 287
 - nuclear resonance fluorescence 317
 - orthopedic implants 286
 - photonuclear activation 312
 - platinum determination 288
 - prompt gamma-rays from neutron-capture 304
 - sample preparation 280
 - total body measurements 362
- aluminium (in brain) 287
- analysis of
 - air particulate matter 67, 162
 - Al (in brain) 287
 - Ba (in gunshot residue) 41
 - body fluids 166
 - Br (in blood) 82, 88, 154
 - Ca (in bone) 360
 - cataract lens 172
 - Cd 293
 - Cd (in kidney) 110
 - Cd (in serum) 294
 - erythrocyte 168
 - erythrocyte survival 87
 - extracellular fluid space 88
 - fat content in tissues 191
 - Fe (in blood) 73
 - Fe (in serum) 75
 - Fe (stable tracer) 158
 - granulocyte survival 88
 - gunshot residue 91
 - hair 154
 - I (in thyroid) 112
 - I (stable tracer) 90
 - kidney 110-116
 - orthopedic implants 286
 - pharmaceuticals 174
 - platelet survival 84
 - platinum (in kidney) 116
 - proteins 285
 - Pb 293
 - Pb (in bone) 104
 - Pb (in gunshot residue) 91
 - Pb (in teeth) 114
 - Pb (in serum) 295

- for PIXE-analysis 157
- for XRF-analysis 34-40
- analysis of
 - Rb 85-88
 - red cell volume 89
 - red cell survival 86
 - Se (in blood) 83, 154
 - skin metallization 95
 - Sr (in bone) 110
 - Tl (in serum) 295
 - urinary calculi 98
 - V (in depressive patients) 287
 - water 63, 161
- atomic form factor 30, 205
- atomic structure 20-25
- attenuation coefficient 27
- attenuation
 - effects in scattered radiation 216
 - of radiation 27-33; 182-184
 - differential 185
- background
 - in XRF-analysis 41
 - in PIXE 135
- barium (in gunshot residue) 98
- basic Equations for A.A. 256
- body fluids (trace elements) 73-83; 166-169
- bone
 - mineral content (attenuation measurements) 189
 - lead in 104
 - strontium in 106
 - mineral determination (coherent/Compton ratio) 239
- brain (Al in) 287
- branching factor 35
- bromine (in blood) 82, 88, 154
- cadmium (in kidney) 110 360
- cadmium (in serum) 294
- calcium (by in vivo A.A.) 360
- cataracta senilis (PIXE-analysis) 172
- cesium (in red cells) 89
- characteristic X-rays 125
- coherent scattering 33; 203-207
- coherent to Compton scattering 207-212; 238-246
- comparison between XRF and PIXE 145
- composition of selected tissues 5-11
- Compton
 - differential cross section 31, 199
 - effect 264-266
 - scattering (dual energy) 231
 - scattering techniques 225
- contamination problems 3
- cross section 127
- cyclotrons for A.A. 261
- composition of human
 - blood 9
 - bone 10
 - hair 10
 - kidney 7
 - liver 7
 - lung 7

detection limits for XRF-analysis 40
 detector efficiency
 - for A.A. 276; 351
 - for XRF analysis 40
 detectors for in vivo neutron A.A. 348-359
 - scintillators 351
 - Ge-detectors 353
 - whole body counters 356
 - partial body counters 359
 detectors for in vitro A.A. 263-269
 detectors for XRF-analysis 54-57
 - proportional gas counters 54
 - scintillators 56
 - semiconductor-detectors 56
 differential attenuation 185
 dosimetry for in vivo neutron A.A. 323-328
 dual-energy Compton scattering 231
 effective atomic number 207
 electron density 202, 230
 electronic chain for XRF-analysis 58
 energy resolution for X-ray detectors 55
 enrichment methods 64
 erythrocyte (PIXE-analysis) 168
 excitation sources for XRF-analysis 45-54
 extracellular fluid space 88
 fast neutron irradiation 320-328
 fat content in tissues 191
 filters (for XRF-analysis) 65,66,74
 fluorescence yield 21, 25, 26, 34, 35
 forensic science (XRF-applications) 91-98
 form factor (atomic) 33, 205
 full energy peak efficiency 33, 205
 geometrical arrangement in XRF-analysis 43
 geometrical factor in XRF-analysis 35
 geometry in photon scattering 213
 glomerular filtration rate 90
 gunshot residue XRF-analysis 91
 hair (PIXE-analysis) 154, 155
 imaging techniques using Compton scattering 234
 imaging using differential transmission 192
 incoherent scattering function 31, 200
 inelastic scattering of neutrons 309
 interaction of radiation with matter 27
 iodine
 - in thyroid 112-114
 - stable tracer 90
 ionization 125, 127
 iron
 - in blood 73
 - in serum 75
 - stable tracer in blood 293
 kidney (analysis of)
 - cadmium 110
 - mercury 110
 - platinum 116
 Klein-Nishina cross section 31

- lead analysis
 - in bone 104
 - in gunshot residue 91
 - in teeth 114
 - in serum 295
- macromolecules (characterization with N.A.A.) 284
- mercury (in kidney) 110
- microprobe (proton) 150
- multi-channel analyzer 58
- multiple scattering 221
- neutron capture and prompt gamma-rays 304
- neutron sources for in vivo N.A.A.
 - low-energy sources 329
 - (γ ,n) sources 335
 - accelerator neutron sources 338
 - pulsing of neutron flux 342
 - intensities 342
 - pulsed beams 343
- nonhomogeneity of the sample (in scattering techniques) 223
- nuclear decay 252
- nuclear reactions 249
- nuclear resonance fluorescence 317
- orthopedic implants 286
- pair production 267
- photoelectric effect 28, 264
- photon wavelength 31
- PIGE 152
- PIXE-analysis
 - of air particulates 162
 - of body fluids 166
 - human cataract lens 172
 - of pharmaceuticals 174
 - of water samples 161
 - physical principles 124
 - under vacuum conditions 147
 - with external beam 149
- PIXE-microbeam analysis of biological tissues 170
- photonuclear activation 312
- platelet-survival 84
- platinum (in kidney) 116
- platinum (in antineoplastic treatment) 288
- proportional gas counters 54
- proton activation analysis
 - determination of Cd 293
 - determination of Pb 293
 - determination of Tl 293
 - with prompt gamma emission 295
- proton microbeam 150
- pulsed neutron beams for in vivo N.A.A. 343
- radiochemistry 278
- Rayleigh scattering 33, 203
- reactors for neutron A.A. 258
- red cell volume 89
- red cell survival 86
- resins (ion-exchange) 65
- rubidium (stable tracer for blood cells) 85-88
- samples
 - for in vitro A.A.) 277

scintillation detectors 56
 secondary radiation 48, 49, 50, 51, 52
 secondary target 40
 selenium (in blood) 83, 154
 semiconductor detectors 57, 353
 sensitivity of in vivo N.A.A. 275
 single channel analyzers 59
 skin metallization 95
 sources
 - for in vivo N.A.A. 329-343
 - for PIXE-analysis 148
 - for XRF-analysis 45-53
 strontium (in bone) 110
 synchrotron radiation 52
 survival studies of blood cells 83-88
 - platelets 84
 - red-cells 86
 - granulocytes 88
 target preparation for PIXE-analysis 157
 teeth (lead in) 114, 115
 thallium (in serum) 295
 thick samples for XRF-analysis 34
 thin samples for XRF-analysis 37
 thyroid (iodine in) 112
 trace elements 2-14
 - functions of 2-14
 tracers of blood cells 83-91; 293
 urinary calculi 98
 vanadium (in depressive patients) 287
 water
 - enrichment methods 64, 65
 - PIXE-analysis 161
 - XRF-analysis 63
 XRF-analysis of
 - air particulates 67
 - bromine in blood 82
 - bromine for EFS 88
 - cadmium in kidney 110
 - cesium for RCV measurement 89
 - iodine for GFR measurement 90
 - iodine in thyroid 112
 - iron in blood 73
 - iron in serum 75
 - lead in bone 104
 - lead in teeth 114
 - mercury in kidney 116
 - platinum in kidney 116
 - rubidium in granulocytes 88
 - rubidium in platelets 84
 - rubidium in red cells 86
 - skin metallization 95
 - stable tracers in blood 83-84
 - strontium in bone 106
 - trace elements in serum 78
 - urinary calculi 98
 - water samples 63-67

X-Ray Fluorescence

- apparatus 43
- detectors 54
- excitation sources 45
- minimum detection limits 40
- radiation flux 47
- radioactive sources 45
- synchrotron radiation 52
- theoretical background 34
- thick samples 34
- thin samples 37
- X-ray spectrum 60
- X-ray transitions 126
- X-ray tubes

X-rays

- energies and intensities 21
- emission 125

X-ray spectrum 60

- automatic analysis 62

X-ray transitions 126